Cuyama Valley, California Hydrologic Study: An Assessment of Water Availability

Water resources are under pressure throughout California, particularly in agriculturally dominated valleys. Since 1949, the Cuyama Valley's irrigated acreage has increased from 13 to 35 percent of the valley. Increased agriculture has contributed to the demand for water beyond natural recharge. The tools and information developed for this study can be used to help understand the Cuyama Valley aquifer system, an important resource of Santa Barbara County.

To evaluate the historical use and availability for future use of groundwater, the U.S. Geological Survey (USGS), in cooperation with the Santa Barbara County Water Agency, has recently completed a hydrologic study of Cuyama Valley. The study found continued depletion of groundwater storage in the Main zone of the Valley's groundwater basin and, to a lesser extent, in the Sierra Madre Foothills (figs. 1, 2). Since about 1949, nearly 2.1 million acre-feet (acre-ft) of groundwater has been removed from storage in the Cuyama Valley aquifer system, which, on average, is enough to supply every resident of California with water for 4 months.

To complete the study, the USGS developed hydrologic models of Cuyama Valley (Hanson and others, 2014) to analyze water availability. The Cuyama Valley Hydrologic Model (CUVHM) simultaneously accounts for changing water supply and demand across the landscape and simulates surface-water and groundwater flow across the entire valley.

This new hydrologic modeling tool can be used to address issues related to water-resource sustainability that affect food and water security:

- Land-use change and its effects on water resources.
- Effects of water supply and demand on water quality and land subsidence.
- Effects of climate variability and climate change on available water resources.

Currently, groundwater is the sole source for domestic, agricultural, and municipal water use in the Cuyama Valley. Groundwater withdrawals, mainly for irrigation, have resulted in water-level declines of more than 300 feet (ft) in the area since the 1940s.

Cuyama Valley Water Facts

- There are three groups of subregions in the valley—The Main zone, the Sierra Madre Foothills, and the Ventucopa Uplands (fig. 2). There is minimal groundwater flow between these subregions, which are separated by faults, have different hydrologic and geologic properties, and respond differently to groundwater pumping and recharge. The largest groundwater withdrawals in excess of natural recharge (overdraft) are in the Main zone, with some additional groundwater depletion in the Sierra Madre Foothills, but no permanent depletion in the Ventucopa Uplands.
- Estimated groundwater use for irrigation is twice the 61-year average annual recharge, with about 72 percent of groundwater-storage depletion in the Main-zone subregions.
- Natural recharge and climate have approximately 27-, 22-, 13.5-year cycles that could be used for water-management periods. Groundwater recharge, which occurs primarily in wet years, is not sufficient to replenish the storage depletion driven by current demands.
- Model simulations indicated that a reduction in the amount of water used for irrigation in the Main zone to the amount of average annual recharge would reduce, but not eliminate, groundwater-storage depletion, because most of the recharge is not reaching the aquifers in the Main zone.
- More complete recovery of groundwater storage occurs with cessation of agriculture in the Main zone, but limits valley-wide pumpage to about half of average recharge, which may not allow sustainable agriculture with current practices and land use.
- There are no local criteria for definition of sustainability*, no current water-management practices in place, and no longer term water-management plan for Cuyama Valley.
- Water in the region has historically been of poor quality and continues to be used for ranching, agriculture, and oil and gas production.
- A basin management plan aligned with climate cycles, land use, and planning policies could be developed to reduce groundwater deficits and extend the life of the basin using the CUVHM model.

*Water-resource sustainability is the development and use of water in a manner that can be maintained for an indefinite time without causing unacceptable environmental, economic, or social consequences.

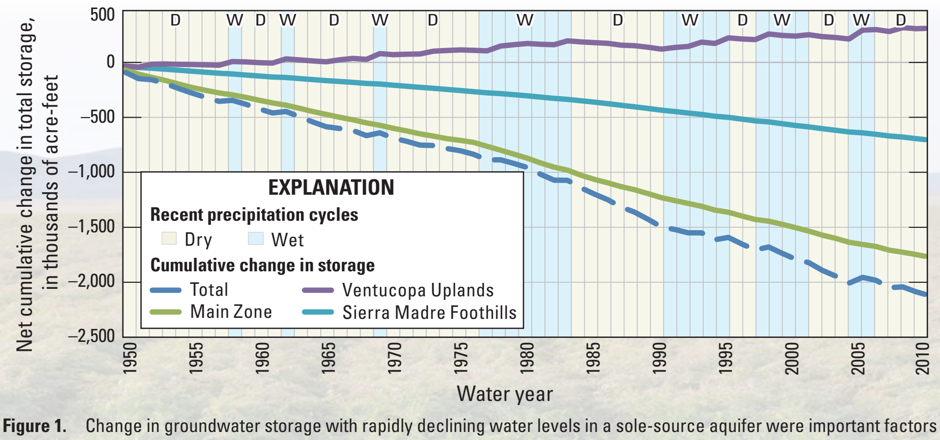

Figure 1. Change in groundwater storage with rapidly declining water levels in a sole-source aquifer were important factors in undertaking and completing this study. To better understand the system, the Cuyama Valley has been split into three groups of subregions: (1) the Main zone, (2) the Sierra Madre Foothills, and (3) the Ventucopa Uplands. Although partially connected hydraulically, the groundwater system in these subregions generally responds independently to different supply sources and demands.

U.S. Department of the Interior
U.S. Geological Survey

Fact Sheet 2014–3075
August 2014

Cuyama Valley Hydrologic Model

The CUVHM is built on previous studies conducted by the USGS, Santa Barbara County Water Agency, and other Federal, State, and local studies. The CUVHM was constrained by comparing simulated and historically observed groundwater levels and subsidence. In the Cuyama Valley, the model simulates unmetered historical pumpage and streamflow for changing land use for 61 water years (1950 to 2010). This model provides a better understanding of valley-wide supply and demand for water.

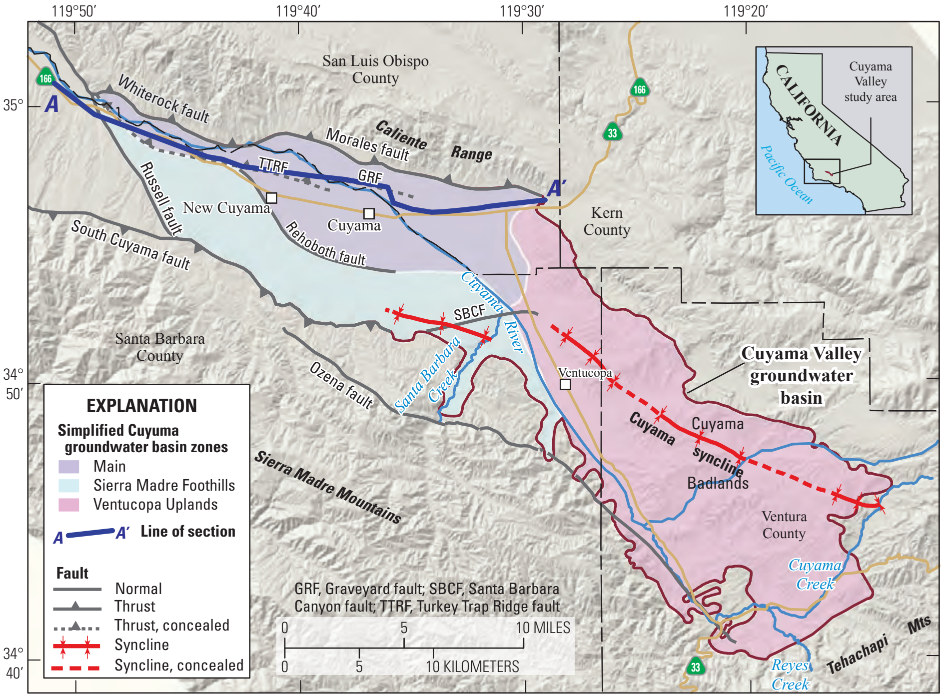

Base modified from U.S. Geological Survey digital data, various scales
Albers Equal Area Projection, North American Datum of 1983

Figure 2. Model framework for the Cuyama Valley Hydrologic Model. To create enough detail to be practical for informing water-management decisions, the aquifer system was divided into 6,817 model cells of 15.4 acres each and, vertically, into 3 model layers as much as 4,710 ft thick. This cell represents the typical land parcel in land-use maps, which will facilitate future linkage of the model to remotely sensed land-use data.

Model Features

- The combined use and movement of water on the landscape, streams, and aquifers were simulated with an integrated hydrologic model called MODFLOW-OWHM (One Water Hydrologic Model, Hanson and others, 2014).
- The Basin Characteristics Model was used to estimate the recharge and runoff from all of the surrounding watersheds (Hanson and others, 2014).
- A 3-D stratigraphic and texture model was developed to characterize the hydraulic properties and the layering and structure of the aquifers (figs. 3, 4; Sweetkind and others, 2013).
- Data were compiled to simulate changing land ownership, land use, wells, streamflow, and climate.

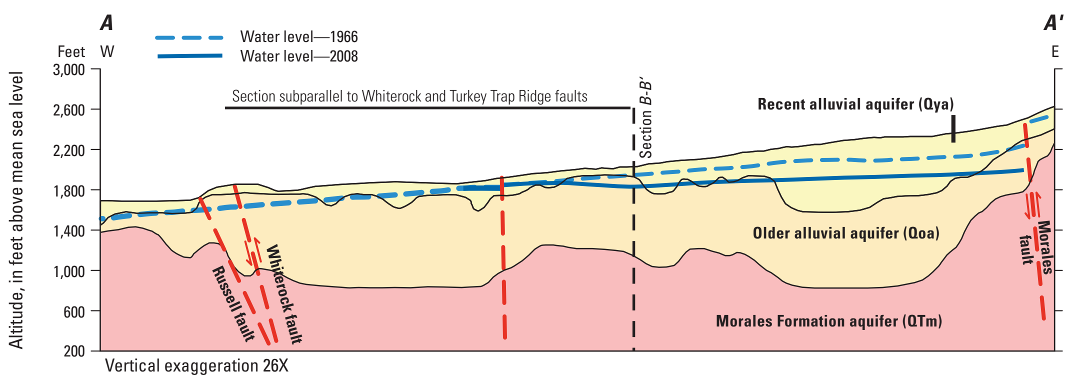

Figure 3. Aquifer-system cross section of the Cuyama Valley Hydrologic Model along line A-A′ in figure 2. The recent alluvial aquifer (model layer 1) reaches a maximum thickness of about 630 ft. The older alluvial aquifer (model layer 2) has an estimated maximum thickness of 1,350 ft. The Morales Formation (model layer 3) has an estimated maximum thickness of 4,710 ft.

3-D Geologic Framework and Texture Model

A 3-D geologic framework model was created to define the stratigraphic units and structure of Cuyama Valley (fig. 4). The units and the textural data, such as grain size, sorting, and bedding characteristics, form the basis for estimating the distribution of aquifer hydraulic properties. The framework model was constructed to represent the subsurface geometry of the primary water-bearing units, Recent Alluvium (Qya), Older Alluvium (Qoa), Morales Formation (QTm), and a composite pre-QTm bedrock unit. Interpretation of these data has redefined the structure, extent, thickness, and properties of the aquifer system of the Cuyama Valley.

The Qya has the highest percentage of coarse-grained deposits (59 percent) and the greatest spatial correlation with current drainages. The Qoa is overall much finer grained (36 percent coarse) than Qya and generally unrelated to the modern active drainages. QTm is much finer grained (31 percent coarse) than the overlying units and represents deposition of alluvial materials prior to the evolution of the modern topography.

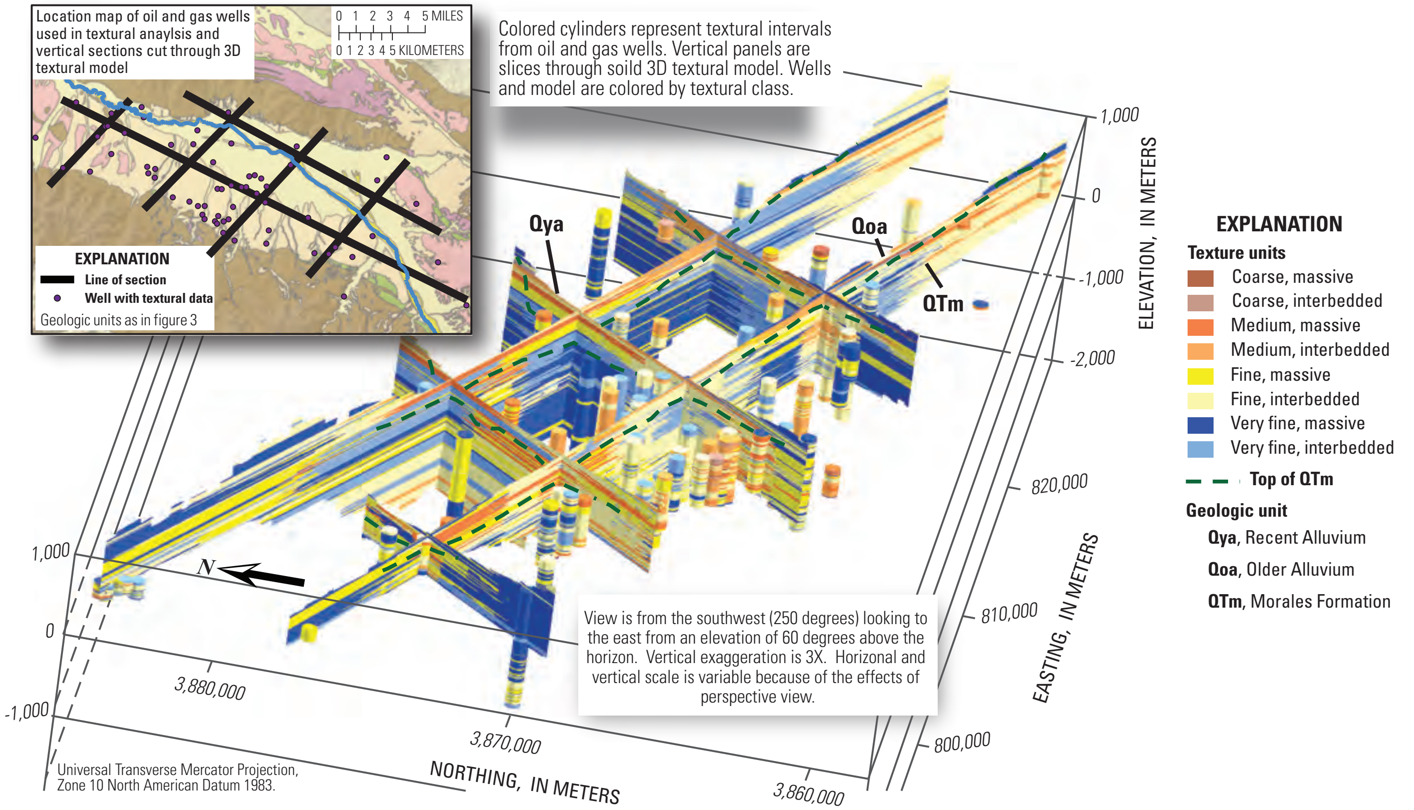

Figure 4. Hydrogeologic framework for Cuyama Valley. Information from lithologic and electrical geophysical logs from 65 oil and gas wells and 153 water wells, cross sections, and geologic maps were used to create a 3-D model of the geologic framework of the aquifer system.

Faults separate the aquifers into distinct zones in which the response to the use, movement, and consumption of water is similar. Thus, Cuyama Valley can be considered a collection of zones that are partially hydraulically connected, but respond differently to natural and anthropogenic stresses. Data indicated that groundwater does not readily flow vertically between the water-bearing units and that faults restrict the lateral movement of groundwater between different zones.

Temporal and Geospatial Database

A temporal and geospatial database was developed to capture, compile, manage, store, and analyze the large quantity of data needed to run the CUVHM. Because the integrated hydrologic model of the Cuyama Valley aquifer system simulates temporally varying processes, the database is extremely useful for recognizing and understanding spatial relations within and between data types.

The USGS completed three multiple-well monitoring sites, which provided detailed information that could not be obtained from conventional wells (Everett and others, 2013). Measurements and observations at these sites provide geophysical data on the alluvial deposits as well as depth-specific data on groundwater levels, hydrologic properties, and water chemistry from selected water-bearing layers within the aquifer system. Measurements at these sites, combined with measurements at existing wells, constitute a new hydrologic monitoring network of the valley. The regional database also includes geomechanical deformation data and data from new upstream streamflow gaging stations on the Cuyama River and Santa Barbara Creek (fig. 2).

Results of Study

Study results showed that human activities such as irrigated agriculture and associated groundwater pumping have adversely affected the availability of water resources in Cuyama Valley (fig. 5). Measured and simulated groundwater levels indicated substantial water-level declines in selected subregions, increased groundwater storage depletion, and seasonal changes in vertical hydraulic head gradients. There is also some additional degradation in already poor water quality, as well as mobilization of natural contaminants and land subsidence in the Main-zone subregions.

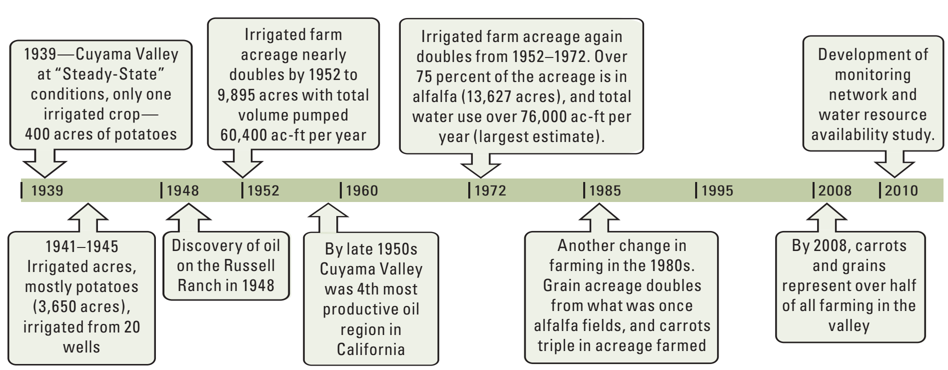

Figure 5. Timeline highlights of Cuyama Valley development.

Table 1. Summary of groundwater-flow budgets for selected regions and periods from the Cuyama Valley Hydrologic Model.
[Average-net flows in acre-feet per year]

Simulated flows	Valley wide		Main zone	Ventucopa Uplands	Sierra Madre Foothills	Base case[1]	Reduced supply[2]	Reduced demand[3]
Simulation period (Water years)	1950–2010[4]	2000–10[5]	2000–10	2000–10	2000–10	2011–71[6]	2011–71	2011–71
Groundwater inflows								
Storage depletion	34,100	34,800	27,500	0	13,800	32,700	500	0
Direct infiltration	5,600	3,100	700	1,500	900	2,400	1,100	1,300
Streamflow infiltration	27,500	30,300	8,300	20,500	1,600	29,500	25,600	29,500
Total recharge	33,100	33,400	9,000	22,000	2,500	31,900	26,700	30,800
Total inflows	67,200	68,200	36,500	22,000	16,300	64,600	27,200	30,800
Groundwater outflows								
Storage accretion	0	0	0	6,000	0	0	0	11,900
Groundwater underflow	3,700	3,100	3,200	15	0	2,900	2,900	3,000
Springs as drains	1,000	600	600	0	0	400	500	600
Domestic pumpage	20	10	6	8	2	7	7	7
Water-supply pumpage	90	190	190	0	0	190	190	190
Agricultural pumpage	65,300	68,100	56,700	10,000	1,400	63,700	32,800	15,800
Total pumpage	65,400	68,300	56,900	10,000	1,400	63,900	33,000	16,000
Total outflow	70,100	68,900	57,500	16,000	1,400	67,200	36,400	31,500
Inflows – Outflows	–2,900	–700	–21,000	6,000	–14,900	–2,600	–9,200	–700

[1]Base case projection of current demand with historical climate.
[2]Base case projection with supply limited to recharge.
[3]Base case projection with no agriculture in the Main-zone subregions.
[4]Historical period that represents two climate cycles.
[5]Historical period that represents recent climate and land-use conditions.
[6]Projection of historical climate and 2010 land use.
[7]Includes water lost to evapotranspiration.
[8]Demand greater than replenishment (overdraft).
[9]Replenishment is greater than demand.

Long-term water demand exceeds replenishment, as shown by simulated overdraft of the groundwater basin of about 2.1 million acre-ft during the 61-year simulation period (1949–2010), with about 72 percent of total groundwater-storage depletion from the Main zone. Groundwater-storage depletion varies considerably from year to year depending on land use, pumpage, and climate conditions. Although interdecadal wet years used to replenish the basin, the predominance of dry and average years with increased water use and sustained storage depletion have diminished the effects of these major recharge events. As a result, large regions have depressed water levels and large unsaturated zones in the Recent and Older alluvium aquifers. These conditions have led to an unsustainable water resource with reduced replenishment, 'overdraft,' poor water quality, and land subsidence.

Hydrographs and simulations of groundwater levels showed annual and seasonal variations, with historical declines of more than 300 ft and rates of decline of 7 feet per year (ft/yr) in parts of the south Main zone. Groundwater-level declines, averaging 1–2 ft/yr, occur throughout most of the basin. Wells in the Ventucopa Uplands corridor showed cyclical fluctuations in water levels associated with climatic variations and related streamflow events.

Analyses of groundwater samples indicated naturally occurring poor-quality water containing elevated levels of total dissolved solids and sulfate throughout the Cuyama Valley. The groundwater generally is very old, indicating limited recharge. Trends indicated that the water quality has been poor historically and showed no indicators of improvement with continued water-level declines. Water quality could be slightly deteriorating with the addition of nitrates and other anthropogenic contaminants and the mobilization of natural contaminants such as sulfate, arsenic, and chromium. An exception to this poor quality is in the Ventucopa area, where local recharge has historically created a small area of relatively better quality water.

Data indicated small amounts of permanent subsidence of up to 0.2 ft since 2000 and reduced storage capacity in the aquifer sediments due to groundwater pumping. Simulations of historical conditions indicate near 1.6 ft of subsidence that is spatially centered near New Cuyama and coincident with the groundwater declines in the Main zone. An additional foot of permanent subsidence is projected in the Main zone if current demands continue.

Continued or reduced supply still would result in groundwater depletion (table 1). Recent conditions (2000–10) showed the largest depletion in the Main zone. Reduced demand would allow aquifer recovery, but may not allow adequate irrigation for agriculture.

The bounds of water-resource availability in Cuyama Valley were assessed, but the criteria for sustainability remain undefined. There is no current management plan, and pumpage is not metered. Projected current demand of water resources (base case) will result in continued groundwater-storage depletion and land subsidence, which probably is not sustainable. Similarly, reducing pumpage to an amount comparable to average recharge (reduced supply) still may not provide a sustainable resource under current agricultural practices and land use. Complete cessation of agriculture in the Main zone (reduced demand) would ensure sustainable water resources but not sustainable agriculture.

For more information contact:

California Water Science Center

6000 J Street, Placer Hall
Sacramento, CA 95819
916-278-3000

Randall T. Hanson

rthanson@usgs.gov
U.S. Geological Survey
4165 Spruance Road, Suite 200
San Diego, CA 92101

Donald Sweetkind

dsweetkind@usgs.gov
U.S Geological Survey,
Denver Federal Center, MS 973
Lakewood, CO 80225-0046

References:

Everett, R.R., Gibbs, D.R., Hanson, R.T., Sweetkind, D.S., Brandt, J.T., Falk, S.E. and Harich, C.R., 2013, Geology, water-quality, hydrology, and geomechanics of the Cuyama Valley groundwater basin, California, 2008–12: U.S. Geological Survey Scientific Investigations Report 2013–5108, 62 p.

Hanson, R.T., Boyce, S.E., Schmid, Wolfgang, Hughes, J.D., Mehl, S.M., Leake, S.A., Maddock, Thomas, III, and Niswonger, R.G., 2014, One-Water Hydrologic Flow Model–MODFLOW-OWHM: U.S. Geological Survey Techniques and Methods 6-A51, 122 p.

Hanson, R.T., Flint, L.E., Faunt, C.C., Gibbs, D., and Schmid, Wolfgang, 2014, Hydrologic models and analysis of water availability in Cuyama Valley, California: U.S. Geological Survey Scientific Investigations Report 2014–5150, 150 p.

Sweetkind, D.S., Faunt, C.C., and Hanson, R.T., 2013, Construction of 3-D geologic framework and textural models for Cuyama Valley groundwater basin, California: U.S. Geological Survey Scientific Investigations Report 2013–5127, 46 p.

Prepared in cooperation with Santa Barbara County Department of Public Works Water Agency

Hydrologic Models and Analysis of Water Availability in Cuyama Valley, California

Scientific Investigations Report 2014–5150

U.S. Department of the Interior
U.S. Geological Survey

Cover. Looking northwest from the south side of Cuyama Valley to the Caliente Range. Photograph taken by Randall T. Hanson, U.S. Geological Survey, September 19, 2009.

Hydrologic Models and Analysis of Water Availability in Cuyama Valley, California

By R.T. Hanson, Lorraine E. Flint, Claudia C. Faunt, Dennis R. Gibbs, and Wolfgang Schmid

In cooperation with Santa Barbara County Department of Public Works Water Agency

Scientific Investigations Report 2014–5150

U.S. Department of the Interior
U.S. Geological Survey

U.S. Department of the Interior
SALLY JEWELL, Secretary

U.S. Geological Survey
Suzette M. Kimball, Acting Director

U.S. Geological Survey, Reston, Virginia: 2014

Suggested citation:
Hanson, R.T., Flint, L.E., Faunt, C.C., Gibbs, D.R., and Schmid, W., 2014, Hydrologic models and analysis of water availability in Cuyama Valley, California: U.S Geological Survey Scientific Investigations Report 2014–5150, 150 p., *http://dx.doi.org/10.3133/sir20145150*.

ISSN 2328-0328 (online)

Contents

Contents—Continued

Figures

Figures—Continued

Figures—Continued

Tables

Conversion Factors

Inch/Pound to SI

Multiply	By	To obtain
	Length	
inch (in.)	2.54	centimeter (cm)
inch (in.)	25.4	millimeter (mm)
foot (ft)	0.3048	meter (m)
mile (mi)	1.609	kilometer (km)
	Area	
Acre	4,047	square meter (m^2)
Acre	0.4047	hectare (ha)
Acre	0.4047	square hectometer (hm^2)
Acre	0.004047	square kilometer (km^2)
square foot (ft^2)	929.0	square centimeter (cm^2)
square foot (ft^2)	0.09290	square meter (m^2)
section (640 acres or 1 square mile)	259.0	square hectometer (hm^2)
	Volume	
acre-foot (acre-ft)	1,233	cubic meter (m^3)
acre-foot (acre-ft)	0.001233	cubic hectometer (hm^3)
	Flow rate	
acre-foot per day (acre-ft/d)	0.01427	cubic meter per second (m^3/s)
acre-foot per year (acre-ft/yr)	1,233	cubic meter per year (m^3/yr)
acre-foot per year (acre-ft/yr)	0.001233	cubic hectometer per year (hm^3/yr)
	Hydraulic conductivity	
foot per day (ft/d)	0.3048	meter per day (m/d)

Abbreviations

BCM	Basin Characteristics Model
CADWR	California Department of Water Resources
CIR	Consumptive irrigation requirement
CUVHM	Cuyama Valley Hydrologic Model
SBDPWWA	Santa Barbara Department of Public Works Water Agency
ENSO	El Nino-Southern Oscillation
ET_h, ET_o	Reference evapotranspiration
ET_{act}	Actual evapotranspiration
K_c	Crop coefficient
K_h	Horizontal hydraulic conductivity
K_v	Vertical hydraulic conductivity
MF2K5	MODFLOW-2005
OWHM	One Water Hydrologic Flow Model
NAMS/PE	North American Monsoon-Pineapple Express
PDO	Pacific Decadal Oscillation
PEST	Parameter Estimation Program
SOSWR	Sum of squared weighted residual
TFDR	Total farm delivery requirement
USGS	U.S. Geological Survey
WBS	Water-balance subregions

Acknowledgments

The authors acknowledge Alan Flint, Chris Harich, Donald Martin, Sarah Falk, and Katherine Paybins, who contributed to the technical content of this study. The authors also thank Larry Schneider of the U.S. Geological Survey for completion of the technical illustrations in this document.

This page intentionally left blank.

Hydrologic Models and Analysis of Water Availability in Cuyama Valley, California

By R.T. Hanson, Lorraine Flint, Claudia C. Faunt, Dennis Gibbs, and Wolfgang Schmid

Abstract

Changes in population, agricultural development practices (including shifts to more water-intensive crops), and climate variability are placing increasingly larger demands on available water resources, particularly groundwater, in the Cuyama Valley, one of the most productive agricultural regions in Santa Barbara County. The goal of this study was to produce a model capable of being accurate at scales relevant to water management decisions that could be considered in the evaluation of the sustainable water supply. The Cuyama Valley Hydrologic Model (CUVHM) was designed to simulate the most important natural and human components of the hydrologic system, including components dependent on variations in climate, thereby providing a reliable assessment of groundwater conditions and processes that can inform water users and help to improve planning for future conditions. Model development included a revision of the conceptual model of the flow system, construction of a precipitation-runoff model using the Basin Characterization Model (BCM), and construction of an integrated hydrologic flow model with MODFLOW-One-Water Hydrologic Flow Model (MF-OWHM). The hydrologic models were calibrated to historical conditions of water and land use and, then, used to assess the use and movement of water throughout the Valley. These tools provide a means to understand the evolution of water use in the Valley, its availability, and the limits of sustainability.

The conceptual model identified inflows and outflows that include the movement and use of water in both natural and anthropogenic systems. The groundwater flow system is characterized by a layered geologic sedimentary sequence that—in combination with the effects of groundwater pumping, natural recharge, and the application of irrigation water at the land surface—displays vertical hydraulic-head gradients. Overall, most of the agricultural demand for water in the Cuyama Valley in the initial part of the growing season is supplied by groundwater, which is augmented by precipitation during wet winter and spring seasons. In addition, the amount of groundwater used for irrigation varies from year to year in response to climate variation and can increase dramatically in dry years. Model simulation results, however, also indicated that irrigation may have been less efficient during wet years. Agricultural pumpage is a major component to simulated outflow that is often poorly recorded. Therefore, an integrated, coupled farm-process model is used to estimate historical pumpage for water-balance subregions that evolved with the development of groundwater in the Valley from 1949 through 2010. The integrated hydrologic model includes these water-balance subregions and delineates natural, municipal, and agricultural land use; streamflow networks; and groundwater flow systems. The redefinition of the geohydrologic framework (including the internal architecture of the sedimentary units) and incorporation of these units into the simulation of the regional groundwater flow system indicated that faults have compartmentalized the alluvial deposits into subregions, which have responded differently to regional groundwater flow, locations of recharge, and the effects of development. The Cuyama Valley comprises nine subregions grouped into three regional zones, the Main, Ventucopa Uplands, and Sierra Madre Foothills, which are fault bounded, represent different proportions of the three alluvial aquifers, and have different water quality.

The CUVHM uses MF-OWHM to simulate and assess the use and movement of water, including the evolution of land use and related water-balance regions. The model is capable of being accurate at annual to interannual time frames and at subregional to valley-wide spatial scales, which allows for analysis of the groundwater hydrologic budget for the water years 1950–2010, as well as potential assessment of the sustainable use of groundwater.

Simulated changes in storage over time showed that significant withdrawals from storage generally occurred not only during drought years (1976–77 and 1988–92) but also during the early stages of industrial agriculture, which was initially dominated by alfalfa production. Since the 1990s, agriculture has shifted to more water-intensive crops. Measured and simulated groundwater levels indicated substantial declines in selected subregions, mining of groundwater that is thousands to tens of thousands of years old, increased groundwater storage depletion, and land subsidence. Most of the recharge occurs in the upland regions of Ventucopa and Sierra Madre Foothills, and the largest fractions of pumpage and storage depletion occur in the Main subregion. The long-term imbalance between inflows and outflows resulted in simulated overdraft (groundwater

withdrawals in excess of natural recharge) of the groundwater basin over the 61-year period of 1949–2010. Changes in storage varied considerably from year to year, depending on land use, pumpage, and climate conditions. Climatically driven factors can greatly affect inflows, outflows, and water use by more than a factor of two between wet and dry years. Although precipitation during inter-decadal wet years previously replenished the basin, the water use and storage depletion have lessened the effects of these major recharge events. Simulated and measured water-level altitudes indicated the presence of large areas where depressed water levels have resulted in large desaturated zones in the younger and Older Alluvium layers in the Main-zone subregions. The results of modeled projection of the base-case scenario 61 years into the future indicated that current supply-and-demand are unsustainable and will result in additional groundwater-level declines and related storage depletion and land subsidence. The reduced-supply and reduced-demand projections reduced groundwater storage depletion but may not allow for sustainable agriculture under current demands, agricultural practices, and land use.

Introduction

Cuyama Valley is north of Sierra Madre Mountains in south-central California (fig. 1) and is one of the most productive agricultural regions in Santa Barbara County. Increases in population in the Valley and transitions to crops that consume additional water have increased the demand for water within Cuyama Valley groundwater basin (CUVGB). Although a small amount of urban supply is provided by groundwater, irrigated agriculture is solely supplied by groundwater pumpage. The aquifers in the Valley have been subject to overdraft (groundwater withdrawals in excess of natural recharge) since the 1950s (Singer and Swarzenski, 1970), and more recently, land subsidence related to increased and sustained groundwater pumpage has occurred (Everett and others, 2013). The water levels throughout most of the central parts of Cuyama Valley have not substantially recovered since the onset of industrial agriculture in the 1970s. As a part of a resource assessment process, the U.S. Geological Survey (USGS) undertook the study described in this report in cooperation with the Santa Barbara Department of Public Works Water Agency (SBDPWWA) to better understand the hydrologic budget and limits of availability and sustainability.

The purpose of the study was to quantify the water availability of the Cuyama Groundwater Basin under varying cultural and climatic scenarios to inform regional stakeholders' potential constraints of water-supply availability options for the aquifer system, which is the sole source of water supply for the basin. A regional hydrologic flow model capable of being accurate at scales relevant to water management decisions was developed with the SBDPWWA for the Cuyama Valley, California.

Purpose and Scope

This report documents (1) an analysis of the conceptual model of the hydrologic system of the Cuyama Valley, (2) the description of the hydrologic features used in the hydrologic flow models of the Valley groundwater system, (3) development and calibration of a three-dimensional (3D) regional flow model, and (4) an analysis of water availability with respect to current water and land use and potential climate variability and change. Because the regional hydrologic model incorporates time-varying inflows and outflows, the model can be used to evaluate the basin-scale effects of temporal changes in groundwater recharge and pumping. Overall, the development of the geohydrologic and hydrologic models, data networks, and hydrologic analyses provide a basis for assessing water availability and formulating and assessing water-resource management strategies.

Approach

The creation of the first set of hydrologic models of Cuyama Valley for this study required the updating of the conceptual model, the geohydrologic framework, and the estimation of the components of the hydrologic cycle. The conceptual model was realigned with recent information about the framework of recharge, land use, and streamflow infiltration (Everett and others, 2013; Sweetkind and others, 2013). Refinement of the geohydrologic framework required the remapping of geologic surfaces and reconciliation of recent geologic information available from wells and investigations (Sweetkind and others, 2013).

The Cuyama Valley Hydrologic Model (CUVHM) was constructed on the basis of the new conceptual and geohydrologic models to simulate the flow and use of water for the period September 1949 through December 2010. This model includes new layering, inflows and outflows, and more detailed representation of the current land cover/land use and vegetation. The new valley-wide model (fig. 1*B*) includes estimates of runoff from the surrounding watersheds simulated by using the Basin Characterization Model (BCM) (Flint and Flint, 2012), a regional-scale precipitation-runoff model (fig. 1*A*).

Description of the Study Area

Cuyama Valley is a high desert watershed with a surface-water drainage area of about 690 square miles (mi^2) and an underlying main alluvial basin covering about 230 mi^2 that straddles the northeastern part of Santa Barbara County and parts of San Luis Obispo, Ventura, and Kern Counties (the Cuyama River forms part of the county boundary) within the CUVGB (figs. 1*A*, 1*B*). This high desert watershed trends northwesterly from the Sierra Madre Mountains on the south to the Caliente Range on the north (fig. 1*A*). Land-surface elevations in the watershed range from 800 feet (ft) above NAVD88 near Twitchell Reservoir to greater than 8,000 ft at Mt. Pinos, and land surface elevations within the groundwater basin proper range from about 1,950 ft to 3,600 ft above NAVD88. The valley is drained by the Cuyama River and its tributaries, of which Santa Barbara Creek is the largest (fig. 1*B*). The valley has been developed predominantly for oil production since the 1950s and for agriculture since the 1930s but also contains the towns of Cuyama and New Cuyama and other small towns (fig. 1*B*). The CUVGB encompasses about 230 mi^2, of which about 30 percent is used for agriculture, about 69 percent is natural vegetation, and one percent is urban land as of 2010. The residents of the valley rely almost exclusively on groundwater for their drinking-water supply and for irrigation (Gibbs, 2010). As a result, the aquifer is susceptible to overdraft (groundwater pumpage in excess of recharge) and related secondary effects such as land subsidence and poor water quality when outflows (including pumpage) exceed inflows for an extended period of time.

Hydrologic and Water-Balance Subregions

The assessment and analysis of groundwater availability relative to the components of the hydrologic cycle required the division of Cuyama Valley into subregions that can be analyzed individually with respect to supply-and-demand components. This study also required a more precise delineation of the groundwater basin. The delineation described by the California Department of Water Resources (2003) includes several extraneous regions that are not part of the main regional aquifer systems within Cuyama Valley. Thus, the extent of the groundwater basin was redefined as a part of this study (fig. 1*B*). The basin was further divided into nine groundwater hydrologic subregions (fig. 2*A,* table 1). These subregions separate the aquifers into regions that: are fault bounded; represent different proportions of the three alluvial aquifer systems; have different water-quality characteristics; and where the response to the use, movement, and consumption of water is similar in specific parts of the aquifers but differ from the responses in the other subregions. In this context, these subregions of Cuyama Valley may be considered a collection of subbasins that are partially hydraulically connected, but have different hydrologic features or hydraulic properties and consequently respond differently to natural and anthropogenic stresses. To facilitate regional water-availability analysis, these nine subregions were grouped into three simplified major regional zones that represent the Main zone, Ventucopa Uplands, and Sierra Madre Foothills (fig. 2*B*).

The valley also was divided into multiple water-accounting units called water-balance subregions (WBS), to create the associations between demand for water for irrigation and supply from wells that link the supply-and-demand components driven by changing land use and land ownership (fig. 2*C*). These subregions comprise a combination of private and public lands from which data can be used to estimate the water-balance components of land use, streamflow, and groundwater flow relative to the use and movement of water at the land surface. The increase in the number—from 2 in 1949 to 83 in 2010—reflect the historical development of the valley across the landscape. The changing number of WBS generally represents changes in land ownership and use that occurred during 10 different periods within the 61 years of simulation. Superimposed on these WBS are cell-by-cell distributions of changes in land use that include different natural vegetation, urban, and agricultural uses throughout the valley (described later in the “Model Development” section). The most recent WBS are based on land-use parcels of 2010 and were sequentially changed for earlier periods to provide a logical progression of land-use and ownership changes over the 61-year simulation period (1949–2010). These WBS are also combined with the nine groundwater subregions for the purposes of water-supply analysis and are generally coincident with those subregions (fig. 2*A*).

Geologic Framework

The Cuyama Valley is a down-faulted block or graben that is bordered on the north by the Morales and Whiterock Faults and on the south by the South Cuyama and Ozena Faults (fig. 3*A*). The eastern part of the valley is underlain by the Cuyama syncline, with a strike parallel to the elongation of the valley, which plunges toward the northwest. The north limb of this fold is truncated against the Morales Fault (Singer and Swarzenski, 1970).

Hydrogeologic Units

The hydrogeologic framework of Cuyama Valley was developed through a reevaluation and synthesis of geologic information from previous studies, which resulted in a simplified grouping of geologic units into hydrogeologic units (Sweetkind and others, 2013). Geologic units within the Cuyama Valley groundwater basin include unconsolidated Pleistocene and Holocene alluvial deposits and fluvial deposits of the Cuyama River drainage, and the underlying, partly consolidated nonmarine Morales Formation of Pliocene to Pleistocene age (Upson and Worts, 1951; Singer and Swarzenski, 1970). These deposits unconformably overlie a late Cretaceous to middle Cenozoic succession of consolidated marine and nonmarine sedimentary rocks, which themselves overlie crystalline granitic and gneissic rocks (Hill and others, 1958; Dibblee, 1982; Lagoe, 1987; Bazeley, 1988; fig. 3*A*). Previous USGS studies of Cuyama Valley (Upson and Worts, 1951; Singer and Swarzenski, 1970) delineated aquifers in the saturated parts of the Recent and Older Alluvium, units that historically have yielded most of the water pumped in the study area. Since these studies were completed, water levels have declined in some areas into the deeper units such as the Morales Formation. The hydrogeologic framework that was used to represent the three discrete hydrologic model layers as determined by Sweetkind and others (2013) is illustrated in figure 3*A*:

1. Recent Alluvium aquifer—one layer of the younger alluvial deposits representing an alluvial deposit layer.
2. Older Alluvium aquifer—one layer of the older alluvial deposits.
3. Morales Formation aquifer—one layer representing the uppermost units of the Morales Formation.

Collectively, these aquifers are variable in areal extent and range in thickness from a few feet up to thousands of feet. The outcrops and extent of these units are superimposed onto the BCM and the CUVHM active model grids (fig. 3*A*).

Faults and the Groundwater Flow System

Faults of hydrologic significance occur at the basin margins, where fault offset juxtaposes basin-fill sediments against older consolidated rocks, and within the basin, where basin-fill units of differing water-transmitting ability are juxtaposed. Faults within the basin fill have been recognized previously as being associated with historical surface springs or lateral changes in groundwater elevations (Singer and Swarzenski, 1970). Sweetkind and others (2013) identified three faults within the basin that offset the basin-filling deposits and are associated with known water-level changes (Upson and Worts, 1951; Singer and Swarzenski, 1970): the thrust faults that bound Turkey Trap Ridge and Graveyard Ridge, the Santa Barbara Canyon Fault, and the Rehoboth Fault (fig. 3*A*). Upson and Worts (1951) reported the presence of springs and seeps along the base of Turkey Trap and Graveyard Ridges in 1946. Singer and Swarenski (1970) reported water-level drawdowns of 80 to 100 feet in the area near these ridges and indicated that water removed by pumping from this region is slow to replenish because faults restrict movement of water. The impediment to flow might be related to the hydraulic properties of the fault itself or fault juxtaposition of older, slightly less permeable material. A fault (or fault zone), here called the Santa Barbara Canyon Fault (SBCF; fig. 3*A*), was suggested by Singer and Swarzenski (1970) as the cause of a steep hydraulic gradient in the southeastern part of Cuyama Valley, where water levels in the vicinity of Ventucopa are at least 100 ft higher than water levels a couple miles to the northwest. The relatively small amount of vertical offset on the Santa Barbara Canyon Fault indicates that changes in water levels across this fault documented in previous studies are caused by distinct fault-zone properties, rather than juxtaposition of units of differing water-transmitting ability. Another fault, here called the Rehoboth Fault (fig. 3*A*), is inferred from lateral water-level changes in the west-central part of the valley. The other major faults in Cuyama Valley (figs. 2*A*, 3*A*), such as the Russell, Morales, South Cuyama, Ozena, and Whiterock Faults, are represented as no-flow groundwater boundaries along the outer edge of the alluvial basin.

Hydrogeologic Framework

A digital 3D hydrogeologic framework model of the alluvial basin was developed and is described in detail by Sweetkind and others (2013). The framework model uses information from a variety of datasets, including existing lithologic and electrical geophysical logs from oil and gas wells and water wells, cross sections, and geologic maps, to delineate the volumes of the aquifer system bounded by faults and relevant depositional or formational boundaries. The model is the digital representation of the interpreted geometry and thickness of subsurface geologic units and the geometry of folds and faults that bound the basin and lie within it. Specifically, the model was constructed to represent the subsurface geometry of the Recent Alluvial aquifer, the Older Alluvial aquifer, the Morales Formation aquifer, and a composite pre-Morales Formation bedrock unit. This model provides the fundamental hydrogeologic framework for the subsequent development of a transient numerical model of groundwater flow in the study area.

The framework model may be explored and visualized by slicing the model volume at any chosen location (for example, figs 3*B*, *C*). Two sections were cut from the framework model along the same two section lines as published by Singer and Swarzenski (1970). One section (A–A', fig. 3*B*) is aligned roughly east-west , parallel to the trace of the interbasin thrust faults that bound the Turkey Trap Ridge and Graveyard Ridge, and a second (B–B', fig. 3*C*) is a roughly north-south section transverse to the major structural grain of the basin. Together with the map, the sections show the extent and thickness of the aquifers. The sections show the thickness of Recent Alluvial aquifer in the axis of the valley, underlain by Older Alluvial aquifer. The Older Alluvial aquifer dominates the southern part of the valley, beneath its outcrop exposures, with the Morales Formation aquifer underlying it. The Morales Formation aquifer predominates in the Cuyama Badlands area, where it is virtually the only permeable stratigraphic unit except for thin Recent Alluvium along the trace of the Cuyama River channel. The Morales Formation aquifer is also exposed at the ground surface in the western part of the valley, where it is locally overlain by thin deposits of alluvium in the channel of the Cuyama River. The effect of fault offset is not obvious at the scale of figure 3*A*, except for the appearance of Older Alluvial aquifer at land surface at Graveyard Ridge and Turkey Trap Ridge.

Three-Dimensional Model of Grain-Size Distribution

An analysis of variability of lithology and grain size was conducted for the three principal basin-filling units, the Recent Alluvial aquifer, Older Alluvial aquifer, and Morales Formation aquifer. The details of this analysis are documented by Sweetkind and others (2013). Textural variability in the basin-filling units is ultimately a function of the sedimentary facies, environment of deposition, and depositional history of the basin. Textural data such as grain size, sorting, and bedding characteristics form the geologic basis for estimating the hydraulic properties within the numerical hydrologic-flow model.

The spatial distribution and the characteristics of the sediments forming the three aquifers are related to the Pliocene and Pleistocene tectonic evolution and uplift of the basin, the progressive narrowing of the valley, and the gradually increasing channelization of the Cuyama River drainage. The Morales Formation is a widespread unit that was deposited prior to the constriction of the basin by encroaching thrust faults. As a result of tectonic uplift, the previously deposited Morales Formation was exposed and eroded. Streams deposited and reworked sediment from the Morales Formation into a narrower basin that resulted in the deposition of the Older Alluvial aquifer. The Recent Alluvial aquifer is confined to the center of Cuyama Valley and alluvial channels tributary to the Cuyama River. Textural variations in the Recent Alluvial aquifer appear to be primarily climate-driven and reflect regional rainfall variations that control stream incision and aggradation.

Sediment grain size, a textural parameter commonly reported in oil-well and water-well data as well as in outcrop observations, was analyzed and modeled. Boulders, gravels and sands are considered coarse-grained, whereas silts and clays are considered fine-grained. As part of a statistical and geostatistical analysis, the percentage of coarse-grained sediment was calculated for the entire thickness of each aquifer for all 218 available wells. Percent coarse-grained sediment was calculated as the total thickness of coarse-grained intervals divided by the total thickness of the aquifer. The global mean percentage of coarse-grained texture is 34 percent, with the Recent Alluvial aquifer being significantly more coarse-grained than the Older Alluvial aquifer or the Morales Formation aquifer.

Initially, the interpreted grain-size and bedding-frequency parameters derived from data from the oil and gas exploration boreholes were used to construct a 3D model of textural variations within the basin by extrapolating data away from boreholes using a nearest-neighbor 3D-gridding process for a cell size of 500 meters (m) horizontally and 10 m vertically (Sweetkind and others, 2013). Using geostatistical methods, this model was refined to a higher resolution 250-meter grid for producing a series of plan-view estimates of texture variation of grain-size variability for each aquifer that is coincident with the gridding of the hydrologic model (fig. 4). The two-dimensional (2D) kriged estimates of percentage of coarse-grained texture highlight textural distributions within and between the aquifers.

The spatial patterns of the percentage of coarse-grained texture for each aquifer show significant heterogeneity in the texture of the sediments, which reflects the depositional environment and the geomorphic evolution of the region since Pliocene time. The texture model of the Recent Alluvial aquifer has the highest percentage of coarse-grained deposits (fig. 4*A*). It is coarsest in the eastern part of the valley, becomes finer grained with distance downstream to the west, and, although not evident at the scale of these maps, is also coarsest in the vicinity of the active Cuyama River channel. The coarse-grained nature of the Recent Alluvial aquifer reflects a number of factors, including the short distances between the sediment sources in the surrounding uplands and the sites of sediment deposition as well as the high-energy nature of Cuyama River and tributary creeks that transport sediments during winter storms and summer monsoonal rains. The spatial structure of the kriged textural model for the Recent Alluvial aquifer can be attributed to the alignment of the active drainages, whereas the textural models of the older aquifers are less correlated to modern topography.

The texture model for the Older Alluvial aquifer differs in spatial structure from the Recent Alluvial aquifer in being overall much finer grained and generally unrelated to the modern active drainages (fig. 4*B*). The Older Alluvial aquifer is moderately coarse-grained in the eastern half of Cuyama Valley, but transitions to fine-grained at the western end of the valley. Much of (the) Older Alluvial aquifer is derived from erosional reworking of uplifted parts of the Morales Formation. The Older Alluvial aquifer is generally coarser than the Morales Formation aquifer and has more numerous medium- and coarse-grained lenses that probably represent alluvial channel deposits.

The Morales Formation aquifer is much finer-grained than the overlying units (fig. 4*C*). This aquifer has relatively few coarse-grained intervals and is characterized by relatively fine-grained material, particularly in the axis of the valley, where Older Alluvial aquifer contains some of the coarsest intervals. The Morales Formation aquifer is particularly fine grained in the western half of Cuyama Valley, where surface geologic mapping identifies a lacustrine facies in this unit (Upson and Worts, 1951; Dibblee and Minch, 2005; DeLong and others, 2008). However, the Morales Formation aquifer becomes more coarse-grained along the southern flank of the valley and to the southeast, perhaps reflecting available sediment supply from uplifting areas outside the valley at the time of deposition.

Hydrologic System

The conceptual model for the hydrologic cycle starts with inflows from precipitation and streamflow. Streamflow enters Cuyama Valley through the Cuyama River and as runoff from the side slopes and local stream networks that drain the surrounding mountains. Infiltration of runoff along with percolation of some precipitation and irrigation below the root zone contribute to groundwater recharge. Additional underflow of groundwater occurs along the Cuyama River channel as inflows at the eastern and outflows at the western boundaries of the valley in all three aquifers (fig. 2*A*). Outflow also occurs as evapotranspiration from natural vegetation, urban landscapes, and irrigated agriculture. Additional outflow occurs as groundwater pumpage for agricultural, urban, and domestic uses. These natural and man-made inflows and outflows represent the supply-and-demand components of water use within the hydrologic cycle in Cuyama Valley. Since the 1990s, the developed hydrologic system now also includes the pumpage of water in one groundwater subregion that is exported to adjacent subregions for irrigation use.

Climate

The climate of the Cuyama Valley is arid, with hot summers and cool winters. The record of cumulative departure from the mean of precipitation for the late 1940s or 1950s (depending on when records were available) to 2010 shows that major and minor wet periods and dry periods are typical of the climate variability for Cuyama Valley (figs. 5, 6*A*). The map of average annual precipitation indicates that higher precipitation occurs within the large mountain-front inland regions (fig. 6*A*).

On figure 5, 16 wet and dry periods are shown, and 15 major wet and dry periods are coincident with the period of simulation and related stress periods from October 1949 through December 2010 (fig. 5; table 2). Average rainfall ranges from about 7 inches per year on the valley floor to about 15 inches per year in the eastern part of Cuyama Valley (Gibbs, 2010; fig. 6*A*).

Time-series analysis of the residuals from the cumulative departure of precipitation from the Santa Barbara Canyon (Reyes Ranch) long-term hydrologic time series from Cuyama Valley suggest a significant influence in climate variability. The estimated periodicities include 6 percent of the oscillations coincident with the El Nino-Southern Oscillation (ENSO, 2–6 years), 0 percent of cycles from the North American Monsoon-Pineapple Express (NAMS/PE, 7–10 years), and 94 percent of the variation from the Pacific Decadal Oscillation (PDO, 10–30 years) (Hanson and others, 2006; Dickinson and others, 2014). This long-term record shows periods of 27 years (55 percent of the variation), 22 years (36 percent of the variation), 13.5 years (3 percent of the variation) (PDO), and 2–6 years (ENSO) that explain variation in precipitation (fig. 5). Thus, almost all of the variation in precipitation and streamflow occurs in the longer climate cycles. No records of streamflow or groundwater levels are long enough for estimation of climate cycles. The longer cycles will be important periods for the evaluation of interdecadal sustainability of the water resources.

The average annual reference evapotranspiration (ET_h) values show the orographic effects similar to those in the precipitation values. The ET_h in the Cuyama Valley transitions from values of about 55 to 56 inches per year (in/yr) at the base of the Caliente Mountains to lower values of about 45 to 53 in/yr toward the south end of the Cuyama Valley near Ventucopa (fig. 6*B*). Values of ET_h in the inland areas of Cuyama Valley consistently range from 53 to 55 in/yr with very little variation (fig. 6*B*). Variations in ET_h are higher in the southeastern part of Valley, where they range from 45 to 57 in/yr due to shading effects from the rugged terrain.

Effects of Water Use on the Landscape

An integral part of the hydrologic system is the use and movement of water across the landscape, which in this study includes the shallow subsurface defined by the root zone. This includes the evolution of the development and use of land in Cuyama Valley, from the tracts of the Spanish land grants to modern agriculture, urbanization, and industry. Several major periods of development occurred in Cuyama Valley, including the transformation of the land grants into cattle ranches with the eventual need for alfalfa, the introduction of the petroleum industry and founding of the town of Cuyama by the Atlantic Richfield Company (ARCO) , and the introduction of large-scale agriculture with orchards, vineyards, and organic farming (fig. 7). Also farming has evolved from the planting of predominantly potatoes and alfalfa during the 1940s–1970s to a doubling of the acreage of grain crops and a tripling of the acreage in carrot crops by the mid-1980s (fig. 7*A*). Carrot and grains represent more than half of the crops grown in the Cuyama Valley in recent decades (fig. 7*A*).

Population growth in Cuyama Valley was estimated from census tract data (U.S. Census Bureau, 2014a, b) and showed a steady increase from just over 1,000 inhabitants to more than 8,600 inhabitants from 1950 through 2010 (fig. 7). The town of Cuyama was established along with the discovery and development of petroleum resources (fig. 7). Cuyama, along with New Cuyama and the smaller town of Ventucopa, represent the three clusters of housing in the valley. These urban clusters represent less than 1 percent of the land on the valley floor. The towns of Cuyama and New Cuyama are served water from the Cuyama Community Service District supply wells, while the schools and other residents are served water by their own local wells.

The evolution of the landscape occurred as a combination of changes in land use and related land ownership in Cuyama Valley. For the purpose of modeling the hydrologic system, temporal changes in the land ownership were represented by using a sequence of 10 different periods over the 61 years of historical simulation 1949–2010 (figs. 2*C*, 5). These periods were first defined for 2010 on the basis of current land use and ownership and then discretized from recent years to past years to represent the multi-year periods of 1943–50, 1951–59, 1960–69, 1970–79, 1980–85, 1986–92, 1993–95, 1996–2000, 2001–09, and 2010 (fig. 5). The changing water-balance subregions (WBS; fig. 2*C*) reflect the evolution of land ownership and land-use that required groundwater pumpage, as well as regions of native vegetation using precipitation only, and urban and domestic areas served by separate specified sources of groundwater pumpage. The more detailed land-use changes that cover 14 periods (fig. 5) are described later in the "Land Use" section.

Surface Water

Streamflow infiltration together with deep percolation of precipitation, is a major source of natural recharge in Cuyama Valley. Streamflow within the valley occurs primarily from runoff that originates from rainfall and snowmelt in upstream tributary drainages, entering the valley through the Cuyama River and Reyes Creek and other ungaged tributaries. During occasional large storms that can result in flood flows, runoff is also generated within Cuyama Valley and flows through the tributaries to the Cuyama River (fig. 8). Streamflow is currently measured at two gages that record the flow into Cuyama Valley: the Cuyama River near Ventucopa (11136500, 1937–58; 11136501, 2002–10); and, Santa Barbara Canyon Creek near Ventucopa (11136600, 2002–10; fig. 8). There is no downstream gage to measure outflow prior to the streamgage at Buckhorn and inflow to Twitchell Reservoir (fig. 1), which include flows from other large tributary watersheds downstream of Cuyama Valley. The remainder of the tributary canyons and outflow from the Valley along the Cuyama River remain ungaged with the exception of occasional flood-flow measurements.

Groundwater

Under predevelopment conditions, groundwater flowed from the foothills of the surrounding mountains of the Cuyama Valley toward the Pacific Ocean. Under developed conditions, pumpage in excess of recharge has occurred for decades, altering the predevelopment flows in response to groundwater storage depletion and regional cones of depression (or drawdown) in groundwater levels in the center of the valley. Groundwater levels in these persistent depressions show additional seasonal declines that are driven by a combination of agricultural and water-supply pumpage. Groundwater inflows include recharge from infiltration of precipitation, streamflow (figs. 6*A*, 8), and applied water from irrigation. Additional inflow occurs as underflow across the southeastern boundary of the valley, beneath the stream channel of the Cuyama River and Reyes Creek. Outflow from groundwater includes pumpage, base flow or rejected recharge along streams, evapotranspiration, and subsurface underflow to the west from the aquifer systems (fig. 9).

Development of groundwater in the Cuyama Valley has resulted in the construction and pumpage of several hundred wells between 1949 and 2010. This includes about 120 domestic wells, two municipal-supply wells, and more than 100 agricultural irrigation wells (fig. 9). Total pumpage for water supply grew from less than 50 acre-feet (acre-ft) prior to 1982 to more than 150 acre-ft from 1983 to 2010, with an increase around 1982, which was coincident with the increase in population in the valley (fig. 10). The domestic pumpage was estimated on the basis of population growth and an assumed consumption of about 0.54 acre-ft per year per land parcel for each "domestic" (household) well. A minor amount of the increase can also be attributed to the increase in rural residential (domestic) pumpage between 2000 and 2010 (fig. 10). Most of the drinking-water supply is pumped by the Cuyama Valley Community Service District. For the period 1949–2010, the overall distribution of pumpage for drinking-water supply is estimated to be about 88 percent urban, and 12 percent domestic. Temperature difference logs indicated that all three aquifers are contributing to groundwater flow and pumpage in various parts of the valley (Everett and others, 2013).

Model Development

Two hydrologic models were developed for the Cuyama Valley watershed. One is a water-balance model representing the watersheds in the mountains surrounding the valley that was developed by using the Basin Characterization Model (BCM) (Flint and Flint, 2012; Flint and others, 2012; Thorne and others, 2012). Simulations made with this model provided runoff estimates for all of the ungaged ephemeral streams and arroyos that form a drainage network that carries mountain-front recharge from streamflow infiltration of flood flows along the boundary of the alluvial groundwater basin. The second model, referred to herein as the Cuyama Valley Hydrologic Model (CUVHM), is an integrated hydrologic model that was developed using an integrated hydrologic flow model with MODFLOW-One-Water Hydrologic Flow Model (MF-OWHM) (Schmid and others, 2006a, b; Schmid and Hanson, 2009, 2013; Hanson and others, 2010, 2014) to simulate the use and movement of water throughout the groundwater basin.

Water-Balance Model

Estimation of Recharge and Runoff

Rainfall-runoff models require streamflow data for calibration and, then, can be used to simulate flow at gaged and ungaged locations. Rainfall-runoff models do not provide an estimate of spatially distributed recharge to complement runoff estimates, but do provide a more complete picture of the hydrologic processes in data-sparse basins. The Basin Characterization Model (BCM) is a grid-based, regional water-balance model that can provide process-based estimates of recharge and runoff for ungaged locations. BCM was used in this study to provide flow boundary conditions for the CUVHM. The BCM model domain includes the 144 subwatersheds that surround and drain into the alluvial/structural valley (fig. 11).

BCM is a distributed parameter water-balance model that performs a multi-year simulation of surface and shallow subsurface hydrologic processes. The water balance calculations are performed at a monthly time step and independently at an evenly distributed 270 square meters (m^2) grid cell spacing. The model inputs include (1) topography, soil properties, and geology datasets, which are virtually static with time; (2) monthly gridded precipitation and temperature datasets (Parameter–Elevation Regressions on Independent Slopes Model, PRISM; Daly and others, 2008; 800-m transient dataset); and (3) monthly gridded potential evapotranspiration (PET). The monthly gridded PET is simulated using an hourly energy-balance calculation that is based on solar radiation, air temperature, and the Priestley–Taylor equation (Flint and Childs, 1987) to calculate potential evapotranspiration (Flint and Childs, 1991). Clear sky PET is calculated using a solar radiation model that incorporates seasonal atmospheric transmissivity parameters and site-specific parameters of slope, aspect, and topographic shading. Hourly PET is averaged to a monthly rate and cloudiness corrections are made using cloudiness data from National Renewable Energy (2014). Modeled PET for the southwestern United States was calibrated to the measured PET rates from California Irrigation Management Information System (CIMIS) (California Department of Water Resources, 2007) and Arizona Meterological Network (University of Arizona, 2012) stations, and is comparable to the estimates from Cuyama Valley CIMIS station No. 88 (figs. 6*B*, 12). No error analysis was made for the PET. There is a bias in the comparison to CIMIS measured ET_o on the valley floor equivalent of approximately −10 percent (BCM estimates are lower than measured at the CIMAS station), or approximately −0.8 inches per month for the months with the highest PET, and less than −0.1 inches per month for low PET months (fig. 12).

For the Cuyama Valley, the precipitation, air temperature, and monthly PET maps were combined with maps of elevation, bedrock permeability (estimated on the basis of geology (Jennings, 1977) and iteratively modified in the model calibration process), and soil-water storage from the SSURGO soil databases (U.S. Department of Agriculture Natural Resources Conservation Service, 2006). Once available monthly water is calculated, if available water exceeds total soil storage, this excess water becomes runoff, and the amount of water between total soil storage and field capacity storage becomes potential recharge. If available water is less than total soil storage but greater than field capacity, the water exceeding field capacity becomes potential recharge. If potential recharge is greater than bedrock permeability (K), then recharge equals K and potential recharge that exceeds K becomes runoff, or else it will recharge at K until it reaches field capacity. Any water less than field capacity will be lost to actual evapotranspiration at the rate of PET for that month until it reaches wilting point. Additional details of model operation and input and output datasets can be found in Thorne and others (2012).

Calibration and Comparison With Measured Streamflows

The BCM is calibrated to partition excess water into recharge and runoff by comparing simulation results for runoff with measured surface-water flow and iteratively changing K until a reasonable match is achieved. This was done for seven basins (fig. 11) with varying amounts of impairment (regulated flow) and representing three main geologic units, sandstone, conglomerate, and alluvium (fig. 11, table 3). Finally, basin discharge was calculated from recharge and runoff accumulated from grid cells upstream of “pour points,” to more accurately reflect stream channel losses and gains between stream gages and to create surface-water flow recession and baseflow that can extend throughout the dry season (Flint and others, 2012). The “pour points” represent locations where outflow from each of the surrounding watersheds flows into the valley. The portions of the recharge and runoff estimated by BCM simulations then become the inflow at 144 pour-point locations within the streamflow network that is simulated by MF-OWHM in the CUVHM model (fig.8). The fractions of recharge and runoff that are ultimately used within CUVHM were adjusted for the two largest inflows along the Cuyama River and Santa Barbara Creek during BCM calibration.

The BCM was calibrated against selected monthly streamflows at seven USGS streamgages (fig. 13, table 4). Comparisons of BCM-estimated basin discharge and measured streamflow indicate a relatively good match with BCM results. By adjusting the parameter controlling baseflow, the total measured streamflow volume for the period of record for each streamgage was matched exactly by BCM estimates. Calibration statistics indicate relatively good goodness-of-fit on the basis of the Nash-Sutcliffe Efficiency (NSE) statistic, and monthly and annual r^2 values (table 4). The majority of the runoff is derived from the watersheds that drain the Cuyama River and Santa Barbara Canyon, with lesser amounts of storm flows from other ungaged creeks such as Aliso, Apache, Quatal, Berringer, and Reyes Creeks.

Development of BCM Results for CUVHM model

The average annual areal recharge for 1980–2009 ranges from 0 to 11.8 in/yr. The relative proportions of (1) shallow subsurface flow from recharge that becomes baseflow, (2) runoff that becomes streamflow, and (3) runoff that become deep recharge to the mountain-block or alluvial-basin areas were calculated and are indicated in table 4. These were used to develop scaling factors for 144 ungaged basins surrounding the fault-defined valley in two main geologic types, and 13 pour points within the alluvial valley. The first two columns in table 3 indicate the scaling coefficients used to distribute the total potential stream inflow estimates for the MF-OWHM SFR Package that were the initial estimates of inflow used for model calibration. The third column is an estimate of the recharge upstream of each basin's pour point that becomes mountain block recharge. It was assumed that no mountain block recharge would cross the fault boundaries that surround most of the valley and would discharge upgradient of the fault. Therefore only the scaling factors for the SFR recharge and SFR runoff were used and selectively adjusted to estimate the fractions of runoff and rejected recharge that become inflow along the mountain fronts during the CUVHM model calibration for the largest contributing drainages, the Cuyama River and Santa Barbara Canyon Creek. The scaling factor for each column of table 3 was multiplied by the accumulated recharge or runoff for each subwatershed for each geologic type and summed to provide the SFR boundary condition for each of the 144 basins as a monthly recharge and a runoff flow. Average annual streamflow applied to SFR boundaries is approximately 1,500 acre-ft, ranging from 0 to 120,000 acre-feet per year (acre-ft/yr) (fig. 14*A*). Annual streamflow exceeds 10 acre-ft in only 14 of 144 basins for any of the last 40 years, and with the exception of the two largest basins in the southeastern conglomerates, all are on the southern side of the valley, an area dominated by sandstones. These 14 basins contribute more than 60 percent of the total streamflow.

The Cuyama Valley is classified as semiarid, which means that average annual precipitation is between 20 and 50 percent of potential evapotranspiration, indicating little potential for runoff or recharge. However, recharge in a semiarid basin does not occur on the basis of average annual conditions. In certain areas of a basin, such as at higher elevations on the southern slopes of Cuyama Valley, precipitation in some months can exceed potential evapotranspiration and soil storage, and runoff and (or) recharge can occur. Note that there is commonly little streamflow in the Cuyama Valley (fig. 14*A*), and significant streamflow (greater than 10,000 acre-ft/yr) occurs in only 23 of 71 years (1939–2010), or about 32 percent of the time. The relation of streamflow and especially recharge to precipitation is nonlinear in arid and semiarid environments (Flint and others, 2012), which is confirmed in Cuyama Valley (fig. 14*B*).

For application to the CUVHM, the monthly streamflows developed through simulations with the BCM for the 144 pour points are used as inflow rates for the monthly periods and provide the intermittent inflows along the outer boundary of the active CUVHM model area. The overall estimate of gaged and ungaged inflow for the period 1950–2010 averaged 29,500 acre-ft/yr, with about 19,100 acre-ft/yr as runoff (65 percent) and 10,400 acre-ft/yr as recharge (35 percent) for the watersheds surrounding and draining into the valley. Recharge occurring as underflow (mountain-block recharge) was considered negligible, because faults bound most of the valley and the age of many groundwater samples from wells along the mountain-fronts are thousands to tens of thousands of years old (Everett and others, 2013). Consequently, the BCM recharge as groundwater underflow into the valley (mountain-block recharge) was considered to discharge locally through ET or additional baseflow as rejected mountain-front recharge. The reader is referred to BCM documentation for more details on limitations associated with monthly stress periods (Flint and Flint, 2012; Flint and others, 2012; Thorne and others, 2012).

Integrated Hydrologic Model—CUVHM

The Cuyama Valley Hydrologic Model, or CUVHM, was developed to (1) characterize the historical conditions for the analysis of the use and movement of water throughout the valley, and (2) provide a tool for stakeholders to address water availability and water-use issues in the valley. In order to maintain the usefulness of the CUVHM, periodic updates will be required as changing conditions in the actual hydrologic system continue to respond to the stresses imposed upon it, and as new information on the surface-water and groundwater systems become available. The CUVHM is a numerical hydrologic flow model developed with the finite-difference hydrologic modeling software One Water Hydrologic Flow Model (MF-OWHM) (Hanson and Schmid, 2013; Hanson and others, 2014a, b) that includes MODFLOW-2005 (MF2K5) (Harbaugh and others, 2000; Hill and others, 2000; Harbaugh, 2005) and incorporates an updated version of the Farm Process (FMP3) (Hanson and others, 2014b). The MF-OWHM is the newest version of MODFLOW-2005 with the Farm Process (Schmid and others, 2006a, b; Schmid and Hanson, 2009) that incorporates a dynamically integrated water supply-and-demand accounting within agricultural areas and areas of native vegetation. The MF-OWHM enables a more-detailed and realistic simulation of hydrologic systems than do earlier versions of MODFLOW. The MF-OWHM code incorporates the simulation of conjunctive use with linkages of supply-constrained and demand-driven use and movement of water across the landscape, surface-water, and groundwater flow systems throughout the Cuyama Valley (Hanson and others, 2010, 2014b; Hanson and Schmid, 2013).

The CUVHM was constructed in three major phases. The first phase was the collection of new data and compilation of existing data (Everett and others, 2013). The geohydrologic framework model was then developed on the basis of work in previous studies and analysis of new data (Sweetkind and others, 2013). This framework was further modified to include the inflow and outflows of the updated conceptual model, geohydrologic model development to determine the distribution of hydraulic properties, and finally, development of the hydrologic models. These components of model development were completed iteratively during the development and calibration of the model. The final components of MF-OWHM (processes and packages) used for the CUVHM are summarized in table 5.

Input parameters to the CUVHM were adjusted during implementation of these model development phases. Input parameters to the CUVHM were adjusted, with the aid of trial-and-error and automated parameter estimation calibration. The parameter estimation codes UCODE-2005 (Poeter and others, 2005) and PEST (Doherty, 2004, 2010a, b, c; Doherty and Hunt, 2010) were used to help with the calculation of sensitivities and parameter estimation. The model was calibrated to heads (groundwater levels), head differences, head changes with time, and land subsidence. During construction and calibration of the model, it became evident that several updates and enhancements were needed within MF2K5, the FMP, and some post-processing software. These updates and enhancements are summarized in the documentation of MF-OWHM (Hanson and others, 2014a, b). The CUVHM model components can be grouped in terms of the discretization and boundaries, land-use, streamflow, aquifer characteristics, initial conditions, and water budgets. The next few sections of the report describe the model components within these groups.

Discretization

The CUVHM domain includes the major alluvial deposits of the entire Cuyama Valley. The valley extends from east of Ventucopa and the confluence of Reyes Creek with Cuyama River to the narrows along Cuyama River northwest of New Cuyama, to the headlands of the foothills of the Sierra Madre Mountains on the southwest and west, and is bounded on the northeast by Caliente Range and Cuyama badlands (fig. 2*A*). The finite-difference model grid used to represent the land surface and subsurface alluvial deposits consists of a series of orthogonal square model cells. Spatial and temporal discretizations are held to uniform increments throughout space and time.

Spatial Discretization and Layering

The total active modeled area is 164 mi^2 on a finite-difference grid consisting of 135 rows, 300 columns (40,500 cells), and 3 layers having a varying number of active cells per layer, for a total of 15,577 active model cells (figs. 1*B*, 3*A*). In the horizontal dimension, about 17 percent of the cells (6,813 cells) are used to define the active part of the hydrologic model grid. The model has a uniform horizontal discretization of 15.4 acres per cell (820.2 ft by 820.2 ft equal to 250 m by 250 m) and is oriented subparallel to the tectonic structure of the Cuyama Valley and to the Cuyama River, 33 degrees west of due north (fig. 1*B*). This cell size was chosen to be comparable to the typical land parcel size and to facilitate the future linkage of the CUVHM model with remotely sensed land-use data for potential updates of land use and other landscape properties. The bounding coordinates for the total model grid are summarized in table 6.

The model includes three layers that are aligned with the hydrostratigraphic units described previously (Sweetkind and others, 2013). The top of the model is represented by the altitude of the land surface and is a composite of model layers 1, 2, and 3. The uppermost, Recent Alluvial aquifer model layer (layer 1) ranges in thickness from an assumed minimum of 16 ft (5 m) to an estimated maximum of about 633 ft (193 m). The second layer is coincident with the Older Alluvial aquifer system and ranges in thickness from an assumed minimum of 16 ft (5 m) to an estimated maximum of about 1,350 ft (411 m). The third layer is coincident with the extent of the upper portion of the Morales Formation and ranges in thickness from an assumed minimum of 16 ft (5 m) to an estimated maximum of about 4,710 ft (1,436 m).

Temporal Discretization

In order to adequately represent the dynamics of changing precipitation and streamflow, as well as the dynamics of the growing season, including the irrigation supply and demand components, the CUVHM is discretized into monthly stress periods and bimonthly time steps. Periods of user-specified (or BCM simulated) model inflows and outflows and boundary heads are referred to as stress periods. A model stress period is an interval of time in which the user-specified inflows and outflows are held constant. Variations in stresses are simulated by changing inflows and outflows and boundary heads from one stress period to the next. These inflows, outflows and boundary heads that include pumping, precipitation, reference evapotranspiration (ET_h), stream inflows, irrigation, and underflow beneath the Cuyama River are assumed to be constant within each stress period. Stress periods are further divided into bimonthly (approximately 15-day) time steps, which are units of time for which water levels and flows are calculated throughout all model cells. The total simulation period was 61.25 years (or 735 monthly stress periods) from October 1949 through December 2010.

Initial Conditions and Recent Conditions

Initial conditions are the distribution of water levels at every active cell within each of the three model layers estimated for 1947 and assumed to apply to October 1949. Data for 1947–66 drawdowns (fig. 15*A*) were used because more data were available for 1947 than for 1949, and any water-level changes during those 2 years early in development are assumed to have been negligible. Also, because very little data are available for the late 1940s, water-level data for years 1938–1955 were used to create the 1947 composite water-level contour map. The spring 1966 water-level contour map from Singer and Swarzenski (1970; fig. 15*B*) was used to help identify spatial trends in water levels on the 1947 map. A map of drawdown between 1947 and 1966 was developed by Singer and Swarzenski (1970). In order to check the accuracy of the 1947 map having more limited data, the contour maps were converted to raster grids, and the spring 1966 water-level and the 1947–66 drawdown raster grids were differenced. A good match was found with the Singer and Swarzenski (1970) water-level change map. In this study, all model layers were simulated as confined yet still represent the drawdown and evolution of the large cones of depression in the water table in the central subregions of the Cuyama Valley. For the parts of model layers that represent areas of the aquifers that are actually unconfined, the saturated thickness is held constant during declining or rising water levels. Though all layers are treated as confined in the model during the simulation, only parts of model layers 2 and 3 actually remain confined while other parts remain unconfined. Storage properties in the outcrop subregions (fig. 3*A*) of the uppermost layers (1, 2, or 3) are represented by specific yield and aare coincident with the unconfined portion of the system (see "Storage Properties" section). The regions of large water-level declines and related large unsaturated zones in the central zones of the valley are illustrated by the water-level maps from summer 1966 (fig. 15*B*), and from spring and summer of 2010 (fig. 15*C*, *D*). The geologic cross sections indicate that, after sustained groundwater-level declines between 1966 and 2008, portions or all of the shallower zones of these aquifers were drained (figs. 3*B, C*).

Boundary Conditions

Boundary conditions are applied at some model cells to simulate the inflows and outflows from the active model region as groundwater underflow (both inflows and outflows) and aquifer interaction along intermittent streams, as well as interaction with landscape processes (figs. 8 and 16). Two general types of boundary conditions are used in the model: no-flow and general-head. Inflows and outflows simulated across the hydrologic boundaries include recharge to and discharge from the groundwater system as well as interdependent flows between the groundwater, streams, and landscape processes such as ET and irrigation. The intermittent stream-aquifer interaction and landscape process interactions are discussed in later sections.

No-Flow Boundaries

No-flow boundaries were used for the bottom of the model and the lateral boundaries that are coincident with faults. The lower boundary was limited to the bottom of the Morales Formation or a total thickness for the formation of 300 m (980 ft), which is deeper than the deepest supply wells. Lateral no-flow boundaries represent the contact between the low-permeability rocks and thrust faults that bound the foothills and the unconsolidated alluvial sediments of Cuyama Valley (figs. 3*A*, 16).

General-Head Boundaries

The upstream northern and downstream regions of the Cuyama River are lateral hydrologic boundaries of the groundwater flow system that are simulated as head-dependent flow boundaries (figs. 3*A*, 16). These regions were simulated by using the General Head Boundary Package (GHB) of MODFLOW (Harbaugh, 2005). General-head boundaries were specified for model cells in layers 1 through 3 for the inflow region with spatially and temporally constant boundary heads and cell-specific hydraulic conductance. The hydraulic conductances of the lateral boundary cells were initially based on the texture-derived hydraulic conductivity of the aquifer sediments (described in the section "Aquifer Characteristics"). Hydraulic conductances were adjusted during model calibration.

Surface-Water Inflows and Outflows

Surface-water inflows and outflows were simulated with a streamflow routing network comprising 708 individual stream segments that represent the Cuyama River and its major and minor tributaries. This network was used to simulate the inflows from 144 major and minor drainages from the surrounding mountains, streamflow infiltration, and occasional outflows along the Cuyama River network (fig. 8). Additional stream inflow also was specified from the discharge of the waste-water treatment plant for the period 1938–2010. These features were simulated by using the Streamflow Routing Package (SFR2) (Prudic and others, 2004; Niswonger and Prudic, 2005); the head-dependent boundary condition used in SFR2 allows for streamflow routing, the capture and conveyance of overland runoff, streamflow infiltration into the aquifer (losing stream reaches), and any potential base flow as groundwater discharge to streams (gaining stream reaches). Runoff estimated by FMP is redirected to the streamflow networks and provides a substantial component of groundwater recharge and streamflow during the wettest months. Each of the major and minor drainages is represented by a collection of stream cells (referred to as reaches). The cells or reaches are combined between tributary points to form a collection of cells or reaches known as a segment. The stage-discharge relations were assumed to be constant for each segment in the SFR stream network. The details on how the relation is specified are given in the SFR manual (Niswonger and Prudic, 2005). The streambed elevations for the beginning and end of each segment are specified, along with the stream channel width, streambed thickness, and the vertical hydraulic conductivity of reaches within each segment (fig. 8).

In addition to intermittent and ephemeral streamflows, and about 9 springs and groups of seeps historically discharged shallow groundwater in Cuyama Valley prior to the 1970s (Singer and Swarzenski, 1970). Prior to groundwater development, these springs flowed at rates from 0.01 cubic feet per second (ft^3/sec) (5 gallons per minute, gpm) to as much as 1.9 ft^3/sec (860 gpm) along the outcrop boundaries that are aligned with the Turkey Trap and Graveyard Ridge Faults in the center of the valley along the northwestern segments of the Cuyama River channel (fig. 16). These springs and seeps are no longer flowing since the 1970s.

Groundwater Pumpage

Groundwater pumpage is a major component of the hydrologic budget of Cuyama Valley, and is grouped into two categories of pumpage for this study: agricultural and water supply. Agricultural pumpage includes water withdrawn from all farm wells used to supply water for irrigation, and water supply includes groundwater withdrawn for municipal, domestic/rural residential and industrial uses. Farm wells were simulated as a combination of single-aquifer wells (Schmid and others, 2006a) and multi-aquifer wells. Farm wells that are single-aquifer wells are simulated in a similar manner as used in the WEL Package (Harbaugh and others, 2000), while multi-aquifer wells are simulated by the multi-node well (MNW) Package (Halford and Hanson, 2002). The total pumpage for each WBS (that is, virtual farm) is distributed among each of the farm wells (both single-aquifer wells and multi-aquifer wells) that collectively supply groundwater to that WBS needed for irrigation for each monthly stress period (fig. 2*C*). The distribution of pumpage between wells is based on the average pumping rate up to the maximum yield of each well (Schmid and others, 2006a). Agricultural pumpage is estimated within FMP of the MF-OWHM model. Pumpage from wells used for municipal and domestic supply is specified on the basis of reported and estimated values. A select number of farm wells and municipal wells are simulated as multi-aquifer (MNW) wells that derive water from up to three aquifer model layers. Because some wells in the valley were not located in the DWR well-permit database, additional “virtual wells” were simulated to satisfy simulated delivery of groundwater to selected WBSs. In this report, a virtual well is one for which there is no specific information available for the existing well.

Agricultural Supply

Because pumpage from agricultural wells has never been metered in the Cuyama Valley, those values must be indirectly estimated for simulating and analyzing water use. The two most common methods of indirectly estimating pumpage are through analysis of data for power consumption by well pumps and data for consumptive use of water. Because many wells are driven by either electric or diesel power sources, and because of the inherent complexity of accounting for additional uses for electricity on a farm by farm basis, the use of electric power records is considered unreliable for estimating agricultural pumpage here. Consumptive-use estimates are also considered unreliable because this method does not account for the combined consumption of precipitation and water applied for irrigation and does not capture the variability in consumption with changing climate. The estimation of agricultural pumpage through application of FMP provides physically-based, dynamic, and linked pumpage estimates as an alternative to these other indirect methods (Hanson and others, 2014b; Schmid and Hanson, 2009).

Pumpage for agricultural supply is estimated as a combination of crop irrigation requirement and inefficient losses required to satisfy the total farm delivery requirement for all wells that deliver water to a particular WBS. Inefficient losses include those from in-farm conveyance of irrigation water, as well as potential losses from runoff and deep percolation below the root zone during irrigation. The crop irrigation requirement in this context refers to all evaporation and transpiration of water by a particular crop within a model cell, and is a part of the total consumptive use. Total consumptive use is the water consumed by evaporation and transpiration from all sources of water. Groundwater pumpage needed to satisfy the total farm delivery requirement can be estimated by taking into account any potential surface-water supply, the efficiency of irrigation, additional effective precipitation, fractions of transpiration and evaporation within each model cell, and the fractions of inefficient losses to runoff and deep percolation. Because all irrigation in Cuyama Valley is supplied by groundwater pumpage, surface-water supplies are not simulated. Unmetered pumpage is estimated through consumptive use by the FMP on the basis of a suite of land-use estimates applied to selected periods of the entire simulation period (table 2). Data from as many as 94 actual farm wells (fig. 9) were used for simulating pumpage for irrigation and the number of active wells for any given month varies through time on the basis of reported drill dates and destruction dates. There is no known reported agricultural pumpage data for Cuyama Valley that can be used as corroborative observations for calibration of simulated pumpage.

Pumpage for each well was allocated to the model layers on the basis of the construction information available. The open-screen interval was used to identify the model layers from which water was withdrawn, with the model assuming full penetration of each layer. If no construction information was available for “real” wells, or virtual wells were needed for irrigation, top and bottom model layer for each well were assigned on the basis of data from other wells in the area. The FMP allocated pumpage on a well-by-well basis, using the average fraction of total required pumpage within a particular WBS up to the pumping capacity of each well’s screened interval that supplies water. The capacity of the farm wells ranges from several hundred to several thousand gallons per minute, and the casing diameters range from 6 to 16 inches. However, during model calibration pumping capacities were set to a larger value to insure that supply would meet demand. In addition, the deficit irrigation scenario was used with FMP to reduce demand to available supply, and virtual wells were used for farms with simulated demand that did not have a known well a priori.

Water Supply

Pumpage information for municipal and industrial (M and I) uses and for domestic water supply was based on available reported monthly to annual pumpage on a well-by-well basis. As many as 17 wells, including the 2 Cuyama Community Service District (CCSD) production wells, were used to represent M and I wells at various periods during the 61-year simulation. The actual locations of municipal-supply wells were used in the model. The MNW Package is used to simulate municipal-supply groundwater pumpage. The open-screen interval or total depth was used to identify the model layers from which pumping occurred.

For domestic wells, either actual locations were used, or, if the actual locations were unknown for a select land parcel, the parcel was assigned a single virtual well (fig. 9). The well package was used to simulate the domestic pumpage from single aquifer model layers. The number of the domestic wells varies for each stress period. Drilling and destruction dates were used when available, or otherwise, wells were assumed to be present for the entire period of simulation. Total domestic pumpage was estimated to range from about 8 to 37 acre-ft/yr from as many as 95 domestic wells (figs. 9 and 10). Domestic pumpage was estimated on the basis of an assumed consumption rate of 0.25 to 0.94 acre-ft/yr and averaged about 0.54 acre-ft/yr per well (fig. 10). Overall, the combined M and I and domestic pumpage is minor compared to agricultural pumpage, but is important locally. For example, the CCSD wells supplied between 165 and 206 acre-ft/yr for the period 1998 to 2007 (U.S. Wilson, Cuyama Community Service District, written commun., 2008).

Landscape Use and Movement of Water

The FMP provides coupled simulation of the groundwater and surface-water components of the hydrologic cycle for irrigated and non-irrigated areas. A dynamic allocation of groundwater recharge and groundwater pumping is simulated on the basis of residual crop-water demand after surface-water deliveries and root uptake from shallow groundwater. The estimation of irrigation pumpage in FMP is dependent on contributions of water from precipitation and variable irrigation efficiencies and is also connected to irrigation inefficiency losses as return flows (deep percolation and runoff combined). The FMP not only estimates supply and demand, movement, and consumption of agricultural irrigation water, but also estimates these components for natural vegetation and for landscape irrigation in urban areas. Thus, the use of FMP in MF-OWHM represents the simulation of fully coupled flow of water through surface-water, land-use, and groundwater processes and is also dependent on atmospheric conditions through precipitation and reference evapotranspiration (Schmid and others, 2006b; Schmid and Hanson, 2009; Hanson and others, 2014b). MF-OWHM simulates the demand components representing crop irrigation requirements that are subject to crop and farm-specific inefficiency losses, and the supply components representing precipitation, direct uptake from groundwater, and irrigation from pumped groundwater. Soil moisture is not considered a significant source or storage component of the water budget in well managed, irrigated agriculture. The FMP also simulates additional head-dependent inflows and outflows from the landscape, such as a monthly approximation of surface runoff from precipitation and surface-water return flows to the streamflow network, and groundwater recharge by way of deep percolation of water in excess of actual evapotranspiration (ET_{act}) and runoff (Schmid and others, 2006a, b; Schmid and Hanson, 2009).

Inflows and outflows throughout the WBSs on the landscape are simulated by FMP as mass balances within each WBS and are calculated and balanced for each simulation time step. The following summarizes how FMP accounts for inflows and outflows for each WBS; more details can be found in the FMP and MF-OWHM documentation step (Schmid and others, 2006a, b; Schmid and Hanson, 2009; Hanson and others, 2014). The FMP dynamically integrates irrigation water demand from evapotranspiration with water supply and inefficiency losses. FMP allocates water, simulates processes, and computes the surface-water and groundwater inflows and outflows for each WBS in the active model domain induced by irrigated and non-irrigated agriculture and natural vegetation. On the basis of cell-by-cell estimations for each WBS, the FMP first calculates water demand as the transpiration from plant-water consumption and the related evaporation. The FMP then determines a residual water demand that cannot be satisfied by precipitation and (or) by root uptake from shallow groundwater near the root zone. Next, the FMP equates this residual water demand with the irrigation requirement for the cells with irrigated crops (that is, exclusive of any natural vegetation), which is called the crop irrigation requirement (CIR).

The CIR is then adjusted (increased) by accounting for evaporative losses from irrigation and other inefficiency losses to yield a final total farm delivery requirement (TFDR). For Cuyama Valley, where groundwater is the sole source of water used for irrigation, FMP attempts to satisfy the TFDR using only pumped groundwater. The amount of excess water from irrigation and (or) precipitation that is not effectively used for crop growth or is otherwise “lost” as described above then becomes either overland runoff to nearby streams or groundwater recharge as deep percolation below the root zone. Thus, the FMP dynamically links the demand, supply, and related change in aquifer storage. All of the supply and demand components are then tabulated into WBS landscape budgets that complement the groundwater-flow and streamflow budgets that collectively represent the hydrologic cycle within Cuyama Valley.

In order to estimate the inflows and outflows, the FMP integrates various components of supply and demand data that can be specified over time or held constant for the entire simulation. The FMP requires soil, crop, and climate data to compute consumptive use and the groundwater pumping capacity of all wells that serve a WBS.

The FMP dynamically simulates these supply and demand components for a WBS within MF-OWHM by integrating the following computational components specific to Cuyama Valley's hydrologic setting:

1. TFDR, which is largely dependent on the CIR but also depends on efficiency, changing climate (ET and precipitation), and variable aquifer head.
2. Supplemental groundwater pumpage, which is estimated as the TFDR, but is limited by a specified maximum WBS well-pumping capacity on a well-by-well basis.
3. Net recharge (deep percolation) to groundwater, which is taken to be the sum of excess irrigation and precipitation minus the sum of surface-water runoff and ET from groundwater (Schmid and others, 2006a, p. 20). (Groundwater discharge to streams is accounted for by SFR2).

The MF-OWHM code maintains a mass balance of the landscape for each WBS, for the streamflow network, and for the groundwater-flow system. Flows between these budgets are accommodated by head-and flow-dependent inflows and outflows, such as the actual ET, runoff and infiltration, or transpiration from groundwater. Quantities of interest, such as TFDR, surface-water and groundwater supply, and excess applied irrigation water depend on these head-dependent inflows and outflows.

For the CUVHM, the processes of evaporation, transpiration, runoff, deep percolation to groundwater, and groundwater pumpage were estimated using MF-OWHM. The simulated deliveries and groundwater pumpage reflect climatic differences, differences in agricultural practices among defined WBSs, changes in the water-delivery system, and changes in the distribution of the WBSs that reflect changing land use and water usage during the 1939–2010 simulation period. The CUVHM model provides a detailed transient analysis of changes in groundwater availability in relation to climatic variability, urbanization, land use, WBS, and changes in irrigated agriculture.

Delivery Requirement

The TFDR is determined as the sum of consumptive use of all WBS cells for irrigated crops and inefficient losses of applied irrigation water with respect to plant consumption. In order to calculate the components of the water budget, the FMP also requires estimates of both the irrigation and groundwater components and ET as a whole. Consumption of water by individual crops in each WBS is simulated with steady-state transpiration, varying with changing water level, which is approximated in FMP by an analytical solution. Thus, the amount of evaporation and transpiration from the water table are both a function of soil type, water-table altitude, the root depth of each crop type, and the user-specified anoxia and wilting point of each crop. As mentioned previously, soil moisture is not accounted for directly other than by a capillary fringe based on soil type. Therefore, the TFDR requires soil, land use (specifically distribution of crop types), and climate data to compute consumptive use on a cell-by-cell basis.

Soils

The CUVHM soils were simplified into four categories—sand, sandy loam, silty clay, and silt—on the basis of data from the Soil Survey Geographic Database (SSURGO; U.S. Department of Agriculture Natural Resources Conservation Service, 2005, 2006; fig. 17). The capillary fringe was also estimated for each soil type, and ranges from 4 to 6 feet thick. These soil attributes are used for the entire simulation period and the cell-by-cell distribution is independent of the crop and WBS. The FMP associates the distributed soil types with the specified capillary fringes and internal coefficients that allow individual analytical solutions for the calculation of ET (Schmid and others, 2006a).

Land Use

The FMP can be used to estimate components of consumptive water use for a wide variety of land-uses, including vegetation in irrigated or non-irrigated agriculture, fallow fields, riparian or natural vegetation, and urban landscape settings. FMP also can be used to simulate an assortment of irrigation settings that span the spectrum from flooded fields such as rice and cotton, to drip irrigation of truck crops, vineyards, and orchards. Applications with zero transpiration, such as artificial recharge systems (including Aquifer Storage and Recovery, or ASR, systems) also can be simulated with FMP (Hanson and others, 2010, 2014a).

For the Cuyama Valley, the land-use attributes are defined on a cell-by-cell basis and include urban and agricultural areas, as well as areas of natural vegetation. The land use that covered the largest fraction of each cell was used as the use representative of that cell. The CUVHM model employs a standardized land-use category system that combines the classification systems for agricultural and native vegetation as well as generalized land uses from historical maps. This system combines the USGS National Land Cover Database (NLCD) (Anderson and others, 1976; Homer and others, 2012), the USDA National Vegetation Classification System (NVCS) (Brohman and Bryant, 2005; Federal Geographic Data Committee, 2008), and the U.S. Forest Service CALVEG ("Classification and Assessment with Landsat of Visible Ecological Groupings") system (U.S. Department of Agriculture, 2007). The CUVHM has 41 land-use categories that represent 41 agricultural, urban vegetation, native vegetation, general, and non-vegetation land uses. This includes a split in crop attributes for the period prior to 1993 and for 1993–2010. Crops that are represented at various land-use periods include 8 hay and grain crops, 8 vegetable crops, 10 orchard crops, 4 natural vegetation types, 4 non-vegetation land uses, and 5 generalized land-use categories (table 7). Constructing maps of land use, including crops, is problematic because of the complex pattern that is subject to rapid change in the dynamic environment of modern agriculture. Despite the uncertainty and complexity, land-use maps were developed for 14 different periods during the entire period of simulation. Most of the more recent maps (2007–10) were based on interpreted high-altitude aerial photography that is supplemented with published land-use maps and CropScape images (Mueller and others, 2011; U.S. Department of Agriculture, 2012) and confirmed with the NAIP photo imagery. Land-use changes may occur gradually or rapidly in response to changes in climate, urbanization, zoning, or farming practices. This required making decisions as to how and when to assign land-use changes to the modeled domain. For this simulation, the seven land-use patterns were generally aligned with the wet-dry climate cycle for which they were compiled (table 2, fig. 5).

From 13 to 34 percent of the valley floor is developed land that is not native trees or shrub land (table 7). Most of this land is agricultural land that was further subdivided into agricultural classifications. The agricultural categories were augmented with more general classes for earlier years, when the delineation of land use was less detailed. In general, the class-1 categories represent groups of vegetation that have similar amounts of water consumption and similar growth cycles that drive their consumption of water. Because of the interest by water managers in water use by vegetables and by orchard and field crops, selected varieties that are grown in Cuyama Valley were simulated individually when their distribution was available from the land-use maps. These land-use categories were then defined on the basis of land-use maps and these groups of similar crops are herein referred to as “virtual crops” (table 7, figs. 5, 18–22). For the entire simulation period, these virtual crops were used to drive the use and demand for water for each WBS. Each of the virtual crops was represented by an index number in the FMP (table 7). Many of the virtual crops were amalgamations of the multiple crop types (table 7, grouping of other classes). For example, virtual crops such as “Irrigated Row and Vegetables Crop” or “Field Crops” were amalgamations of other more detailed virtual crops. Because the virtual crop maps for the earlier periods were more generalized, some of the more permanent or more established land cover, such as “native vegetation” and orchard crops, which were mapped more recently, were assumed to be active earlier and were embedded in the earlier land-use maps on the basis of the most recent land-use period (2010). The land-use periods simulated are the multi-year periods of 1949–55, 1955–62, 1962–76, 1976–79, 1980–84; biannually for 1985–86, 1987–88, 1989–90, 1991–92, 1993–94, 1995–96, 1997–98, 1999–2000, 2001–02, 2003–04; and annually from 2005–10 (fig. 5).

Land-Use Maps

For the period 1945–79, land use was based on the Anderson level II classifications (Anderson and others, 1976) for the 1977 land-use map (fig. 18), and stored in the Geographic Information Retrieval and Analysis System (GIRAS) (U.S. Geological Survey, 1990). Data were compiled by geographic quadrangle from the mid-1970s to the early 1980s. The original 1977 land-use map includes 22 vegetation classes that matched 8 of the CUVHM virtual crops (fig. 18). Five of these classes are different types of native vegetation, and six classes represent developed land uses. Because of this generalized classification, the agricultural virtual crop classes were replaced with the virtual crop of identical extent from the 2000 virtual-crop map. For example, where only “cropland” was specified in 1977, the virtual crops interpreted on the 2000 virtual crop map were embedded. This assumes the farmer would be growing the same type of crop in a given area through the period of the hydrologic simulation. For some crops, such as for orchards, this is generally a good assumption; for other crop types, however, the type of crop may have changed several times. Despite the general nature of the map, it shows that approximately 66 percent of the valley was covered by native vegetation, 34 percent was agricultural land and less than 1 percent was urban land use (fig. 18*D;* table 7). Because earlier land-use maps were not available, land-ownership parcels were used to define the evolution from native vegetation to agricultural land use (fig. 18*A*–*C*).

For the period 1980–94, land use was based on the NLCD land-use map (fig. 19*A*). The NLCD classification, is a 21-class hierarchical, modified, Anderson Land Cover Classification (U.S. Geological Survey, 1999). The NLCD data are derived from images acquired by Landsat’s Thematic Mapper (TM) sensor, and several ancillary data sources. The NLCD is based on imagery acquired throughout the 1980s (U.S. Geological Survey, 1999). It is the first national land-cover dataset produced since the early 1970s, effectively replacing the GIRAS datasets. Despite the availability of more recent datasets, however, many of the land-use categories were more general than those in the original 1977 land-use map. Therefore, the general land-use categories were replaced with the more detailed classifications from the 1977 land-use map (fig. 18*A*).

For the period 1995 through 2000, land use was assigned on the basis of land-use data for 2000 (fig. 19*B*), which were obtained in digital format from the California Department of Water Resources (2000). The county land-use survey data were developed by CADWR, through its Division of Planning and Local Assistance, from aerial photography and extensive field surveys. The land uses that were compiled were detailed agricultural uses and less detailed urban and native vegetation land uses. The agricultural classifications can be correlated to the 12 CADWR class-1 categories (California Department of Water Resources, 2000). Such level of spatial detail is ideal for this study, because the crop types are aggregated into classes that have similar water-use characteristics. The

CADWR prepares these detailed county maps of agricultural land use every 6–7 years. Because the virtual-crop map for 2000 represents a composite map of land use from the late 1990s, this type of map also lacks the temporal detail needed to accurately reflect the dynamics of changing agriculture or urbanization. Although the data are suitable for representing regional spatial patterns of land use and crop patterns, there are some discrepancies across county boundaries. The agricultural classes were used instead of the more detailed crops that were identified. The land use was grouped into 14 classes, and the crop that covers the majority of each model cell was identified as the virtual crop for that cell. Upland areas omitted from the CADWR maps were classified as native vegetation. For the period 2001–2002, land-use parcels were used to define the change in agricultural land use (fig. 19*C*). For all these maps, approximately 65 percent of the valley was covered by native vegetation, 34 percent was agricultural land, and less than 1 percent was urban land (fig. 19; table 7).

For the period of 2004–09, land use was assigned on the basis of the use in 2000 (California Department of Water Resources, 2000; figs. 20, 21). As in prior years, land-use parcels were used to define the change in agricultural land use. The spatial distribution is similar to that in 2000, with only small local changes. Approximately 65 percent of the valley was covered by native vegetation, 34 percent was agricultural land, and less than 1 percent was urban land (figs. 20, 21; table 7).

For 2010, land-use data were obtained in digital format from the CropScape (U.S. Department of Agriculture, 2012; fig. 22). These data were based on parcel maps and show more detailed crop distributions than the CADWR land-use maps (California Department of Water Resources, 2000). These data, however, do not cover the entire valley and were supplemented and modified with the CADWR land-use maps (California Department of Water Resources, 2000) in areas where the data were missing. The spatial distribution of different land use is similar to that of 1997 and 2000, with only small local changes. Approximately 65 percent of the valley was covered by native vegetation, 35 percent was agricultural land, and less than 1 percent was urban land (fig. 22). The actual land use (fig. 22*A*) and the model discretized land use (fig. 22*B*) are shown for this most detailed land-use cover to demonstrate the alignment of actual and modeled land use over the active model area. Overall, the changes in total land use include a small decrease in natural vegetation, a small increase in total percentage of agricultural land use, but multiple changes in the types of crops grown on that agricultural land.

Crop-Type Data

The virtual crops provide a basis for estimating the consumptive use of water at the land surface, a key component of the TFDR (Schmid and others, 2006a). The TFDR is largely determined by the consumptive irrigation requirement (CIR). The CIR is determined from the product of a reference ET (ET_h) and an area-weighted crop coefficient (K_c) on a cell-by-cell basis; these products are summed over all cells within each WBS. Because so many factors affect ET (including weather conditions, soil properties, and plant characteristics), it is difficult to formulate an equation that can produce estimates of ET under different sets of conditions (California Department of Water Resources, 2013). Therefore, the reference crop ET was developed (California Department of Water Resources, 2013). The reference ET from a uniform (evenly mowed) grass surface is commonly denoted as ET_o or ET_h from the CIMIS station 88 (fig. 6*B*).

Specified root depths, suction pressures for the unsaturated root zone, K_cs, and fractions of transpiration and evaporation affect the consumption and movement of water for each crop category (Schmid and Hanson, 2009). For the CUVHM, the root depths and root uptake pressures were held constant for the entire simulation and are based on values from the literature (table 8). Pressure heads for suction pressures in the root zone are a range of negative (unsaturated) pressures for agriculture and native vegetation such as grasses, shrubs, and trees.

Direct transpiration (T) and evaporation (E) from groundwater occur at a rising water table when the top of the capillary fringe above the water table reaches the bottom of the root zone of plants or when the top of the capillary fringe above the water table reaches the land surface, respectively. For changing water tables, the direct T and E from groundwater are eliminated when the top of the capillary fringe above the water table reaches the land surface or when the top of the capillary fringe above the water table falls below the land surface (Schmid and others, 2006a).

Crop water demand, which is the product of the K_c values and a crop stress coefficient, can be related to crop growth stages. The K_c values used in this study were based on an unstressed crop growth curve. This growth curve was divided into twelve monthly stages spanning the initial growth stage, the rapid growth stage, the mid-season stage, the late-season stage, and a period of no planting (fig. 23). Although the specific growth dates for each virtual crop vary depending on the planting date and climatic zone, growth dates are assumed to be spatially uniform throughout the valley. The only change in K_c value at a given location is based on a change in virtual-crop type with land-use changes and with changes in the crop stress coefficient for different wet- and dry-year seasons.

The K_c values were derived from several sources (figs. 23*A*, *B*, *C*, *D*, *E*). When available, published K_c values for similar coastal areas were used (Brouwer and others, 1985; Brouwer and Heibloem, 1986; Snyder and others, 1987a, b; Allen and others, 1998). If no published K_c values were available for similar coastal areas, published K_c values for the western San Joaquin Valley compiled by Brush and others (2004), for turf grass (Gibeault and others, 1989), and for various Central coast field and vegetable crops (Snyder and Schullbach, 1992) were used. In many cases, multiple crops were area-weighted to produce a composite virtual K_c value. The K_c values were divided into two periods of agriculture, representing an early period of more traditional seasonal agriculture in the Cuyama Valley (1949–92) and a more recent period of more intensified agriculture (1993–2010). The transition between these periods of agriculture was placed at the end of the last multi-year drought (1984–92). Finally, the K_c values were multiplied by a crop-stress coefficient (Schmid and Hanson, 2009), the values of which depended on climatic conditions and other factors. The climatic stress on irrigated agriculture can vary by more than 20 percent between wet and dry seasons (Hanson and others, 2010). Eight stress coefficients were used to represent the wet- and dry-year seasons. These stress coefficients were adjusted during model calibration.

Other WBS and crop-related properties that were specified include the fraction of transpiration (F_{tr}), fraction of evaporation from precipitation (F_{ep}), and fraction of evaporation from irrigation (F_{ei}), and the irrigation efficiencies. These fractions (F_{tr}, F_{ep}, and F_{ei}) vary linearly with the respective area occupied by crops and the area open to soil-evaporation (Schmid and others, 2006a). Because the cropped area and the exposed wetted area amount to the entire area, F_{tr} plus F_{ep} equals one. In addition, F_{ei} must be less than or equal to F_{ep}. The F_{tr} is assumed to be independent of whether the transpiratory consumptive use is satisfied by irrigation, precipitation, or groundwater uptake. The fraction of the consumptive use that is transpiratory (F_{tr}) or evaporative (F_{ep} and F_{ei}) depends highly on type of crop and growth stage. When the vegetation cover reaches nearly 100 percent, then $F_{tr} = 1$, with F_{ep} and $F_{ei} = 0$. As a result, the fractions of transpiration and evaporation vary by virtual crop for different months of the year (table 9).

Irrigation efficiency is defined as the fraction of applied water actually consumed. The applied water that is not consumed, as a result of excess irrigation and excess precipitation, becomes losses to runoff and deep percolation (Schmid and others, 2006a). In the CUVHM, the irrigation efficiencies are specified as a matrix of efficiencies for each WBS and each crop for each of the monthly stress periods (Schmid and Hanson, 2009). In this way, the efficiencies differ from crop to crop for different WBSs and can change through time. The range in irrigation efficiency for each crop or crop group is tabulated in table 10. Irrigation efficiencies are assumed to have varied in time, reflecting improvements in irrigation application technologies and changes in the cost and availability of water (Brush and others, 2004). In general, the efficiencies have improved through time with technological advances in irrigation systems, changes in cropping patterns, and better leveling of the fields (California Department of Water Resources, 1994). The increase in efficiency is taken into account during calibration by applying fractional irrigation efficiencies that were estimated to increase through time.

In general, irrigation efficiencies are poorly known (California Department of Water Resources, 1994; and Brush and others, 2004). The CUVHM efficiencies specified in the FMP are typically quite variable, with lower values in wet seasons and in early years with less efficient means of irrigation and higher values in dry seasons and in more recent years with improved irrigation methods. However, irrigation efficiencies also can vary between seasons, and this variability can differ between wet-year and dry-year periods. Thus, irrigation efficiencies were also scaled on the basis of wet- and dry-year seasons. These scale factors were adjusted during model calibration.

Climate Data

The consumptive use of water, specifically the TFDR, is directly related to the climate. Although several of the properties specified previously take into account yearly or monthly variations, and some have a climatic component, the main climatic contributors to the FMP are precipitation and potential or reference evapotranspiration (ET_h). In constructing the CUVHM, climate data were developed for precipitation and potential evapotranspiration and distributed spatially and temporally for all months and active model cells (Hanson and others, 2012; Flint and Flint, 2012).

Precipitation

Precipitation for the CUVHM is specified through the FMP at the uppermost active cells across the entire active model grid. For each month of the entire period of simulation the total monthly precipitation is specified at an equivalent average daily rate. Gridded regional estimates of precipitation and temperature are obtained at a 800-m spatial resolution from the Parameter-elevation Regression on Independent Slopes Model (PRISM, *www.prism.oregonstate.edu*) (Daly and others, 2008), transient monthly dataset, downscaled to a 270-m grid resolution (Flint and Flint, 2012). PRISM uses instrumental observations and a digital elevation model, making adjustments for features such as elevation, aspect, slope, and rain shadows. Flint and Flint (2012) downscaled the PRISM precipitation estimates from 800-m to 270-m using a gradient-inverse-distance-squared approach that incorporates northing, easting, and elevation. A monthly precipitation rate was bilinearly interpolated from the 270-meter monthly raster estimates to the center of each 15-acre model cell of the rotated model grid, and varies month to month with the general distribution reflected by the long-term average (fig. 6*A*).

Portions of the precipitation are simulated as consumption through evaporation and transpiration from the WBS on a cell-by-cell basis. If precipitation in excess of ET occurs, a portion of this precipitation becomes runoff and the remaining portion becomes deep percolation as natural groundwater recharge from precipitation or artificial groundwater recharge from excess irrigation. The portions of runoff from precipitation vary by land-use type specified through the estimation of virtual-crop properties (table 8). Certain types of crops have additional runoff, such as some pistachio orchards on which a plastic mulch is applied. Larger fractions of runoff for irrigation and precipitation were specified for these types of agricultural practices.

Reference Evapotranspiration (ET_h)

Estimates of ET_h can be derived by using either complex parameter-based equations or simpler empirical equations. The main difficulty encountered in the use of parameter-based equations is the lack of accurate or complete data with a sufficient spatial and temporal distribution for the parameters and the general requirement to make estimates on a daily basis. In addition, the detailed climatological data required for the parameter-based equations (such as the Penman-Monteith equation) are not available for many sites in California, especially prior to the operation of the California Irrigation Management Information System (CIMIS) stations started in 1987. For the CUVHM, ET_h was developed on the basis of an hourly energy-balance calculation that is based on solar radiation, air temperature, and the Priestley–Taylor equation (Flint and Childs, 1987) to calculate potential evapotranspiration (ET_h; Flint and Childs, 1991). Clear-sky ET_h is calculated using a solar radiation model that incorporates seasonal atmospheric transmissivity parameters and site parameters of slope, aspect, and topographic shading (to define the percentage of sky exposing every grid cell) (Flint and Flint, 2007). Hourly ET_h is aggregated to a monthly rate and cloudiness corrections are made using cloudiness data from NREL (National Renewable Energy Lab, 2014). Modeled ET_h for the southwestern United States was then calibrated to the measured ET_h rates from CIMIS and Arizona Meterological Network (AZMET) stations (Flint and Flint, 2007).

One CIMIS station has been operated in Cuyama Valley since 1989 (Cuyama Station No. 88; fig.6*B*). The Cuyama Valley station has an average annual ET_h of 60.8 inches. The comparison with simulated potential ET (ET_h) is shown for CIMIS Station No. 88 (fig. 12). Simulated ET_h has an average annual value of 60.0 inches and underestimates measured ET_h for all months, with a standard error of the regression of 0.37 inches/month for the entire year. Monthly differences between measured ET_h and simulated ET_h range from 2 percent to 14 percent, with the highest differences in the summer months (table 11). When forced through zero, the regression equation has a slope of 1.1097, indicating an underestimation of the evapotranspiration in general relative to the CIMIS data.

Groundwater Agricultural Supply

The groundwater supplied to each WBS is simulated by a series of single-model-layer “farm wells” or through multi-aquifer wells simulated with the MNW1 Package (Halford and Hanson, 2002). The multi-aquifer farm wells that are simulated by MNW1 were reduced to a single priority well in each cell when more than one multi-aquifer well occurred in same cell. The priority for the multi-aquifer farm wells was given to wells with more than 10 percent screened interval in more than one layer, largest capacity, and longest history of potential pumpage. All remaining wells were simulated as single-aquifer farm wells through the farms-wells feature in the FMP. In addition, any multi-aquifer farm wells that did not include more than about 10 percent of the second model-layer thickness were also treated as single-aquifer farm wells. This resulted in as many as 103 single-aquifer farm wells and 29 multi-aquifer farms wells.

Agricultural groundwater pumpage requirements are estimated by the FMP after water supplied by precipitation is subtracted from the total actual ET on a cell-by-cell basis. The remainder of the water needed for agricultural land-use is the crop irrigation requirement that is summed on a cell-by-cell basis within each WBS as the TFDR which is the CIR combined with other potential losses from inefficient irrigation. The TFDR that is required from groundwater pumpage is estimated from this sole-source aquifer. This allows a way to simulate an estimate of historical unmetered pumpage for the period 1949–2010.

Net Recharge

The net recharge in a WBS is defined as losses after consumption due to excess irrigation and excess precipitation, reduced by losses to surface-water runoff and ET from groundwater (Schmid and others, 2006a). The fraction of losses to surface-water runoff depends on whether the runoff is related to irrigation or to precipitation. Losses based on irrigation depend on different irrigation methods, which, in turn, depend on the virtual crop type and related fractions of runoff from precipitation and irrigation (table 8) as well as other factors such as soil type and irrigation efficiency. The ET from groundwater is subtracted from the potential net downward flux to the uppermost aquifer. Hence, net recharge to groundwater can be affected by both user-specified and head-dependent parameters. This definition of net recharge requires the following assumptions: deep percolation below the active root zone is equal to groundwater recharge, ET from groundwater equals an instantaneous outflow from aquifer storage within any time step, and the net change in soil moisture storage for well managed (irrigated) agricultural areas for periods of weeks to months is negligible (Schmid and others, 2006a). The net recharge to the aquifers is applied to each uppermost active model cell in each WBS.

Aquifer Characteristics

The unconsolidated alluvial deposits and the Morales Formation form a three-layered aquifer system within the regional aquifer system defined by the three hydrogeologic units in the Cuyama Valley. Each aquifer can be characterized by variations in hydraulic properties, which are based on the textural distribution of coarse and fine-grained sediments and zones representing subregions in which the sediments accumulated in particular depositional environments. The hydraulic properties represent the ability for the aquifer to transmit water and to store or release water and are functions of depositional environment and lithology. Variations in depositional environments and lithology cause differences in grain size, grain shape, grain orientation, and the degree of sorting. This causes considerable spatial variation in the hydraulic properties of the deposits. Thus, variable lithology and depositional environments determine spatial variation in the hydraulic properties of the deposits. The hydraulic water-transmitting properties of the aquifer sediments are represented by horizontal (K_h) and vertical (K_v) hydraulic conductivity and hydraulic storage properties of the hydrogeologic units that constitute the aquifer system are represented by hydraulic conductivity and the storativity, respectively. The relation between hydrogeologic units in the aquifer system, lithology, and hydraulic properties has been developed in many previous studies that include both the properties of the aquifers and those of any fine-grained interbeds or confining units (Hanson and others, 1990, 2003, 2004, 2014a, b; Laudon and Belitz, 1991; Phillips and Belitz, 1991; Hanson and Benedict, 1993; Leighton and others, 1994; Fio and Leighton, 1995; Belitz and Phillips, 1995; Burow and others, 2004, Phillips and others, 2007; and Faunt and others, 2009a, b).

Textural Analysis

Lateral and vertical variations in sediment texture affect the direction and rate of groundwater flow as well as the magnitude and distribution of aquifer-system storativity. The textural distribution was used to define the vertical and lateral hydraulic conductivity and storage property distributions for the hydrologic model (Sweetkind and others, 2013). As in many of the previous studies identified above, the textural distribution was based on drillers' and geophysical logs. The primary variable selected for the textural analysis was the percentage of coarse-grained sediment, with the complement being the percentage of fine-grained sediment.

Based on the distribution of texture in the Cuyama Valley and the reanalysis of the hydrogeology (Sweetkind and others, 2013) the groundwater system was split into three aquifers. Within each hydrogeologic model layer, the fraction of coarse- and fine-grained sediments within the thickness of each layer was estimated on a cell-by-cell basis. Texture was estimated at the model-cell centers of the model grid for each of the model layers that are coincident with the hydrogeologic units. The fraction of coarse- and fine-grained sediments within the thickness of each layer was estimated on a cell-by-cell basis.

Hydraulic Properties

Estimates of textural-based hydraulic properties were segregated into three hydrogeologic units that were delineated on the basis of the distribution of sediment texture derived from drillers' logs, geologic logs, and geophysical logs. The hydraulic properties of an aquifer are its transmission and storage properties. The transmission properties of the Cuyama Valley aquifer are represented by the hydraulic conductivity (K) in this study. Equivalent horizontal and vertical hydraulic conductivities are assumed to be correlated to sediment texture (the fraction of coarse-grained and fine-grained sediment). The method uses the estimated binary sediment texture for each model cell and horizontal and vertical hydraulic conductivity estimates for each textural end member.

Faunt and others (2009a) identify the power mean as useful for defining hydraulic conductivity values. In addition, their work also includes a review of the literature that describes the use of power mean for estimating hydraulic conductivity. A power mean is a mean of the following form:

$$M^p(x) = \left(\frac{1}{n}\sum_{k=1}^{n} x_k^p\right)^{1/p} \quad (1)$$

where

- p is the averaging power-mean exponent,
- n is the number of elements being averaged, and
- X_k is the k^{th} element in the list.

The horizontal hydraulic conductivity ($K_{h,i}$) was calculated as the weighted arithmetic mean (also equivalent to the power mean to the zero power) of the hydraulic conductivities of the coarse-grained (K_c) and fine-grained (K_f) lithologic end members and the distribution of sediment texture for each (i^{th}) model cell:

$$K_{h,i} = \left[K_c F_{c,i} + K_f F_{f,i}\right] \quad (2)$$

where

- $F_{c,i}$ is the fraction of coarse-grained sediment in a cell, estimated from sediment texture data, as described in the previous section, and
- $F_{f,i}$ is the fraction of fine-grained sediment in a cell ($1 - F_{c,i}$).

Because K_f is much smaller than K_c, the arithmetic mean heavily weights the coarse-grained end member for horizontal hydraulic conductivity.

Vertical hydraulic conductivity between model layers ($K_{v,k+½}$) was calculated as the p^{th} weighted power mean of the hydraulic conductivities of the coarse-and fine-grained lithologic end members, and k is the model-layer number (Faunt and others, 2009b):

$$K_{v,k+1/2} = \left[F_{c,k+1/2} K_c^p + F_{f,k+1/2} K_f^p\right]^{1/p} \quad (3)$$

where

- $F_{c,k+½}$ is the fraction of coarse-grained sediment between layer midpoints, and
- $F_{f,k+½}$ is the fraction of fine-grained sediment between layer midpoints of k^{th} element in the list.

The harmonic mean is a weighted power mean with the exponent $p = -1.0$ in eqn. 3 and results in increased vertical anisotropy. The geometric mean is a weighted power mean with $p = 0.0$ in eqn. 3 and results in decreased vertical anisotropy. Phillips and Belitz (1991) determined that vertical conductivities could be calculated using either weighted harmonic or weighted geometric means. Belitz and others (1993) represented the vertical conductivities with the weighted harmonic mean. The vertical conductivities can be represented as power means in which p varied between −1.0 (the harmonic mean) and 0.0 (the geometric mean) (Faunt and others, 2009b; Hanson and others, 2014a). The relation between hydraulic conductivity and percentage of coarse-grained deposits based on hydraulic conductivity end members and exponent of the power mean is nonlinear. The resulting value is a function of the power mean and as a result is sensitive to the power used (averaging method). Both the harmonic and geometric means weight the fine-grained end members more heavily, and as a result, the vertical hydraulic conductivities are much lower than the horizontal. Dimitrakopoulos and Desbarats (1993) determined that the value of p depended to some extent on the size and thickness of the grid blocks used to discretize the model domain; smaller grid cells resulted in smaller values of p. The exponent p was specified for each model layer and adjusted during model calibration. The resulting K_f values of the exponent, p were −0.9 for the Recent Alluvium aquifer (layer 1), −0.5 for the Older Alluvium aquifer (layer 2), and −0.7 for the Morales Formation aquifer (layer 3).

Data from aquifer tests in the Cuyama Valley that generally represent short-term pump tests that were compiled and used to provide selected transmissivity and hydraulic conductivity values (Everett and others, 2013; fig 24*A*). The estimated hydraulic conductivity values from these tests ranged from 0.3 to 39 feet per day (ft/d) from an estimated transmissivity derived from Jacob's method (Jacob, 1946). Additional estimates of hydraulic conductivity for the three aquifers include slug tests from the three multiple-well monitoring sites and range between 1.6 and 28 ft/d (Everett and others, 2011, 2013). These estimates were used as additional observations during model calibration to constrain the hydraulic conductivity of the model layers in select regions (table 12).

Hydraulic Conductivity of Lithologic End Members

Parameter estimation, in combination with the texture model developed for the region on the basis of the known stratigraphic units and kriged subsurface texture based on reported lithology, was used to estimate K_c and K_f, the end-member hydraulic conductivities (Sweetkind and others, 2013). These end members were used to estimate the horizontal and vertical K for each cell in the model, which are then related to zonal subareas (table 13; figs. 24*B–D*) that are used to estimate final values derived from model calibration. The Layer Property Flow Package (LPF) is used to simulate the hydraulic properties and groundwater flow process for the application of MF-OWHM to Cuyama Valley's aquifer systems. The final parameters from model calibration representing hydraulic properties and related scale factors are included in the summary of parameter values in table 14 discussed in the section "Model Calibration."

The hydrostratigraphic layers of the aquifer system in Cuyama Valley formed in somewhat different depositional environments and have textural compositions that affect the end-member K values. In the model, each of these layers was further subdivided into subareas that helped facilitate model calibration and better represent subareas that are different depositional environments (table 12; fig. 24). These also were used to define the subareas distribution of vertical hydraulic conductivity (fig. 24). In subareas where the Older Alluvium (layer 2) was estimated to be missing between the Recent Alluvium and Morales Formation, the hydraulic properties are represented by assumed values that allow communication between the Recent Alluvium and the Morales Formation model layers.

Because the hydraulic properties differ for each of the hydrostratigraphic units, they were estimated separately. The parameters used to control these subareas within each model layer represent unconfined aquifers in the outcrop areas as well as subareas of confined aquifers where the Older Alluvium or Morales Formation underlie the other aquifers. In addition, the subareas where the Older Alluvium aquifer is missing is also treated separately and represent subareas where the hydraulic properties allow the surrounding units to communicate. Therefore, the hydraulic properties of each of these subareas were estimated with separate model parameters during model calibration (table 13). The estimated values of K_f range from $3.9\text{x}10^{-03}$ ft/d for the alluvial aquifer layer to $2.9\text{x}10^{-03}$ ft/d for the Morales Formation; K_c range from 20.3 ft/d for the alluvial aquifers to 0.8 ft/d for the sediments of the Morales Formation layer. For each unit, the distributions of horizontal and vertical *K*'s vary with the distribution of sediment texture within each zone of each layer (figs. 4, 24). During calibration, a multiplier was used for each zone, and the final range in vertical and horizontal hydraulic conductivities was calculated based on this formulation (fig. 24; tables 12, 13, 14).

Unlike previous analysis of the valley in which the hydraulic conductivity was not differentiated for the various aquifers, the recent and Older Alluvium were delineated as separate units with separate estimates and zonation of the coarse- and fine-grained end-member values of the hydraulic conductivity. Hydraulic conductivities generally decrease with depth and with increasing distances from the original source of the sediments (eroded and (or) transported from the adjacent mountain ranges and river channels), which is consistent with the fining down and fining toward the center sequences observed in the aquifer sediments and textural model (Sweetkind and others, 2013). In several subregions, however, smaller values of hydraulic conductivity have been estimated at depth because of fine-grained textures and secondary alteration such as cementation (Everett and other, 2013; Sweetkind and others, 2013). Coarser grained sediments were simulated near stream channels in the alluvium in the outcrop parts of all three layers. The hydraulic property zones used in CUVHM also were aligned with the textural zones and with the internal fault boundaries.

Storage Properties

The hydraulic properties used to simulate the changes in storage of water within the saturated parts of the aquifer system consist of three components (Hanson, 1988):

1. Specific yield.
2. Elastic specific storage.
3. Inelastic specific storage.

The first two components, specific yield and the elastic specific storage, represent and govern the reversible uptake and release of water to and from storage. Specific yield is unconfined storage and represents gravity-driven draining or filling (resaturation) of sediments with changes of the water table. The elastic storage coefficient represents the component of confined storage because of the compressibility of water and the reversible compressibility of the matrix or the skeletal framework of the aquifer system (Jacob, 1940; Hanson, 1988). The inelastic storage coefficient governs the irreversible release of water from the inelastic compaction of the fine-grained deposits or permanent reduction of pore space, which can also lead to land subsidence. Changes in inelastic storage in fine-grained beds is beginning to occur. Because this is potentially a significant source of water, as a result of the relatively large water-level declines in the Main-zone subregions in the Cuyama Valley, the estimation of water derived from inelastic compaction was included as a feature in this hydrologic model. Given the fine-grained nature of parts of the three aquifers in the Cuyama Valley, the elastic components of storage for the coarse and fine-grained sediments were simulated separately with the Subsidence Package (SUB) in MF-OWHM. Thus, separate values of elastic storage for coarse and fine-grained sediments were used to simulate elastic specific storage for the aquifers and fine-grained interbeds that were applied to all layers. Specific yield typically is orders of magnitude larger than specific storage and is volumetrically the dominant storage parameter for the outcrop regions of all three aquifers.

The Layer Property Flow Package (LPF) and SUB were collectively used to define storage properties in each of the aquifers represented in the model. The LPF and multiplier (MULT) Packages were used to calculate and specify the aquifer-storage components, which included the compressibility of water for all model layers and the specific yield for the portions of the uppermost active layers (layers 1, 2, 3; fig. 3*A*). The SUB Package was used to specify the specific storage related to the skeletal elastic compressibility of the coarse and fine-grained portions of the aquifers and the inelastic compressibility of the fine-grained portions of the aquifers. The resulting equation for the composite storage is represented (Hanson and others, 2014) as follows:

$$S^* = S + S' + S_y \tag{4}$$

where

- S* is the total storage of the aquifer layer,
- S is the elastic storage of the coarse-grained component,
- S’ is the elastic and inelastic storage of the fine-grained component, and
- S_y is the specific yield from the water table drainage for the unconfined portions of an aquifer.

Both S and S’ can be further represented by its respective components:

$$S = b * S_s = \rho g(\alpha + n\beta) * b \tag{5}$$

where

- ρg is the weight of water,
- α is the compressibility of the coarse- or fine-grained matrix material,
- n is the total porosity of the coarse- or fine-grained material,
- b is the fractional thickness of the total model-layer thickness of the coarse- or fine-grained material, and
- β is the compressibility of water.

The aquifer-system specific storage for each model layer on a cell-by-cell basis can be further subdivided into its components for coarse- and fine-grained material, resulting in a complete equation of storage based on textural fractions of total porosity and the matrix compressibility:

$$S_s = S_{sFc} + S_{sFf} = \rho g\left[(\alpha_{Fc} + n_{Fc}\beta) * Fc_I + (\alpha_{Ff} + n_{Ff}\beta) * Ff_I\right] \tag{6}$$

where

total porosity, ${}_{nT} = {}_{nFc} + {}_{nFf}$,
is the sum of the coarse and fine-grained fractions of porosity, with ${}_{nFc} = {}_{nFc} \times F_{c\,I}$ and ${}_{nFf} = {}_{nFf} \times F_{f\,I}$

- α_{Fc} and α_{Ff} are the compressibility of the coarse or fine-grained matrix material, respectively;
- $F_{c\,I}$ is the fraction of coarse-grained sediment in cell (I,J); and
- $F_{f\,I}$ is the fraction of fine-grained sediment in the i^{th} model cell ($1 - F_{c\,I}$).

Although all model layers are simulated as convertible from confined to unconfined, portions of uppermost active model layer represent unconfined conditions, and are therefore assigned a specific yield. Specific yield, which is a function of sediment porosity and moisture-retention characteristics, cannot exceed sediment porosity. The zones used to specify the subareas of the storage properties are similar to the layers used for the other hydraulic properties (tables 13, 14; fig. 24) except for the unconfined subareas of the uppermost layers.

The compressibility of water as well as the compressibility of the aquifer skeleton is dependent on the specified porosities for the coarse- and fine-grained fractions of each hydrostratigraphic unit (model layer). The estimated total porosities from selected core samples from alluvial sediments in nearby Santa Clara Valley ranged from 23 to 43 percent, and the effective porosity ranged from 22 to 40 percent on the basis of laboratory tests of selected cores (Newhouse and others, 2004). For this model, porosity values range from 20 percent for the coarse-grained sediments of the Recent Alluvium to 29 percent for fine-grained sediments within the Morales Formation aquifer sediments (table 14). The products of these average porosity and the respective cell-by-cell average coarse- and fine-grained fractional aggregate thicknesses are summed and multiplied by the compressibility of water (1.4×10^{-6} ft^{-1}) to yield one part of the composite aquifer specific storage value for each active cell of every layer.

Specific yield was specified for all active cells of each layer where those model cells represent the uppermost model cell and unconfined conditions. Specific yield was calculated by using a linear relationship between the fraction of coarse grained deposits, between 0 and 1, and an upper maximum estimated specific yield value ranging from 0.14 for the alluvial to 0.25 for the Morales Formation (table 14). During calibration, a multiplier was used for each zone and to determine the final range in specific yield (fig. 24; tables 12, 13, 14).

Hydrogeologic Structures

The subregions of the Main zone are bounded by faults. The faults along the edges of these zones delineate the no-flow boundaries of the active flow region. The Morales, Graveyard, Turkey Track, Santa Barbara Canyon, and Rehoboth Faults subdivide and compartmentalize the Main-zone subregions from the bounding subregions of the Sierra Madre Foothills and Ventucopa zones (Sweetkind and others, 2013; fig. 2*A*). These interior faults separate the Cuyama Valley into a set of subregions that respond differently to climate and water-resource development. The Horizontal Flow Barrier Package (Hsieh and Freckelton, 1993) was used to simulate resistance to flow across these structures. The effectiveness of these faults as partial flow barriers was then estimated by a parameter representing the conductance of the vertical model cell faces aligned with the fault trace (table 14). All faults were essentially barriers to groundwater flow, although some leakage occurs across the Rehoboth Fault (fig. 3*A*).

Initial Conditions

For transient models, initial conditions define the system state at the beginning of the simulation. There is a long history of groundwater development and irrigation in the study area. Despite the fact that the system has been under stress since the 1940s, historical water levels and other data sufficient for estimating stresses are not available until about the 1960s (figs. 25, 26). The combined effects of groundwater pumping for irrigation and water supply have greatly depressed the groundwater levels in the Main zone. The pumpage has also increased the vertical head differences in some parts of the Main zone; however, the vertical head difference remains small in other regions, such as Ventucopa. In addition, head differences vary seasonally, ranging from about 40 ft in a downward gradient direction during the pumping season to about 8 ft of upward gradient during the nonpumping winter months at the multiple-well monitoring site (CVKR) in the Main-zone subregions. There are almost no head differences less than 5 ft away from the main regions of pumping (CVFR; fig. 26*A;* Everett and others, 2011, 2013). While the effects of climate variability may preclude the occurrence of true steady-state conditions for this hydrologic system, prior to development that started in the 1940s the basin was virtually full and in a quasi-steady-state condition, responding to changes driven by the natural cycles of climate variability. Initially, groundwater levels may have been shallow in many parts of the basin, as evidenced by the presence of cottonwood riparian areas along some reaches of the Cuyama River and the discharge of springs along the Graveyard and Turkey Track Faults that separate the Main zone ssubregions near the Cuyama River (fig. 2*A*). As a result of these subsurface conditions combined with the exceptionally wet climatic conditions for the initial years (1939–45), which reflect regional climate variability in the years prior to the simulation, the initial conditions used in the model do not represent steady-state conditions but rather estimates of hydrologic conditions in 1949. These initial conditions were derived from a combination of land-surface data and model-derived initial water levels. The groundwater flow simulation starts in October 1949, for which there are no data to map the undifferentiated groundwater levels throughout the regional aquifer system. Thus, initial heads were further refined by periodically using the simulated heads from the end of the first year (October 1950) of simulation as initial heads during calibration. This substitution was made in concert with scaling parameters of the overall elevation of initial water levels that helped refine the initial heads for all three model layers during parameter estimation.

The range in water levels over which elastic and inelastic compaction occur is controlled by the previous maximum stresses imposed on the aquifer system from the history of geologic loading and water-level declines (Terzaghi and Peck, 1948; Riley, 1969), as well as secondary effects such as cementation. The previous maximum stress can be expressed as a critical head—the previous minimum head—so that head changes in the stress range above the critical head (elastic stress range) that result in elastic deformation (reversible compaction and expansion) of the aquifer system, and head declines in the stress range below the critical head (inelastic stress range) result in inelastic compaction (largely irreversible) of the system. A head decline below the previous critical head establishes a new critical head so that any subsequent head increase results in elastic expansion of the aquifer system. The specification of the critical heads that control the transition from elastic to inelastic compaction within the fine-grained deposits of the aquifers is initially unknown for each aquifer. This threshold in pressure can typically vary from 50 to more than 200 feet below predevelopment water levels for alluvial basins and usually represents sediments that are overconsolidated because of geologic and hydrologic stresses and secondary lithification (Holzer, 1981; Hanson and others, 1990, 2003; Hanson and Benedict, 1993). Because these are initially unknown, the critical heads were specified as a constant depth below land surface and were modified during model calibration with respect to recent land subsidence observations.

When the simulation is started, the simulated heads and flows change in response to the initially specified and ongoing inflows and outflows. Because the irrigation and pumping stresses on the system change rapidly, the inconsistencies between the initially specified conditions and the simulated initial processes and properties generally are not problematic because the next stress regime soon dominates the solution (Hill and Tiedeman, 2007). As a result, comparing observed and simulated values becomes meaningful after a relatively short simulation time. This study and previous studies (Belitz and Phillips, 1995; Faunt and others, 2009a) show that the time frame for the stabilization is typically less than several months to years of the simulation.

Model Calibration and Sensitivity

The CUHM was calibrated through a combination of trial-and-error and an automated process of minimizing differences between “real-world” observations and model output. The hydrologic framework and definitions of water balance zones were modified as part of this process. Simulation with the CUVHM requires specification of several hundred parameters that vary spatially and temporally, making it a challenge to develop an optimized set of calibrated parameter values. As a result, a parameterization procedure was employed to allow a limited number of parameter values to control the temporal and spatial variability of a much larger number of model inputs. The parameterization procedure followed that of Hill and Tiedeman (2007) in defining the term “parameters” to mean model inputs of hydraulic and hydrologic properties but also included landscape and crop-related properties from FMP and fractions of BCM-simulated surface inflow from runoff and recharge of surrounding watersheds. As mentioned earlier, all inflow to the model domain is combined in the SFR2 inflows. Calibration consisted of a systematic application of the parameter estimation method to limit the range of possible solutions. Even though some parameters demonstrated significant correlations, those parameters selected for model calibration were assumed to be independent. Parameter estimation software packages (UCODE, Poeter and others, 2005; PEST, Doherty, 2010a, b, c; Doherty and Hunt, 2010) were used directly for all sensitivity analyses and parameter estimation. Initially, UCODE was used to estimate parameters. In order to use some of the extended capabilities in PEST, a combination of PEST and manual adjustments were used to conduct the final parameter estimation and sensitivity analyses.

Calibration of transient-state conditions was dependent on the components of the use and movement of water across the landscape and their interplay with the streamflow network and groundwater flow system. Calibration started with adjustments of all parameters from the landscape, such as fractions of transpiration, irrigation efficiencies, stress factors for K_cs, and fractions of runoff, as well as aquifer properties, including fault conductances across fault planes or zones. Then, adjustments were made to other factors related to movement of water on the land surface, such as the hydraulic conductivity of the streambeds in the upstream portions of the streamflow network, and the recharge areas of the groundwater flow system. The calibration of the groundwater flow simulations involved adjustment of parameters that control the inflows and outflows to the groundwater flow system. The dominant sources of inflow to the groundwater system are streamflow infiltration and recharge from landscape processes. Therefore, parameters controlling inflow included vertical hydraulic conductivity of the streambed and runoff parameters. Parameters controlling outflow include pumpage and evapotranspiration. Some of the water-budget components are specified values of inflows and outflows that were not adjusted during calibration; these include the runoff component from the BCM model of stream inflows, urban and domestic pumpage, monthly precipitation and reference evapotranspiration, and water-balance area and crop properties (table 14). The remaining water-budget components that are calculated by the model include streamflow gains/losses, outflow through the stream network, actual evaporation and transpiration, groundwater pumpage from agricultural uses, runoff from irrigation and from precipitation, farm-net recharge, wellbore flow through MNW wells, and changes in groundwater storage. The implementation of the multi-node well package maintained the net pumpage but redistributed groundwater flow vertically and related vertical head differences between model layers, by intra-wellbore flow. This wellbore flow occurs not only during periods of pumpage and for undestroyed and unused wells but also in wells that are only used periodically for water supply or during the irrigation season. A total of 200 parameters were initially created to facilitate model calibration, but this number was reduced to 65 parameters after initial global sensitivity and calibration analysis (table 14).

Observations Used In Model Calibration

The ability of the transient hydrologic flow model to simulate the hydrologic system was evaluated on the basis of comparisons with select hydrologic observations, hydrologic time series, and groundwater-level maps. These comparisons were used to assess the capacity of the model to predict the effects of changing inflows and outflows on the hydrologic system, based on reasonable estimates of hydraulic, river, and landscape properties used to estimate pumpage, recharge, and changes in groundwater storage. Model calibration was based primarily on comparisons of spatially and temporally distributed groundwater and subsidence components. Simulated changes in water levels and water-level differences were compared to those measured in long-term, long-screened supply wells used as part of the new valley-wide monitoring network and from recent depth-specific multiple-well monitoring sites (Everett and others, 2013). Recent land subsidence observations from GPS and InSAR satellite images (Everett and others, 2013) were also used for calibration. Some limited estimates of hydraulic properties from aquifer tests and slug tests were also used (Everett and others, 2013) to help constrain parameters adjusted during calibration. Calibration adjustments were based on the combined fit of simulated values to these observations (figs. 26 and 27). The simulated values were compared to all observed values and provided a measure of model performance through various historical time intervals and subregions of the valley. The resulting error distributions constrain the model parameters, and the comparison between simulated and observed values provided a basis for sensitivity analysis of selected parameters. In addition, groundwater-level maps were used for qualitative comparisons. However, these maps were considered less reliable than time-series data because the composite water-level measurements and manually drawn contour lines represent averaged conditions. In many areas there are vertical-head differences within some parts of the aquifer systems. These differences are not well represented by composite water-level measurements and the manual contour lines. An overall estimate of model fit was made using all available groundwater level data.

Although the CUVHM was calibrated to available observations, model uncertainty exists because of the large number of variables that were adjusted as part of the calibration procedure. In addition, limitations are inherent in the necessary simplifications and assumptions needed to represent a complex hydrologic system with a numerical model. These uncertainties and model limitations are discussed later in this report in the section “Model Uncertainty, Limitations, and Potential Improvements.”

Groundwater Observations

The largest set of observed values used for calibration consisted of the groundwater levels and changes in groundwater levels over time. SBDPWWA maintains a database of key wells in the Cuyama Valley that are regularly measured as part of their monitoring network for their annual summary of the valley. These data were combined to form a database of available water levels throughout the Cuyama Valley from 1949 to 2010. About 4,465 water-level measurements (herein referred to as observations) from 258 single and multiple-aquifer wells and the recently installed multi-well monitoring sites were used for model calibration (fig. 25). Despite the number of wells, the lack of wells in southern and southeastern part of the basin means that the model calibration has greater uncertainty in these areas. The well data included 258 initial head observations and 4,207 drawdown observations. Hydrographs for 36 observation wells were developed and used to represent the Main-zone, Ventucopa Upland, and Sierra Madre Foothills subregions of the Cuyama Valley (fig. 26).

In order to represent the overall trends in heads throughout the region and to minimize the potential effects of initial conditions, a set of observations were made for each well based on the overall change in head relative to the first observation for the time span of measurements from each well. In addition to changes in water levels, 45 water-level differences were estimated between 17 pairs of observation wells completed in vertically adjacent aquifers (fig. 25). These observations were used to help with the calibration of vertical hydraulic conductivity and distribution of pumpage during parameter estimation.

Hydrographs that show both simulated and measured heads for select wells help to illustrate the match of water levels throughout the upper and lower parts of the system (fig. 26). The minimum period over which model simulations can accurately reproduce fluctuations in the groundwater flow system (the response time of the model) varies with the depth to water, hydrologic setting, hydraulic properties, climate, and land use. The amplitude of monthly fluctuations in simulated heads are generally less than fluctuations in measured heads, are smallest at the water table, and increase with depth below the land surface, because of the varying pumping rates during monthly stress periods, applications of irrigation water, transition between unconfined and confined conditions, and depth of unsaturated zone.

The overall model fit for water-level comparisons is generally good when the simulated head values are compared with the measured water levels over the combined 1,200 ft range of measured levels. About 37 percent of the residuals were between −20 and +20 ft, and 49 percent were between −30 and +30 ft. (fig. 27*A*). Simulated water levels generally match measured water levels, as indicated by an average residual of 15.6 ft and a sum of squared weighted residual (SOSWR) of 1.02 ft; the residuals ranged from –198 to 371 ft and the standard deviation was 52 ft. The residuals calculated from results of the CUVHM simulations are generally within 30 ft of the measured values, which represents about 2.5 percent of the total elevation range of the aquifers. The simulated water levels tend to underestimate water levels (positive residuals), which is considered a conservative bias. The total change in measured water levels in wells ranged from –345 ft (rise) to 142 ft (decline) and the total simulated change in water levels at these well locations range from –475 to 136 feet. The larger range in observed changes may reflect some values that are instantaneous water-levels affected by nearby pumping. The crossplot of simulated versus measured water levels (herein referred to as correlation diagrams) also indicate a generally good fit across the wide range of altitudes in the valley (fig. 27*B*). Most of the outliers are a result of underestimation of measured water-level changes in the southern Ventucopa subregion, where large interannual fluctuations in wells near the Cuyama River are related to climate cycles. Overall, the time series of simulated and measured water levels across the valley indicates the model is fairly accurate in the Main-zone and Ventucopa subregions, but does not replicate the elevated water levels of wells in parts of the Sierra Madre Foothill subregions (fig. 26*C*). The water levels fit better in recent times (the last 10 years of the simulation, 2000–10), when the land use and related crop information is better defined.

The hydrographs for the Main-zone subregions generally indicate a reasonable fit of rates of water-level decline, and in some regions show similar water-levels altitudes. For example, in the northern Main zone, water levels match for the early years but are underestimated for some wells in the more recent decades, which could reflect incomplete land-use data for the 1980s through 2010. Similarly, for the Western Main-zone subregion, the rates of decline are similar to those in historical records but some of the temporal changes are missing, which also could be a function of incomplete land-use data. In the Southern Main-zone subregion, the simulated rates of decline show variable matches with observed rates and may overestimate some declines for select subregions, which also could be a result of incomplete land-use data. The hydrographs in the Ventucopa subregions are similar to those constructed from historical records but do not capture the interannual fluctuations for some of the wells near the Cuyama River. This could be a function of the delay in runoff from surrounding watersheds as has been observed in similar settings, such as the Santa Clara–Calleguas basin, where there is multi-year recession of wet-year baseflow (Hanson and others, 2003). Although the simulated trend is similar to that of the historical record for most wells, some of the annual fluctuations were not captured by the simulated water levels. This again is probably a function of incomplete land-use data used to drive the demand for irrigation and related groundwater pumpage. The hydrographs in the Sierra Madre Foothills are more variable, matching trends in parts of the northern and central subregions for some wells, and over- or underestimating trends for other wells. The number of water-level observations and the land-use data precluded a better match in this region. Additional refinements of the model combined with more detailed land-use and well data likely will allow for a better match with subsequent updates of the model.

Variations in matches of individual hydrographs indicate that simulation results generally provide a reasonable fit, given the general lack of information on the use and movement of water in the valley. The monthly to interannual fluctuations indicate the influence of climate, streamflow infiltration, and annual changes in land use. The goal of the model calibration was to try to match individual groups of hydrographs, and to minimize the sum of squared weighted residuals (SOSWR) for all simulated heads. As mentioned previously, there are large areas for which no water-level data are available (fig. 25). The use of WBSs that represent multiple farms, estimated pumpage rates, spatially and temporally coarse (multi-year) land-use and crop distributions for the periods prior to the last two decades, and assumptions made in spatially distributing pumpage may limit the ability of the model to accurately simulate water levels for the periods before detailed land-use data became available (about 1999). The spatial distribution of the residuals and water-level matches is discussed in more detail in the "Groundwater Levels Map" section. Much of the error, and the primary source of the average error, could be associated with the lack of spatial and temporal detail in land-use estimates in the valley that ultimately drives ET consumption through irrigation and pumping.

Vertical water-level differences range between –54 ft (upward gradient) and 49 ft (downward gradient; fig. 27*C*). Residuals between observed and simulated vertical water-level differences generally ranged from –14.1 to 1.1 ft and were largest between the upper and lower alluvium in the Main-zone subregions of the model. The water-level differences have a median residual of –0.8 ft, and the model fit is best for the shallower layers, such as in the 10N26W region of the Southern Main-zone subregion (fig. 26). About 58 percent of the simulated vertical head differences are within 5 ft of the measured head differences. Overall, the simulated and observed vertical water-level differences are similar in magnitude and sign and for many sites improve in later (more recent) years with improved information on land use that drives agricultural consumption and related pumpage. Despite the matches, there are areas in which agreement between observed and simulated values could be improved. For example, measured vertical head differences range about 100 ft, whereas simulated differences range only 15 ft, indicating that the simulated vertical hydraulic conductivity may be too large in some areas.

Water-Level Maps

The spatial comparison of the CUVHM-simulated data to observed data allow compilation of water-level maps for the Cuyama Valley aquifer system for September 1966 (fig. 28*A*), and Spring and Fall of 2010 (figs. 28*B*, *C*). The simulated groundwater levels (fig. 28) are in general agreement with the water-level maps for these periods. The thematic pixels from the simulated water levels are a thickness weighted average of composite water levels. The thickness weighted average was used because this is consistent with the observation process in MF-OWHM and is more consistent with the composite water levels derived from wells that were used to create the hand-contoured water level maps and the composite simulated water levels derived from the HOB Package (Hill and others, 2000; Harbaugh, 2005). The water-level maps were useful during the model calibration by providing additional information on the effects of internal flow boundaries along faults and the adjustments to select model hydraulic properties such as vertical hydraulic conductivities.

The sequence of simulated and measured water-level maps both indicate regions in the center of Cuyama Valley where water levels continue to decline and that the declines are concentrated in the Main-zone subregions (fig. 28). Changes in measured and simulated groundwater levels from spring to fall in 2010 range between –3 (rise) and 90 ft (fig. 28*B*, *C*). By the fall of 2010, water levels below 1,900 ft persisted in the Main-zone subregions, a pattern replicated by output of the CUVHM (fig. 28*C*). However, simulated water levels underestimate the hand-drawn contours in northeastern parts of the model (northeast of Ventucopa) where additional refinement of aquifer properties, land use, or recharge may be required (fig. 28).

Land-Subsidence Observations

Measurements of land subsidence were made at two continuous GPS sites and five reference point InSAR sites (fig. 29*A*). A total of 308 monthly observations were derived from the GPS and InSAR data. These observations show from little to no subsidence to a maximum of about 0.2 feet between 2000 and 2010 when measurements were available. The CUVHM model matches the relative deformation in the Main zone and Ventucopa Upland subregions based on both observed data types. Overall, the CUVHM underestimates the relative vertical displacements but the rates are comparable in the Southern Main-zone subregion at the Cuyama High School Plate Boundary Observation (PBO) site (fig. 29*A*). The simulated subsidence is generally restricted to the fault-bounded regions of the Main-zone subregions for the period 1950–2010 with 0.1–1.6 ft of simulated subsidence in this region (fig. 29*B*). Although these magnitudes and rates are currently relatively small compared to the 30 feet of subsidence at rates approaching 1 foot per year at times in the Central Valley (Faunt and others, 2009a), if water-levels in the Cuyama Valley continue to decline there will be more subsidence. Despite the small magnitude, much of this subsidence is inelastic, resulting in a small permanent loss of storage in the aquifer system. The simulated subsidence indicates the initiation of inelastic subsidence in the late 1970s. Because the amounts of subsidence were so small and the number of observations is sparse, no estimation of residual errors was calculated on this limited set of data.

Pumpage Observations

Observations of agricultural pumpage included previous estimates based on land-use and power records reported for the period 1947–66 by Singer and Swarzenski (table 1, 1970). These annual pumpage estimates were used to guide the final adjustments of landscape properties and irrigation efficiencies but were not used in the formal parameter estimation. The CUVHM model matches the annual agricultural pumpage within 14 percent of the reported values for any particular year and underestimates average annual agricultural pumpages by 1.6 percent for the early dry years (1949–58) and by 2.0 percent for early wet years (such as 1959, 1964, and 1969). Reported pumpage for the early years can vary by as much as 20 percent and is aligned with climate variability to some degree, but indicates persistent pumpage even during the wet years. Overall, the agricultural pumpage increases with changes in land use in more recent years and shows considerable variability that is aligned with changes in climate conditions, with simulated pumpage from 1967 to 2010 ranging from about 42,000 to 88,000 acre-ft/yr (fig. 30). For example, simulated pumpage increases rapidly in 1977, which is coincident with increased agricultural land use, such as alfalfa production, with pumpage for irrigation estimated to have increased to about 76,000 acre-ft/yr. (fig. 7*A*).

Model Parameters

Although many parameters were originally defined in the model (tables 14 and 15), only about 69 parameters were determined to be relatively sensitive and were subsequently considered and included in the automated calibration process. These parameters included landscape and crop-related properties, hydraulic parameters of the aquifers and multi-node wells, fault conductances (table 14), streamflow vertical conductivities, and fractions of BCM-simulated combined runoff and recharge inflowing along the Cuyama River and Santa Barbara Creek into the SFR2 Package (table 15). Hydraulic properties were initially assigned values based on published values and earlier modeling studies, then adjusted during model calibration. Model parameters were adjusted within ranges of reasonable values to best-fit historical hydrologic conditions measured in the aquifer, the stream network, and the landscape.

Calibration started with the landscape processes, followed by adjustment of hydraulic properties, streambed properties, multi-aquifer well properties, general-head boundary conductances, and fault conductances. Because many of these properties are head dependent or were correlated through their exchange of water, these properties were adjusted recursively through automated and trial-and-error analysis. The calibration process also required modifications to the parameter framework. For example, calibration also required additional partitions of hydraulic-property-zone parameters and observations for the alluvium. By using the sensitivities calculated as a function of the observations, only those parameters that were determined to be sensitive were adjusted during automated calibration.

Farm Process Parameters

Farm Process parameters that were adjusted during calibration included selected crop properties. Some parameters were fixed, some were adjusted manually, and some were adjusted using PEST. Tables 13–15 indicate which parameters were estimated at some point during the calibration. These included scale factors for seasonal K_cs, percent runoff from inefficient losses from precipitation and irrigation for select crops and natural vegetation, and seasonal scale factors for irrigation efficiencies. The scale factors for seasonal K_cs are used to represent the stress factors (Allen and others, 1998) that amplify or reduce the K_cs, which were estimated under unstressed conditions. Because published K_cs are estimated under unstressed conditions (K_c less than or equal to 1), the K_cs used in this study required reductions for wet winters, summers, and falls of 19–44 percent for the early years and increases of 2–15 percent for later years. Stress factors for K_cs for wet springs were reduced for early and late years by 20 and 13 percent, respectively. Similarly, stress factors for dry-year seasons were increased by 65 percent for dry, late-year summers and 20–24 percent for early- and late-year dry winters (table 14) to align estimated agricultural pumpage with water-level declines. Part of this adjustment could be related to antecedent soil moisture not being accounted for by the FMP, but this would represent a relatively small amount of water. The scale factors for K_cs were adjusted to reach somewhat subjective matches to observations of ET and agricultural pumpage estimates for 1950 and 1966 (Singer and Swarzenski, 1970). Irrigation efficiencies for the early decades were adjusted for dry-year seasons, with spring values increased by 10 percent, fall values reduced by 7 percent, and summer values reduced by 2 percent during calibration. For the greater efficiencies of the recent decades, irrigation efficiencies for all seasons were increased by 10 percent except for dry springs. Irrigation efficiencies for early-year wet-year seasons were increased by 8–11 percent. Irrigation efficiencies for later years were increased relative to the initial estimates by 10–20 percent for winters, springs, and summers (table 14) and reduced relative to initial estimates by 20 percent for wet-year springs. This could indicate that irrigation is less efficient during wetter periods or could include pre-wetting of soils for vegetable crops. Runoff from selected crops and native vegetation is a direct control on the water available for deep percolation or for overland runoff to the streamflow network. The fractions of inefficient losses to runoff were initially adjusted for truck and vegetable crops, orchards, field, pasture, and grain-and-hay crops, but were finally held constant at 97 percent excess water to runoff after ET consumption of irrigation and precipitation for final calibration. Similarly, fractions of runoff from precipitation were increased to about 92 percent to control the deep percolation and additional runoff from the native vegetation, which is the largest component of the land use in Cuyama Valley. The multiple caliche layers that are common in many parts of the Main-zone subregions of the valley may also enhance runoff and further impede deep percolation from precipitation and irrigation.

Hydraulic Parameters

The model was used to determine the values of 15 hydraulic properties within each model layer during calibration. The values of K_c and K_f for each model layer were adjusted to produce simulated heads representing the long-term trends in the aquifer and to produce heads that best matched the measured heads and estimated streamflow losses. Because of the differences in depositional environments within the various zones of each layer, the hydraulic properties were also adjusted subregionally by using 72 related parameter scale factors for the parameter subregions that are multipliers for horizontal and vertical hydraulic conductivity and storage properties (fig. 24*B*–*D*). The hydraulic properties that were adjusted included coarse- and fine-grained values for hydraulic conductivity, porosities, specific yields, and skeletal specific storage for coarse- and fine-grained end-members, and the exponent of the vertical hydraulic conductivity (eqn. 4). Specifying a single exponent value of p of –0.9 for the vertical hydraulic conductivity was replaced with individual values for each model layer of –0.9, –0.5, and –0.7 for model layers 1–3, respectively. This resulted in values of K_c (coarse-grained) and K_f (fine-grained) which are relatively close to the harmonic mean of vertical hydraulic conductivity (eqns. 2 and 4) for the Recent Alluvium and Morales Formation aquifer layers and closer to the geometric mean for the Older Alluvium model layer. The compressibility of water was specified as a component of the storage properties proportional to the coarse- and fine-grained porosities and was held constant.

The calibration of hydraulic properties required the adjustment and rescaling of these intrinsic properties based on water-level hydrographs (fig. 26). The most sensitive parameters were vertical hydraulic conductivities (represented by the hydraulic conductivity of the fine-grained fraction) that, in part, controlled the seasonal amplitudes and vertical water-level differences between aquifer layers. Scaled reductions in vertical hydraulic conductivity and storage properties were required for select confined zones and scaled increases in these properties were required for unconfined zones. Horizontal hydraulic conductivities (represented by the hydraulic conductivity of the coarse-grained fraction) were increased during model calibration in many of the aquifer layers (table 13). Because the model was relatively less sensitive to values of porosity and specific yield, these were not included in automated parameter estimation.

Streamflow Properties

The model also required calibration of the streambed vertical hydraulic conductivity parameters. Groups of stream segments where stream channels are similar were represented by 30 parameters of streambed vertical hydraulic conductivity (figs. 8; table 15). The groupings and calibrated vertical hydraulic conductivity values range from 0.2 ft/d in tributaries crossing the alluvium of the western Main-zone subregion to as much as 49 ft/d in the Cuyama River and select tributaries crossing the Recent Alluvium of the southern Ventucopa Uplands (table 15). Because there are no downstream gages, no downstream streamflows or differences between gages as gains and losses on rivers or tributaries were available for calibration of streambed conductivities. The final distribution of streambed vertical hydraulic conductivities for each of the 577 segments is summarized in figure 8 and table 15.

Multi-Aquifer Well Parameters

The skin factors in the MNW Package define the friction losses to water flowing from the aquifer into the well due to the screen and to formation damage. They affect the interlayer flow and related water-level difference between model layers. Three skin factors were used as parameters to control the retardation of wellbore flow within each layer for the multi-aquifer wells (table 14). Skin factors were relatively high to maintain the observed vertical head differences and to control wellbore flow between layers. The final calibrated skin factors ranged between 395 square feet per day (ft^2/d) for the Recent Alluvium layer and 1,625 ft^2/d for the Morales Formation (table 14).

General-Head Boundary Parameters

The conductance factors in the GHB Package for the groundwater underflow were constant model values. These conductances controlled the small inflows beneath Reyes Creek and the Cuyama River and outflows beneath the Cuyama River at its western groundwater outflow from the valley. The final conductances that controlled lateral outflow were set relatively large in comparison to typical hydraulic conductances to promote underflow from the western boundaries, ranging from 5.4×10^6 to 8.6×10^6 ft^2/d. The conductances for the inflows were held small, ranging from 1.1 to 0.1 ft^2/d for the alluvium and Morales Formation layers, respectively (table 14). This small conductance restricts flow from the adjacent watersheds through the very narrow alluvial channel in the upper layer. The majority of the inflow from the adjacent watersheds is relatively small and is incorporated into the inflows of the SFR2 Package based on the BCM data.

Horizontal Flow Barrier Parameters

The conductance factors in the HFB Package affected the subsurface flow of water between the groundwater subregions that collectively represent Cuyama Valley. In turn, these flows not only affected water levels but also indirectly affect the propagation of storage depletion and subsurface recharge from underflow. Six parameters were used for the interior faults—Morales, Graveyard, Turkey Track Hill, Rehoboth, and Santa Barbara Faults—as delineated by Sweetkind and others (2013). The Santa Barbara Fault was split into two modeled flow barriers with one representing the fault within the Older Alluvium and Morales Formation and a second representing the flow barrier in the Recent Alluvium. Fault conductances were initially model-estimated parameters but ultimately specified at low values and were held constant for final calibration. These low conductances are consistent with the discontinuities in the water levels mapped by Singer and Swarzenski (1970) and the concept of subregions with limited groundwater flow between them. For example, the Santa Barbara Fault appears to separate the southern Ventucopa Uplands subregion from the Southern Main-zone subregion. The Morales, Graveyard and Turkey Track Hill Faults separate the Southern Main zone from the Western and Northern Main-zone subregions, and the Rehoboth Fault impedes underflow along the Sierra Madre Foothills region in the Older Alluvium and Morales Formation that would potentially replenish the Southern and Western Main-zone subregions. The final calibrated conductances for the faults are summarized in table 14.

Subsidence Parameters

The simulation of land subsidence and related changes in groundwater storage were controlled by nine model parameters that scaled the critical head, elastic skeletal storage, and inelastic skeletal storage for each model layer (table 14). Specified critical heads represent initial conditions in 1949 of overconsolidation and were estimated with PEST during calibration using scaling factors. The majority of the aquifer and interbed confined storage resides in the skeletal elastic storage values used with the SUB Package. These values were estimated using PEST during model calibration with scale factors of initial estimates; the final values were reduced to 42 percent for the Older Alluvium and increased to 34 and 50 percent for the Recent Alluvium and Morales Formation, respectively.

Sensitivity Analysis

The simulated equivalents of the suite of observations in CUVHM were most sensitive to scaling factors for initial heads in layers 1 and 2, secondarily to changes in select climate and landscape properties, and to a lesser extent to selected scaling factors for hydraulic properties for the aquifers, streambed vertical hydraulic conductivities, and horizontal hydraulic conductivities. Systematic parameter-estimation techniques were primarily used to estimate select model parameters and related sensitivities that are based on perturbation approaches with limited guidance from trial-and-error analysis. Although the sensitivity to initial conditions might be partially solved by simulating a longer initialization period, because groundwater levels adjust relatively slowly, it would take many decades with little information on stresses to arrive at a potentially more uncertain set of initial conditions.

The sensitivity process in PEST identifies the sensitivity of computed values at the locations of measurements to changes in model parameters, and was used to identify which parameters to include and to adjust during calibration (Hill and others, 2000; Doherty and Hunt, 2010). Results of the sensitivity analysis indicated that the model was most sensitive to scaling factors for adjusting the initial heads within the Recent and Older Alluvium aquifer layers. Parameter sensitivities for an additional 29 parameters related to hydraulic properties, stress coefficients of K_cs, and scale factors for the runoff from precipitation for native vegetation are shown in declining order of sensitivity on figure 31. The model is next most sensitive to runoff from precipitation over native vegetation, which not only controls a major contribution to recharge through deep percolation but also intermittent ungaged runoff contributions to streamflow and stream channel infiltration. Included within the 20 most sensitive parameters are spring and summer scale factors for K_cs and irrigation efficiencies. The most sensitive streamflow parameters were the vertical hydraulic conductivity related to sections of Cuyama River channel (wvc_qyacc), various creeks in the unconfined Recent Alluvium in the Ventucopa Uplands subregion (vc_qyauc), the Western Main-zone subregion Cuyama River channel (wmz_qyacc), and northern tributary reaches of the Sierra Madre Foothills (wsmfh_qoan) subregion.

Model Uncertainty, Limitations, and Potential Improvements

The CUVHM is a simplification of the real flow system, and, as such, has some inherent limitations. The accuracy of simulation results is related strongly to the quality and resolution (both spatial and temporal) of input data and of measurements of the system (such as precipitation, water levels, streamflow, and pumpage) used to constrain the calibration. The inflows and outflows in the model were a combination of measured values, adjustments to parameters to represent conceptualizations of the system, estimated inflows provided by the BCM model, and values specified through the use of the model code, MF-OWHM. Differences between simulated and actual hydrologic conditions arise from a number of sources and are collectively known as model error.

While the CUVHM was designed with the capability to be accurate everywhere, the conceptual and numerical models were developed on the basis of assumptions and simplifications that may restrict the use of the model to regional and subregional levels of spatial analysis within seasonal to interannual temporal scales. Potential future refinements and enhancements will continue to improve the level of resolution and model accuracy. In general, proper design and calibration of flow models, along with better estimates of inflows and outflows and changing spatial data such as climate and land use, can minimize some of the inherent model limitations. Limitations of the modeling software, assumptions made during model development, and results of model calibration and sensitivity analysis all are factors that may constrain the appropriate use of this model and can be used to identify where potential future improvements in the simulation of specific processes are needed or where new data are needed to constrain simulations.

Model discretization in space and time can be a potential source of error and uncertainty. Models represent a hydrologic system as a series of discrete spatial units, through which intrinsic properties and flows are assumed to be uniform. The use of a discretized model to represent a hydrologic system introduces limitations for features that occur at scales smaller than the discretization. Transient models are further discretized into a series of discrete units of time, during which specified hydrologic inflows and outflows are held constant. The use of monthly stress periods and two time steps per month in the CUVHM assumes that the variations of inflows and outflows and changes in water levels are piecewise linear changes. Changes at smaller time scales are not simulated, and are not discernable in the model results, which may contribute to some additional temporal uncertainty. For example, the distribution of daily precipitation and soil moisture within each monthly period used by the BCM and CUVHM can result in large variations in simulated recharge and runoff (for example, precipitation occurring as a large one-day storm rather than as a series of smaller storms), and this cannot be accounted for with the existing model. The temporal scale used in the CUVHM was expressly designed to separate the supply and demand components of water use and movement for agriculture.

Differences between simulated and measured hydrologic features also can arise from the numerical solution that attempts to provide a cell-by-cell mass balance of inflows and outflows. Mass-balance errors are minimized by ensuring the model solution reaches a reasonable state of mass balance within each biweekly period. The twice a month time steps were used to remain consistent with the assumptions of the current version of the FMP process. The cumulative mass balance of the model was within 1 percent of the total flow over the 61 years of simulation.

An additional component of model error arises as a consequence of how well model-input values represent the actual hydrologic system. The accuracy of the calibrated model is contingent on the accuracy of the specified inflows and of the specified observed flows used for model comparison. Model calibration provides a means to use comparisons to indirectly constrain the differences between the real-world and simulated mass flows. Thus, the degree to which a simulated condition provides a reasonable representation of the hydrologic system can be evaluated through comparing simulated hydrologic conditions with those observed in the field, which in turn provides a mass-constrained calibration. The performance and accuracy of CUVHM are constrained primarily by groundwater levels, and to a lesser degree by recent land subsidence and vertical groundwater-level differences. The model is used for developing a conceptual understanding of the flow system by quantifying the regional inflows and outflows and their relative proportions. Because the Cuyama Valley flow system is inherently complex, like all models, simplifying assumptions were made in developing and applying the numerical code, MF-OWHM. The model solves for average conditions within each 15-acre cell for each two-week period, with the parameters interpolated or extrapolated from measurements, and (or) estimated during calibration. Modeling the regional aquifer system without the delayed recharge of unconfined conditions also may affect the timing and magnitude of groundwater recharge and can be a potential source of error and uncertainty. Thus, results from the model should be interpreted at the sub-regional to regional scale and multi-year periods for comparative analysis and generalized estimates of flows.

Several elements of the revised model remain uncertain and will require additional investigation to help further improve the accuracy of the simulation of the groundwater and surface-water flow, the simulation of regional storage changes, and the simulation of the use and movement of water across the landscape. For example, some of the crop, soil, and landscape features that are inputs to the Farm Process and are used to calculate water use remain uncertain. Thus, model features such as pumpage and recharge are sensitive to some of these parameters such as K_cs, irrigation efficiencies, multiple cropping, or monthly land use. In particular, the distribution and change in land-use patterns needs to be improved to annual or even monthly scales to significantly increase accuracy of the simulation. Many of the stresses that are driven by these land uses varied throughout the simulation period at higher frequencies than the multi-year estimates of most of the historical land use. This is evident by the improved simulation since 2000, when land use estimates used in the model were more frequent. These variations also are driven by climatic conditions as well as growing periods. Hence, the changes appear seasonally and by climate-driven events that can be yearly or multi-year in length. Because the land use was based on generalized classification for the early years and select crop categories, some of the agricultural composite crop classes were replaced with the composite crop of identical extent from the 2000 land-use map. For example, where only generalized categories of land use were specified, the composite crops interpreted on the 2000 land-use map were embedded. This assumes the farmer would be growing the same type of crop in a given area over the time frame of the hydrologic simulation when that land-use map was used (figs. 18–22). In some cases, such as orchards, this is generally a good assumption; in other cases, the crops being grown may have changed several times during the years represented by the land-use map. Estimates of ET_o and growing periods are uncertain and should be better delineated, especially in terms of their relation to climate changes. Finally, the natural vegetation represents between about 87 percent (historically) to 65 percent (recently) of the land use and, as such, is an important control for runoff and recharge in the upland regions of Cuyama Valley. Another potential future refinement to the model could include separation of the natural vegetation into several separate land-use subregions in different parts of the valley. This may improve simulated recharge and runoff in these areas. Though some additional uncertainties may be associated with estimating runoff as a fraction of precipitation and irrigation by crop type that does not consider the effect of soil properties on runoff, improving this feature would require prohibitively small time steps and longer simulation run times. Because the desert caliche layers and not the soils probably control much of the runoff and deep percolation, additional mapping of these layers may be needed to improve the simulation of runoff for these biweekly time intervals.

Some inflows and outflows, such as outflow along the Cuyama River, remain relatively uncertain, and the accuracy of the model could benefit from additional observations of streamflow from other major ungaged drainages such as Reyes Creek, especially if more constraints are needed to improve the overall hydrologic budget and estimates of local recharge and runoff. Continued monitoring of the inflows from the Cuyama River and Santa Barbara Creek will also be useful in maintaining an inventory of the major components of runoff from surrounding mountains.

The CUVHM may benefit from refinement of the location of the trace of the Santa Barbara and Rehoboth Faults, which may change the locations and extents of the flow barriers and potentially segregate the subregions of the valley into subbasins. The accuracy of the model could also be improved if the input values of selected hydraulic properties, such as horizontal and vertical hydraulic conductivities and storages, could be adjusted on the basis of additional field estimates. Additional estimates of horizontal hydraulic conductivity to further constrain the model properties could be obtained from aquifer tests at select supply well sites or well specific-capacity tests at single-aquifer supply wells. In addition, uncertainty in the data used to distribute the textural data is both more sparse and larger with increasing depth. The difference between simulated and measured heads generally increases with depth below the land surface. This may reflect decreasing accuracy with depth within the texture distribution used to estimate the hydraulic conductivities. Uncertainty in the values for the hydraulic properties of the Morales Formation may be especially large even though many wells currently produce water from this unit in the Cuyama Valley. Thus, textural-data uncertainty is smaller for the younger and Older Alluvium and larger for parts of the Morales Formation.

Several of the processes within the model could also potentially allow for refined simulation of selected flow features. Improved simulation of multi-aquifer wells to account for partial penetration and better estimates of actual pumping capacities of all wells could increase the accuracy of simulated pumpage. Some WBS required virtual wells, so the additional location of wells or water conveyances that are used to service these properties requires additional investigation. Similarly, the simulation of runoff within the Farm Process could be enhanced to better simulate the intensity of wet-year winter precipitation events that would facilitate better estimates of runoff within the valley. Also, the simulation of unconfined conditions and the lowering of the water table in the Main-zone subregions could be improved by the use of the Unsaturated Zone Package (Niswonger and others, 2006) and related Newton-Raphson Solver (Niswonger and others, 2011). However, this upgrade could result in significant increases in total run time of the historical and future simulations.

In summary, some potential components that could improve the accuracy and reduce uncertainty of the simulation could include but are not limited to the following:

1. Improved temporal estimates of land use from annual to seasonal or monthly.
2. Improved estimation and application of crop and irrigation properties.
3. Improved segregation of natural vegetation into multiple classes in different parts of the valley.
4. Improved estimates of ungaged stream inflows and outflows through additional streamflow gaging (either used directly or to improve the calibration of BCM).
5. Refined location and extents of the trace of the Santa Barbara and Rehoboth Faults.
6. Improved estimates of hydraulic properties through additional field tests.
7. Improved texture estimates at depth and refined zonation of the Morales Formation.
8. Improved simulation of multi-aquifer wells to account for partial penetration and farm well pumping capacities and additional location of potential wells.
9. Improved groundwater, streamflow, land subsidence, and land cover observations for better model evaluation and calibration.

Despite all of these potential limitations, the CUVHM represents a realistic, reasonably accurate, and reliable means for understanding many aspects of the Cuyama Valley groundwater basin that are needed for planning and evaluating alternatives for managing water resources. Additional observed hydrologic and land-use data could also be used to improve the model calibration. When used correctly, CUVHM can help to continue developing understanding as more data and more capabilities are added. Additional observed hydrologic and land-use data could also be used to improve the model calibration

Hydrologic Budget and Flow Analysis

The CUVHM simulation of the conjunctive use and movement of water in Cuyama Valley indicates that, overall, the storage depletion and onset of land subsidence are driven by sustained and increased agriculture and related demand for water, thus resulting in a condition of overdraft. While periodic events of recharge occur from natural climate cycles, the current and historical sustained demand for water exceeds the long-term replenishment rate from these quasi-periodic events. The CUVHM confirms that the overdraft conditions have persisted since the onset of increased development in the 1970s up through 2010. The CUVHM indicates a level of pumpage that is consistent with estimates from the early years of reported pumpage and an increase in water demand with increased agricultural development. The overdraft is predominantly the result of cycles of storage depletion in the Main-zone subregions, which are also climatically driven over seasonal to interdecadal periods.

As with groundwater storage depletion and replenishment, the temporal distribution of inflows and outflows to the landscape and surface-water systems also indicates a strong climatic influence. The total inflows to the landscape range from about 100,000 to more than 250,000 acre-ft/yr (fig. 32*A*), which includes inflows, that are, on average, 53 percent precipitation, 44 percent irrigation from groundwater pumpage, and 3 percent direct uptake of groundwater through ET (fig. 32*B*). Similarly, the average total outflow from the landscape consists of 25 percent runoff, 8 percent deep percolation to groundwater recharge, 36 percent ET from precipitation, 29 percent ET from irrigation, and less than 3 percent ET directly from uptake of groundwater (fig. 32*B*). Thus, about half the inflow of water to the landscape comes from precipitation and half from irrigation, and about a third of the outflows occur as each of ET from irrigation, runoff and recharge, and ET from precipitation and groundwater. ET from groundwater is a minor component of inflow to the landscape, and runoff, predominantly from precipitation, is a major outflow from the landscape. Deep percolation from precipitation and irrigation persists for all years but generally is larger during wet years.

In 50 of the 60 years (fig. 33*A*), the total demand for water on the landscape for agriculture is much greater than the natural inflows in this high desert valley, with irrigation from groundwater supplementing the water needed for agriculture. Groundwater recharge from precipitation and irrigation is about half the groundwater pumpage in the wettest years (for example, in 1998 and 2005) and typically is 10 to 25 percent of groundwater pumpage for most years, resulting in sustained groundwater storage depletion and overdraft. Estimated agricultural pumpage during wetter years is sometimes comparable to that in dry years, which may reflect lower irrigation efficiencies during wet years.

The components of the net annual groundwater budget (fig. 33) are similar to inflows and outflows for the landscape, and vary with climate and changes in land use (fig. 33*A*). The average hydrologic budget overall and for the most recent decade (2000–10) indicates that streamflow infiltration and recharge from precipitation and irrigation are the largest inflows, and pumpage is the largest component of outflow, as summarized for select periods (fig. 33*B;* table 16). The percentages of these groundwater inflow and outflow components are summarized in a pie diagram (fig. 33*C*). Except for the occasional wet years, the major outflow is agricultural pumpage, and most of this outflow is supplied by a decrease in groundwater storage. The net groundwater budget averages about 70,000 acre-ft/yr (in and out of the groundwater system) but can vary widely as shown by the large replenishment of about 53,000 acre-ft that can occur in wet years such as 2005 or additional depletion of about 44,000 acre-ft in dry years such as 2009 (table 16). On average and valley wide, water released from storage contributes 68 percent to the total groundwater outflow, along with a contribution of 25 percent stream leakage and 6 percent farm-net recharge. About 38 percent of the groundwater outflow flows back into aquifer storage, for a net storage depletion of about 30 percent of groundwater flow (fig. 33*C*). The largest component (44 percent) of groundwater outflow is pumpage, (wells, farm wells, and multi-node wells), which is combined with 9 percent outflow to streams, 5 percent farm-net recharge (groundwater recharge minus ET from groundwater), and 4 percent as groundwater underflow (general head boundary) and spring discharges (drains; fig. 33*C*). Though some storage replenishment occurs during wet years, which offsets some of the storage depletion in dry years, the overall temporal distribution of net flows shows an increase in storage depletion (inflow of water from net storage; fig. 33*D*). This is largely focused in the Main-zone subregions, with small amounts of depletion in the Ventucopa Uplands subregions and a small accretion in storage in the Sierra Madre Foothills subregions. The total simulated storage depletion is about 2.1 million acre-ft for the period 1950–2010. The average storage depletion represents about half of the average agricultural pumpage (65,400 acre-ft/yr) per year. The estimates of recharge and underflow are about 30 percent larger than the flows estimated for the earliest years of development (1947–66) by Singer and Swarzenski (1970). About 72 percent of the average storage depletion and 87 percent of the agricultural pumpage occurs in the Main-zone subregion and the remaining average depletion and 11 percent of the agricultural pumpage occurs in the Sierra Madre Foothills region for the historical period. Conversely, about 57 percent of the total average recharge and 64 percent of the average net streamflow infiltration occurs in the Ventucopa Uplands subregion.

The temporal distribution of groundwater pumpage is dominated by agricultural pumpage. Most of the flow of groundwater to wells is from the Recent Alluvium and ranges from 40 to 93 percent (fig. 34). Additional water is derived from the Morales Formation in the early years (1950–77) and from the Older Alluvium in the subsequent years (1978–2010) with shifts in development and related land use in the valley. The relative reductions in pumpage during the intervening wet periods show the sensitivity of the climate built into FMP calculations. For example, agriculture and related irrigation is very sensitive to climate as irrigation is supplemented by precipitation, a portion of which is consumptively used by crops, as demonstrated by the comparison with estimated pumpage for the early years (fig. 30).

More than 70 percent of the recharge occurs within the Recent Alluvium layer during the years of greatest land-use development prior to the 1980s (fig. 35*A*). An additional 20 percent enters the groundwater flow system through the Older Alluvium. The fractions of recharge to the Morales Formation could be an artifact of the model's initial conditions. There is some variation with climate in the relative proportions of recharge from year to year (deep percolation, fig. 32), but the overall percentages remain relatively constant valley wide. This exchange of water between aquifers largely occurs across layer boundaries and in relatively small amounts by intraborehole flow through long-screened supply wells that are open to both formations. As indicated from the depth-specific water level histories of the multiple-well monitoring sites (fig. 26*A*), the vertical head gradients can be downward during the growing season and upward during the non-growing season. Most of the vertical interlayer flow occurs across layer boundaries and is focused in the regions where coarse-grained sediments are more prevalent, such as along the stream channels in the Recent Alluvium. The majority of the vertical flow is to the Older Alluvium or the Morales Formation from the Recent Alluvium, where the majority of the recharge is occurring (fig. 35*B*).

Projection of Potential Water Availability

Three 61-year projections were made to begin the assessment of the sustainability of the water resources in Cuyama Valley. This assessment included a base-case projection of "business-as usual" land use, a reduced-supply projection, and a reduced-demand projection with cessation of agriculture in the Main-zone subregion. Since there is no basin management plan, these three hypothetical scenarios are used to assess potential water availability beyond 2010 using existing land- and water-use conditions from 2010. All three projections use information on historical hydrologic conditions (streamflows and related climate data) and 2010 land use, wells, and land ownership distributions, with 2010 crop and irrigation properties, to simulate 61 years of potential future hydrologic conditions under current supply-and-demand conditions. This assumes that there is no additional growth or reductions in demand for water resources or additional development of land for agriculture, urban, or domestic uses. Though downscaled and bias-corrected climate-model projections could have been used to create future climate conditions (Hanson and others, 2012), historical climate data were used for these initial projections to ensure that climate variability and climate cycles were similar to recent historical conditions. This assures that the historical variability in inflows and demand from ET is maintained from the historical wet and dry periods. The monthly climate data and streamflows for each water year are used starting with the most recent year (2010) and working backward in years (but forward in the months of each year) to 1950 to make a projection for the period 2011–71 so that year 2071 uses conditions from 1950.

The second scenario is called a reduced-supply scenario that represents a potential management scenario through reduction in supply in which a target yield of the basin would be determined and some acreage-based reduction would have to be made to bring demand in line with the long-term average recharge of the valley. The long-term average recharge was determined from data for the historical period 1950–2010 because conditions in this period are fairly similar and aligned with the PDO climate cycles (1947–77 dry period, 1978–99 wet period, and 2000–10 partial dry period) that control runoff and resulting recharge. The long-term (61-year) average recharge rate from this historical period is about 33,000 acre-ft/yr and the recharge for 2010 was estimated at about 35,000 acre-ft/yr. The distribution of this recharge is 57 percent in the Ventucopa Uplands, 36 percent in the Main-zone, and 7 percent in the Sierra Madre Foothill subregions. The fraction of total recharge within each of the three groups of subregions was prorated by percentage of area in 2010 over the various WBS that are designated as agriculture within each group of subregions. In addition, the distribution of the portions of long-term recharge were distributed for each WBS based on the monthly fractions of simulated monthly usage for 27 agricultural WBS that are part of the total 83 WBS in 2010.

The third scenario is called a reduced-demand scenario that represents the alternative to a reduced supply, a reduced demand projection, by retiring all agriculture in the Main zone. The difference is a reduced supply or a reduction in the amount of water that would be supplied from groundwater pumpage, while a reduced demand could represent a reduction in the acreages or types of crops grown that drives irrigation demand. This reduced demand scenario was implemented by simulating the return of all WBS agricultural land back to native vegetation without irrigation within the Main-zone subregions.

A reduction in supply may have a different effect in the three major subregions of Cuyama Valley. For example, in the Ventucopa region, where there is a lesser long-term storage depletion, less storage depletion may occur, which may increase stream baseflows during dry years. In wetter years, streamflow could pass farther west past the Santa Barbara Fault and into the Main-zone subregion and flow farther for more days of the year. In contrast, reduced supply in the Main-zone subregion will result in less artificial recharge from irrigation, which results in a reduced replenishment, as well as reduced demand from deficit irrigation or reduced acres of agriculture that can be sustained with reduced supply.

For the first base-case scenario, the projected supply-and-demand indicates the potential for additional water-level declines of more than 350 ft in the Main-zone subregion, with a sustained agricultural pumpage of about 64,000 acre-ft/yr (fig. 36). The projected change in cumulative storage indicates that an additional 2.5 million acre-ft of water would be removed above and beyond any potential recharge (fig. 37*A*). The projected groundwater levels for the end of the projection period show sustained declines in areas of substantial agricultural demand in the Main zone and Sierra Madre Foothills subregions (figs. 2*A,* 36, 37B). With these sustained declines also comes additional potential land subsidence of almost two feet near Cuyama (fig. 37*C*) that is mainly focused in the areas of sustained agricultural demand in the Main-zone subregions. Conversely, the Ventucopa Uplands subregion appears to retain conditions similar to current conditions and there is only modest storage depletion in the Sierra Madre Foothills subregion. The combination of storage depletion with continued drawdowns in the aquifers within the younger and Older Alluvium combined with additional potential land subsidence is probably not a sustainable scenario in the Main-zone subregions.

The second scenario represents reduced supply with the use of groundwater allotments within FMP to limit the pumpage within each WBS to a proportional fraction of long-term recharge. This scenario still shows some small amount of long-term storage depletion of about 28,000 acre-ft (fig. 37*A*). There is about a 30- to 70-foot recovery of water levels in parts of the Main-zone; levels in other regions such as the Sierra Madre Foothills region show continued declines with additional storage depletion that may be the result of continued pumping from wells that actually serve the Main zone (fig. 37*B*). While there is a general cessation of additional land subsidence and some elastic rebound for this scenario (fig. 37*C*), there is still some potential land subsidence occurring in parts of the Main zone. The overall average rate of storage depletion is greatly reduced with pumpage held close to the average long-term recharge rate (table 16). This scenario indicates that while the storage depletion is largely arrested in the Main zone, there still may not be a sustainable resource after the projection of 61 years because of reduced artificial recharge from irrigation in the Main zone and lack of overall long-term storage recovery. This scenario is comparable to the scenarios that describe the relation between safe yield, sustainability, and the water-budget myth

(Bredeheoft and others, 1982; Bredeheoft, 1997, 2002; Alley and Leake, 2004). The reduced pumpage may not allow the current intensity and extent of agriculture to be sustainable even if irrigation was more efficient, for example, by transition from sprinkler to drip or soaker irrigation, or if mulching, canopy, deficit irrigation, and other practices were used to reduce demand from irrigation (ET).

The third scenario that represents reduced demand with cessation of agriculture in the Main-zone subregions results in widespread recovery of water levels except within the Sierra Madre Foothills subregions. This scenario results in storage accretion averaging about 11,900 acre-ft/yr (fig. 37*A*), that results in about a 170-ft to a more than 200-ft of recovery in groundwater levels in parts of the Main zone but continued declines in parts of the Sierra Madre Foothills (fig. 37*B)* and cessation of potential land subsidence with some minor elastic recovery (relative uplift) (fig. 37*C*). Average recharge is again reduced by reduction in direct infiltration from irrigation supplied by pumpage that is about half the average recharge rate (table 16). This scenario represents a radical change in land use that is probably not realistic, but serves to demonstrate the changes that would need to made and long time frames needed to not only arrest storage depletion but to only partially recover the basin's aquifers. This scenario may also not be feasible with respect to sustainable agriculture in the valley. The three scenarios indicate that other sources of water, combined with managed aquifer recharge, possibly through redistribution of streamflows further into the Main zone, and a comprehensive basin management plan could be needed to augment the current levels of water demand and reduce the disparity between supply and demand. Wet years alone cannot overcome the sustained deficit between supply and demand based on recent climate, land-use conditions and demand for water for irrigation at twice the long-term average recharge rate.

Additional projection scenarios with CUVHM could be simulated with alternative future climate conditions and adaptation of land-use and agricultural practices such as improved irrigation efficiencies to further assess the mitigation of potential overdraft conditions. Alternatively, simulations could be made to assess potential projects such as new land ordinances or reductions in agricultural acreage, groundwater management projects such as managed aquifer recharge that could redistribute streamflow from the Ventucopa Uplands corridor into the Main-zone subregions, climate-change adaptation that would facilitate capturing and replenishing water through managed aquifer recharge, or new policies regarding water use and reuse. These types of scenarios and analysis require a management structure that could develop and evaluate the feasibility of social, political, and engineering solutions and their costs, before a given management strategy and related policies and projects could be evaluated using the CUVHM model. This analysis could help to form the basis for evaluating a potential water-resource management plan by using alternative policies and projects. Though not simulated in this version of CUVHM, as the water table is lowered with a growing unsaturated zone, recharge can be delayed or reduced when the streamflow becomes hydraulically disconnected from the groundwater water table.

Suggestions for Future Work

Future work could include refinement and temporal updates of the Cuyama Valley Hydrologic Model, through additional calibration, with additional model observations, and development of alternative projection scenarios based on a comprehensive basin management plan. An expanded monitoring network would allow a better understanding of changes in groundwater flow, streamflow, and streamflow infiltration, which are the main sources of recharge in the valley. In particular, the additional monitoring of stream inflow, groundwater pumpage, land subsidence, and groundwater levels throughout the valley would help to better quantify the state of the resources as well as provide valuable comparison to model performance. However, monitoring Cuyama River outflows or inflows from other major tributaries and continued monitoring of the inflows on Cuyama River and Santa Barbara Creek are also needed refine the hydrologic budget as well as to maintain and improve the accuracy of the CUVHM. The calibration of the model, based predominantly on groundwater levels, could be supplemented with additional calibration That include observations from remote-sensing estimates of ET and with additional streamflow values to help improve model accuracy. Additional verification of the numbers and conditions of wells used for irrigation and cropping practices would also potentially improve the accuracy of the model. Projections of water availability and sustainability of supply could include the analysis of alternative scenarios of land use, crops, and irrigation practices, as well as additional capture of intermittent runoff from wet years for managed aquifer recharge.

Summary and Conclusions

Cuyama Valley is north of Sierra Madre Mountains in south-central California (fig. 1*A*) and is one of the most productive agricultural regions in Santa Barbara County. However, increases in population and transitions to crops that consume additional water have increased the demand for water within the Cuyama Valley groundwater basin (CUVGB). While a small amount of urban supply is pumped from groundwater, irrigated agriculture is supplied solely by groundwater pumpage. This study provided a refined conceptual model, geohydrologic framework, and an integrated hydrologic model, the Cuyama Valley Hydrologic Model, or CUVHM. The goal of this study was to produce a model capable of being accurate at scales relevant to water-supply analysis needed for the evaluation of water availability and sustainability. The CUVHM is the first hydrologic model of this high desert basin. The Basin Characteristics Model (BCM) and the CUVHM were calibrated to historical conditions of water and land use and were used with the new geohydrologic and conceptual models to assess the use and movement of water throughout the Valley. These tools provide a means to understand the evolution of water use, its availability, and the limits of sustainability.

The conceptual model identified inflows and outflows, which include the movement and use of water from natural and human components. The groundwater flow system is characterized by a layered geologic sedimentary system that results in vertical hydraulic gradients due to the combined effects of the application of irrigation water and natural recharge from streamflow infiltration and direct infiltration at the land surface combined with groundwater pumpage, evapotranspiration (ET), and underflow as outflows. Overall, groundwater supplies most of the agricultural demand in the initial part of the growing season, which is augmented by precipitation during wet winter and spring seasons. In addition, the amount of groundwater used for irrigation varies from year to year in response to climate variation and can increase dramatically in dry years, but the model also indicates that irrigation may have been less efficient during wet years. While agricultural irrigation is not measured, it is the largest demand for water along with transpiration by native vegetation. The integrated hydrologic model, CUVHM, includes new water-balance subregions, delineation of natural, municipal, and agricultural land use, streamflow networks, and groundwater flow systems. The redefinition of the geohydrologic framework (including the internal architecture of the deposits) and incorporation of these units into the simulation of the regional groundwater flow system indicate the importance of faults in compartmentalizing the alluvial deposits into subregions that have responded differently with respect to regional groundwater flow, locations of recharge, and the effects of development. The Cuyama Valley comprises nine subregions that are fault bounded, represent different proportions of the three layers of the valley's aquifer system, and show differences in generally poor-quality water (Everett and others, 2013).

The BCM was used to estimate the monthly runoff and recharge in the 144 subbasin watershed that surround the alluvial basin of Cuyama Valley. The BCM of the surrounding watershed indicates that about 65 percent of water leaving the landscape after ET becomes runoff that flows into Cuyama Valley. Some additional recharge within these surrounding watersheds may also become rejected recharge and contribute to runoff into the valley. The BCM generally fits the limited streamflow data that were available from the region and provides a systematic estimate of runoff and recharge for the largely ungaged watersheds surrounding Cuyama Valley. Average annual streamflow applied to streamflow network boundaries is approximately 1,500 acre-ft/yr (acre-feet per year) and ranges from 0 to120,000 acre-ft/yr. Only 14 of 144 subbasin watersheds exceed 10 . for any of the last 40 years, and with the exception of the two largest subbasins in the southeastern conglomerates, all are present on the southern side of the valley, an area dominated by sandstones. These 14 subbasins contribute more than 60 percent of the total streamflow.

The Cuyama Valley Hydrologic Model was designed to reproduce the most important natural and human components of the hydrologic system, including components dependent on variations in climate, permitting an accurate assessment of groundwater conditions and processes that can inform water users, and help to improve planning for future conditions. Model development included a revised conceptual model of the flow system, construction of a precipitation-runoff model using the Basin Characterization Model, and construction of an integrated hydrologic flow model with MODFLOW-One-Water Hydrologic Flow Model (MF-OWHM). The new geohydrologic, conceptual, and hydrologic models were developed, and the hydrologic models were calibrated to historical conditions of water and land use, and then used to assess the use and movement of water throughout the Valley. These tools provide a means to understand the evolution of water use, its availability, and the limits of sustainability.

The CUVHM uses MF-OWHM to simulate and assess the use and movement of water, which includes the evolution of changing land use and related water-balance regions. The model is capable of being accurate at annual to interannual time frames and subregional to valley-wide spatial scales that allow for analysis of the assessment of the groundwater hydrologic budget for water years 1949–2010, as well as potential assessment of the sustainability of groundwater use. Overall, the model provides a good representation of the regional flow system and the movement and use of all water.

Simulated changes in storage over time show that significant withdrawals from storage generally occurred not only during drought years (1976–77 and 1988–92) but also during the early stages of industrial agriculture that was initially dominated by alfalfa production. Since the 1990s, growers in the Cuyama Valley have shifted to more water-intensive organic vegetable crops such as carrots, broccoli, and potatoes that are rotated with field crops such as onions and grains. Combined with an extended growing season and increased irrigated acres, the shift in land use has increased demand on limited groundwater resources in excess of natural and artificial recharge. Measured and simulated groundwater levels indicate substantial declines in selected subregions, mining of groundwater that is thousands to tens of thousands of year old, increased storage depletion, and land subsidence. Simulated groundwater flow indicates that vertical gradients between aquifer layers fluctuate and even reverse in several parts of the basin as recharge and pumpage rates change seasonally and annually. The majority of recharge to the Cuyama Valley occurs from stream loss in the upland regions of Ventucopa and Sierra Madre Foothills, and the largest fractions of pumpage and storage depletion occur in the Main-zone subregions. The long-term imbalance between inflows and outflows results in modeled overdraft of the groundwater basin over the 61-year period 1949–2010. Changes in storage vary considerably from year to year, depending on land use, pumpage, and climate conditions. Climate-driven factors can greatly affect inflows, outflows, and water use by as much as a factor of two between wet and dry years. While inflows during inter-decadal wet years partly replenish water in the basin, the longer-term water use and storage depletion from pumping have restricted the effects of these major recharge events. Maps of simulated and measured water-level altitudes indicate large regions where depressed water levels have resulted in large desaturated zones in the recent and Older Alluvium layers in the Main-zone subregions. The projections of the base-case scenario and 2010 land use 61 years into the future indicates that current supply-and-demand are not sustainable (assuming that the past 61 years are representative of future climate) and will result in the potential for additional groundwater-level declines and related storage depletion and land subsidence.

References Cited

Allen, R.G., Pereira, L.S., Raes, D., and Smith, M., 1998, Crop evapotranspiration—Guidelines for computing crop water requirements: Food and Agriculture Organization of the United Nations, Irrigation and Drainage Paper 56, 300 p.

Alley, W.M., and Leake, S.A., 2004, The journey from safe yield to sustainability: Ground Water, v. 42, no. 1, p. 12–16.

Anderson, J.R., Hardy, E.E., Roach, J.T., and Witmer, R.E., 1976, A land use and land cover classification system for use with remote sensor data: U.S. Geological Survey Professional Paper 964, 28 p.

Bazeley, W.J.M., ed., 1988, Tertiary tectonics and sedimentation in the Cuyama basin, San Luis Obispo, Santa Barbara, and Ventura Counties, California: Society of Economic Paleontologists and Mineralogists, Pacific Section, Book 59, p. 87–98.

Belitz, Kenneth, and Phillips, S.P., 1995, Alternative to agricultural drains in California's San Joaquin Valley: Results of a regional-scale hydrogeologic approach: Water Resources Research, v. 31, no. 8, p. 1845–1862.

Belitz, Kenneth, Phillips, S.P., and Gronberg, J.M., 1993, Numerical simulation of ground-water flow in the central part of the Western San Joaquin Valley, California: U.S. Geological Survey Water-Supply Paper 2396, 69 p.

Bredehoeft, J. D., 1997, Safe yield and the water budget myth, Ground Water, v. 35, no. 6, p. 929

Bredehoeft, J. D., 2002, The water budget myth revisited: why hydrogeologists model: Ground Water, vol. 40., no. 4, p. 340–345.

Bredehoeft, J.D., Papadopolous, S.S., and Cooper Jr., H.H., 1982, The water budget myth, *in* Scientific Basis of Water Resources Management: National Academy Press, Washington, D.C., p. 51–57.

Brohman, R., and Bryant, L. eds., 2005, Existing vegetation classification and mapping technical guide: Gen. Tech. Rep. WO–67, Washington, DC: U.S. Department of Agriculture Forest Service, Ecosystem Management Coordination Staff, 305 p.

Brouwer, C. and Heibloem, M., 1986, Irrigation water management: training manual no. 3—Irrigation water needs: Food and Agriculture Organization of the United Nations, Land and Water Development Division.

Brouwer, C., Goffeau, A., and Heibloem, M., 1985, Irrigation water management: Training manual no. 1— Introduction into Irrigation. Food and Agriculture Organization of the United Nations, Land and Water Development Division, 91p.

Brush, C.F., Belitz, K., and Phillips, S.P., 2004, Estimation of a water budget for 1972–2000 for the Grasslands Area, Central Part of the Western San Joaquin Valley, California: U.S. Geological Survey Scientific Investigations Report 2004–5180, 51p.

Burow, K.R., Shelton, J.L., Hevesi, J.A., and Weissmann, G.S., 2004, Hydrogeologic characterization of the Modesto area, San Joaquin Valley, California: U.S. Geological Survey Scientific Investigations Report 2004–5232, 54 p.

California Department of Water Resources, 1994, California water plan update: Bulletin 160-93, California Department of Water Resources, Sacramento, Calif.

California Department of Water Resources, 2000, Explanations of land use attributes used in database files associated with shape files: Land and Water Use Section, 11 p.

California Department of Water Resources, 2003, California's Groundwater: Bulletin 118 Update 2003, Chapter 6: Basic Groundwater Concepts: accessed May 1, 2012, *http://www.water.ca.gov/pubs/groundwater/bulletin_118/california%27s_groundwater__bulletin_11_-_update_2003_/bulletin118-chapter6.pdf*.

California Department of Water Resources, 2007, California Irrigation Management Information System: *http://www.cimis.water.ca.gov/cimis/welcome.jsp*.

California Department of Water Resources, 2013, California Irrigation Management Information System: accessed January 20, 2013, *http://wwwcimis.water.ca.gov/cimis/welcome.jsp*.

Daly, C., Halbleib, M., Smith, J. I., Gibson, W. P., Doggett, M. K., Taylor, G. H., Curtis, J., and Pasteris, P. A., 2008, Physiographically sensitive mapping of temperature and precipitation across the conterminous United States: International Journal of Climatology, v. 28, no. 15, p. 2031–2064, *http://onlinelibrary.wiley.com/doi/10.1002/joc.1688/abstract*.

DeLong, S.B., Pelletier, J.D., and Arnold, L.J., 2008, Climate change triggered sedimentation and progressive tectonic uplift in a coupled piedmont-axial system—Cuyama Valley, California, USA: Earth Surface Processes and Landforms, v. 33, p. 1033–1046.

Dibblee, T.W., and Minch, J.A., ed., 2005, Geologic map of the Peak Mountain quadrangle, San Luis Obispo and Santa Barbara Counties, California: Dibblee Geological Foundation Map DF–181, scale 1:24,000.

Dibblee, T.W. Jr., 1982, Geology of the Alamo Mountain, Frazier Mountain, Lockwood Valley, Mount Pinos, and Cuyama Badlands areas, Southern California, *in* Fife, D.L. and Minch, J.A., eds., Geology and mineral wealth of the California Transverse Ranges: Mason Hill Volume: South Coast Geological Society, p. 57–77.

Dickinson, J.E., Hanson, R.T., and Predmore, S.K., 2014, HydroClimATe—Hydrologic and climatic analysis toolkit: U.S. Geological Survey Techniques and Methods 4–A9, 49 p.

Dimitrakopoulos, Roussos, and Desbarats, A.J., 1993, Geostatistical modeling of grid block permeabilities for 3D reservoir simulators: Reservoir Engineering, v. 8, p. 13–18.

Doherty, J., 2004, PEST Model-independent Parameter Estimation, User Manual: fifth ed. Watermark Numerical Computing Inc.

Doherty, J., 2010a, PEST, Model-independent parameter estimation—User manual (5th ed., with slight additions): Brisbane, Australia, Watermark Numerical Computing.

Doherty, J., 2010b, Addendum to the PEST manual: Brisbane, Australia, Watermark Numerical Computing.

Doherty, J., 2010c, BeoPEST for Windows: Brisbane, Australia, Watermark Numerical Computing.

Doherty, J.E., and Hunt, R.J., 2010, Approaches to highly parameterized inversion—A guide to using PEST for groundwater-model calibration: U.S. Geological Survey Scientific Investigations Report 2010–5169, 59 p.

Everett. R.R., Hanson, R.T., and Sweetkind, D.S., 2011, Kirschenmann Road multi-well monitoring site, Cuyama Valley, Santa Barbara County, California: U.S. Geological Survey Open-File Report 2011–1292, 4 p., *http://pubs.usgs.gov/of/2011/1292/*.

Everett, R.R., Gibbs, D.R., Hanson, R.T., Sweetkind, D.S., Brandt, J.T., Falk, S.E. and Harich, C.R., 2013, Geology, water-quality, hydrology, and geomechanics of the Cuyama Valley groundwater basin, California, 2008–12: U.S. Geological Survey Scientific Investigations Report 2013–5108, 62 p.

Faunt, C.C., Hanson R.T., Schmid, Wolfgang, Belitz, K., and Predmore, S., 2009a, Documentation of the Ground-water Flow Model, Chap. C *of* Faunt, Claudia, ed., Ground-Water Availability of California's Central Valley: U.S. Geological Survey Professional Paper 1766, p. 121–212

Faunt, C.C., Belitz, K., and Hanson, R.T., 2009b, Texture Model of the Valley Fill Deposits of the Central Valley, California: Hydrogeology Journal, DOI 10.1007/s10040-009-0539-7, 25p.

Federal Geographic Data Committee, 2008, National vegetation classification standard, Ver. 2: FGDC-STD-005-2008, accessed May 5, 2014, *https://www.fgdc.gov/standards/projects/FGDC-standards-projects/vegetation*.

Fio, J.L., and Leighton, D.A., 1995, Geohydrologic framework, historical development of the ground-water system, and general hydrologic and water-quality conditions in 1990, South San Francisco Bay and Peninsula area, California: U.S. Geological Survey Open-File Report 94–357, 46 p.

Flint, A.L. and Childs, S.W., 1987, Calculation of solar radiation in mountainous terrain: Journal of Agricultural and Forest Meteorology, v. 40, p. 233–249.

Flint, A.L. and Childs, S.W., 1991, Modification of the Priestley-Taylor equation to estimate evapotranspiration for soil water limited conditions: Journal of Agricultural and Forest Meteorology, v. 56, p. 247–260.

Flint, L.E. and Flint, A.L., 2007, Regional analysis of ground-water recharge, *in* Stonestrom, D. A.; Constantz, J.; Ferr´e, T. P. A.; and Leake, S.A., eds., Ground-water recharge in the arid and semiarid southwestern United States, U.S. Geological Survey Professional Paper 1703, p. 29–59.

Flint, L.E. and Flint, A.L., 2012, Simulation of climate change in San Francisco Bay Basins, California: Case studies in the Russian River Valley and Santa Cruz Mountains: U.S. Geological Survey Scientific Investigations Report 2012–5132, 55 p.

Flint, L.E., Flint, A.L., Stolp, B.J., and Danskin, W.R., 2012, A basin-scale approach for assessing water resources in a semiarid environment: San Diego region, California and Mexico, Hydrology and Earth System Sciences, v. 16, p. 1–17.

Gibbs, D., 2010, Cuyama Groundwater Basin: Department of Public Works, Santa Barbara County, 8 p.

Gibeault, V.A., Cocker-ham, S., Henry, J.M., and Meyer, J., 1989, California Turfgrass: It's use, water requirement, and irrigation: California Turfgrass Culture, University of California Cooperative Extension, v. 39, no. 3–4, 14 p.

Halford, K.J. and Hanson, R.T., 2002, User guide for the drawdown-limited, multi-node well (MNW) package for the U.S. Geological Survey's modular three-dimensional finite-difference ground-water flow model, versions MODFLOW-96 and MODFLOW-2000: U.S. Geological Survey Open-File Report 02–293, 33 p., *http://water.usgs.gov/pubs/of/2002/ofr02293/*.

Hanson, R.T., 1988, Aquifer-system compaction, Tucson basin and Avra Valley, Arizona: U.S. Geological Survey Water-Resources Investigation Report 88–4172, 69 p.

Hanson, R.T., and Benedict, J.F., 1993, Simulation of ground-water flow and potential land subsidence, upper Santa Cruz River Basin, Arizona: U.S. Geological Survey Water-Resources Investigation Report 93–4196, 47 p., *http://pubs.er.usgs.gov/usgspubs/wri/wri934196*.

Hanson, R.T., and Leake, S.A., 1998, Documentation for HYDMOD, A program for time-series data from the U.S. Geological Survey's modular three-dimensional finite-difference ground-water flow model: U.S. Geological Survey Water-Resources Investigations Report 98–564, 57 p.

Hanson, R.T., Anderson, S.R., and Pool, D.R., 1990, Simulation of ground-water flow and potential land subsidence, Avra Valley, Arizona: U.S. Geological Survey Water-Resources Investigation Report 90–4178, 41 p., *http://pubs.er.usgs.gov/usgspubs/wri/wri904178*.

Hanson, R.T., Martin, P., and Koczot, K.M., 2003, Simulation of ground-water/surface-water flow in the Santa Clara-Calleguas Basin, Ventura County, California: U.S. Geological Survey Water-Resources Investigation 02–4136, 214 p.

Hanson, R.T., Li, Z., and Faunt C., 2004, Documentation of the Santa Clara Valley regional ground-water/surface-water flow model, Santa Clara County, California: Scientific Investigations Report 2004–5231, 75 p., *http://pubs.water.usgs.gov/sir2004-5231/*.

Hanson, R.T., Dettinger, M.D., and Newhouse, M.W., 2006, Relations between climate variability and hydrologic time series from four alluvial basins across the southwestern United States: Hydrogeology Journal, v. 14, no. 7, p. 1122–1146

Hanson, R.T., Schmid, Wolfgang, Faunt, C.C., and Lockwood, B., 2010, Simulation and Analysis of Conjunctive Use with MODFLOW's Farm Process: Groundwater, v. 48, no. 5, p. 674–689, doi: 10.1111/j.1745-6584.2010.00730.x.

Hanson, R.T., Flint, L.E., Flint, A.L., Dettinger, M.D., Faunt, C.C., Cayan, D., and, Schmid, Wolfgang, 2012, A method for physically based model analysis of conjunctive use in response to potential climate changes: Water Resources Research, v. 48, 23p., doi:10.1029/2011WR010774

Hanson, R.T., and Schmid, Wolfgang, 2013, Economic Resilience through "One-Water" Management: U.S. Geological Survey Open-File Report 2013–1175, 2 p.

Hanson, R.T., Schmid, Wolfgang, Faunt, C. C., Lear, J., and Lockwood, B., 2014a, Integrated Hydrologic Model of Pajaro Valley, Santa Cruz and Monterey Counties, California: U.S. Geological Survey Scientific Investigations Report 2014–5111, 166 p.

Hanson, R.T., Boyce, S.E., Schmid, Wolfgang, Hughes, J.D., Mehl, S.M., Leake, S.A., Maddock, Thomas, III, and Niswonger, R.G., 2014b, One-Water Hydrologic Flow Model (OWHM): U.S. Geological Survey Techniques and Methods 6-A51, 122 p.

Harbaugh, A.W., 2005, MODFLOW-2005, the U.S. Geological Survey modular ground-water model-the Ground-Water Flow Process: U.S. Geological Survey Techniques and Methods 6–A16, variously paginated.

Harbaugh, A.W., Banta, E.R., Hill, M.C., and McDonald, M.G., 2000, MODFLOW-2000: U.S. Geological Survey modular ground-water model—User guide to modularization concepts and the ground-water flow process: U.S. Geological Survey Open-File Report 00–92, 121 p.

Hill, MC., 1990, Preconditioned conjugate-gradient 2 (PCG2), a computer program for solving ground-water flow equations: U.S. Geological Survey Water-Resources Investigations Report 90–4048, 43 p.

Hill, M.C., and Tiedeman, C.R., 2007, Effective groundwater model calibration: with analysis of data, sensitivities, predictions, and uncertainty: New York, Wiley and Sons, 464 p.

Hill, M.C., Banta, E.R, Harbaugh, A.W., and Anderman, E.R., 2000, MODFLOW-2000, The U.S Geological Survey modular ground-water model—User guide to the observation, sensitivity, and parameter-estimation processes and three post-processing programs: U.S. Geological Survey Open-File Report 00–184, 209 p.

Hill, M.L., Carlson, S.A., and Dibblee, T.W., Jr., 1958, Stratigraphy of Cuyama Valley-Caliente Range Area, California: American Association of Petroleum Geologists Bulletin, v. 42, p. 2973–3000.

Holzer, T.L., 1981, Preconsolidation stress of aquifer systems in areas of induced land subsidence: Water Resources Research, v. 17, no. 3, p. 693–704.

Homer, C.H., Fry, J.A., and Barnes C.A., 2012, The national land cover database: U.S. Geological Survey Fact Sheet 2012–3020, 4 p.

Hsieh, P.A., and Freckelton, J.R., 1993, Documentation of a computer program to simulate horizontal-flow barriers using the U.S. Geological Survey's modular three-dimensional finite-difference ground-water-flow model: U.S. Geological Survey Open-File Report 92–477, 32 p.

Jacob, C. E., 1940, On the flow of water in an elastic artesian aquifer: Transactions of the American Geophysical Union, v. 21, no. 2, p. 574–586.

Jacob, C. E., 1946, Drawdown test to determine effective radius of artesian well: American Society of Civil Engineers Proceedings, v. 72, May.

Jennings, C. W., 1977, Geologic map of California: California Division of Mines and Geology Geologic Data Map Number 2, scale 1:750,000.

Lagoe, M.B., 1987, Middle Cenozoic basin development, Cuyama Basin, California, *in* Ingersoll, R.V. and Ernst, W.G., eds., Cenozoic basin development of coastal California, Rubey volume VI : Prentice-Hall, Englewood Cliffs, New Jersey, p. 172–206.

Lantis, D.W., Steiner, R., Karinen, A.E., 1977, California, Land of Contrast, 3d ed: Kendall/Hunt Publishing Company, Dubuque, Iowa.

Laudon, Julie, and Belitz, Kenneth, 1991, Texture and depositional history of late pleistocene-holocene alluvium in the central part of the western San Joaquin Valley, California: Bulletin of the Association of Engineering Geologists, v. 28, no. 1, p. 73–88.

Leighton, D.A., Fio, J.L., and Metzger, L.F., 1994, Database of well and areal data, South San Francisco Bay and Peninsula area, California: U.S. Geological Survey Water-Resources Investigations Report 94–4151, 47 p.

Mueller, R., Yang, Z., Han, W., and Di, L., 2011, CropScape: A new web based visualization portal for the dissemination of NASS geospatial cropland products: USDA National Agricultural Statistics Service, 33 p, *http://www.nass.usda.gov/Education_and_Outreach/Reports,_Presentations_and_Conferences/Presentations/Mueller_WSS11_CropScape.pdf*.

National Renewable Energy Laboratory, 2014, Measurement and instrumentation data center (MODC): U.S. Department of Energy, Golden, Colo., *http://www.nrel.gov/midc/, last accessed June 15, 2014*.

Newhouse, M.W., Hanson, R.T., Wentworth, C.M., Everett, R., Williams, C. F., Tinsley J., Noce, T. E., and Carkin, B.A., 2004, Geologic, water-chemistry, and hydrologic data from multiple-well monitoring sites and selected water-supply wells in the Santa Clara Valley, California, 1999–2003: U.S. Geological Survey Scientific Investigations Report 2004–5250, 134 p.

Niswonger, R.G., and Prudic, D.E., 2005, Documentation of the Streamflow-Routing (SFR2) Package to include unsaturated flow beneath streams—A modification to SFR1: U.S. Geological Survey Techniques and Methods 6-A13.

Niswonger, R.G., Prudic, D.E., and Regan, R.S., 2006, Documentation of the Unsaturated-Zone Flow (UZF1) Package for modeling unsaturated flow between the land surface and the water table with MODFLOW-2005: U.S. Geological Survey Techniques and Methods 6-A19, 62 p.

Niswonger, R.G., Panday, Sorab, and Ibaraki, Motomu, 2011, MODFLOW-NWT, A Newton formulation for MODFLOW-2005: U.S. Geological Survey Techniques and Methods 6–A37, 44 p.

Phillips, S.P., and Belitz, Kenneth, 1991, Calibration of a textured-based model of a ground-water flow system, western San Joaquin Valley, California: Groundwater, v. 29, no. 5, p. 702–715.

Phillips, S.P, Green, C.T., Burow, K.R., Shelton, J.L., and Rewis, D.L., 2007, Simulation of multiscale ground-water flow in part of the northeastern San Joaquin Valley, California: U.S. Geological Survey Scientific Investigations Report 2007–5009, 43 p.

Poeter, E.P., Hill, M.C., Banta, E.R., Mehl, Steffen, and Christensen, Steen, 2005, UCODE_2005 and six other computer codes for universal sensitivity analysis, calibration, and uncertainty evaluation: U.S. Geological Survey Techniques and Methods 6–A11, 283 p.

Prudic, D.E., Konikow, L.F., and Banta, E.A., 2004, A new Streamflow-Routing (SFR1) package to simulate stream-aquifer interaction with MODFLOW-2000: U.S. Geological Survey Open-File Report 04–1042, 95 p.

Riley, F.S., 1969, Analysis of borehole extensometer data from central California, *in* Tison, L.J., ed., Land subsidence: Volume 2: Proceedings of the Tokyo Symposium, September 1969, International Association of Scientific Hydrology Publication 89, p. 423–431, accessed November 23, 2007, *http://www.cig.ensmp.fr/~iahs/redbooks/a088/088047.pdf*.

Schmid, Wolfgang, and Hanson R.T., 2009, The farm process version 2 (FMP2) for MODFLOW-2005—Modifications and upgrades to FMP1: U.S. Geological Survey Techniques in Water Resources Investigations, Book 6, Chapter A32, 102 p.

Schmid, Wolfgang, Hanson, R.T., Maddock III, T.M., and Leake, S.A., 2006a, User’s guide for the farm process (FMP) for the U.S. Geological Survey’s modular three-dimensional finite-difference ground-water flow model, MODFLOW-2000: U.S. Geological Survey Techniques and Methods 6-A17, 127 p.

Schmid, Wolfgang, Hanson, R.T., and Maddock III, Thomas, 2006b, Overview and advances of the farm process for MODFLOW-2000: Managing groundwater systems: Conference Proceedings, International Groundwater Modeling Center, Golden, Colo., May 21–24, 2006, p. 23–27

Singer, J.A., and Swarzenski, W.V., 1970, Pumpage and ground-water storage depletion in Cuyama Valley California, 1947–66: U.S. Geological Survey Open-File Report 70–304, 24 p.

Snyder, R.L., and Schullbach, K.F., 1992, Central coast Crop Coefficients for Field and Vegetable Crops: California Department of Water Resources, Water Conservation Office, Drought Tips No. 92-45, 12 p.

Snyder, R.L., Lamina, B.J., Shaw, D.A., and Pruitt, W.O., 1987a, Using reference evapotranspiration (ET_o) and crop coefficients to estimate crop evapotranspiration (Et_{ch}) for agronomic crops, grasses, and vegetable crops: Leaflet 21427, Cooperative Extension of the University of California Division of Agriculture and Natural Resources, Berkeley, Calif., 12 p.

Snyder, R.L., Lamina, B.J., Shaw, D.A., and Pruitt, W.O., 1987b, Using reference evapotranspiration (ET_o) and crop coefficients to estimate crop evapotranspiration (Et_{ch}) for trees and vines: Leaflet 21428, Cooperative Extension of the University of California, Division of Agriculture and Natural Resources, Berkeley, Calif., 8 p.

Sweetkind, D.S., Faunt, C.C., and Hanson, R.T., 2013, Construction of 3-D geologic framework and textural models for Cuyama Valley groundwater basin, California: U.S. Geological Survey Scientific Investigations Report 2013–5127, 46 p.

Terzaghi, Karl, and Peck, R.B., 1948, Soil mechanics in engineering practice: New York, John Wiley and Sons, Inc. 566 p.

Thorne, J.H., Flint, L.E., Flint, A.L., Boynton, R., and Thuy- N'goc Le, 2012, Development and application of downscaled hydroclimatic predictor variables for use in climate vulnerability and assessment studies: California Energy Commission, Publication number: CEC-500-2012-010.

University of Arizona, 2012, The Arizona meteorological network: Arizona Cooperative Extension, College of Agriculture and Life Sciences, accessed May 2013, *http://ag.arizona.edu/azmet/*.

Upson, J.E., and Worts, G.F., 1951, Ground water in the Cuyama Valley, California: U.S. Geological Survey Water Supply Paper 1110–B, 81 p.

U.S. Census Bureau, 2014a, , Census data 1950 and 1960: U.S. Census Bureau, accessed March 27, 2014, *http://www.census.gov/population/cencounts/ca190090.txt*.

U.S. Census Bureau, 2014b, Census data for 2010: U.S. Census Bureau, accessed March 25, 2014, *http://www.census.gov/2010census/popmap/*

U.S. Department of Agriculture Natural Resources Conservation Service, 2005, Soil survey geographic (SSURGO) database: USDA Natural Resources Conservation Service, accessed September 12, 2005, *http://www.ncgc.nrcs.usda.gov/products/datasets/ssurgo/*.

U.S. Department of Agriculture Natural Resources Conservation Service, 2006, State soil survey map (SSURGO): U.S. Department of Agriculture, accessed July 2010, *http://soildatamart.nrcs.usda.gov*.

U.S. Department of Agriculture, 2007, Existing Vegetation—CALVEG, [ESRI personal geodatabase], McClellan, CA: USDA Forest Service, Pacific Southwest Region, Remote Sensing Laboratory, accessed August 19, 2011, *http://www.fs.usda.gov/detail/r5/landmanagement/resourcemanagement/?cid=stelprdb5347188*.

U.S. Department of Agriculture, 2012, Cropscape raster data sets: U.S. Department of Agriculture, accessed, January 2013, *http://nassgeodata.gmu.edu/CropScape/*.

U.S. Geological Survey, 1990, Land use and land cover digital data from 1:250,000- and 1:100,000-scale maps—Data User Guide 4.: U.S. Geological Survey, Reston, Va.

U.S. Geological Survey, 1999a, National land cover digital data: U.S. Geological Survey, *http://edc.usgs.gov/products/landcover/nlcd.html*.

Figures

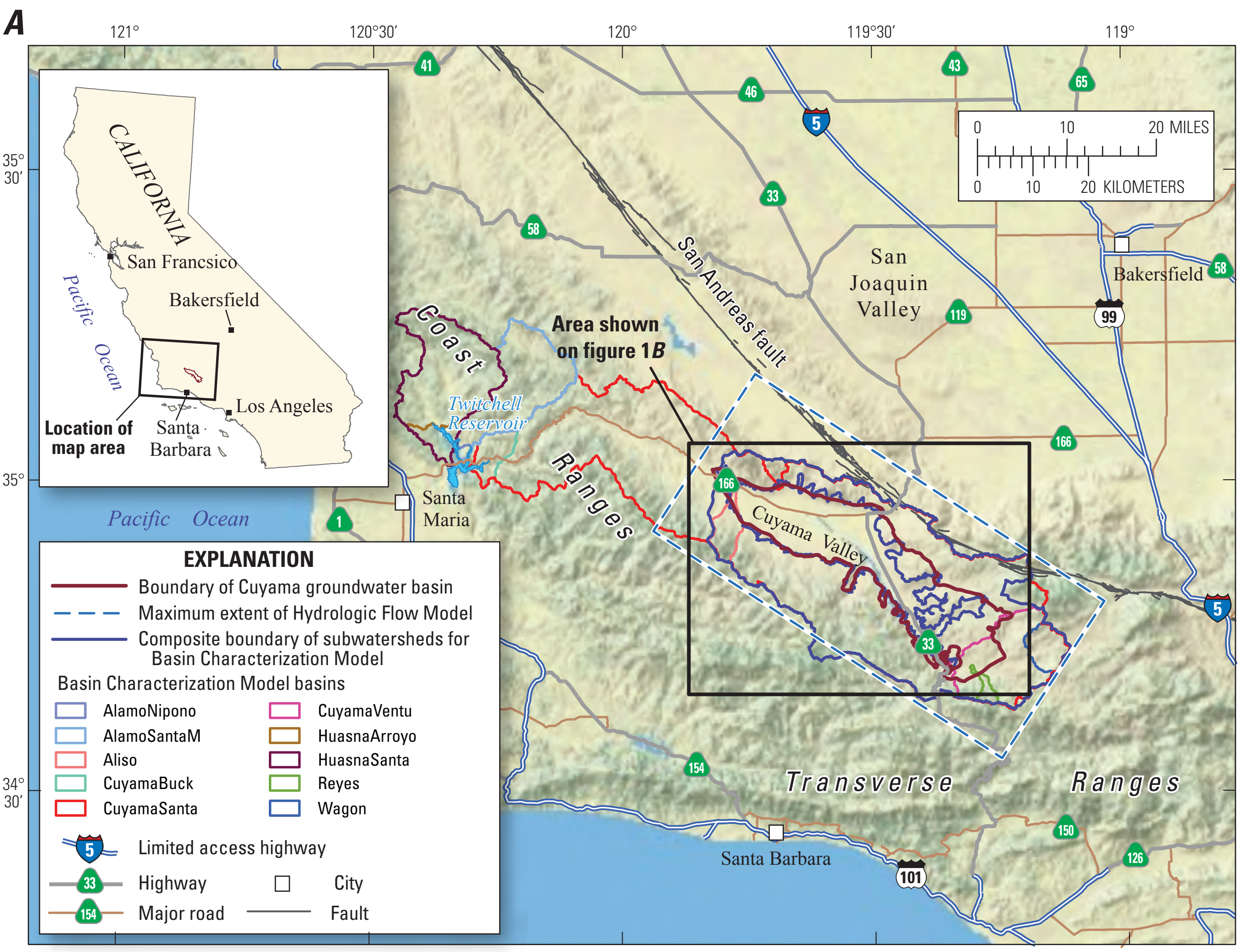

Shaded relief base from ESRI ArcGIS Online Map Service
http://services.arcgisonline.com/arcgis/services: ESRI_ShadedRelief_World_2D.
Roads from Cal-Atlas Geospatial Clearinghouse http://atlas.ca.gov/download.html
Place names sourced from USGS Geographic Names Information System,
1974-2009. San Andreas fault from Bryant (2005). Albers Projection, NAD83

Figure 1. *A*, Cuyama Valley watershed and groundwater basin, and *B*, detailed location map with the active hydrologic model grid, groundwater basin, and major rivers, Cuyama Valley, California.

B

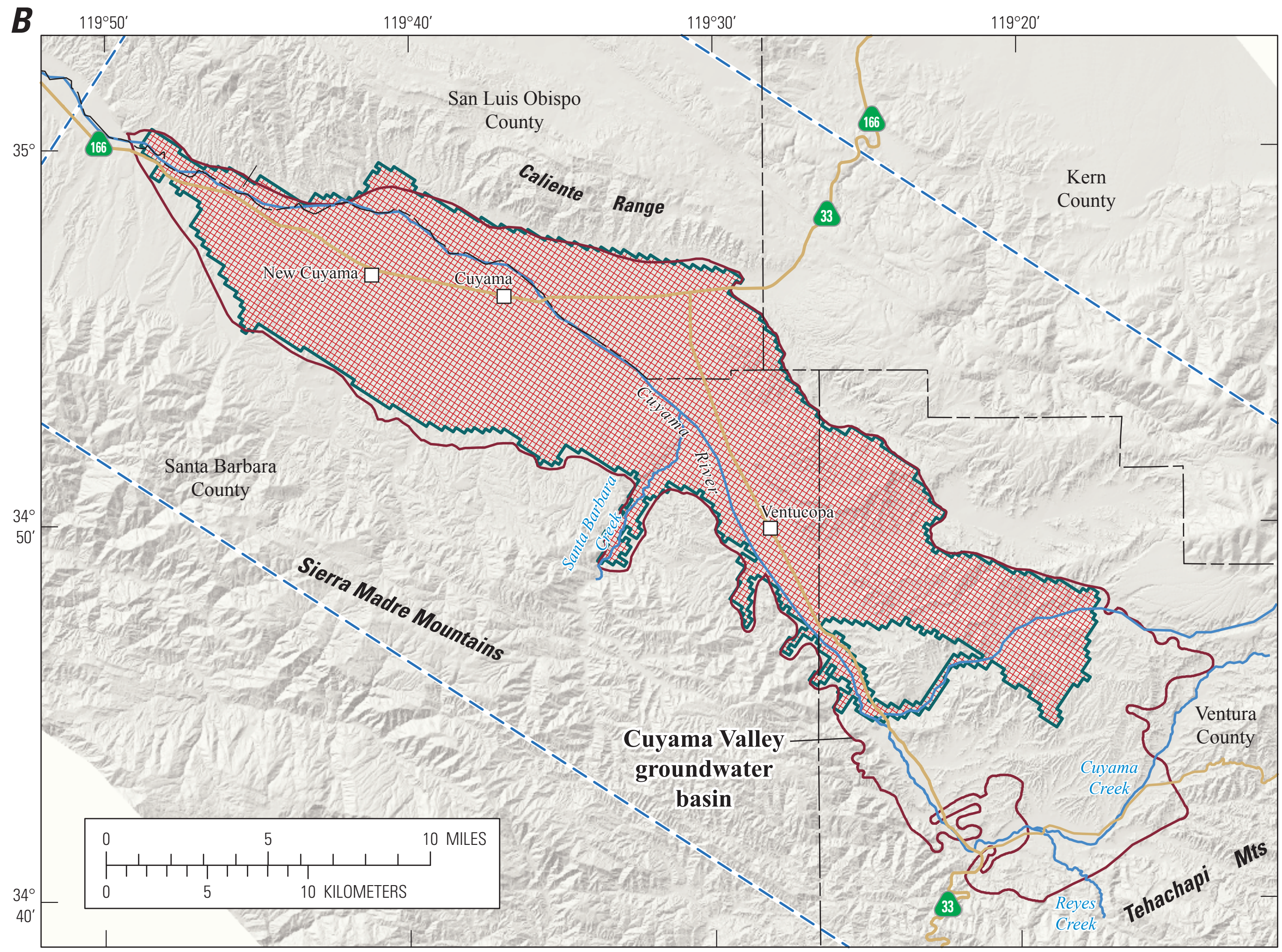

Shaded relief base created from 30-m digital elevation model from USGS National Elevation Dataset (NED); North America Vertical Datum 1983 (NAVD83). Hydrology sourced from 1:24,000-scale National Hydrography Dataset, 1974-2009. Place names sourced from USGS Geographic Names Information System, 1974-2009. Albers Projection, NAD83.

EXPLANATION

Figure 1. —Continued

A

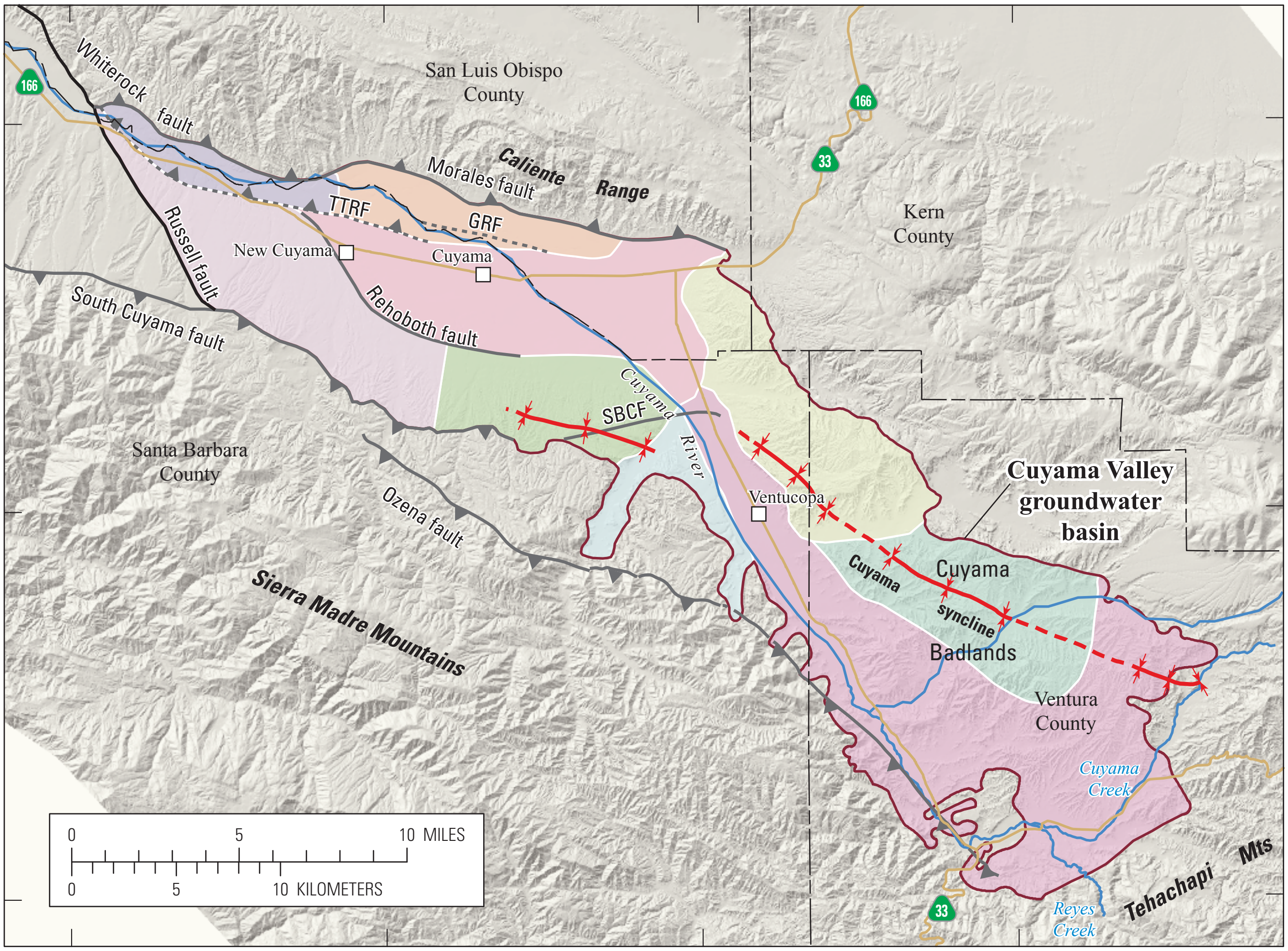

Shaded relief base created from 30-m digital elevation model from USGS National Elevation Dataset (NED); North America Vertical Datum 1983 (NAVD83). Hydrology sourced from 1:24,000-scale National Hydrography Dataset, 1974-2009. Place names sourced from USGS Geographic Names Information System, 1974-2009. Albers Projection, NAD83.

EXPLANATION

Cuyoma groundwater basin subregions (table 1)

- Caliente/Northern-Main (CNMZ)
- Central Sierra Madre Foothills (CSMFH)
- Northeast Ventucopa Uplands (NEVU)
- Northwestern Sierra Madre Foothills (NSMFH)
- Northern Ventucopa Uplands (NVU)
- Southern Sierra Madre Foothills (SSMFH)
- Southern Ventucopa Uplands (SVU)
- Southern-Main (SMZ)
- Western-Main (WMZ)

See table 1 for subregion designation

Normal fault

Thrust fault

Thrust fault, concealed

Syncline

Syncline, concealed

GRF, Graveyard fault;
SBCF, Santa Barbara Canyon fault;
TTRF, Turkey Trap Ridge fault

Figure 2. *A*, Groundwater hydrologic subregions and related geologic structures; *B*, simplified Cuyama major groundwater regions; and C, groups of landscape water-balance subregions for 1943–2010 in Cuyama Valley, California.

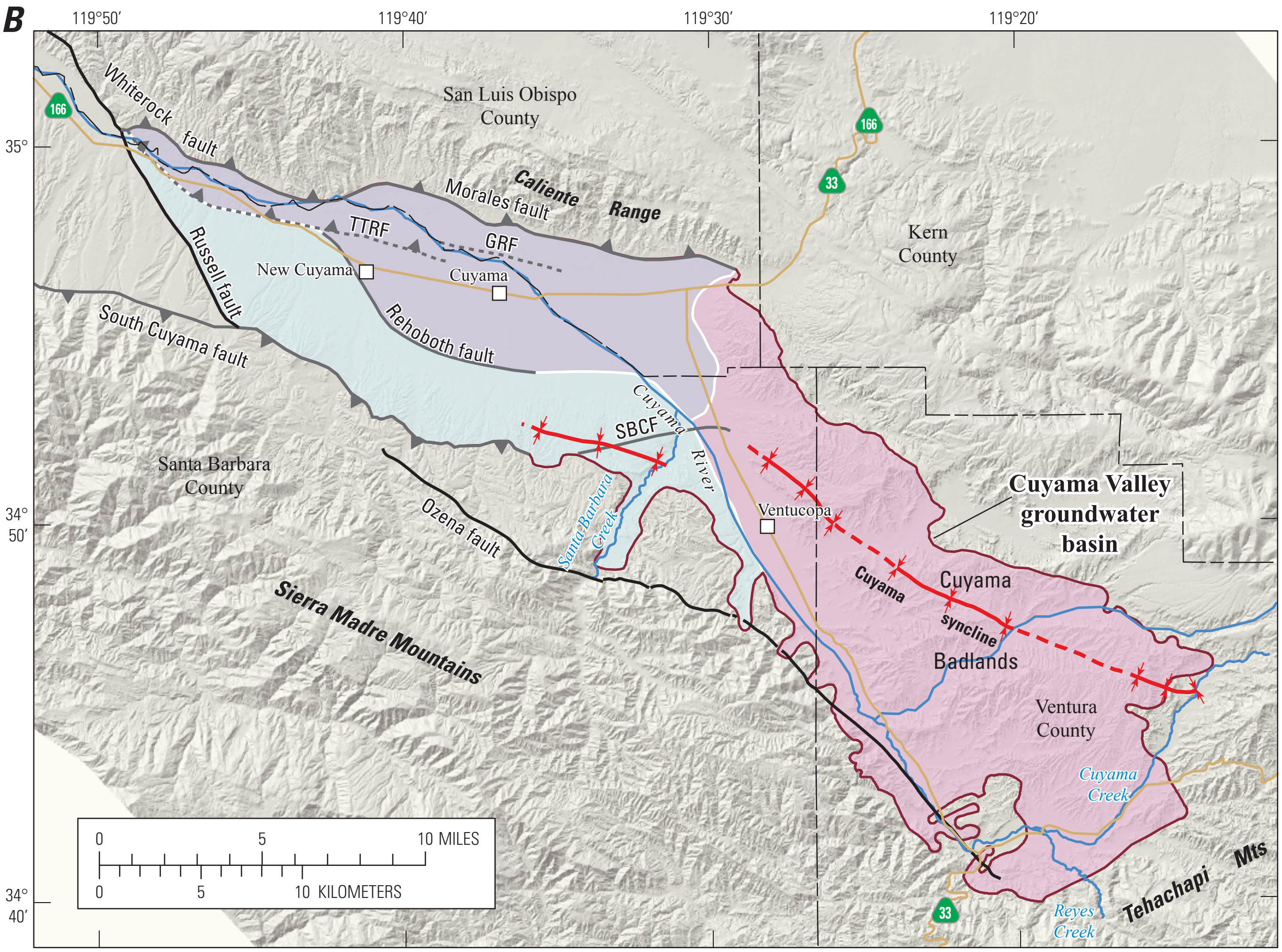

Shaded relief base created from 30-m digital elevation model from USGS National Elevation Dataset (NED); North America Vertical Datum 1983 (NAVD83). Hydrology sourced from 1:24,000-scale National Hydrography Dataset, 1974-2009. Place names sourced from USGS Geographic Names Information System, 1974-2009. Albers Projection, NAD83.

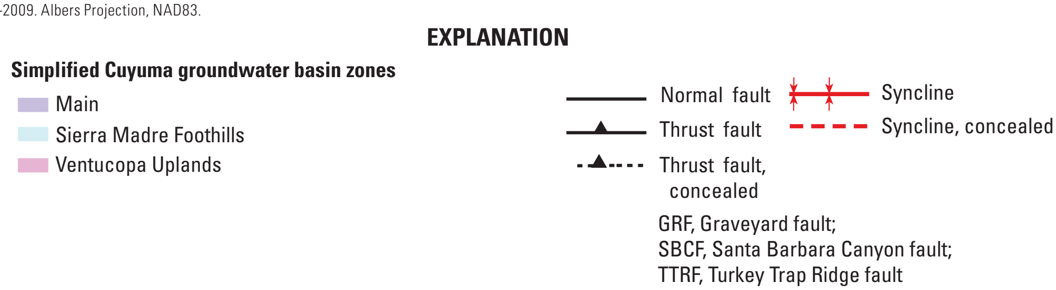

Figure 2. —Continued

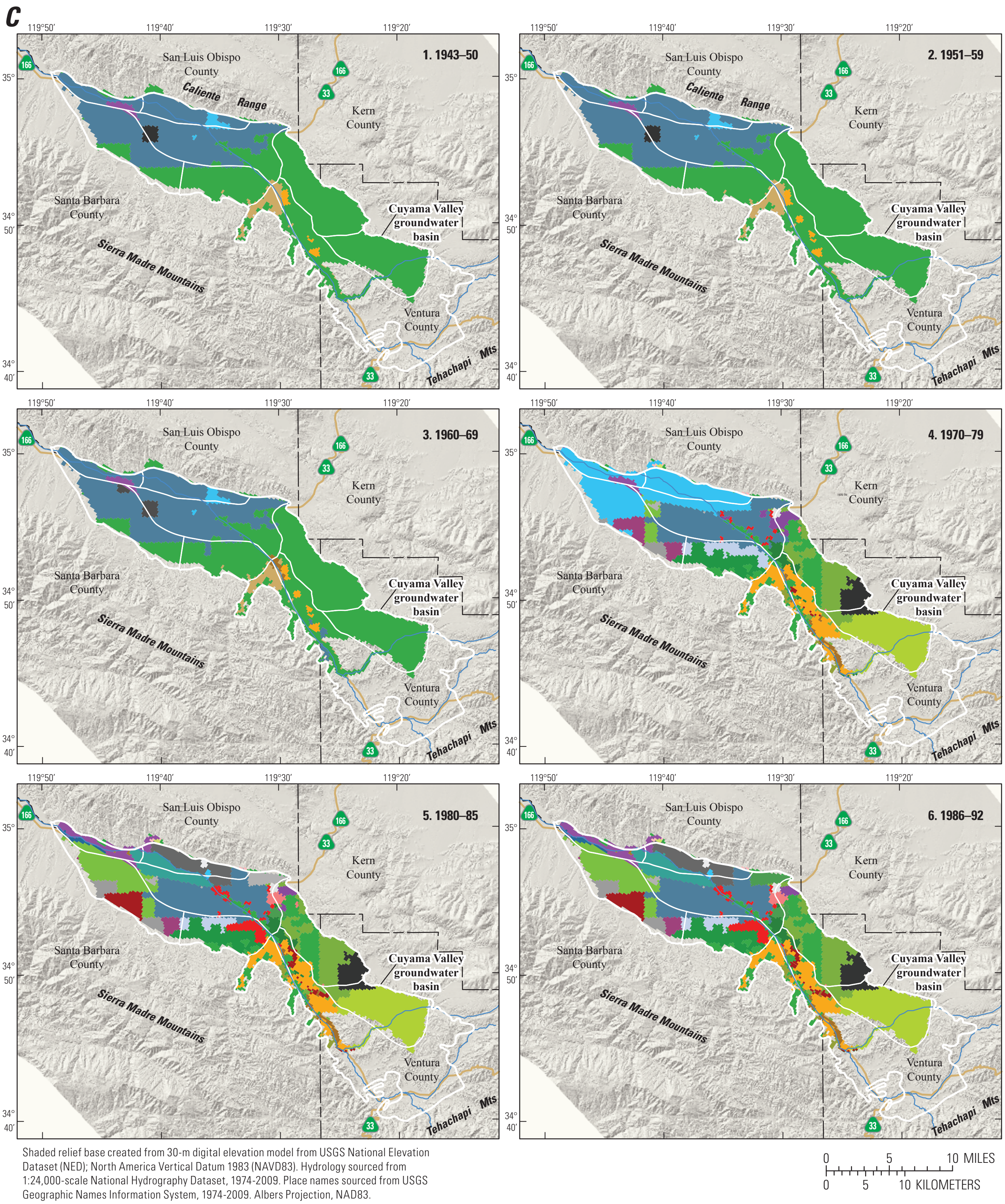

Figure 2. —Continued

C (Continued)

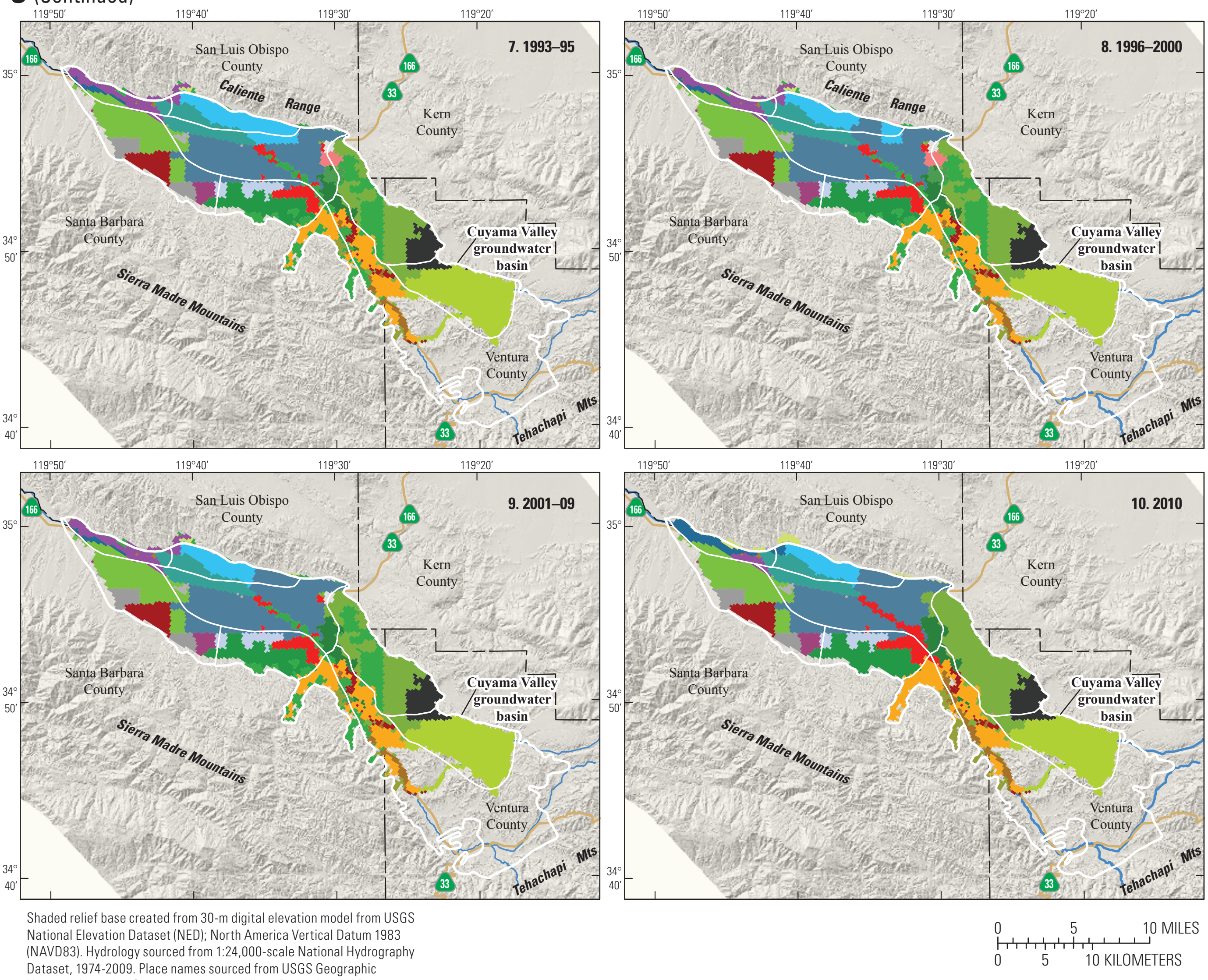

Shaded relief base created from 30-m digital elevation model from USGS National Elevation Dataset (NED); North America Vertical Datum 1983 (NAVD83). Hydrology sourced from 1:24,000-scale National Hydrography Dataset, 1974-2009. Place names sourced from USGS Geographic Names Information System, 1974-2009. Albers Projection, NAD83.

EXPLANATION

Farm groundwater ID for 1943 to 1969

Zone_primary use

- CNMZ_Ag
- SMZ_Ag
- SMZ_Dom
- SMZ_Ind
- SSMFH_Rch
- SVU_Ag
- SVU_Ind
- WMZ_Ag
- Native

See table 1 and figure 2A for zone designation

Farm groundwater ID for 1970 to 2010

Zone_primary use	Zone_primary use	Zone_primary use	
CNMZ_Ag	NVU_Ag	NSMZ_Nat	Native
CNMZ_Dom	NVU_Dom	SSMFH_Nat	
CNMZ_Ind	NVU_Ind	SVU_Ag	
CNMZ_Nat	NVU_Nat	SVU_Dom	
CNMZ_Urb	NVU_Urb	SVU_Ind	
CSMFH_Ag	SMZ_Ag	SVU_Nat	
CSMFH_Nat	SMZ_Dom	SVU_Rch	
NEVU_Nat	SMZ_Nat	WMZ_Ag	
NSMFH_Ag	SMZ_Rch	WMZ_Nat	
NSMFH_Urb	SMZ_Urb	WMZ_Rch	

Figure 2. —Continued

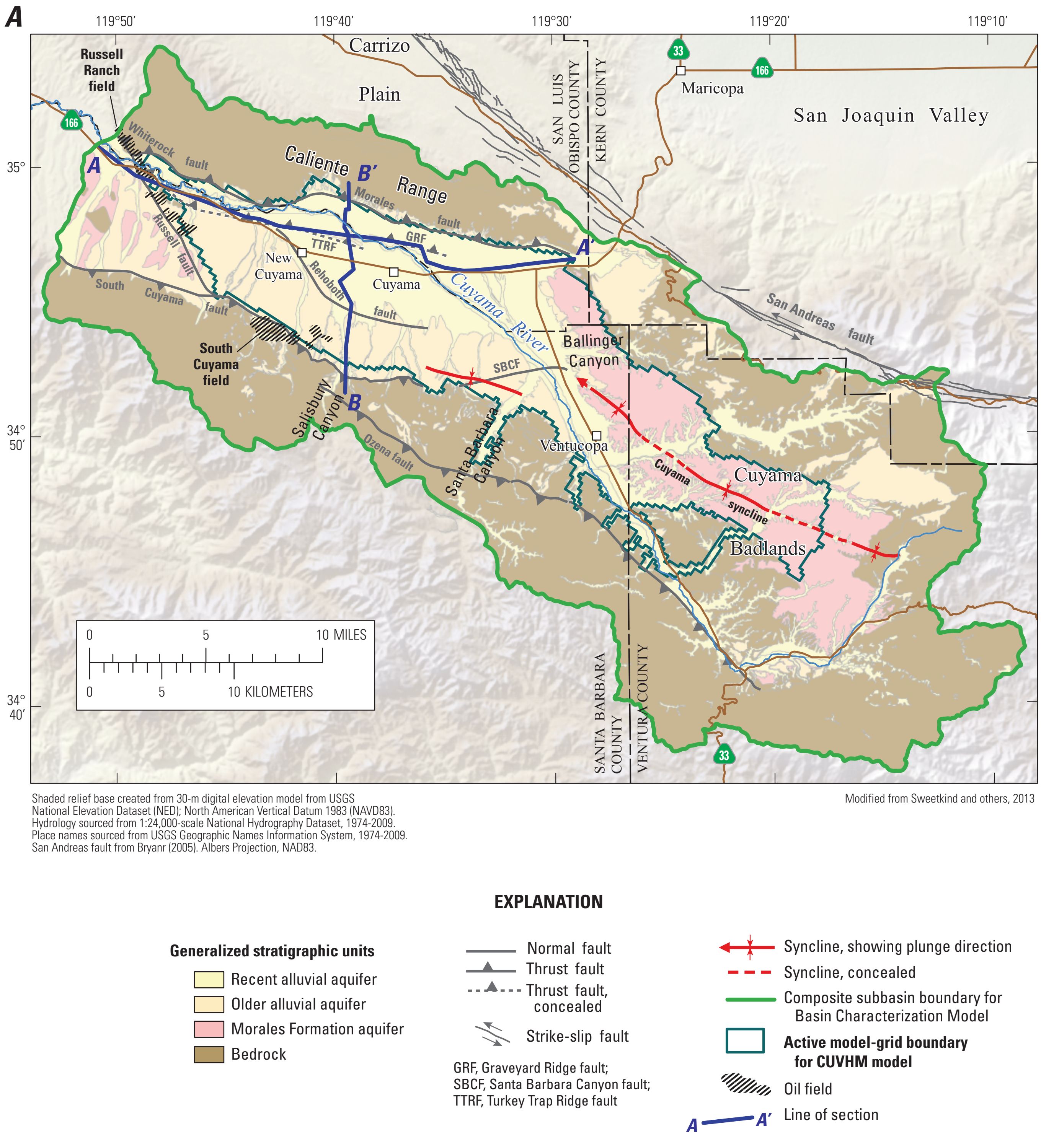

Figure 3. Generalized *A*, outcrops of geologic units and major faults within model grid; *B*, axial hydrogeologic cross-section (A–A′); and C, transverse hydrogeologic cross-section (B–B′) of Cuyama Valley, California.

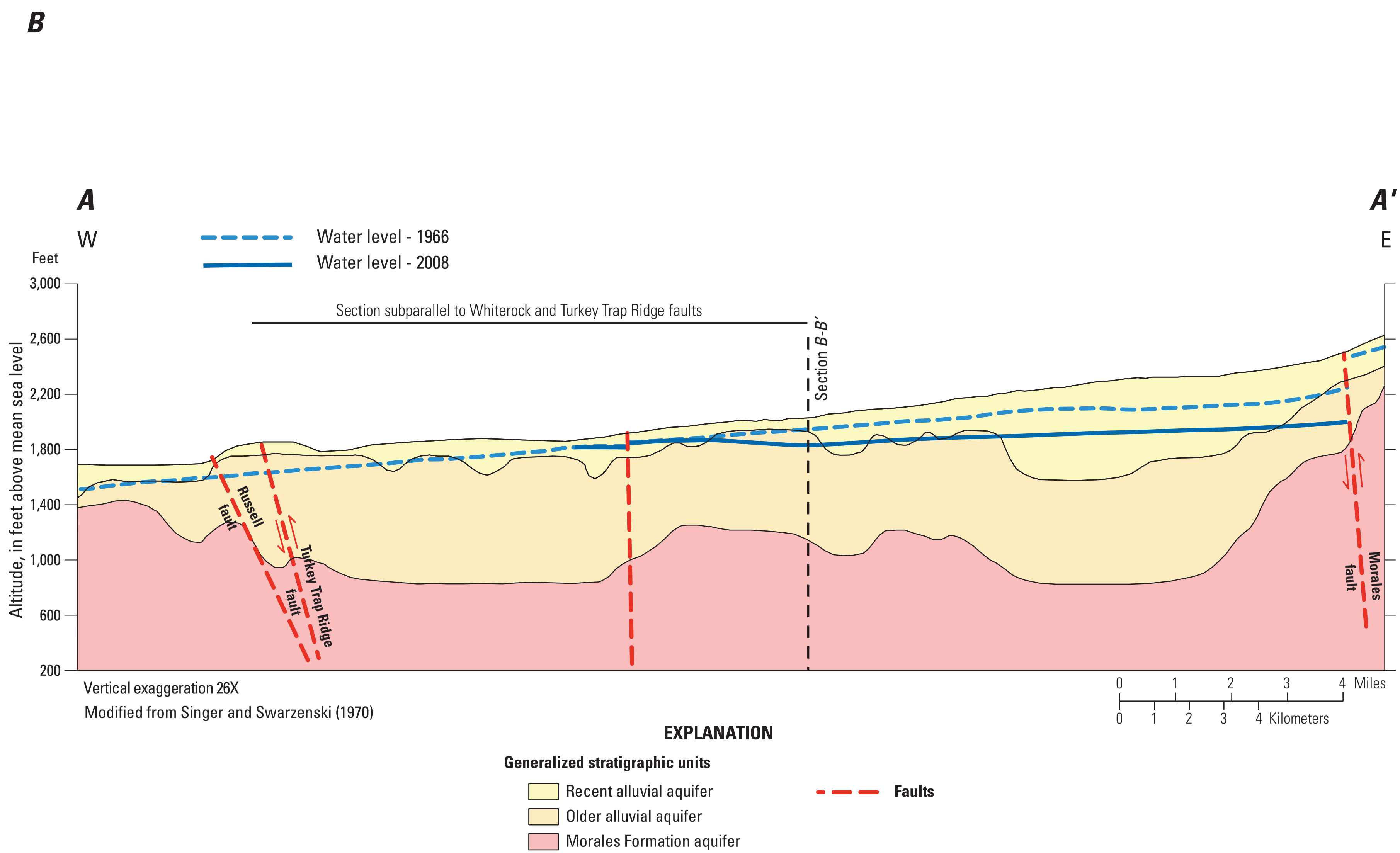

Figure 3. —Continued

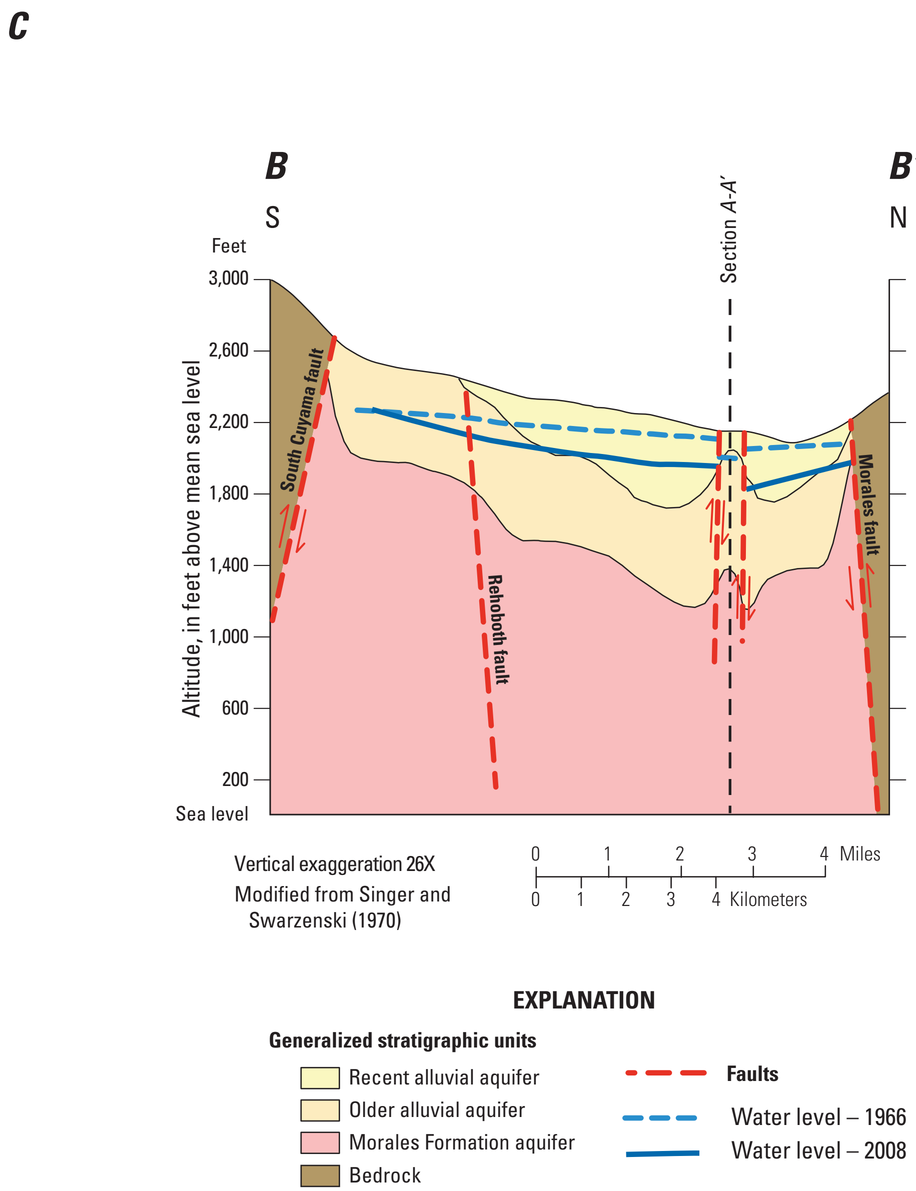

Figure 3. —Continued

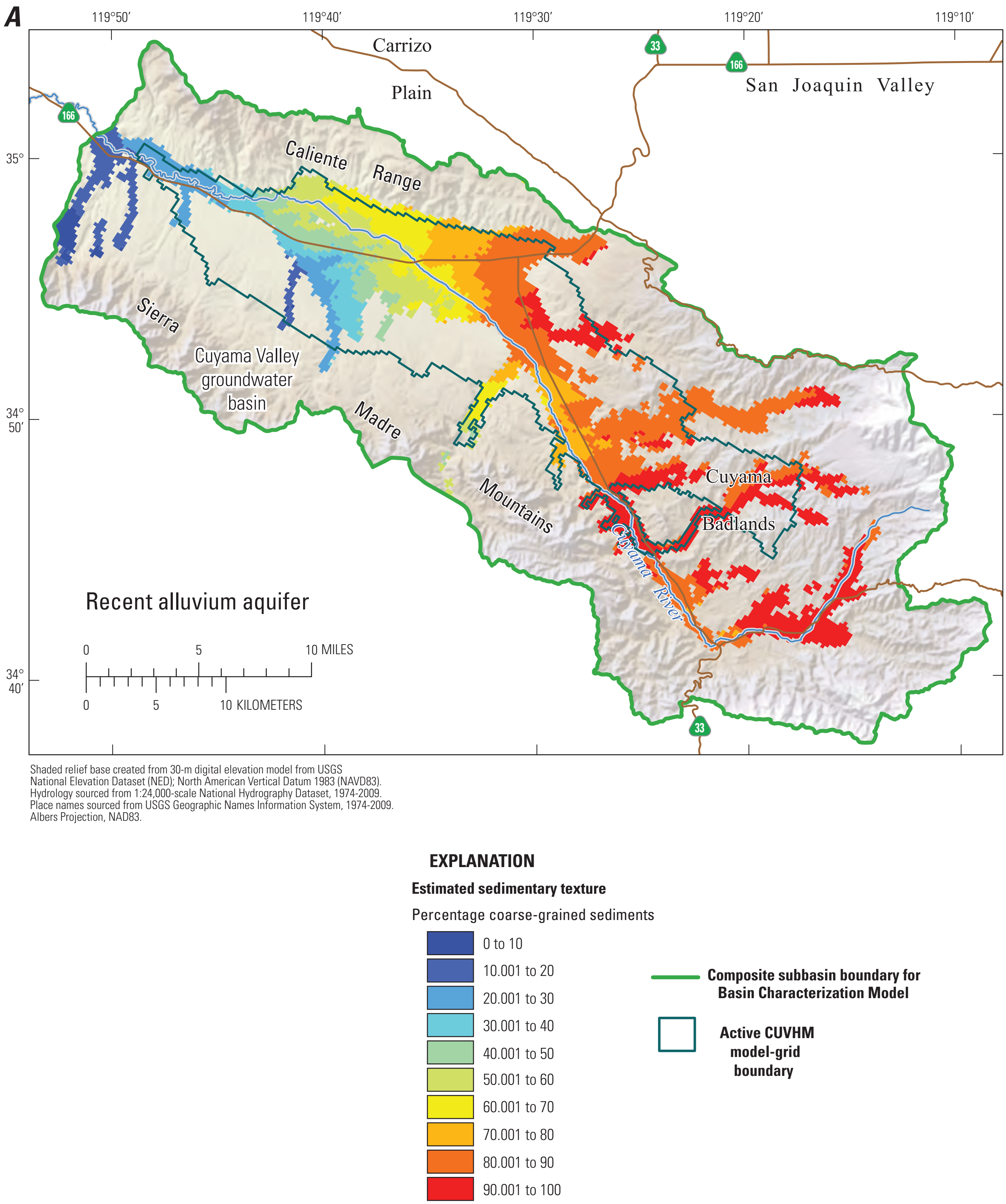

Figure 4. Extent and percentage of coarse-grained deposits for the *A*, Recent Alluvial aquifer; *B*, Older Alluvial aquifer; and *C*, Morales Formation aquifer of Cuyama Valley, California.

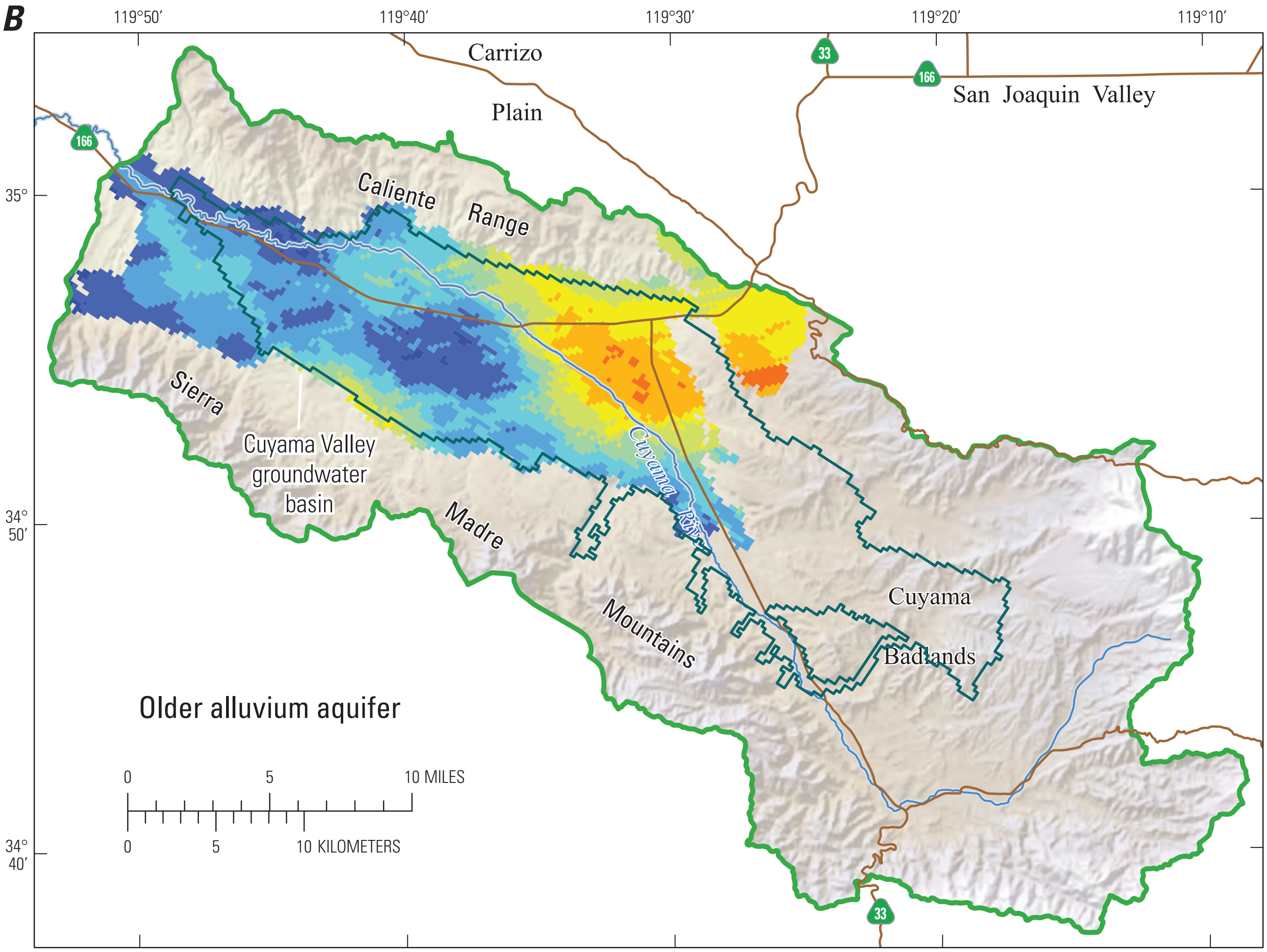

Shaded relief base created from 30-m digital elevation model from USGS National Elevation Dataset (NED); North American Vertical Datum 1983 (NAVD83).
Hydrology sourced from 1:24,000-scale National Hydrography Dataset, 1974-2009.
Place names sourced from USGS Geographic Names Information System, 1974-2009.
Albers Projection, NAD83.

EXPLANATION

Estimated sedimentary texture

Percentage coarse-grained sediments

- 0 to 10
- 10.001 to 20
- 20.001 to 30
- 30.001 to 40
- 40.001 to 50
- 50.001 to 60
- 60.001 to 70
- 70.001 to 80
- 80.001 to 90
- 90.001 to 100

Composite subbasin boundary for Basin Characterization Model

Active CUVHM model-grid boundary

Figure 4. —Continued

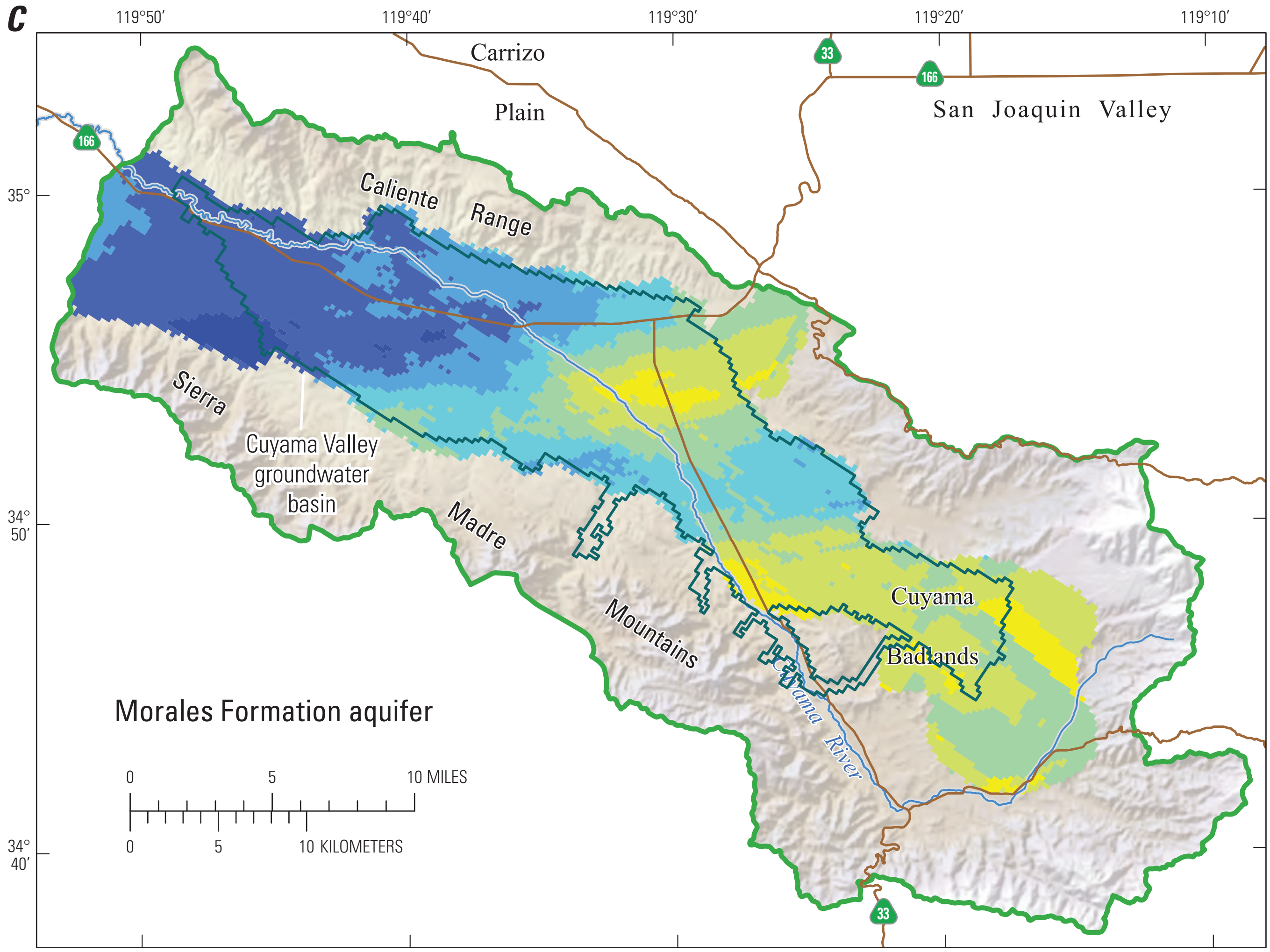

Shaded relief base created from 30-m digital elevation model from USGS National Elevation Dataset (NED); North American Vertical Datum 1983 (NAVD83).
Hydrology sourced from 1:24,000-scale National Hydrography Dataset, 1974-2009.
Place names sourced from USGS Geographic Names Information System, 1974-2009.
Albers Projection, NAD83.

EXPLANATION

Estimated sedimentary texture

Percentage coarse-grained sediments

- 0 to 10
- 10.001 to 20
- 20.001 to 30
- 30.001 to 40
- 40.001 to 50
- 50.001 to 60
- 60.001 to 70
- 70.001 to 80
- 80.001 to 90
- 90.001 to 100

Composite subbasin boundary for Basin Characterization Model

Active CUVHM model-grid boundary

Figure 4. —Continued

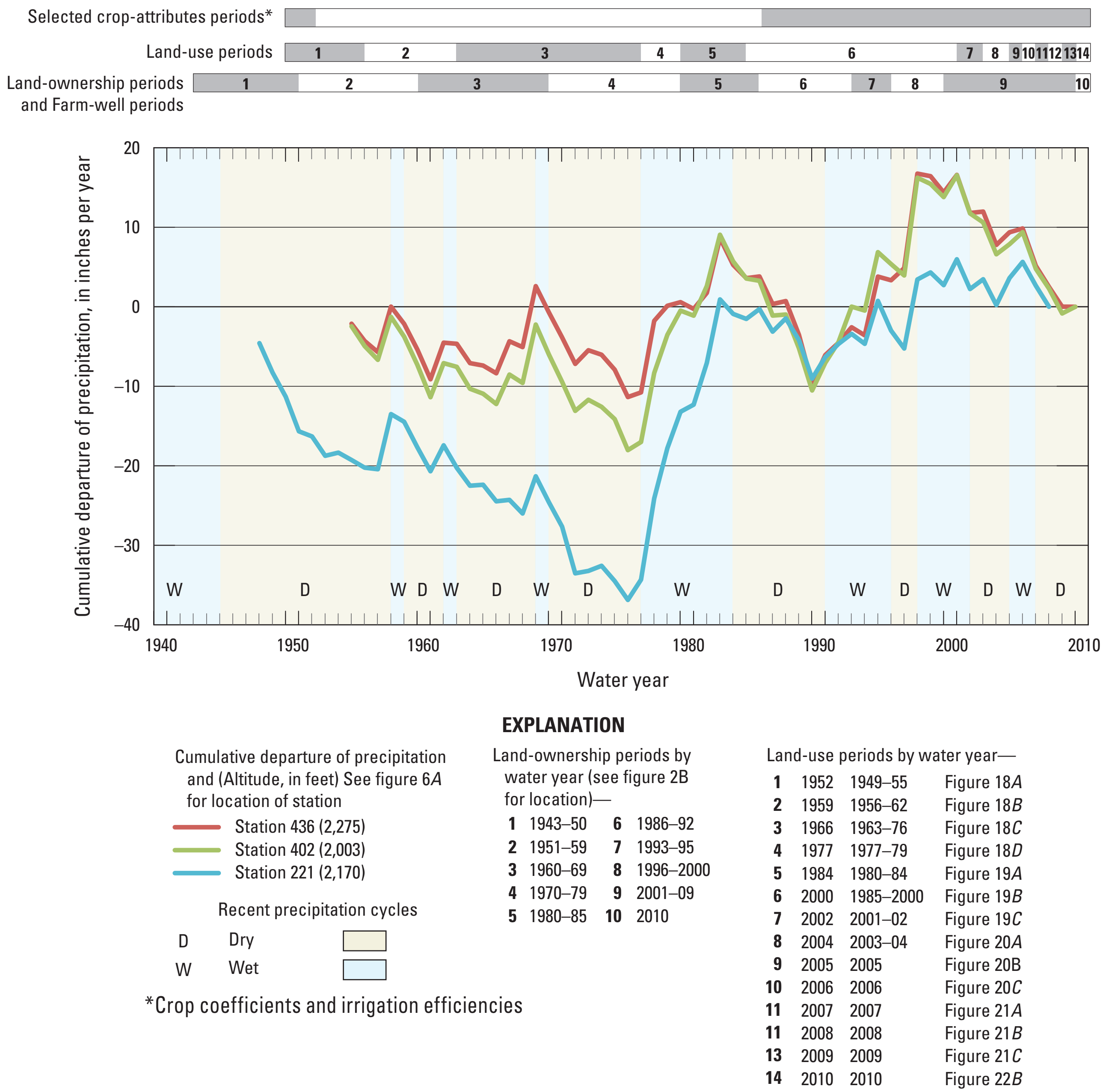

Figure 5. Cumulative departure of precipitation along with wet-dry periods, land-use map periods, periods of application for land-use, land-ownership (WBS) and related farm wells, and selected crop attributes for Cuyama Valley, California.

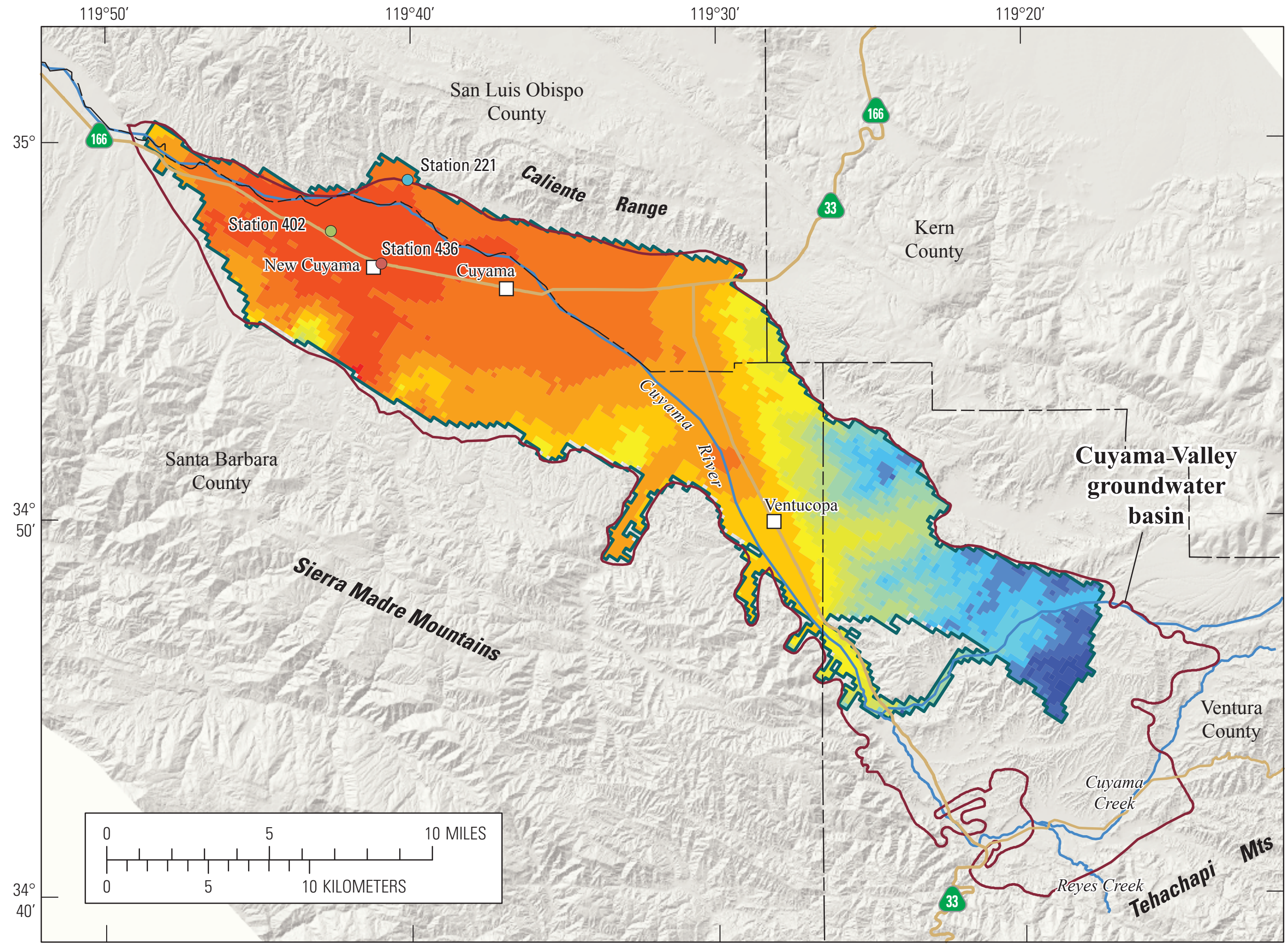

Shaded relief base created from 30-m digital elevation model from USGS National Elevation Dataset (NED); North America Vertical Datum 1983 (NAVD83). Hydrology sourced from 1:24,000-scale National Hydrography Dataset, 1974-2009. Place names sourced from USGS Geographic Names Information System, 1974-2009. Albers Projection, NAD83.

EXPLANATION

Active model-grid boundary

Rainfall gages

- Cuyama Ranch (1948-2008), Station 221
- CalTrans New Cuyama (1955-2010), Station 402
- Fire Station (1955-2010), Station 436

Average precipitation, in inches per year

6.94 to 7.0
>7.0 to 7.5
>7.5 to 8.0
>8.0 to 8.5
>8.5 to 9.0
>9.0 to 9.5
>9.5 to 10.0
>10.0 to 10.5
>10.5 to 11.0
>11.0 to 11.5
>11.5 to 12.0
>12.0 to 12.5
>12.5 to 13.0
>13.0 to 13.5
>13.5 to 14.0
>14.0 to 14.5
>14.5 to 15.0

Figure 6. Average annual *A*, precipitation, and *B*, potential evapotranspiration for the simulation period (1949–2010) for Cuyama Valley, California.

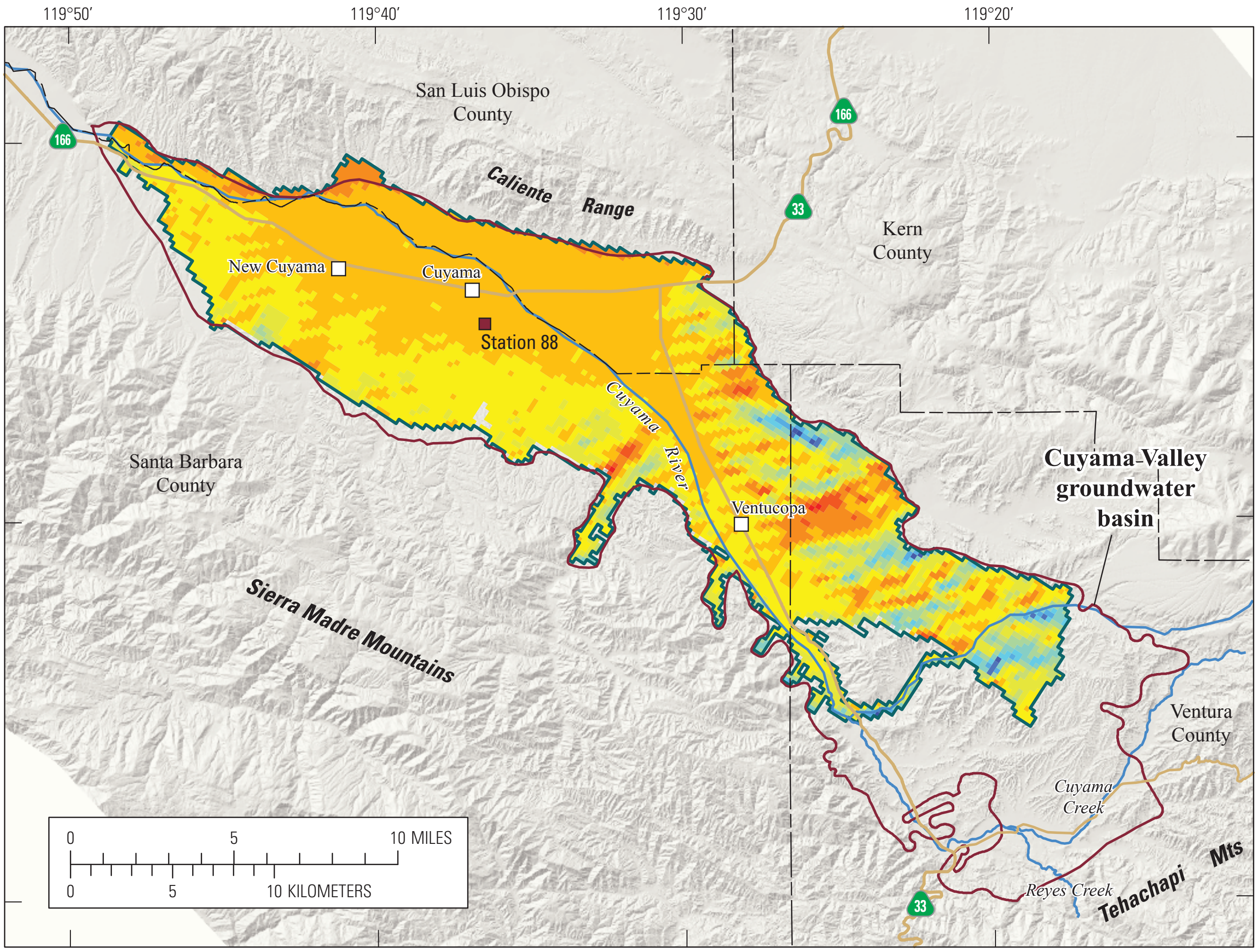

Shaded relief base created from 30-m digital elevation model from USGS National Elevation Dataset (NED); North America Vertical Datum 1983 (NAVD83). Hydrology sourced from 1:24,000-scale National Hydrography Dataset, 1974-2009. Place names sourced from USGS Geographic Names Information System, 1974-2009. Albers Projection, NAD83.

EXPLANATION

Active model-grid boundary

California irrigation management information system (CIMIS)—Station 88

Average potential evapotranspiration, in inches per year

44.6 to 45
>45 to 46
>46 to 47
>47 to 48
>48 to 49
>49 to 50
>50 to 51
>51 to 52
>52 to 53
>53 to 54
>54 to 55
>55 to 56
>56 to 57
>57

Figure 6. —Continued

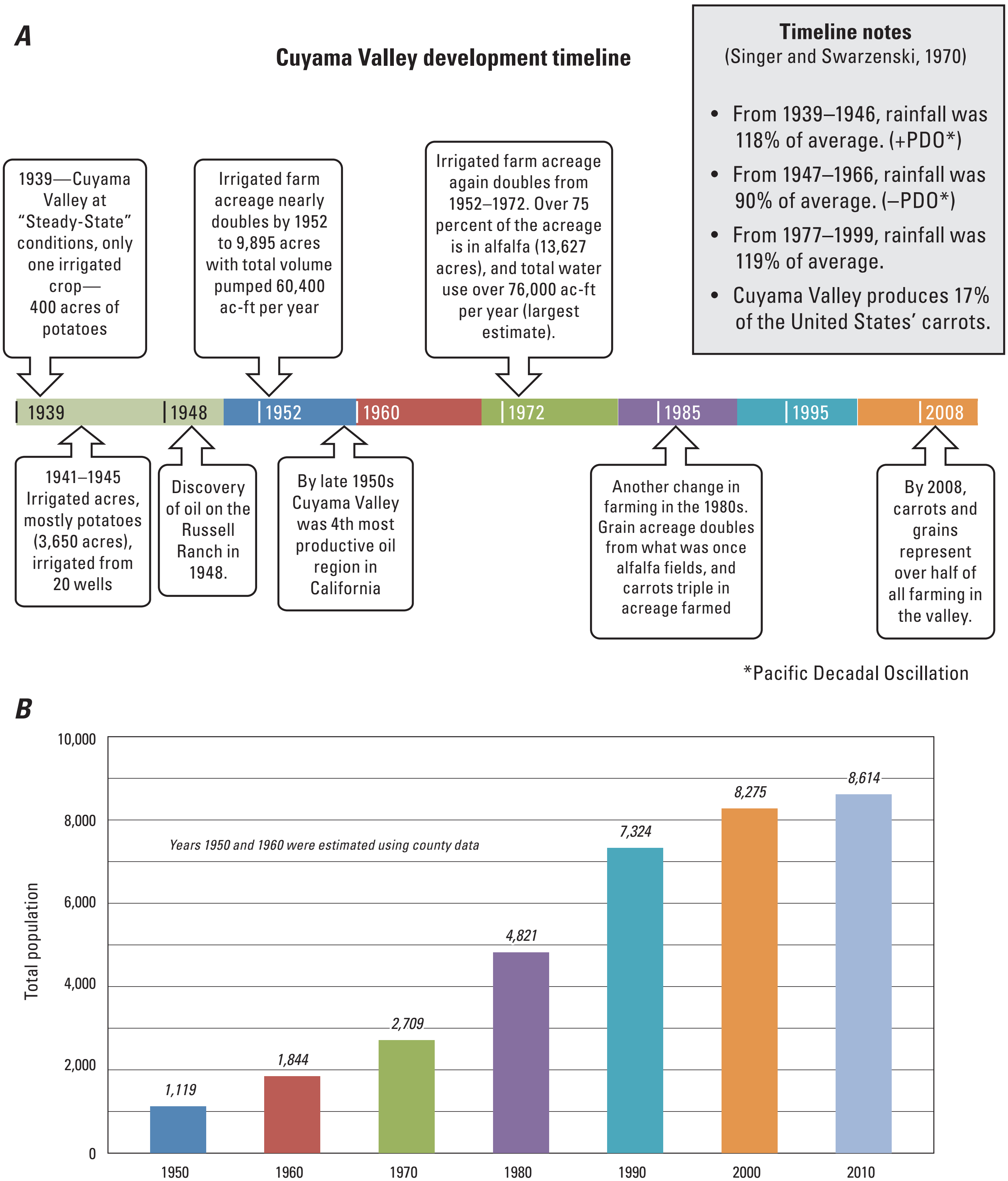

Figure 7. Generalized *A*, history of water and land-use development through time, and *B*, population growth for Cuyama Valley, California.

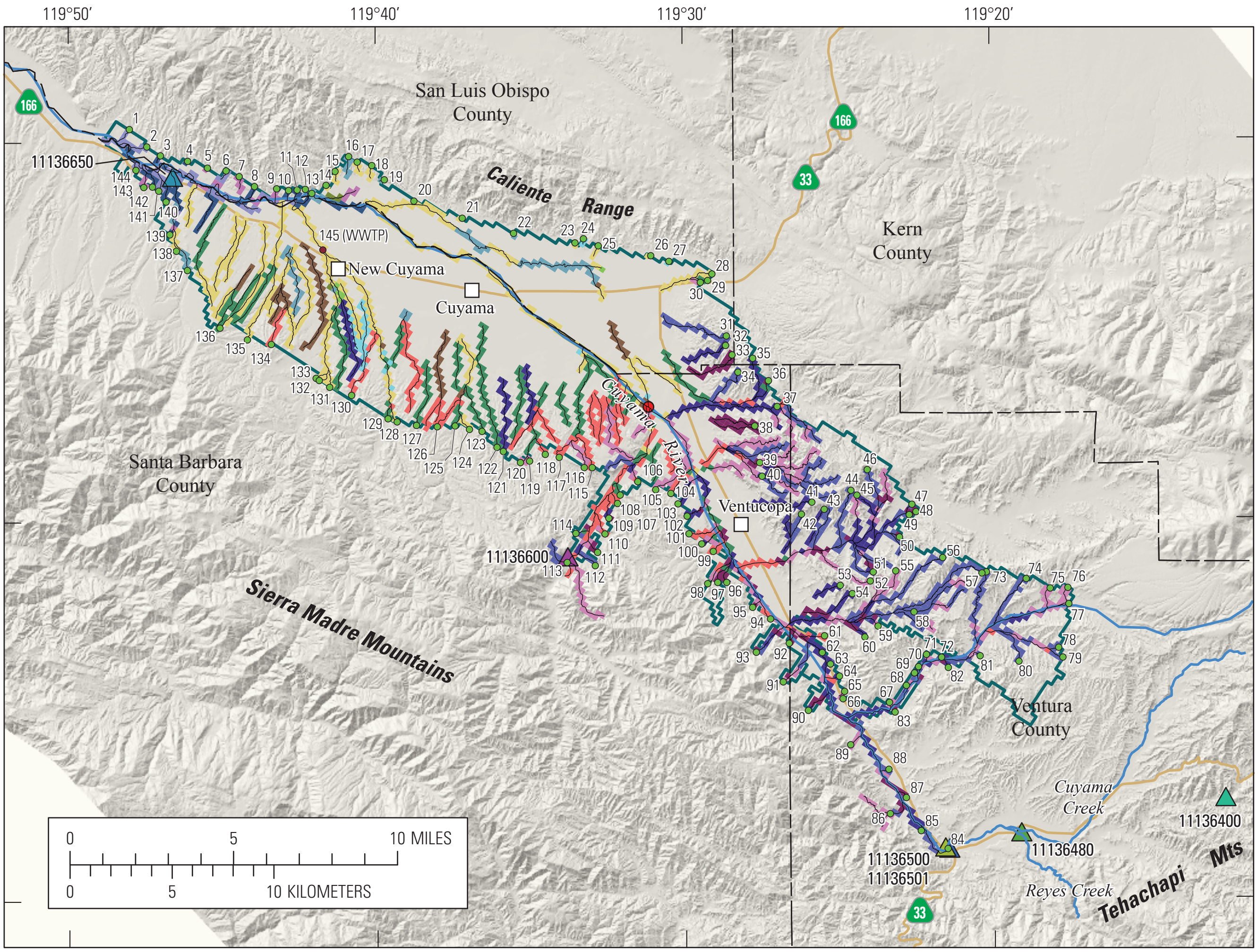

Shaded relief base created from 30-m digital elevation model from USGS National Elevation Dataset (NED); North America Vertical Datum 1983 (NAVD83). Hydrology sourced from 1:24,000-scale National Hydrography Dataset, 1974-2009. Place names sourced from USGS Geographic Names Information System, 1974-2009. Albers Projection, NAD83.

EXPLANATION

Active CUVHM model-grid boundary

Stream channel parameter names

Western zone
- QYA
- QYACC
- QOA

North Main zone
- QYA
- QYACC
- QOA

South Main zone
- QYA
- QYACC

Sierra Madre Foothills
- QOA-North
- QOA-Middle
- QOA-South

Ventucopa Uplands
- QYAUC
- QYACC
- QOA
- MOCU

QYA is Quaternary young alluvium
QOA is Quaternary older alluvium
MOUC is Morales unconfined
CC is Cuyama Channel
UC is unconfined

USGS stream gage and number
- Aliso Canyon Creek near New Cuyama—11136650
- Santa Barbara Canyon Creek near Ventucopa—11136600
- Cuyama River near Ventucopa—11136500
- Cuyama River near Ventucopa—11136501
- Reyes Creek near Ventucopa—11136480
- Wagon Road Creek near Stauffer—11136400

Diversion location

84 **Inflow points**—Numbers represent streamflow identifiers for inflow points for runoff from BCM model and from the Waste-water Treatment Plant (WWTP-145)

Figure 8. Distribution of streams with streamflow routing cells and segments, and location of inflows, Cuyama Valley, California.

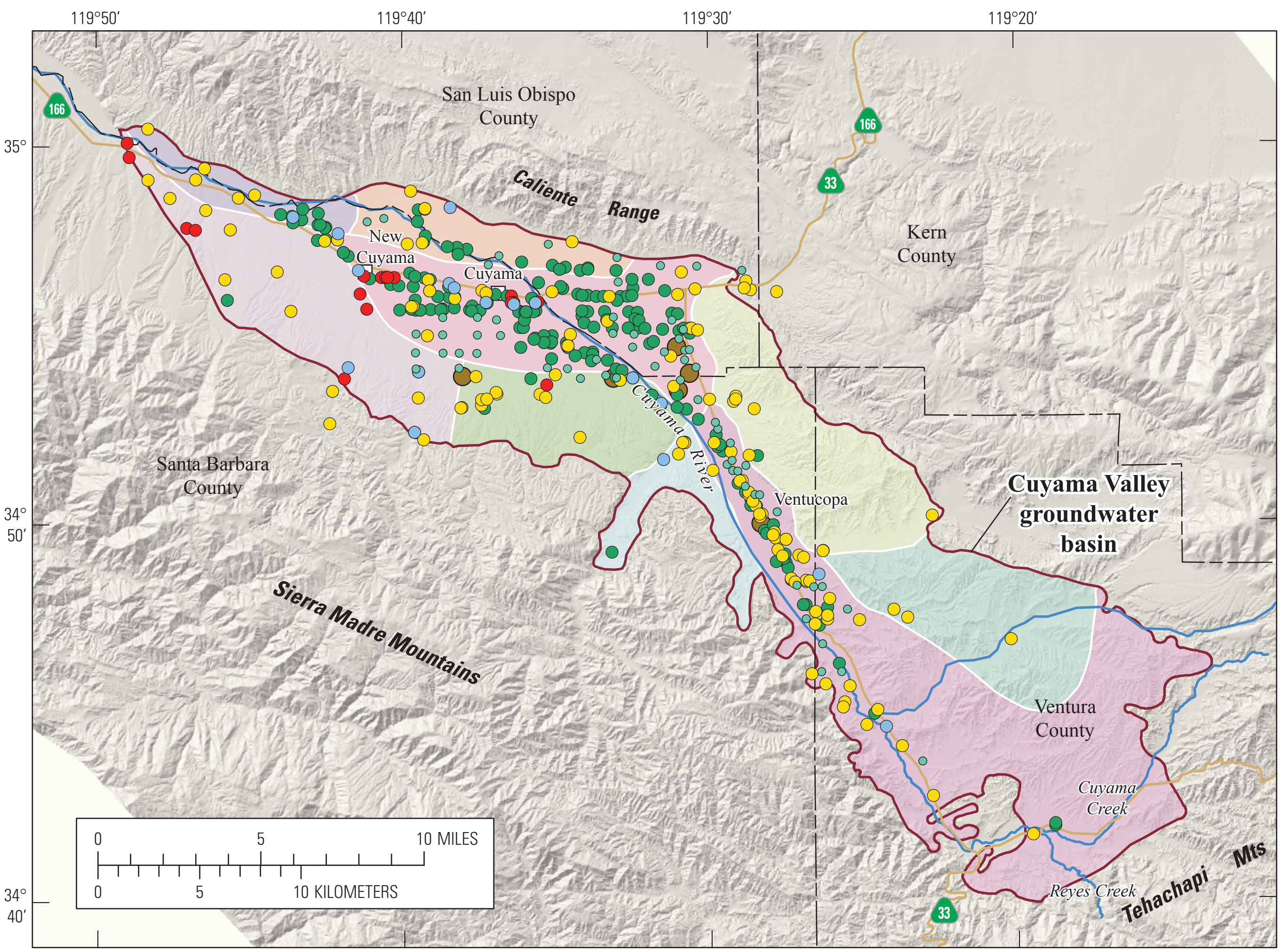

Shaded relief base created from 30-m digital elevation model from USGS National Elevation Dataset (NED); North America Vertical Datum 1983 (NAVD83). Hydrology sourced from 1:24,000-scale National Hydrography Dataset, 1974-2009. Place names sourced from USGS Geographic Names Information System, 1974-2009. Albers Projection, NAD83.

EXPLANATION

Cuyuma groundwater basin subregion

- Caliente Northern-Main
- Central Sierra Madre Foothills
- Northeast Ventucopa Uplands
- Northwestern Sierra Madre Foothills
- Northern Ventucopa Uplands
- Southern Sierra Madre Foothills
- Southern Ventucopa Uplands
- Southern-Main
- Western Basin

Well and type

- Agriculture
- Other agriculture
- Domestic
- Municipal and industrial
- Observation
- Virtual

Figure 9. Distribution of agricultural, urban-supply, and domestic wells, Cuyama Valley, California.

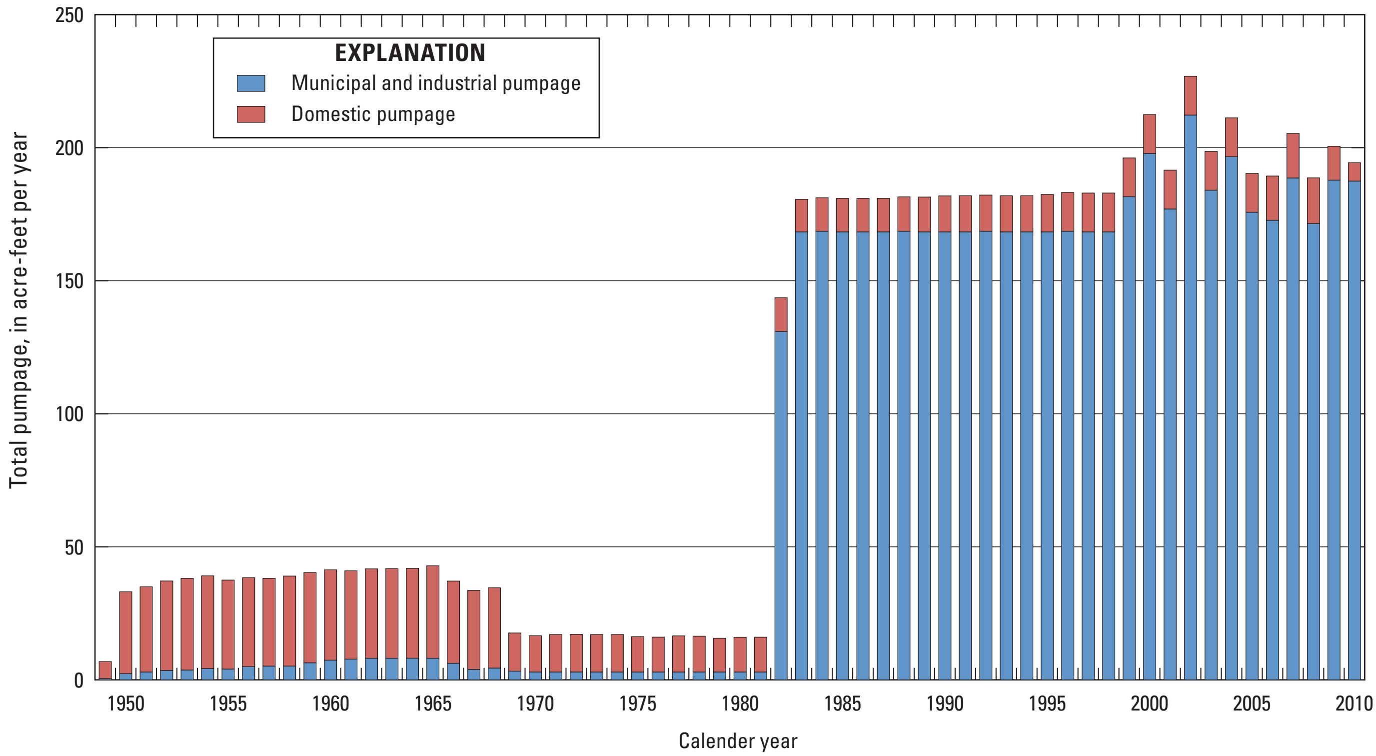

Figure 10. Estimated groundwater pumpage from municipal and domestic wells, Cuyama Valley, California.

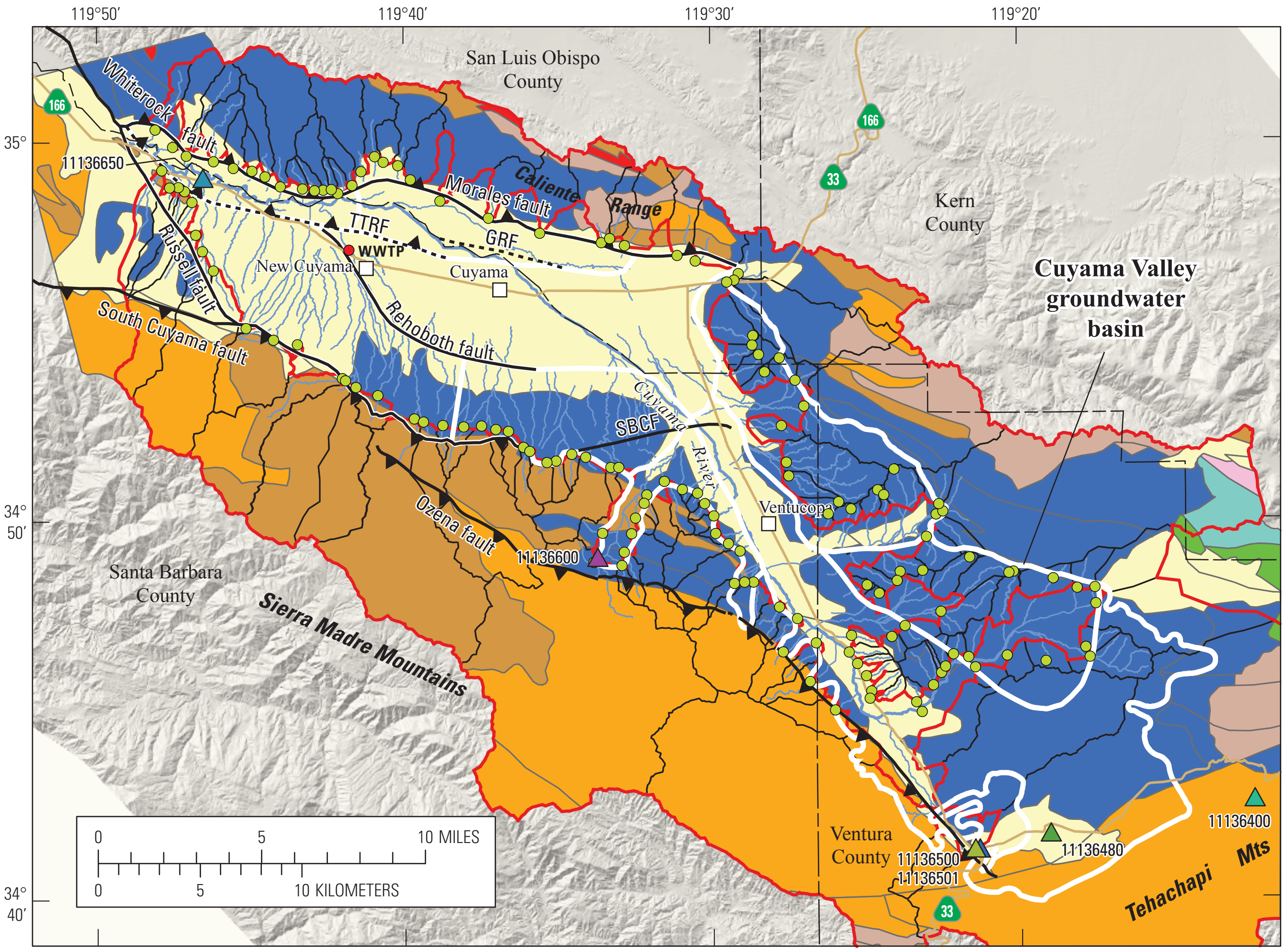

Shaded relief base created from 30-m digital elevation model from USGS National Elevation Dataset (NED); North America Vertical Datum 1983 (NAVD83). Hydrology sourced from 1:24,000-scale National Hydrography Dataset, 1974-2009. Place names sourced from USGS Geographic Names Information System, 1974-2009. Albers Projection, NAD83.

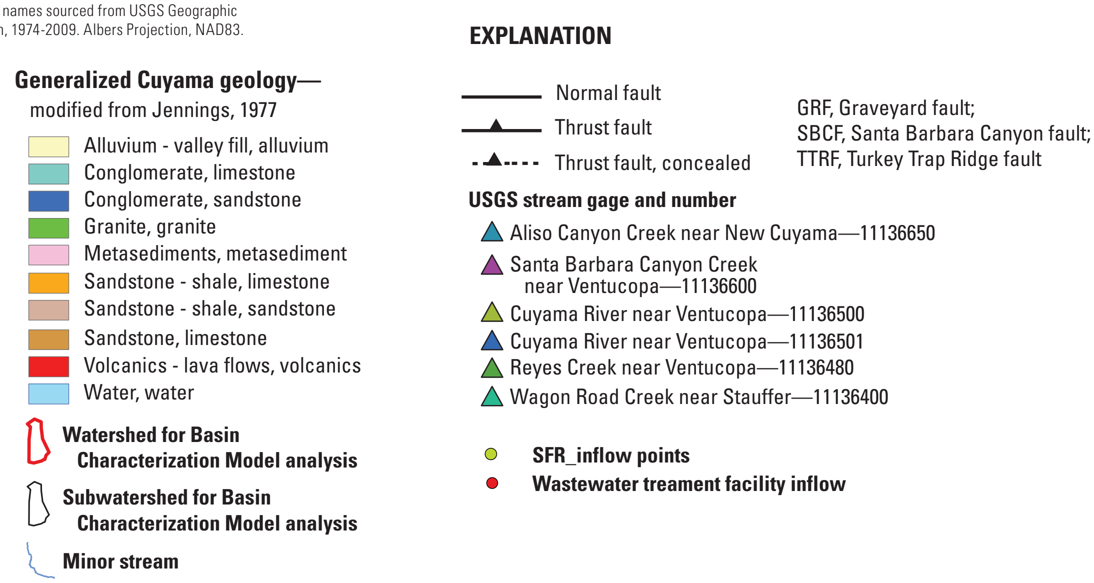

Figure 11. The generalized distribution of bedrock, subwatersheds and related inflow points used with the Basin Characterization Model (BCM) recharge-runoff estimates for Cuyama Valley.

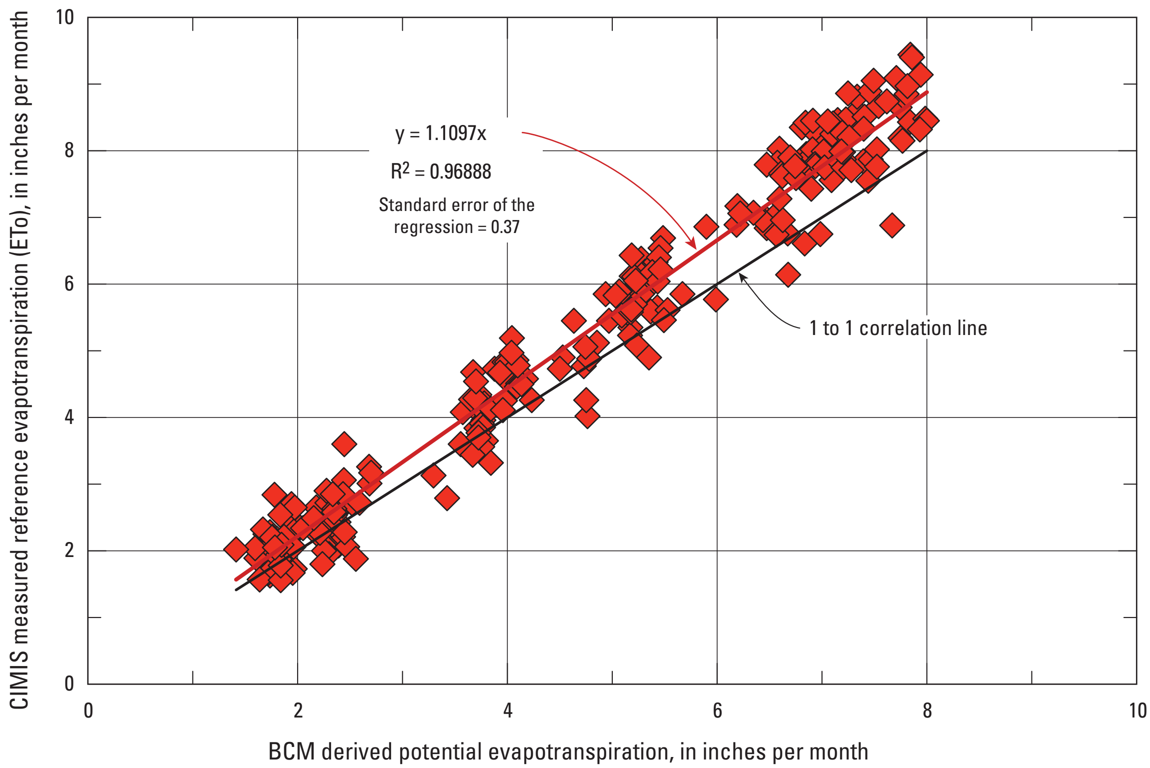

Figure 12. Comparison of Basic Characteristics Model (BCM) simulated potential evapotranspiration using the Priestley-Taylor approach with measured reference evapotranspiration (ET_o) from California Irrigation Management Information System (CIMIS) station in Cuyama Valley, California.

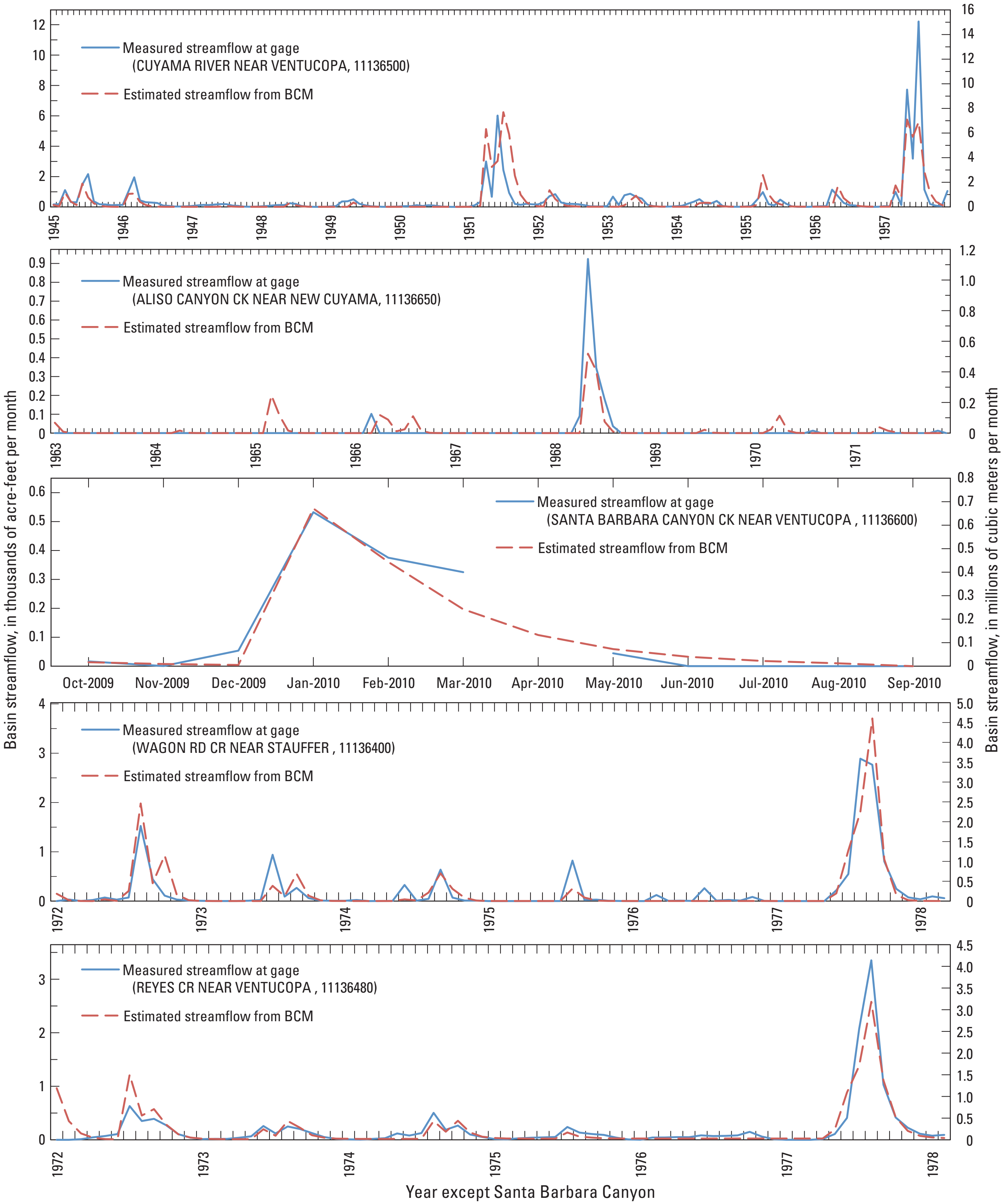

Figure 13. Comparisons of basin discharge, estimated by using the Basin Characterization Model (BCM), with measured streamflow for gaged basins in the Cuyama Valley model domain.

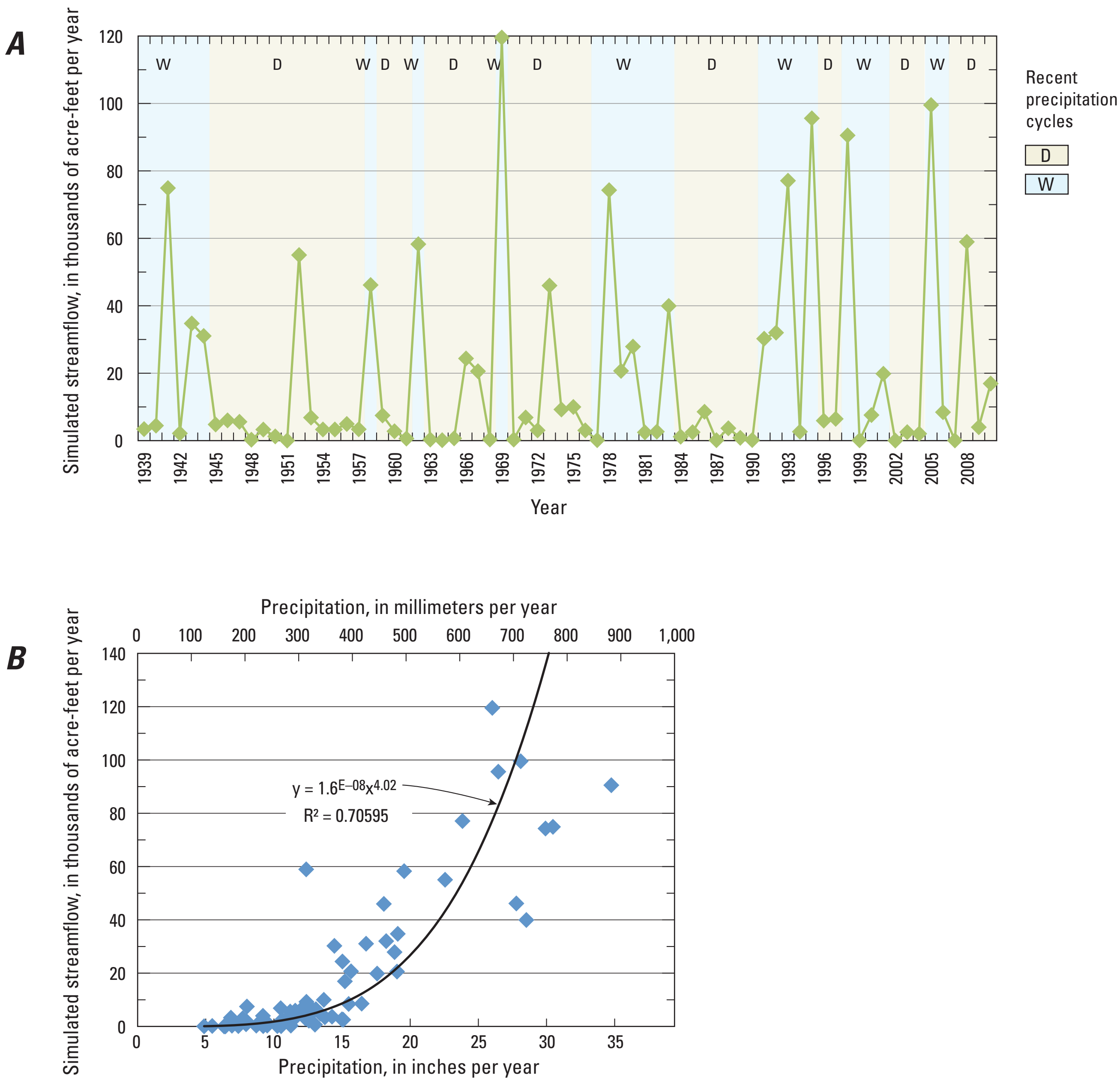

Figure 14. Annual streamflow for all Streamflow Routing (SFR) inflows in Cuyama Valley, California, *A*, for 1939–2009, and *B*, in comparison to precipitation.

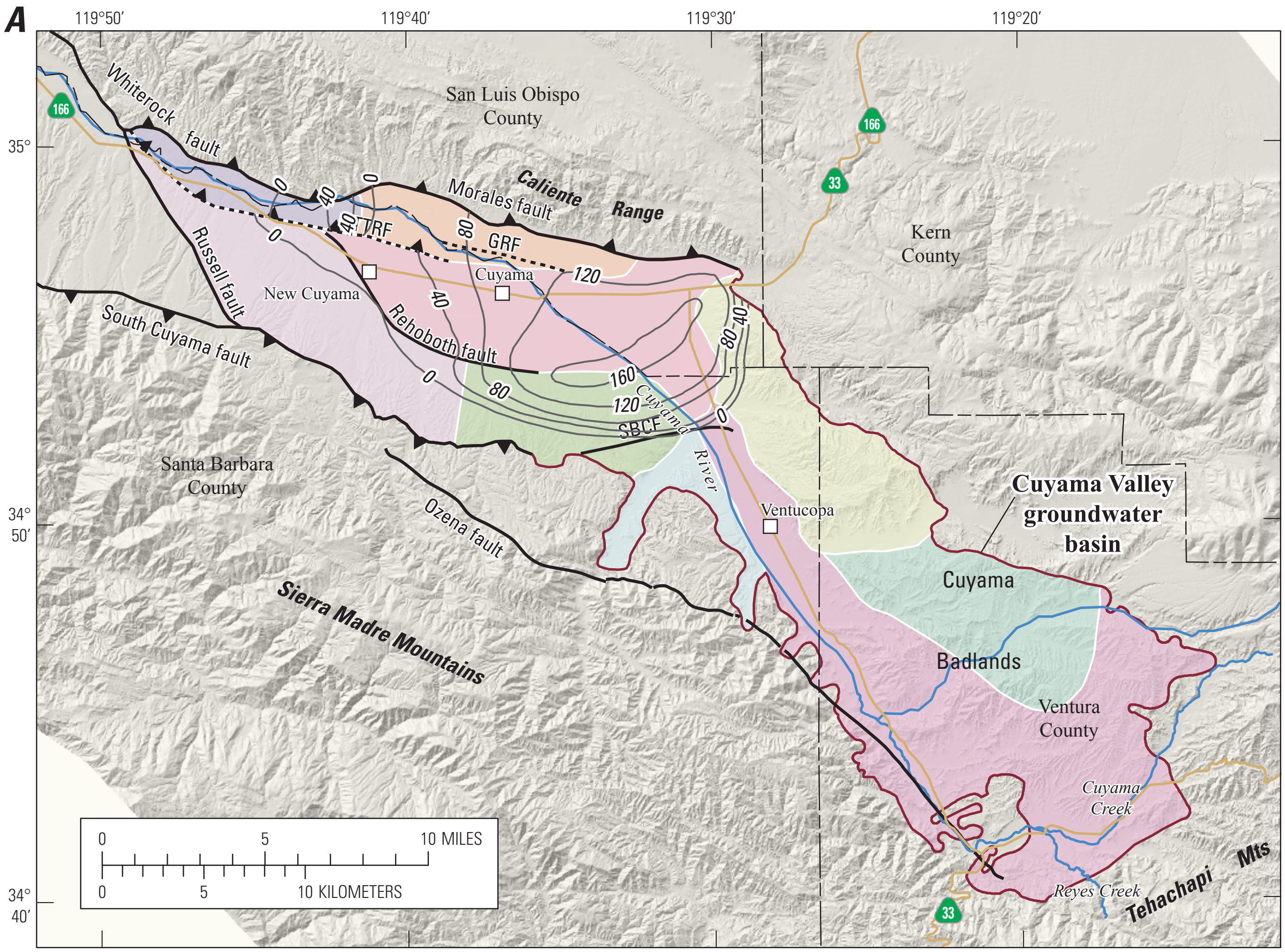

Shaded relief base created from 30-m digital elevation model from USGS National Elevation Dataset (NED); North America Vertical Datum 1983 (NAVD83). Hydrology sourced from 1:24,000-scale National Hydrography Dataset, 1974-2009. Place names sourced from USGS Geographic Names Information System, 1974-2009. Albers Projection, NAD83.

Modified from Singer and Swarzenski, 1970

EXPLANATION

Cuyuma groundwater basin subregion

- Caliente Northern-Main
- Central Sierra Madre Foothills
- Northeast Ventucopa Uplands
- Northwestern Sierra Madre Foothills
- Northern Ventucopa Uplands
- Southern Sierra Madre Foothills
- Southern Ventucopa Uplands
- Southern-Main
- Western Basin

Normal fault

Thrust fault

Thrust fault, concealed

GRF, Graveyard fault;
SBCF, Santa Barbara Canyon fault;
TTRF, Turkey Trap Ridge fault

160 **Estimated drawdown contour (1966–1947). Interval is 40 feet**

Figure 15. *A*, drawdown contours for 1947–66; and groundwater-level contours for *B*, summer 1966, *C*, spring 2010, and *D*, summer 2010 for Cuyama Valley, California.

B

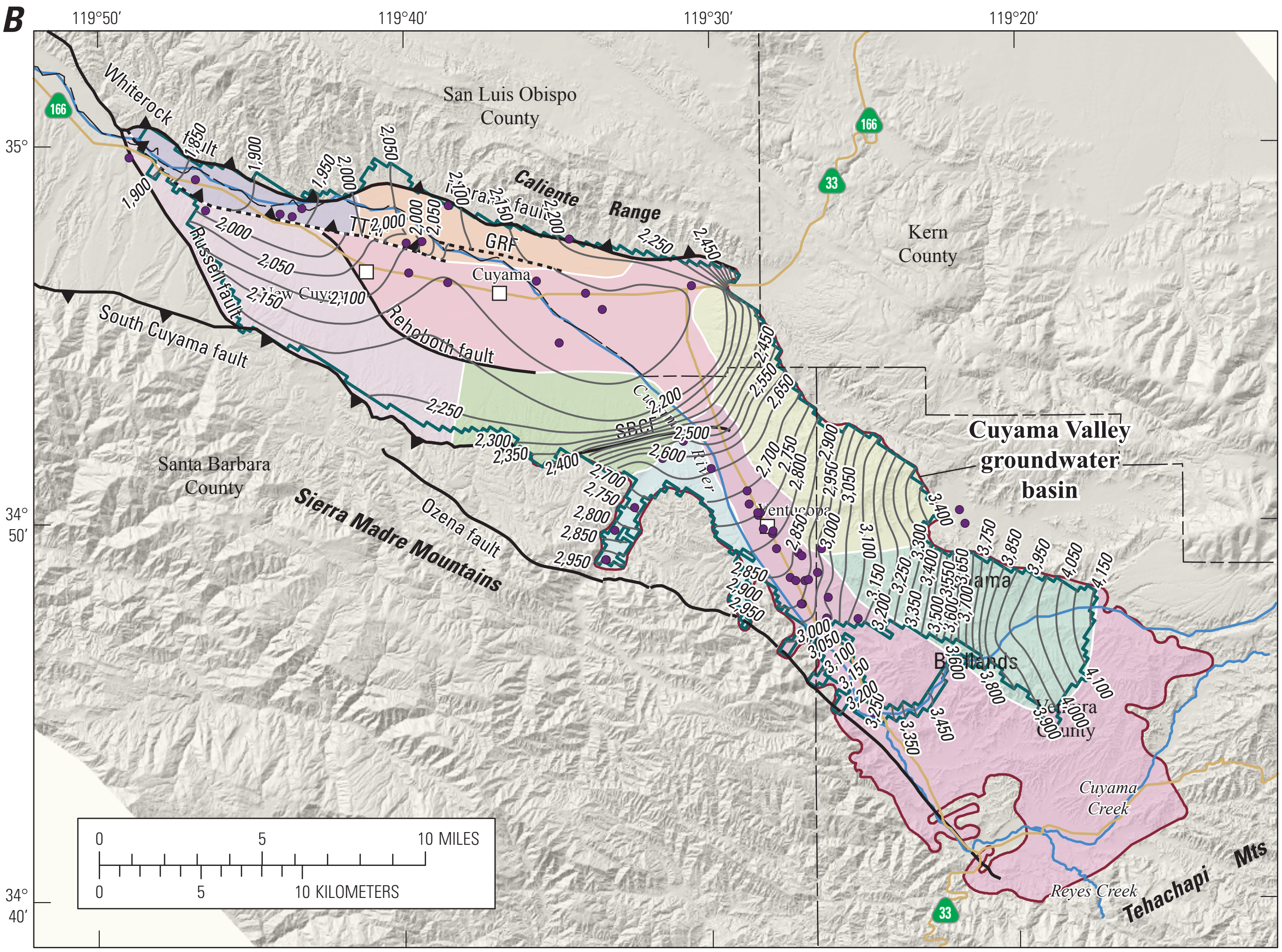

Shaded relief base created from 30-m digital elevation model from USGS National Elevation Dataset (NED); North America Vertical Datum 1983 (NAVD83). Hydrology sourced from 1:24,000-scale National Hydrography Dataset, 1974-2009. Place names sourced from USGS Geographic Names Information System, 1974-2009. Albers Projection, NAD83.

Modified from Singer and Swarzenski, 1970

EXPLANATION

Cuyuma groundwater basin subregion

- Caliente Northern-Main
- Central Sierra Madre Foothills
- Northeast Ventucopa Uplands
- Northwestern Sierra Madre Foothills
- Northern Ventucopa Uplands
- Southern Sierra Madre Foothills
- Southern Ventucopa Uplands
- Southern-Main
- Western Basin

Normal fault

Thrust fault

Thrust fault, concealed

GRF, Graveyard fault;
SBCF, Santa Barbara Canyon fault;
TTRF, Turkey Trap Ridge fault

Active model-grid boundary

2,250 **Water-level altitude, summer 1966 ; interval is 50 feet**

Control point

Figure 15. —Continued

C

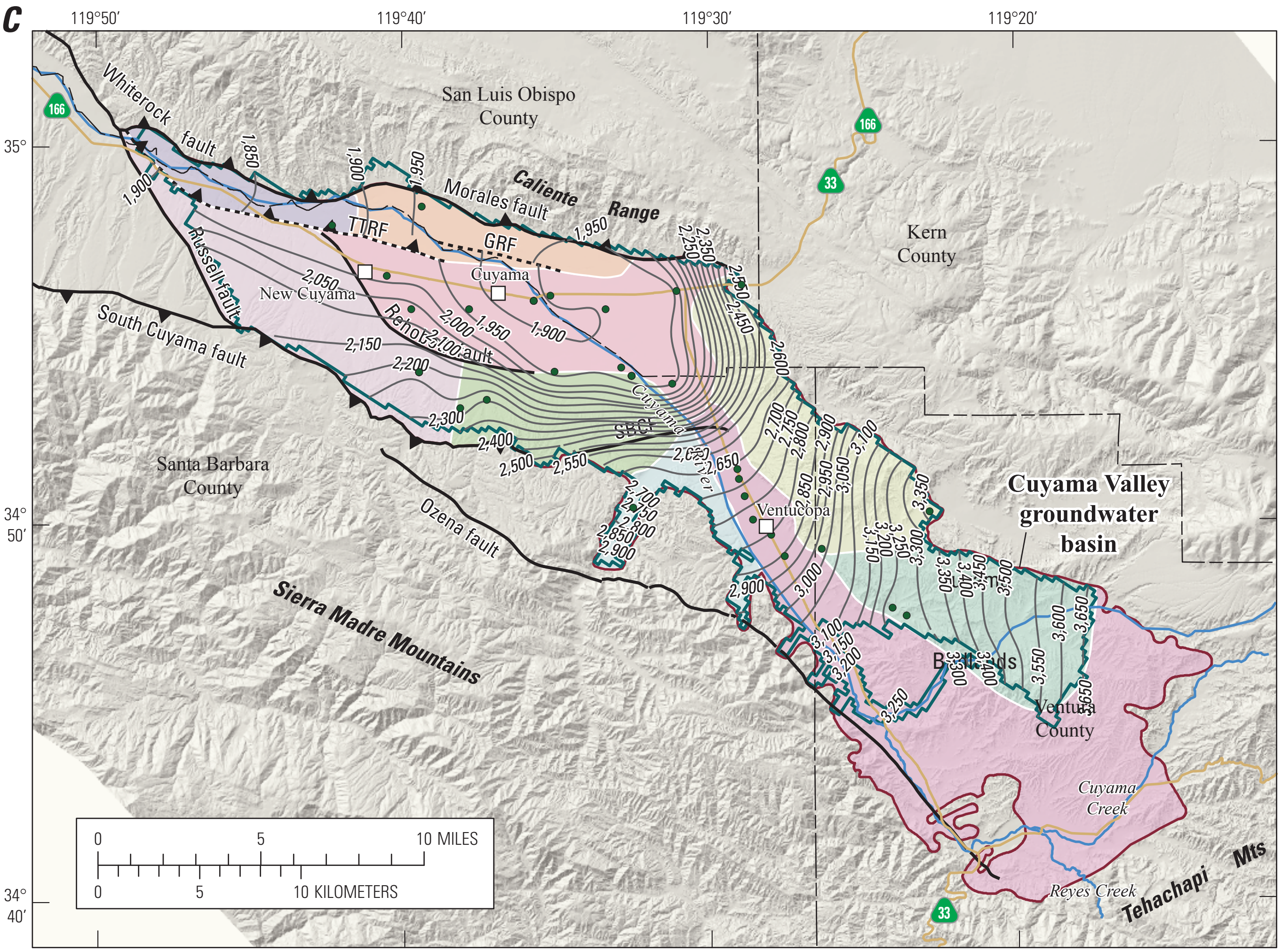

Shaded relief base created from 30-m digital elevation model from USGS National Elevation Dataset (NED); North America Vertical Datum 1983 (NAVD83). Hydrology sourced from 1:24,000-scale National Hydrography Dataset, 1974-2009. Place names sourced from USGS Geographic Names Information System, 1974-2009. Albers Projection, NAD83.

EXPLANATION

Cuyuma groundwater basin subregion

- Caliente Northern-Main
- Central Sierra Madre Foothills
- Northeast Ventucopa Uplands
- Northwestern Sierra Madre Foothills
- Northern Ventucopa Uplands
- Southern Sierra Madre Foothills
- Southern Ventucopa Uplands
- Southern-Main
- Western Basin

Normal fault

Thrust fault

Thrust fault, concealed

GRF, Graveyard fault;
SBCF, Santa Barbara Canyon fault;
TTRF, Turkey Trap Ridge fault

Active model-grid boundary

2,250 **Water-level altitude, spring 2010; interval is 50 feet**

Control point

Figure 15. —Continued

D

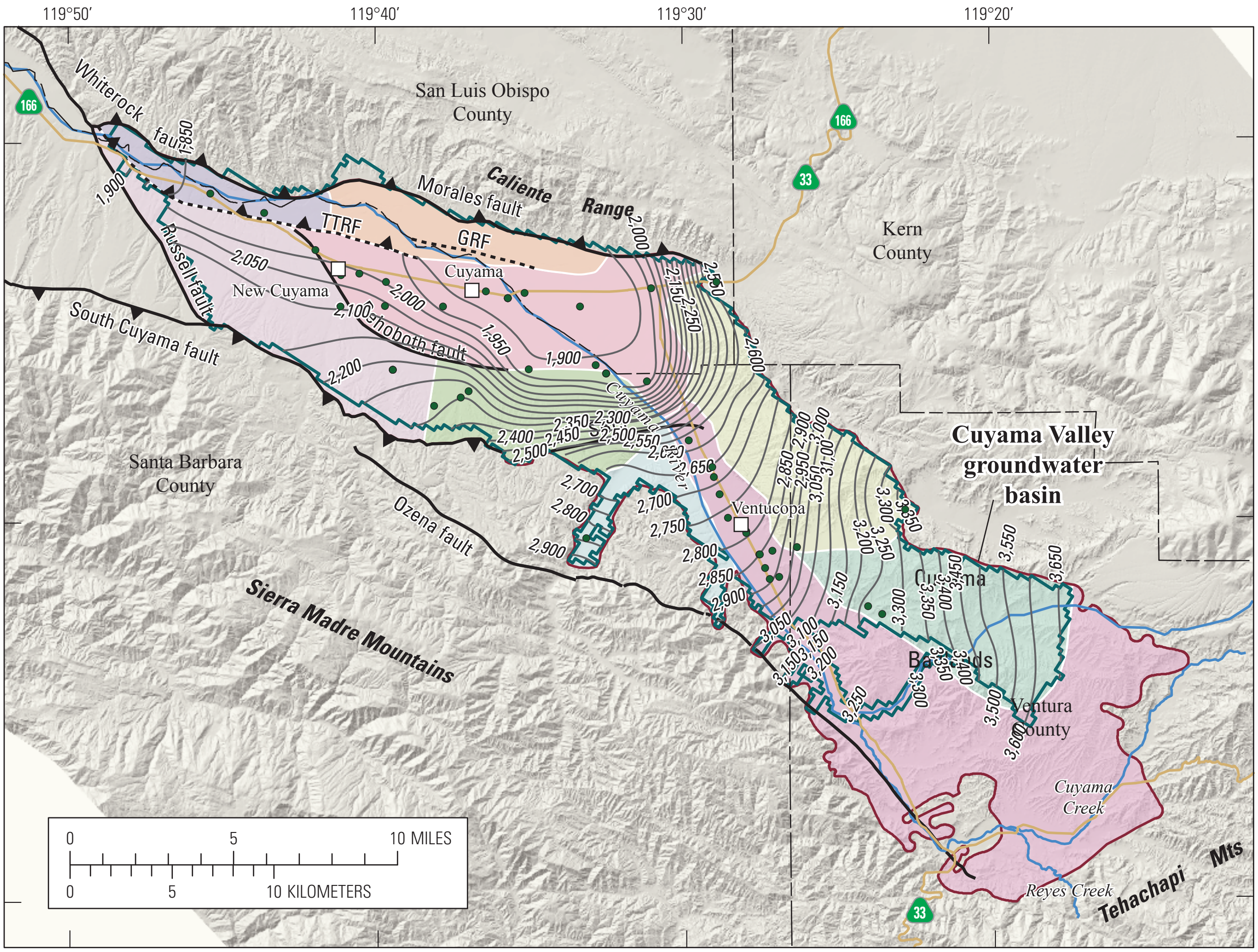

Shaded relief base created from 30-m digital elevation model from USGS National Elevation Dataset (NED); North America Vertical Datum 1983 (NAVD83). Hydrology sourced from 1:24,000-scale National Hydrography Dataset, 1974-2009. Place names sourced from USGS Geographic Names Information System, 1974-2009. Albers Projection, NAD83.

EXPLANATION

Cuyuma groundwater basin subregion

- Caliente Northern-Main
- Central Sierra Madre Foothills
- Northeast Ventucopa Uplands
- Northwestern Sierra Madre Foothills
- Northern Ventucopa Uplands
- Southern Sierra Madre Foothills
- Southern Ventucopa Uplands
- Southern-Main
- Western Basin

Normal fault

Thrust fault

Thrust fault, concealed

GRF, Graveyard fault;
SBCF, Santa Barbara Canyon fault;
TTRF, Turkey Trap Ridge fault

Active model-grid boundary

2,250 **Water-level altitude, summer 2010; interval is 50 feet**

Control point

Figure 15. —Continued

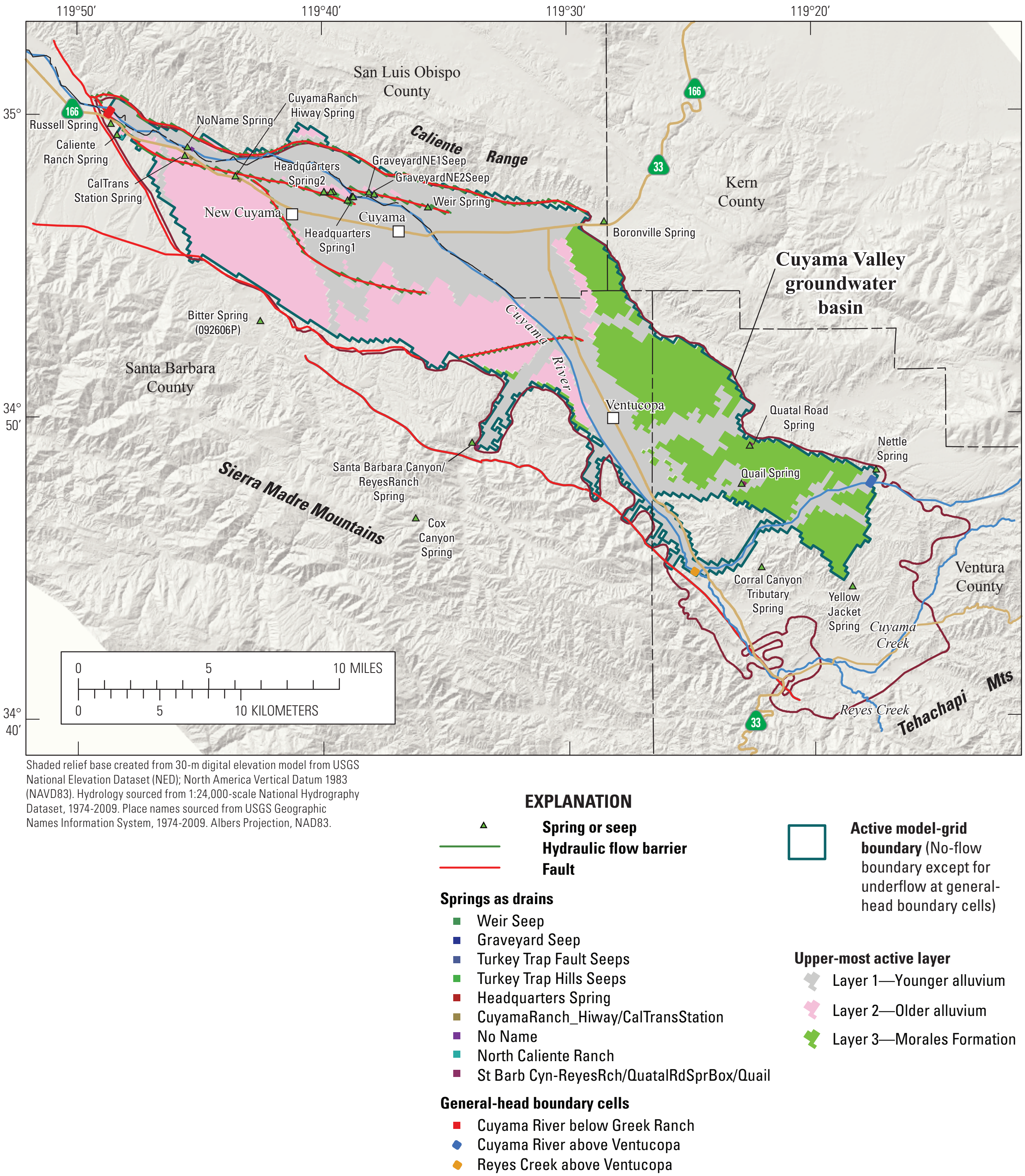

Shaded relief base created from 30-m digital elevation model from USGS National Elevation Dataset (NED); North America Vertical Datum 1983 (NAVD83). Hydrology sourced from 1:24,000-scale National Hydrography Dataset, 1974-2009. Place names sourced from USGS Geographic Names Information System, 1974-2009. Albers Projection, NAD83.

Figure 16. Distribution of model cells representing no-flow, groundwater underflow, springs, streams, and horizontal groundwater flow barrier boundaries in the Cuyama Valley, California.

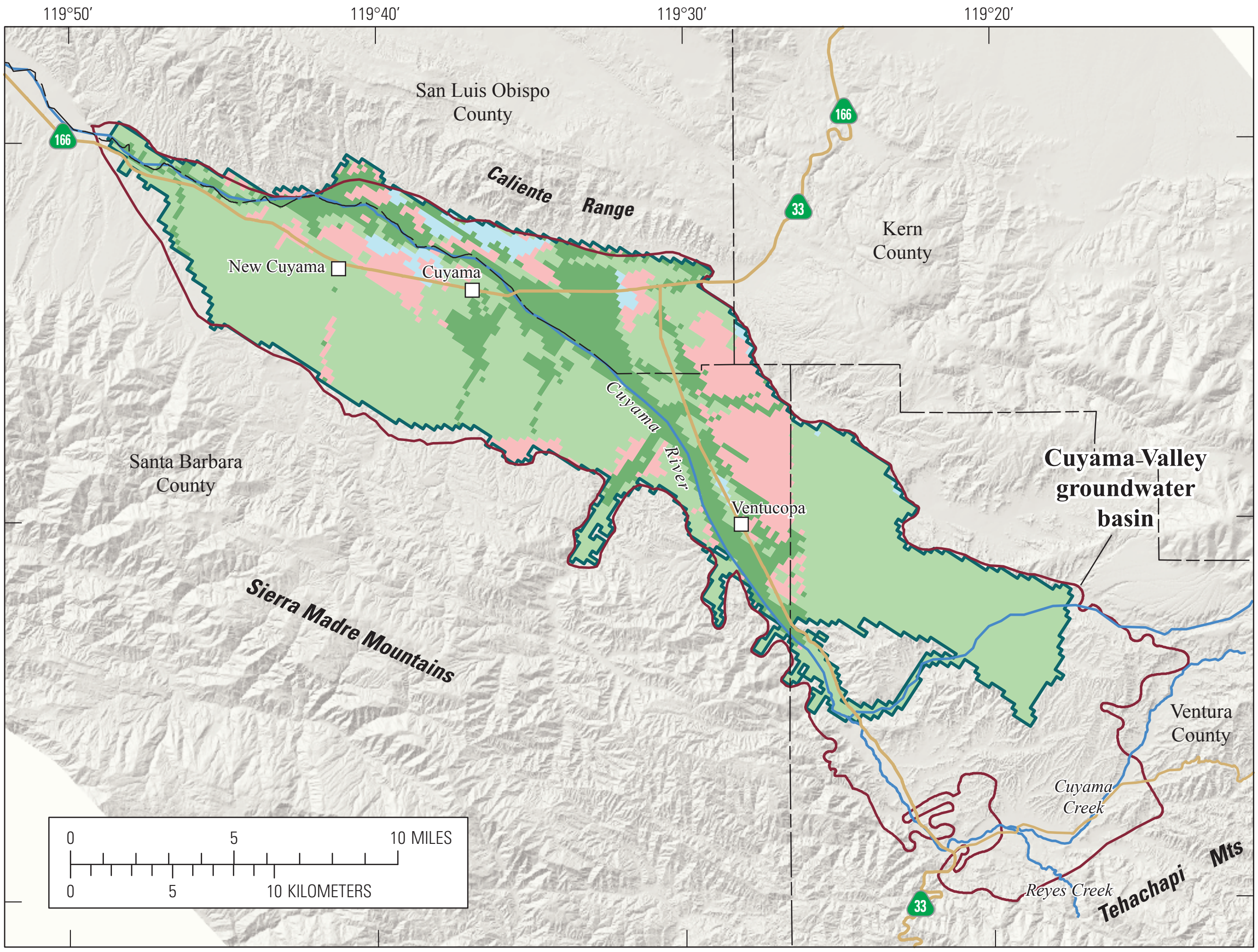

Shaded relief base created from 30-m digital elevation model from USGS National Elevation Dataset (NED); North America Vertical Datum 1983 (NAVD83). Hydrology sourced from 1:24,000-scale National Hydrography Dataset, 1974-2009. Place names sourced from USGS Geographic Names Information System, 1974-2009. Albers Projection, NAD83.

EXPLANATION

CUVHM model grid soil texture and (capillary fringe)

- Silty clay (4.9 feet)
- Sandy loam (2.5 feet)
- Silt (3.3 feet)
- Sand (1.6 feet)

Active model-grid boundary

Figure 17. Agricultural soils for the Cuyama Valley simplified from Soil Survey Geographic Database (SSURGO) (U.S. Department of Agriculture Natural Resources Conservation Service, 2005).

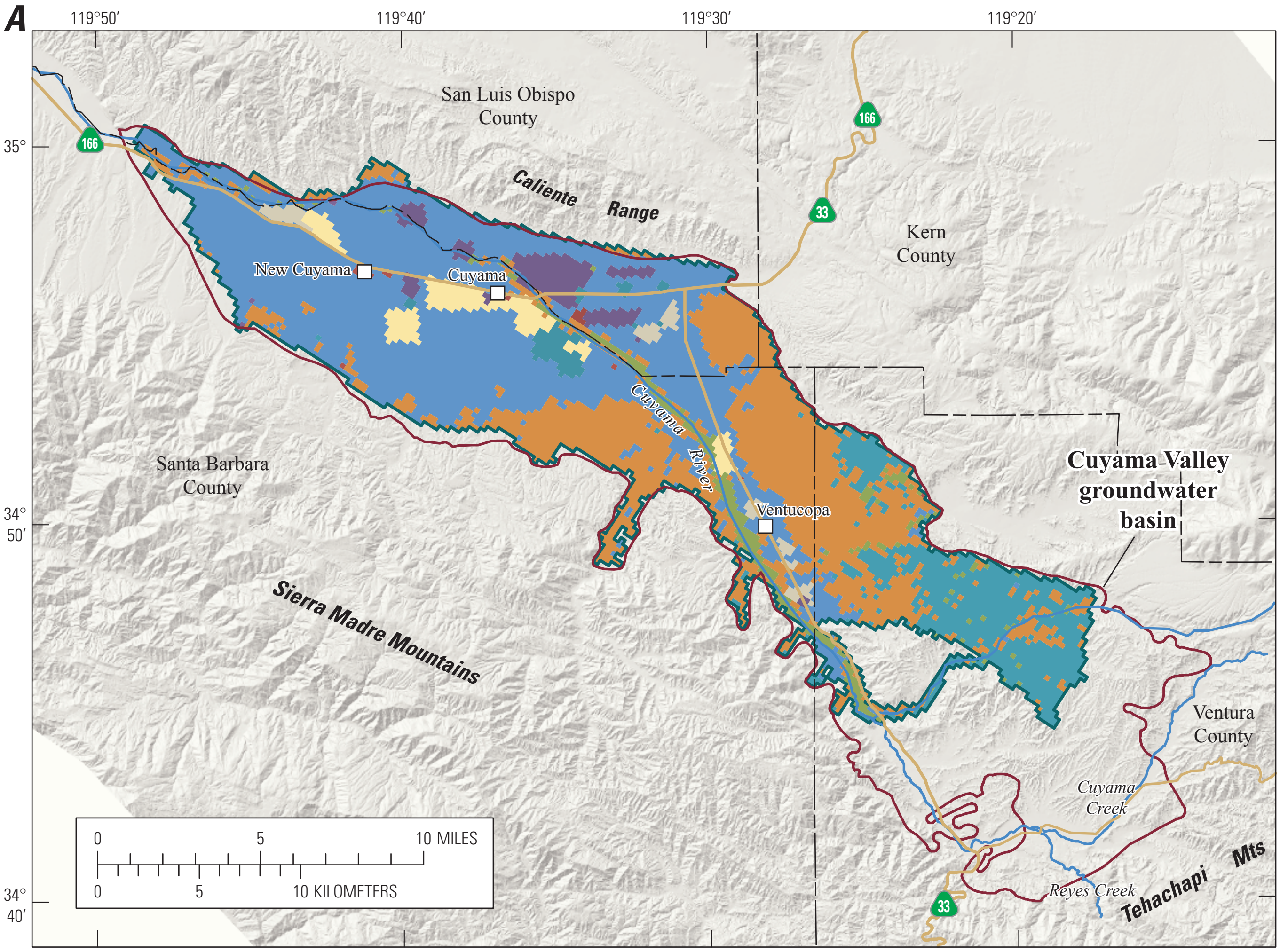

Shaded relief base created from 30-m digital elevation model from USGS National Elevation Dataset (NED); North America Vertical Datum 1983 (NAVD83). Hydrology sourced from 1:24,000-scale National Hydrography Dataset, 1974-2009. Place names sourced from USGS Geographic Names Information System, 1974-2009. Albers Projection, NAD83.

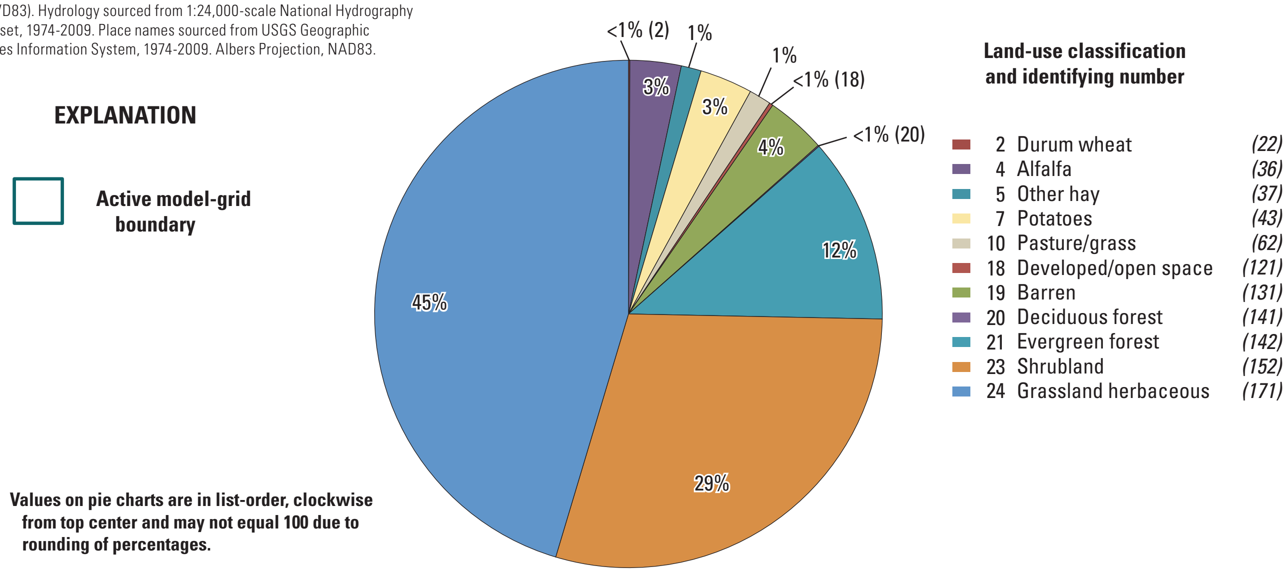

Figure 18. Early periods of land-use (virtual crop) groups discretized to the model grid, and pie chart of percentages of total land use over the modeled area for *A*, 1952; *B*, 1959; *C*, 1966; and *D*, 1977 for Cuyama Valley, California.

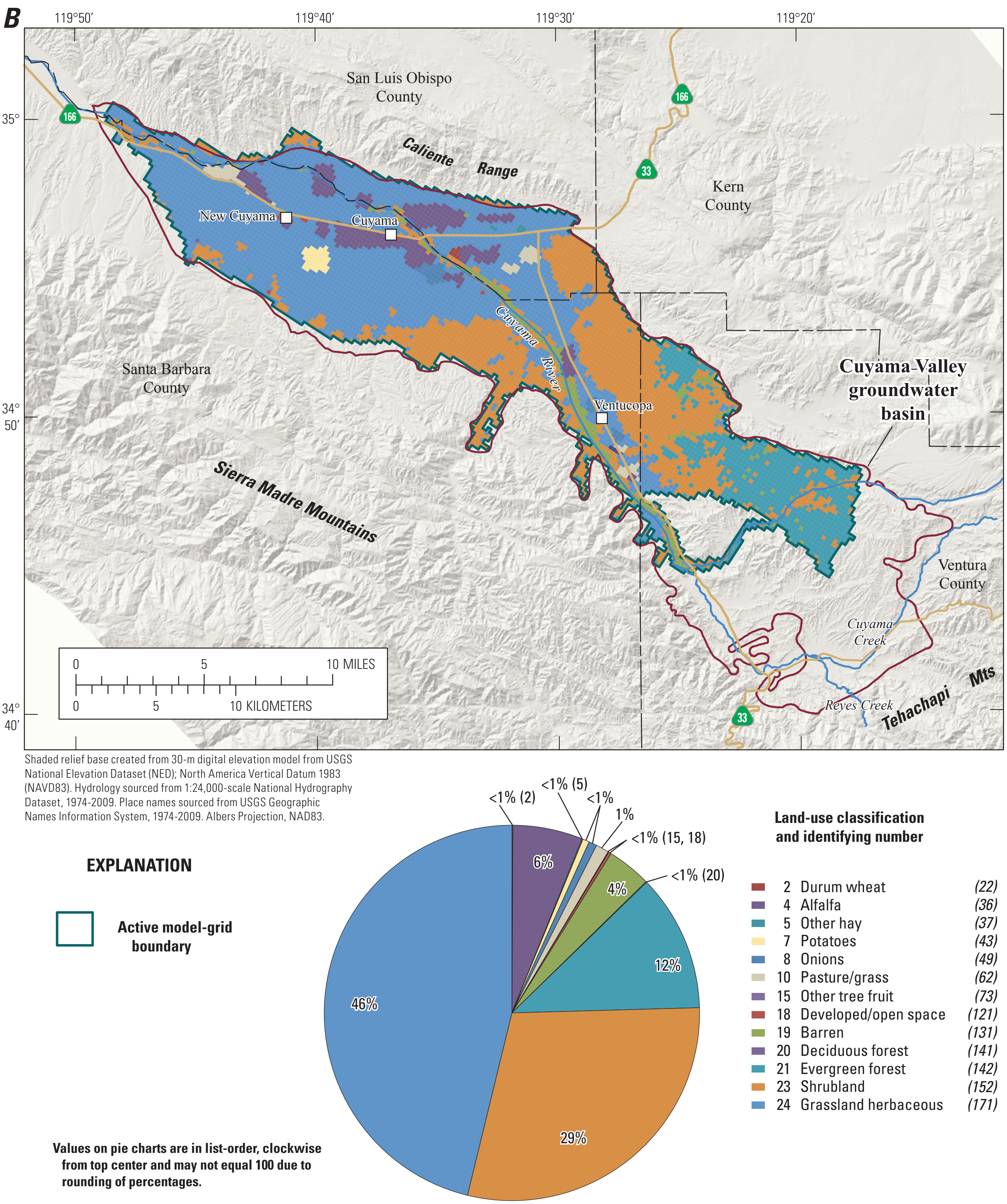

Figure 18. —Continued

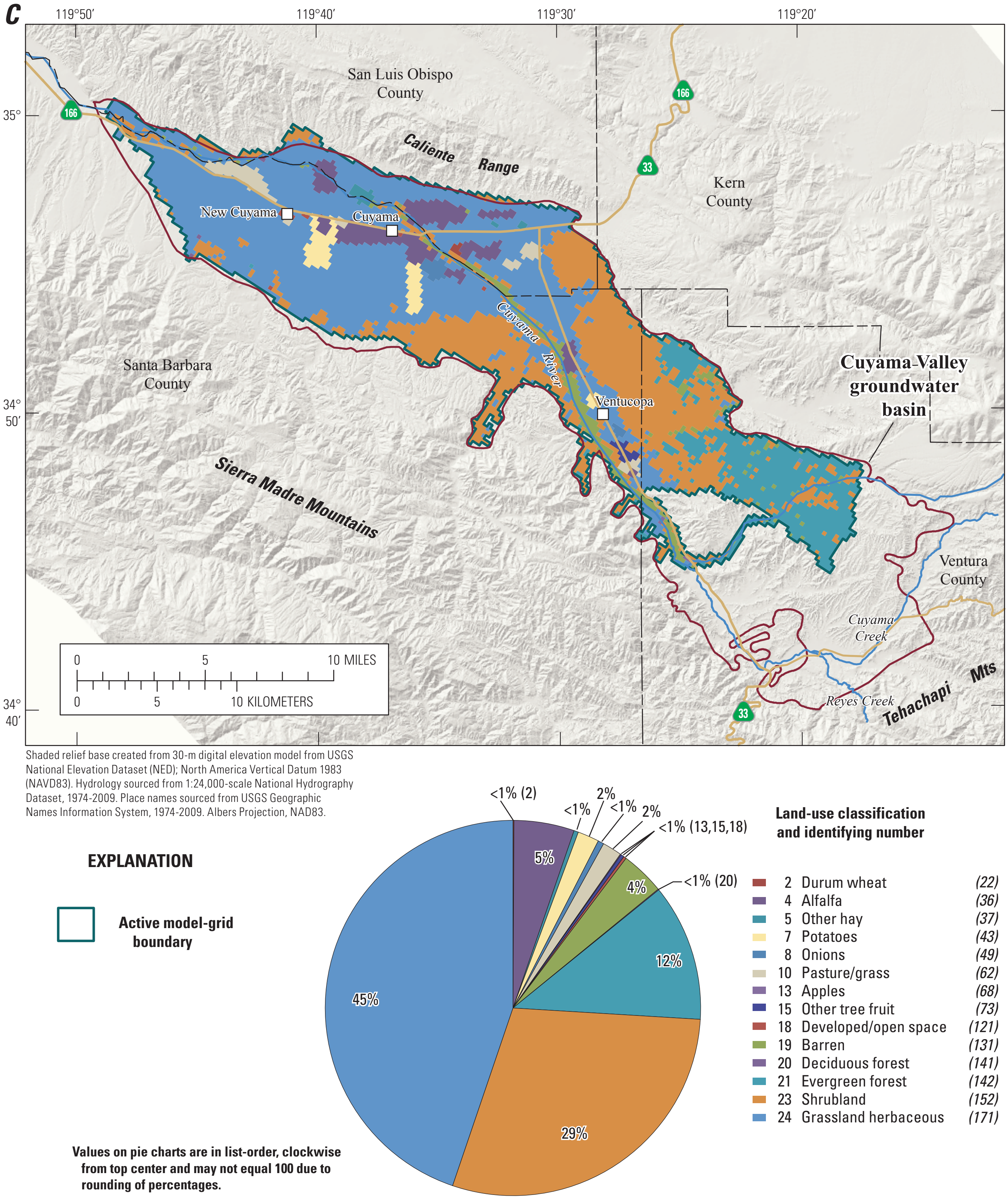

Figure 18. —Continued

D

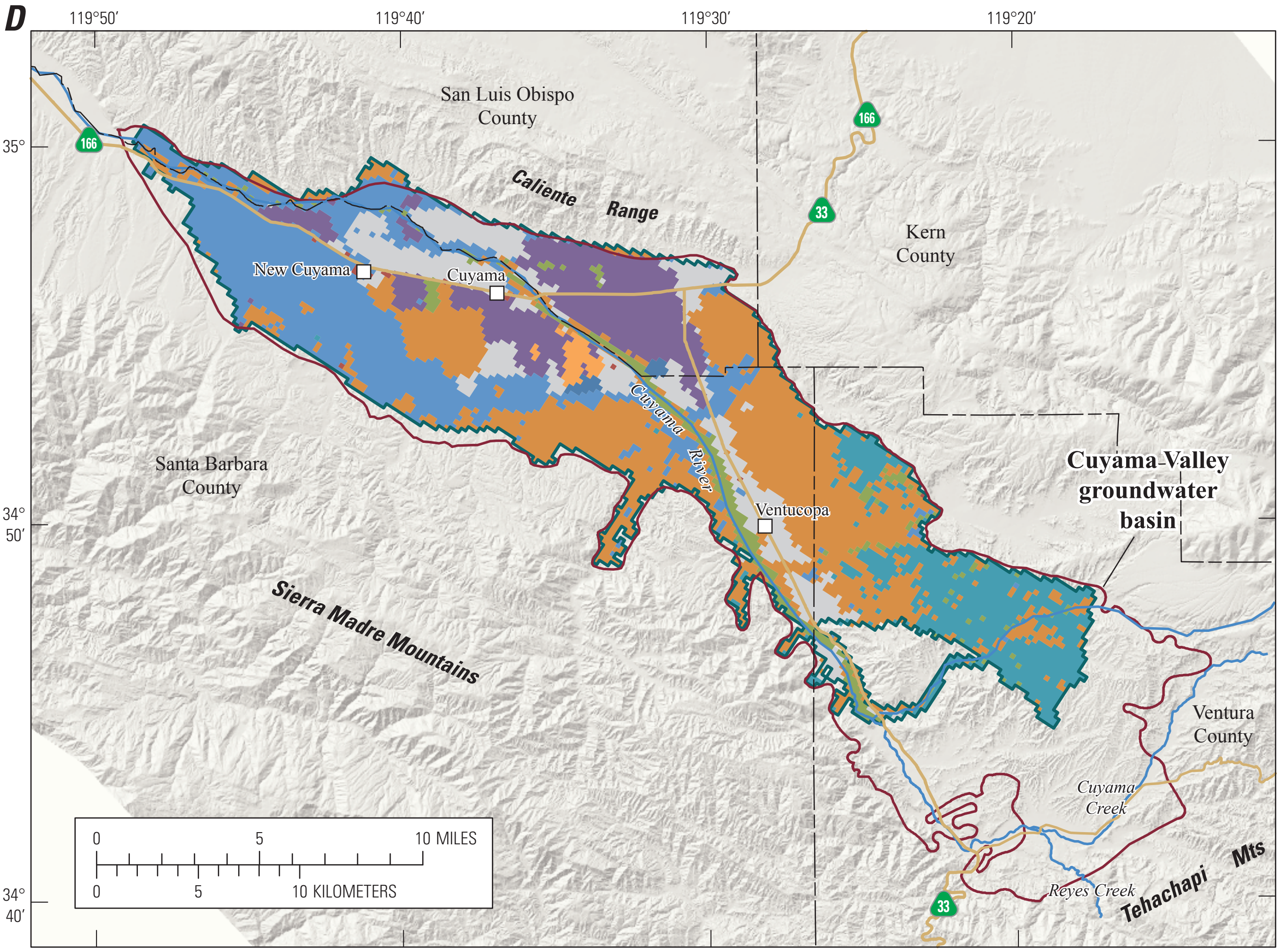

Shaded relief base created from 30-m digital elevation model from USGS National Elevation Dataset (NED); North America Vertical Datum 1983 (NAVD83). Hydrology sourced from 1:24,000-scale National Hydrography Dataset, 1974-2009. Place names sourced from USGS Geographic Names Information System, 1974-2009. Albers Projection, NAD83.

EXPLANATION

Active model-grid boundary

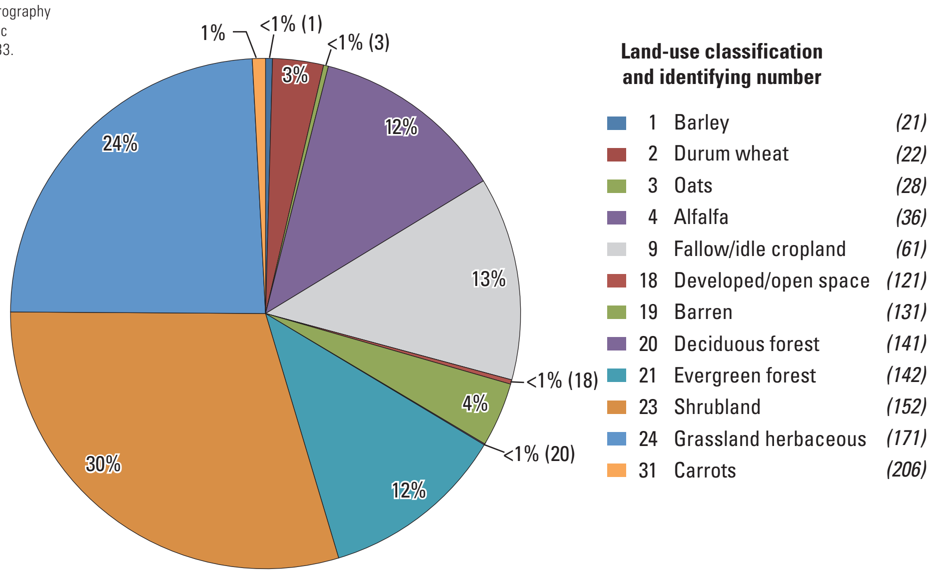

Values on pie charts are in list-order, clockwise from top center and may not equal 100 due to rounding of percentages.

Figure 18. —Continued

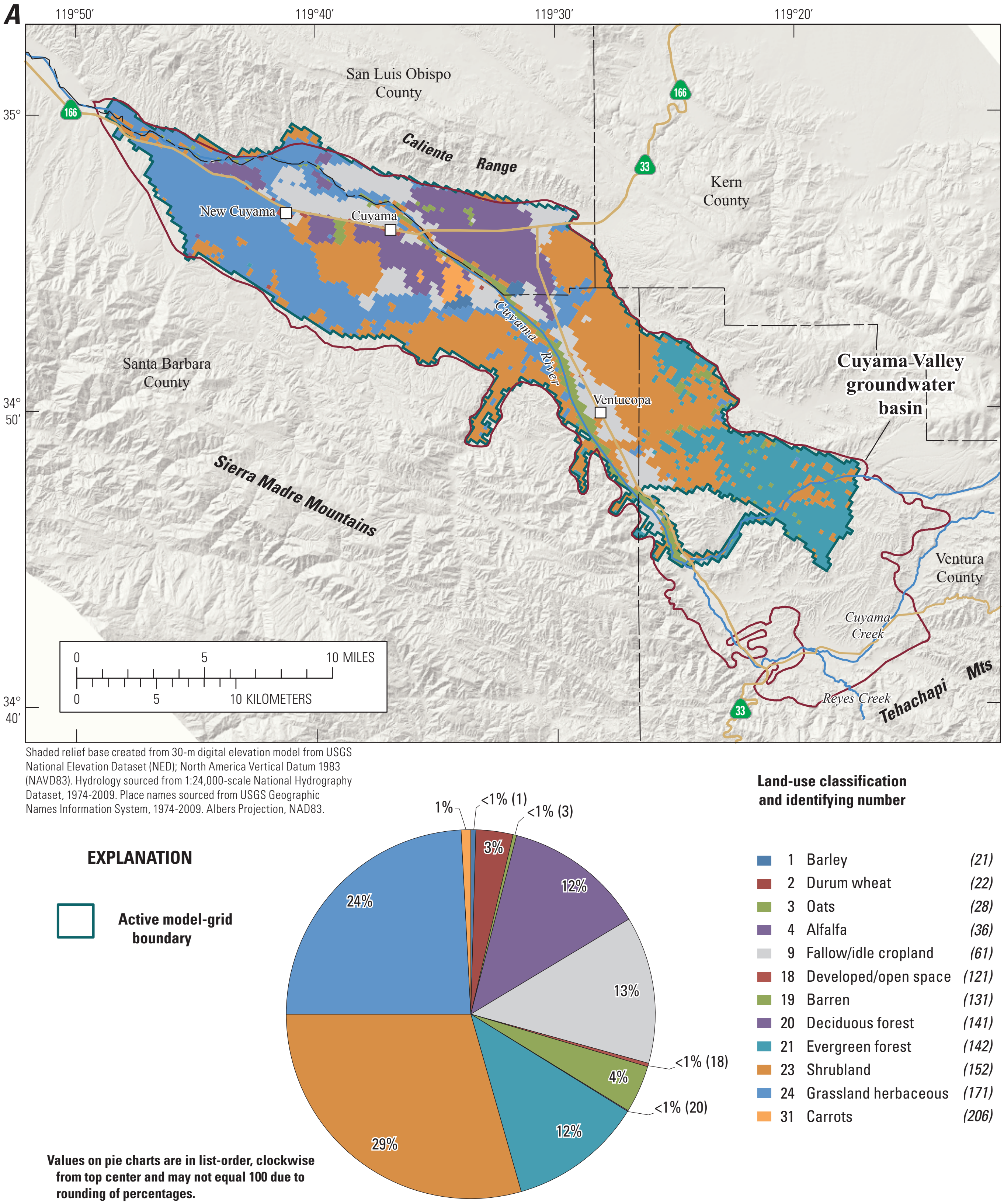

Figure 19. Land-use (virtual crop) groups discretized to the model grid, and pie chart of percentages of total land use over the modeled area for *A*, 1984; *B*, 2000; and *C*, 2002 for Cuyama Valley, California.

B

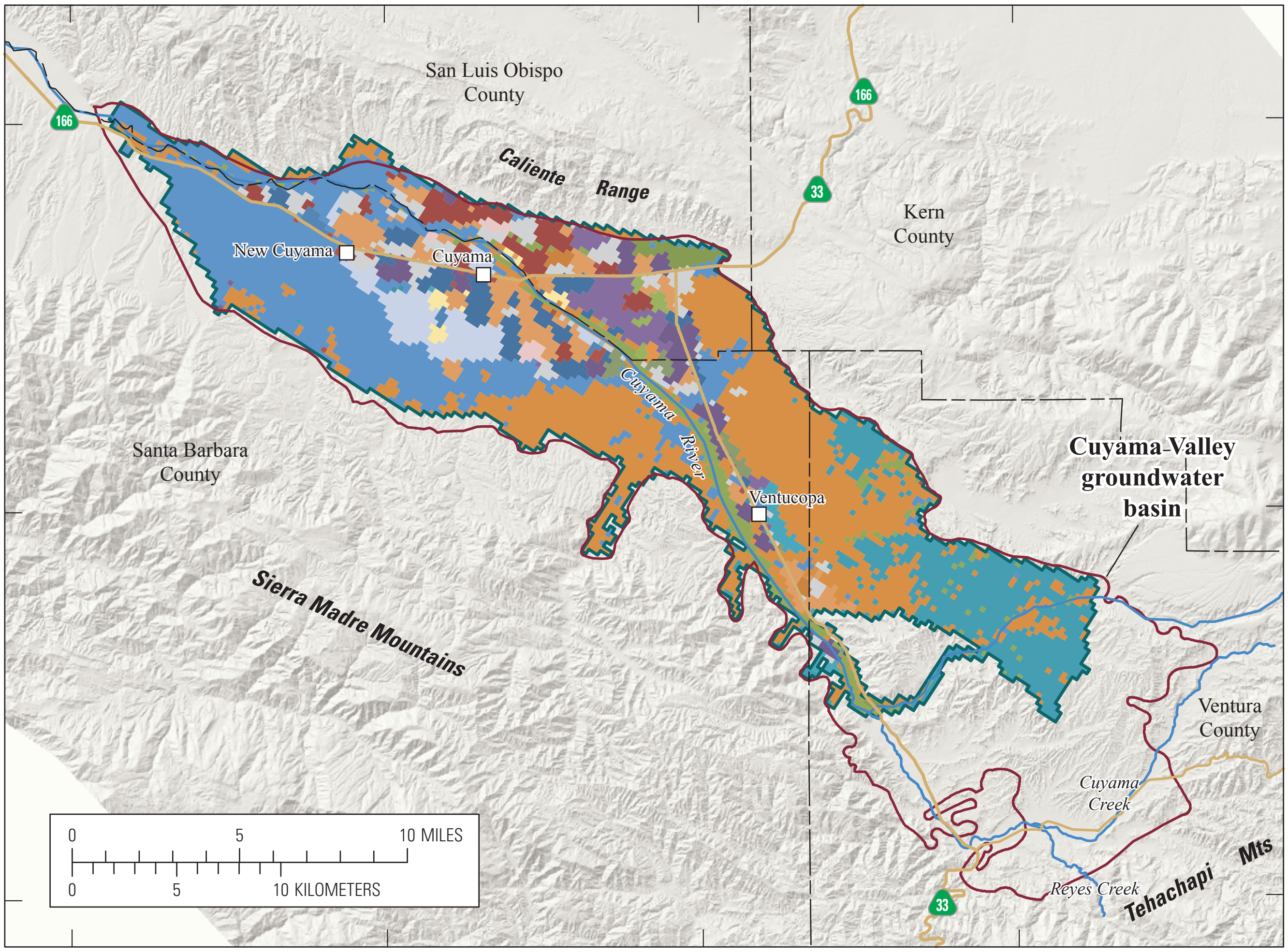

Shaded relief base created from 30-m digital elevation model from USGS National Elevation Dataset (NED); North America Vertical Datum 1983 (NAVD83). Hydrology sourced from 1:24,000-scale National Hydrography Dataset, 1974-2009. Place names sourced from USGS Geographic Names Information System, 1974-2009. Albers Projection, NAD83.

EXPLANATION

Active model-grid boundary

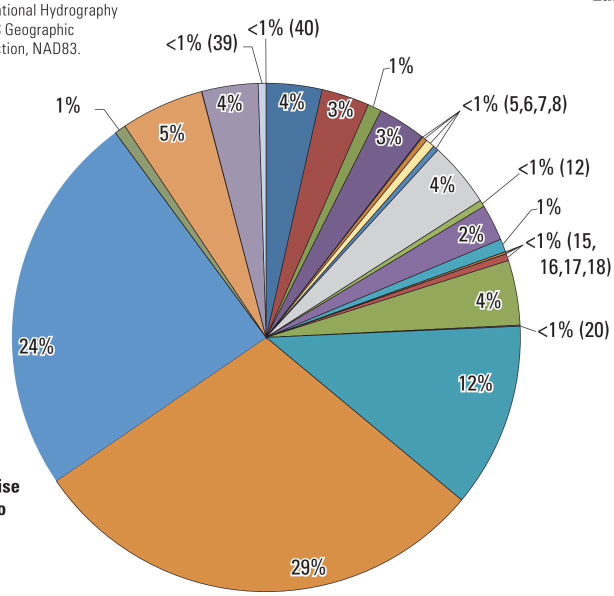

Values on pie charts are in list-order, clockwise from top center and may not equal 100 due to rounding of percentages.

Land-use classification and identifying number

1	Barley	*(21)*
2	Durum wheat	*(22)*
3	Oats	*(28)*
4	Alfalfa	*(36)*
5	Other hay	*(37)*
6	Dry beans	*(42)*
7	Potatoes	*(43)*
8	Onions	*(49)*
9	Fallow/idle cropland	*(61)*
12	Peaches	*(67)*
13	Apples	*(68)*
14	Grapes, wine vinyards	*(69)*
15	Other tree fruit	*(73)*
16	Walnuts	*(76)*
17	Open water	*(111)*
18	Developed/open space	*(121)*
19	Barren	*(131)*
20	Deciduous forest	*(141)*
21	Evergreen forest	*(142)*
23	Shrubland	*(152)*
24	Grassland herbaceous	*(171)*
30	Pistachios	*(204)*
31	Carrots	*(206)*
35	Nectarines	*(218)*
39	Irrigated field crops	*(258)*
40	Irrigated row vegetables crop	*(259)*

Figure 19. —Continued

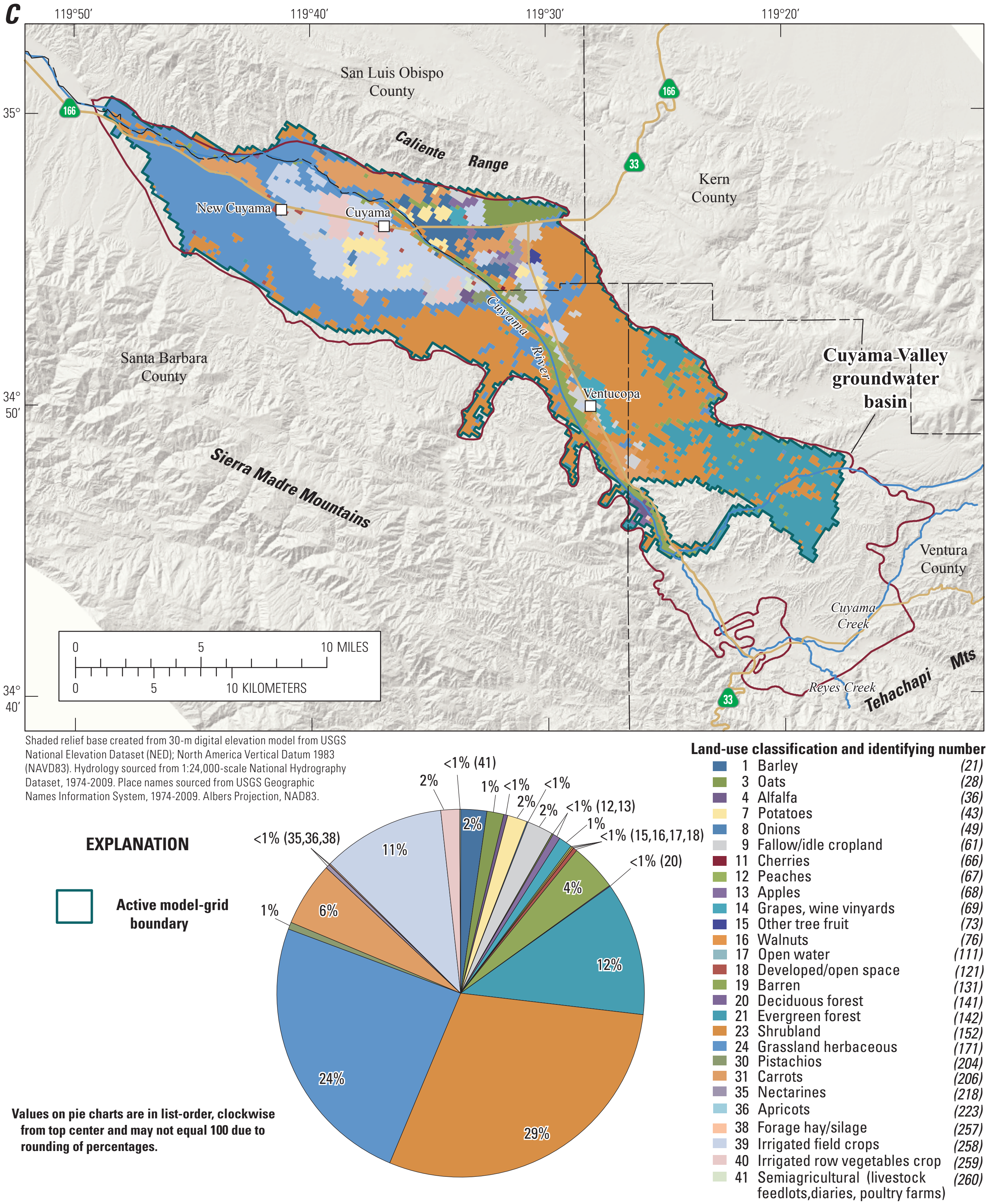

Figure 19. —Continued

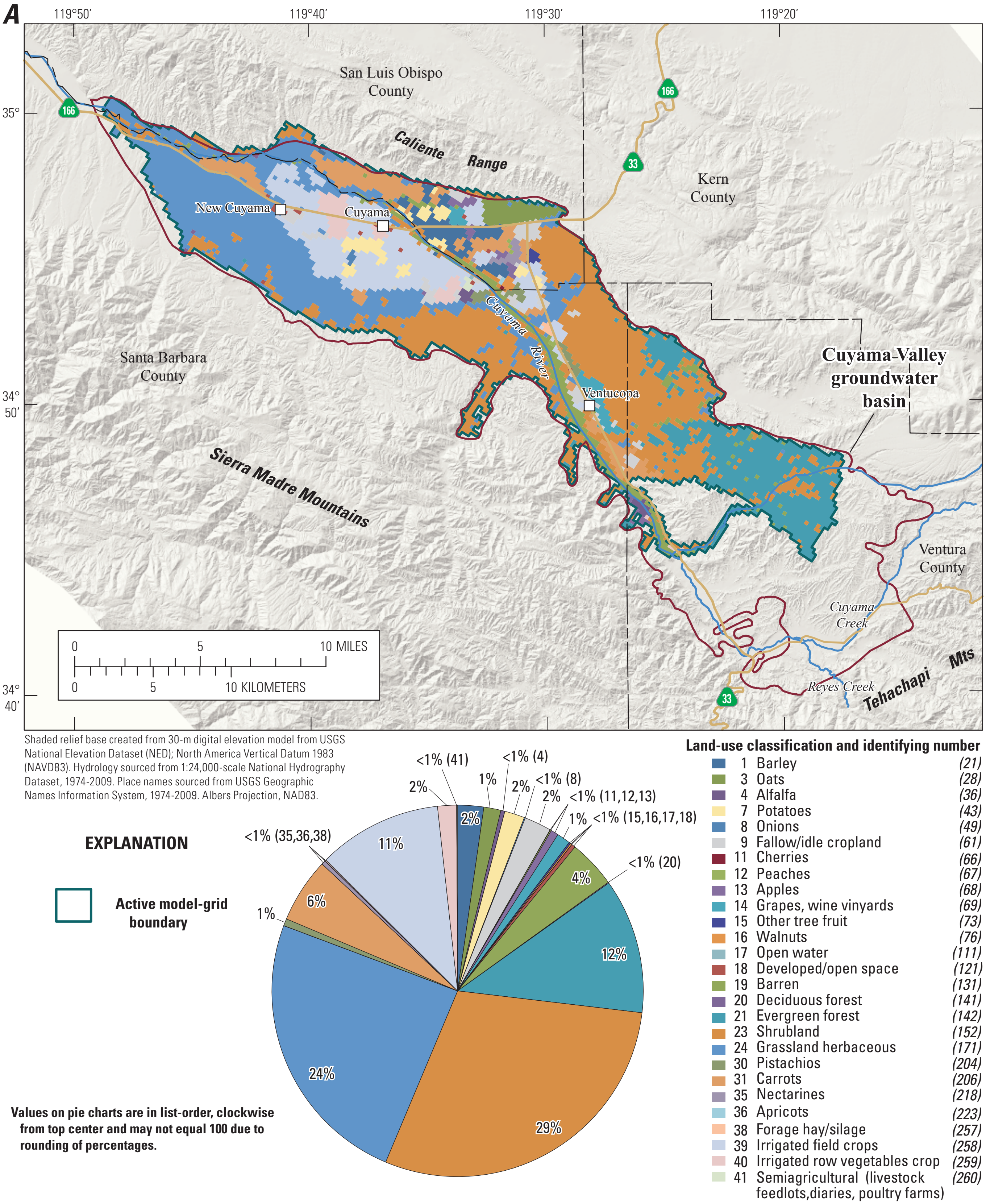

Figure 20. 2004–06 periods of land-use (virtual crop) groups discretized to the model grid, and pie chart of percentages of total land use over the modeled area for *A*, 2004; *B*, 2005; and *C*, 2006 for Cuyama Valley, California.

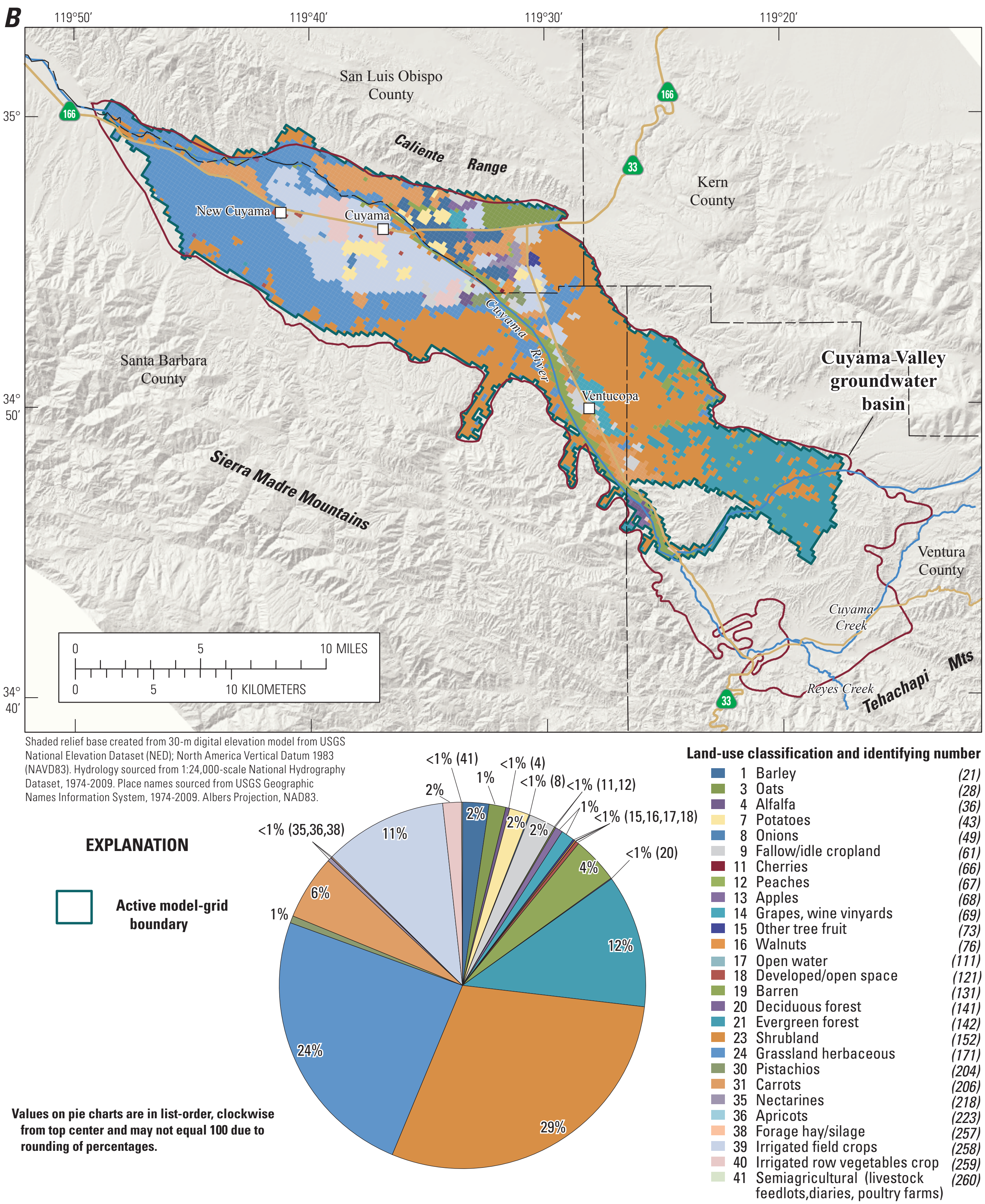

Figure 20. —Continued

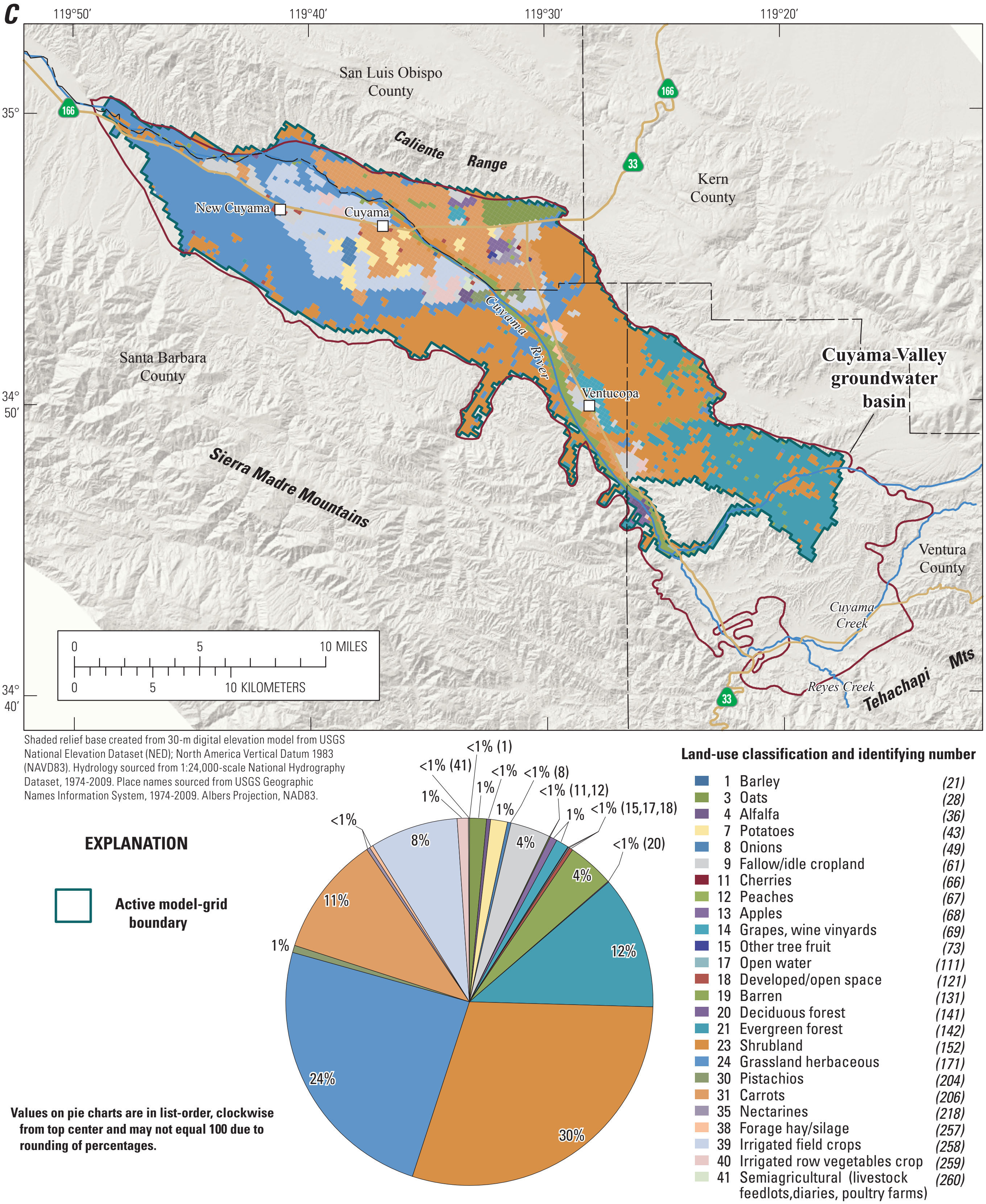

Figure 20. —Continued

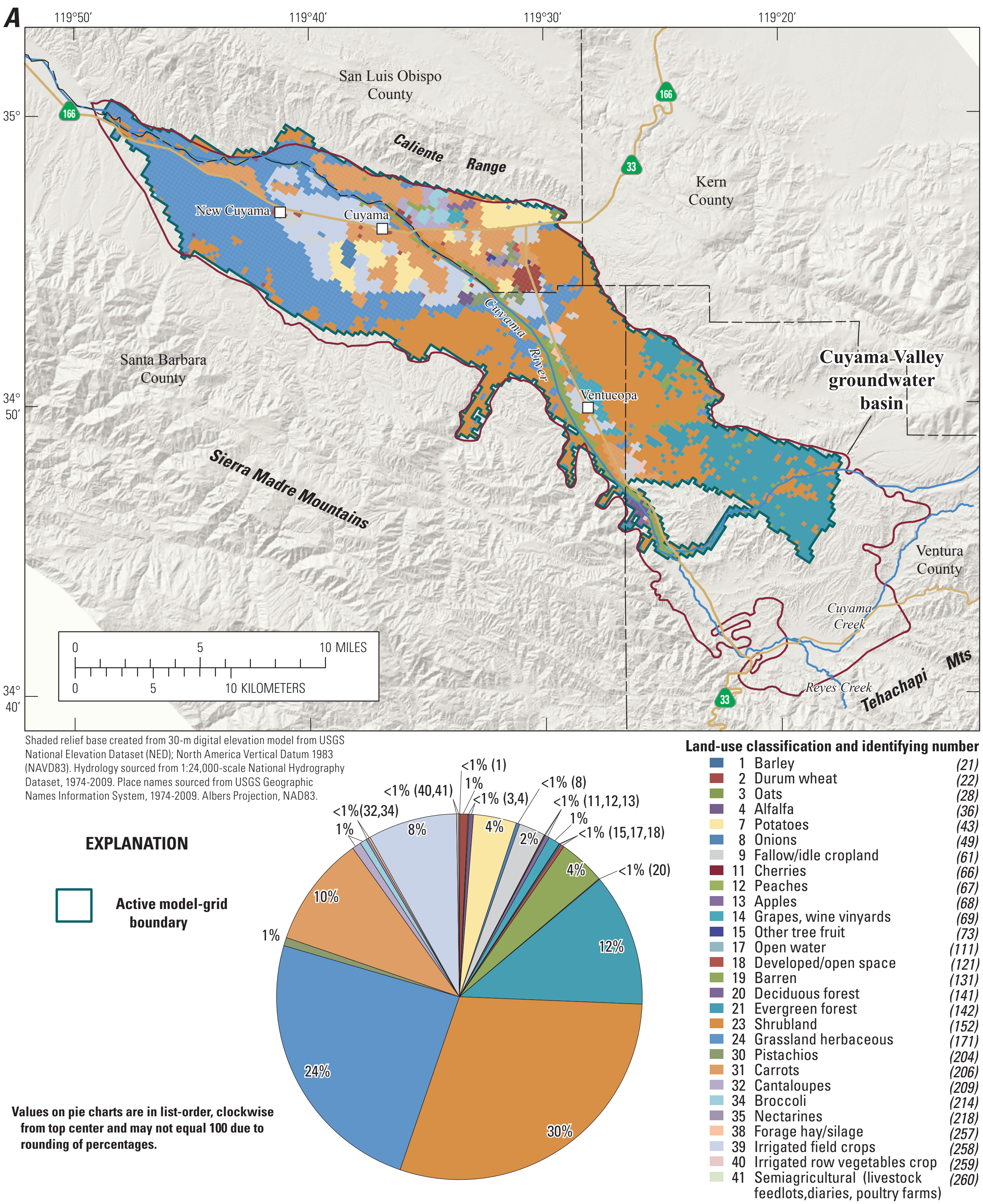

Figure 21. 2007–09 periods of land-use (virtual crop) groups discretized to the model grid, and pie chart of percentages of total land use over the modeled area for *A*, 2007; *B*, 2008; and *C*, 2009 for Cuyama Valley, California.

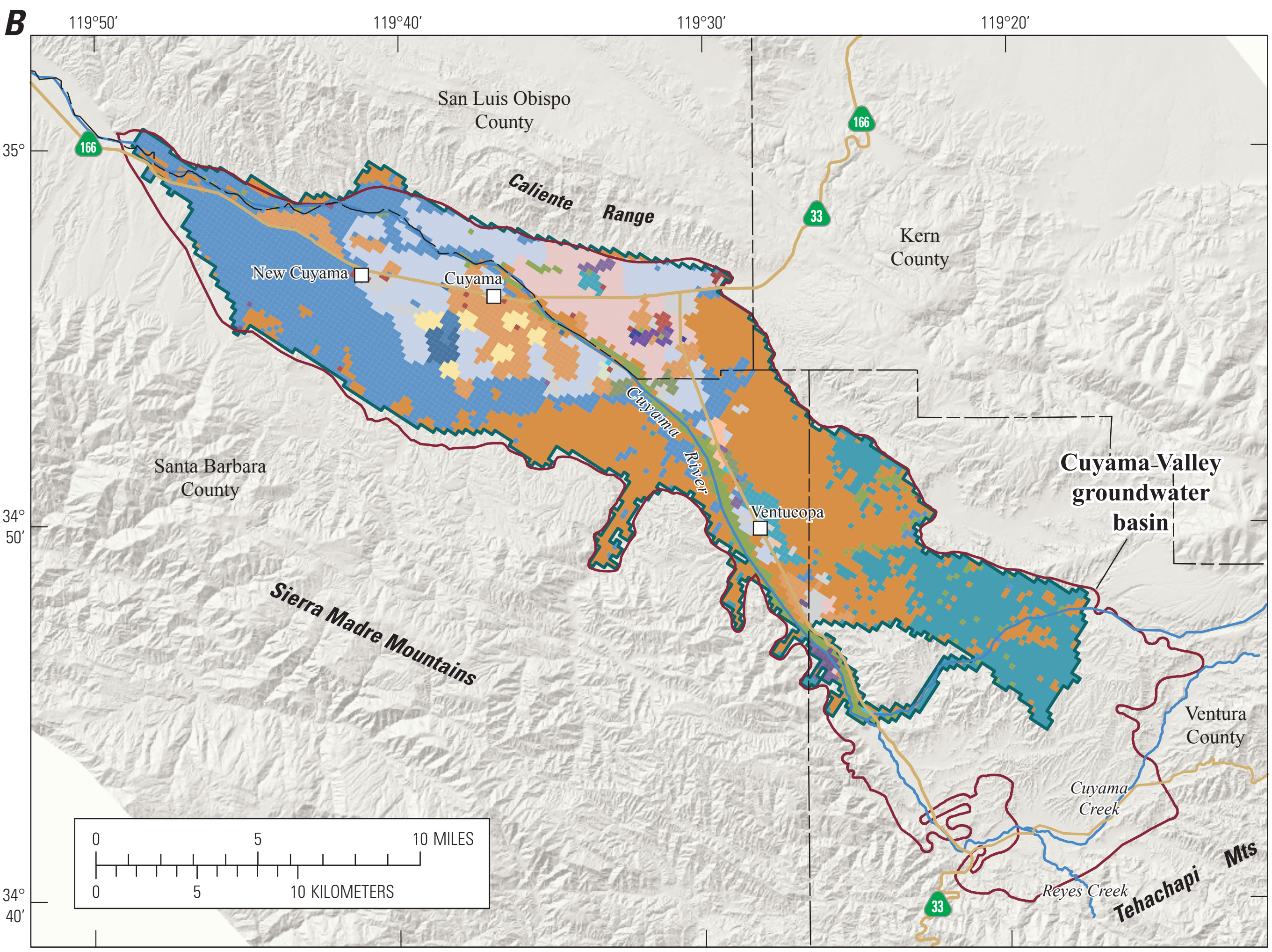

Shaded relief base created from 30-m digital elevation model from USGS National Elevation Dataset (NED); North America Vertical Datum 1983 (NAVD83). Hydrology sourced from 1:24,000-scale National Hydrography Dataset, 1974-2009. Place names sourced from USGS Geographic Names Information System, 1974-2009. Albers Projection, NAD83.

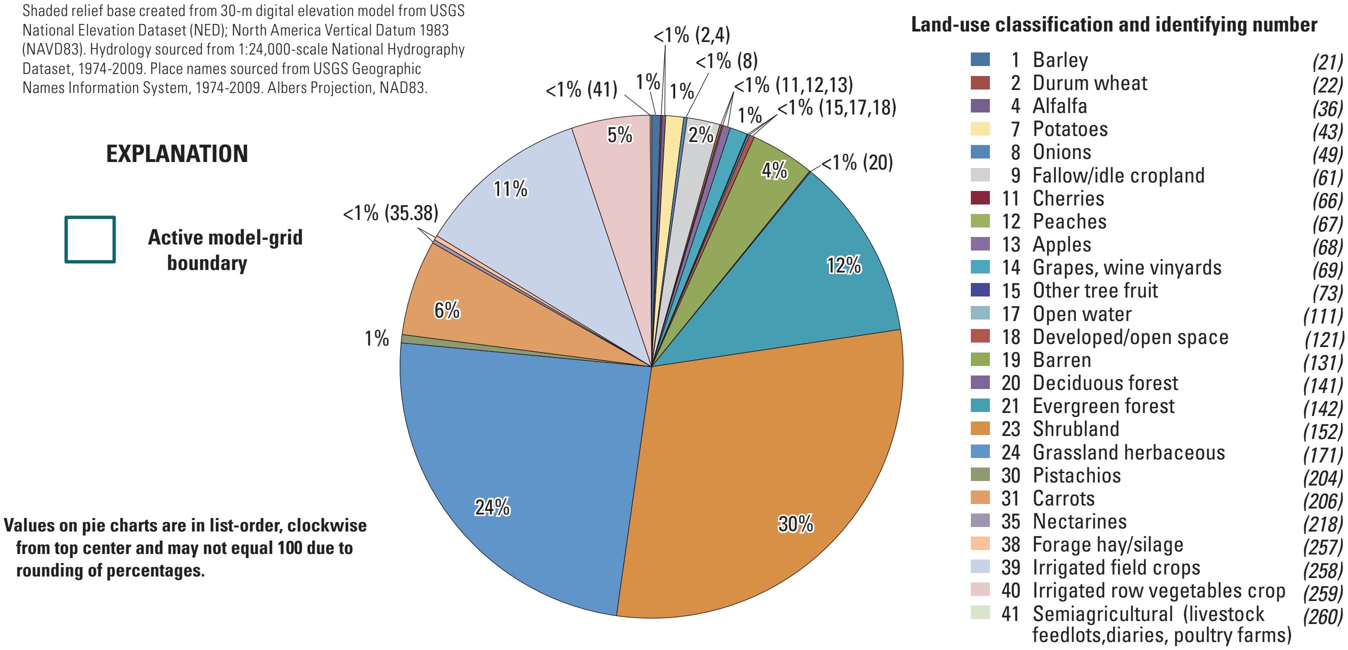

Figure 21. —Continued

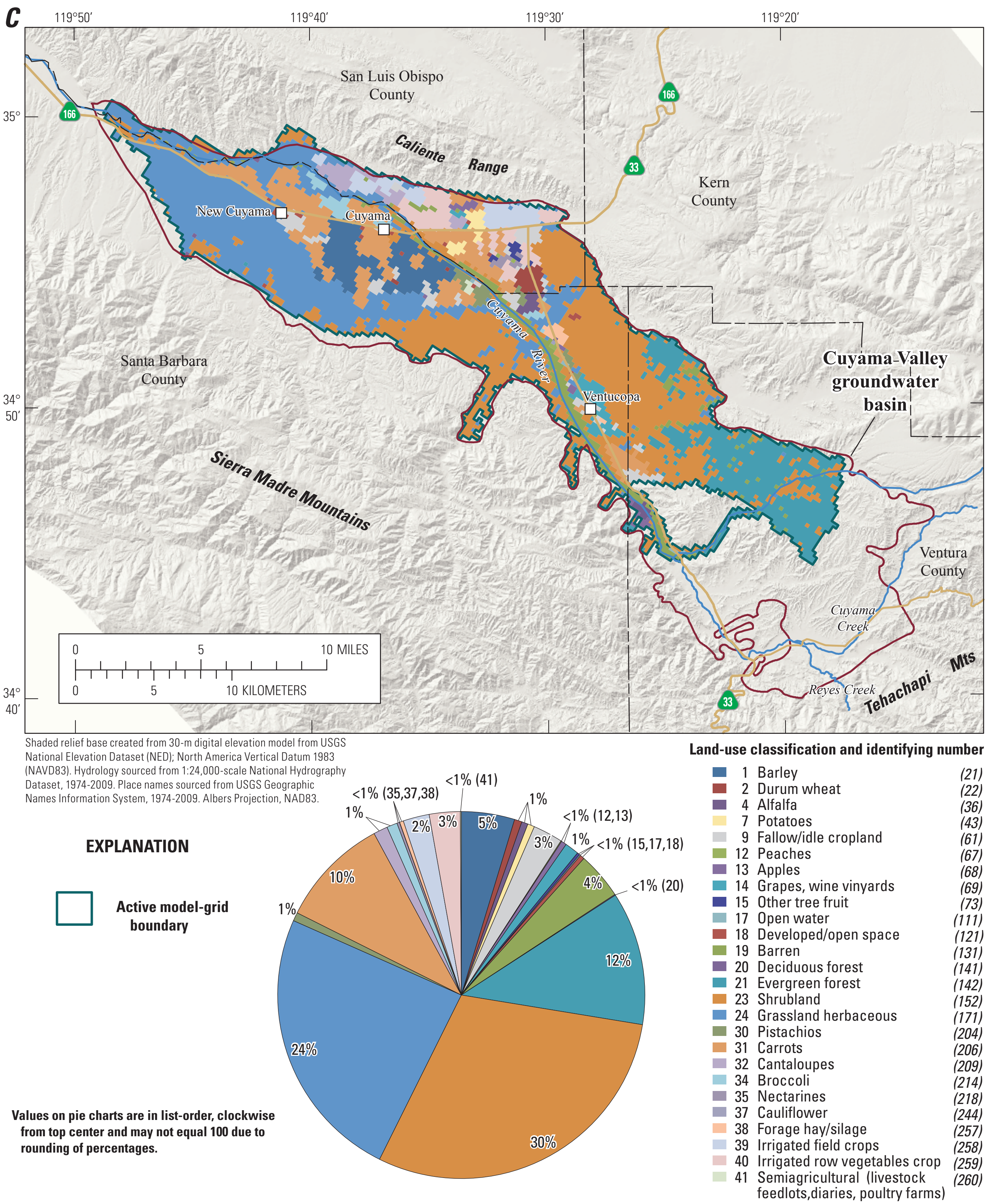

Figure 21. —Continued

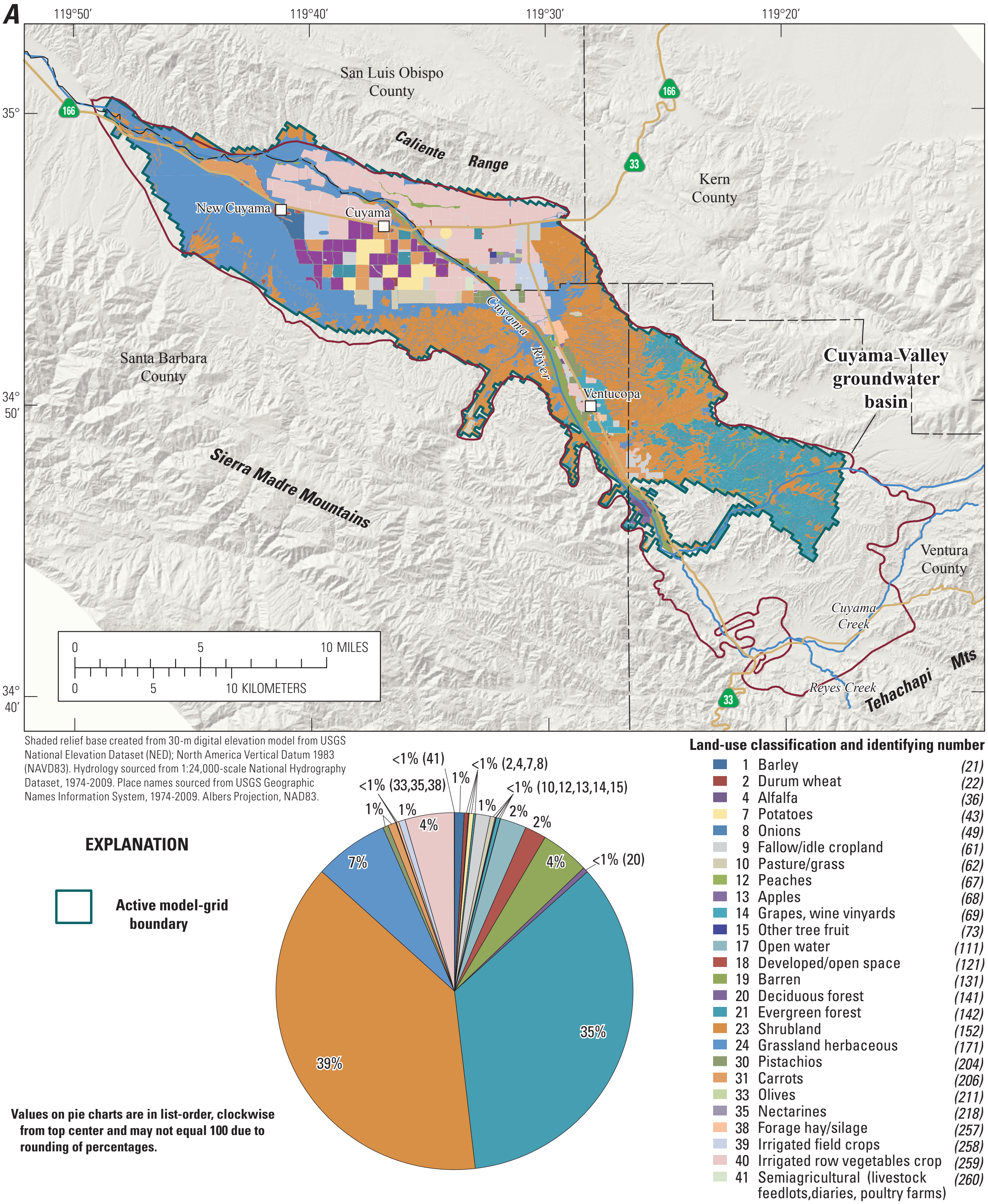

Figure 22. *A*, actual major categories of land-use for 2010; *B*, equivalent land-use (virtual crop) groups discretized to the model grid, and pie chart of percentage of total land use over the entire model area; and *C*, changes in percentages of selected land use through time, Cuyama Valley, California.

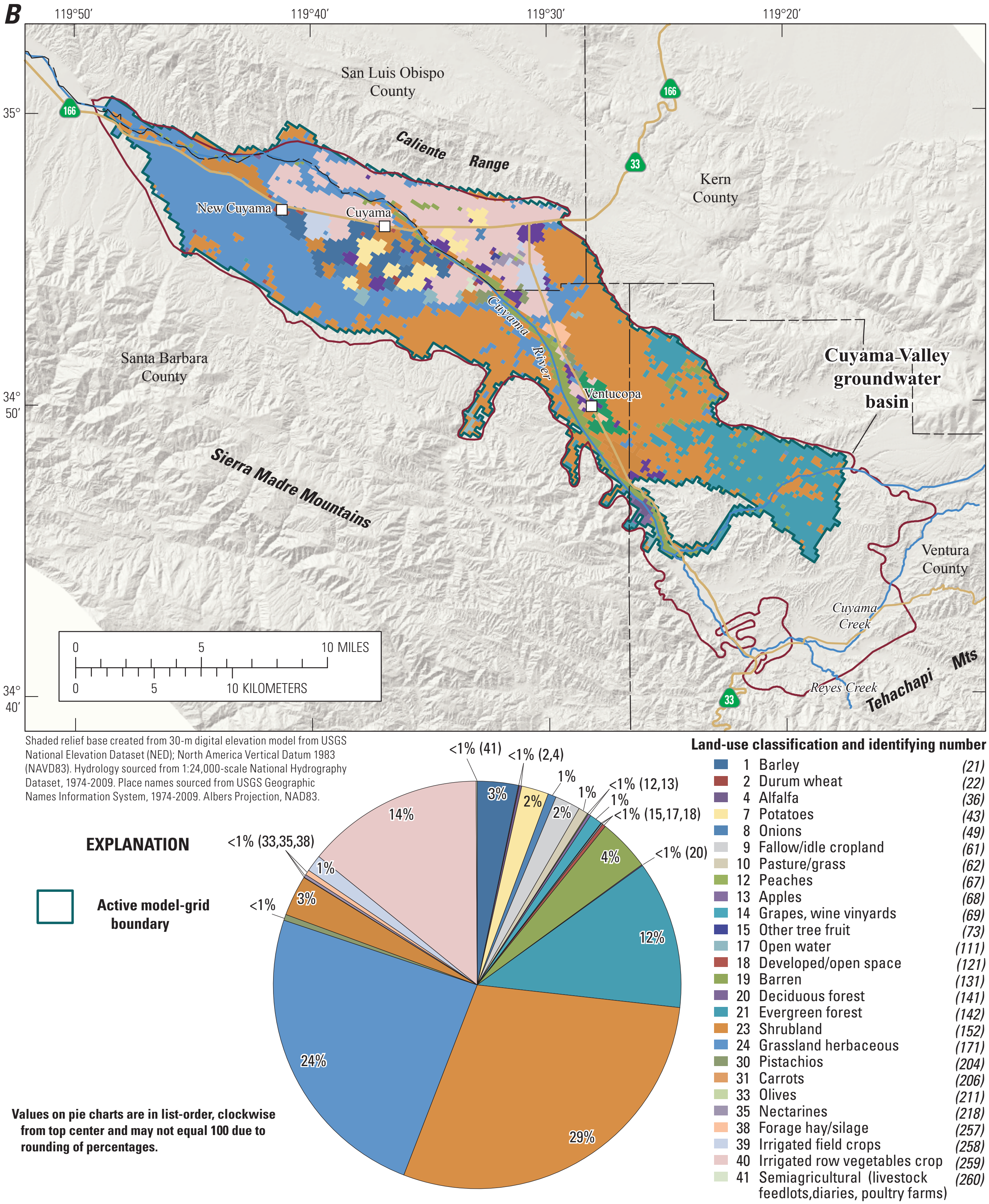

Figure 22. —Continued

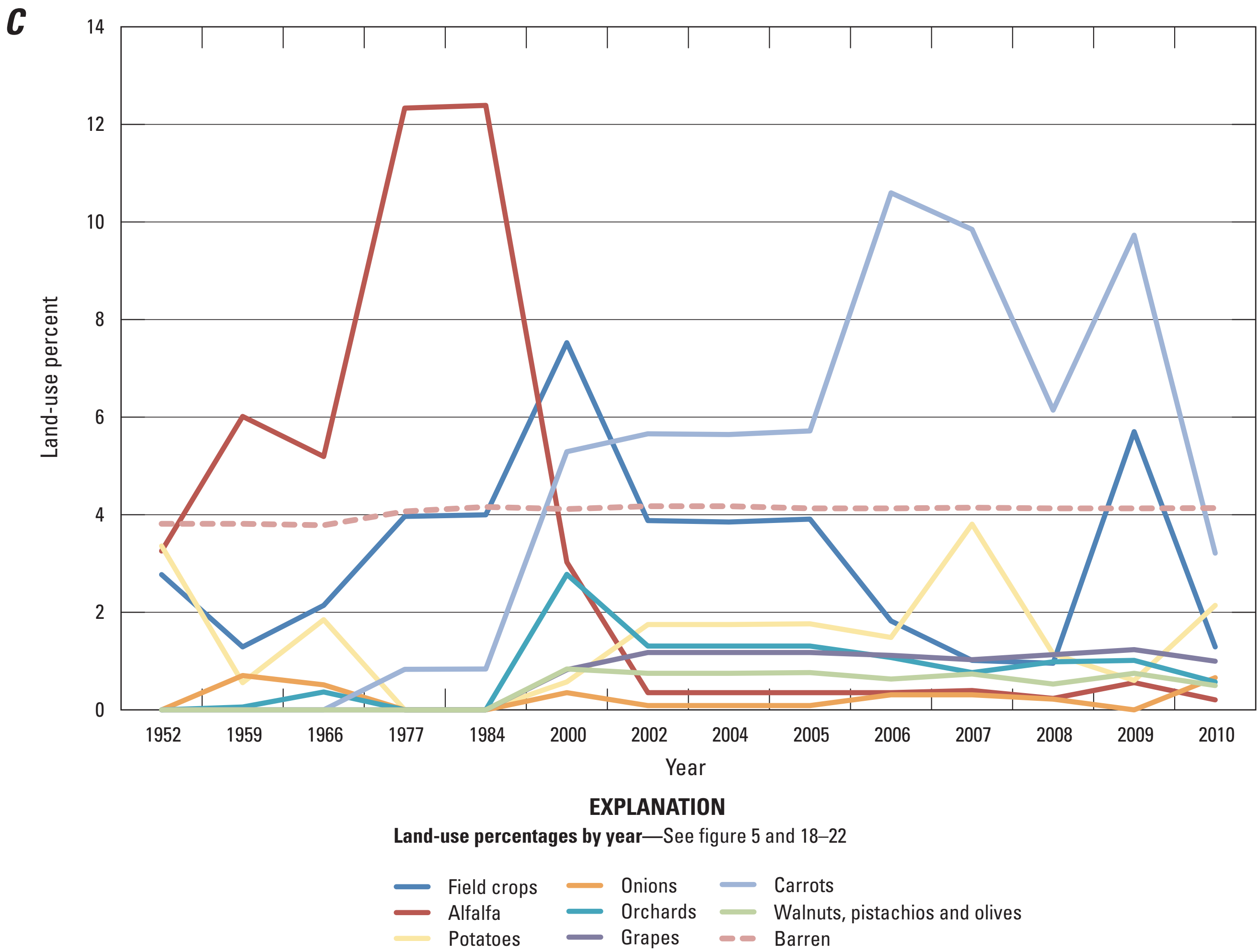

Figure 22. —Continued

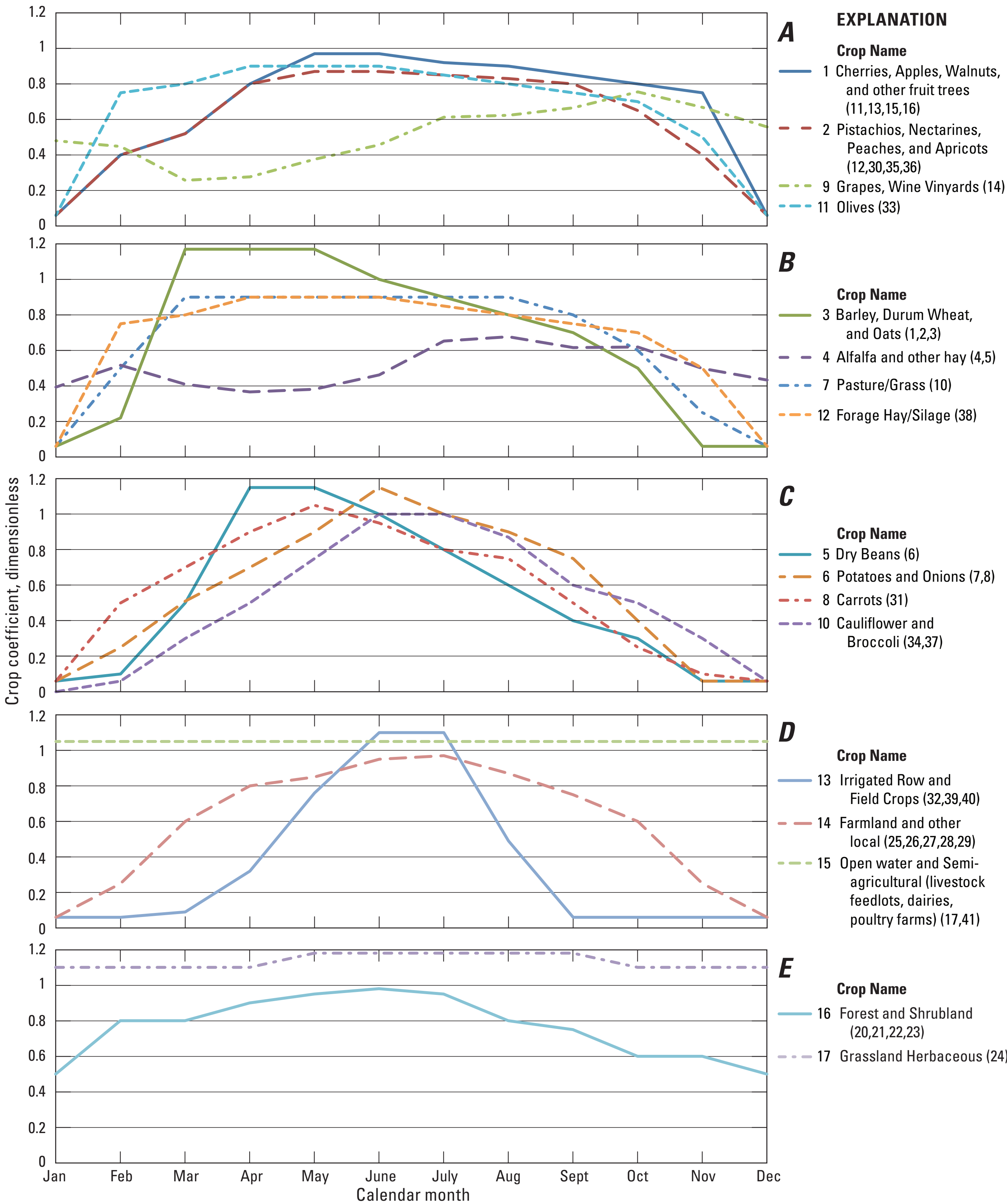

Figure 23. Monthly crop coefficients for *A*, orchards; *B*, grains and hay; *C* vegetables; *D*, general land use; and *E*, native vegetation in the Cuyama Valley, California.

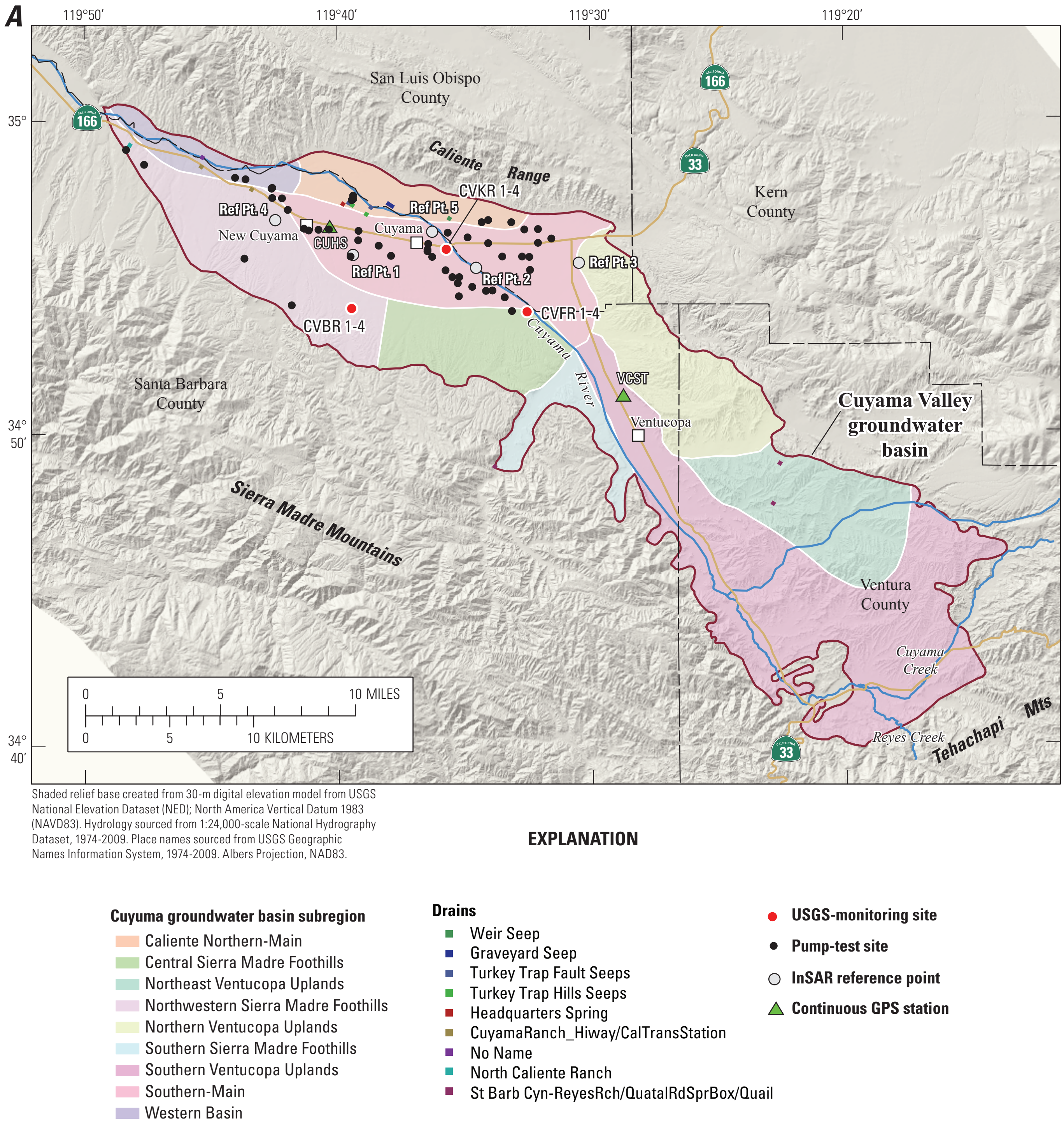

Figure 24. *A*, locations of wells with pumping tests, and the distribution of parameter zones used for model calibration of hydraulic properties for *B*, model layer 1, *C*, model layer 2, and *D*, model layer 3 in the Cuyama Valley, California.

B

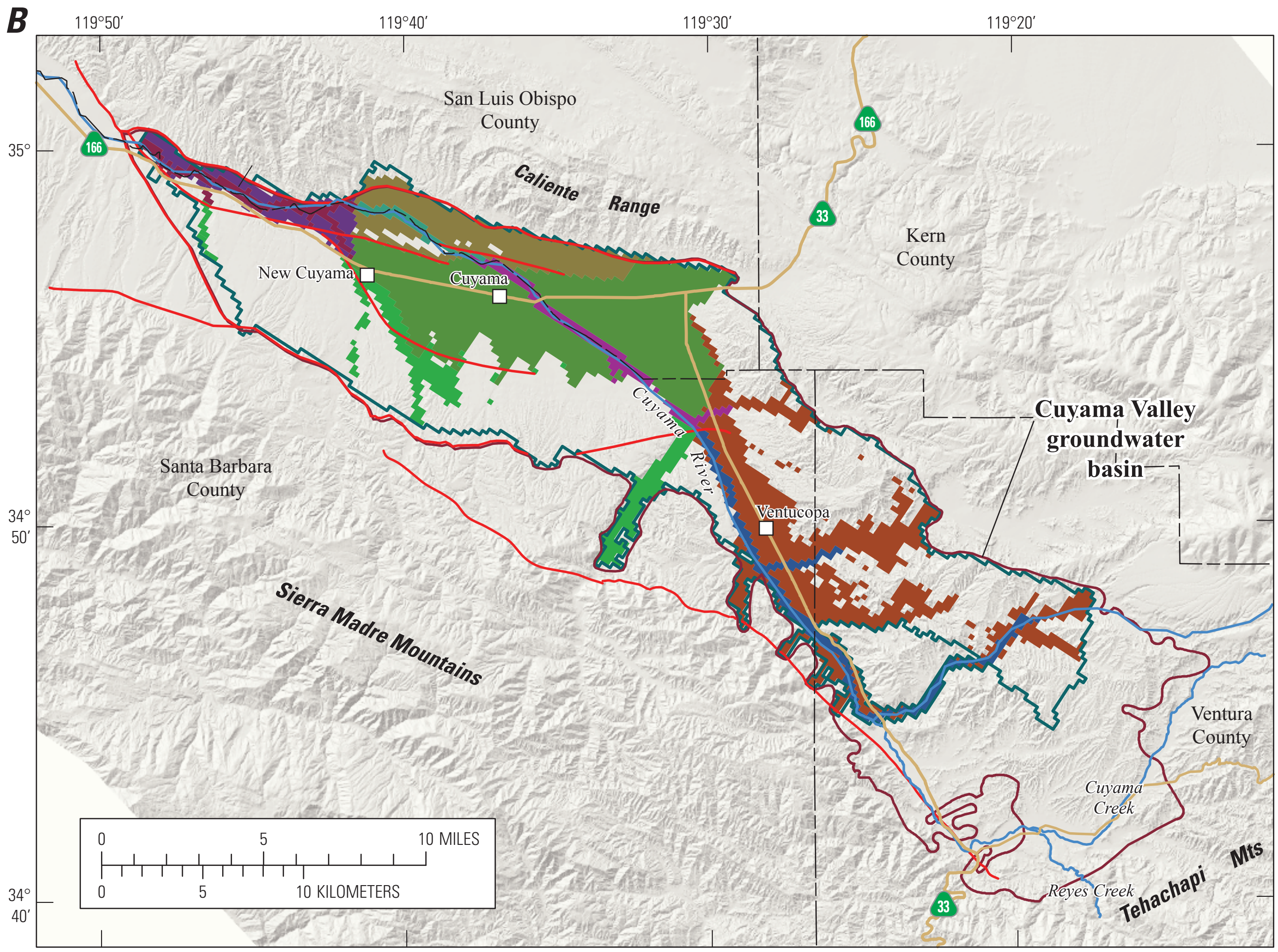

Shaded relief base created from 30-m digital elevation model from USGS National Elevation Dataset (NED); North America Vertical Datum 1983 (NAVD83). Hydrology sourced from 1:24,000-scale National Hydrography Dataset, 1974-2009. Place names sourced from USGS Geographic Names Information System, 1974-2009. Albers Projection, NAD83.

EXPLANATION

Layer 1 hydraulic property zone and (zone number)—
(See table 13 for description of acronyms)

Northern Main
- NMZ_QYA (1)
- NMZQYACC (2)

Southern Main
- SMZ_QYA (4)
- SMZ_QYACC (5)

Western
- WZ_QYA (8)
- WZ_QYACC (9)

Sierra Madre Foothills
- SMFHQYA (3)

Ventucopa Uplands
- VC_QYACC (6)
- VC_QYAUC (7)

Active model-grid boundary

Fault

Figure 24. —Continued

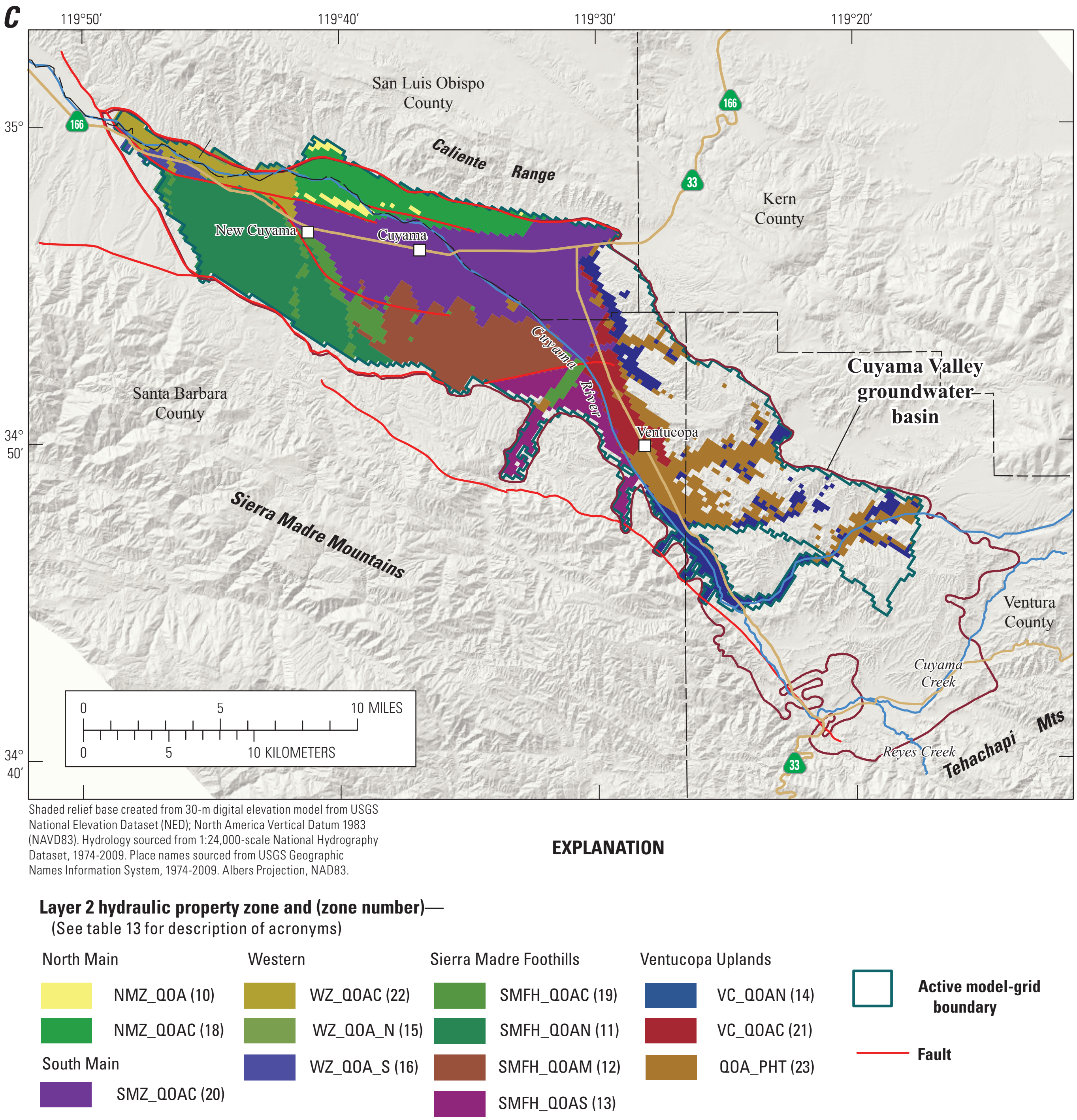

Figure 24. —Continued

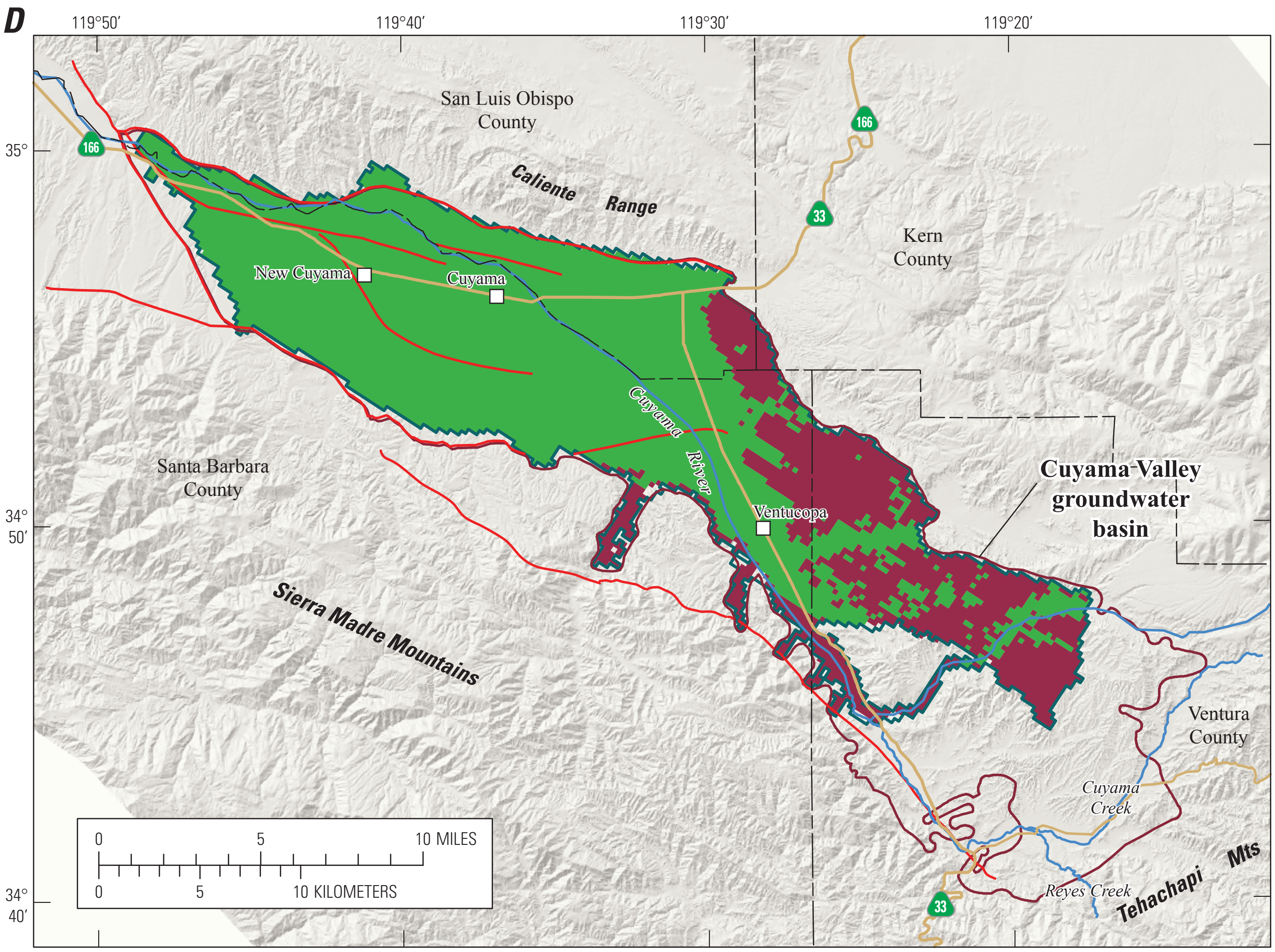

Shaded relief base created from 30-m digital elevation model from USGS National Elevation Dataset (NED); North America Vertical Datum 1983 (NAVD83). Hydrology sourced from 1:24,000-scale National Hydrography Dataset, 1974-2009. Place names sourced from USGS Geographic Names Information System, 1974-2009. Albers Projection, NAD83.

EXPLANATION

Layer 3 hydraulic property zone and (zone number)—
(See table 13 for description of acronyms)

Morales Formation — MO_C (24)

Ventucopa Uplands — VC_MOUC (17)

Active model-grid boundary

Fault

Figure 24. —Continued

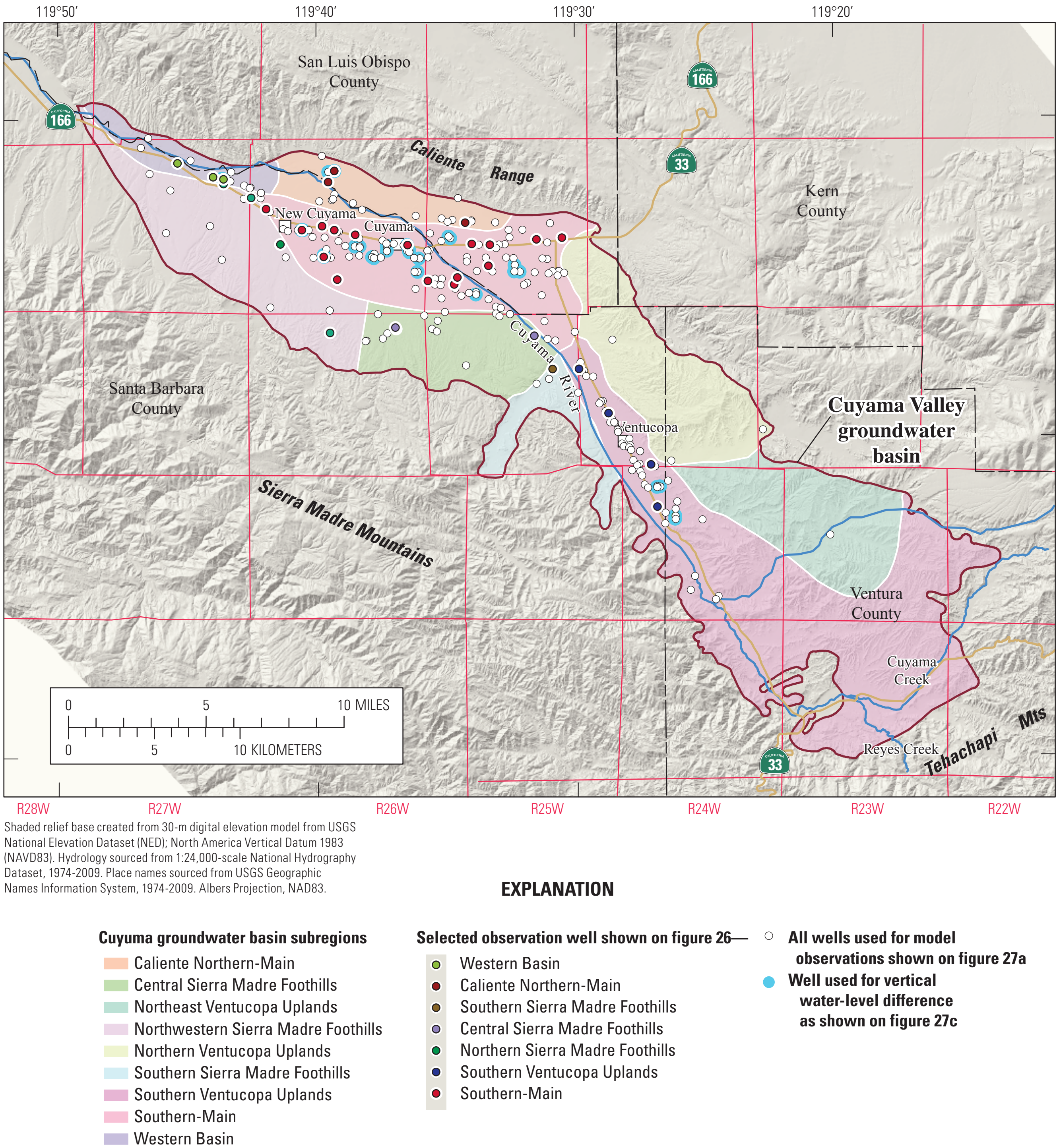

Figure 25. Calibration data sites of wells for groundwater levels and water-level differences for the Cuyama Valley Hydrologic Model, Cuyama Valley, California.

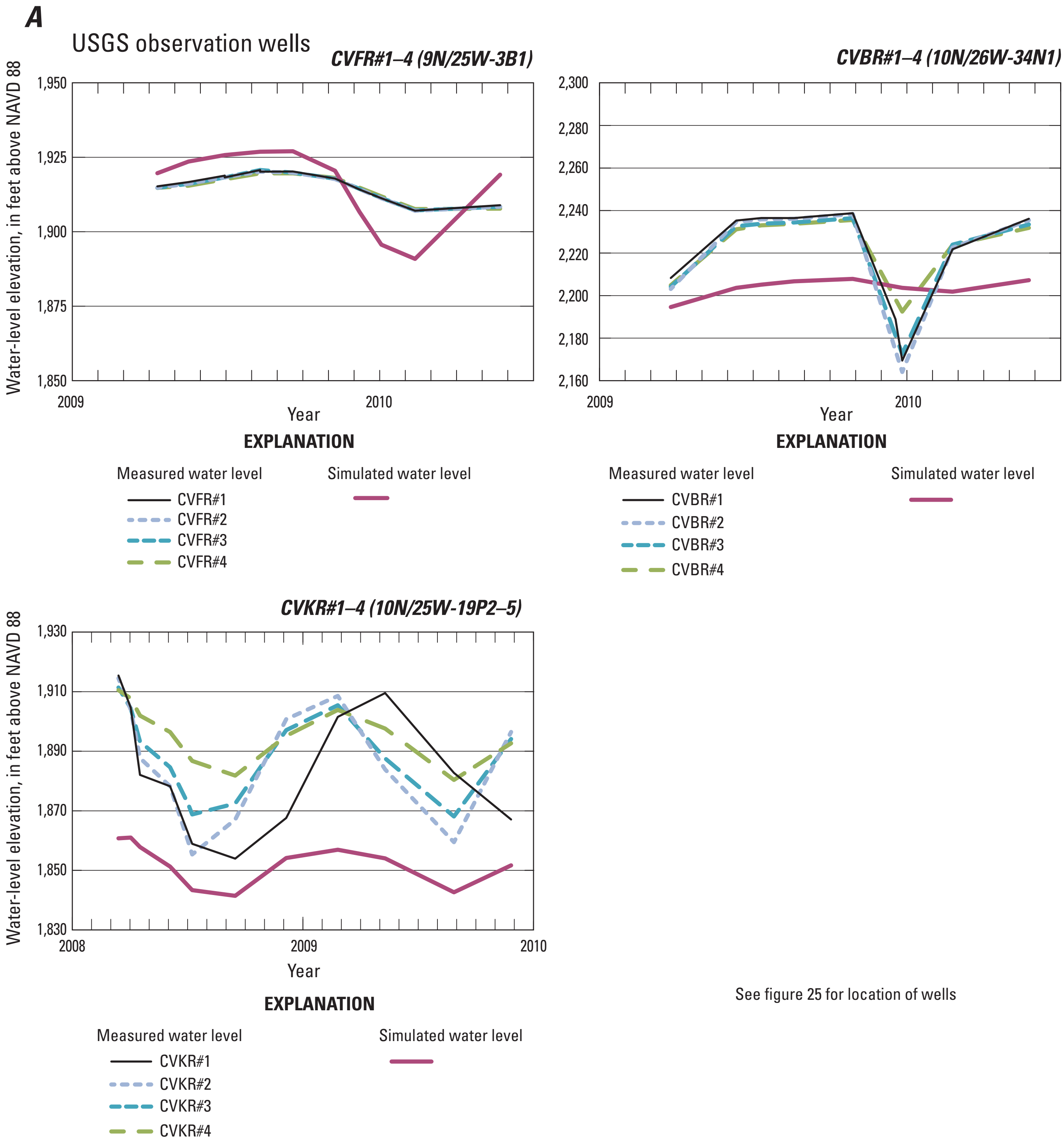

Figure 26. Simulated and measured hydrographs for selected wells in *A*, Main-zone, *B*, Ventucopa Upland, and *C*, Sierra Madre Foothills subregions, Cuyama Valley, California.

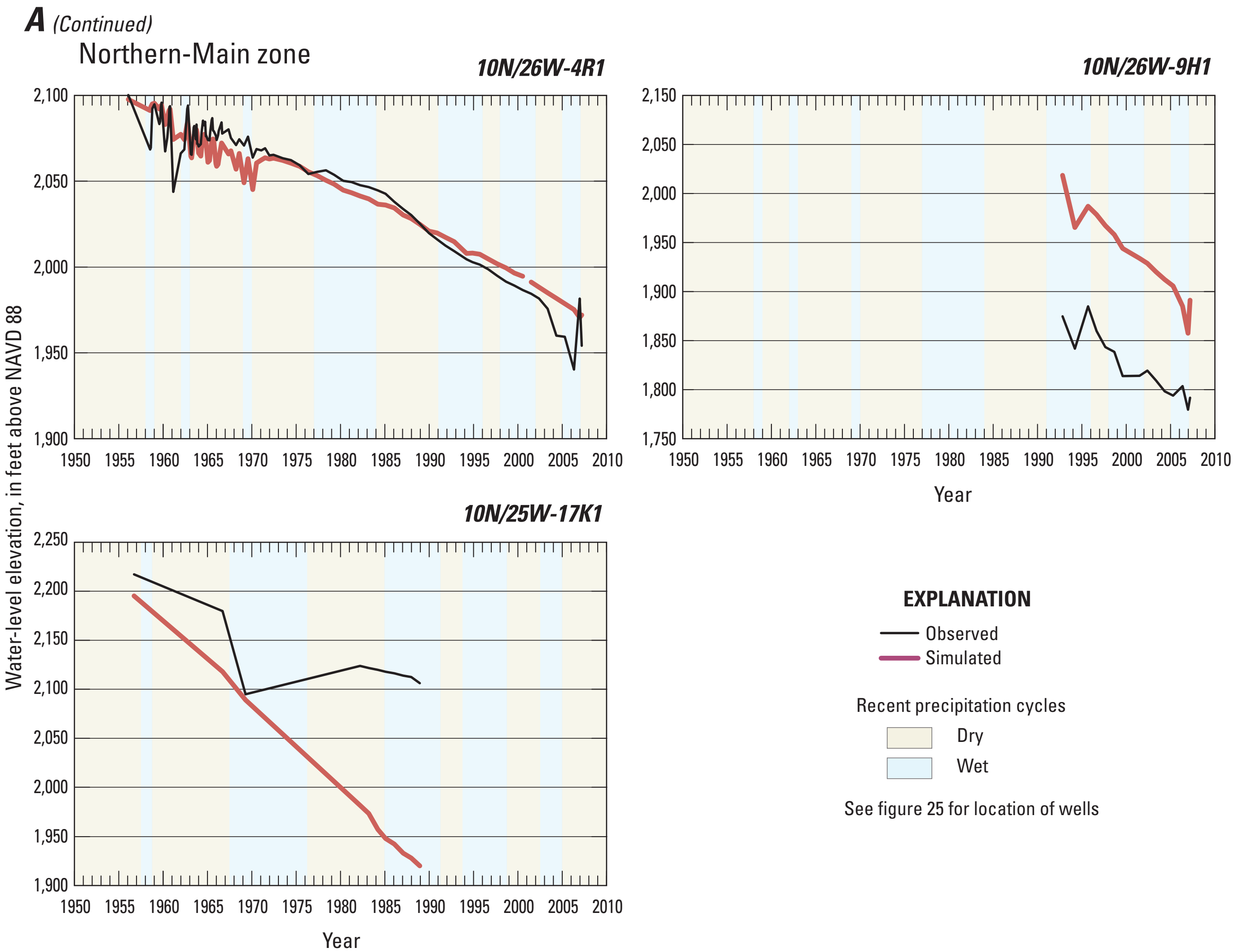

Figure 26. —Continued

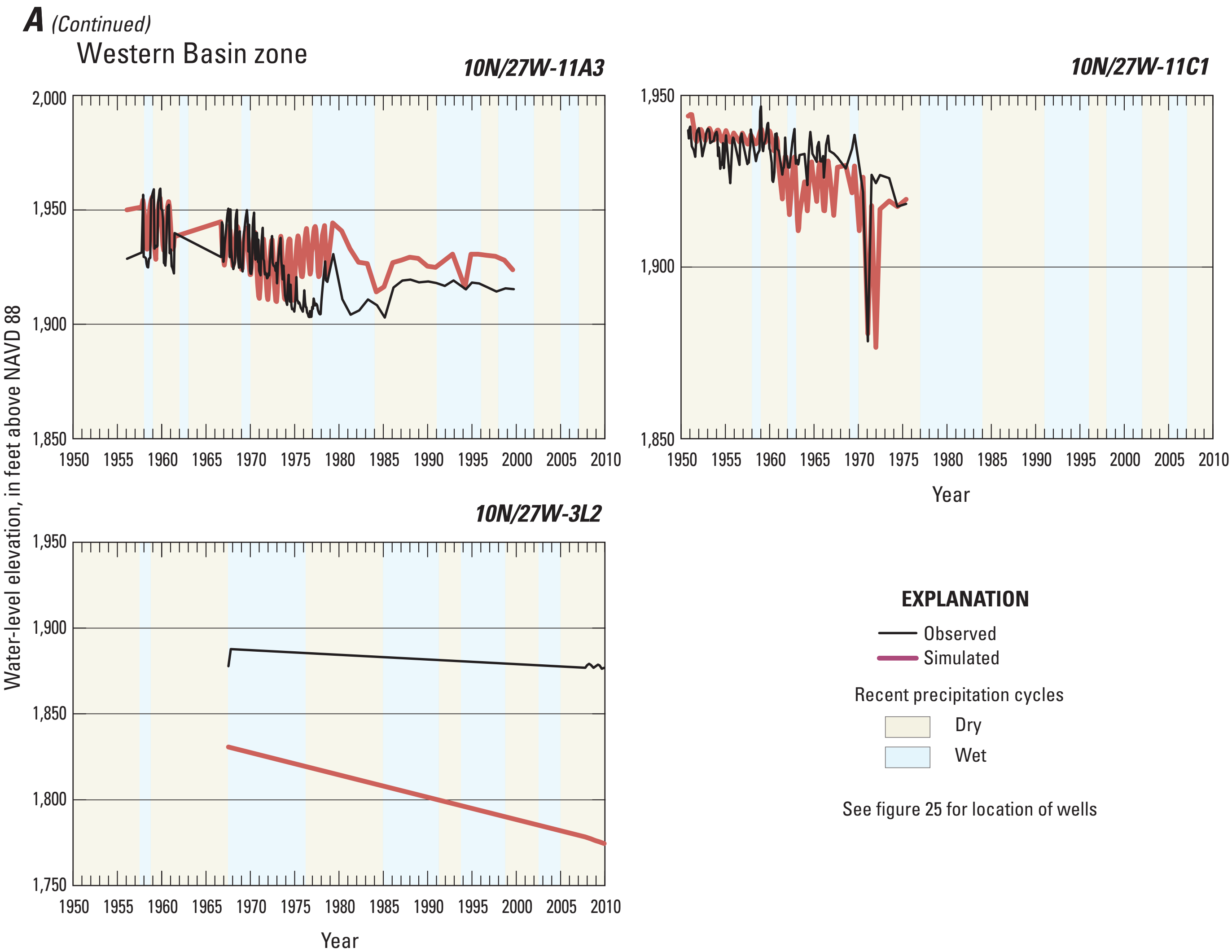

Figure 26. —Continued

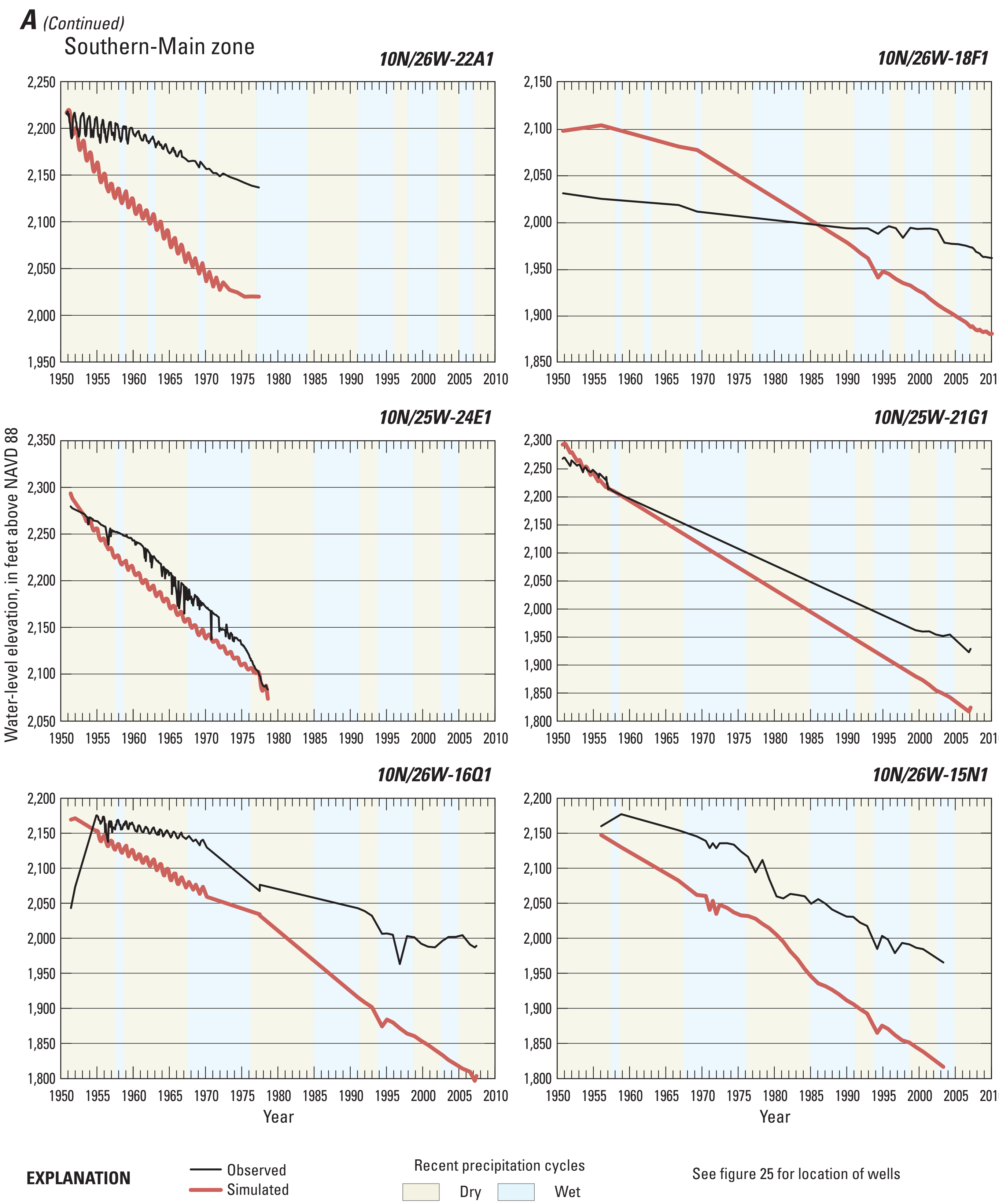

Figure 26. —Continued

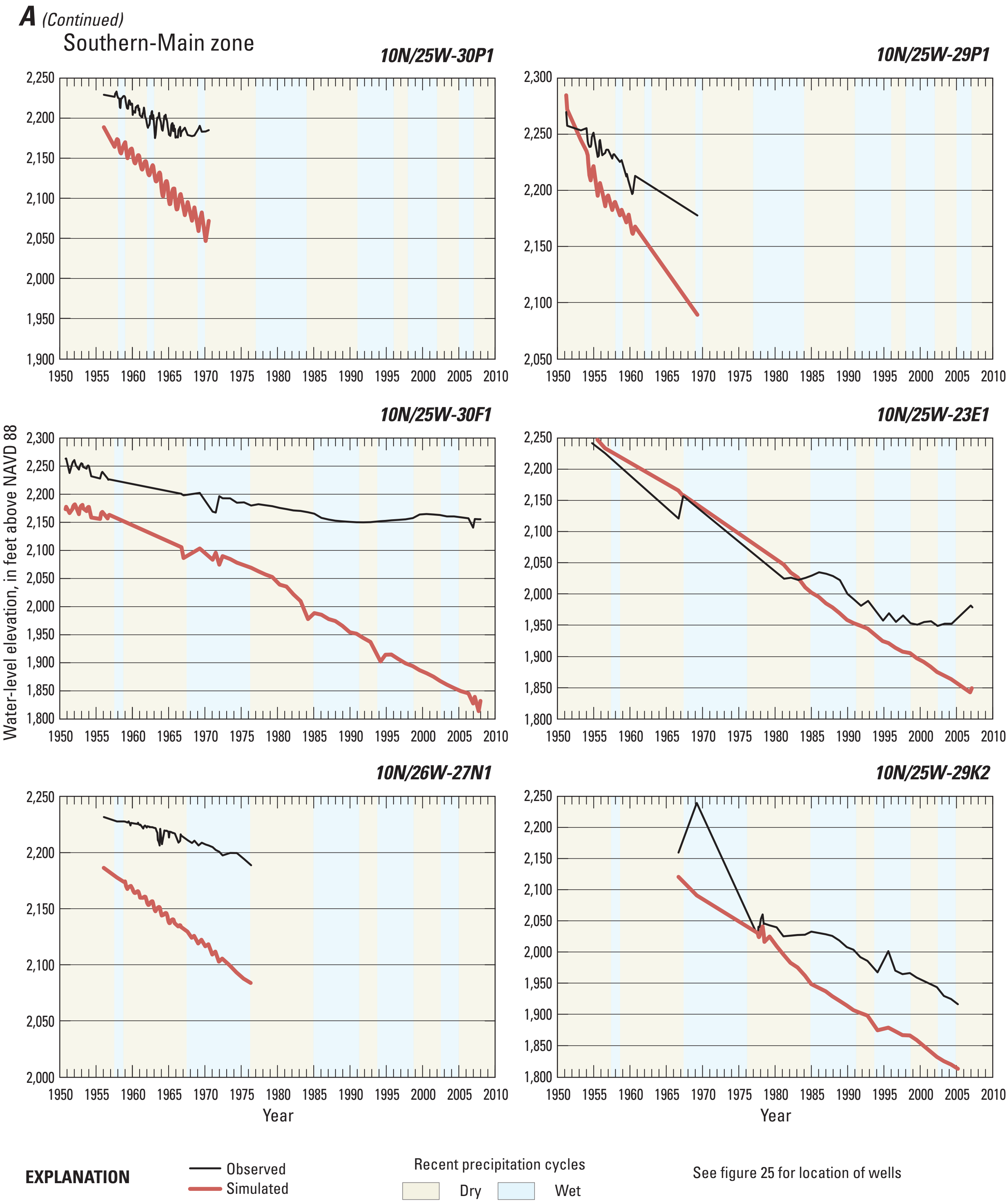

Figure 26. —Continued

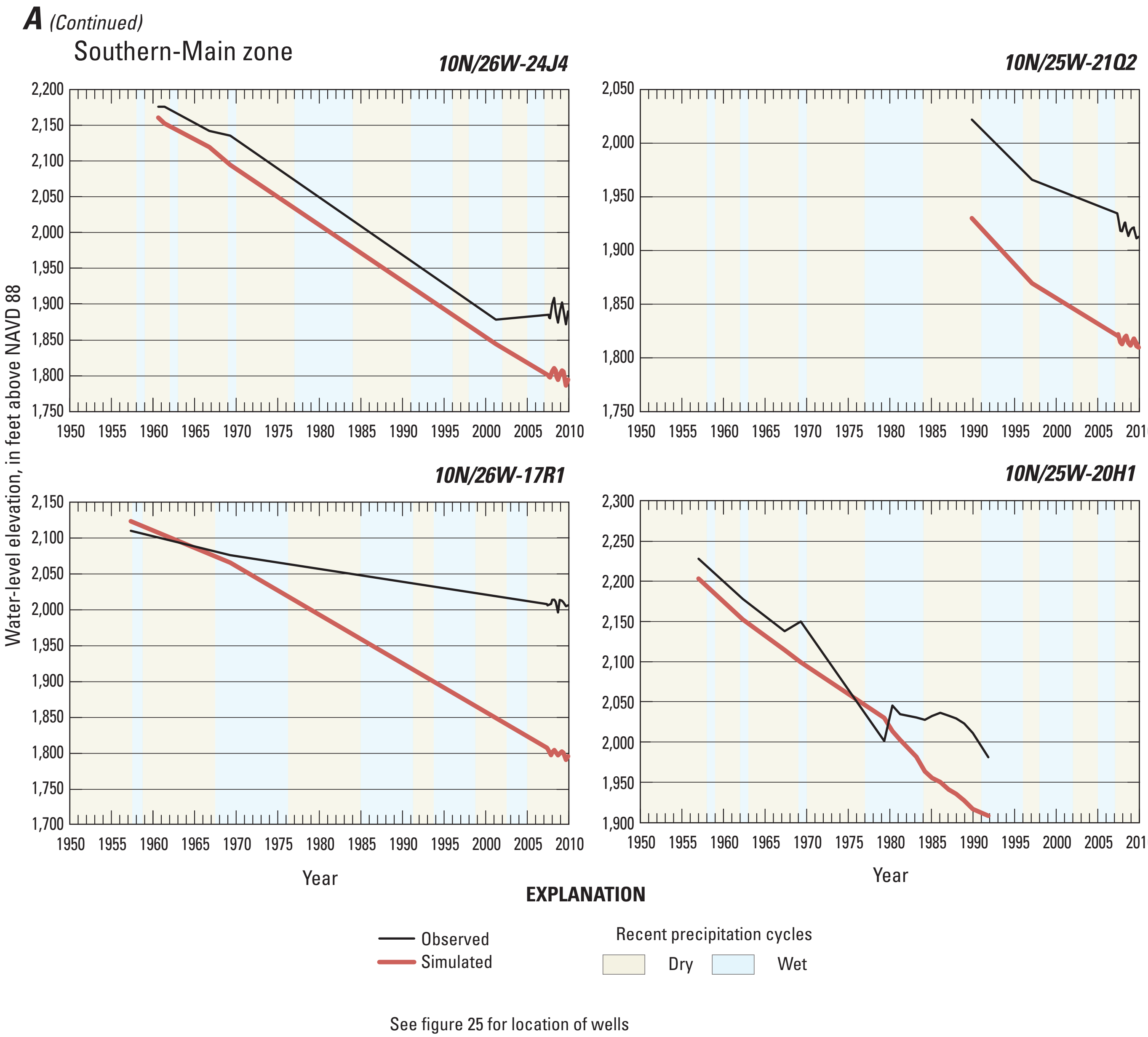

Figure 26. —Continued

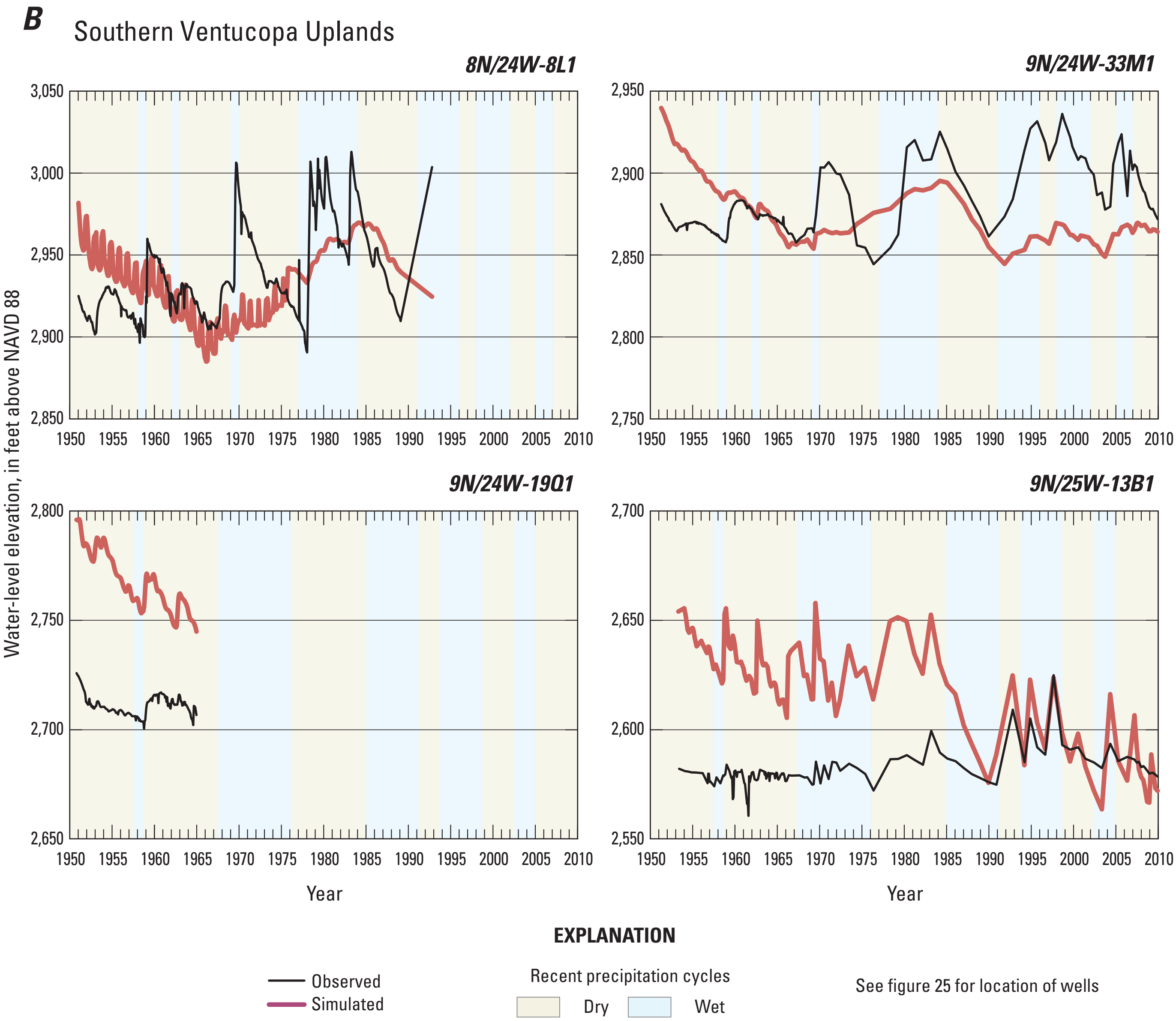

Figure 26. —Continued

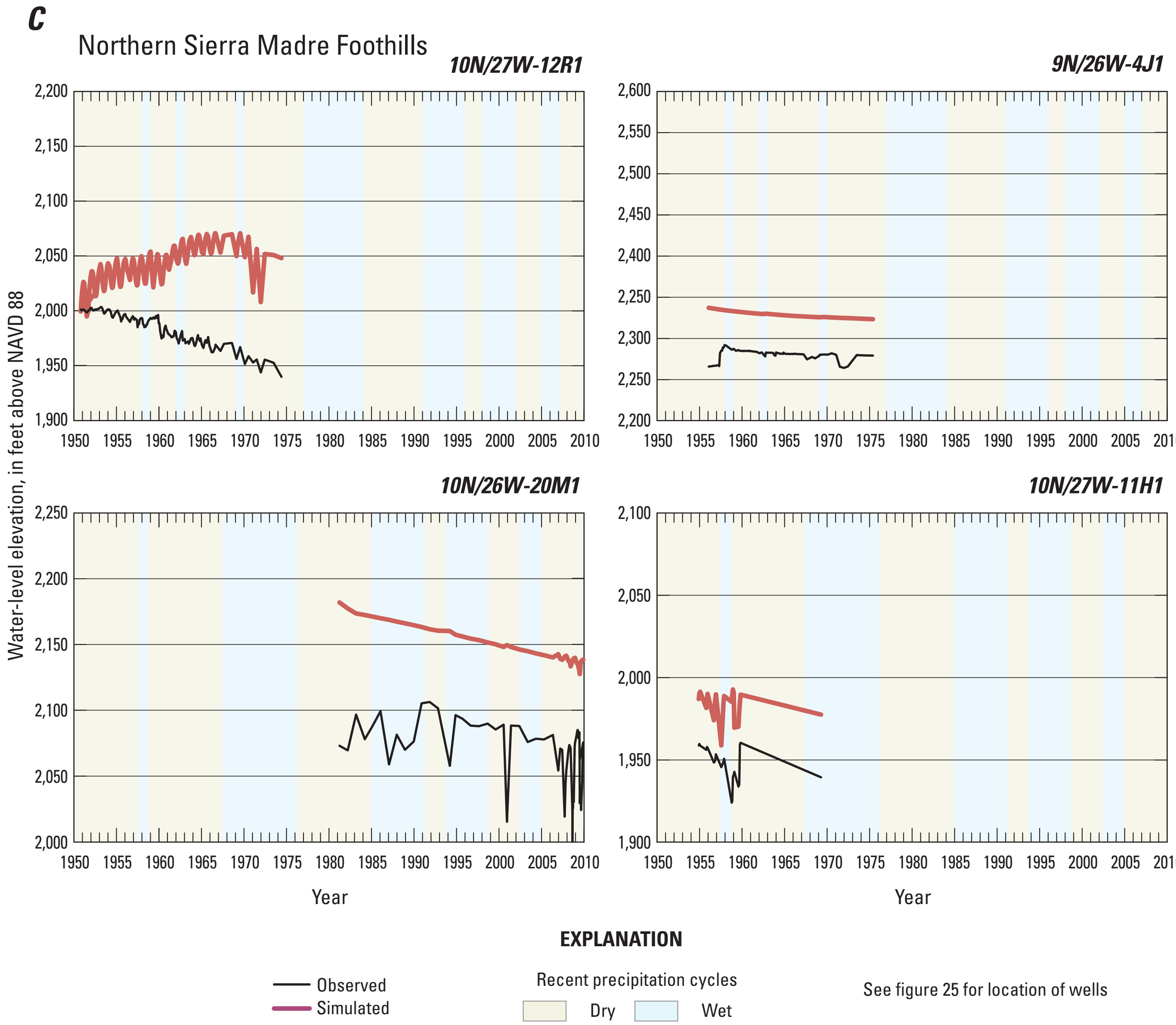

Figure 26. —Continued

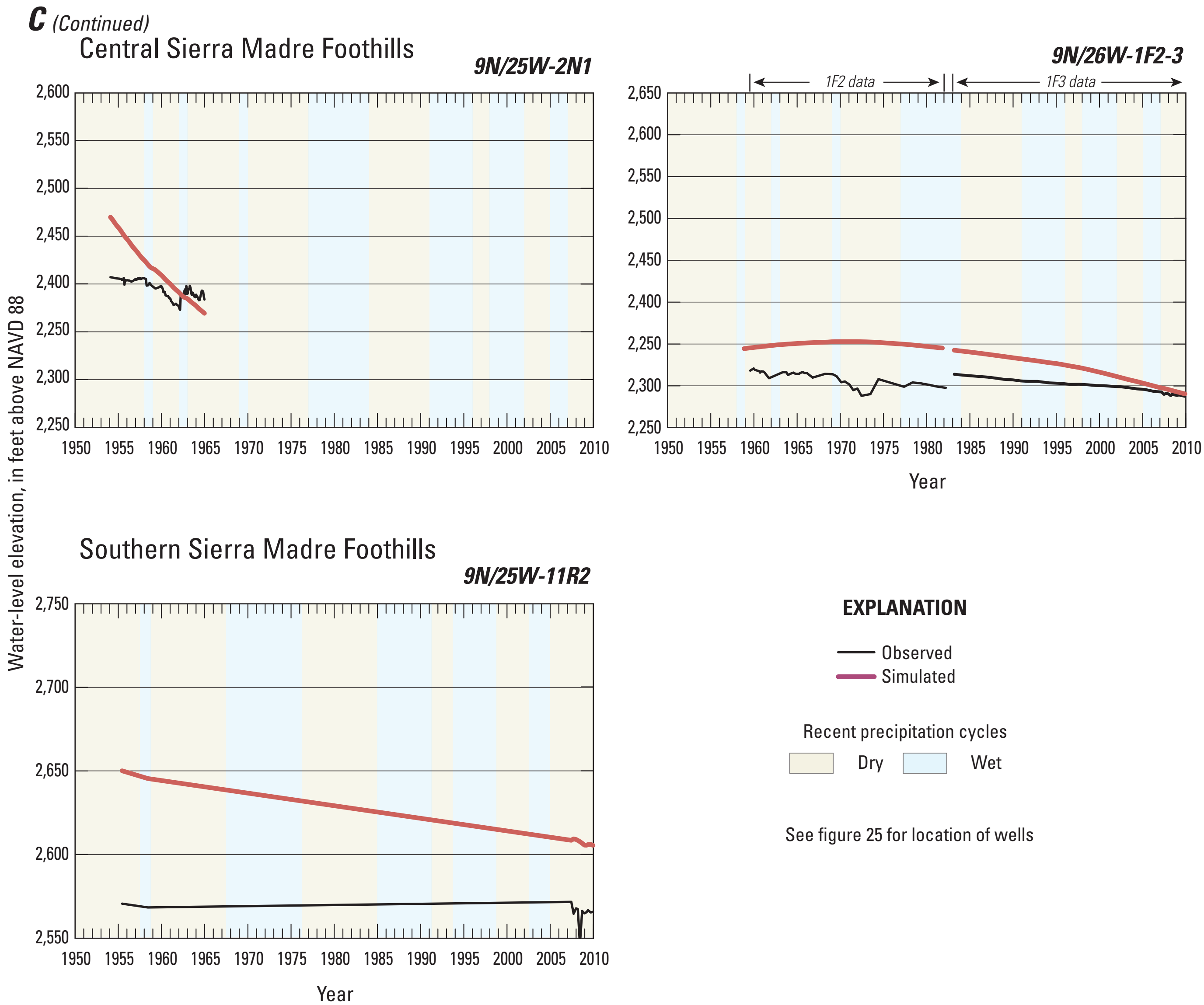

Figure 26. —Continued

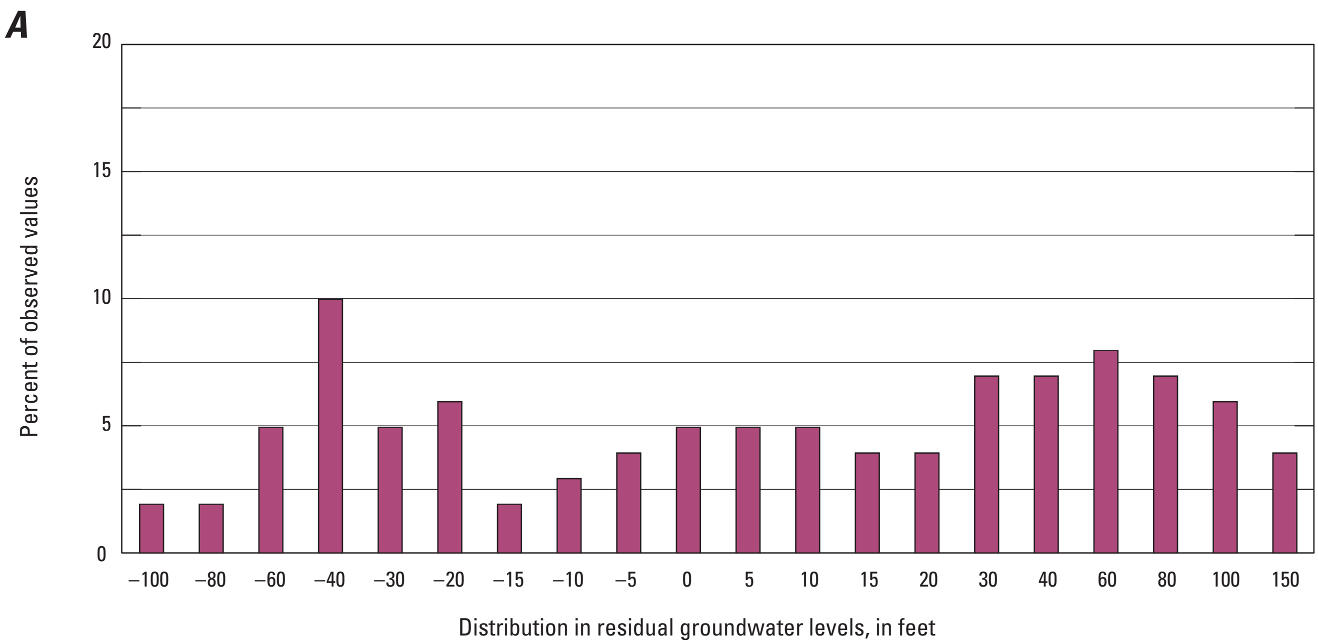

Figure 27. *A*, histogram of distribution of water-level residuals (observed minus simulated) for the Cuyama Valley hydrologic model (CUVHM) model, *B*, correlation graph by subregions of measured versus simulated water levels, and *C*, correlation between simulated and measured vertical water-level differences for selected wells, Cuyama Valley, California.

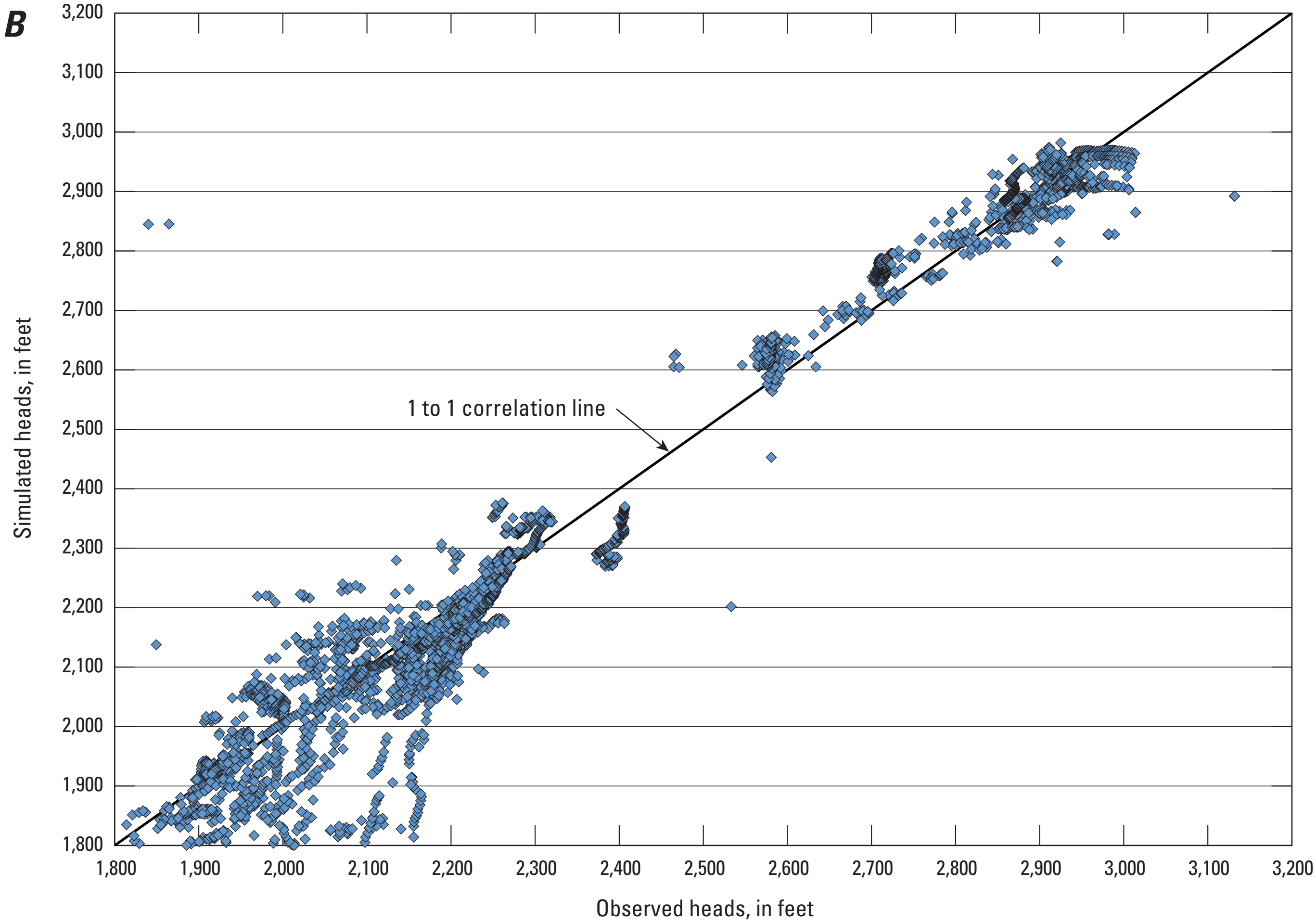

Figure 27. —Continued

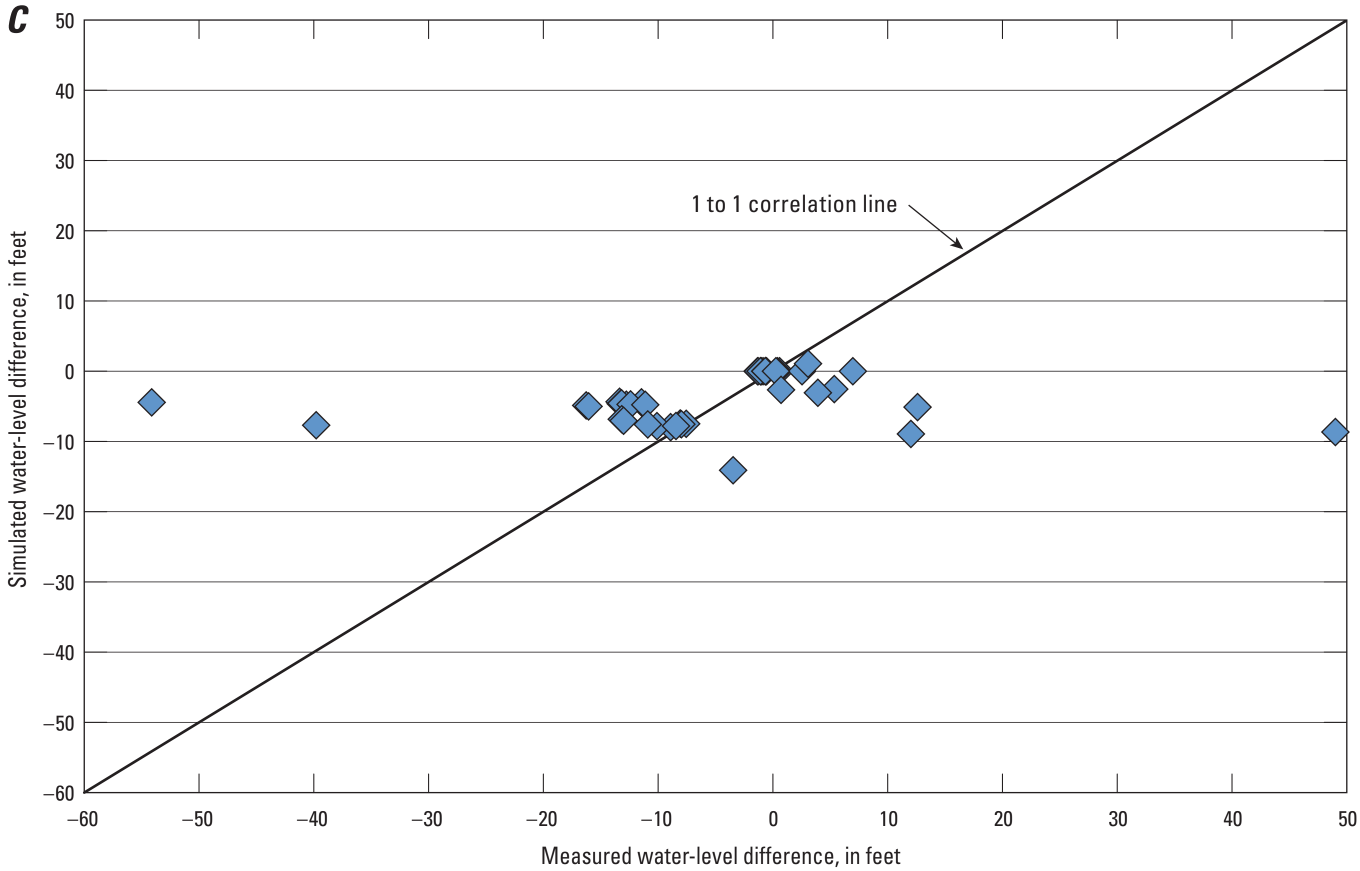

Figure 27. —Continued

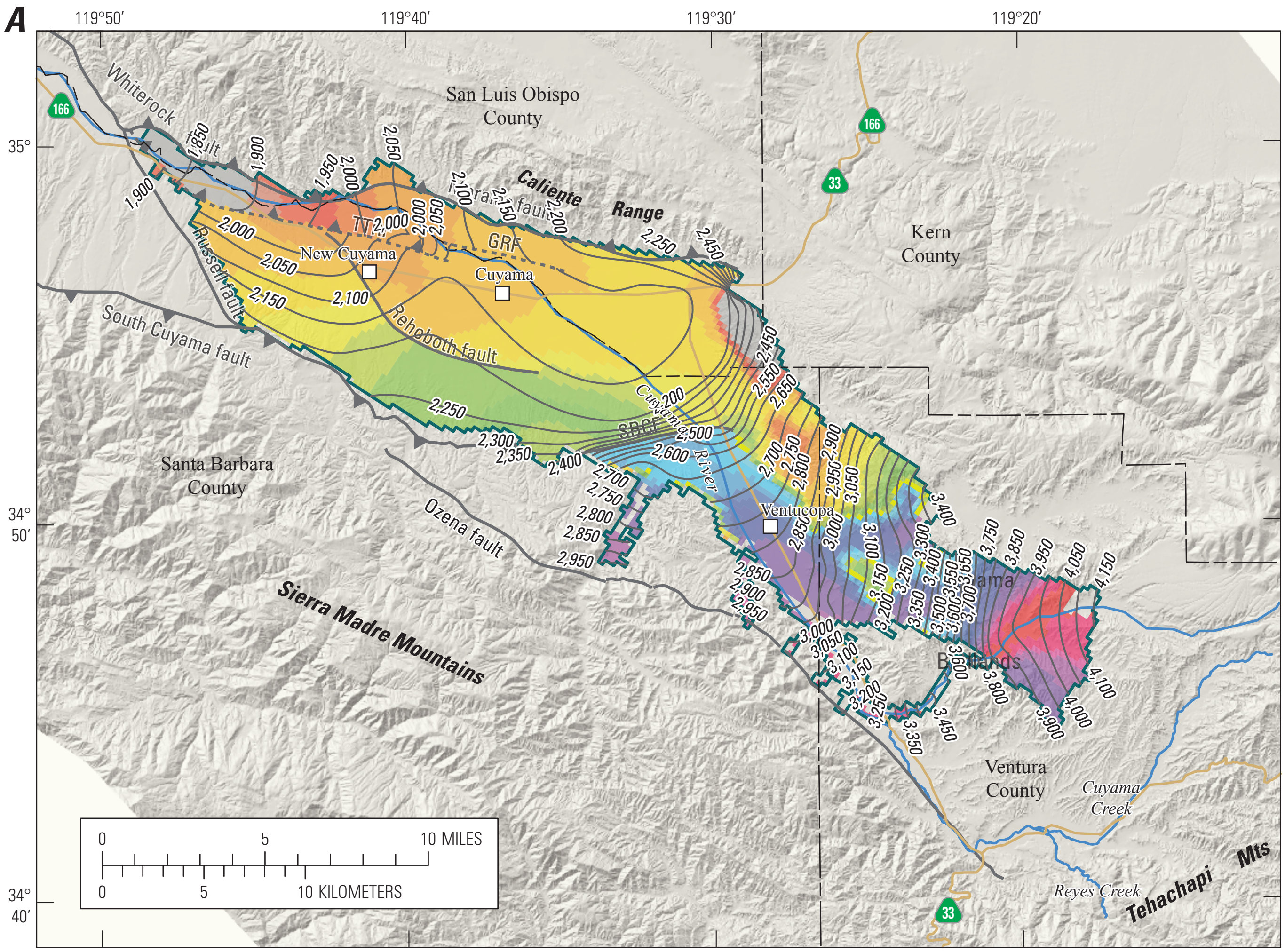

Shaded relief base created from 30-m digital elevation model from USGS National Elevation Dataset (NED); North America Vertical Datum 1983 (NAVD83). Hydrology sourced from 1:24,000-scale National Hydrography Dataset, 1974-2009. Place names sourced from USGS Geographic Names Information System, 1974-2009. Albers Projection, NAD83.

EXPLANATION

Simulated water-level altitude, summer 1966; interval is 50 feet

- <1,850
- >1,850 to 1,900
- >1,900 to 1,950
- >1,950 to 2,000
- >2,000 to 2,050
- >2,050 to 2,100
- >2,100 to 2,150
- >2,150 to 2,200
- >2,200 to 2,250
- >2,250 to 2,300
- >2,300 to 2,350
- >2,350 to 2,400
- >2,400 to 2,450
- >2,450 to 2,500
- >2,500 to 2,550
- >2,550 to 2,600
- >2,600 to 2,650
- >2,650 to 2,700
- >2,700 to 2,750
- >2,750 to 2,800
- >2,800 to 2,850
- >2,850 to 2,900
- >2,900 to 3,000
- >3,000 to 3,100
- >3,100

Active model-grid boundary

2,250 **Water-level altitude, summer 1966; interval is 50 feet**

Normal fault

Thrust fault

Thrust fault, concealed

GRF, Graveyard fault;
SBCF, Santa Barbara Canyon fault;
TTRF, Turkey Trap Ridge fault

Figure 28. Comparison of the contoured measured water levels with simulated water levels *A*, for fall 1966, *B*, for spring 2010, and *C*, for fall 2010, Cuyama Valley, California.

B

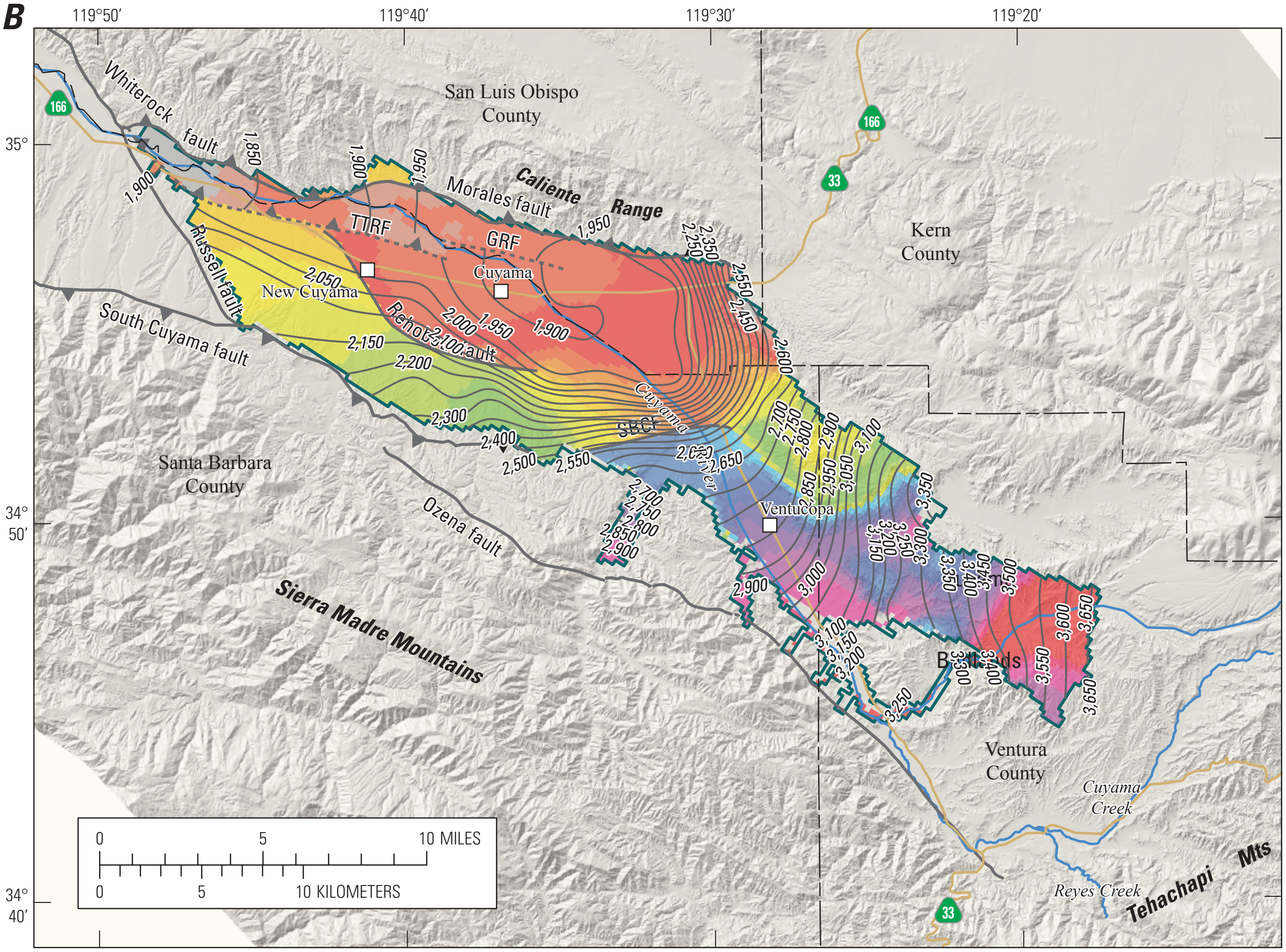

Shaded relief base created from 30-m digital elevation model from USGS National Elevation Dataset (NED); North America Vertical Datum 1983 (NAVD83). Hydrology sourced from 1:24,000-scale National Hydrography Dataset, 1974-2009. Place names sourced from USGS Geographic Names Information System, 1974-2009. Albers Projection, NAD83.

EXPLANATION

Simulated water-level altitude, spring 2010; interval is 50 feet

<1,750	>2,400 to 2,450
>1,750 to 1,800	>2,450 to 2,500
>1,850 to 1,850	>2,500 to 2,550
>1,850 to 1,900	>2,550 to 2,600
>1,900 to 1,950	>2,600 to 2,650
>1,950 to 2,000	>2,650 to 2,700
>2,000 to 2,050	>2,700 to 2,750
>2,050 to 2,100	>2,750 to 2,800
>2,100 to 2,150	>2,800 to 2,850
>2,150 to 2,200	>2,850 to 2,900
>2,200 to 2,250	>2,900 to 3,000
>2,250 to 2,300	>3,000 to 3,100
>2,300 to 2,350	>3,100
>2,350 to 2,400	

Active model-grid boundary

~2,250 **Water-level altitude, spring 2010; interval is 50 feet**

Normal fault

Thrust fault

Thrust fault, concealed

GRF, Graveyard fault;
SBCF, Santa Barbara Canyon fault;
TTRF, Turkey Trap Ridge fault

Figure 28. —Continued

C

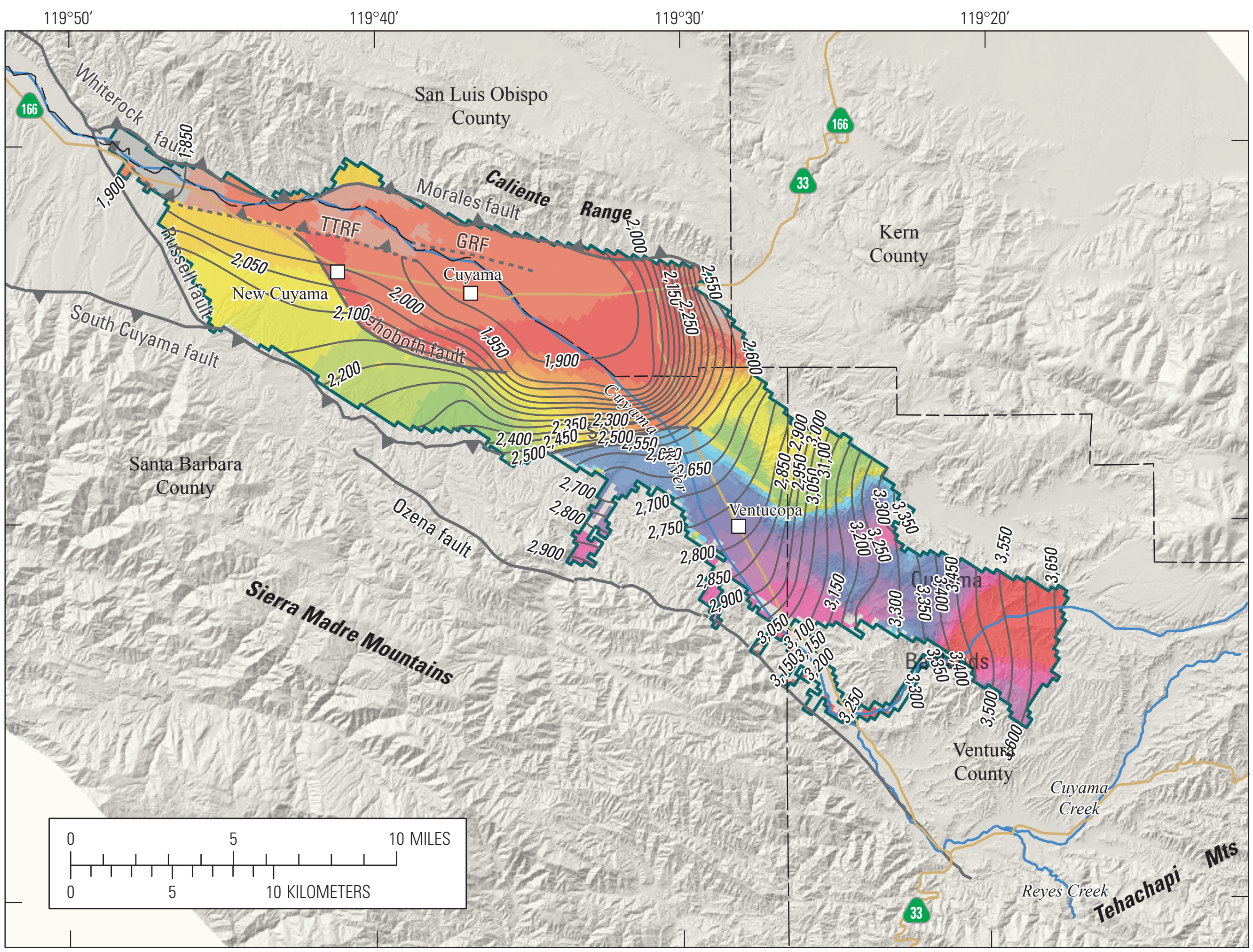

Shaded relief base created from 30-m digital elevation model from USGS National Elevation Dataset (NED); North America Vertical Datum 1983 (NAVD83). Hydrology sourced from 1:24,000-scale National Hydrography Dataset, 1974-2009. Place names sourced from USGS Geographic Names Information System, 1974-2009. Albers Projection, NAD83.

EXPLANATION

Simulated water-level altitude, summer 2010; interval is 50 feet

- <1,750
- >1,750 to 1,800
- >1,850 to 1,850
- >1,850 to 1,900
- >1,900 to 1,950
- >1,950 to 2,000
- >2,000 to 2,050
- >2,050 to 2,100
- >2,100 to 2,150
- >2,150 to 2,200
- >2,200 to 2,250
- >2,250 to 2,300
- >2,300 to 2,350
- >2,350 to 2,400
- >2,400 to 2,450
- >2,450 to 2,500
- >2,500 to 2,550
- >2,550 to 2,600
- >2,600 to 2,650
- >2,650 to 2,700
- >2,700 to 2,750
- >2,750 to 2,800
- >2,800 to 2,850
- >2,850 to 2,900
- >2,900 to 3,000
- >3,000 to 3,100
- >3,100

Active model-grid boundary

2,250 **Water-level altitude, summer 2010; interval is 50 feet**

Normal fault

Thrust fault

Thrust fault, concealed

GRF, Graveyard fault;
SBCF, Santa Barbara Canyon fault;
TTRF, Turkey Trap Ridge fault

Figure 28. —Continued

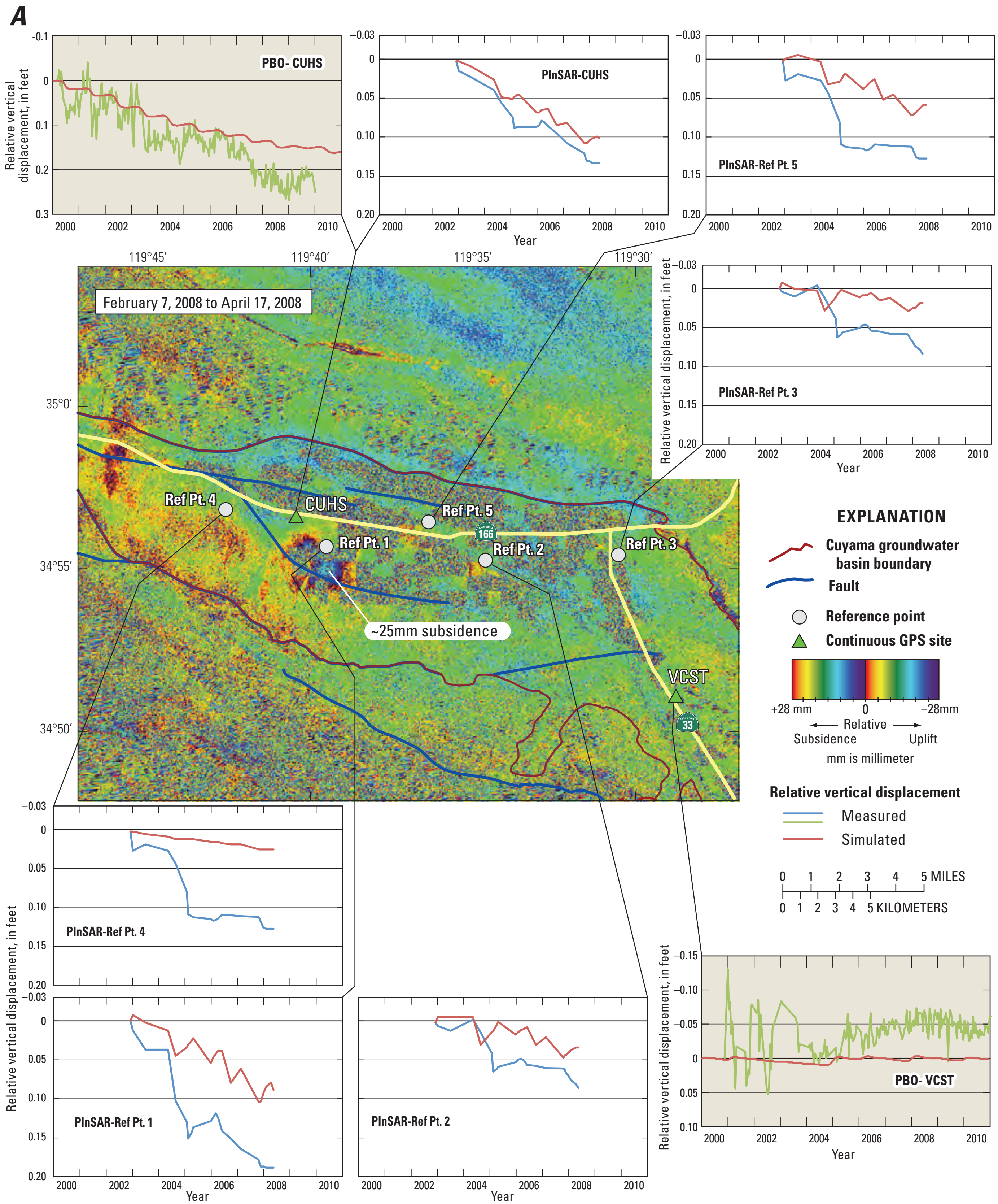

Figure 29. Historical subsidence as *A*, map of seasonal InSAR with graphs of simulated and measured time series for selected locations of relative land-surface deformation from Plate-Boundary Observation (PBO) sites and Point InSAR targets, and *B*, simulated total subsidence 1950–2010 for the calibrated hydrologic flow model, Cuyama Valley, California.

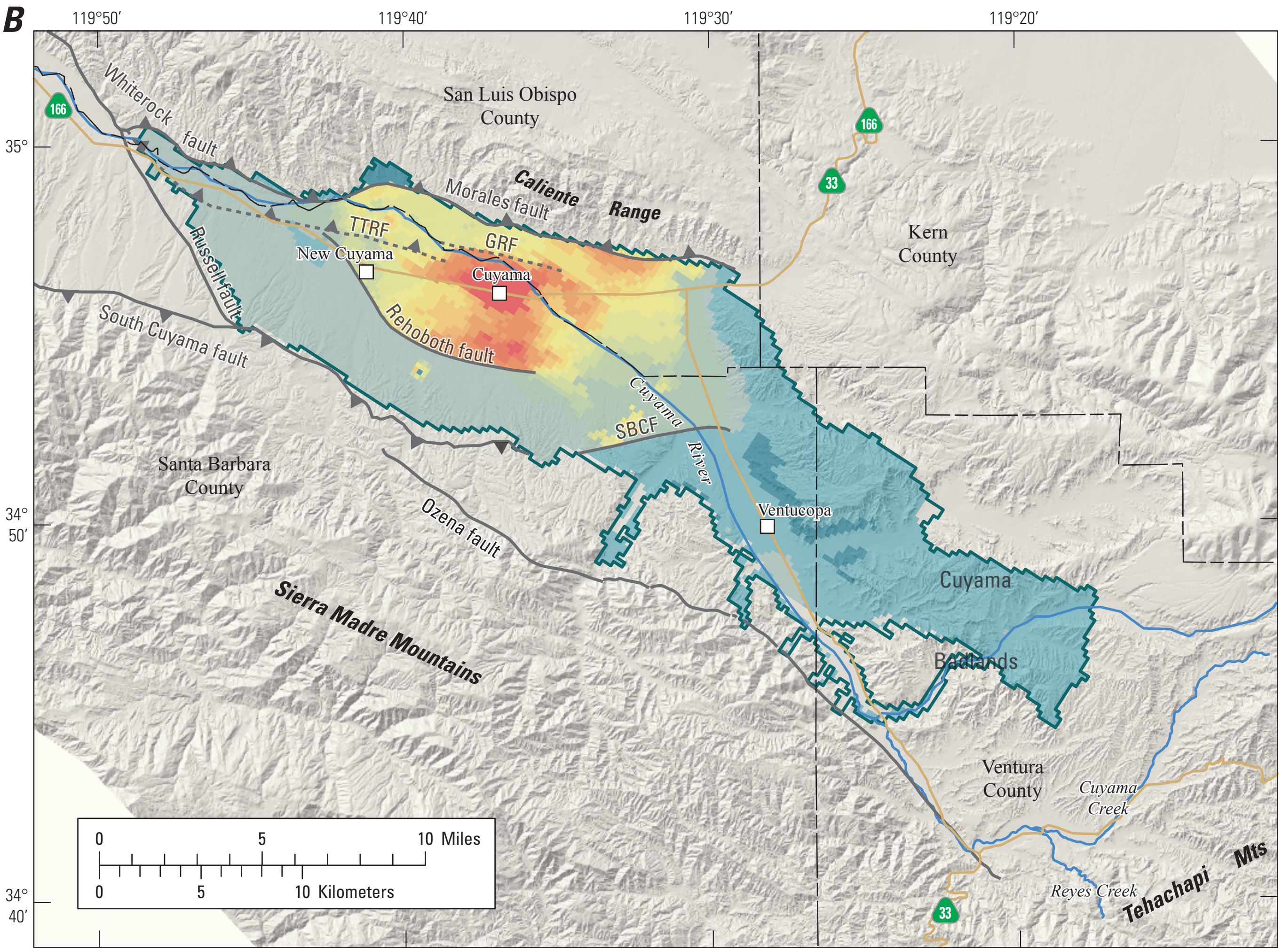

Shaded relief base created from 30-m digital elevation model from USGS National Elevation Dataset (NED); North America Vertical Datum 1983 (NAVD83). Hydrology sourced from 1:24,000-scale National Hydrography Dataset, 1974-2009. Place names sourced from USGS Geographic Names Information System, 1974-2009. Albers Projection, NAD83.

EXPLANATION

Simulated subsidence, in feet negative values are uplift

- –0.2559 to –0.1
- >–0.1 to 0
- >0 to 0.10
- >0.10 to 0.20
- >0.20 to 0.30
- >0.30 to 0.40
- >0.40 to 0.50
- >0.50 to 0.60
- >0.60 to 0.70
- >0.70 to 0.80
- >0.80 to 0.90
- >0.90 to 1.00
- >1.00 to 1.10
- >1.10 to 1.20
- >1.20 to 1.59

Active model-grid boundary

Normal fault

Thrust fault

Thrust fault, concealed

GRF, Graveyard fault;
SBCF, Santa Barbara Canyon fault;
TTRF, Turkey Trap Ridge fault

Figure 29. —Continued

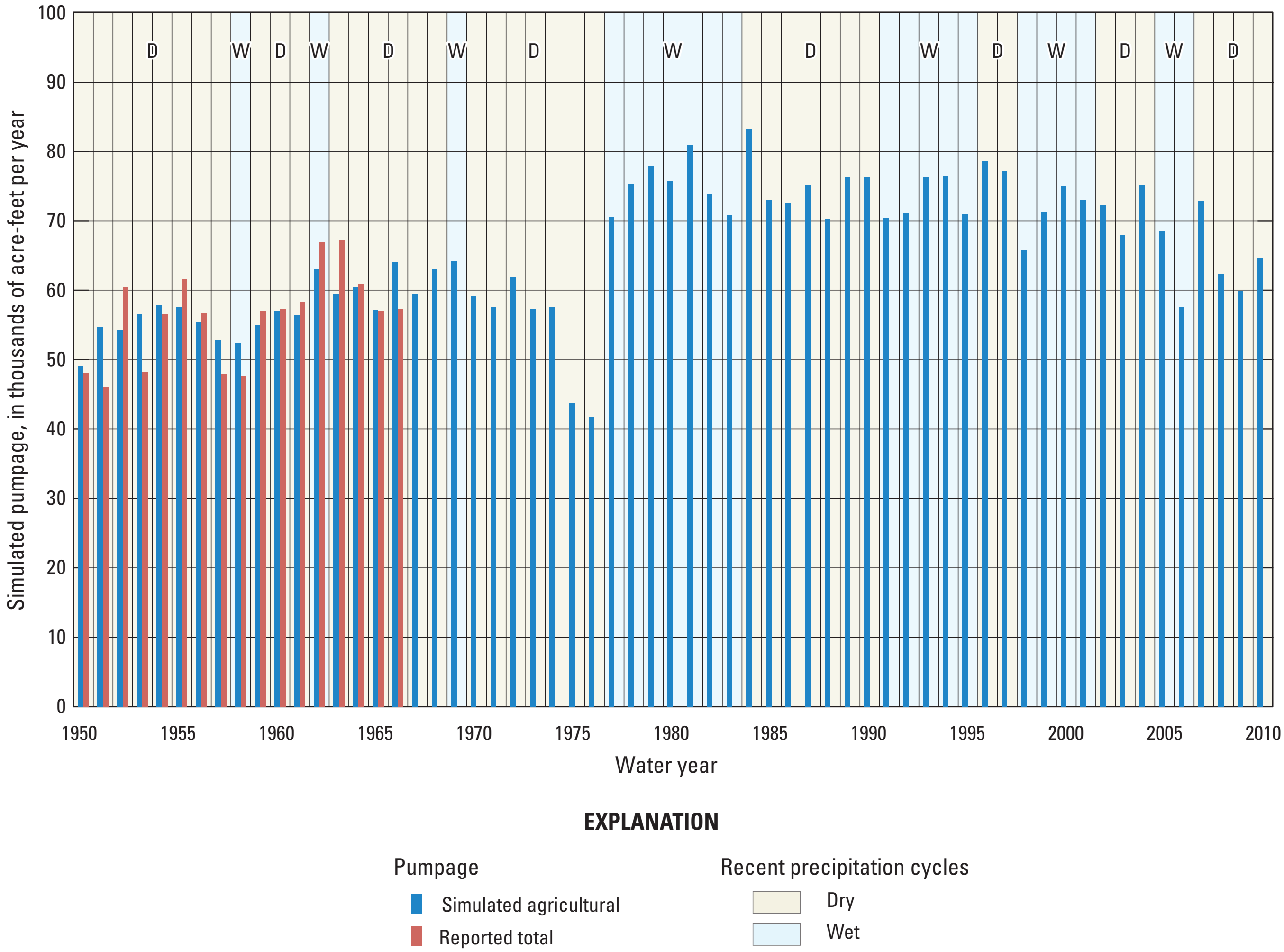

Figure 30. Reported and simulated agricultural pumpage for Cuyama Valley, California.

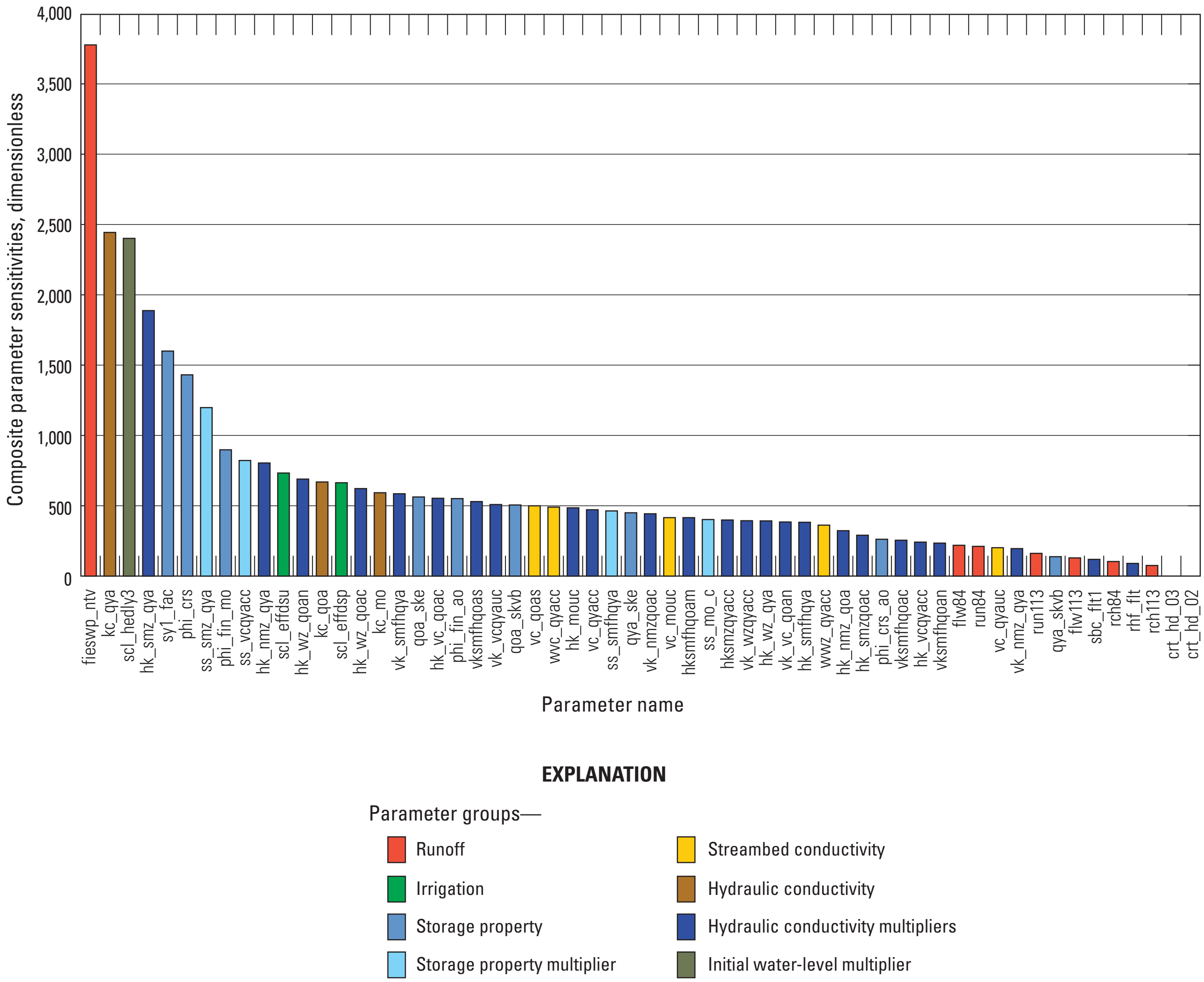

See tables 14 and 15 for names and explanations of all parameter identifiers.

Figure 31. Relative composite sensitivity of computed observations at calibration points to changes in selected parameters from analysis with PEST.

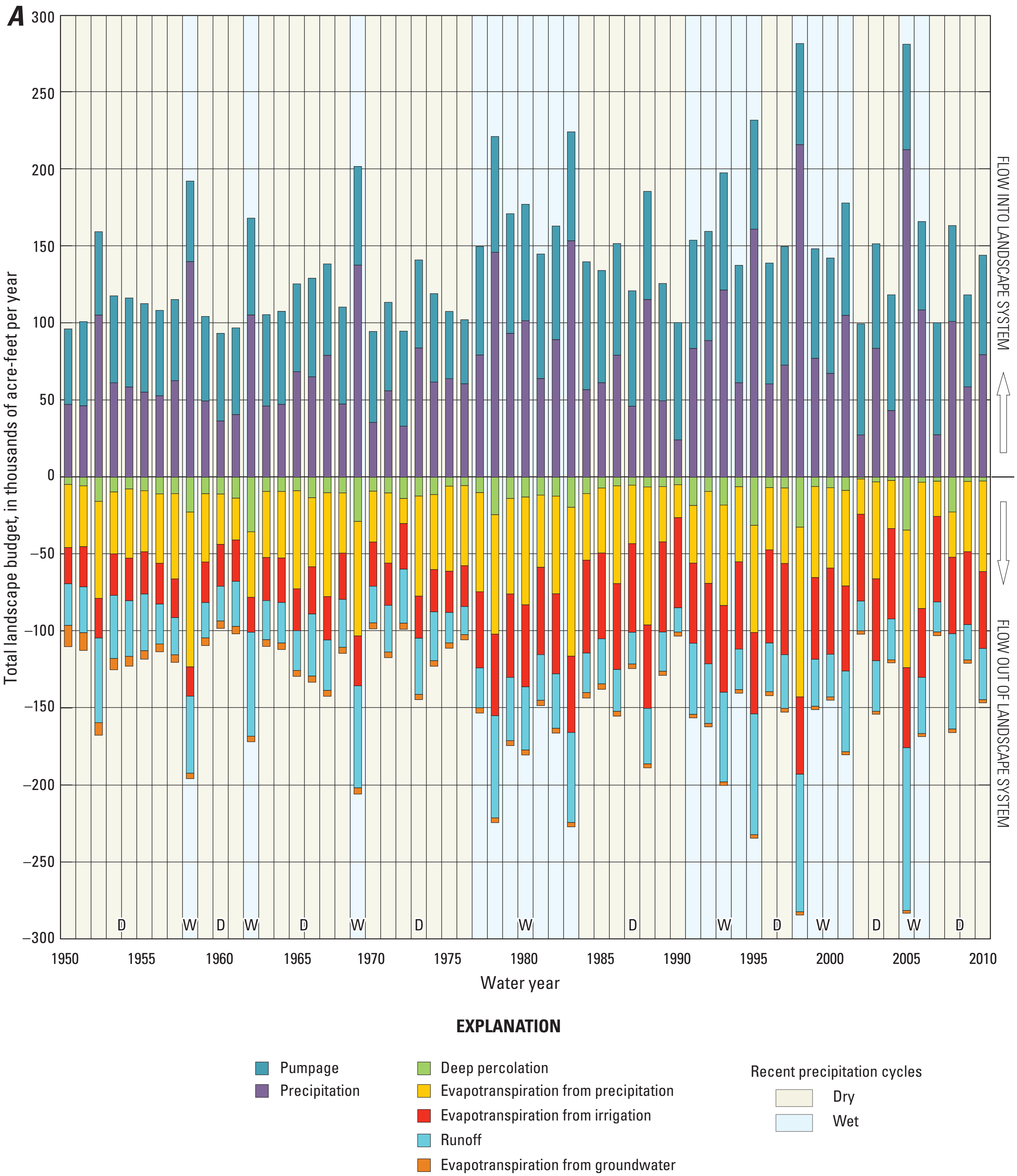

Figure 32. Hydrologic budget for the landscape with *A*, the temporal distribution of total landscape inflows and outflows, and *B*, average annual components of farm budget of the simulated landscape flow system within the Cuyama Valley Hydrologic Model (CUVHM), Cuyama Valley, California.

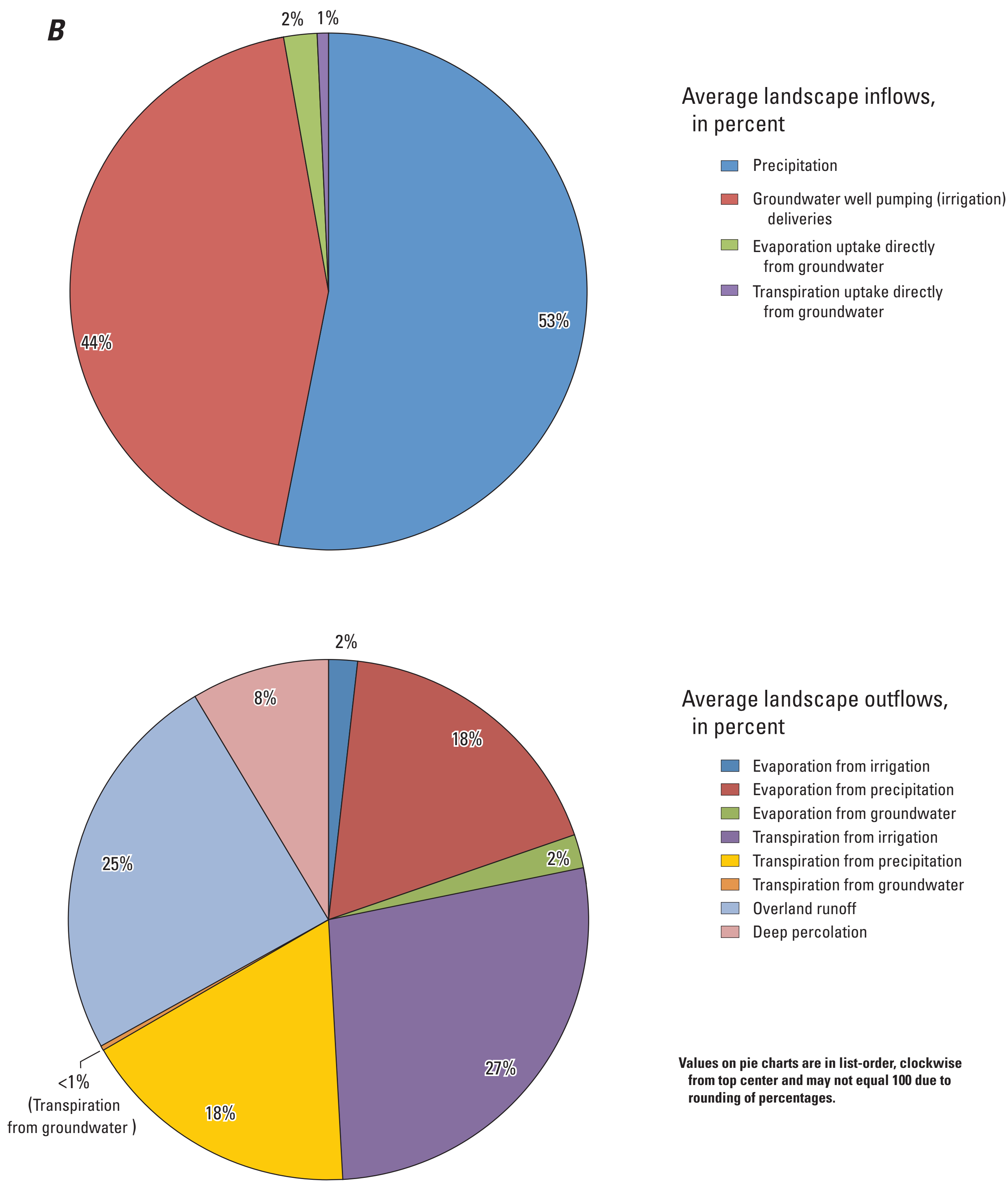

Figure 32. —Continued

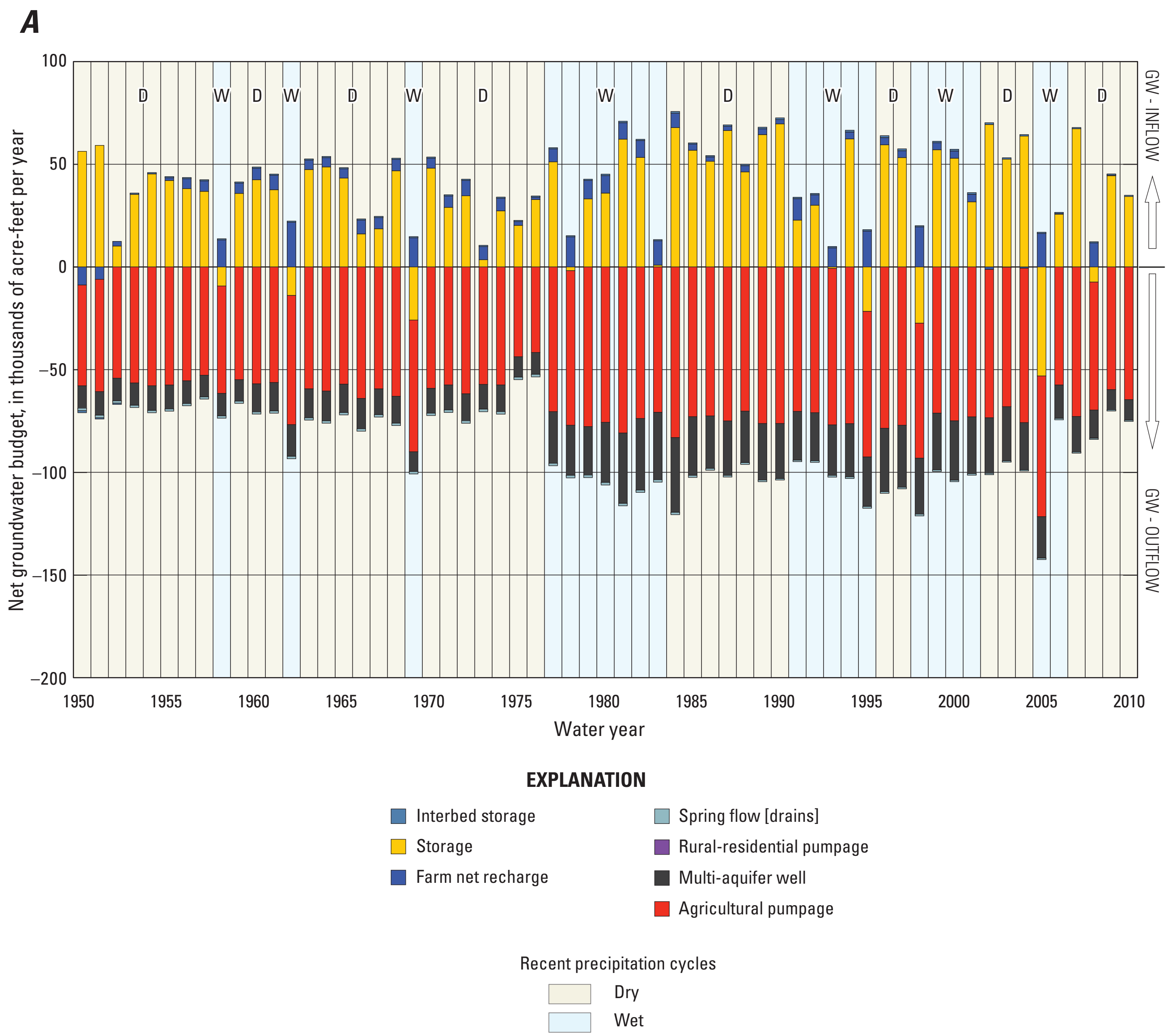

Figure 33. *A*, the simulated net flow of groundwater in the hydrologic cycle, *B*, average annual components of simulated groundwater flow, and *C*, the cumulative change in storage and *D*, changes in groundwater storage, Cuyama Valley, California.

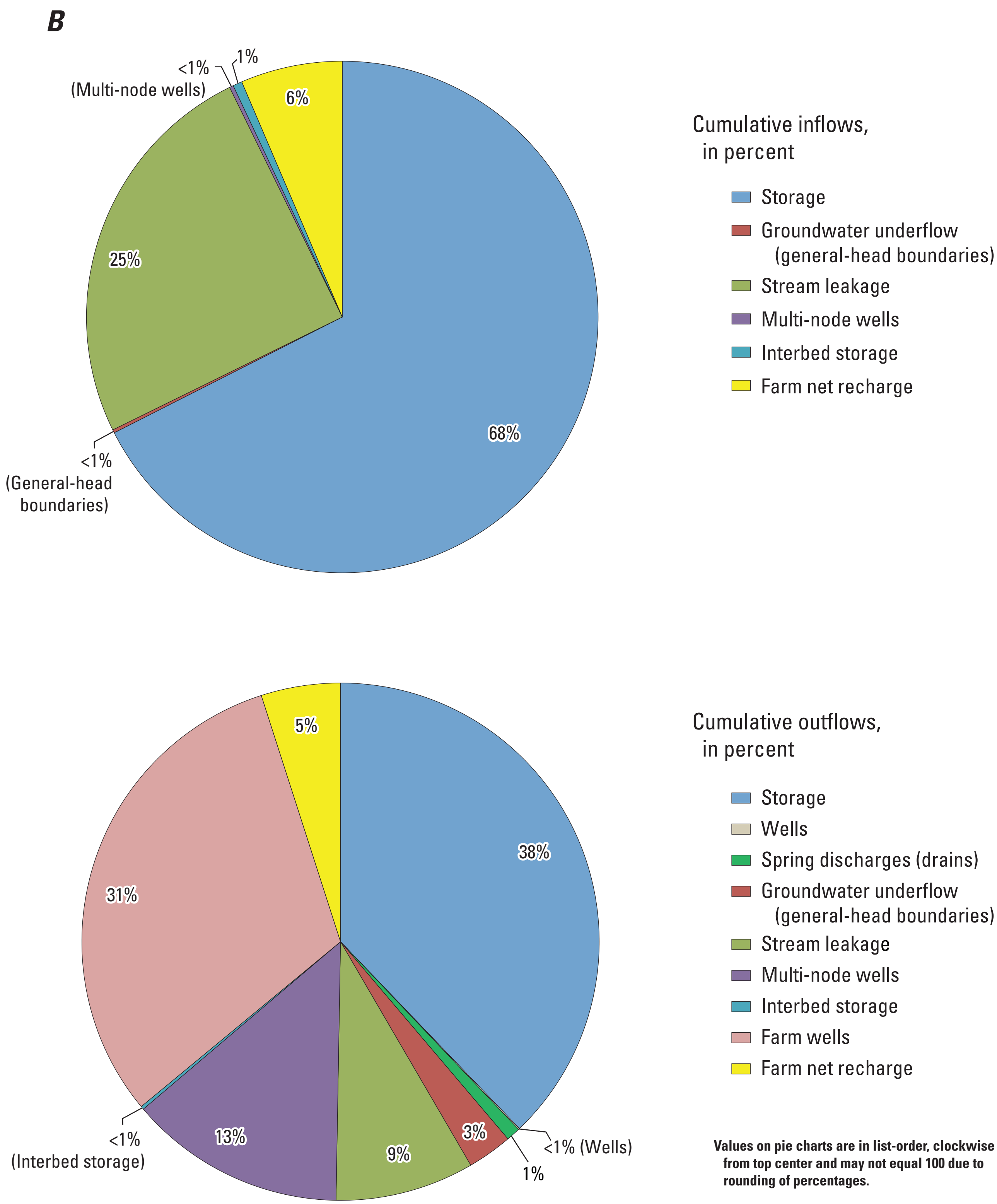

Figure 33. —Continued

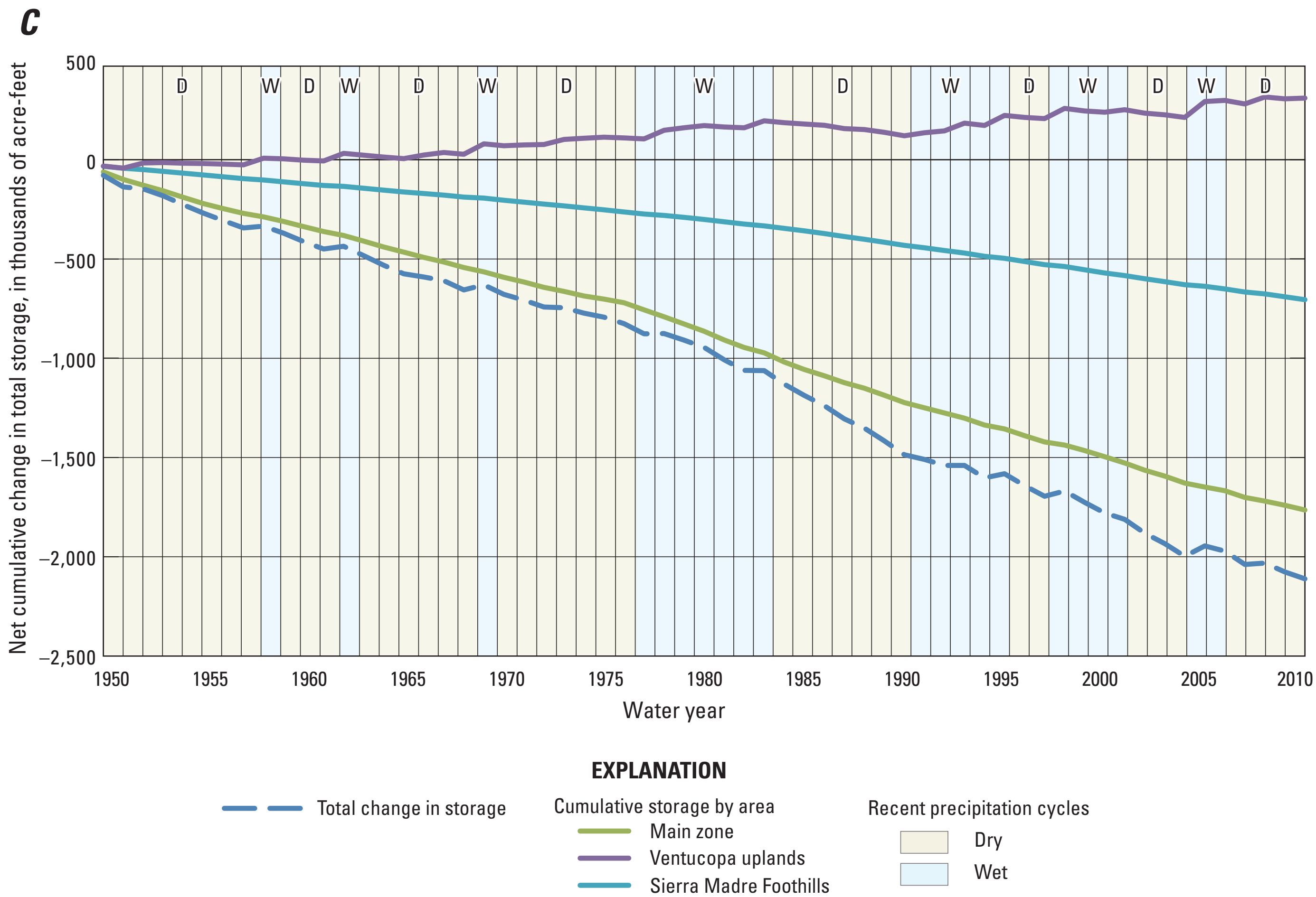

Figure 33. —Continued

B

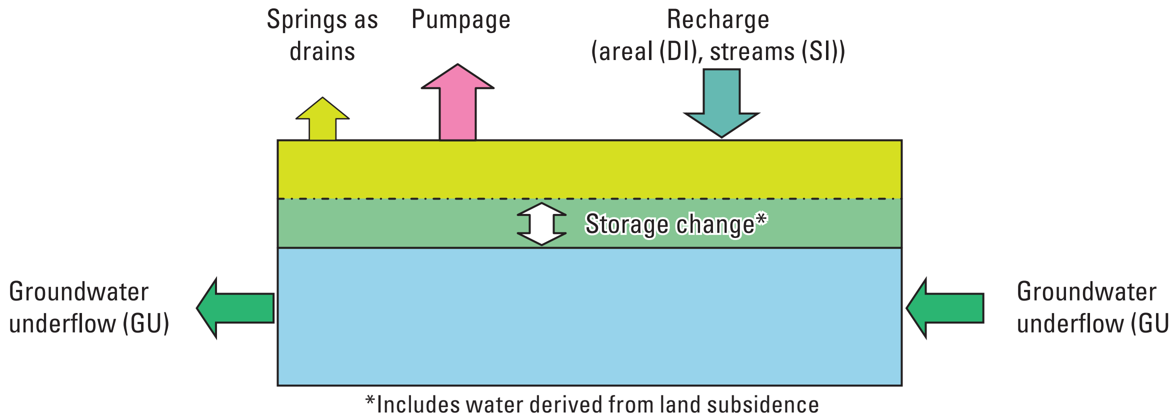

GROUNDWATER-FLOW BUDGET SUMMARY

(Average-net flows in acre-feet per year)

Source	Valley wide				Main zone	Ventucopa Uplands	Sierra Madre Foothills	Base case[1]	Reduced supply[2]	Reduced demand[3]
Time period (Water years)	1950–2010[4]	2000–2010[5]	2005 (Wet)	2009 (Dry)	2000–2010	2000–2010	2000–2010	2011–2071[6]	2011–2071	2011–2071
Inflows:										
Storage depletion:	34,100	34,800	0	45,860	27,500	0	13,800	32,700	500	0
Direct infiltration (DI)[7]	5,600	3,100	16,600	100	700	1,500	900	2,400	1,100	1,300
Streamflow infiltration (SI)	27,500	30,300	93,600	16,700	8,300	20,500	1,600	29,500	25,600	29,500
Total recharge (DI+SI):	33,100	33,400	110,200	16,800	9,000	22,000	2,500	31,900	26,700	30,800
Total inflows:	67,200	68,200	164,210	62,660	36,500	22,000	16,300	64,600	27,200	30,800
Outflows:										
Storage accretion:	0	0	54,010	0	0	6,000	0	0	0	11,900
Underflow (GU):	3,700	3,100	700	500	3,200	15	0	2,900	3,700	3,000
Springs as drains:	1,000	600	700	500	600	0	0	400	500	600
Domestic pumpage:	20	10	10	10	6	8	2	7	7	7
Water-supply pumpage:	90	190	180	1900	190	0	0	190	190	190
Agricultural pumpage:	65,300	68,100	68,100	61,000	56,700	10,000	1,400	63,700	32,800	15,800
Total pumpage:	65,400	68,300	68,290	61,200	56,900	10,000	1,400	63,900	33,000	16,000
Total outflows:	70,100	68,900	123,000	107,560	57,500	16,000	1,400	67,200	36,400	31,500
Inflows - Outflows =	–2,900[8]	–700[8]	41,210[9]	–44,900[8]	–21,000[8]	6,000[9]	–14,900[8]	–2,600[8]	–9,200[8]	–700[9]

[1] Base Case projection of current demand with historical climate
[2] Base Case projection with supply limited to recharge
[3] Base Case pojection with no agriculture in the Main-zone subregions
[4] Historical period that represents two climate cycles
[5] Historical period that represents recent climate and land use conditions
[6] Projection of historical climate and 2010 land use
[7] Includes water lost to evapotranspiration
[8] Demand greater than replenishment (overdraft)
[9] Replenishment is greater than demand

Figure 33. —Continued

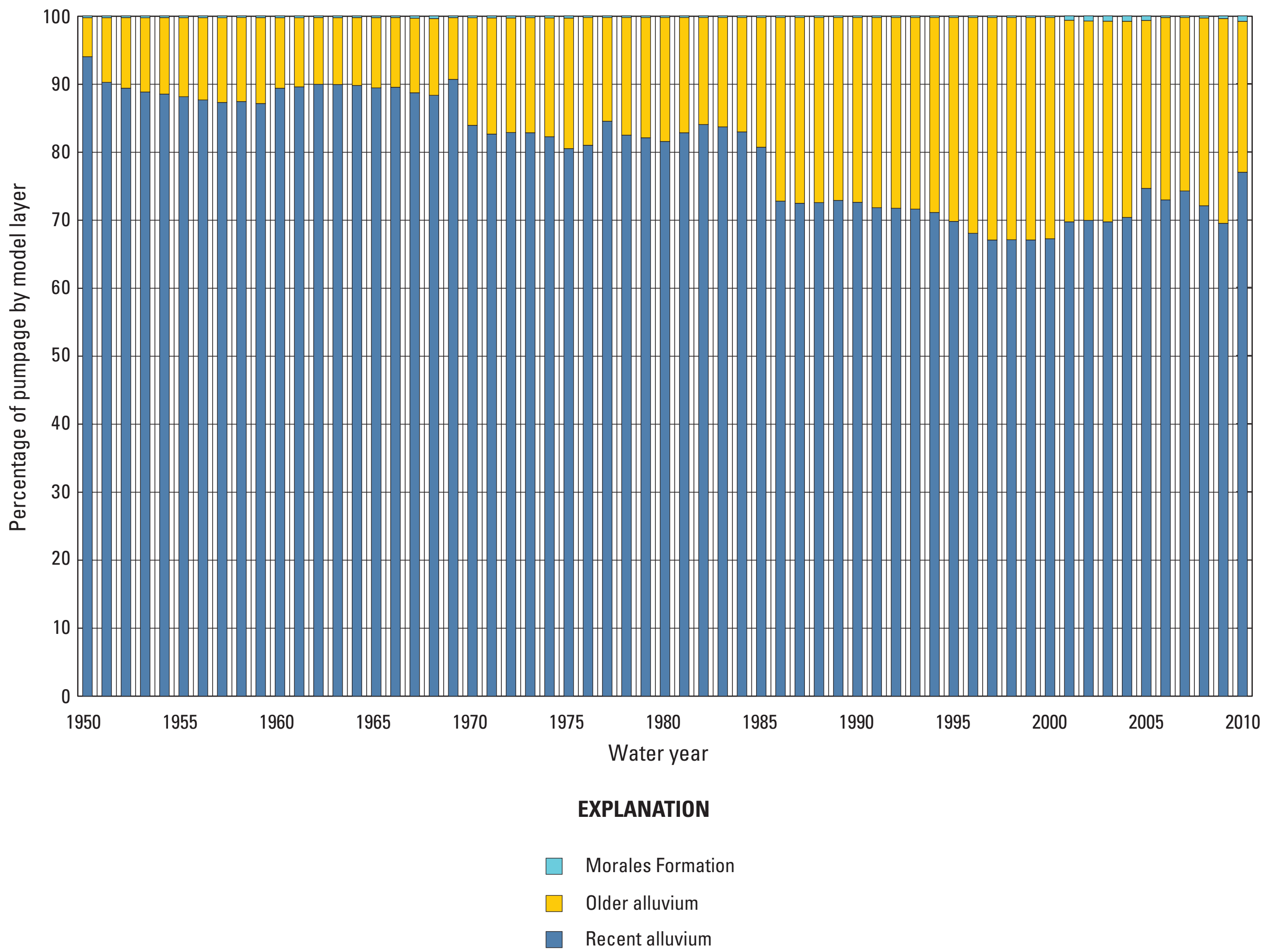

Figure 34. Percentage of simulated groundwater pumpage for the water years 1950–2010 for all three model layers, Cuyama Valley, California.

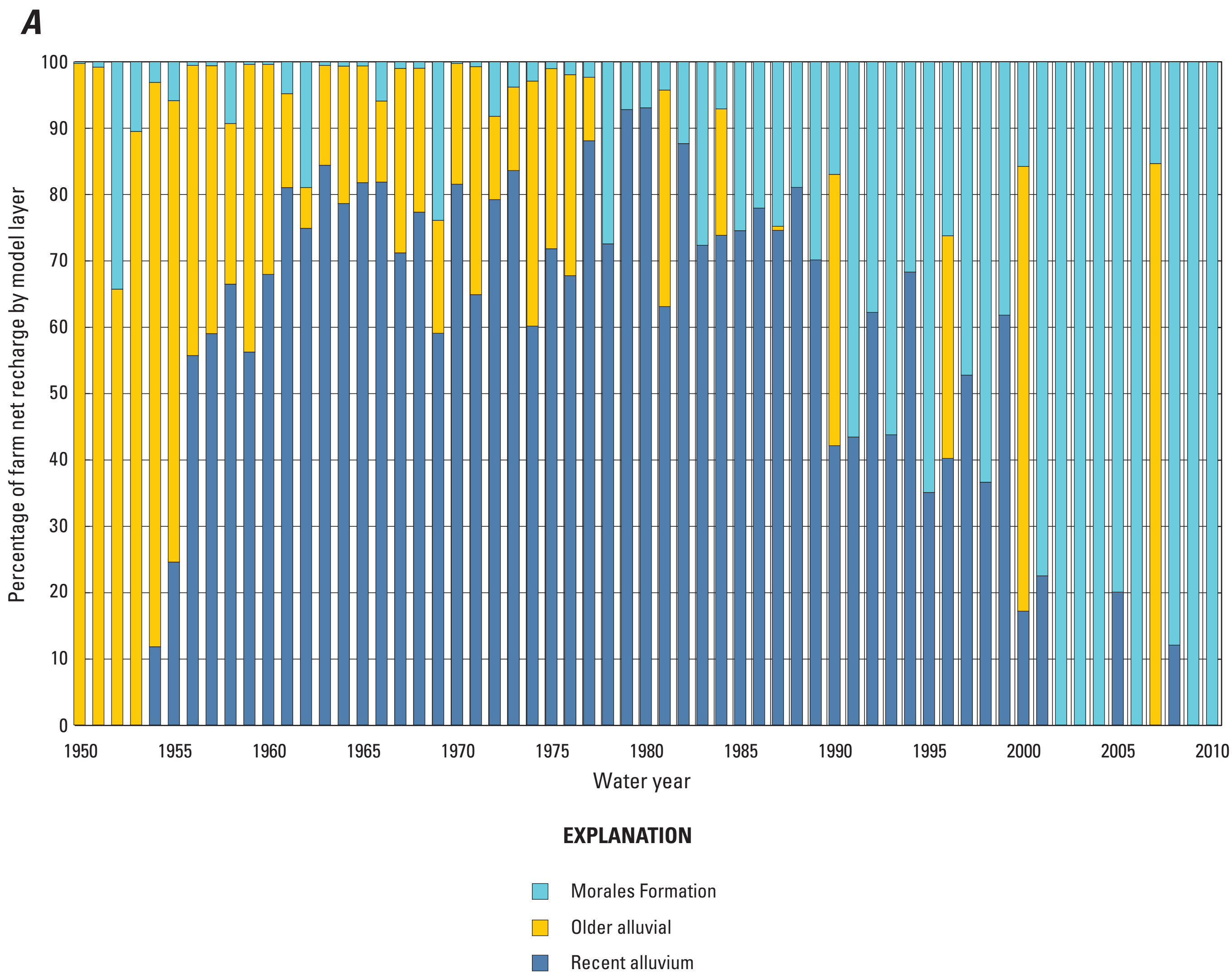

Figure 35. Stacked bar chart showing *A*, percentage of total recharge by aquifer model layers, and *B*, Net downward flow between model layers, Cuyama Valley, California.

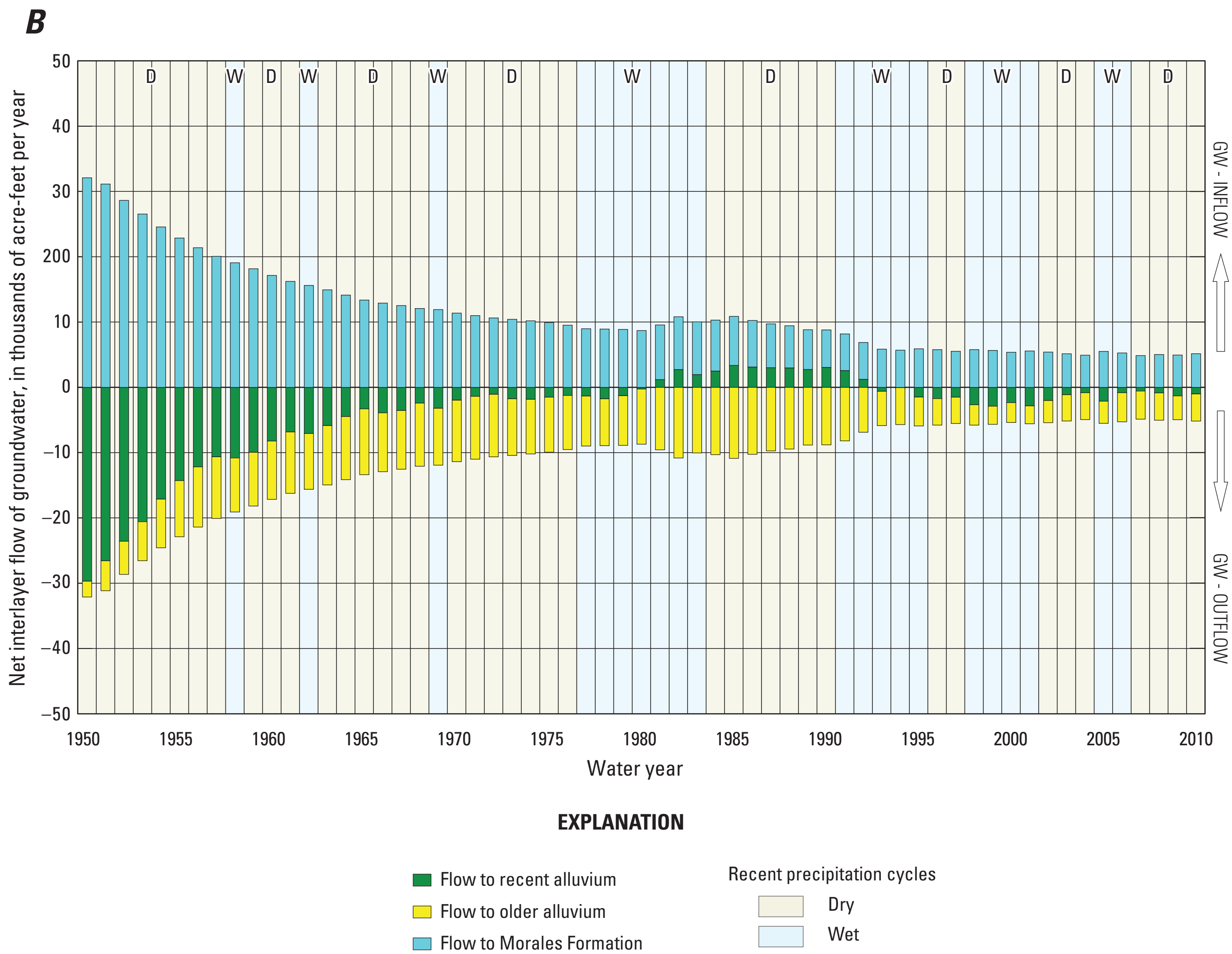

Figure 35. —Continued

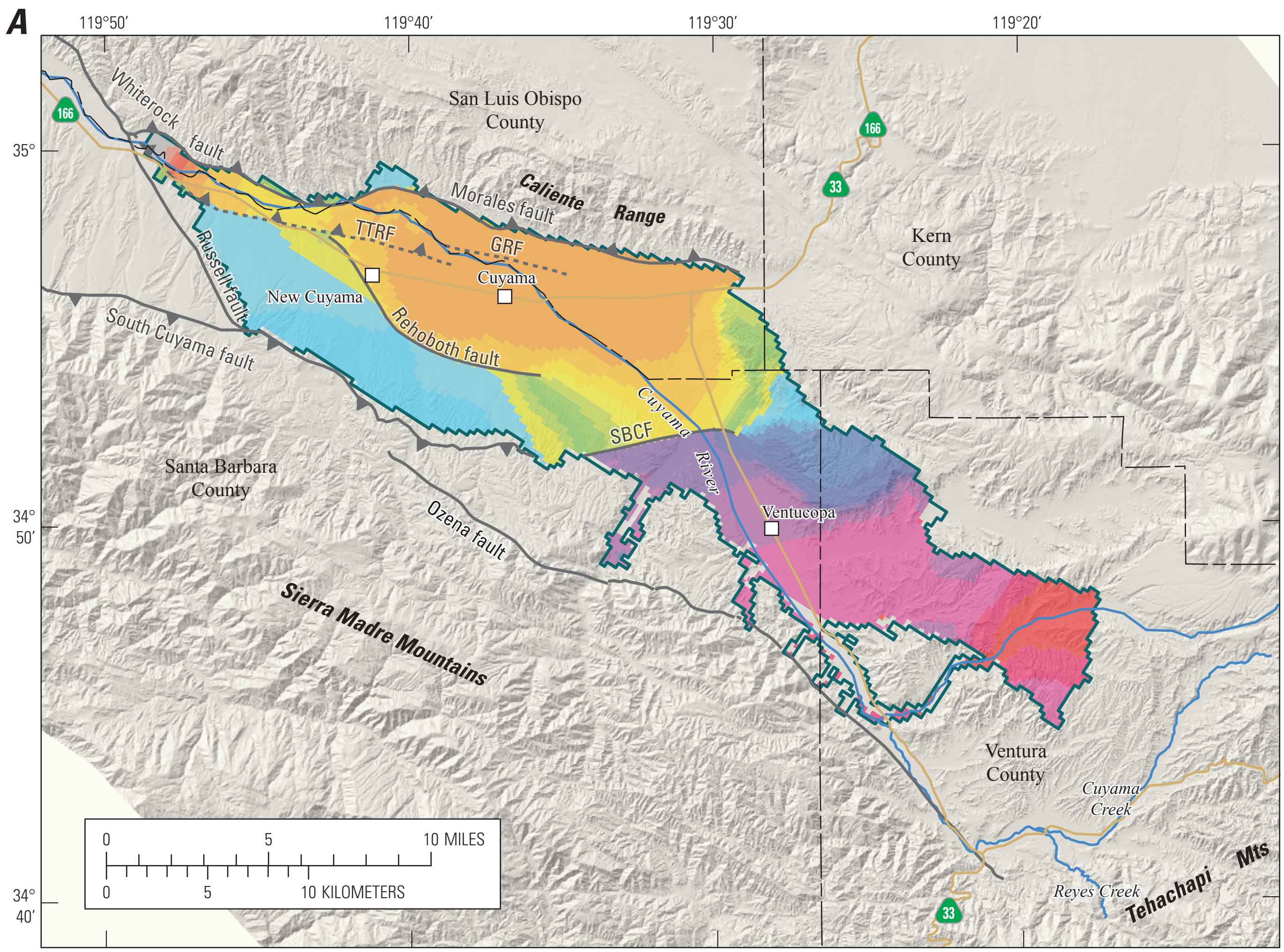

Shaded relief base created from 30-m digital elevation model from USGS National Elevation Dataset (NED); North America Vertical Datum 1983 (NAVD83). Hydrology sourced from 1:24,000-scale National Hydrography Dataset, 1974-2009. Place names sourced from USGS Geographic Names Information System, 1974-2009. Albers Projection, NAD83.

EXPLANATION

Simulated water-level altitude, in feet, summer 2071; contour interval varies

- <1,400
- >1,400 to 1,450
- >1,450 to 1,500
- >1,500 to 1,550
- >1,550 to 1,600
- >1,600 to 1,650
- >1,650 to 1,700
- >1,700 to 1,750
- >1,750 to 1,800
- >1,800 to 1,850
- >1,850 to 1,900
- >1,900 to 1,950
- >1,950 to 2,000
- >2,000 to 2,050
- >2,050 to 2,100
- >2,100 to 2,150
- >2,150 to 2,200
- >2,200 to 2,300
- >2,300 to 2,400
- >2,400 to 2,500
- >2,500 to 2,600
- >2,600 to 2,800
- >2,800 to 3,000
- >3,000 to 3,400
- >3,400

Active model-grid boundary

Normal fault

Thrust fault

Thrust fault, concealed

GRF, Graveyard fault;
SBCF, Santa Barbara Canyon fault;
TTRF, Turkey Trap Ridge fault

Figure 36. *A*, projected simulated water levels and *B*, the difference in water levels between projection of simulated water levels in fall 2071 and simulated water levels in fall 2010 for the hydrologic flow model of Cuyama Valley, California.

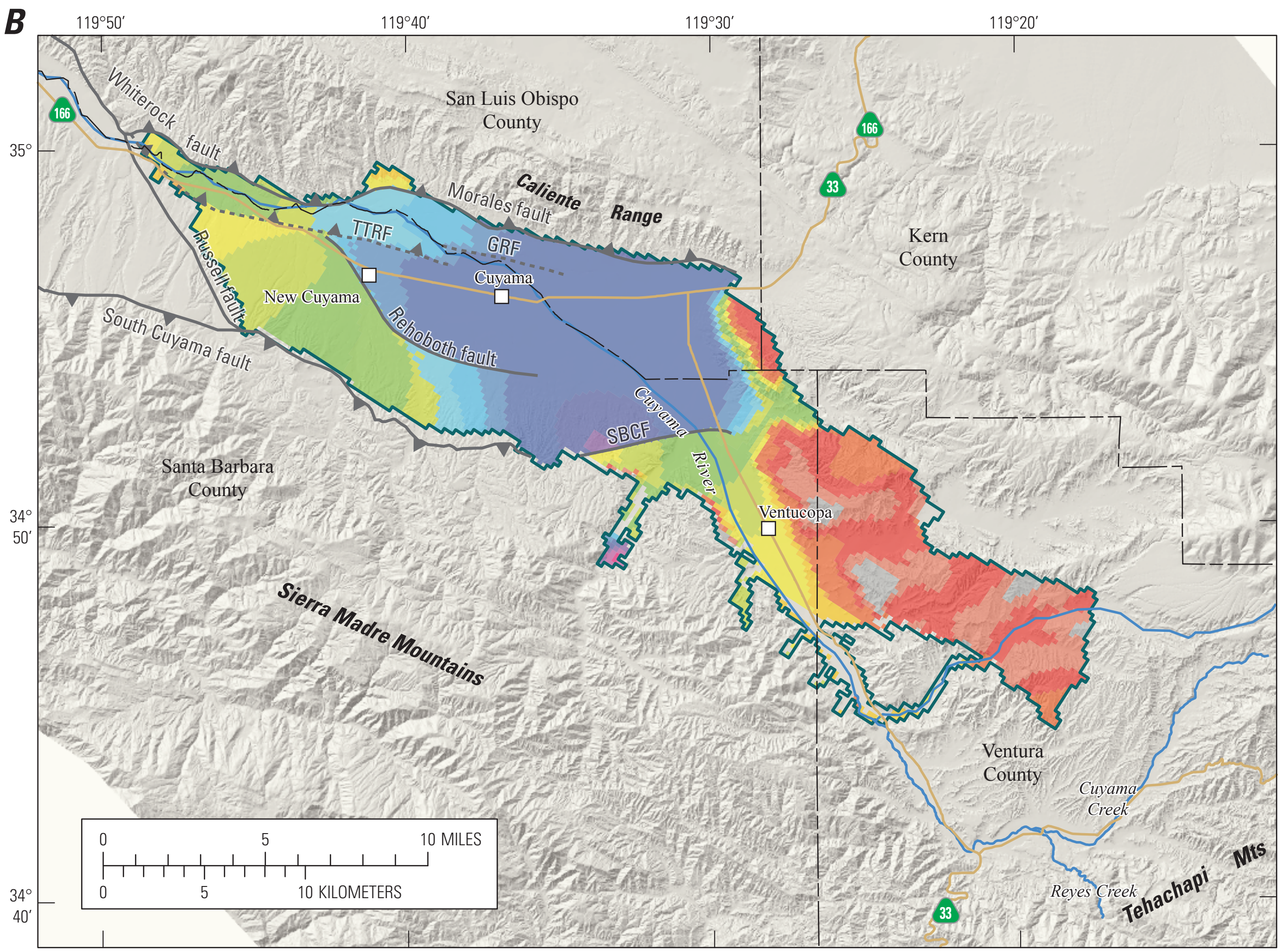

Shaded relief base created from 30-m digital elevation model from USGS National Elevation Dataset (NED); North America Vertical Datum 1983 (NAVD83). Hydrology sourced from 1:24,000-scale National Hydrography Dataset, 1974-2009. Place names sourced from USGS Geographic Names Information System, 1974-2009. Albers Projection, NAD83.

EXPLANATION

Simulated difference in water-level altitude, in feet, summer 2010 minus summer 2071; interval varies

- <–150
- >–150 to –100
- >–100 to –50
- >–50 to 0
- >0 to 1
- >1 to 10
- >10 to 25
- >25 to 50
- >50 to 75
- >75 to 100
- >100 to 125
- >125 to 150
- >150 to 175
- >175 to 200
- >200 to 250
- >250 to 275
- >275 to 300
- >300 to 350
- >350 to 400

Active model-grid boundary

Normal fault

Thrust fault

Thrust fault, concealed

Figure 36. —Continued

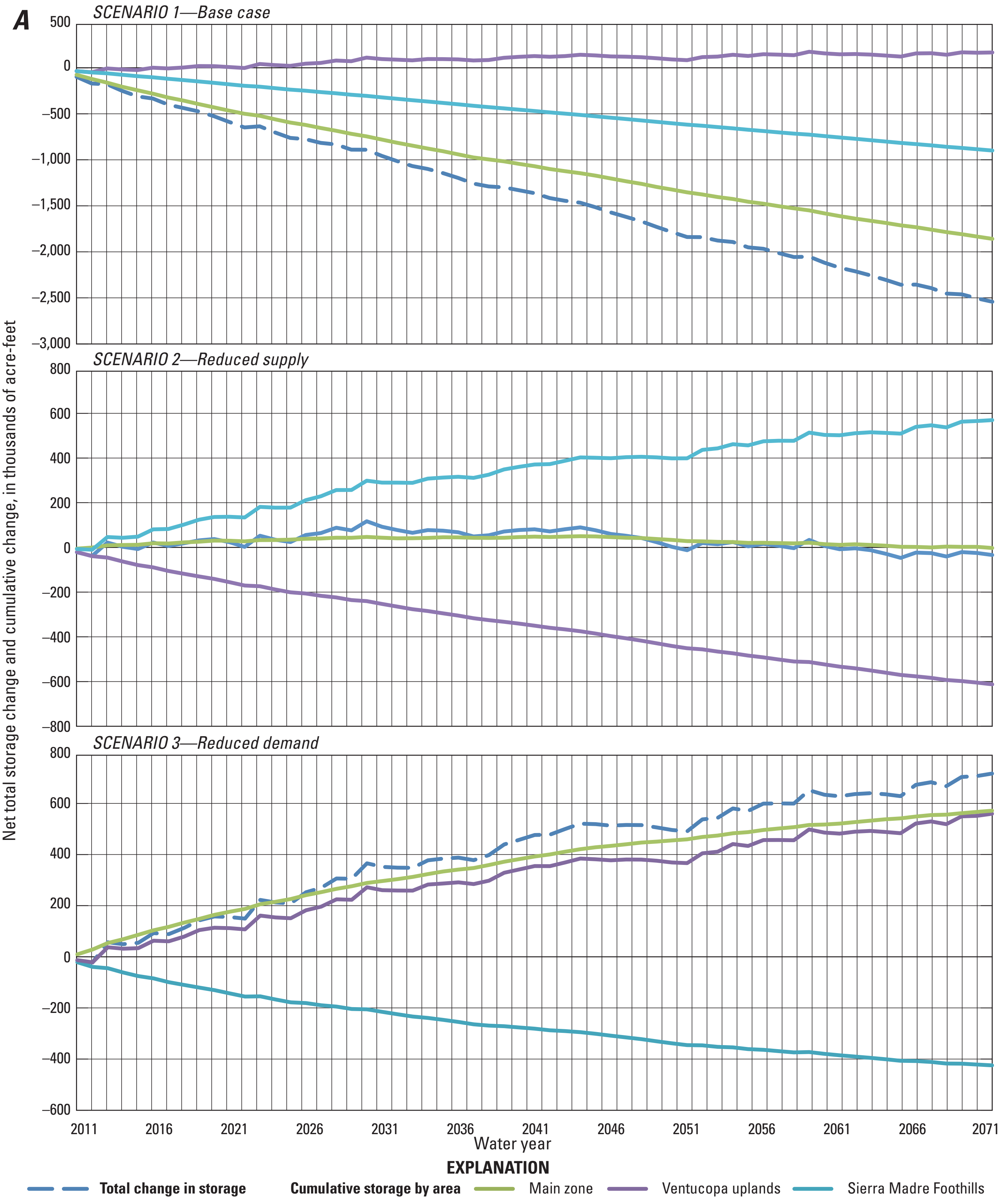

Figure 37. Three projected scenarios showing projected *A*, cumulative change in net groundwater storage, *B*, potential groundwater levels at CVKR and CVBR monitoring sites, and *C*, potential land subsidence near Cuyama, Cuyama Valley, California.

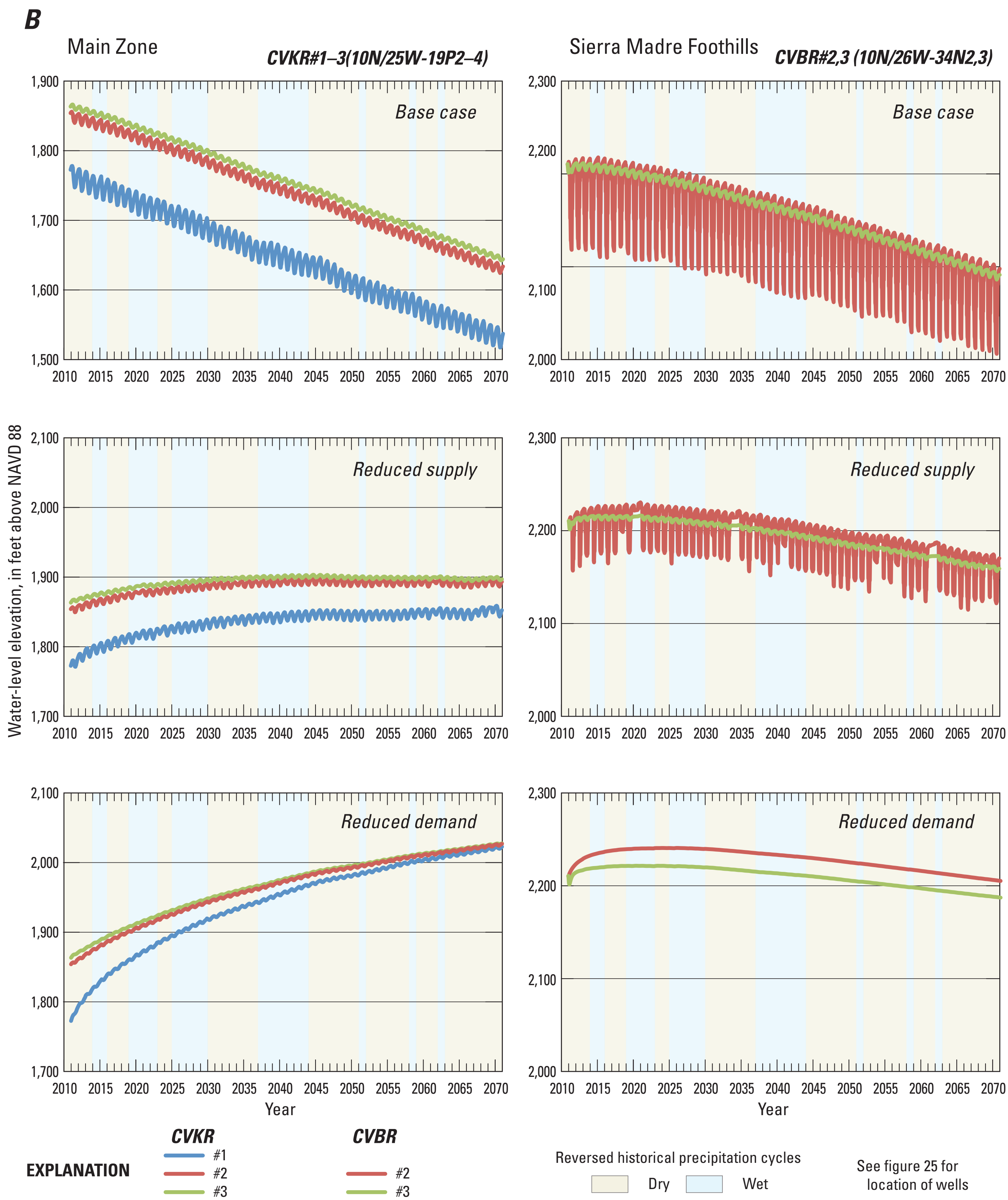

Figure 37. —Continued

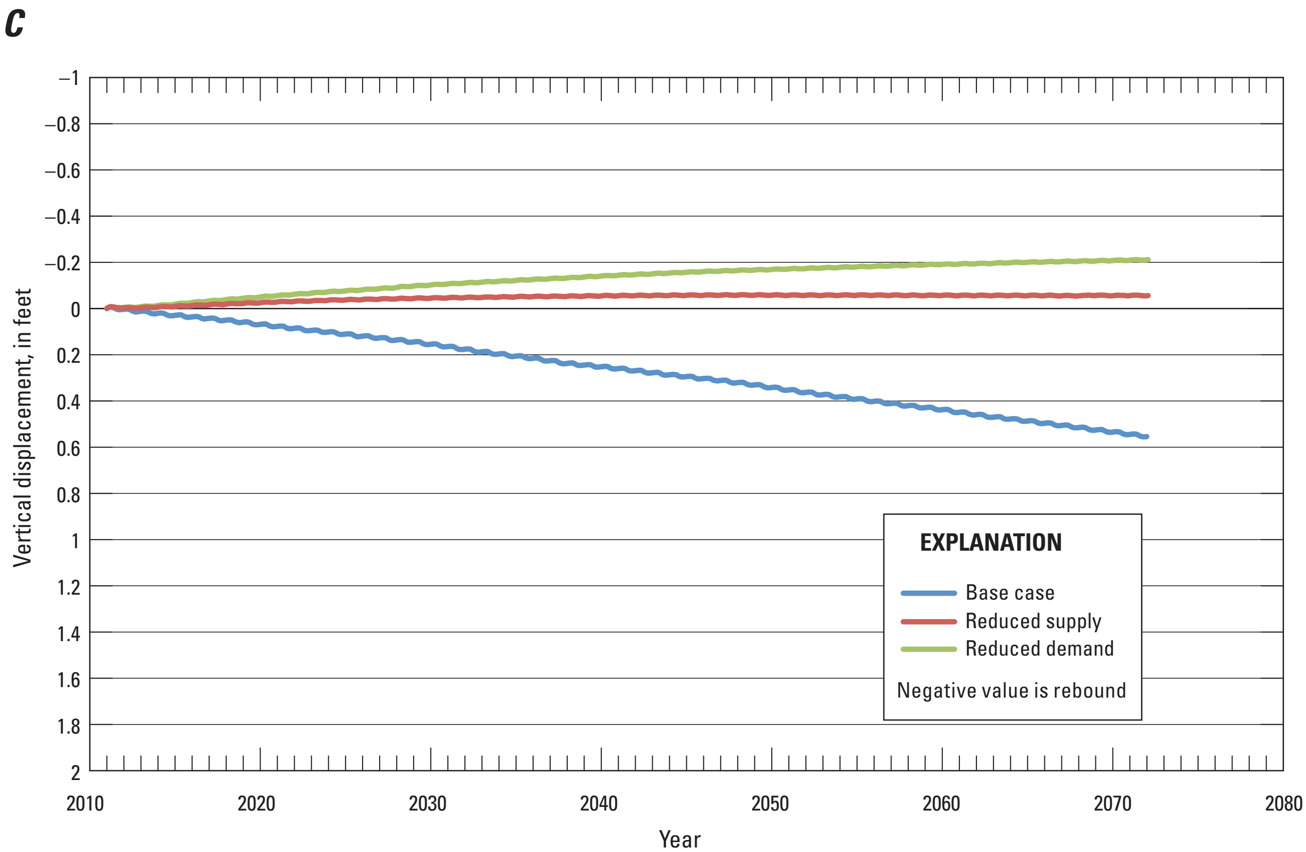

Figure 37. —Continued

Tables

Table 1. Summary of groundwater regional zones and subregions for the Cuyama Valley Hydrologic Model (CUVHM), Cuyama Valley, California.

CUVHM hydrologic subregion zone number	Groundwater subregions group name (fig. 2*A*)	Regional zone groups (fig. 2*B*)	Groundwater subregional zone description
1	Caliente northern main zone (CNMZ)	Main zone	Tributaries to Cuyama River draining the Caliente Foothills Badlands
2	Central Sierra Madre foothills (CSMFH)	Sierra Madre foothills	Central subregion of tributaries draining the Sierra Madre foothills between Salsbury Canyon and Santa Barbara Canyon
3	Northeast Ventucopa uplands (NEVU)	Ventucopa uplands	Northeastern Upper Cuyama Creek Drainage and related tributaries and Reyes Creek
4	Northwestern Sierra Madre foothills (NSMFH)	Sierra Madre foothills	Northwestern subregion of tributaries draining the Sierra Madre foothills north of Salsbury Canyon
5	Northern Ventucopa uplands (NVU)	Ventucopa uplands	Region surrounding Berringer Canyon and draining the Morales formation outcrop region
6	Southern Sierra Madre foothills (SSMFH)	Sierra Madre foothills	Southern subregion of tributaries draining the Sierra Madre foothills south of Santa Barbara Canyon
7	Southern Ventucopa uplands (SVU)	Ventucopa uplands	Southern Ventucopa adjacent to Cuyama River uplands corridor
8	Southern main zone (SMZ)	Main zone	South-Central Cuyama bounded by faults on north and south
9	Western main zone (WMZ)	Main zone	Western region surrounding Cuyama River at outflow of Cuyama groundwater basin

Table 2. Summary of climate periods for the Cuyama Valley Hydrologic Model, Cuyama Valley, California (as shown in figure 5).

Climate period[1] (year)		Climate
1939	1944[2]	Wet
1945	1957[2]	Dry
1958	1958	Wet
1959	1961	Dry
1962	1962	Wet
1963	1968	Dry
1969	1969	Wet
1970	1976	Dry
1977	1983	Wet
1984	1990	Dry
1991	1995	Wet
1996	1997	Dry
1998	2001	Wet
2002	2004	Dry
2005	2006	Wet
2007	2010	Dry

[1]Calendar years.

[2]Climate periods prior to model simulation period that begins in October, 1949.

Table 3. Scaling coefficients for estimation of streamflow for MODFLOW Streamflow Routing (SFR) from recharge and runoff maps developed by the Basin Characterization Model for ungaged basins in three geologic types in Cuyama Valley.

[**Abbreviation**: —, no estimate made]

Geologic type	Shallow subsurface flow from recharge that becomes baseflow (SFR recharge)	Runoff that becomes streamflow (SFR runoff)	Runoff that becomes deep recharge (subsurface recharge)
Alluvium	0.01	0.05	—
Sandstone	0.04	0.4	0.2
Conglomerate	0.01	0.2	0.3

Table 4. Streamgages used for Basin Characterization Model (BCM) calibration with calibration statistics for Cuyama Valley, California.

[**Abbreviations**: BL, below; CA, California; CK, creek; CR, creek; CYN, Canyon; ID, identification; NR, near; NSE, Nash-Sutcliffe Efficiency statistic; R, river; RD, road]

Gage[1]	Station ID	Period of record (year)	NSE	Calibration statistics		Recharge and runoff returning as baseflow (percent)	Recharge and runoff that is streamflow (percent)	Total streamflow that is subsurface recharge to mountain block (percent)
				R^2 monthly	R^2 annual			
WAGON RD CR NEAR STAUFFER	11136400	1972–1978	0.81	0.81	0.9	0	15	36
REYES CR NEAR VENTUCOPA	11136480	1972–1987	0.76	0.82	0.87	5	53	1
CUYAMA RIVER NEAR VENTUCOPA	11136500	1945–1958	0.44	0.56	0.83	1	22	11
SANTA BARBARA CANYON CK NEAR VENTUCOPA	11136600	2009–2010	0.84	0.95	—	0	12	24
ALISO CANYON CK NEAR NEW CUYAMA	11136650	1963–1972		0.68	0.82	0	5	0
CUYAMA R BL BUCKHORN CYN NR SANTA MARIA CA[2]	11136800	1963–2009		0.80	0.82	0	13	37
CUYAMA R NR SANTA MARIA CA[2]	11137000	1939–1962		0.50	0.84	0	5	16

[1]Locations are shown on figure 11.

[2]Outside of basin area and downstream of study area.

Table 5. Summary of One-Water Hydrologic Flow Model (OWHM) Packages and processes used with the hydrologic flow model of Cuyama Valley, California.

[**Abbreviations**: FMP, farm process; MF-FMP, MODFLOW with the farm process; OBS, Observation Package]

Computer program (packages, processes, parameter estimation)	Function	References cited
	Processes and solver	
Groundwater flow (GWF) processes of MOD-FLOW-2005	Setup and solve equations simulating a basic groundwater flow model.	Harbaugh (2005), Harbaugh and others (2000), Hill and others (2000)
Preconditioned conjugate-gradient (PCG)	Solves groundwater flow equations; requires convergence of heads and (or) flow rates.	Hill (1990); Harbaugh (2005)
Farm process (FMP)	Setup and solve equations simulating use and movement of water on the landscape as irrigated agriculture, urban landscape, and natural vegetation.	Schmid and Hanson (2009), Schmid and others (2006a, b), Hanson and others (2014b)
	Files	
Name file (Name)	Controls the capabilities of MF-FMP utilized during a simulation. Lists most of the files used by the OBS, and FMP processes.	Harbaugh (2005)
Output control option (OC)	Used in conjunction with flags in other packages to output head, drawdown, and budget information for specified time periods into separate files.	Harbaugh (2005)
List file (LIST)	Output file for allocation information, values used by the GWF process, and calculated results such as head, drawdown, and the water budget.	Harbaugh (2005)
	Discretization	
Basic package (BAS6)	Defines the initial conditions and some of the boundary conditions of the model.	Harbaugh (2005)
Discretization package (DIS)	Space and time information.	Harbaugh (2005)
Multiplier package (MULT)	Defines multiplier arrays for calculation of model-layer characteristics from parameter values.	Harbaugh (2005), Schmid and Hanson (2009)
Zones (ZONE)	Defines arrays of different zones. Parameters may be composed of one or many zones.	Harbaugh (2005)
	Aquifer parameters	
Layer property flow package (LPF)	Calculates the hydraulic conductance between cell centers.	Harbaugh (2005)
Hydrologic flow barriers (HFB6)	Simulates a groundwater barrier by defining a hydraulic conductance between two adjacent cells in the same layer.	Hsieh and Freckelton (1993)
	Boundary conditions	
General head boundaries (GHB)	Head-dependent boundary condition used along the edge of the model to allow groundwater to flow into or out of the model under a regional gradient.	Harbaugh (2005)
	Recharge and discharge	
Multi-node wells (MNW1)	Simulates pumpage from wells with screens that span multiple layers.	Halford and Hanson (2002)
Streamflow routing (SFR2)	Simulates the routed streamflow, infiltration, exfiltration, runoff, and returnflows from FMP.	Niswonger and Prudic (2005)
	Output, observations and sensitivity	
Headobservation (HOB)	Defines the head observation and weight by layer(s), row, column, and time and generates simulated values for comparison with observed values.	Hill and others (2000), Harbaugh (2005)
Hydmod (HYD)	Generates simulated values for specified locations at each time-step for groundwater levels and streamflow attributes.	Hanson and Leake (1998)
Sensitivity (PVAL)	Specifies parameter values used in other packages.	Harbaugh (2005)

Table 6. Coordinates of the hydrologic flow model of Cuyama Valley, California.

[Model grid is rotated 33 degrees west of north; coordinates below are calculated at the outer corner of the model grid using the North American Datum of 1983 in the Universal Transverse Mercator (UTM) Projection of North America, Zone 11; each model cell is 250 meters by 250 meters. **Abbreviation**: DMS, degree, minute, second]

Corner of model grid	Model coordinates X (column)	Model coordinates Y (row)	Latitude (DMS)	Longitude (DMS)	UTM coordinates X (easting) (meters)	UTM coordinates Y (northing) (meters)
Northwest	1	1	34° 54' 57"	119° 56' 36"	–231,090	3,867,673
Northeast	135	1	35° 10' 07"	119° 44' 23"	–250,476	3,895,182
Southwest	1	300	34° 32' 54"	119° 15' 10"	–293,276	3,825,260
Southeast	135	300	34° 48' 00"	119° 02' 53"	–312,648	3,852,769

Table 7. Percentage of different virtual crop categories in Cuyama Valley Hydrologic Model for selected land-use periods.

[**Abbreviations**: FMP ID, farm process identification; no., number]

Description (FMP ID/cropsScape land-use no.)	Percentage of active model area													
	1952	1959	1966	1977	1984	2000	2002	2004	2005	2006	2007	2008	2009	2010
Field crops[1]	2.8	1.2	2.1	4	4	7.5	3.9	3.8	3.9	1.8	1	1	5.7	4.5
Alfalfa (4/36)	3.3	6.0	5.2	12.3	12.4	3.03	0.35	0.35	0.35	0.35	0.4	0.24	0.56	0.21
Dry beans (6/42)	0	0	0	0	0	0.32	0	0	0	0	0	0	0	0
Potatoes (7/43)	3.4	0.6	1.9	0	0	0.57	1.75	1.75	1.76	1.48	3.81	1.15	0.6	2.14
Onions (8/49)	0	0.7	0.5	0	0	0.35	0.09	0.09	0.09	0.31	0.31	0.22	0	0.66
Various orchards[2]	0	0.1	0.4	0	0	2.78	1.28	1.28	1.28	1.07	2.15	0.98	3.19	0.6
Grapes (14/69)	0	0	0	0	0	0.8	1.2	1.2	1.2	1.1	1	1.1	1.2	1
Walnuts (16/76)	0	0	0	0	0	0.1	0.1	0.1	0.1	0	0	0	0	0
Native trees[3]	12	11.9	11.9	11.8	11.8	11.8	11.8	11.8	11.8	11.8	11.8	11.8	11.8	11.9
Native shrubland (23/152) and grassland (24/171)	74.7	75.4	74.1	53.8	53.6	53.9	53.8	53.8	53.7	53.9	53.9	53.9	54	53.4
Various farmland categories[4]	4.1	0	3.8	4	4.2	4.1	4.2	4.2	4.1	4.1	4.1	4.1	4.1	4.1
Pistachios (30/204)	0	0	0	0	0	0.7	0.6	0.6	0.6	0.6	0.7	0.5	0.8	0.5
Carrots (31/206)	0	0	0	0.8	0.8	5.3	5.7	5.6	5.7	10.6	9.9	6	9.7	3.2
Cantaloupes (32/209)	0	0	0	0	0	0	0	0	0	0	0.8	0	1.3	0
Broccoli (34/214) and cauliflower (37/244)	0	0	0	0	0	0	0	0	0	0	0.6	0	0.9	0
Irrigated row and vegetable crops (40/259)	0	0	0	0	0	0.5	1.7	1.7	1.7	1	0.2	5	2.7	14
Fallow/idle cropland (9/61)	0	0	0	12.9	12.9	4.2	2.3	2.4	2.4	3.5	2.3	2.1	2.6	2

[1]Field crops were simulated separately as they occurred historically. Summaries of areas and percentages represent collective area for this group of crops that includes barley (1/21), durham wheat (2/22), oats (3/28), other hay (5/37), pasture/grass (10/62), forage hay/silage (38/257), and irrigated field crops (39/258).

[2]Various fruit trees were simulated separately as they occurred historically. Summaries of areas and percentages represent collective area for this group of crops that includes cherries (11/66), peaches (12/67), apples (13/68), other fruit trees (15/73), nectarines (34/218), apricots (35/223), and olives (33/211).

[3]Native trees were simulated separately as they occurred historically. Summaries of areas and percentages represent collective area for this group of crops that includes deciduous (20/141), evergreen (21/142), and mixed forest (22/143) vegetation.

[4]Various farmland categories were simulated separately as they occurred historically. Summaries of areas and percentages represent collective area for this group of crops that includes prime farmland (25/183), statewide importance (26/184), unique farmland (27/185), local importance (28/186), and local potential (29/187), developed/open space (19/282).

Table 8. Summary of Cuyama Valley Farm process (FMP) virtual-crop crop category, crop-index number, and select properties for the Cuyama Valley Hydrologic Model (CUVHM), Cuyama Valley, California.

Farm process (FMP) crop index number and virtual-crop crop category[1]	Root depth (feet)	Root uptake pressure heads (feet)				Fraction of surface-water runoff (dimensionless)	
		Anoxia	Lower optimal range	Upper optimal range	Wilting	Precipitation	Irrigation
Field crops (1, 2, 3, 5, 10, 38)	4.4–12	-0.49–-0.24	-0.98–-0.66	-171–-18	-525– -262	0.8–0.99	0.24–0.97
Alfalfa (4)	12.0	-0.49	-0.98	-18	-262	0.9	0.6
Dry beans (6)	5.5	-0.43	-0.89	-23	-36	0.97	0.97
Potatoes (7)	4.7	-0.49	-0.98	-20	-262	0.97	0.97
Onions (8)	3.3	-0.49	-0.98	-24	-262	0.8	0.21
Various orchards (11, 12, 13, 15, 33, 35)	1.5–6.6	-0.49– -0.43	-0.98– -0.89	-37– -0.18	-377– -262	0.95–0.97	0.05–0.97
Grapes (14)	5.0	-0.49	-0.98	-18	-262	0.97	0.25
Walnuts (16)	6.0	-0.49	-0.98	-18	-262	0.95	0.04
Native trees (20, 21, 22)	6.6–10.8	-0.49	-0.98	-18	-262	0.92	0.05
Native shrubland and grassland (23, 24)	5.3–15.4	-0.49	-0.98	-18	-262	0–0.9	0.05
Various farmland categories (19, 25, 26, 27, 28, 29)	0.3–12	-0.49–0	-0.98–0	-98– -20	-406– -262	0.8–0.97	0.21–0.97
Pistachios (30)	1.6	-0.49	-0.98	-171	-525	0.97	0.97
Carrots (31)	1.5	-0.43	-0.92	-37	-262	0.97	0.97
Cantaloupes (32)	1.5	-0.49	0	-27	-377	0.95	0.05
Broccoli (34) and cauliflower (37)	2.5–6.5	-0.49– -0.43	-0.98–0.33	-37– -1.0	-262– -1.31	0.97	0.97
Irrigated row and vegetable crops (40)	1.5	-0.49	-0.98	-18	-262	0.97	0.97
Fallow/idle cropland (9)	5.3	-0.49	-0.98	-18	-262	0.97	0.97

[1]Refer to table 7 for explanation of crop and vegetation groupings. For groups of crops, the root uptake pressure heads represent the range in values for this grouping of crops.

Table 9. Summary of fractions of transpiration and evaporation by month, for Cuyama Valley crop categories (virtual crops).

[**Abbreviations**: FEI, fraction of evaporation from irrigation; FEP, fraction of evaporation from precipitation; FTR, fraction of transpiration]

Crop	January			February			March			April		
	FTR	FEP	FEI	FTR	FEP	FEI	FTR	FEP	FEI	FTR	FEP	FEI
Field crops	0.05–0.58	0.43–0.95	0–0.5	0.05–0.78	0.23–0.95	0–0.5	0.05–0.88	0.13–0.95	0–0.5	0.15–0.97	0.03–0.85	0–0.1
Alfalfa	0.5–0.5	0.5–0.5	0.1–0.1	0.6–0.6	0.4–0.4	0.1–0.1	0.78–0.78	0.22–0.22	0.15–0.15	0.97–0.97	0.03–0.03	0.03–0.03
Dry beans	0.5–0.58	0.43–0.5	0.1–0.1	0.7–0.78	0.23–0.3	0.1–0.1	0.8–0.88	0.13–0.2	0.1–0.1	0.5–0.58	0.43–0.5	0.3–0.3
Potatoes	0.2–0.28	0.73–0.8	0.1–0.1	0.3–0.38	0.63–0.7	0.1–0.1	0.5–0.58	0.43–0.5	0.1–0.1	0.6–0.68	0.33–0.4	0.2–0.2
Onions	0.5–0.58	0.43–0.5	0.05–0.05	0.7–0.78	0.23–0.3	0.05–0.05	0.8–0.88	0.13–0.2	0.05–0.05	0.5–0.58	0.43–0.5	0.05–0.05
Various orchards	0.03–0.58	0.43–0.97	0–0.1	0.03–0.78	0.23–0.97	0–0.1	0.1–0.88	0.13–0.9	0–0.1	0.5–0.68	0.33–0.5	0–0.1
Grapes	0.05–0.13	0.88–0.95	0.1–0.1	0.05–0.13	0.88–0.95	0.1–0.1	0.28–0.36	0.65–0.72	0.1–0.1	0.4–0.48	0.53–0.6	0.1–0.1
Walnuts	0.03–0.11	0.9–0.97	0.05–0.05	0.03–0.11	0.9–0.97	0.05–0.05	0.1–0.18	0.83–0.9	0.05–0.05	0.5–0.58	0.43–0.5	0.05–0.05
Native trees	0.03–0.28	0.73–0.97	0–0.1	0.03–0.28	0.73–0.97	0–0.1	0.1–0.48	0.53–0.9	0–0.1	0.5–0.58	0.43–0.5	0–0.1
Native shrubland and grassland	0.23–0.36	0.65–0.77	0–0.1	0.23–0.36	0.65–0.77	0–0.1	0.61–0.74	0.27–0.39	0–0.15	0.61–0.74	0.27–0.39	0–0.15
Various farmland categories	0–0.5	0.5–1	0–0.1	0–0.5	0.5–1	0–0.1	0–0.5	0.5–1	0–0.2	0–0.97	0.03–1	0–0.03
Pistachios	0.03–0.11	0.9–0.97	0.1–0.1	0.03–0.11	0.9–0.97	0.1–0.1	0.1–0.18	0.83–0.9	0.2–0.2	0.5–0.58	0.43–0.5	0.2–0.2
Carrots	0.5–0.58	0.43–0.5	0–0	0.7–0.78	0.23–0.3	0–0	0.8–0.88	0.13–0.2	0–0	0.5–0.58	0.43–0.5	0–0
Cantaloupes	0.2–0.28	0.73–0.8	0–0	0.3–0.38	0.63–0.7	0–0	0.5–0.58	0.43–0.5	0–0	0.6–0.68	0.33–0.4	0–0
Broccoli and cauliflower	0.5–0.58	0.43–0.5	0.1–0.1	0.7–0.78	0.23–0.3	0.1–0.1	0.8–0.88	0.13–0.2	0.1–0.1	0.5–0.58	0.43–0.5	0.1–0.1
Irrigated row and vegetable crops	0.2–0.28	0.73–0.8	0–0	0.3–0.38	0.63–0.7	0–0	0.5–0.58	0.43–0.5	0–0	0.6–0.68	0.33–0.4	0–0
Fallow/idle cropland	0–0	1–1	0.1–0.1	0–0	1–1	0.1–0.1	0–0	1–1	0.1–0.1	0–0	1–1	0.03–0.03

Table 9. Summary of fractions of transpiration and evaporation by month for Cuyama Valley crop categories (virtual crops).—Continued

[**Abbreviations**: FEI, fraction of evaporation from irrigation; FEP, fraction of evaporation from precipitation; FTR, fraction of transpiration]

Crop	May			June			July			August		
	FTR	FEP	FEI	FTR	FEP	FEI	FTR	FEP	FEI	FTR	FEP	FEI
Field crops	0.25–0.97	0.03–0.75	0–0.3	0.65–0.97	0.03–0.35	0.03–0.2	0.7–0.96	0.04–0.3	0.03–0.2	0.8–0.97	0.03–0.2	0.03–0.2
Alfalfa	0.97–0.97	0.03–0.03	0.02–0.02	0.97–0.97	0.03–0.03	0.02–0.02	0.96–0.96	0.04–0.04	0.02–0.02	0.97–0.97	0.03–0.03	0.02–0.02
Dry beans	0.6–0.68	0.33–0.4	0.3–0.3	0.65–0.73	0.28–0.35	0.03–0.03	0.7–0.78	0.23–0.3	0.03–0.03	0.8–0.88	0.13–0.2	0.03–0.03
Potatoes	0.7–0.78	0.23–0.3	0.2–0.2	0.8–0.88	0.13–0.2	0.1–0.2	0.8–0.88	0.13–0.2	0.1–0.2	0.8–0.88	0.13–0.2	0.1–0.2
Onions	0.6–0.68	0.33–0.4	0.05–0.05	0.65–0.73	0.28–0.35	0.05–0.05	0.7–0.78	0.23–0.3	0.05–0.05	0.8–0.88	0.13–0.2	0.05–0.05
Various orchards	0.6–0.78	0.23–0.4	0–0.1	0.65–0.88	0.13–0.35	0–0.1	0–0.1	0.7–0.88	0.13–0.3	0–0.1	0.8–0.98	0.03–0.2
Grapes	0.38–0.46	0.55–0.62	0.1–0.1	0.36–0.44	0.57–0.64	0.1–0.1	0.36–0.44	0.57–0.64	0.1–0.1	0.36–0.44	0.57–0.64	0.1–0.1
Walnuts	0.6–0.68	0.33–0.4	0.05–0.05	0.7–0.78	0.23–0.3	0.05–0.05	0.8–0.88	0.13–0.2	0.05–0.05	0.9–0.98	0.03–0.1	0.02–0.05
Native trees	0.6–0.68	0.33–0.4	0–0.3	0.7–0.78	0.23–0.3	0–0.2	0.8–0.88	0.13–0.2	0–0.2	0.9–0.98	0.03–0.1	0–0.1
Native shrubland and grassland	0.61–0.74	0.27–0.39	0–0.15	0.61–0.74	0.27–0.39	0.1–0.15	0.61–0.74	0.27–0.39	0.1–0.15	0.61–0.74	0.27–0.39	0.1–0.15
Various farmland categories	0–0.97	0.03–1	0–0.03	0–0.97	0.03–1	0–0.03	0–0.96	0.04–1	0–0.04	0–0.97	0.03–1	0–0.03
Pistachios	0.6–0.68	0.33–0.4	0.3–0.3	0.7–0.78	0.23–0.3	0.2–0.3	0.8–0.88	0.13–0.2	0.1–0.2	0.9–0.98	0.03–0.1	0.02–0.1
Carrots	0.6–0.68	0.33–0.4	0–0	0.65–0.73	0.28–0.35	0–0	0.7–0.78	0.23–0.3	0–0	0.8–0.88	0.13–0.2	0–0
Cantaloupes	0.7–0.78	0.23–0.3	0–0	0.8–0.88	0.13–0.2	0–0	0.8–0.88	0.13–0.2	0–0	0.8–0.88	0.13–0.2	0–0
Broccoli and cauliflower	0.6–0.68	0.33–0.4	0.1–0.3	0.65–0.73	0.28–0.35	0.1–0.2	0.1–0.2	0.7–0.78	0.23–0.3	0.1–0.2	0.8–0.88	0.13–0.2
Irrigated row and vegetable crops	0.7–0.78	0.23–0.3	0–0	0.8–0.88	0.13–0.2	0–0	0.8–0.88	0.13–0.2	0–0	0.8–0.88	0.13–0.2	0–0
Fallow/idle cropland	0–0	1–1	0.03–0.03	0–0	1–1	0.03–0.03	0–0	1–1	0.04–0.04	0–0	1–1	0.03–0.03

Table 9. Summary of fractions of transpiration and evaporation by month for Cuyama Valley crop categories (virtual crops).—Continued

[**Abbreviations**: FEI, fraction of evaporation from irrigation; FEP, fraction of evaporation from precipitation; FTR, fraction of transpiration]

Crop	September			October			November			December		
	FTR	FEP	FEI	FTR	FEP	FEI	FTR	FEP	FEI	FTR	FEP	FEI
Field crops	0.7–0.97	0.03–0.3	0.03–0.2	0.33–0.83	0.18–0.67	0.01–0.5	0.05–0.88	0.13–0.95	0.1–0.5	0.05–0.88	0.13–0.95	0.1–0.5
Alfalfa	0.97–0.97	0.03–0.03	0.02–0.02	0.78–0.78	0.22–0.22	0.2–0.2	0.6–0.6	0.4–0.4	0.15–0.15	0.5–0.5	0.5–0.5	0.1–0.1
Dry beans	0.8–0.88	0.13–0.2	0.03–0.03	0.75–0.83	0.18–0.25	0.1–0.25	0.8–0.88	0.13–0.2	0.1–0.2	0.8–0.88	0.13–0.2	0.1–0.1
Potatoes	0.8–0.88	0.13–0.2	0.1–0.2	0.7–0.78	0.23–0.3	0.2–0.2	0.8–0.88	0.13–0.2	0.1–0.1	0.8–0.88	0.13–0.2	0.1–0.1
Onions	0.8–0.88	0.13–0.2	0.05–0.05	0.75–0.83	0.18–0.25	0.05–0.05	0.8–0.88	0.13–0.2	0.05–0.05	0.8–0.88	0.13–0.2	0.05–0.05
Various orchards	0–0.1	0.8–0.98	0.03–0.2	0–0.1	0.7–0.83	0.18–0.3	0–0.3	0.1–0.88	0.13–0.9	0–0.1	0.03–0.88	0.13–0.97
Grapes	0.36–0.44	0.57–0.64	0.1–0.1	0.36–0.44	0.57–0.64	0.1–0.1	0.2–0.28	0.73–0.8	0.1–0.1	0.05–0.13	0.88–0.95	0.1–0.1
Walnuts	0.9–0.98	0.03–0.1	0.02–0.05	0.7–0.78	0.23–0.3	0.05–0.05	0.1–0.18	0.83–0.9	0.05–0.05	0.03–0.11	0.9–0.97	0.05–0.05
Native trees	0.9–0.98	0.03–0.1	0–0.1	0.7–0.78	0.23–0.3	0–0.3	0.1–0.28	0.73–0.9	0–0.5	0.03–0.28	0.73–0.97	0–0.1
Native shrubland and grassland	0.61–0.74	0.27–0.39	0.1–0.2	0.61–0.74	0.27–0.39	0.1–0.2	0.61–0.74	0.27–0.39	0.1–0.15	0.23–0.36	0.65–0.77	0.1–0.1
Various farmland categories	0–0.97	0.03–1	0–0.03	0–0.5	0.5–1	0–0.3	0–0.5	0.5–1	0–0.25	0–0.5	0.5–1	0–0.1
Pistachios	0.9–0.98	0.03–0.1	0.02–0.1	0.7–0.78	0.23–0.3	0.2–0.2	0.1–0.18	0.83–0.9	0.1–0.1	0.03–0.11	0.9–0.97	0.1–0.1
Carrots	0.8–0.88	0.13–0.2	0–0	0.75–0.83	0.18–0.25	0–0	0.8–0.88	0.13–0.2	0–0	0.8–0.88	0.13–0.2	0–0
Cantaloupes	0.8–0.88	0.13–0.2	0–0	0.7–0.78	0.23–0.3	0–0	0.5–0.58	0.43–0.5	0–0	0.3–0.38	0.63–0.7	0–0
Broccoli and cauliflower	0.1–0.2	0.8–0.88	0.13–0.2	0.1–0.2	0.75–0.83	0.18–0.25	0.01–0.2	0.8–0.88	0.13–0.2	0.1–0.2	0.8–0.88	0.13–0.2
Irrigated row and vegetable crops	0.8–0.88	0.13–0.2	0–0	0.7–0.78	0.23–0.3	0–0	0.5–0.58	0.43–0.5	0–0	0.3–0.38	0.63–0.7	0–0
Fallow/idle cropland	0–0	1–1	0.03–0.03	0–0	1–1	0.3–0.3	0–0	1–1	0.1–0.1	0–0	1–1	0.1–0.1

[1]Refer to table 7 for explanation of crop and vegetation groupings.

Table 10. Irrigation efficiency, by month, for each crop of the Cuyama Valley, California.[1, 2]

[Efficiencies are adjusted seasonally for wet and dry climatic periods with multipliers (see Model Calibration section). Refer to table 7 for explanation of crop and vegetation groupings.]

Crop categories	January	February	March	April	May	June	July	August	September	October	November	December
Field crops	0.5–0.75	0.5–0.75	0.5–0.75	0.5–0.75	0.5–0.75	0.5–0.75	0.5–0.75	0.5–0.75	0.5–0.75	0.5–0.75	0.5–0.75	0.5–0.75
Alfalfa	0.5–0.675	0.5–0.675	0.5–0.675	0.5–0.675	0.5–0.675	0.5–0.675	0.5–0.675	0.5–0.675	0.5–0.675	0.5–0.675	0.5–0.675	0.5–0.675
Dry beans	0.5–0.7	0.5–0.7	0.5–0.7	0.5–0.7	0.5–0.7	0.5–0.7	0.5–0.7	0.5–0.7	0.5–0.7	0.5–0.7	0.5–0.7	0.5–0.7
Potatoes	0.5–0.6	0.5–0.6	0.5–0.6	0.5–0.6	0.5–0.6	0.5–0.6	0.5–0.6	0.5–0.6	0.5–0.6	0.5–0.6	0.5–0.6	0.5–0.6
Onions	0.5–0.65	0.5–0.65	0.5–0.65	0.5–0.65	0.5–0.65	0.5–0.65	0.5–0.65	0.5–0.65	0.5–0.65	0.5–0.65	0.5–0.65	0.5–0.65
Various orchards	0.5–0.75	0.5–0.75	0.5–0.75	0.5–0.75	0.5–0.75	0.5–0.75	0.5–0.75	0.5–0.75	0.5–0.75	0.5–0.75	0.5–0.75	0.5–0.75
Grapes	0.5–0.875	0.5–0.875	0.5–0.875	0.5–0.875	0.5–0.875	0.5–0.875	0.5–0.875	0.5–0.875	0.5–0.875	0.5–0.875	0.5–0.875	0.5–0.875
Walnuts	0.5–0.75	0.5–0.75	0.5–0.75	0.5–0.75	0.5–0.75	0.5–0.75	0.5–0.75	0.5–0.75	0.5–0.75	0.5–0.75	0.5–0.75	0.5–0.75
Native trees	0.5–0.5	0.5–0.5	0.5–0.5	0.5–0.5	0.5–0.5	0.5–0.5	0.5–0.5	0.5–0.5	0.5–0.5	0.5–0.5	0.5–0.5	0.5–0.5
Native shrubland and grassland	0.5–0.5	0.5–0.5	0.5–0.5	0.5–0.5	0.5–0.5	0.5–0.5	0.5–0.5	0.5–0.5	0.5–0.5	0.5–0.5	0.5–0.5	0.5–0.5
Various farmland categories	0.5–0.75	0.5–0.75	0.5–0.75	0.5–0.75	0.5–0.75	0.5–0.75	0.5–0.75	0.5–0.75	0.5–0.75	0.5–0.75	0.5–0.75	0.5–0.75
Pistachios	0.5–0.7	0.5–0.7	0.5–0.7	0.5–0.7	0.5–0.7	0.5–0.7	0.5–0.7	0.5–0.7	0.5–0.7	0.5–0.7	0.5–0.7	0.5–0.7
Carrots	0.5–0.8	0.5–0.8	0.5–0.8	0.5–0.8	0.5–0.8	0.5–0.8	0.5–0.8	0.5–0.8	0.5–0.8	0.5–0.8	0.5–0.8	0.5–0.8
Cantaloupes	0.5–0.75	0.5–0.75	0.5–0.75	0.5–0.75	0.5–0.75	0.5–0.75	0.5–0.75	0.5–0.75	0.5–0.75	0.5–0.75	0.5–0.75	0.5–0.75
Broccoli and cauliflower	0.5–0.75	0.5–0.75	0.5–0.75	0.5–0.75	0.5–0.75	0.5–0.75	0.5–0.75	0.5–0.75	0.5–0.75	0.5–0.75	0.5–0.75	0.5–0.75
Irrigated row and vegetable crops	0.5–0.75	0.5–0.75	0.5–0.75	0.5–0.75	0.5–0.75	0.5–0.75	0.5–0.75	0.5–0.75	0.5–0.75	0.5–0.75	0.5–0.75	0.5–0.75
Fallow/idle cropland	0.5–0.8	0.5–0.8	0.5–0.8	0.5–0.8	0.5–0.8	0.5–0.8	0.5–0.8	0.5–0.8	0.5–0.8	0.5–0.8	0.5–0.8	0.5–0.8

[1]Efficiencies are adjusted seasonally for wet and dry climatic periods with multipliers (see Model Calibration section)

[2]Refer to table 7 for explanation of crop and vegetation groupings.

Table 11. Summary of reference evapotranspiration (ET_h) comparisons between Pennman-Montieth from California Irrigation Management Information System (CIMIS) stations and Priestley-Taylor estimates from regional climate data, Cuyama Valley, California.

[**Abbreviations**: Apr., April; Aug., August; Dec., December; Feb., February; Jan., January; Mar., March; Nov., November; Oct., October; Sept., September]

ET_h average monthly value (inches/month)	Jan.	Feb.	Mar.	Apr.	May	June	July	Aug.	Sept.	Oct.	Nov.	Dec.
[1]CIMIS station 88 (California Department of Water Resources, 2013)	2.10	2.43	3.97	5.33	7.07	8.06	8.55	7.84	6.01	4.39	2.58	1.94
Priestley-Taylor estimate	1.90	2.38	3.80	4.96	6.49	7.16	7.71	6.90	5.35	3.87	2.35	1.70
Adjusted fraction of CIMIS value of P-T estimate [dimensionless]	1.11	1.02	1.05	1.07	1.09	1.13	1.11	1.14	1.12	1.13	1.10	1.14

[1]Average monthly values for 1989–2011.

Table 12. Summary of hydraulic properties estimated from the Cuyama Valley hydrologic model (CUVHM) calibration.

Aquifer (model layer)	Lateral hydraulic conductivity (feet/day)	Specific storage [1/foot]	Specific yield [dimensionless]	Vertical hydraulic conductivity [feet/day] (leakance, in feet/day/feet)	Skeletal elastic storage, coarse and fine-grained layers [dimensionless]	Skeletal inelastic storage, fine-grained layers [dimensionless]
Recent Alluvium (1)	5.2–85	2.2e-05–9.34e-03	0.02–0.14	0.0–12.3	5.9e-06–4.8e-04	6.37e-07–4.7e-03
Older Alluvium (2)	0.3–15.5	1.3e-06–8.0e-03	0.05–0.19	6.1e-04–0.34	7.4e-07–3.3e-04	1.5e-05–2.3e-02
Morales Formation (3)	0.02–0.4	1.3e-06–2.3e-02	0.06–0.25	3.4e-03–0.01	1.05e-05–4.5e-03	7.3e-05–9.2e-03

Table 13. Summary of parameter zones and related property parameter names used to calibrate horizontal hydraulic conductivity (K_H), vertical hydraulic conductivity (K_V), and aquifer specific storage and specific yield (S_S) in the Cuyama Valley hydrologic model (CUVHM), Cuyama Valley, California.

Feature/parameter zone	Root subregion model parameter names[1] (zone number)	Description
Aquifer (model layer)		
Recent alluvial aquifer (layer 1)	**Unconfined Ventucopa**	**Unconfined Ventucopa**
	VC_QYAUC (7)	Ventucopa
	Unconfined main zones	**Unconfined Main zones**
	NMZ_QYA (1)	Northern Main
	SMZ_QYA (4)	Southern Main
	WZ_QYA (8)	Western
	Sierra Madre foothills zones	**Sierra Madre foothills zones**
	SMFHQYA (3)	Sierra Madre foothills
	River channel	**River channel**
	NMZQYACC (2)	Northern Main
	SMZ_QYACC (5)	Southern Main
	VC_QYACC (6)	Ventucopa
	WZ_QYACC (9)	Western (includes selected tributary channels)
Older alluvial aquifer (layer 2)	**Unconfined Ventucopa**	**Unconfined/confined Ventucopa**
	VC_QOAN (14)	Northern Ventucopa foothills unconfined
	VC_QOAC (21)	Ventucopa confined
	Unconfined main zones	**Unconfined Main Zones**
	NMZ_QOA (10)	Northern Main
	WZ_QOA_N (15)	Northern western—Badlands foothills
	WZ_QOA_S (16)	Southern western
	Sierra Madre foothills zones	**Sierra Madre foothills zones**
	SMFH_QOAN (11)	Northern
	SMFH_QOAM (12)	Middle
	SMFH_QOAS (13)	Southern
	River channel	**River channel**
	None	None
	Confined zone	**Confined Ventucopa**
	NMZ_QOAC (18)	None
	SMFH_QOAC (19)	Confined Main zones
	SMZ_QOAC (20)	Northern Main
	WZ_QOAC (22)	Sierra Madre foothills
	QOA_PHT (23)	Southern Main
		Western
		Phantom layer cells
Morales formation (layer 3)	**Unconfined Ventucopa**	**Unconfined Ventucopa**
	VC_MOUC (17)	Ventucopa foothills
	Unconfined main zones	**Unconfined Main zones**
	None	None
	Sierra Madre foothills zones	**Sierra Madre foothills zones**
	None	None
	River channel	**River channel**
	None	None
	Confined zone	**Confined Ventucopa and Main zones**
	MO_C (24)	Entire active model grid where Morales Formation is not uppermost model layer

[1]Root names have H_K, V_K, and SS added to the front of these names for parameter names used in PVAL and LPF input files.

Table 14. Summary of selected parameter values estimated for the Cuyama Valley hydrologic model (CUVHM), Cuyama Valley, California.

Parameter type [model layers]	Parameter name	Parameter description	Final values	Units	Estimated using automated methods[1]	Rank and composite scaled sensitivity	Package/process-parameter group
			Crop properties				
Early	Dry seasons	Stress coefficient	0.85	Multiplier	No	16/54.9	FMP—K_c-value
years	SCL_KCSDFL	for early (1963–92)	1.10		No	101/30.3	properties
[1–3]	SCL_KCSDWN	agriculture crop	1.10		No	20/53.2	
	SCL_KCSDSP	coefficients	0.82		Yes	95/31.7	
	SCL_KCSDSU		====		Yes	====	
	Wet seasons		0.67		No	84/34.3	
	SCL_KCSWFL		0.71		No	102/29.8	
	SCL_KCSWWN		0.80		No	91/32.7	
	SCL_KCSWSP		0.80			44/46.7	
	SCL_KCSWSU						
Recent	Dry seasons	Stress coefficient	1.17	Multiplier	No	117/25.4	FMP—K_c-value
years	SCL_KCSDFL2	for recent-	1.14		No	111/27.0	properties
[1–3]	SCL_KCSDWN2	(1993–2006)	1.20		Yes	71/38.3	
	SCL_KCSDSP2	agriculture	1.03		Yes	126/18.4	
	SCL_KCSDSU2	crop coefficients	====		No	====	
	Wet seasons		1.03		No	115/26.2	
	SCL_KCSWFL2		1.15		No	112/26.7	
	SCL_KCSWWN2		0.87		No	94/31.8	
	SCL_KCSWSP2		1.11			99/30.7	
	SCL_KCSWSU2						
			Runoff				
[1–3]	Fractions of inefficient losses	Fraction runoff from	0.97	Fraction	No	7/7.40	FMP—runoff
	to runoff from precipitation	precipitation for	0.97		No	66/40.4	
	for truck-vegetable crops	selected land use	0.97		No	70/38.5	
	FIESWP_TVR	class	0.97		No	59/41.6	
	field crops FIESWP_FLD		0.92		Yes	48/45.4	
	orchards FIESWP_ORC						
	pasture FIESWP_PAS						
	native FIESWP_NTV						
[1–3]	Fractions of inefficient losses	Fraction runoff from	0.97	Fraction	No	127/17.2	FMP—runoff
	to runoff from irrigation for	irrigation for	0.97		No	5/65.1	
	truck-vegetable crops	selected land-use	0.97		No	86/33.9	
	FIESWI_TVR	class	0.97		No	28/49.9	
	field crops FIESWI_FLD						
	orchards FIESWI_ORC						
	pasture FIESWI_PAS						
			Irrigation efficiency				
Early	Dry seasons	Multiplier on	0.88	Multiplier	No	166/<0.1	FMP—irrigation
years	SCL_EFFDFL	irrigation	0.89		No	167/<0.1	
[1–3]	SCL_EFFDWN	efficiency for wet	1.06		Yes	168/<0.1	
	SCL_EFFDSP	and dry seasons	0.92		Yes	169/<0.1	
	SCL_EFFDSU		0.70		No	158/<0.1	
	Wet seasons		0.70		No	159/<0.1	
	SCL_EFFWFL		0.70		No	160/<0.1	
	SCL_EFFWWN		0.72		No	161/<0.1	
	SCL_EFFWSP						
	SCL_EFFWSU						

Table 14. Summary of parameter values estimated for the Cuyama Valley hydrologic model (CUVHM), Cuyama Valley, California.—Continued

Parameter type [model layers]	Parameter name	Parameter description	Final values	Units	Estimated using automated methods[1]	Rank and composite scaled sensitivity	Package/process-parameter group
Irrigation efficiency—Continued							
Recent	Dry seasons	Multiplier on irrigation	1.1	Multiplier	No	162/<0.1	FMP—irrigation
years	SCL_EFFDFL2	efficiency for wet	1.1		No	163/<0.1	
[1–3]	SCL_EFFDWN2	and dry seasons	1.0		Yes	164/<0.1	
	SCL_EFFDSP2		1.1		Yes	165/<0.1	
	SCL_EFFDSU2		1.1		No	170/<0.1	
	Wet seasons		1.1		No	171/<0.1	
	SCL_EFFWFL2		0.8		Yes	172/<0.1	
	SCL_EFFWWN2		1.1		Yes	173/<0.1	
	SCL_EFFWSP2						
	SCL_EFFWSU2						
Lateral hydraulic conductivity							
[1–3]	KC_QYA	Hydraulic conductivity	20.3	Feet/day	Yes	81/35.5	LPF/MULT—
	KC_ QOA	of coarse-grained	12.6		Yes	10/57.4	hydraulic
	KC_MO	deposits for each	0.76		Yes	58/41.6	conductivity
		model layer					
[1–3]	KF_ QYA	Hydraulic conductivity	0.004	Feet/day	No	12/57.2	LPF/MULT—
	KF_ QOA	of fine-grained	0.004		No	80/35.6	hydraulic
	KF_MO	deposits for each	0.003		No	122/21.6	conductivity
		model layer					
[1]	HK_NMZ_QYA	Hydraulic conductivity	1.95	Multiplier	Yes	109/27.1	LPF/PVAL—
	HKNMZQYACC	of the Recent	2.61		No	113/26.6	hydraulic
	HK_SMFHQYA	Alluvium zones	1.3		Yes	69/39.6	conductivity
	HK_SMZ_QYA		4.87		Yes	33/49.2	multipliers
	HKSMZQYACC		4.20		Yes	9/57.9	
	HK_VCQYACC		4.20		Yes	98/30.8	
	HK_VCQYAUC		1.58		No	55/42.3	
	HK_WZ_QYA		2.55		Yes	18/53.4	
	HK_WZQYACC		2.62		No	93/32.5	
[2]	HK_NMZ_QOA	Hydraulic conductivity	2.3	Multiplier	Yes	34/49.1	LPF/PVAL—
	HKSMFHQOAN	of the older alluvial	0.42		No	50/44.1	hydraulic
	HKSMFHQOAM	zones	0.38		Yes	82/35.4	conductivity
	HKSMFHQOAS		0.47		No	25/50.7	multipliers
	HK_VC_QOAN		1.47		No	83/34.7	
	HK_WZ_QOAN		1.36		Yes	85/34.1	
	HK_WZ_QOAS		2.16		No	21/52.9	
	HK_NMZQOAC		1.52		No	4/71.5	
	HKSMFHQOAC		0.52		No	32/49.3	
	HK_SMZQOAC		2.02		Yes	49/44.3	
	HK_VC_QOAC		0.48		Yes	110/27.1	
	HK_WZ_QOAC		0.94		Yes	65/40.6	
	HK_QOA_PHT		1.00		No	====	
[3]	HK_MO_C	Hydraulic conductivity	0.73	Multiplier	No	53/42.5	LPF/PVAL—
	HK_MOUC	of the Morales	0.10		Yes	6/64.3	hydraulic
		formation zones					conductivity

Table 14. Summary of parameter values estimated for the Cuyama Valley hydrologic model (CUVHM), Cuyama Valley, California.—Continued

Parameter type [model layers]	Parameter name	Parameter description	Final values	Units	Estimated using automated methods[1]	Rank and composite scaled sensitivity	Package/process-parameter group
Vertical hydraulic conductivity							
[1]	VK_NMZ_QYA	Vertical hydraulic conductivity of the Recent Alluvium zones	0.03	Multiplier	Yes	36/48.7	LPF/PVAL—hydraulic conductivity multipliers
	VKNMZQYACC		2.52		No	123/21.6	
	VK_SMFHQYA		1.00		Yes	72/37.8	
	VK_SMZ_QYA		0.09		No	31/49.3	
	VKSMZQYACC		4.75		No	96/31.6	
	VK_VCQYACC		3.56		No	13/56.3	
	VK_VCQYAUC		2.00		No	67/40.2	
	VK_WZ_QYA		2.64		No	114/26.3	
	VK_WZQYACC		1.72		Yes	23/52.1	
[2]	VK_NMZ_QOA	Vertical hydraulic conductivity of the older alluvial zones	0.94	Multiplier	No	42/46.9	LPF/PVAL—hydraulic conductivity multipliers
	VKSMFHQOAN		0.50		Yes	22/52.8	
	VKSMFHQOAM		1.10		No	119/25.1	
	VKSMFHQOAS		0.18		Yes	78/36.3	
	VK_VC_QOAN		0.80		Yes	90/33.5	
	VK_WZ_QOAN		0.80		No	37/48.7	
	VK_WZ_QOAS		1.02		No	76/36.4	
	VK_NMZQOAC		0.11		Yes	3/77.8	
	VKSMFHQOAC		0.45		Yes	108/28.1	
	VK_SMZQOAC		2.84		No	61/41.2	
	VK_VC_QOAC		2.16		No	17/54.8	
	VK_WZ_QOAC		2.25		No	2/80.6	
	VK_QOA_PHT		1.00		No	====	
[3]	VK_MO_C	Vertical hydraulic conductivity of the Morales formation zones	1.04	Multiplier	No	38/48.6	LPF/PVAL—hydraulic conductivity multipliers
	VK_MOUC		0.95		No	68/40.1	
Storage properties							
[1]	SY1_FAC	Specific yield of Recent Alluvium	0.13	Fraction	Yes	51/43.1	LPF/MULT—storage properties
[2]	SY2_FAC	Specific yield of Older Alluvium	0.10	Fraction	No	63/40.7	LPF/MULT—storage properties
[3]	SY3_FAC	Specific yield of Morales Formation	0.08	Fraction	No	87/33.8	LPF/MULT—storage properties
[1]	PHI_CRS	Porosity of Recent Alluvium	20	Percentage	Yes	57/42.1	LPF/MULT—storage properties
	PHI_FIN		37		No	46/46.3	

Table 14. Summary of parameter values estimated for the Cuyama Valley hydrologic model (CUVHM), Cuyama Valley, California.—Continued

Parameter type [model layers]	Parameter name	Parameter description	Final values	Units	Estimated using automated methods[1]	Rank and composite scaled sensitivity	Package/process-parameter group
Storage properties—Continued							
[2]	PHI_CRS_AO	Porosity of Older Alluvium	12	Percentage	Yes	26/50.7	LPF/MULT—storage properties
	PHI_FIN_AO		17		Yes	7/61.8	
[3]	PHI_CRS_MO	Porosity of Morales formation	10	Percentage	No	104/29.1	LPF/MULT—storage properties
	PHI_FIN_MO		29		Yes	45/46.7	
[1]	SS_NMZ_QYA	Specific storage of Recent Alluvium zones	1.21	Multiplier	No	89/33.7	LPF/MULT—storage properties
	SSNMZQYACC		1.15		No	47/46.2	
	SS_SMFHQYA		2.00		Yes	43/46.9	
	SS_SMZ_QYA		0.21		Yes	88/33.7	
	SSSMZQYACC		1.12		No	100/30.5	
	SS_VCQYACC		1.0		Yes	105/29.1	
	SS_VCQYAUC		1.00		No	118/25.2	
	SS_WZ_QYA		0.66		No	30/49.5	
	SS_WZQYACC		1.24		No	11/57.2	
[2]	SS_NMZ_QOA	Specific storage of Older Alluvium zones	2.00	Multiplier	No	39/47.9	LPF/PVAL—storage properties
	SSSMFHQOAN		0.86		No	56/42.1	
	SSSMFHQOAM		1.95		No	120/23.9	
	SSSMFHQOAS		1.25		No	15/54.9	
	SS_VC_QOAN		2.00		No	74/37.1	
	SS_WZ_QOAN		0.92		No	41/47.2	
	SS_WZ_QOAS		0.81		No	92/32.7	
	SS_NMZQOAC		2.09		No	106/28.51	
	SSSMFHQOAC		0.03		No	24/52.1	
	SS_SMZQOAC		1.32		No	77/36.4	
	SS_VC_QOAC		2.22		No	14/56.3	
	SS_WZ_QOAC		1.65		No	60/41.4	
	SS_QOA_PHT		1.00		No	====	
[3]	SS_MO_C	Specific storage of Morales formation zones	0.37	Multiplier	Yes	79/36.0	LPF/PVAL—storage properties
	SS_MOUC		1.06		No	19/53.3	
Subsidence properties							
[1–3]	crt_hd_01	Critical heads for each layer	0.91	Multiplier as fraction of initial groundwater levels	No	1/97.7	SUB—storage properties
	crt_hd_02		0.90		Yes	64/40.6	
	crt_hd_03		0.72		No	52/42.9	
[1–3]	QYA_SKE	Skeletal elastic storage coefficient for each layer	0.90	Multiplier	Yes	54/42.5	SUB—storage properties
	QOA_SKE		0.32		Yes	124/21.3	
	MO_SKE		0.80		No	73/37.1	
[1–3]	QYA_SKVB	Skeletal inelastic storage coefficient for each layer	1.62e-05	1/Foot	Yes	97/31.6	SUB—storage properties
	QOA_SKVB		2.30e-05		Yes	75/36.5	
	MO_SKVBR		1.00e-05		No	103/29.6	

Table 14. Summary of parameter values estimated for the Cuyama Valley hydrologic model (CUVHM), Cuyama Valley, California.—Continued

Parameter type [model layers]	Parameter name	Parameter description	Final values	Units	Estimated using automated methods[1]	Rank and composite scaled sensitivity	Package/process-parameter group
		SKIN factor for multi-node wells					
[1–3]	SKIN_LY1	Skin factor for recent	395	ft²/day	No	27/50.6	MNW1 hydraulic
	SKIN_LY2	and Older Alluvium,	1,536		No	35/48.8	property
	SKIN_LY3	and Morales	1,622		No	8/60.7	
		formation layers					
		Horizontal flow-barrier conductance[2]					
[1–3]	MO_FLT [2–3]	Conductance of	7.5e-12	ft²/day	No		HFB—hydraulic
	GRV_FLT [1–3]	internal faults	1.4e-10		No	107/28.3	conductance factor
	TTHL_FLT [1–3]		7.2e-10		No	40/47.7	
	SBC_FLT [2–3]		1.9e-13		No	62/40.9	
	SBC_FLT1 [1]		1.9e-13		No	29/49.7	
	RHF_FLT [2–3]		4.0e-04		Yes	121/23.8	
		Initial groundwater levels[3]					
[1–3]	SCL_HEDLY1	Scale factor for	1.006	Multiplier	Yes	====	Scale factor of initial
	SCL_HEDLY2	adjusting initial	1.00		Yes		groundwater levels
	SCL_HEDLY3	groundwater levels	1.00		Yes		

[1]Parameters used in calibration varies between calibration runs and indicators here reflect parameters that were generally estimated through the automated process. An additional 15 parameters for scaling precipitation and potential ET were included in the model but remained fixed at the standard values of units conversion.

[2]MO_FLT is the Morales Fault, GRV_FLT is the Graveyard Fault, TTHL_FLT is the Turkey Track Hill Fault, SBC_FLT is the Santa Barbara Canyon Fault, and RHF_FLT is the Rehobith Farm Fault. Numbers within brackets are layers where flow barriers are present.

[3]Scale factors for initial head not part of original sensitivity run. These parameters were added later and were then the most sensitive parameters.

Table 15. Summary of streambed conductivity parameters and current values, Cuyama Valley, California.

Segment categories	Segment conductance group name[1]	Stream segment conductivity (foot per day)	Estimated using automated methods[2]	Rank and composite scaled sensitivity (=== not estimated)
Tributary channels and Cuyama River channel on Recent Alluvium	**Ventucopa**	52.5	Yes	148/1.65
	VC_QYAUC	1.91	No	146/1.74
	WVC_QYAUC	0.98	No	129/2.89
	Main zones	1.50	No	153/1.40
	NMZ_QYA	5.38	No	150/1.44
	SMZ_QYA	0.29	No	145/1.77
	WZ_QYA	0.23	No	152/1.44
	WNMZ_QYA	0.21	No	144/1.78
	WSMZ_QYA	==	None	==
	WWZ_QYA	2.23	No	134/2.28
	Sierra Madre Foothills zones	0.75	No	130/2.84
	None	2.11	No	141/1.85
	Cuyama River channel	52.5	Yes	128/3.34
	NMZ_QYACC	0.29	No	157/0.90
	SMZ_QYACC	1.06	No	139/1.89
	WZ_QYACC	4.95	Yes	143/1.80
	VC_QYACC	10.85	Yes	135/2.25
	WNMZ_QYACC			
	WSMZ_QYACC			
	WVC_QYACC			
	WWZ_QYACC			
Tributary channels and Cuyama River channel on Older Alluvium	**Ventucopa**	2.16	Yes	156/1.09
	VC_QOAS	2.99	No	140/1.88
	WVC_QOAS	0.40	No	138/1.94
	Main zones	0.65	No	151/1.44
	NMZ_QOA	1.73	No	147/1.72
	WWZ_QOAS	0.11	No	155/1.39
	WNMZ_QOA	0.18	No	132/2.49
	WZ_QOAS	0.71	No	154/1.40
	Sierra Madre Foothills zones	0.27	No	131/2.75
	SMFH_QOAN	0.27	No	133/2.42
	SMFH_QOAM	6.87	No	137/1.94
	SMFH_QOAS	0.34	No	136/2.07
	WSMFH_QOAM		None	
	WSMFH_QOAN			
	WSMFH_QOAS			
	Cuyama River channel			
	None			
Tributary channels and Cuyama River channel on Morales formation	**Ventucopa**	3.15	Yes	149/1.60
	VC_MOUC	3.40	No	142/1.81
	WVC_MOUC		None	
	Main zones		None	
	None		None	
	Sierra Madre Foothills zones			
	None			
	Cuyama River channel			
	None			

Table 15. Summary of streambed conductivity parameters and current values, Cuyama Valley, California.—Continued

Segment categories	Segment conductance group name[1]	Stream segment conductivity (foot per day)	Estimated using automated methods[2]	Rank and composite scaled sensitivity (=== not estimated)
Fraction of inflows as recharge plus runoff from basin characterization model				
	Total inflow Cuyama River	1.00	No	====
	Flw84	1.00	No	
	Total Inflow Santa Barbara Canyon			
	Flw113			
Fraction of inflows as recharge or runoff from basin characterization model				
	Inflow Cuyama River as runoff or recharge	1.00	No	====
		0.78	Yes	
	Run84	1.00	No	
	Rch84	0.76	Yes	
	Inflow Santa Barbara as runoff or recharge Canyon			
	Run113			
	Rch113			

[1]Refer to figures 5 and 10 for distribution of stream segments and parameter distributions.

Table 16. Summary of groundwater-flow budgets for selected periods, Cuyama Valley, California.

[Average flows in acre-feet per year. Water Year is October through September of the following year. **Abbreviations**: CUVHM, Cuyama Valley hydrologic model; SMFH, Sierra Madre Foothills; +, plus]

Region/subregion and time period	Average-net inflows					Average-net outflows									Inflow – outflow[1]
	Storage depletion	Direct infiltration (DI)	Stream flow infiltration (SI)	Total recharge (DI + SI)	Total inflows	Storage accretion	Net under flow	Outflow as springs	Domestic pumpage	Water-supply pumpage	Agricultural pumpage	Total pumpage	Total discharge	
CUVHM 1950–2010	34,100	5,600	27,500	33,100	67,200	0	3,700	1,000	16	90	65,300	65,400	70,100	–2,900
CUVHM 2000–10	34,800	3,100	30,300	33,400	68,200	0	3,100	600	10	190	68,100	68,300	78,900	–700
CUVHM 2005 (wet year)	0	16,600	93,200	109,800	162,900	53,100	3,200	700	10	180	68,500	68,700	122,500	40,400
CUVHM 2009 (dry year)	44,900	100	16,700	16,800	61,700	0	3,000	500	10	190	59,800	60,000	105,400	–43,700
Main zone 1950–2010	28,800	3,800	8,000	11,800	40,600	0	3,700	1,000	6	90	57,000	57,100	61,800	–21,200
Ventucopa uplands 1950–2010	0	1,100	17,700	18,800	18,800	5,500	15	0	8	0	7,400	7,400	12,900	5,900
SMFH 1950–2010	11,300	600	1,800	2,400	13,700	0	0	0	2	0	900	900	900	12,800
Main zone 2000–10	27,479	700	8,300	9,000	36,500	0	3,200	600	6	190	56,700	56,900	57,500	–21,000
Ventucopa uplands 2000–10	0	1,500	20,500	22,000	22,000	6,000	15	0	8	0	10,000	10,000	10,000	12,000
SMFH 2000–10	13,800	900	1,600	2,400	16,300	0	0	0	2	0	1,400	1,400	15,200	1,000
Base-case projection CUVHM 2011–71	32,700	2,400	29,500	31,900	64,600	0	2,900	400	7	190	63,700	63,900	67,200	–2,600
Reduced supply projection 2011–71	500	1,100	25,600	26,700	27,200	0	2,900	500	7	190	32,800	33,000	36,400	–9,200
Reduced demand projection 2011–71	0	1,300	29,500	30,800	30,800	11,900	3,000	600	7	190	15,800	16,000	31,500	–700

[1]Negative difference is net depletion and positive difference is net accretion of groundwater flow.

This page intentionally left blank.

Prepared by the Sacramento Publishing Service Center.

For more information concerning this report, contact:

Director
U.S. Geological Survey
California Water Science Center
6000 J Street, Placer Hall
Sacramento, CA 95819
dc_ca@usgs.gov

or visit our Web site at:
http://ca.water.usgs.gov

Hanson and others—**Hydrologic Models and Analysis of Water Availability in Cuyama Valley, California**—SIR 2014–5150

ISSN 2328-0328 (online)

http://dx.doi.org/10.3133/sir20145150

Prepared in cooperation with the Santa Barbara County Water Agency

Construction of 3-D Geologic Framework and Textural Models for Cuyama Valley Groundwater Basin, California

Scientific Investigations Report 2013-5127

U.S. Department of the Interior
U.S. Geological Survey

Cover. Looking northwest from the south side of Cuyama Valley to the Caliente Range. Photograph taken by Donald S. Sweetkind, U.S. Geological Survey, August 2, 2011.

Construction of 3-D Geologic Framework and Textural Models for Cuyama Valley Groundwater Basin, California

By Donald S. Sweetkind, Claudia C. Faunt, and Randall T. Hanson

Prepared in cooperation with the Santa Barbara County Water Agency

Scientific Investigations Report 2013–5127

U.S. Department of the Interior
U.S. Geological Survey

U.S. Department of the Interior
Sally Jewell, Secretary

U.S. Geological Survey
Suzette M. Kimball, Acting Director

U.S. Geological Survey, Reston, Virginia: 2013

Suggested citation:
Sweetkind, D.S., Faunt, C.C., and Hanson, R.T., 2013, Construction of 3-D geologic framework and textural models for Cuyama Valley groundwater basin, California: U.S. Geological Survey Scientific Investigations Report 2013–5127, 46 p.

Contents

Figures

Tables

Conversion Factors, Datums, and Abbreviated Water-Quality Units

Inch/Pound to SI

Multiply	By	To obtain
	Length	
foot (ft)	0.3048	meter (m)
mile (mi)	1.609	kilometer (km)
	Volume	
barrel (bbl), (petroleum, 1 barrel=42 gal)	0.1590	cubic meter (m^3)
	Flow rate	
gallon per minute (gal/min)	0.06309	liter per second (L/s)
inch per year (in/yr)	25.4	millimeter per year (mm/yr)
	Specific capacity	
gallon per minute per foot [(gal/min)/ft)]	0.2070	liter per second per meter [(L/s)/m]

Vertical coordinate information is referenced to the National Geodetic Vertical Datum of 1988 (NGVD 88).

Horizontal coordinate information is referenced to the North American Datum of 1983 (NAD 83).

Altitude, as used in this report, refers to distance above the vertical datum.

Abbreviations

2-D	two-dimensional
3-D	three-dimensional
API	American Petroleum Institute
BR1	bedrock unit 1
BR2	bedrock unit 2
CA DOGGR	California Department of Conservation, Division of Oil, Gas, and Geothermal Resources
CA DWR	California Division of Water Resources
DEM	Digital Evaluation Model
ESRI	Environmental Science Research Institute
GIS	geographic information system
GPS	Global Positioning System
GT	greater than
HUF	Hydrogeologic-Unit Flow
InSAR	Interferometric Synthetic Aperture Radar
LT	less than
Ma	mega-annum
NAD 83	North American Datum of 1983
NGVD88	National Geodedic Vertical Datum of 1988
NWIS	National Water Information System
Qc	Active stream deposits
Qoa	Older alluvium
QTm	Morales Formation
Qya	Younger alluvium
SBCF	Santa Barbara Canyon fault
SP	spontaneous potential
Tq	Quatal Formation
USGS	U.S. Geological Survey

Acknowledgments

Emily Taylor, U.S. Geological Survey, Denver; Meghan Patterson, Metropolitan State College of Colorado; and Lauren Shumaker, University of California-Santa Cruz, transcribed paper drill-hole records into digital files, and Shumaker assigned textural parameters to down-hole lithologic intervals on the basis of analysis of geophysical electric logs.

Staff at the U.S. Geological Survey California Water Science Center, San Diego District Office, digitized electric logs, georeferenced scanned large-format plates, and provided accurate locations for water wells in the valley. In addition to U.S. Geological Survey technical reviews, a draft of this report was improved by comments and insight and informal reviews from Victoria Langenhiem and Daniel Scheirer of the U.S. Geological Survey and from Dennis Gibbs of Santa Barbara County Department of Public Works, California. Funding for this study provided in part from the U.S. Geological Survey National Cooperative Geologic Mapping Program.

Construction of 3-D Geologic Framework and Textural Models for Cuyama Valley Groundwater Basin, California

By Donald S. Sweetkind, Claudia C. Faunt, and Randall T. Hanson

Abstract

Groundwater is the sole source of water supply in Cuyama Valley, a rural agricultural area in Santa Barbara County, California, in the southeasternmost part of the Coast Ranges of California. Continued groundwater withdrawals and associated water-resource management concerns have prompted an evaluation of the hydrogeology and water availability for the Cuyama Valley groundwater basin by the U.S. Geological Survey, in cooperation with the Water Agency Division of the Santa Barbara County Department of Public Works. As a part of the overall groundwater evaluation, this report documents the construction of a digital three-dimensional geologic framework model of the groundwater basin suitable for use within a numerical hydrologic-flow model. The report also includes an analysis of the spatial variability of lithology and grain size, which forms the geologic basis for estimating aquifer hydraulic properties.

The geologic framework was constructed as a digital representation of the interpreted geometry and thickness of the principal stratigraphic units within the Cuyama Valley groundwater basin, which include younger alluvium, older alluvium, and the Morales Formation, and underlying consolidated bedrock. The framework model was constructed by creating gridded surfaces representing the altitude of the top of each stratigraphic unit from various input data, including lithologic and electric logs from oil and gas wells and water wells, cross sections, and geologic maps.

Sediment grain-size data were analyzed in both two and three dimensions to help define textural variations in the Cuyama Valley groundwater basin and identify areas with similar geologic materials that potentially have fairly uniform hydraulic properties. Sediment grain size was used to construct three-dimensional textural models that employed simple interpolation between drill holes and two-dimensional textural models for each stratigraphic unit that incorporated spatial structure of the textural data.

Introduction

Cuyama Valley is a rural agricultural area about 55 kilometers (km) north of Santa Barbara and approximately 65 km southwest of Bakersfield, California, in the southeasternmost part of the Coast Ranges of California (fig. 1). It lies west of the San Joaquin Valley and north of the west-trending Transverse Ranges (fig. 1). The valley is bounded on the north by the Caliente Range and on the southwest by the Sierra Madre Mountains, and it is drained by the Cuyama River (fig. 2). Cuyama Valley sits at the intersection of four counties: most of the valley is within Santa Barbara and San Luis Obispo Counties, regions near the headwaters of the Cuyama River lie in Ventura County, and a small eastern part of the Valley lies within Kern County (fig. 2). Although located within the Coast Ranges, Cuyama Valley has many of the climatic features of a desert basin because it is far from the coast and surrounded by relatively high mountains. The main economic activities in Cuyama Valley are ranching, agriculture, and oil and gas production.

Topographically, Cuyama Valley overlies and is part of a broader geologic domain, which was a depocenter for marine and nonmarine sediments during the Oligocene and Miocene epochs (Lagoe, 1984, 1987; Bazeley, 1988; Fritsche, 1988) and for continental deposits and alluvial sediments several hundred meters-thick during the Pliocene and Pleistocene epochs (Vedder and Repenning, 1975; Ellis and others, 1993). These continental deposits and alluvial sediments constitute the principal groundwater aquifer of the Cuyama Valley groundwater basin (California Department of Water Resources, 2003; fig. 2). Groundwater is currently the sole source of water supply for Cuyama Valley. Groundwater withdrawal, mainly for the irrigation of crops, has resulted in water-level declines of as much as 100 meters (m) since the 1940s (Singer and Swarzenski, 1970; Pierotti and Lewy, 1998). Groundwater is found in permeable Holocene alluvial fill and underlying less permeable Pliocene-Pleistocene continental deposits (Upson and Worts, 1951; California Department of Water Resources, 2003). In areas where drawdown is greatest, water-level declines have left the more productive shallow aquifers unsaturated and have dropped the water table into the less-productive, deeper aquifers. In response to these changes, the U.S. Geological Survey (USGS), in cooperation with the Water Agency Division of the Santa Barbara County

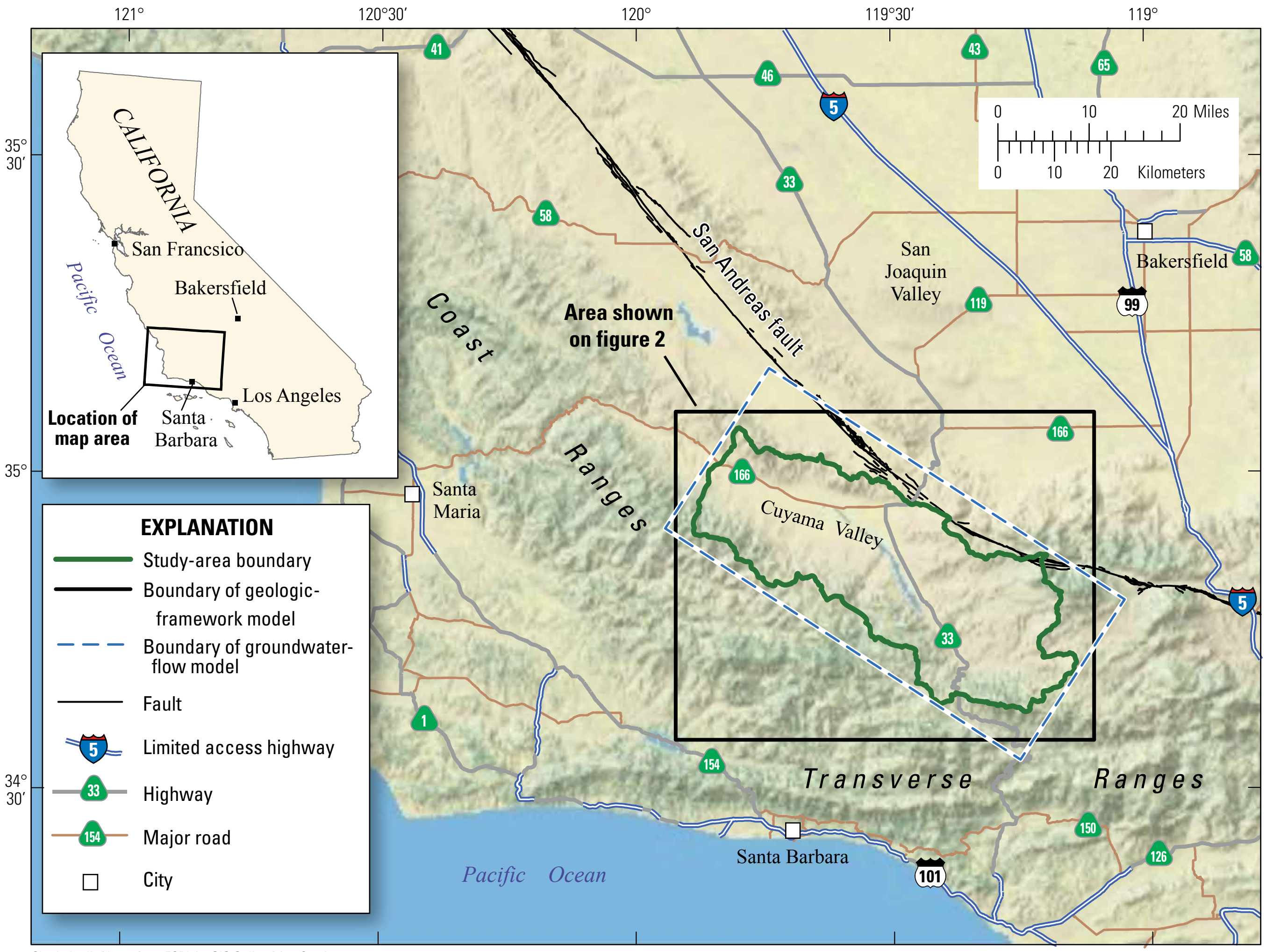

Shaded relief base from ESRI ArcGIS Online Map Service
http://services.arcgisonline.com/arcgis/services: ESRI_ShadedRelief_World_2D
Roads from Cal-Atlas Geospatial Clearinghouse *http://atlas.ca.gov/download.html*
Place names sourced from USGS Geographic Names Information System, 1974–2009
San Andreas fault from Bryant (2005)
Albers Projection, NAD83

Figure 1. Location of Cuyama Valley within the California Coast Ranges.

Department of Public Works, is evaluating the hydrogeology and water availability of the groundwater basin. The intent of the overall study is to develop a greater understanding of the occurrence and availability of groundwater and to evaluate the potential effects of future groundwater withdrawals on different parts of the valley.

An evaluation and simulation of groundwater resources are most effectively achieved through an understanding of the subsurface geologic framework through which the water moves. As a part of the overall groundwater evaluation of Cuyama Valley, this report provides a conceptual understanding of the geologic setting of the Cuyama Valley groundwater basin and documents the construction of three-dimensional (3-D) digital models of the geologic framework and grain-size variations within the study area. These data provide the physical geologic framework that is used within a numerical hydrologic-flow model being developed concurrently (Randall Hanson, U.S. Geological Survey, written commun., 2013).

Purpose and Scope

This report describes the geology in the vicinity of Cuyama Valley, with an emphasis on the Pliocene through Holocene terrestrial sediments that have the greatest bearing on the Cuyama Valley groundwater basin. This report documents the use of surface and subsurface geologic data in the construction of a digital 3-D geologic framework model of the basin. The 3-D model is the digital representation of the interpreted geometry and thickness of subsurface geologic units and the geometry of folds and faults that bound the basin and lie within it. Previous work has outlined the overall shape of the basin and geometry of faulting along specific geologic profiles across the basin (Singer and Swarzenski, 1970; Vedder and Repenning, 1975; Davis and others, 1988), but the 3-D geometry of the geologic units must be defined for the purposes of the numerical flow model. Most previous geologic

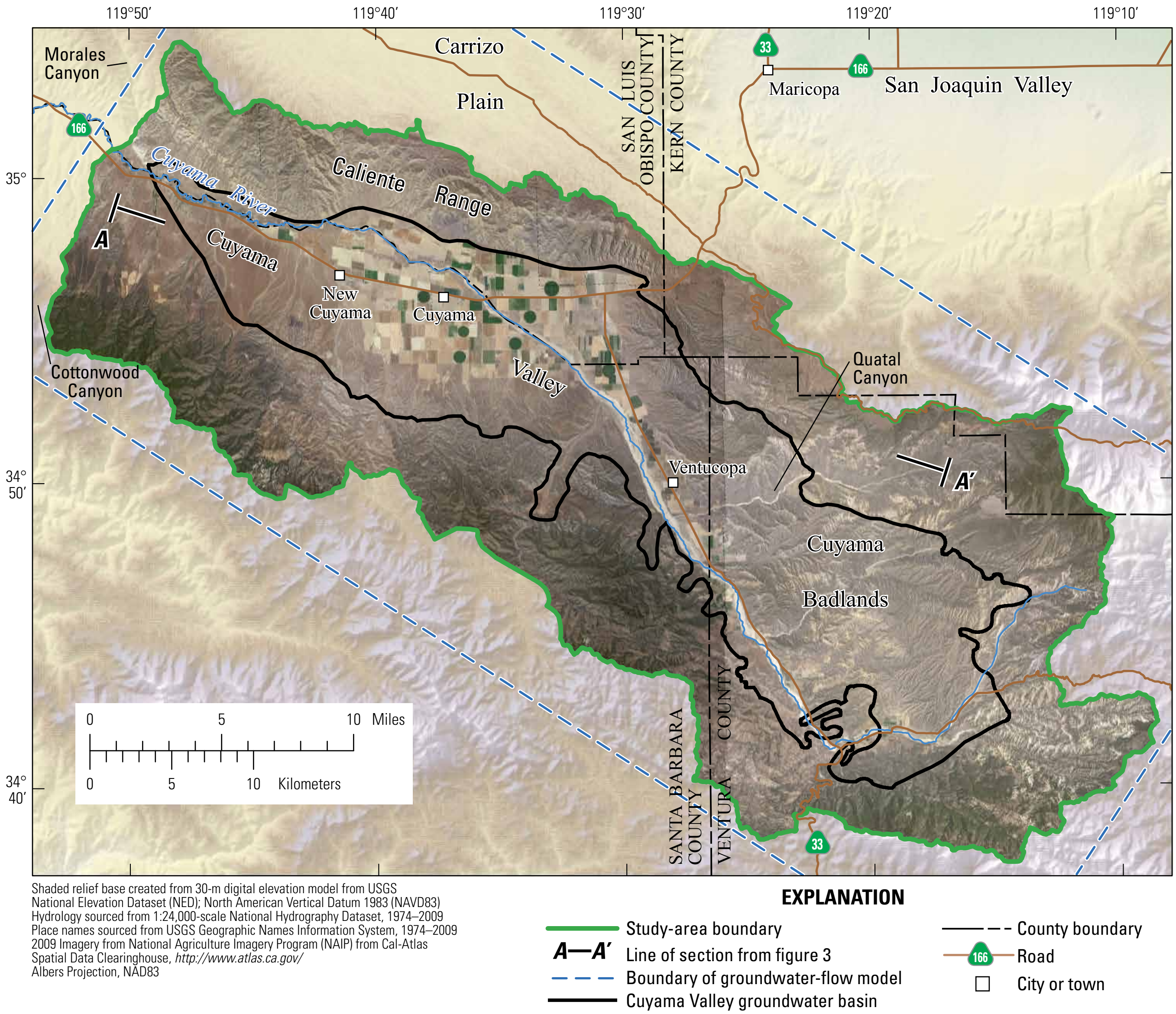

Figure 2. The Cuyama Valley study area.

investigations in Cuyama Valley have focused on the deeper, oil-bearing rocks (Hill and others, 1958; Lagoe, 1987; Bartow, 1990). Here, the geologic framework model uses information from a variety of datasets, including existing lithologic and electrical geophysical logs from oil and gas wells and water wells, cross sections, and geologic maps, to delineate the volumes of the aquifer system bounded by faults and relevant depositional or formational boundaries.

This report also documents the development of the 3-D spatial distribution of grain size of the basin-filling deposits. Textural characteristics such as grain size form the basis by which aquifer hydraulic properties are assigned within the numerical hydrologic-flow model (Hanson and others, 2003, 2004; Faunt, 2009). Previous USGS studies of Cuyama Valley (Upson and Worts, 1951; Singer and Swarzenski, 1970) delineated aquifers in the saturated parts of the younger and older alluvium, which are the units that, historically, have yielded most of the water pumped in the study area. Since these studies were completed, water levels have declined in some areas into the deeper formations, such as the Morales Formation, that were not previously investigated in detail, requiring an investigation of the geometry and water-bearing properties of all of the basin-filling units, including the deeper stratigraphic sections of the groundwater basin.

The focus of this investigation is the alluvial basin that underlies the valley and constitutes the principal groundwater reservoir beneath Cuyama Valley and adjacent areas at the basin margins, where Pliocene and younger continental sediments are exposed in outcrop and could serve as active recharge areas for the groundwater basin. The study area of interest thus includes the agricultural areas between the town of New Cuyama on the west and State Highway 33 on the east (fig. 2) and the part of the Cuyama River drainage extending southeastward along the Cuyama River to its headwaters south of the Cuyama Badlands (fig. 2). The western boundary of the study area is located in the vicinity of the tributary washes of Morales Canyon on the north and Cottonwood Canyon on the south (fig. 2) to include all thick occurrences of young alluvium (Upson and Worts, 1951; Vedder and Repenning, 1975).

Although the Cuyama Valley groundwater basin is the primary interest of this study, for computational reasons the geologic framework model covers a large rectangular area slightly larger than the boundaries of figure 2, and thus includes much bedrock of little hydrologic interest. The overall hydrogeologic evaluation of Cuyama Valley involves the use of a numerical hydrologic-flow model and a linked watershed model; the boundary of this numerical simulation forms an elongate, northwest-trending rectangular polygon aligned with the valley axis (fig. 2).

Geologic Setting

Aquifer units within the Cuyama Valley groundwater basin include unconsolidated Pleistocene and Holocene alluvial deposits and fluvial deposits of the Cuyama River drainage and the underlying partly consolidated nonmarine Morales Formation of Pliocene to Pleistocene age (Upson and Worts, 1951; Singer and Swarzenski, 1970). These deposits unconformably overlie a late Cretaceous to middle Cenozoic succession of consolidated marine and nonmarine sedimentary rocks, which themselves overlie crystalline granitic and gneissic rocks (Hill and others, 1958; Dibblee, 1982; Lagoe, 1987; Bazeley, 1988; fig. 3).

Cuyama Valley has cumulative production plus reserves of about 290 million barrels of oil (Stanley, 1995; California Department of Conservation, 2009). Most of the production comes from the South Cuyama and Russell Ranch fields, located next to the Russell fault (fig. 4; Stanley, 1995). Abundant subsurface geologic data for this study have come from oil and gas wells from these fields and from exploration holes scattered across the valley (Nevins, 1982; Schwing, 1984; Calhoun, 1986; Spitz, 1986; Sweetkind and others, 2013).

Stratigraphic Units

The shallow alluvial section is subdivided into three units: Qc, fluvial channel deposits associated with the Cuyama River; Qya, younger alluvium; and Qoa, older alluvium (figs. 3 and 4; table 1). Previous studies did not separate the younger and older alluvium as separate units (Upson and Worts, 1951; Singer and Swarzenski, 1970), but the two are distinguishable as mappable units at the surface (fig. 4) and, in the subsurface, can often be identified by differences in electric log signature.

Younger alluvium (Qya, figs. 3 and 4) consists of unconsolidated sand, gravel, and boulders, with some clay, deposited as alluvium in stream channels, floodplains, alluvial fans, and stream terraces. The unit is mainly Holocene in age, but locally can be late Pleistocene in part. Active stream deposits (Qc, figs. 3 and 4) consist of river-bed gravels of the Cuyama River and other active channels (Vedder and Repenning, 1975; DeLong and others, 2008, 2011). These deposits are incorporated into Qya within the geologic framework model.

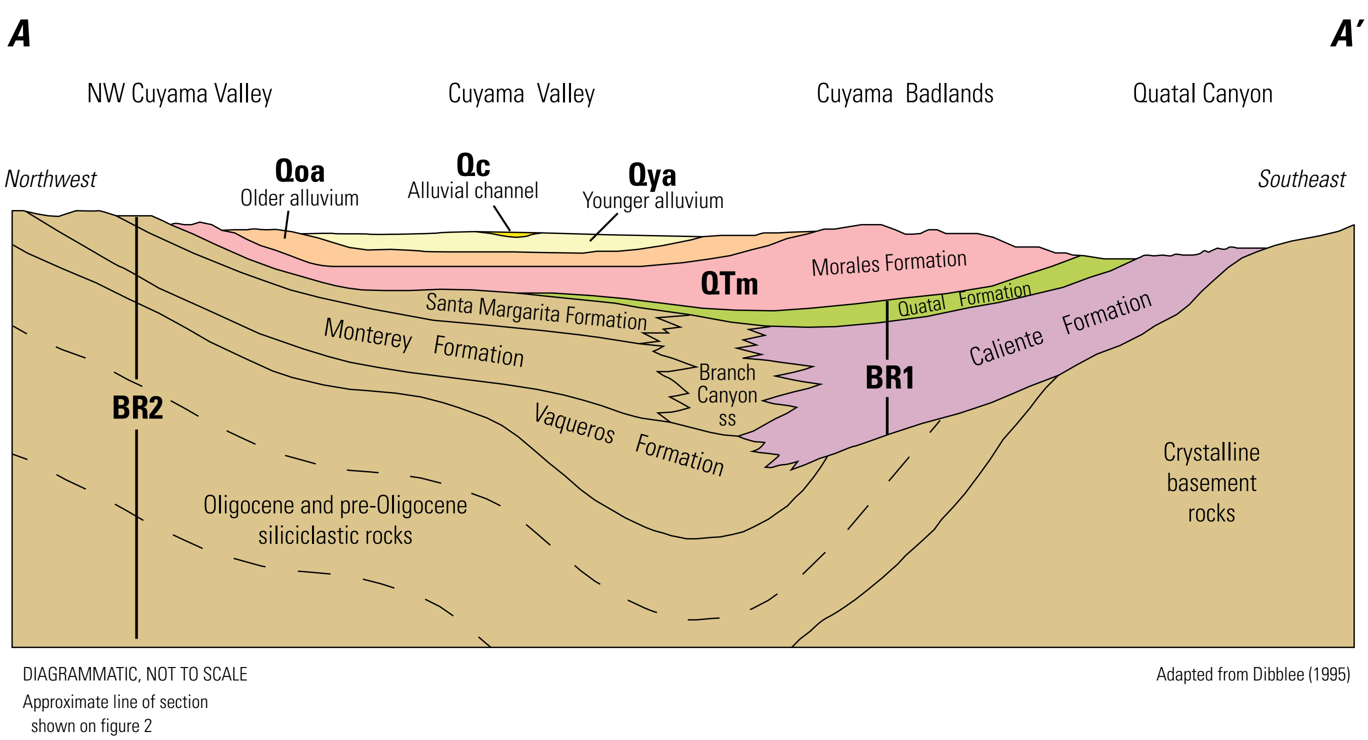

Figure 3. Generalized stratigraphic diagram of the Cuyama Valley study area.

Older alluvium (Qoa, figs. 3 and 4) consists of unconsolidated to partly consolidated sand, gravel, and boulders, with some clay, and the percentage of clay increases in the western part of the valley (Singer and Swarzenski, 1970; Vedder and Repenning, 1975; DeLong and others, 2008). Interpretation of geophysical logs from oil-exploration wells indicates that this unit is typically 125 to 200 m thick, but as thick as 300 m near the axis of Cuyama Valley (Schwing, 1984; Spitz, 1986). In the study area, older alluvium includes dissected alluvial fans, colluvial deposits, and sediments on multiple terraces and alluvial surfaces (Hill and others, 1958; DeLong and others, 2008). Older alluvium is exposed on uplifted alluvial surfaces along the south side of Cuyama Valley and in the center of the valley along the Turkey Trap and Graveyard Ridge faults (fig. 4; Vedder and Repenning, 1975; DeLong and others, 2008). A greater degree of consolidation, dissection, and local deformation distinguishes the older alluvial deposits from young alluvium in outcrop.

The Pliocene-Pleistocene Morales Formation (QTm, figs. 3 and 4) is an alluvial and fluvial deposit throughout most of the study area. The unit is as thick as 1,500 m and consists of massive- to thick-bedded, partly consolidated deposits of gravelly

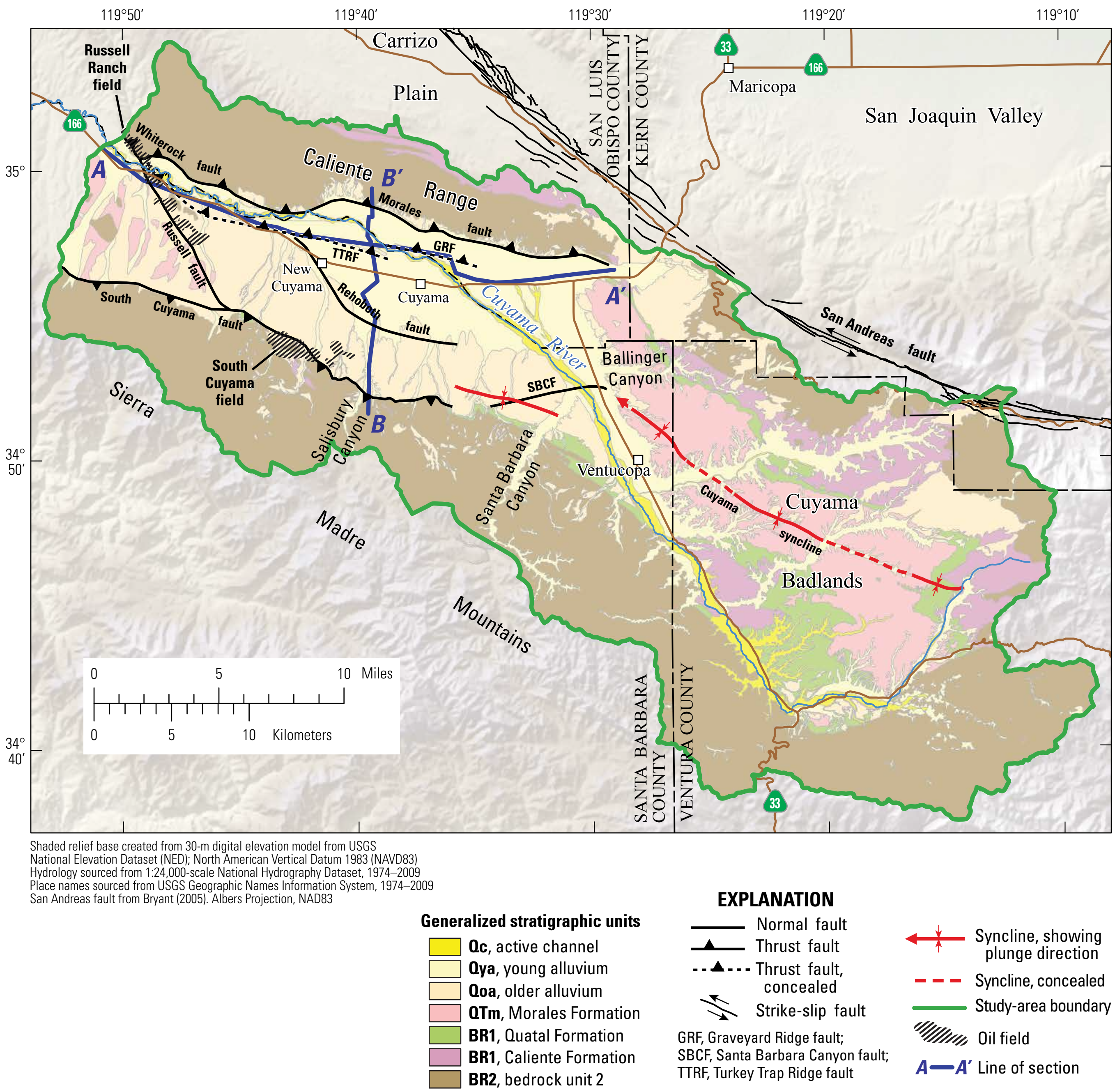

Figure 4. Generalized geology of the Cuyama Valley study area.

Table 1. Correspondence between map units from source geologic maps to geologic units.

Geologic unit (abbreviation)	Unit description	Corresponding geologic units (Kellogg and others, 2008)	Corresponding geologic units (Graham and others, 1999)
Quaternary channel deposits (Qc)	Includes active channel of the Cuyama River and recent meander cutoffs.	Qa, active alluvium.	Not shown
Younger alluvium (Qya)	Young unconsolidated alluvium on valley floor and in tributary washes.	Qya, younger (inactive) alluvium.	Qa, alluvium
Older alluvium (Qoa)	Older alluvial deposits, partly consolidated. Dissected and deformed into gentle folds.	Qoa, older alluvium; QTa, old alluvium, locally deformed.	Qoa, older alluvium
Morales Formation (QTm)	Weakly to moderately indurated arkosic, lithic sandstone and conglomerate. Fine-grained lacustrine facies in western part of study area.	QTm and subunits, Morales Formation; QTt, Tulare Formation	Tmo, Morales Formation; QTp, Paso Robles Formation
Quatal Formation (Tq)	Predominantly fine-grained fluvial to lacustrine siltstone and fine-grained sandstone. Underlies Morales Formation in eastern half of the study area, pinches to zero thickness in the vicinity of the town of Cuyama.	Tq and subunits, Quatal Formation; Tlc, Lockwood Clay.	Tq, Quatal Formation.
Bedrock unit 1 (BR1)	Continental sedimentary rocks of the Caliente Formation. In the subsurface the Caliente Formation interfingers westward with Middle Miocene consolidated marine rocks.	Tc and subunits, Caliente Formation.	Tc, Caliente Formation.
Bedrock unit 2 (BR2)	Includes all Miocene and older consolidated bedrock units (except for continental Caliente Formation). Tertiary basalts that are interbedded with Caliente Formation in the Caliente Range were included in this unit.	Tcb, Alkalic olivine basalt flow; Ti, Intrusive olivine diabase; Tsm and subunits, Santa Margarita Sandstone; Tb and subunits, Branch Canyon Sandstone; Tm and subunits, Monterey Formation; Tv and subunits, Vaqueros Formation; all older units.	Tb, basalt; Tsm and subunits, Santa Margarita Formation; Tbs, Branch Canyon Sandstone; Tm and subunits, Monterey Formation; Tv and subunits, Vaqueros Formation; all older units.

arkosic sand with local gravel beds and siltstone (Hill and others, 1958; Ellis and others, 1993; DeLong and others, 2008, 2011; Kellogg and others, 2008). In the western part of the study area, the unit is predominantly fine-grained and consists chiefly of lacustrine clay (Upson and Worts, 1951; Dibblee and Minch, 2005d; DeLong and others, 2008). The Morales Formation is widely exposed as badland topography east of the Cuyama River (fig. 4; Dibblee, 1982; Dibblee and Minch, 2005a, 2006; Kellogg and others, 2008).

For the purposes of this study, non-water-bearing consolidated rocks that lie beneath the Morales Formation are divided into two generalized geologic units: BR1 and BR2. Most of the middle Miocene and older consolidated rocks were included in the deeper unit, bedrock unit 2 (BR2; figs. 3 and 4; table 1). This unit forms the bedrock highlands on the north, south, and east sides of the study area and includes consolidated marine and continental deposits of great thickness. Stratigraphic units that compose BR2 include the Santa Margarita Formation, the Branch Canyon Sandstone, the Monterey Formation, the Vaqueros Formation, and older rocks (fig. 3; table 1).

Continental sedimentary rocks of the Caliente Formation and the Quatal Formation were retained as a separate bedrock unit (BR1; figs. 3 and 4; table 1) because they are significantly less consolidated than the underlying units, which can result in different water-transmitting properties. The Quatal Formation is a nonmarine claystone and sandstone sequence that conformably underlies the Morales Formation (Hill and others, 1958). At its type locality in the Cuyama Badlands, it consists of about 250 m of gypsiferous claystone, although elsewhere in the study area, nonmarine sandstones are interbedded with the claystone (Vedder, 1968; Kellogg and others, 2008). The unit is readily identified in the subsurface throughout the eastern part of the study area as a distinctive interval on electric logs; it thins westward and pinches out beneath the central part of Cuyama Valley (fig. 3; Ellis and Spitz, 1987; Ellis, 1994). The Quatal Formation is not part of the active groundwater flow system. It is highlighted on the geologic map because, in the eastern and central parts of the study area, it is a distinctive stratigraphic marker that defines the base of the Morales Formation and the base of the groundwater system (figs. 3 and 4; table 1).

Historically, most of the water pumped from the study area was obtained from the younger and older alluvium (Singer and Swarzenski, 1970). Large-capacity wells perforated in the alluvium yield 1,000–3,000 gallons per minute (gpm) and have specific capacities in the range from 100 to 200 gpm per foot (gpm/ft; Singer and Swarzenski, 1970). The water-bearing properties of the Morales Formation are not well defined, but available data indicate that hydraulic conductivity, the ease with which water passes through the formation, varies greatly both areally and with depth. Wells perforated in the Morales Formation along the northern margin of the central valley have specific capacities of 25–50 gpm/ft; wells perforated in the finer-grained facies in the western part of the valley have specific capacities of 5 to 25 gpm/ft (Singer and Swarzenski, 1970). Inspection of available geologic and geophysical logs indicate that the hydraulic conductivity of the Morales Formation decreases with depth.

Structural Setting

In the Cuyama Valley region, Oligocene extension and Miocene strike-slip faulting are overprinted and obscured by Pliocene- to Pleistocene-aged thrust faults that bound the ranges surrounding the current topographic valley (Calhoun, 1986; Davis and others, 1988). Rocks of Miocene age and older are known from deep oil and gas wells to be affected by older, now inactive faults largely buried by the Morales Formation and younger units (Yeats and others, 1989). The most significant of these older faults is the Russell fault at the west edge of the study area (fig. 4). This fault localizes the oil-producing fields in Cuyama Valley by trapping petroleum in faulted updip ends of sandstones within the Miocene Vaqueros Formation (Stanley, 1995). Up to 29 km of right-lateral offset has been documented on the northwest-striking Russell fault in the northwest part of Cuyama Valley to have occurred between 23 and 4 mega-annum (Ma), but the fault has little to no offset in Morales Formation or younger units (Yeats and others, 1989; Ellis and others, 1993).

During Pliocene time, the deformational style in Cuyama Valley changed to a predominantly compressional mode during the deposition of the Morales Formation (Ellis and others, 1993; Ellis, 1994). Resultant deformation has created the Cuyama structural basin and produced the converging thrust faults that bound Cuyama Valley: the south-directed Whiterock and Morales faults on the north and the north-directed South Cuyama fault on the south (fig. 4; Vedder and Repenning, 1975; Davis and others, 1988). Based on the magnetostratigraphy of the Morales Formation, uplift of the Caliente Range began between 3.0 and 2.6 Ma (Ellis and others, 1993; Ellis, 1994). Thrust motion continued into Quaternary time, with Miocene-aged rocks of the Caliente Range to the north of Cuyama Valley being thrust southward over Quaternary alluvium on the Morales fault (Vedder and Repenning, 1975). DeLong and others (2008) report thrust-fault interaction with Quaternary piedmont deposits in the western part of the study area indicateing ongoing contraction through 0.1 Ma.

Contraction of the Cuyama structural basin is driven by transpressional forces resulting from northwest-directed transport of the crustal block containing Cuyama Valley around the Big Bend of the San Andreas fault system to the east (Argus and Gordon, 2001; Hardebeck and Michael, 2004). Geodetic results from various models indicate that the San Andreas fault system and central California Coast Ranges accommodate northwest-directed motion relative to the North American plate of about 39 mm/yr, mainly by strike-slip faulting (Meade and Hager, 2005), with a small and variable amount of fault-perpendicular convergence (Argus and Gordon, 2001). The greatest amount of convergence along the length of the San Andreas fault system is in the vicinity of the Big Bend of the San Andreas fault (Argus and Gordon, 2001), an area that includes Cuyama Valley. Inversion of focal mechanisms of small earthquakes near the San Andreas fault showed that the direction of maximum horizontal compressive stress in the vicinity of the Big Bend of the San Andreas fault is between 40 and 60 degrees to the strike of the fault (Hardebeck and Michael, 2004). In the vicinity of Cuyama Valley, this direction is approximately perpendicular to the valley axis and tectonically consistent with the orientation of thrust faults that bound the north and south sides of the valley.

The Morales Formation and older alluvium are folded into tight synclines along the north and south margins of the valley near the bounding thrust faults (Spitz, 1986; Kellogg and others, 2008). The Cuyama syncline plunges northwestward beneath the valley from the Cuyama Badlands to the southeast (fig. 4; Dibblee, 1982; Ellis and Spitz, 1987; Dibblee and Minch, 2005a; 2006; Kellogg and others, 2008). It is exposed in the Ventucopa area and the Cuyama Badlands (fig. 4; Dibblee and Minch, 2005a; 2006; Kellogg and others, 2008) and is known from subsurface data from oil exploration wells beneath the valley itself (Spitz, 1986; Ellis and Spitz, 1987; Ellis, 1994).

Faults and the Groundwater Flow System

Faults of hydrologic significance in Cuyama Valley area are those that involve the aquifers. Such faults occur at the basin margin, where fault offset juxtaposes basin-fill sediments against older consolidated rocks, and within the basin, where basin-fill units of differing water-transmitting ability are juxtaposed. Faults that offset the consolidated rocks are known principally from oil and gas exploration; faults within the basin fill have been recognized previously as being associated with historic surface springs or changes in groundwater elevations (Singer and Swarzenski, 1970). Three faults within the basin offset the basin-filling deposits and are associated with known water-level changes (Upson and Worts, 1951, Singer and Swarzenski, 1970): the thrust faults that bound Turkey Trap and Graveyard Ridges, the Santa Barbara Canyon fault, and the Rehoboth fault (fig. 4).

Graveyard and Turkey Trap Ridges in the center of Cuyama Valley, north of Highway 166, trend slightly north of west, are oriented in a left-stepping, en echelon pattern and contain exposures of older alluvium (Qoa; fig. 4). Geologic mapping and north-south seismic reflection profiles collected across these ridges showed that these ridges are bounded by north-dipping, south-directed, reverse faults along their south sides (Upson and Worts, 1951; Vedder and Repenning, 1975; Ellis, 1994). Upson and Worts (1951) reported the presence of springs and seeps along the base of Turkey Trap and Graveyard Ridges in 1946. Singer and Swarenski (1970) reported water-level drawdowns of 80 to 100 feet (ft) in the area near these ridges and indicated that water removed by pumping from this region was slow to replenish because faults restrict movement of water from neighboring areas. The impediment to flow could be related to the hydraulic properties of the fault itself or fault juxtaposition of older, slightly less permeable Qoa, to the north, against Qya to the south of the faults.

A fault, here called the Santa Barbara Canyon fault (SBCF, fig. 4), was suggested by Singer and Swarzenski (1970) to be the cause of a steep hydraulic gradient in the southeastern part of Cuyama Valley, where water levels in the vicinity of Ventucopa are at least 30 m higher than water levels 3 km to the north. Singer and Swarzenski (1970) suggest that this fault could be a projection of east-northeast-striking faults mapped west of Santa Barbara Canyon by Dibblee and Minch (2007) on the basis of anomalous topographic lineaments in older alluvium. No geologic evidence bearing on sense or amount of offset has been found in the field, although some confirmation of faulting is provided by truncation of distinctive gravel beds in the older alluvium along the west wall of Santa Barbara Canyon, near its mouth, on trend with the lineaments. Very minor throw, southeast-side down, is indicated by distinctive markers in the Morales Formation on geophysical logs from wells on either side of the lineaments, and Dibblee and Minch (2007) showed about 1,500 m of left-lateral offset on fold axes across the lineaments. Such lateral slip on east-northeast-striking faults is consistent with the present northward-directed compressive tectonic regime of Cuyama Valley. Although a single fault is shown on figure 4, the topographic lineaments mapped in the piedmont upland and the width of the zone where there are water-level changes indicate that there could be a zone of subparallel faults. No deep-well data constrain how these faults project northeastward across the Cuyama River; analysis of formation contacts, dip amounts, and dip directions in Ballinger Canyon on the east side of the Cuyama River reveals no obvious continuation of this fault trend. The relatively small amount of vertical offset on the Santa Barbara Canyon fault indicate that changes in water levels across this fault documented in previous studies are perhaps the result of distinct fault-zone properties, rather than juxtaposition of units of differing water-transmitting ability.

Another fault, here called the Rehoboth fault (fig. 4), is inferred from water-level changes in the west-central part of the valley. The fault is interpreted to trend southeastward near the town of Cuyama and to project beneath the Salisbury Canyon drainage (Lane-Western Company, written commun. to developers of Rehoboth Farms property, 1982). Comparison of the elevation of distinctive marker horizons within the Morales Formation on geophysical logs of exploration wells drilled on either side of the fault indicates that the top of the Morales Formation is offset about 50 m down on the northeast side of the fault; offset at the base of the Morales Formation is greater. Surface exposures of Qoa do not appear to be offset along the trace of the fault, indicating that motion on this fault may have ceased prior to deposition of the youngest part of Qoa.

Regional Tectonics and Uplift Rates

Geologic evidence indicates that Cuyama Valley has been the site of contractile deformation for the past 4 Ma (Ellis and others, 1993). Geologic relations along the southern flank of the Caliente Range, which forms the northern margin of Cuyama Valley, indicate contraction until as recently as 100,000 yr (Ellis and others, 1993; DeLong and others, 2008). In addition to this shortening, ongoing compression manifests itself by broad regional tectonic uplift. Although the valley is low relative to the surrounding thrust-bounded ranges, it is elevated by 500–700 m relative to the San Joaquin Valley to the northeast of the San Andreas fault (Argus and Gordon, 2001). The Pliocene and Pleistocene Morales Formation was deposited within Cuyama Valley structural basin as a result of uplift along valley-margin structures, erosion of those marginal rocks, and sedimentation in the basin (Spitz, 1986; Ellis, 1994). As regional uplift continued, and the axial part of the valley narrowed, the Morales Formation and older Quaternary alluvium were themselves uplifted, exposed to fluvial erosion, and moderately deformed (Spitz, 1986; DeLong and others, 2008). On the south side of Cuyama Valley, young Quaternary deposits unconformably overlie deformed older Quaternary deposits and the Morales Formation as a result of ongoing tectonic uplift and erosion (DeLong and others, 2008; Kellogg and others, 2008). The Cuyama River and its major tributaries are currently incised into Holocene alluvium in the axial part of the valley as a result of progressive regional tectonic uplift (DeLong and others, 2008, 2011).

Continuously monitored global positioning system (GPS) stations are located in Cuyama Valley and surrounding uplands as part of an integrated GPS Network designed to monitor deformation throughout southern California (Hudnut and others, 2002; Meade and Hager, 2005). The GPS stations record variations in position and elevation that can result from either tectonic motions or from deformation associated with anthropogenic activities such as groundwater withdrawal. Land-surface position was recorded at two GPS monitoring stations within the valley—at Cuyama High School near the center of the valley and near Ventucopa in the southeastern part of the valley—and three stations in the uplands to the east, south, and southwest of the valley (Everett and others, 2013). Running 31-day averages of GPS observations acquired between 2000 and 2012 (2008–2012 for one of the upland stations) indicated a slight net upward motion at Ventucopa and the three upland stations outside the valley (Everett and others, 2013). In contrast, land surface position for the GPS station at Cuyama High School records a long-term downward trend between 2000 and 2012 with cyclic, annual seasonal variations in elevation. This cyclic variation correlates with pumping records and variations in water levels measured in nearby wells (Everett and others, 2013). It is likely that the long-term trend in subsidence at Cuyama High School represents inelastic, irreversible deformation of the underlying aquifer as a result of permanent changes in the pore volume and resulting loss of storage capacity within the aquifer, whereas short-term seasonal trends represent elastic deformation associated with seasonal groundwater withdrawals (Everett and others, 2013). The magnitude of subsidence between 2002 to 2008 was estimated at five points in the central part of the valley from analysis of satellite interferometric synthetic aperture radar (InSAR) images, a remote sensing technique that can detect centimeter-level elevation changes (Everett and others, 2013). Point analysis of the InSAR images confirmed downward movement throughout the central subregions of the basin where groundwater pumpage and related water-level declines are largest (Everett and others, 2013).

Compilation of Surface and Subsurface Data

Construction of the geologic framework model utilized data from multiple sources to define the top surface and extent of each geologic unit. Input data sources include topographic data, geologic maps, stratigraphic tops interpreted from borehole data, and structure contour maps. Textural properties of the basin-filling deposits were interpreted from borehole lithologic and electric logs.

Surface Geologic Map Data

A generalized geologic map of the study area (fig. 4) was compiled through the merging of two main digital data sets: (1) a 1:100,000-scale geologic map of the eastern three-quarters of the Cuyama 30′ x 60′ quadrangle (Kellogg and others, 2008) that covers the main part of Cuyama Valley, the Cuyama Badlands, and the bedrock geology in a wide area to the south and east of Cuyama Valley, and (2) a 1:125,000-scale geologic compilation of geology along the San Andreas faults (Dibblee, 1973), as rendered digitally by Graham and others (1999), that was used to compile the geology at the northwest end of Cuyama Valley and in the Caliente Range. Larger-scale, non-digital geologic maps of parts of the basin were consulted for local geologic relations (Vedder, 1968; Vedder and Repenning, 1975; Calhoun, 1986; Dibblee and Minch, 2005a, 2005b, 2005c, 2005d, 2006, 2007).

Source geologic data were given a common map projection, and correlative geologic units from each of the source maps were merged in a geographic information system. Mapped geologic units were then combined into the limited number of geologic units of table 1.

Stream-channel deposits in the northwestern part of the area were digitized from Vedder and Repenning (1975) and from satellite imagery. Numerous landslide deposits on bedrock units were merged with the underlying bedrock unit. Landslide deposits are generally thin (10–20 m thick) and are composed primarily of rubble from of the underlying bedrock.

Data points representing the location and elevation of stratigraphic contacts exposed in outcrop were generated from the geologic map in combination with a 1 arc-second (approximately 30-m resolution) National Elevation Dataset digital elevation model (Cal-Atlas Geospatial Clearinghouse; *http://atlas.ca.gov/download.html*). Regularly spaced points were digitized along a stratigraphic contact within a geographic information system (GIS). These points were assigned coordinate locations from the map base and elevations from the digital evaluation model (DEM) and exported as a series of files, one for each stratigraphic unit, containing x,y, and z data that were subsequently used in gridding the stratigraphic unit tops.

Subsurface Data

Oil and Gas Wells

Stratigraphic information from oil and gas exploration and development wells from Cuyama Valley, Calif., and surrounding areas have recently been compiled by Sweetkind and others (2013). Most of the oil wells in Cuyama Valley are clustered within two fields with historic and continuing production: the Russell Ranch field (Barger and Zulberti, 1952) at the west edge of the study area and the South Cuyama oil field (Zulberti, 1954) at the southwest edge of the study area (fig. 4). Production wells in those fields are very closely spaced; selected wells were used to represent geologic conditions in the vicinity of the producing fields. Exploratory wells were drilled away from the fields at widely scattered locations across Cuyama Valley. Data from every one of these exploratory wells were compiled for this study. Information on subsurface stratigraphy and lithology from over 200 oil and gas exploration wells was selected for use in the current study.

The California Department of Conservation, Division of Oil, Gas, and Geothermal Resources (CA DOGGR) maintains paper copies of electric logs on file for most of the oil and gas exploration holes in Cuyama Valley. Initially, logs were obtained directly from the CA DOGGR district office in Santa Maria, Calif., by physically scanning paper copies of the electric logs. The CA DOGGR has subsequently made some of the electric logs available on-line (*http://owr.conservation.ca.gov/WellSearch/WellSearch.aspx*).

In the 1980s four masters theses (Nevins, 1982; Schwing, 1984; Calhoun, 1986; Spitz, 1986) and one Ph.D. dissertation (Ellis, 1994) were produced at Oregon State University under the guidance of Professor Robert Yeats. These works, and related publications (Schwing, 1982; Ellis and Spitz, 1987; Yeats and others, 1989), discussed the subsurface geology of Cuyama Valley and focused on the mapping of subsurface formations by using data from oil exploration holes, in particular electric logs. Each thesis contained several stratigraphic cross sections that correlated subsurface formations across the valley (Sweetkind and others, 2013). Although the focus was primarily on the Miocene section, the cross sections showed the interpreted base of the Morales Formation and, occasionally, showed correlation of distinctive marker units within the Morales. These sections served as a starting point for the electric log interpretations of formation tops in this study.

Water Wells

Downhole lithologic data from water-well drillers' logs, used here to interpret formation tops and sediment grain size and sorting parameters, were derived from three sources: a U.S. Geological Survey Water-Supply paper on Cuyama Valley (Upson and Worts, 1951), lithologic data associated with well records obtained from the USGS National Water Information System (NWIS), and well data obtained from the State of California Department of Water Resources (CA DWR). Lithologic data from all wells reported by Upson and Worts (1951) were transcribed from the paper report. The location map that accompanied that report was georeferenced in a GIS, and well locations were digitized. Lithologic data associated with NWIS records and from CA DWR were also transcribed and tied to reported site locations. CA DWR wells were located according to descriptive information included on the well completion reports submitted to the State of California. The specific location of each well differed from GPS locations recently confirmed in the field with differential GPS systems to sketched maps or township, range, section, and quarter-quarter-section information on the well completion reports. Wells that had sufficiently detailed sketch maps were assigned a latitude-longitude by comparing the sketch maps with georeferenced aerial photos in a GIS. Latitude-longitude locations were established for wells listing only the township, range, section and quarter-quarter section locations on the drillers' logs by calculating the center position of the most detailed part of the township and range location. Ultimately, all well locations were cross-checked against locations in the NWIS database, with well compilations for hydrologic data compiled for Cuyama Valley (Everett and others, 2013) and with field-checked locations.

Of the water wells compiled for stratigraphic information, 21 were from Upson and Worts (1951), and 56 wells came from the State of California and other sources. Of the water wells compiled for lithologic information and subsequent textural analysis, 41 were from Upson and Worts (1951), and 110 wells were from the State of California and other sources.

Interpretation of Subsurface Data

Stratigraphic contacts, including the top of Qoa and the top and base of the QTm were interpreted from electric logs and drillers' lithologic logs. For the oil and gas wells, formation tops were almost invariably interpreted from electric logs. Lithologic logs from the oil and gas exploration holes were not helpful in the shallow alluvial section, which was not of interest to the well-site geologists. Lithology in the shallow parts of these holes was typically logged with a single descriptor, such as "sand and gravel," that might apply to hundreds of meters of section. Similarly, the tops of Qoa and the QTm were typically not recorded by these geologists; formation tops were reported only for consolidated rocks below the Morales Formation. In contrast to the oil and gas exploration wells, very few water wells had electric logs. Stratigraphic tops generally were interpreted in the water wells from drillers' lithologic descriptions.

Oil and Gas Wells

An electric log typically consists of a spontaneous potential, or SP, curve placed alongside one or more resistivity curves (fig. 5). Many of the oil and gas exploration wells in Cuyama Valley were drilled in the 1940s and 1950s (Stanley, 1995), when these particular logs were commonly the only geophysical logs run. They are valuable for correlating geologic units between wells, determining unit or bed thickness, distinguishing porous and non-porous rocks in shale-sandstone sequences, and identifying beds containing fresh water (Keys and MacCary, 1971).

Stratigraphic units, and lithologic variations within stratigraphic units, are interpreted on the basis of their characteristic electric log response (Keys and MacCary, 1971; Johnson and Pile, 2002); interpretations are tied, where possible, to lithologic descriptions of cuttings and core and to nearby outcrops. High-porosity quartz-bearing units, such as sandstone and sand and gravel, typically show leftward deflections of the SP-curve (toward more negative values) and rightward deflections of the resistivity curves (toward larger resistivity values). Low-porosity, shaly units tend to have the opposite electric log response, with rightward deflections of the SP-curve (toward more positive values) and leftward deflections of the resistivity curves (toward smaller resistivity values; Keys and MacCary, 1971; Johnson and Pile, 2002). In thin-bedded units, the poor vertical resolution of the SP-logging tool produces an average log response from multiple lithologic units rather than separating the units. Because SP- and resistivity logs measure a response only where the borehole contains fluids—either drilling mud or formation waters—the upper few hundred feet of section potentially would not be captured by these methods (fig. 5), and, in certain wells, the shallowest stratigraphic units were not recorded by the electric logs.

Qya has generally high, but irregular, resistivity values characterized by high amplitude, short wavelength, resistivity peaks (fig. 5). This response is a result of large clast size, poor sorting, and abundant channel deposits of gravelly material inset into finer-grained overbank deposits that create abrupt lithologic contrasts and generate a strong resistivity-log response. The subdued nature of the SP-log response could be the result of thin bedding.

Qoa tends to have a more subdued resistivity-log response when compared to Qya (fig. 5), although some wells have resistivity peaks of moderately-high amplitude and short wavelength when compared to the underlying section. The contact with the underlying Morales Formation is typically

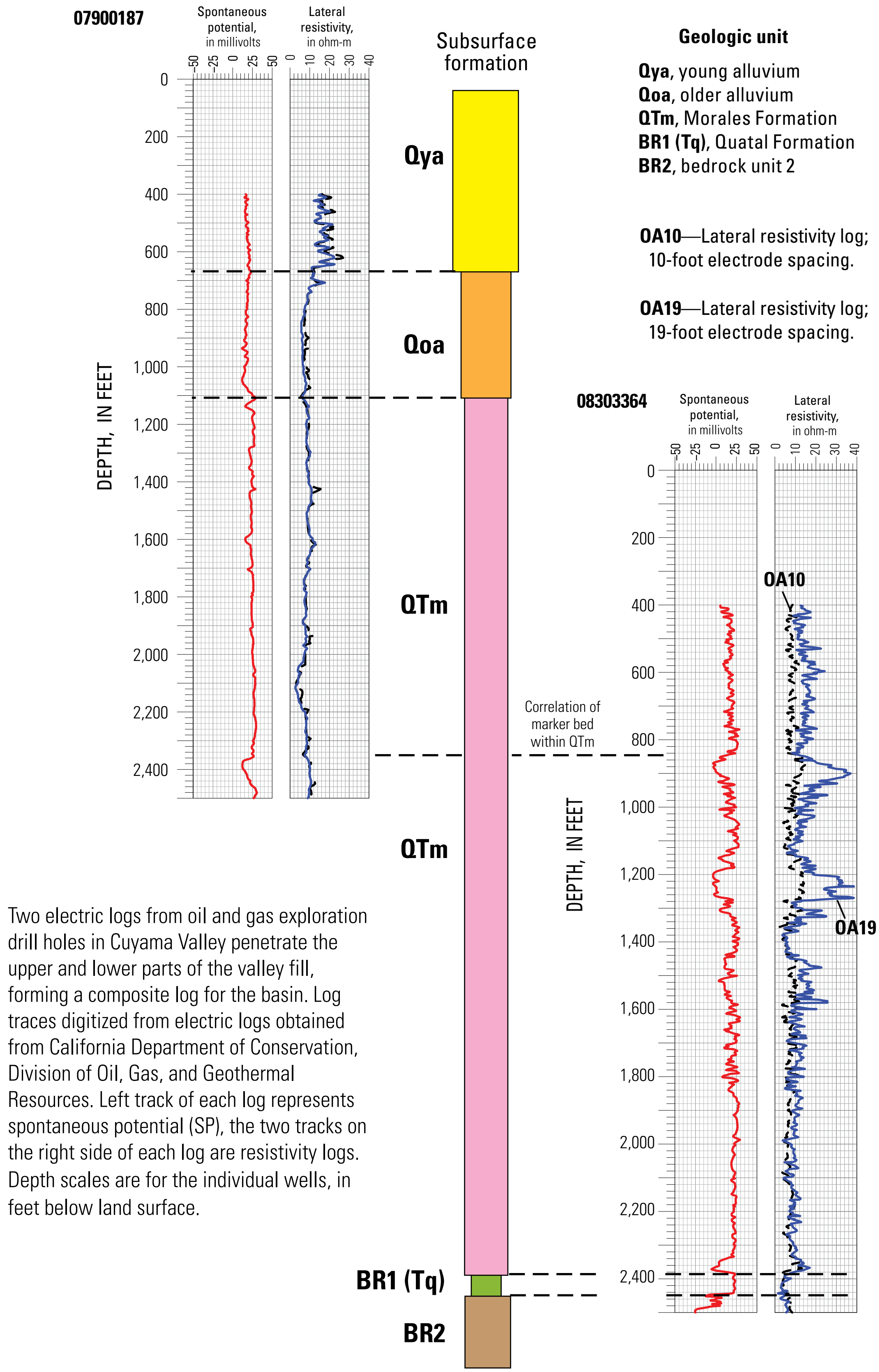

Figure 5. Composite electric log from the Cuyama Valley study area.

marked by a thin zone with inward deflections of the SP-curve (rightward, toward more positive values) and the resistivity curves (leftward, toward smaller resistivity values) (fig. 5; 1,100-ft depth, log 07900187).

The QTm can be broadly subdivided into an upper part that has a generally subdued electric log response in both the SP- and resistivity curves (fig. 5; between 1,100 and 2,350-ft depth, log 07900187) and a lower part that has several distinct coarse-grained intervals (fig. 5, log 08303364). In outcrop, this upper unit is poorly-sorted, consisting of pebbles and cobbles in a fine sand matrix (Dibblee and Minch, 2005a, 2006; Kellogg and others, 2008). The subdued log response in the upper part of the QTm could be the result of the lack of distinct bedding and lithologic contrast between beds of differing grain size. In this interval, the Morales Formation tends to be a massively-bedded arkosic clayey sandstone derived from granitic and metamorphic rocks (Hill and others, 1958). In the lower part of the QTm, boulder trains and gravelly channel deposits create deflections to lower values on both SP- and resistivity logs (fig. 5, log 08303364). The Quatal Formation (Tq, fig. 5, log 08303364) below the QTm is picked as a distinctive interval characterized by inward deflection of both the SP- and resistivity curves.

Ideally, an oil and gas exploration well would intersect a partial thickness of Qya and the full thickness of Qoa and the QTm (fig. 5). As a result of the variable stratigraphic and structural setting across the basin, few individual wells encounter all of these stratigraphic units (fig. 6). Exploration wells drilled in upland areas to the south of the valley are spudded in Qoa, such that only the top and base of the QTm are intersected. In some cases, the electric logging begins below the top of the QTm, such that only the base of the unit is recorded (fig. 6). Previous workers (Nevins, 1982; Schwing, 1984; Calhoun, 1986; Spitz, 1986), who interpreted electric-log data in Cuyama Valley, tended not to pick the top of the Morales Formation but, instead, identified distinctive marker beds within the Morales Formation that allowed correlation between wells in the upper part of the sedimentary section (fig. 6). The most readily identifiable horizons within the Morales Formation are distinctive fine-grained units that represent periods of depositional quiescence across parts of the basin. Similarly, coarse sand bodies can be correlated over more limited areas, but the fine-grained units tend to be more widely distributed and can be correlated over broad areas (fig. 6). These fine-grained units serve as stratigraphic marker horizons within the Morales Formation and serve as guides to the relative elevations of the top and base of the formation in any borehole.

Water Wells

Water well drillers' lithologic descriptions were highly variable in terms of the number and thickness of subsurface intervals described, the detail of the descriptions, and the words used to describe specific sediment types and textures. The descriptions required geologic interpretation to obtain consistency between wells and to identify the unit penetrated. Key descriptive elements used to identify stratigraphic units included the degree of cementation and relative amount of clay; color was considered a secondary element, but was not used as a primary discriminator. Degree of cementation was used to distinguish Qoa from Qya where, in many cases, deeper intervals encountered during drilling would be described as "hard" or "slow drilling," or the intervals would be described as sandstone and conglomerate, instead of sand and gravel, respectively. The Morales Formation was often distinguished from the overlying older alluvium by an abrupt increase in the number of clayey intervals. The clayey, arkosic sands of the Morale Formation were often described by drillers as "decomposed granite," in contrast to overlying intervals described as sand and gravel. Thin intervals described as being yellow, orange, or red in color, where present within a thick interval described by another color, were interpreted as possible paleosols that record an episode of exposure and surficial weathering. These intervals were interpreted as boundaries between units where supported by other factors, such as degree of cementation.

Compilation of Stratigraphic Tops from Well Data

Stratigraphic tops from the oil and gas and water wells were assembled in a single database and checked for internal consistency. The spatial distribution of these tops is shown in a perspective view looking from above and north to the south in figure 7. In this view, water wells appear as a cluster of relatively shallow wells along the center of the basin that mostly intercept the Qya. Oil and gas exploration wells predominantly intercept the Qoa and QTm units. Wells in the far southeast part of the study area (upper left part of figure 7) penetrate thin sections of younger alluvium overlying bedrock units. Stratigraphy was not interpreted for every downhole interval in every well. Where stratigraphic units were not interpreted for specific downhole intervals, they are shown as a thin vertical line (fig. 7).

Contacts interpreted from borehole lithologic and electric logs were assigned x,y, and z coordinate locations for use in the geologic framework model. All boreholes were assumed to be vertical, so that all contacts from a well were assigned the x,y coordinates of the well's surface location. Stratigraphic unit contacts, originally compiled as depth below land surface from the source data, were converted to elevation values by subtracting measured depth from the land-surface altitude at the well. Two types of data were generated from the borehole records: points where the stratigraphic top was explicitly picked from the data and points that only define limiting values for the elevation of the top. Limiting values are defined for cases where the top of the formation is above the start of the electrical geophysical log, such that the top of the log only provides a maximum value for the drilled depth to the top of the stratigraphic unit.

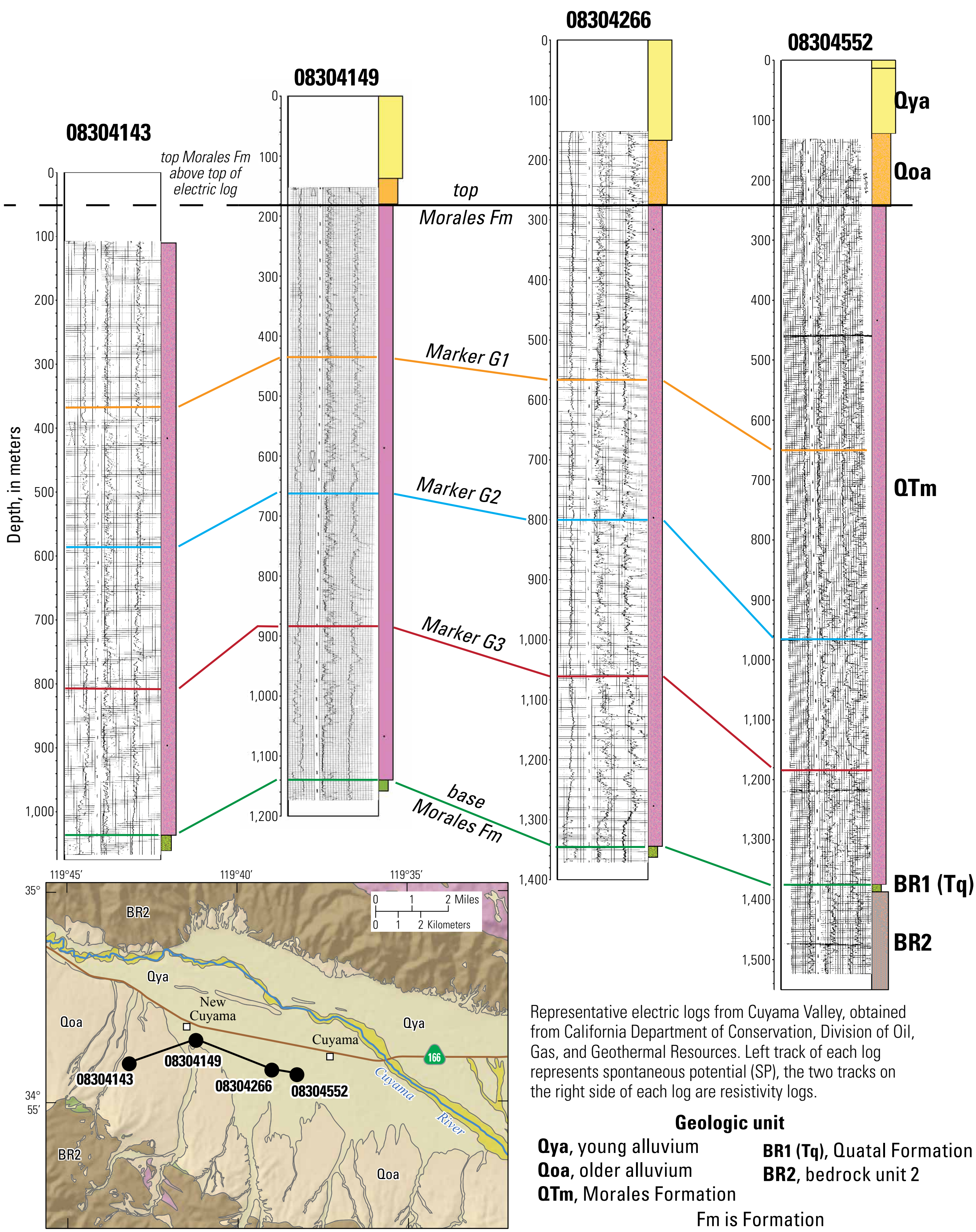

Figure 6. Correlation of electric logs from the central part of the Cuyama Valley study area.

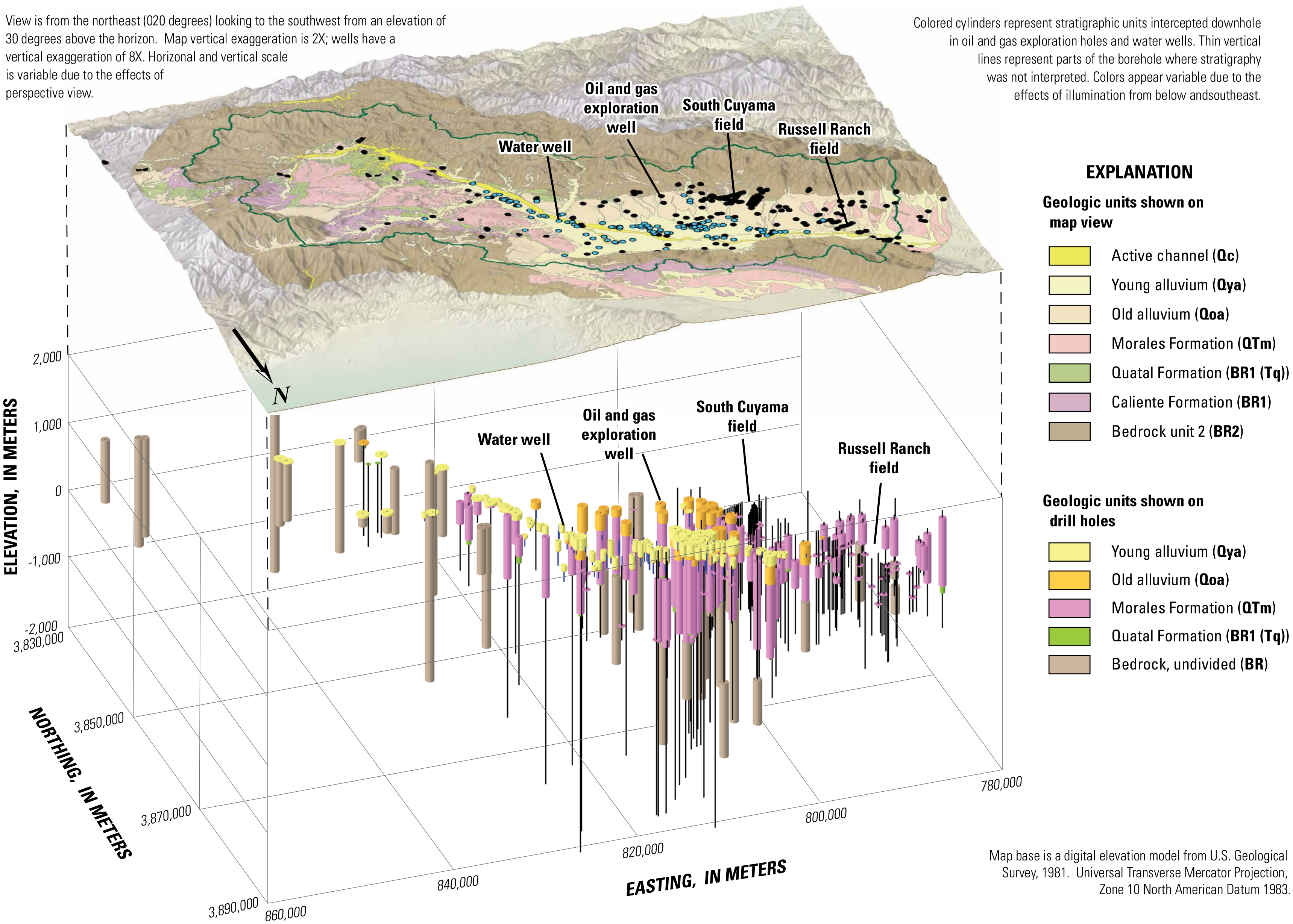

Figure 7. Three-dimensional (3-D) perspective view of geologic units in water wells and oil and gas wells in Cuyama Valley.

3-D Geologic Framework Model

A 3-D geologic framework model was constructed to represent the subsurface geometry of the stratigraphic units, Qya, Qoa, QTm, and a composite pre-QTm bedrock unit. This digital model provides the fundamental geologic framework for the subsequent development of a transient numerical hydrologic-flow model of the study area (Randall Hanson, U.S. Geological Survey, written commun., 2013).

The geologic framework model was constructed by creating surfaces representing the altitude of the top of each stratigraphic unit from the input data and then combining these surfaces within a 3-D geologic modeling software package. Each surface is represented by a grid covering a rectangular area slightly larger than that shown in figure 2, with dimensions of 85,000 m in the east-west direction and 65,000 m in the north-south direction. Square grid cells are 200 m in size, resulting in 426 grid cells in the east-west direction and 326 cells in the north-south direction. Software-based requirements for the grids and 3-D model to be aligned with the cardinal directions resulted in the inclusion of areas to the northeast and southwest of Cuyama Valley far outside the area of interest to this study.

To construct the geologic framework model, spatial data, such as digital elevation, outcrop, and borehole information, were compiled using Environmental Science Research Institute (ESRI) ArcGIS® software. Interpolation of spatial data points into grids representing the stratigraphic unit tops was processed using Rockware Rockworks14® 3-D-modeling software. This software was designed to represent stratigraphic relations within sedimentary basins, including representation of depositional contacts and stratigraphic onlap, erosion, and unconformities. The 3-D-modeling software does not allow explicit entry of fault surfaces into the 3-D framework, so the effect of faulting was accomplished by inserting numerical discontinuities during the gridding of individual horizons. The resultant grids have steep inflections at the fault trace but remain as continuous surfaces within the geologic framework model.

Modeling Approach

The geologic framework model represents the altitude of the top of stratigraphic unit as a grid that spans the entire rectangular framework model domain. Because of the requirement for grids to be continuous, where stratigraphically lower units are exposed at land surface, one or more shallower units are required to have the same land-surface elevation but to have zero thickness (fig. 8). Four general cases describe the elevation and thickness of a particular stratigraphic horizon with respect to the elevations of other horizons in the geologic framework model (fig. 8):

(1) The top of the unit is present in the subsurface beneath other units, where the elevation of the unit top is defined by well data or by the thickness of the overlying unit and the thickness of the unit is defined by well data.

(2) The unit crops out at land surface, such that the eroded top of the unit is defined by the DEM, and the thickness of the unit is defined by well data.

(3) The unit of interest has an elevation defined by the DEM and zero thickness where an underlying unit crops out at the surface.

(4) The unit of interest can crop out at land surface, where the elevation of the top is defined by the DEM, or exist in the subsurface, where the elevation of the top is defined by well data, but thickness of the unit is an arbitrary or assigned value.

As an example, figure 9 depicts these general cases as they were applied to Qoa over the western half of the study area. In the center of the basin (region 1, fig. 9), Qoa is overlain by Qya, and the elevation of the top of Qoa is defined by well data. Where Qoa crops out at land surface (region 2, fig. 9), the top of the unit is defined by the DEM, and the thickness of the unit is defined by well data. The top of the unit in this case is a modeled top based on erosion at land surface, not the true stratigraphic top. In a relatively small area on the extreme eastern edge of the study area (region 3, fig. 9), map data and limited well data indicated the presence of Qoa, but the well data were too limited to create a satisfactory thickness grid, and the unit was assigned an arbitrary thickness (region 3, fig. 9). Finally, in areas of bedrock outcrop (region 4, fig. 9), the top of Qoa is assigned the elevation of land surface and a thickness of zero. Using the cases described above, the elevation grids for each stratigraphic unit were built in an iterative fashion. First, the parts of the unit present in the subsurface were gridded using the well data. These grids were then modified in areas where the unit cropped out or where underlying units were exposed at land surface.

Input data points were pre-processed with a declustering routine prior to surface gridding, such that multiple closely-spaced data points were assigned an averaged location and altitude value that was used as input to the surface-modeling routine. The optimal degree of pre-processing was one that eliminated extreme clusters of data (for example data from closely-spaced production wells in oil fields), but did not result in an overly smoothed trend where all local variation was eliminated. Data representing the altitude of a stratigraphic top were gridded using an inverse distance algorithm, where the value assigned to a grid node was computed as a distance-weighted average of the nearest 12 directionally-distributed neighbors. The value of each of the data points was exponentially weighted according to the inverse of its distance from the grid node; weighting was adjusted to balance the effects of strong, local control with a broader regional average.

For computational convenience, all faults in the study area were generalized as vertical boundaries and dropped from their surface locations. Faults were inserted within the gridding algorithm as two-dimensional (2-D) boundaries that acted as a barrier to information flow during horizon gridding. When point data were gridded, elevation data on one side of a fault were not directly used when calculating grid node values on the other side of the fault. The resultant grids have sharp inflections where the altitude of the surface changes rapidly, but the gridded surface remains continuous and is not split into two segments by the fault.

For the purposes of use within a numerical hydrologic-flow model, the faults were classified according to their recency and the stratigraphic units that each fault offsets (table 2). Motion on the Russell fault is documented to have ended during Morales Formation time, and the fault does not affect younger units (Yeats and others, 1989; Ellis and others, 1993). Well data indicated that the Morales and Santa Barbara Canyon faults create offset in the Morales Formation and the older alluvium (table 4). The thrust faults that bound the Turkey Trap Ridge and Graveyard Ridges (fig. 4) affect all stratigraphic units within the basin, as does the Rehoboth fault (fig. 4, table 2).

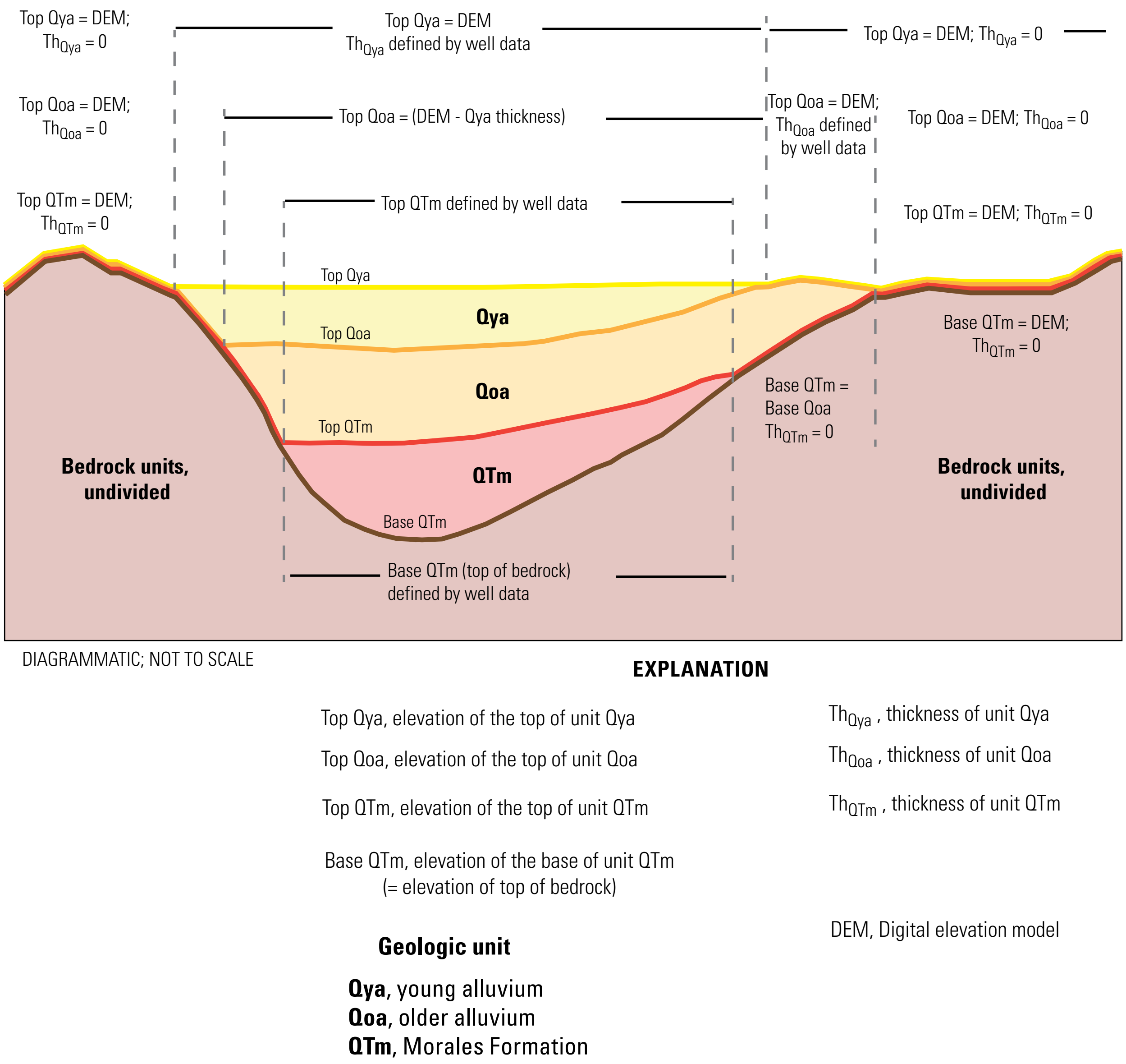

Figure 8. Diagrammatic cross section showing relative elevation of stratigraphic unit tops and resultant thickness within the framework model.

Construction of Gridded Surfaces

Gridded surfaces were interpolated from the data described in the previous sections. The approach for gridding the Qya and Qoa surfaces differed from that used for the QTm and bedrock surfaces as a result of differences and limitations of the data. The strategy for contouring each stratigraphic unit is presented in this section, and the final top altitude grids are presented.

Younger Allvium, Qya

As the stratigraphically highest unit, the top of Qya is everywhere defined by the digital elevation model; the areal

Table 2. Geologic units affected by Cuyama Valley faults.

[Qya, Younger alluvium; Qoa, Older alluvium; QTm, Morales formation]

Fault name	Affected Geologic Units
Whiterock fault	QTm only
Russell fault	QTm only
South Cuyama fault	QTm only
Morales fault	Qoa and QTm
Santa Barbara Canyon fault	Qoa and QTm
Graveyard Ridge fault	Qya, Qoa, and QTm
Turkey Trap Ridge fault	Qya, Qoa, and QTm
Rehoboth fault	Qya, Qoa, and QTm

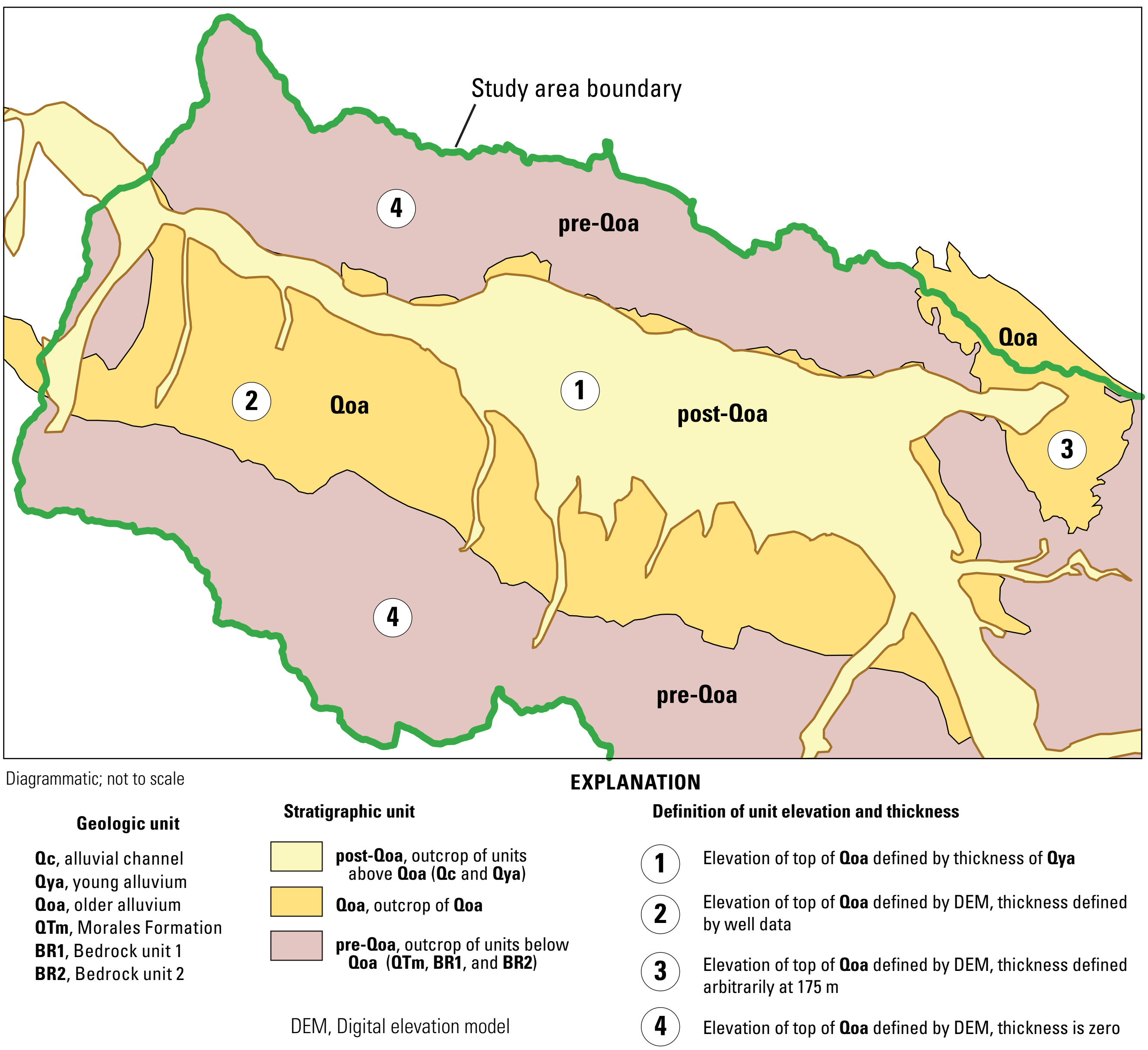

Figure 9. Conceptualization of the elevation and thickness of unit Qoa within the geologic framework model for the western part of the study area.

extent of the unit is defined by the geologic map (fig. 4). In parts of the framework model area, for example in the upstream reach of the Cuyama River, Qya is unconformable on and incises into older units. Accurate portrayal of these stratigraphic relations is aided by the construction of a thickness map for Qya that can then be superimposed upon the older units within the framework model.

A map of the total areal extent of Qya was created by merging the mapped polygons of Qya and Qc in a GIS. Inside of the unit extent polygon, Qya thickness data from oil and gas wells and water wells (fig. 10) were contoured. In cases where a well bottomed within Qya, the thickness of Qya was constrained to be thicker than the total depth of the well at that location. This initial Qya thickness grid was hand-edited in alluvial channel areas that lacked well control as guided by thickness trends evident from well data along the main channel of the Cuyama River and its major tributaries. Qya thickness was assigned according to stream rank, such that the third-order stream of the Cuyama River channel was given the thickest sediments, second-order streams that were tributaries to the Cuyama River were given the next-greatest thickness, and first-order streams that were tributaries to the second-order streams were given the least thickness. The thickness grid was modified with the intent of connecting similar thickness values and creating smoothly-varying changes. The hand-edited grid was smoothed and then clipped with the unit extent boundary to create a final thickness map (fig. 10).

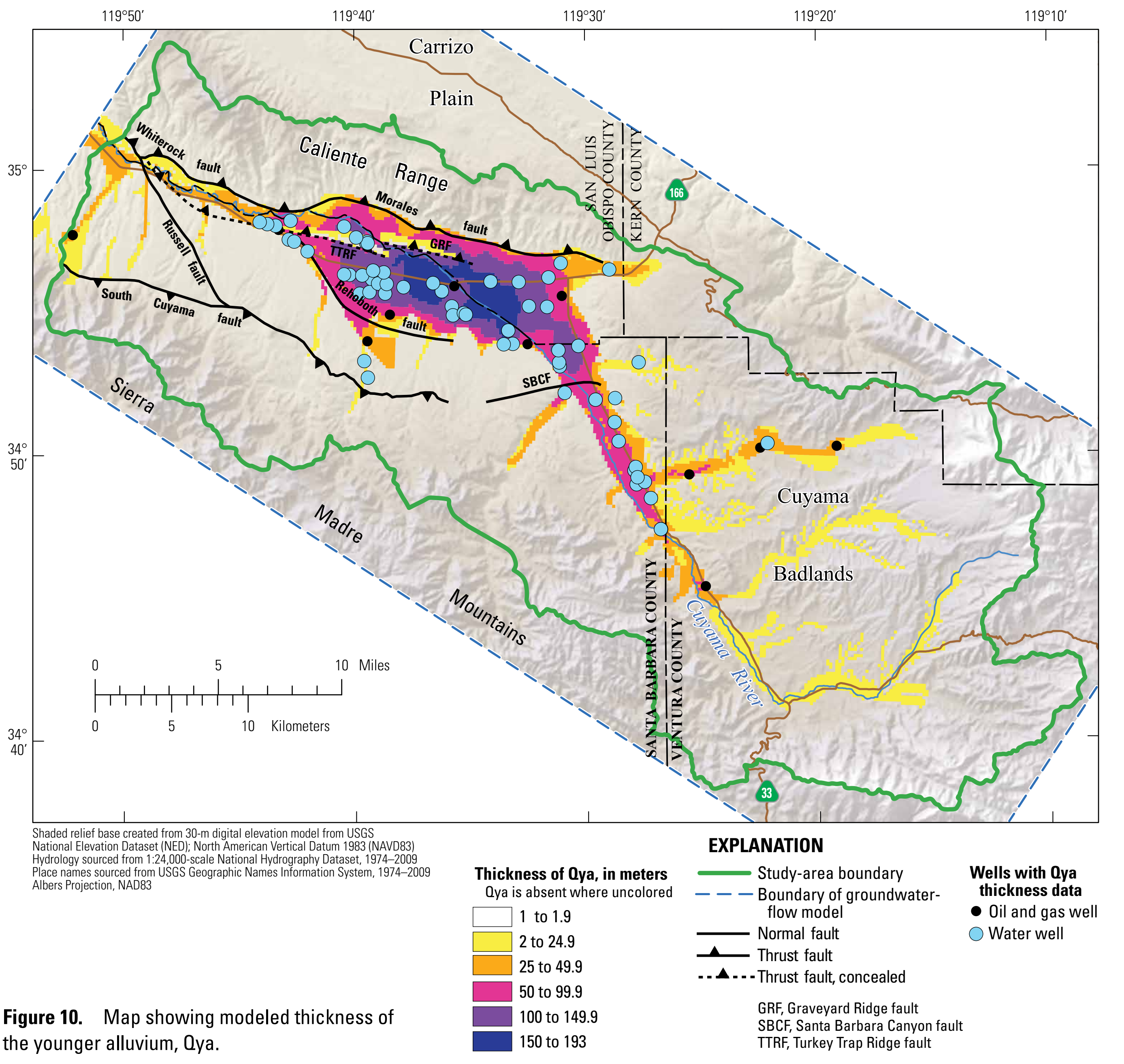

Figure 10. Map showing modeled thickness of the younger alluvium, Qya.

Older Alluvium, Qoa

The elevation of the top of Qoa is defined by the base of Qya, so that the thickness of Qya was subtracted from the digital elevation model to yield the top of Qoa (fig. 11). The top defines a west-northwest to east southeast trending trough that is aligned with axis of the valley, but skewed toward the north side of the basin against the base of the Caliente Range. This pattern is reflected by the surficial geology, where Qoa is uplifted and exposed along the south side of the basin as upland alluvial terraces (fig. 4), but buried by younger materials on the north side of the basin. Local linear troughs are present at alluvial channels draining the Sierra Madre Mountains, such as Santa Barbara Canyon and Salisbury Canyon (fig. 11), and result from incision of the older alluvium by young stream courses during recent uplift of the Sierra Madre Mountains (DeLong and others, 2008, 2011).

Qoa crops out where it is structurally uplifted by the Turkey Trap Ridge and Graveyard Ridge faults (fig. 11). To the south of these faults, well data showed that the top of Qoa is buried by as much as 200 m of Qya. The Rehoboth fault and Santa Barbara Canyon fault do not have a discernible effect on the elevation of Qoa at the scale at which Qoa is contoured (fig. 11).

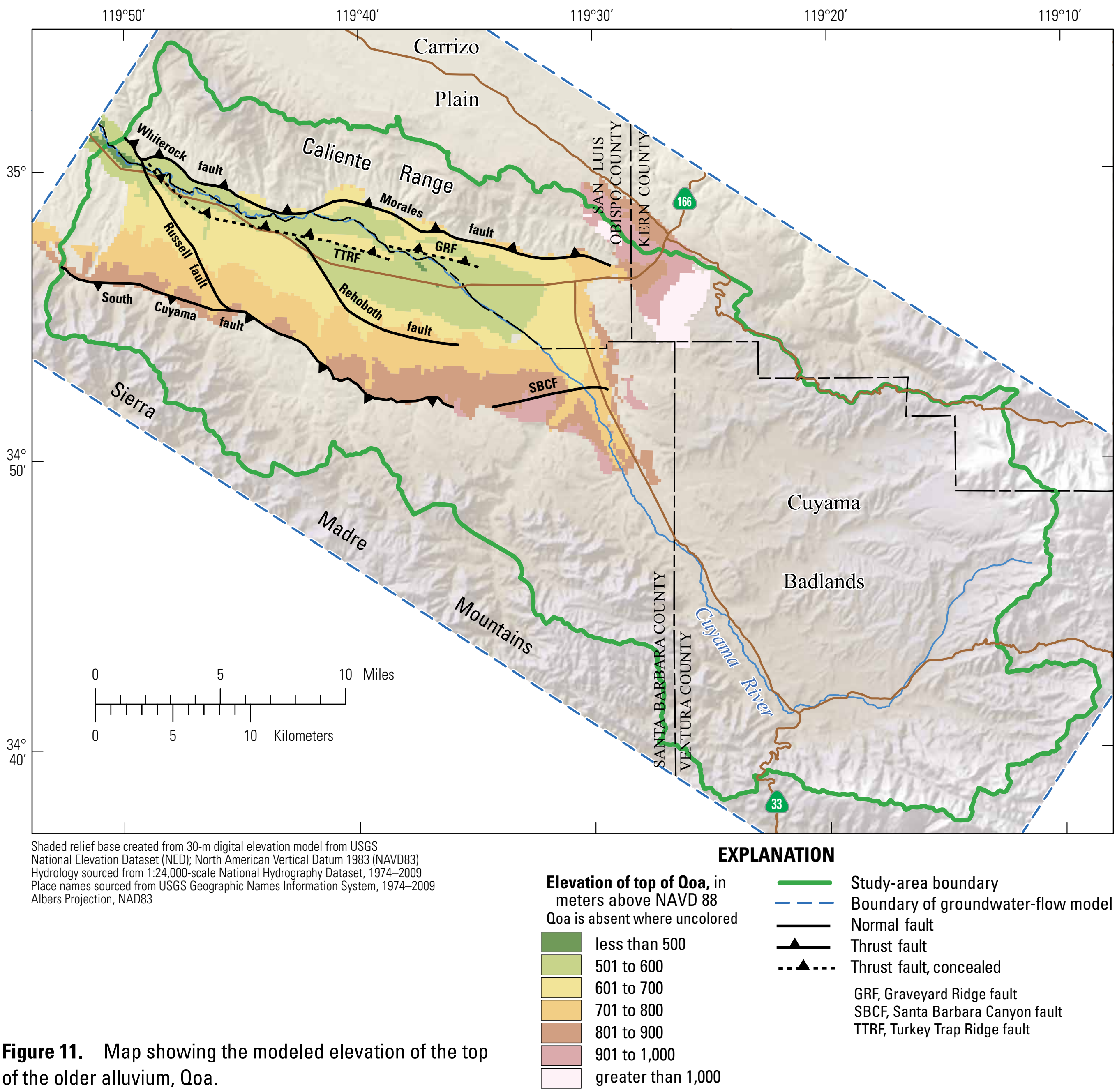

Figure 11. Map showing the modeled elevation of the top of the older alluvium, Qoa.

Morales Formation, QTm

Subsurface data for the QTm are clustered in the vicinity of the two producing oil and gas fields and are sparse in the southeastern part of the study area (black circles in fig. 12). A computer-contoured map of the top of the QTm, generated from only the well and outcrop data, produced unsatisfactory results that did not reflect the synclinal structure in the southeastern part of the study area. To improve horizon gridding, a generalized structural contour map of the top of the QTm was drawn by hand that honored the outcrop data and contact elevation from boreholes and that defined a broad, open syncline consistent with the map trace of the Cuyama syncline and with seismic reflection data (Ellis and Spitz, 1987; Ellis, 1994). Structure contours were converted to a series of regularly-spaced points, which were assigned coordinate locations and given the contoured elevation value (purple dots in fig. 12). These points became part of the input data for horizon gridding of the top of the QTm.

The top of the QTm generally defines an asymmetric west-northwest to east southeast trending trough that is aligned with axis of the valley, such that the unit is deepest along the north side of the basin against the base of the Caliente Range and is shallowest along the south side of the valley (fig. 13). In

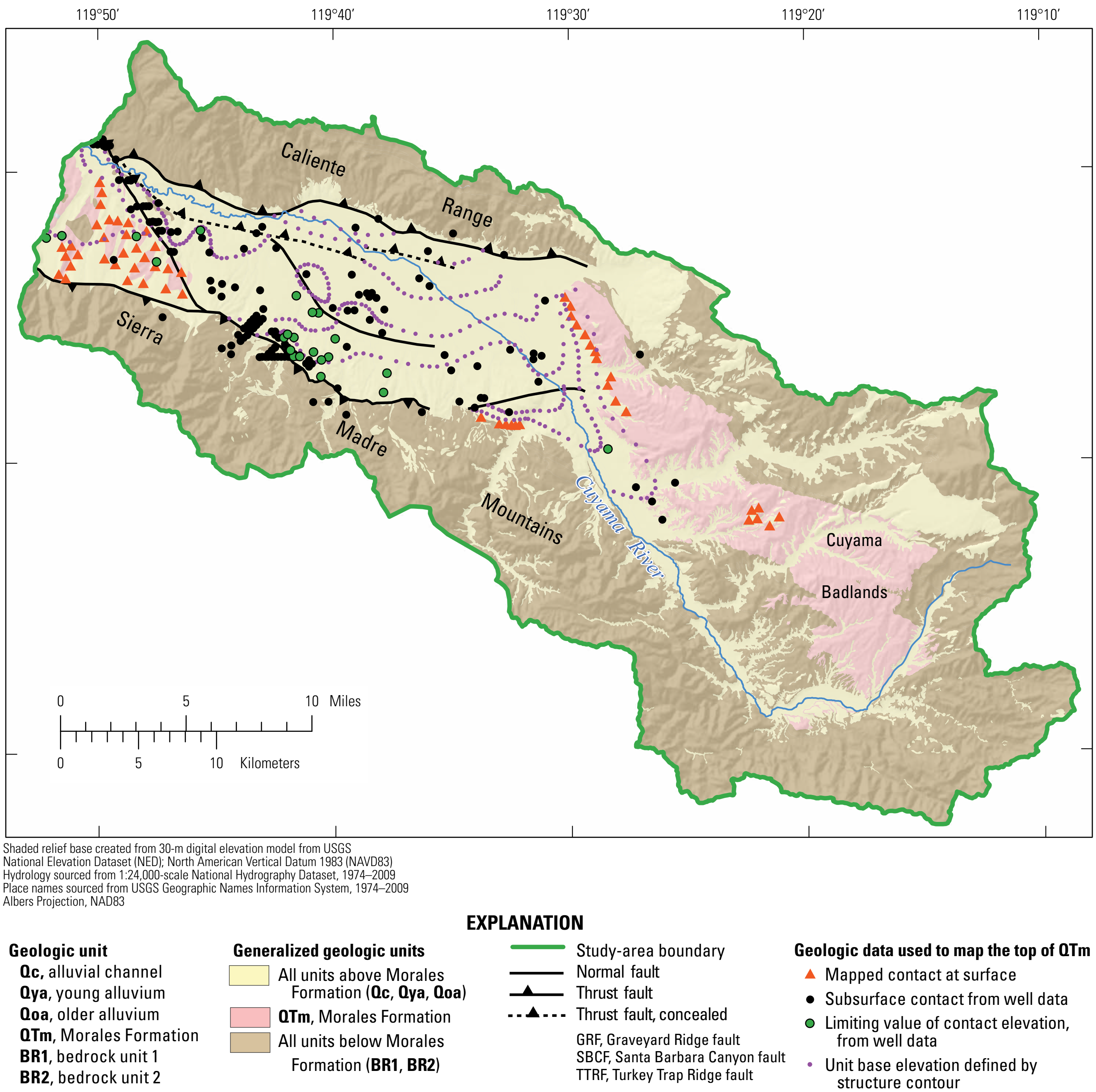

Figure 12. Map showing geologic data used to map the top of the Morales Formation, QTm.

the southeastern end of the valley, the trough trends parallel to the axis of the Cuyama syncline. The northwest-striking Russell and Rehoboth faults are both associated with relative highs in the top of the QTm (fig. 13). The unit is elevated on the southwest side of the Russell fault, whereas the Rehoboth fault roughly is centered on a structural high in the top of the QTm (fig. 13). The structurally elevated Morales Formation, next to the Russell and the Rehoboth faults, could be the result of transpression-related uplift as the tectonic regime changed from transcurrent to compressional faulting in the Pliocene. The small-offset Santa Barbara Canyon fault does not have a discernible effect on the elevation of the QTm at the scale at which the unit is contoured (fig. 13).

Pre-Morales Formation (QTm) Bedrock

Sparse well control on the elevation of pre-QTm bedrock was augmented by a generalized structural contour map of the base of the QTm that used the mapped trace of the Cuyama syncline to define the shape of the contour lines in the south-eastern part of the study area (purple dots in fig. 14). Additional subsurface data (purple dots shown within thesis study areas, fig. 14) were obtained from detailed structure contour maps of the base of the QTm in the vicinity of the Russell Ranch oil field (Nevins, 1982) and the South Cuyama oil field (Schwing, 1984). Structure contours were converted to a series

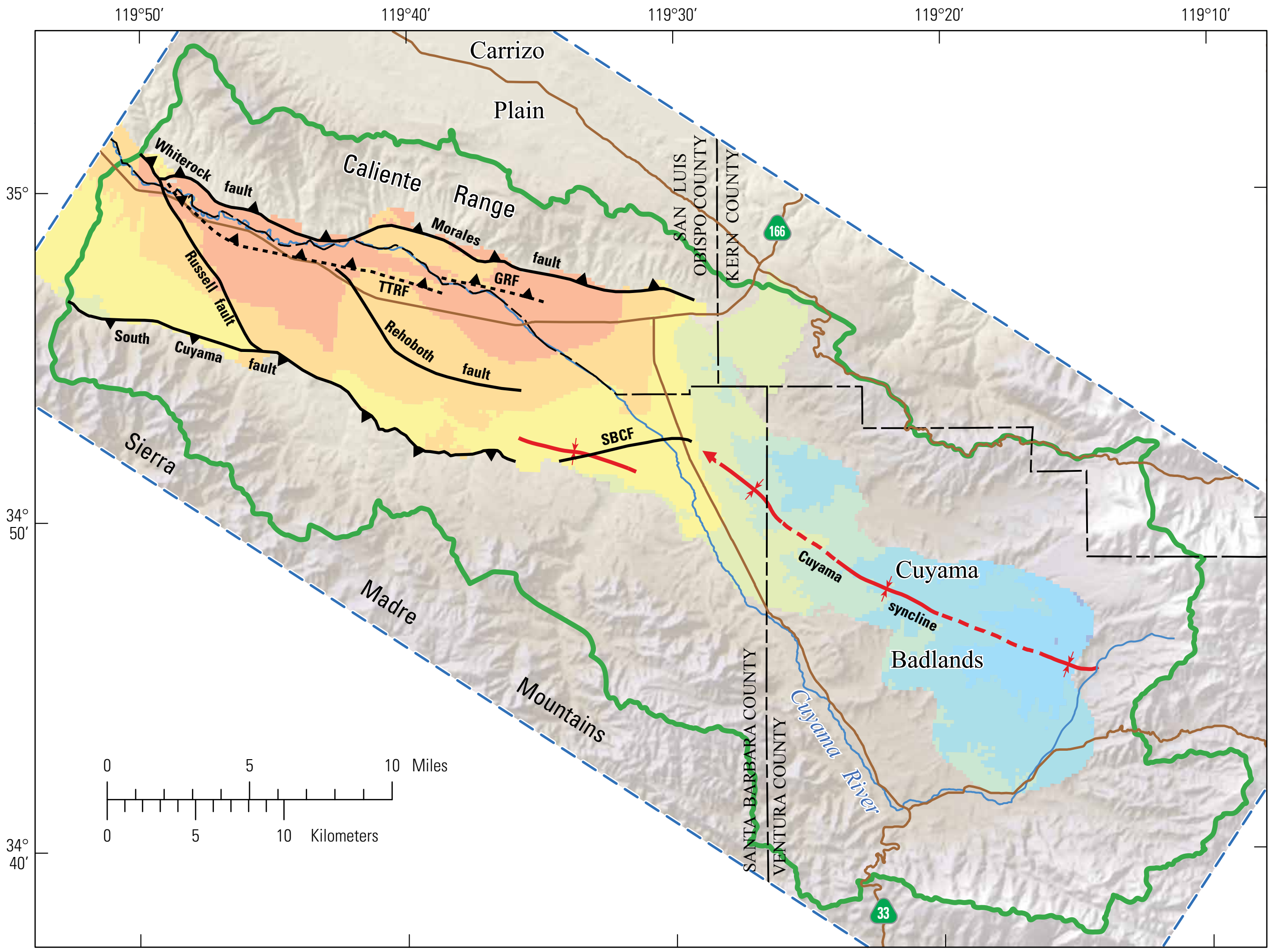

Shaded relief base created from 30-m digital elevation model from USGS National Elevation Dataset (NED); North American Vertical Datum 1983 (NAVD83)
Hydrology sourced from 1:24,000-scale National Hydrography Dataset, 1974–2009
Place names sourced from USGS Geographic Names Information System, 1974–2009
Albers Projection, NAD83

EXPLANATION

Elevation of top of QTm, in meters above NAVD 88
QTm is absent where uncolored

- 201 to 400
- 401 to 600
- 601 to 800
- 801 to 1,000
- 1,001 to 1,200
- 1,201 to 1,400
- 1,401 to 1,600
- 1,601 to 1,800

- Study-area boundary
- Boundary of groundwater-flow model
- Normal fault
- Thrust fault
- Thrust fault, concealed

GRF, Graveyard Ridge fault
SBCF, Santa Barbara Canyon fault
TTRF, Turkey Trap Ridge fault

- Syncline, showing plunge direction
- Syncline, concealed

Figure 13. Modeled elevation of the top of the Morales Foramtion, QTm.

of regularly-spaced points that were assigned coordinate locations and given the contoured elevation value. These points became part of the input data for horizon gridding of the top of the pre-QTm bedrock (fig. 14).

The elevation of the top of the bedrock emphasizes the fault-bounded nature of the basin, where pre-QTm bedrock crops out to the north and south of the basin, but abruptly drops to great depths within the basin (fig. 15). The structural trough of the Cuyama syncline is evident in the eastern half of the basin and in the Cuyama Badlands (fig. 15). The Russell fault offsets the top of bedrock by as much as 500 m (Nevins, 1982). The Rehoboth and Santa Barbara Canyon faults do not disrupt the contoured elevation of the top of bedrock at the contouring interval shown on figure 15.

3-D Geologic Framework Model Results

The final 3-D-geologic framework was compiled with the Rockworks 3-D modeling package, which allows individual gridded surfaces to be stacked in stratigraphic order. Unit

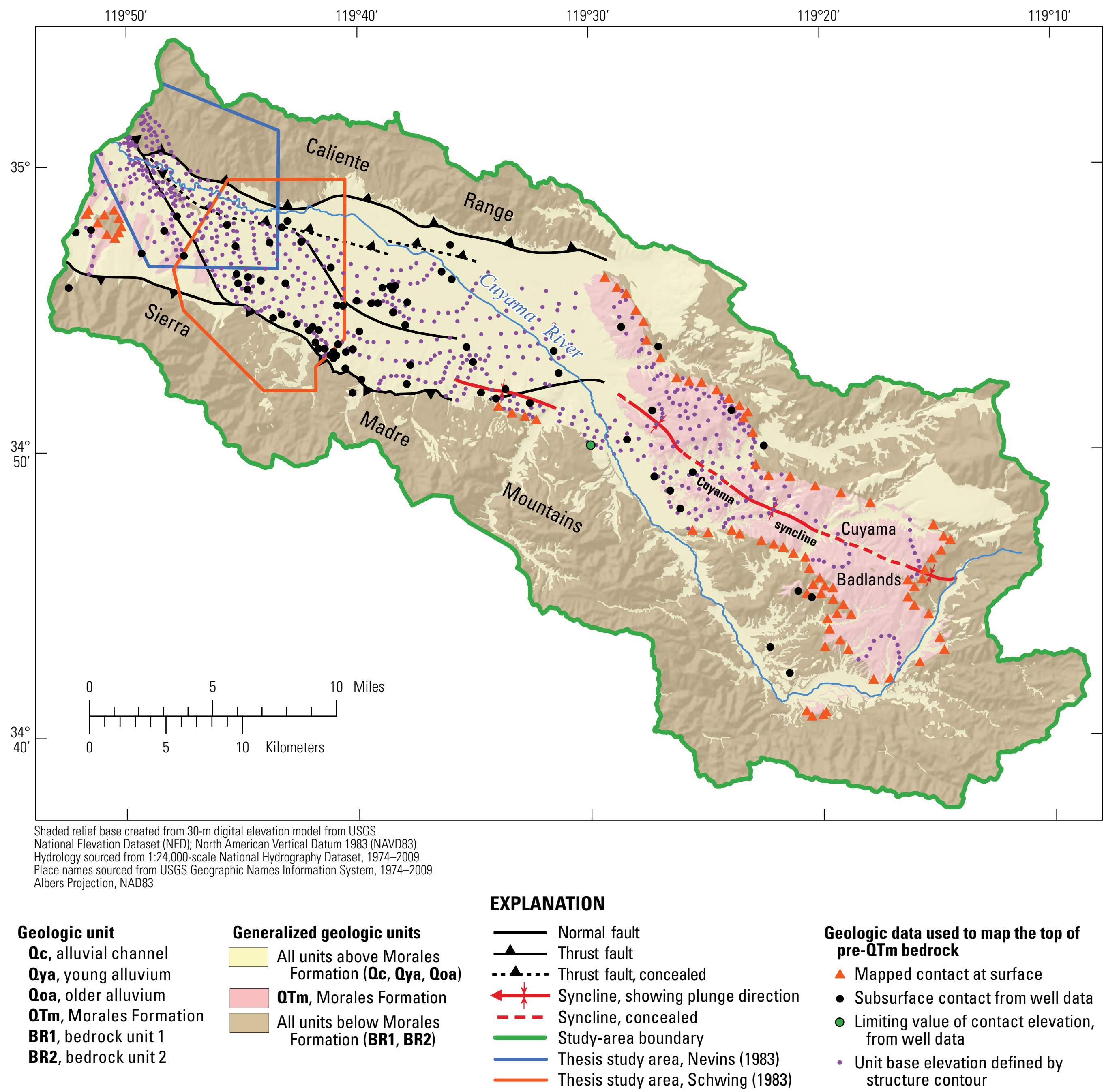

Figure 14. Geologic data used to map the top of the pre-Morales Formation (QTm) bedrock.

thickness is represented by the difference between altitudes of successive stratigraphic tops, such that the altitude of the base of a unit is always equal to the altitude of the top of the unit directly below it in the stacking order.

The results from the geologic framework model can be explored and visualized by slicing the model volume at any chosen location, as shown in a perspective view looking from above to the east (fig. 16). In the upper part of the figure, the

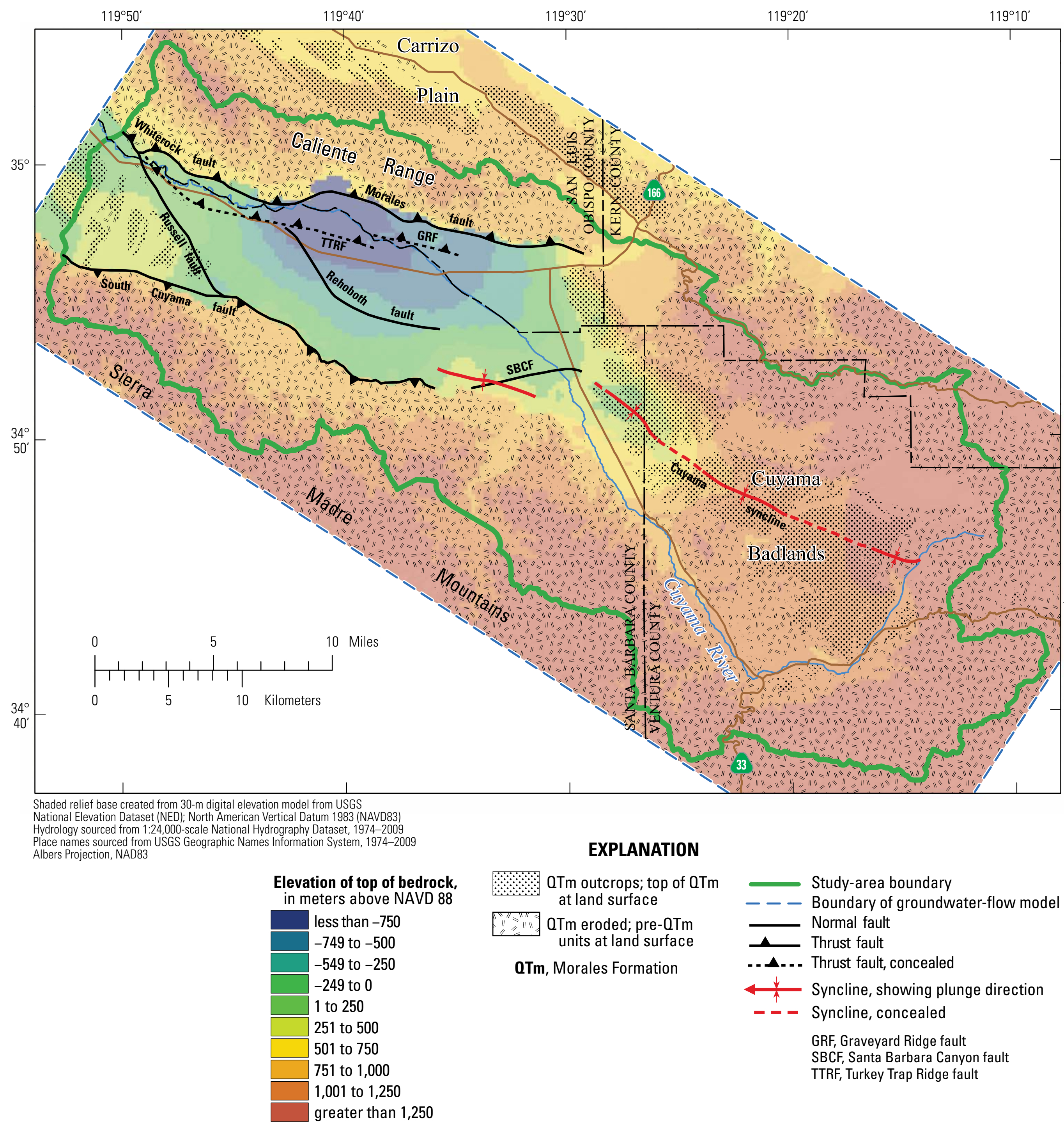

Figure 15. Modeled elevation of the top of bedrock.

upper surface of the geologic framework is trimmed with a digital elevation model, creating a map of the geologic units predicted by the model to be present at land surface. The patterns of the geologic units at land surface are similar to the geologic map of the basin (fig. 4), providing a first-order check on the model's validity. In this view, extensive outcrops of the QTm are present in the Cuyama Badlands and at the western edge of Cuyama Valley; both areas match known surface exposures. Outcrops of Qoa are extensive along the south side of Cuyama Valley and are also present as uplifted blocks at the two fault-bounded ridges at the north side of the valley. The modeled extent of young alluvial Qya occupies the center of the valley and outlines the trace of the Cuyama River channel to the west of the Cuyama Badlands, following mapped surface outcrops.

View is from the west (280 degrees) looking to the east from an elevation of 20 degrees above the horizon. Upper figure has no vertical exaggeration; lower figure has a vertical exaggeration of 3X. Horizonal and vertical scales are variable because of the effects of perspective view.

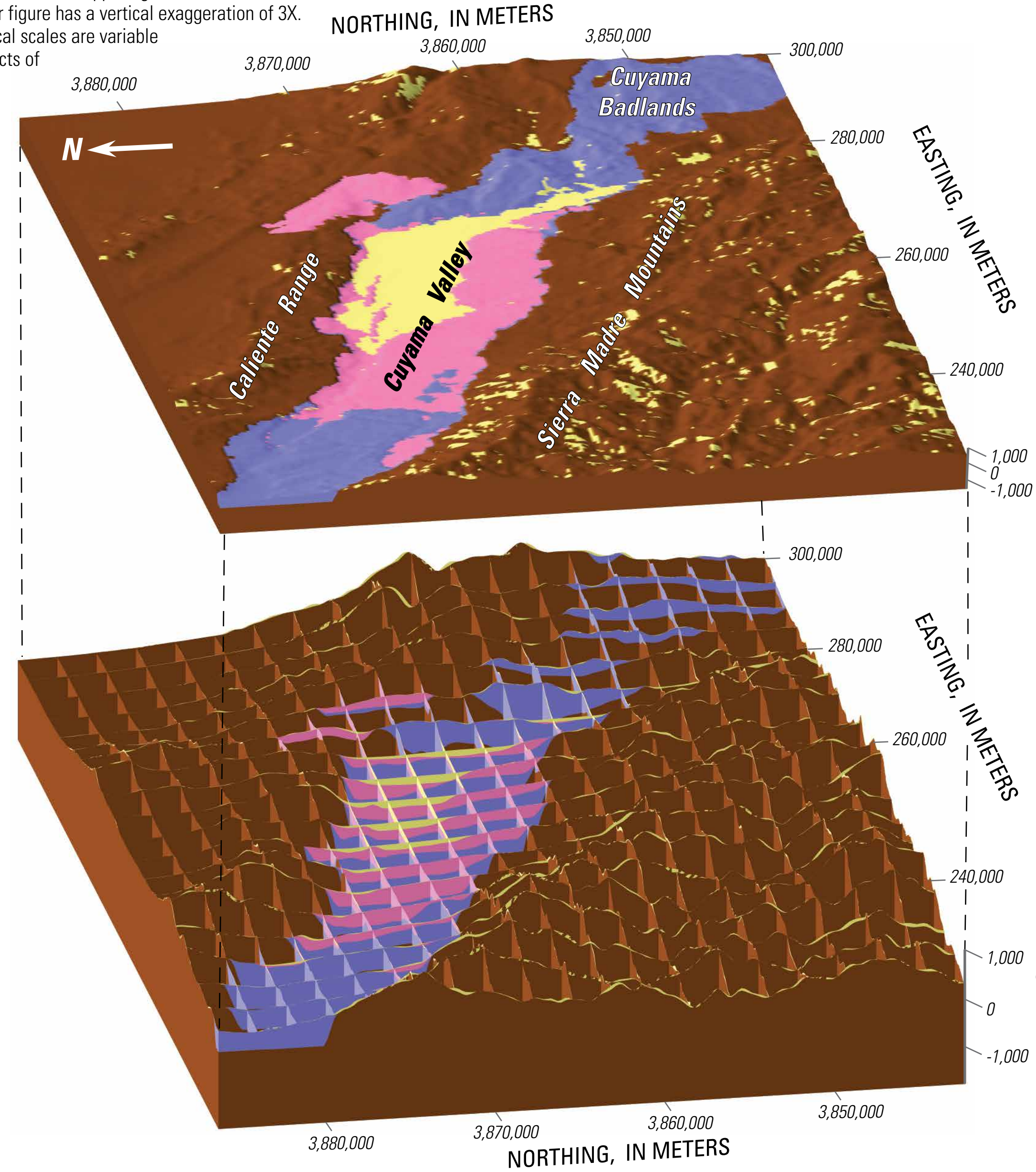

EXPLANATION

Colors appear variable because of the effects of lighting from the north

- Young alluvium (**Qya**)
- Morales Formation (**QTm**)
- Old alluvium (**Qoa**)
- Bedrock, undivided

Upper figure shows the upper surface of the geologic framework model trimmed with a digitial elevation model, such that the upper surface of the geologic framework approximates a geologic map of the study area. The lower figure shows vertical sections that are cut through the geologic framework model in the north-south and east-west directions, showing the configuration of stratigraphic unit tops within the model volume.

Figure 16. Perspective views of vertical slices through the geologic framework model.

The lower part of figure 16 shows a series of east-west and north-south vertical sections cut through the geologic framework model; these vertical sections allow for the visualization of the modeled stratigraphic unit tops beneath the valley. This figure shows the thickness of Qya in the axis of the valley, underlain by Qoa. The Qoa dominates the southern part of the valley, beneath its outcrop exposures, with the QTm underlying it. The QTm predominates in the Cuyama Badlands area, where it is essentially the only permeable stratigraphic unit, except for thin younger alluvium along the trace of the Cuyama River channel. The QTm is also exposed at the surface in the western part of the valley, where it is locally overlain by thin deposits of alluvium in the channel of the Cuyama River. The effect of fault offset is not obvious at the scale of figure 16, except for the appearance of Qoa at land surface at Graveyard Ridge and Turkey Trap Ridge (upper figure, fig. 16) and the abrupt change in elevation of Qoa beneath these ridges that can be identified in two vertical panels (lower figure, fig. 16).

Singer and Swarzenski (1970) published two cross sections showing the configuration of the water-bearing units in Cuyama Valley as interpreted from well control. One cross section was aligned roughly east-west (*A-A′*, fig. 4), parallel to the trace of the interbasin thrust faults that bound the Turkey Trap Ridge and Graveyard Ridge, and a roughly north-south section was transverse to the major structural grain of the basin (*B-B′*, fig. 4). These sections were compared to the modeled elevation of the stratigraphic units from the geologic framework model along the same line of section (fig. 17).

The greatest difference between the previously published sections and the stratigraphic tops, as defined in the geologic framework model, is the elevation of the top of the QTm and the definition of Qoa. The QTm in the geologic framework model is almost everywhere 400 to 600 ft deeper than the previously published interpretation (figs. 17*A* and *B*). The previously published interpretation of the QTm as portrayed on the north-south section *B-B′* (fig. 17*B*) followed the geologic mapping of Dibblee (Dibblee, 1973; Graham and others, 1999; Dibblee and Minch, 2005b,c, 2007), which included all young, deformed, non-marine sediments of the Cuyama area in the Morales Formation. By using these criteria, the upland area that lies to the south of Cuyama Valley and north of the Sierra Madre Mountains was interpreted on the previously published section as being composed of exposed

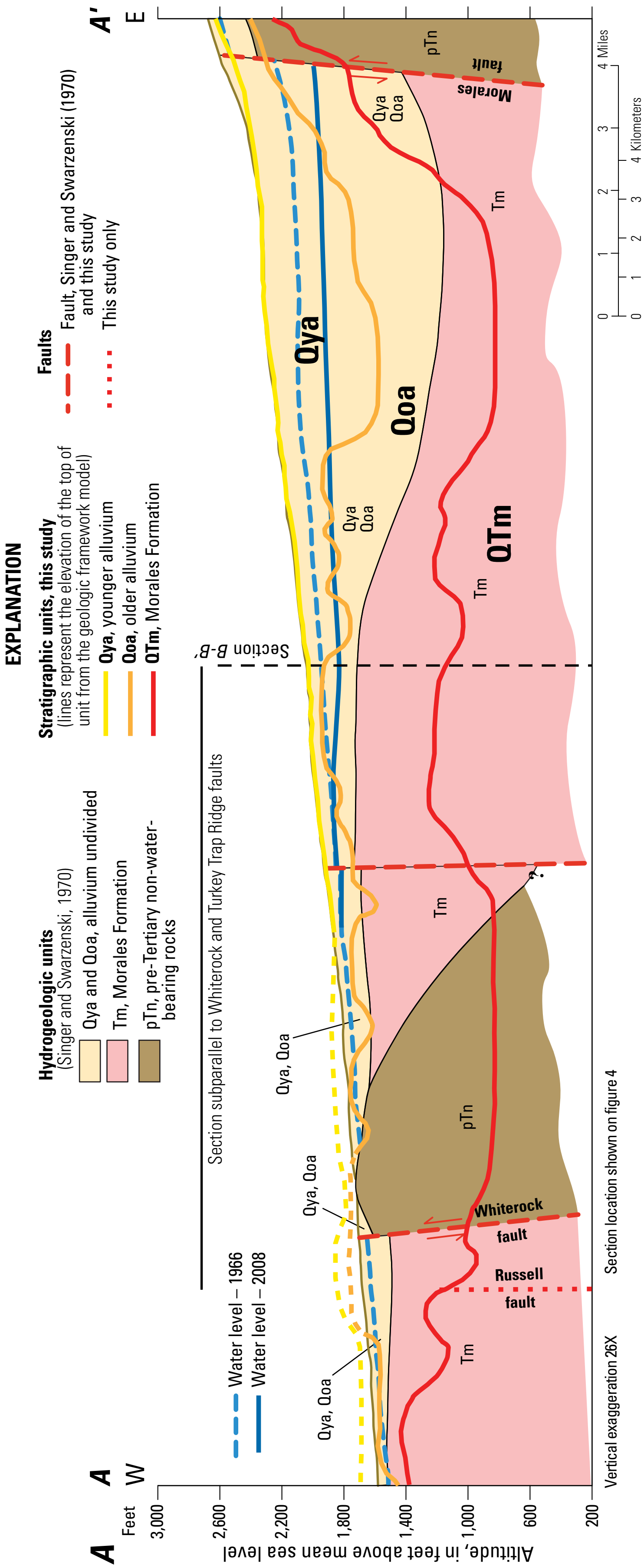

Figure 17. Cross sections showing previous hydrogeologic interpretation and elevation of stratigraphic unit tops from the geologic framework model. *A*, east-west section *A-A′*; *B*, north-south section *B-B′*.

outcrops of Morales Formation (fig. 17*B*). Subsequent workers (Vedder, 1968; Vedder and Repenning, 1975; Schwing, 1984; Spitz, 1986; Kellogg and others, 2008) classified the upper part of Dibblee's mapped Morales Formation as "deformed older Quaternary alluvium," thus putting the Morales Formation a few hundred meters in the subsurface on the south side of Cuyama Valley, rather than exposed at the surface. Data from electric logs that were used in the construction of the geologic framework consistently place the top of the QTm deeper than Singer and Swarzenski (1970).

A second difference between information from previous publications and the model output is the definition of the top of the older alluvial unit Qoa, which was not subdivided from younger alluvium in previously published sections (figs. 17*A* and *B*). Qoa in the geologic framework model includes both the lower part of the previously defined undivided Qya/Qoa and the upper part of the previously defined Morales Formation. For the geologic framework model, Qoa was subdivided from Qya primarily on the basis of degree of cementation. Differences in how such cementation was described in well drillers' reports could account for some of the irregularities in the elevation on the top of Qoa seen in section *A-A′* (fig. 17*A*). The topographic surface used for the previously published sections was generalized and ignored local irregularities, resulting in the shallow modeled unit tops appearing to go above the previously portrayed land surface on the western edge of section *A-A′*. The sections showed general agreement on the location and character of the main basin-bounding faults. The geologic framework model adds the Russell fault at depth on the west edge of section *A-A′* and the Rehoboth fault on section *B-B′* (fig. 16).

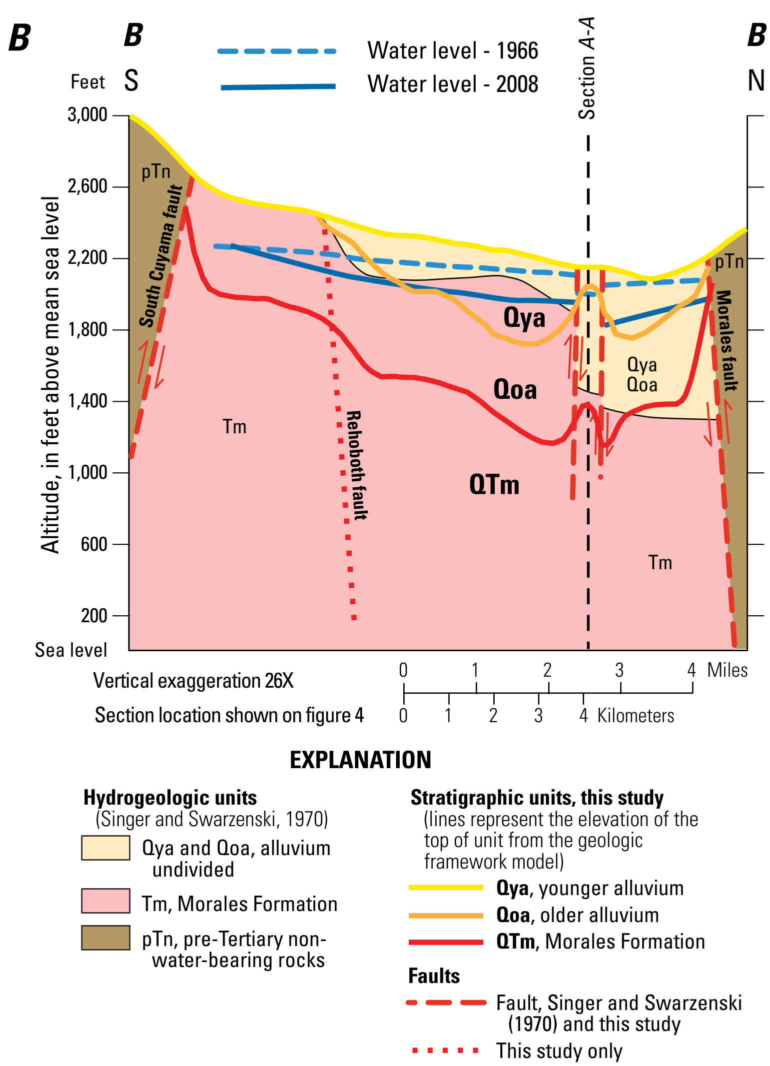

Figure 17. Cross sections showing previous hydrogeologic interpretation and elevation of stratigraphic unit tops from the geologic framework model. *B*, north-south section *B-B′*.—Continued

Textural Analysis of Basin-Filling Unit

An analysis of variability of lithology and grain size was completed for the three principal basin-filling units, Qya, Qoa, and the QTm. Textural data, such as grain size, sorting, and bedding characteristics, form the geologic basis for estimating the hydraulic properties within a numerical hydrologic-flow model (Burow and others, 2004; Faunt and others, 2010). Textural variability in the basin-filling units is ultimately a function of the sedimentary facies, environment of deposition, and depositional history of the basin. Textural data were compiled from 65 oil and gas and 153 water wells in the study area (fig. 18).

Textural Variations Observed in Outcrop

The Morales Formation is composed of up to 1,500 m of weakly indurated fluvial and alluvial sediments deposited in an extensive valley area. The unit is exposed in the Cuyama Badlands, is present in the subsurface beneath Cuyama Valley, and is also exposed on the north flank of the Caliente Range along the edge of the Carrizo Plain (fig. 4), where it was deposited prior to the thrust-related uplift of the range. In outcrop, the Morales Formation can be informally divided into a more poorly sorted, generally coarse-grained upper unit and a well-sorted, generally finer-grained lower unit (Dibblee and Minch, 2005a, 2006; Kellogg and others, 2008). The upper part of the Cuyama Badlands is about 700 m thick and is composed of weakly indurated, poorly sorted, matrix-supported cobble-pebble conglomerate in a sandstone matrix (fig. 19*A*). The

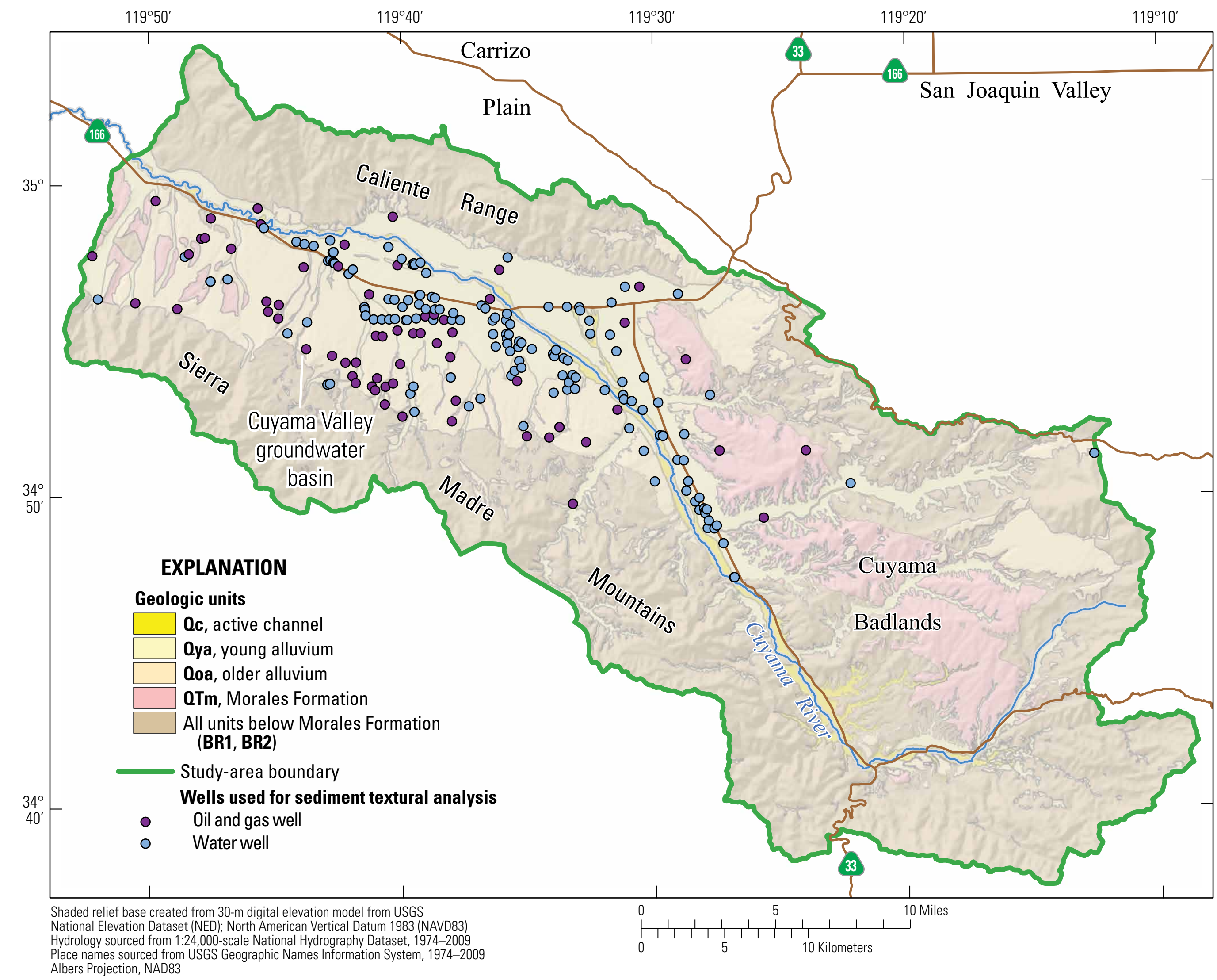

Figure 18. Location of wells used for textural analysis in Cuyama Valley.

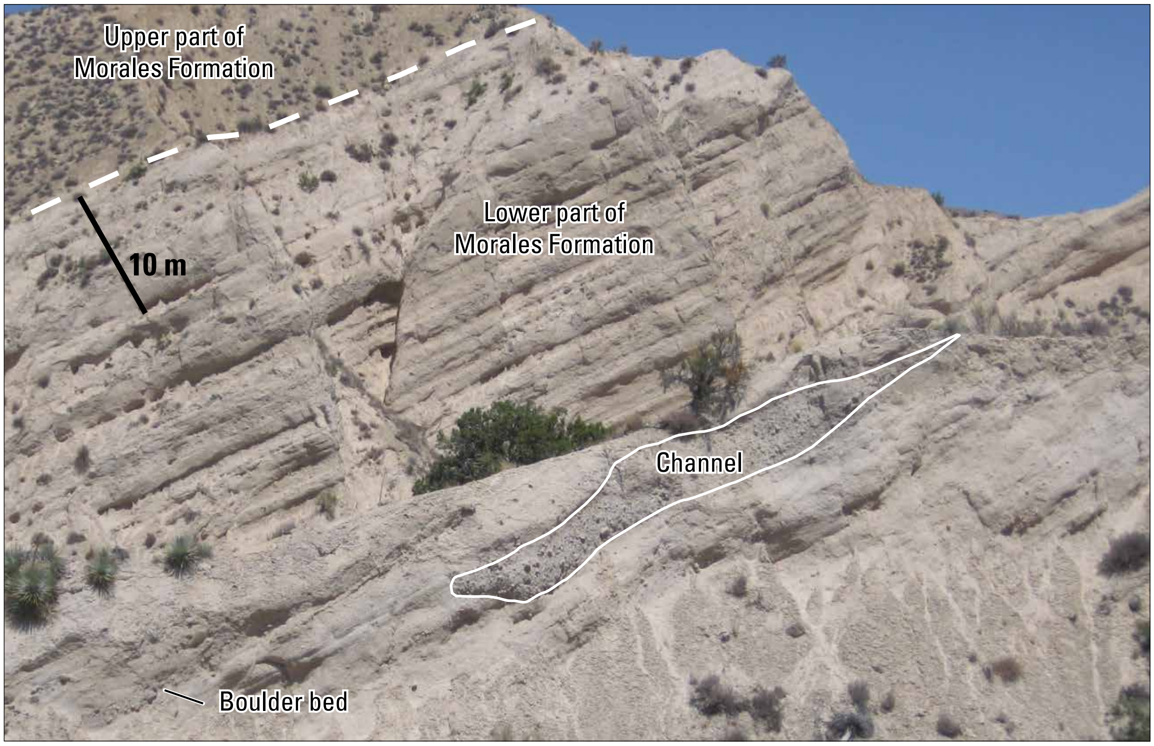

Photograph by Donald Sweetkind, U.S. Geological Survey

A. Morales Formation, Quatal Canyon

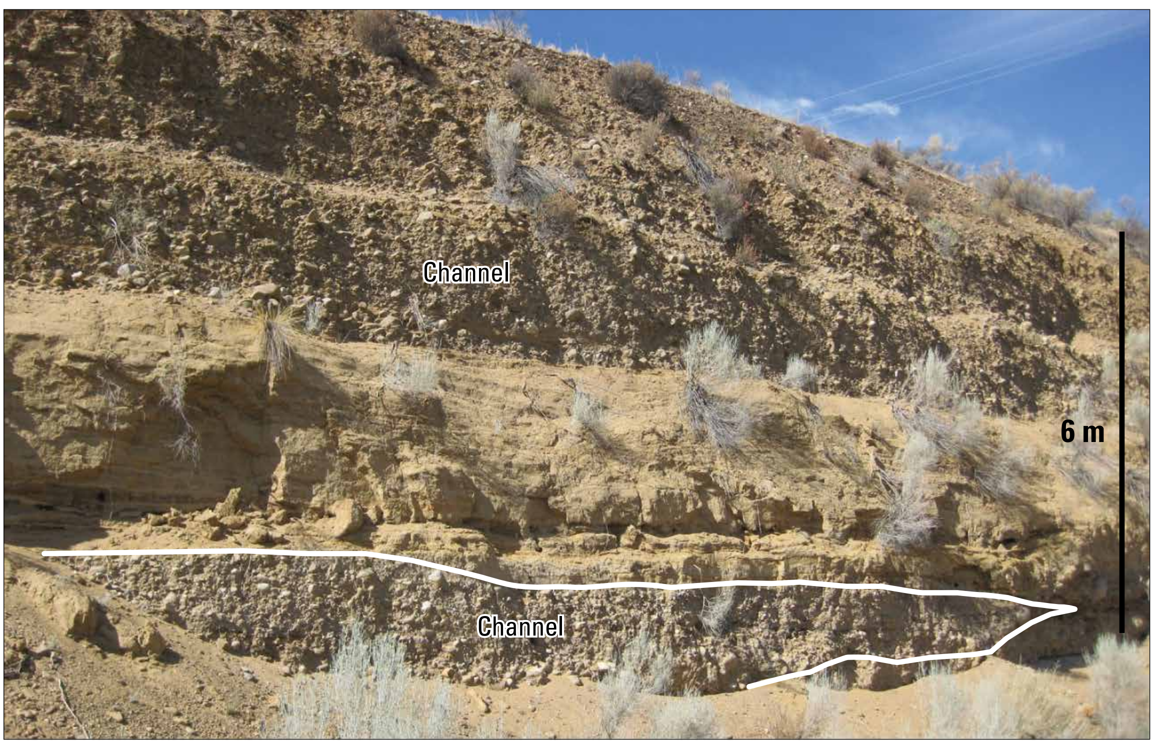

Photograph by Donald Sweetkind, U.S. Geological Survey

B. **Qoa**, along Highway 166, 5 kilometers west of New Cuyama

Figure 19. Outcrop expression of textural variations in basin-filling units: *A,* Morales Formation; *B,* Older alluvium.

lower part is composed of about 650 m of thick- to massively-bedded arkosic sands with interbeds of pebble conglomerate and sandy siltstone (fig. 19*A*). In western Cuyama Valley, the lower part of the Morales Formation consists of about 400 m of gypsiferous lacustrine claystones that are conformably overlain by 500 m of sand and gravel.

The great thickness of thick-bedded to massively bedded arkosic sands, large area of deposition, and general lack of matrix-supported gravel deposits or well-defined channels indicate that the Morales Formation could have been deposited in a large streamflow-dominated alluvial fan system. Comglomerate clasts are a mixture of granitic rocks, gneiss, schist, quartzite, andesite, and basalt, whose sources are outcrops of crystalline rocks near the San Andreas fault, 20–30 km southeast of Cuyama Valley (Dibblee, 1982; Ellis, 1994; Kellogg and others, 2008). These clasts are evidence of long-distance transport from sediment sources at the margins of the broad depositional basin. Well and seismic-reflection data indicated that fine-grained intervals within the Morales Formation can be correlated in the subsurface for several kilometers.

Older alluvial deposits often consist of a sequence of boulder, clast-supported alluvial channel deposits separated by sandy interbeds (fig. 19*B*). Boulder clasts are typically of local origin and reflect nearby sources; deposits on the south side of Cuyama Valley often are dominated by clasts of Eocene sandstones derived from the Sierra Madre Mountains, whereas deposits on the northern side of the valley have a large proportion of Monterey shale clasts derived from the Caliente Range. Channel deposits are local-scale features that cannot be correlated for long distances. Younger alluvial deposits exposed in incised arroyos along the Cuyama River are dominated by tabular beds of fine to medium sand (DeLong and others, 2011).

The spatial distribution and sediment characteristics of the three basin-filling units are related to the Pliocene and Pleistocene tectonic evolution and uplift of the basin, the progressive narrowing of the valley, and the gradually increasing channelization of the Cuyama River drainage. The QTm is a widespread unit that was deposited prior to the constriction of the basin by encroaching thrust faults. The sediment supply to the QTm was from relatively distant sources, and the unit appears to have been deposited by streams in which the channel system was broad and poorly bounded. The inception of Pliocene compression and uplift caused thrust-bounded bedrock highlands to impinge upon the valley, and the drainages became more restricted to channels and, perhaps, higher gradient. As a result of tectonic uplift, previously deposited Morales Formation was exposed and eroded, feeding reworked sediment into a narrower basin, which resulted in the deposition of Qoa. Qya is confined to the center of Cuyama Valley and alluvial channels tributary to the Cuyama River. Textural variations in Qya appear to be primarily climate-driven and reflect regional rainfall variations that control stream incision and aggradation.

Texture Derived from Drill-Hole Data

Textural data were derived by using drillers' lithologic logs from water wells and by interpretation of electric logs from oil and gas wells. Water wells yielded data for lithologic intervals in the younger part of the section, primarily from Qya and the upper part of Qoa, whereas the oil wells yielded data primarily from QTm and the lower part of Qoa. The two types of wells produced different textural parameters; lithologic logs from water wells could be interpreted in terms of sediment grain size and the degree of sorting, whereas oil wells yielded textural parameters of grain size and bedding frequency.

Oil and Gas Wells

Textural data were derived from 65 oil and gas wells (fig. 18) by analyzing the electrical geophysical logs. The presence of fresh water as pore fluids in sand and gravel aquifers results in rightward deflections on resistivity logs to higher resistivity values and in leftward deflections to more negative values on the SP log; clays and shales are generally conductive and have low values of resistivity with rightward deflections to more positive values on the SP logs (Wyllie, 1957; Keys and MacCary, 1971; Johnson and Pile, 2002; fig. 20). Textural analysis used the deflection of the SP curve in the electric logs to approximate the sand-shale ratio, which is a technique often used in consolidated sand-shale sequences (Wyllie, 1957; Johnson and Pile, 2002), although not frequently applied to continental basin-fill deposits. Spontaneous potentials occur near boundaries between shale or clay and coarse-grained deposits. The polarity and amplitude of the SP-log deflection depend on lithology and the salinities of both the formation water and the borehole fluid. Assuming that coarse-grained and fine-grained beds within Qoa and QTm have similar formation water salinities, the sand-shale interpretations were made in reference to a shale baseline that was drawn on each electric log connecting the SP-log deflections to the most positive values. This shale baseline was defined by using SP-log deflections for the entire thickness of QTm and the underlying fine-grained Quatal Formation below. A sand line was constructed roughly parallel to the shale baseline by connecting the maximum deflections to negative values on the SP log. Variation of the SP curve between the maximum deflections is due to a variety of factors, including the relative clay content of the formation and the damping effect of thin beds, which tend to reduce the SP deflection even in cases of clean sands interbedded with pure shale (Wyllie, 1957; Keys and MacCary, 1971; Johnson and Pile, 2002).

The 100-mV scale of the SP curve was divided into four categories that corresponded to relative-size fractions, described as coarse, medium, fine and very fine (fig. 20). The finest and coarsest relative-size fractions were each assigned a 30-mV range (six vertical divisions, fig. 20); the middle two relative-size categories each occupied 20-mV range on either side of the zero value. These divisions were assigned on the basis of the maximum SP-log deflections observed in

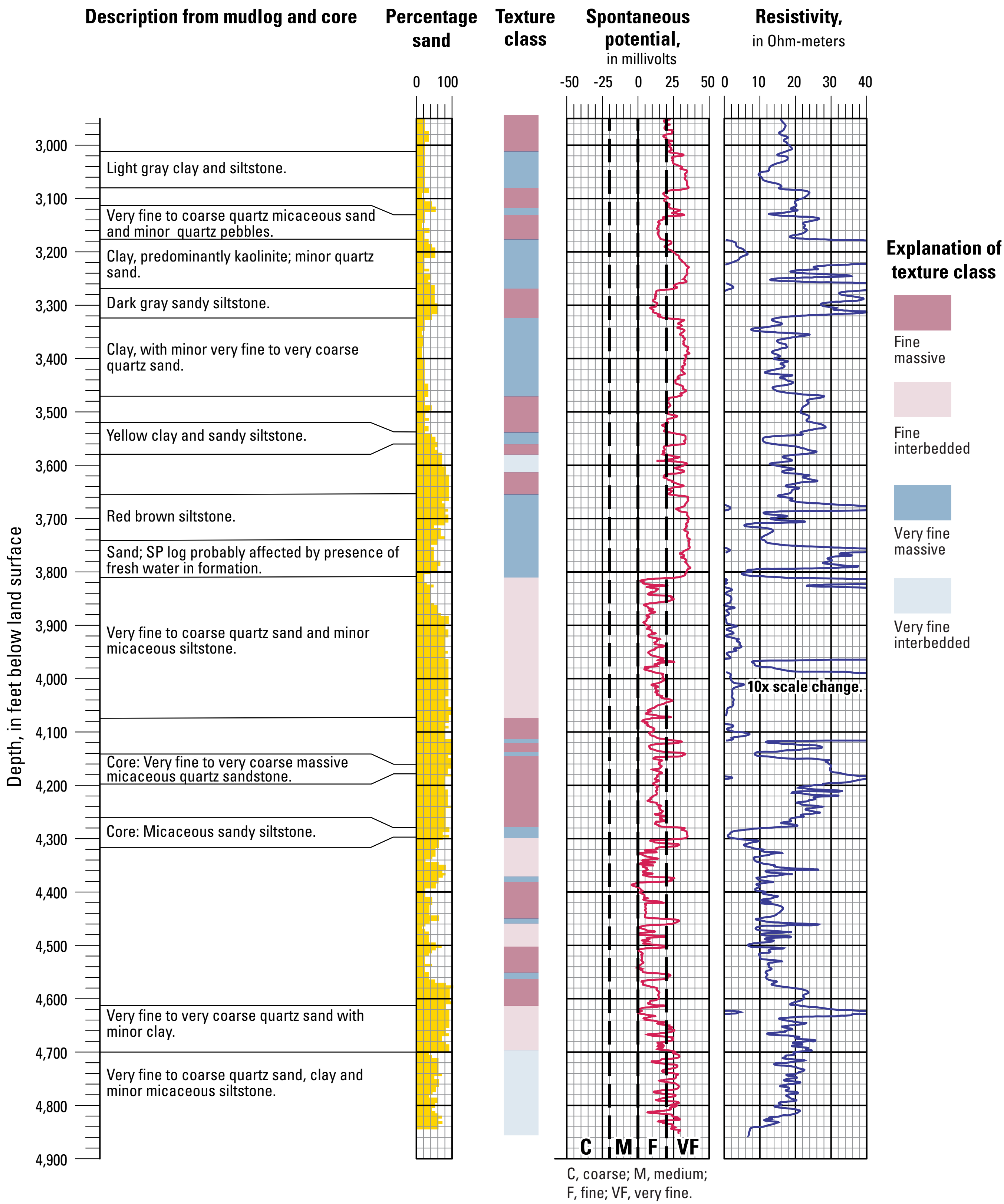

Figure 20. Example electric log from oil and gas well showing derivation of textural data.

the Miocene rocks beneath the Morales Formation, where shale and sandstone were penetrated. The upper parts of the boreholes were logged by using the same SP-log scale as the deeper section, so that the magnitude of the deflection could be roughly calibrated to a known grain size. Down-hole intervals were then assigned a relative grain size on the basis of the location of the SP-log curve with respect to the category boundaries. Qoa tended to be characterized by numerous intervals that had SP-log deflections to large negative values that were described as coarse or medium relative-size fractions, whereas QTm tended to be characterized by relatively monotonous SP-log response in the fine to fine relative-size fractions.

Down-hole intervals were also classified by bedding frequency and described as either massive or interbedded (fig. 20). Massively bedded intervals were those where the SP curve remained within a relative-size category for at least 20 ft; interbedded intervals were characterized by frequent alternation between relative-size fractions at the scale of several feet in thickness. Thin beds tend to dampen the full response of the SP logging tool because the tool spans the thickness of multiple beds and integrates the spontaneous potentials developed at multiple unit contacts. For these units, the SP curve was augmented by the higher-resolution peaks of the resistivity curves to qualitatively discriminate between massively bedded units and thinly interbedded units.

The relative-size fractions derived from SP-log analysis compared favorably to mud-log descriptions, percentage sand analysis, and descriptions from sidewall cores (fig. 20). Although mud-log descriptions include a wide range of grain sizes, intervals described as siltstone corresponded to rightward deflections to more positive values on the SP logs that were classified as very fine, whereas sand-bearing intervals were consistently interpreted in the fine grain size class (fig. 20). Where lithologic descriptions were more general or applied to a large downhole interval, there was a general correspondence between the logged sand percentage and the SP-log results, such that sand-poor intervals corresponded to an interpreted grain-size class of very fine (fig. 20). Correspondence between observed lithology and interpreted grain-size class was strongest where relatively thick beds of uniformly coarse material were penetrated. Thin-bedded deposits tended to be described as mixtures of grain-size fractions in the mud logs. Shale or clay intervals recorded in the mud log rarely correlated well with a clear shale line on the SP-log, which, perhaps, was a result of the interbedded nature of the deposits or of the lag in cutting return coming up the drill hole. In some cases, the fine-grained fraction could have been underrepresented in the mud log when the drill cuttings were washed to remove drilling mud and fluids.

Water Wells

Textural data were derived from drillers' lithologic logs from 153 water wells in the study area (fig. 18). Drillers' descriptions are generally short phrases that accompany a significant lithologic change. Typically, descriptions range from one to ten words that describe a change recognized by the driller as the drill penetrates a different unit; for example, descriptions can include information on grain size, presence or absence of gravel or large rocks, degree of consolidation, and rock type or abrupt color changes. Each lithologic log was divided into a discrete binary texture classification of either "coarse grained" or "fine grained" intervals on the basis of the description in the log. In this study, coarse-grained sediment is defined as consisting of sand, gravel, pebbles, boulders, cobbles, or conglomerate. Fine-grained sediment is defined as consisting principally of clay, lime, loam, mud, or silt. These definitions of "coarse grained" and "fine grained" are similar to those originally defined by Page (1986) and later used by Laudon and Belitz (1991), Belitz and others (1993), and Burow and others (2004).

2-D and 3-D Models of Textural Data

Numerical hydrologic-flow models must represent the hydraulic conductivity of aquifers throughout the model volume. This can be accomplished through a 3-D array of values (Burow and others, 2004; Faunt, 2009) or as a 2-D representation in plan view where the model domain is subdivided into zones that represent areas with the same hydraulic properties within individual aquifers (Faunt, Blainey, and others, 2010). Textural data were analyzed in both 2-D and 3-D to help define textural variations in the Cuyama Valley groundwater basin in ways potentially useful for a numerical hydrologic-flow model. Ultimately, sediment grain size, a textural parameter common to both the oil and water well data, was modeled by using geostatistical methods to produce 2-D estimates of grain-size variability for each principal basin-filling unit.

3-D Model of Textural Data from Oil Wells

The interpreted grain-size and bedding-frequency parameters derived from the oil and gas exploration holes were used to construct a 3-D solid model of textural variations within the basin by extrapolating data away from boreholes by using a nearest-neighbor 3-D-gridding process within a 3-D software modeling package (fig. 21). The 3-D-gridding process is a cell-based modeling approach where solid-model cell nodes are sequentially assigned properties outward horizontally from each borehole in circles of increasing diameter. The approach is a simple spatial interpolation method that does not consider spatial structure of the data. Cell dimensions for the modeling were 500 m in the horizontal dimensions and 10 m in the vertical dimension. The x,y cell dimensions were chosen to mimic the closest spacing of the oil and gas wells, and the vertical dimension was chosen to preserve the textural detail obtained from the SP-log analysis. The extrapolated lithologic data in the resulting solid model have the appearance of stratigraphic units with aspect ratios that emphasize the horizontal dimension relative to the vertical dimension.

A series of vertical northwest-southeast and northeast-southwest sections through the 3-D solid lithologic model

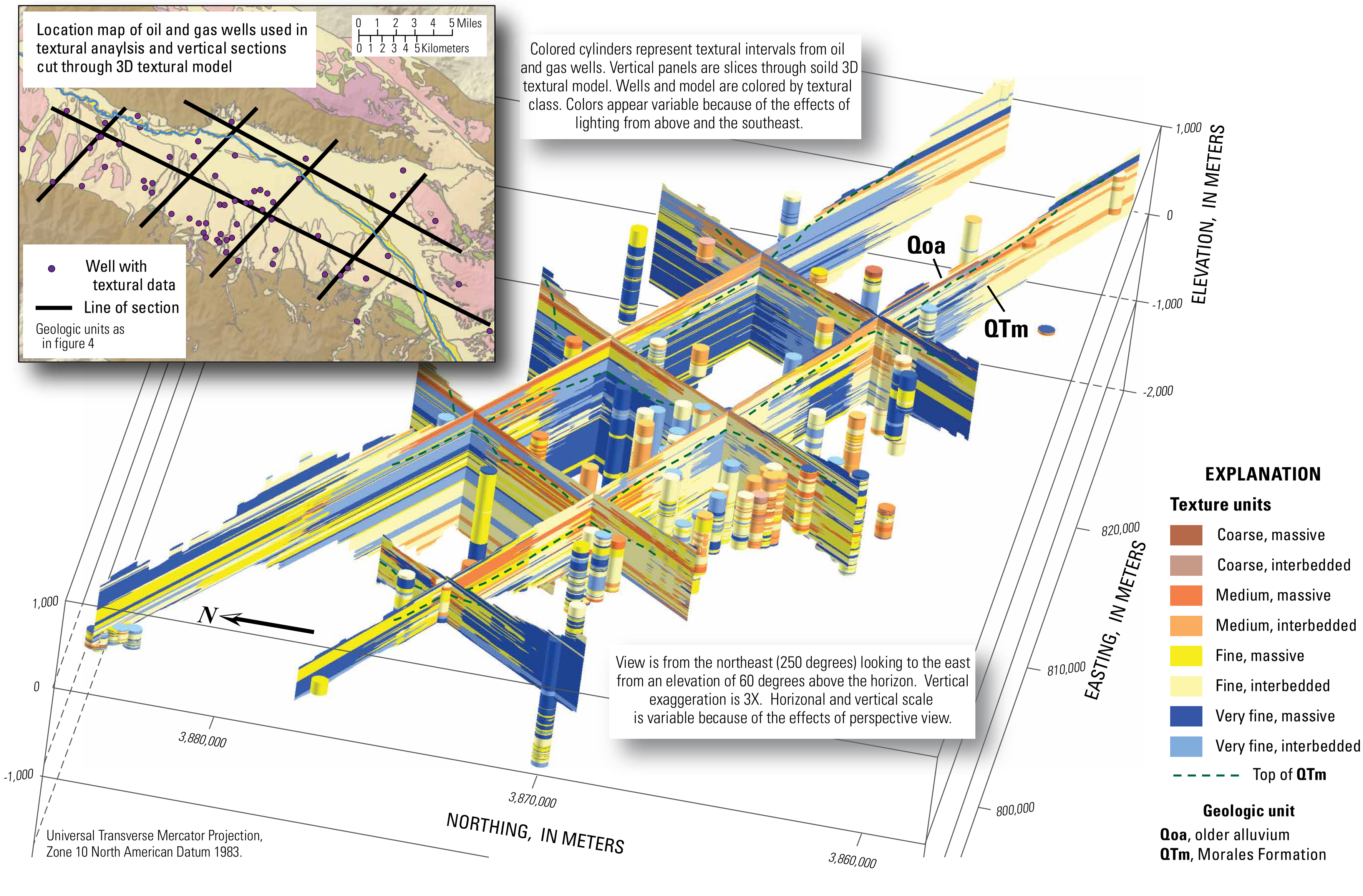

Figure 21. Perspective view showing results of 3-D textural modeling from oil and gas well data.

portray the lithologic variability of the basin fill in the Cuyama Valley region as extrapolated from the oil and gas borehole data (fig. 21). The upper surface of the 3-D solid lithologic model is clipped at the topographic surface by using a digital elevation model; the base of the model is clipped with the modeled base of QTm. Mountainous regions that are underlain by bedrock around the basin margins are uncolored (fig. 21).

The 3-D solid model shows the relative extents of coarse- and fine-grained sediments in the shallow subsurface and highlights textural differences between the Qoa and QTm units (fig. 21). Qoa is generally coarser than the QTm and has more numerous medium- and coarse-grained lenses, which probably represent alluvial channel deposits. The QTm has relatively few coarse-grained intervals and is characterized by relatively fine-grained material, particularly in the axis of the valley where Qoa contains some of the coarsest intervals. The QTm becomes more coarse-grained along the southern flank of the valley and to the southeast, perhaps reflecting available sediment supply from uplifting areas outside the valley.

The 3-D modeling approach was ultimately limited by the extrapolation methodology. The method preserved the local variability of the lithology where data were abundant, but resulted in poorer extrapolation where drill holes were widely spaced and the outlying points influenced a large part of the model volume. A series of plan-view zones of texture variation was envisioned as input for the numerical flow model, and 2-D extrapolation methods, described in the following section, were ultimately used rather than the 3-D approach.

2-D Models of Textural Data

Geologic or hydrogeologic units are the basis for assigning horizontal hydraulic conductivity to the cells of a numerical flow model grid within the groundwater modeling code MODFLOW-2000 (Anderman and Hill, 2000, 2003). Lateral variations in horizontal hydraulic-conductivity,or the material's capacity to transmit water in the x-y plane parallel to bedding, can be assigned through the use of the zonation capability of the Hydrogeologic-Unit Flow (HUF) package of MODFLOW-2000 (Anderman and Hill, 2000). Zones are used to define areas with similar properties within individual geologic or hydrogeologic units. For eventual use within a numerical hydrologic-flow model, 2-D (map view) models of textural data from both oil and water wells were created for the geologic units, Qya, Qoa, and the QTm, to define areas with similar geologic materials that are likely to have fairly uniform hydraulic properties.

Similar to previous studies (Phillips and Belitz, 1991; Burow and others, 2004; Faunt, 2009), the primary variable used in the textural analysis was sediment grain size, tabulated as percentage of coarse-grained texture. Down-hole intervals from both oil and water wells were classified as either coarse or fine grained. For water wells, coarse-grained deposits were those dominated by gravel and sand-size clasts with no clay matrix; all other lithology classes were considered fine-grained. Even units that had a considerable fraction of large clasts were classified as fine-grained if the clasts tended to be suspended in a fine-grained matrix. For oil wells, coarse and medium texture classes derived from the SP-log curve were assigned as coarse grained; fine and very fine classes were assigned as fine grained. The binary classification of intervals as either coarse or fine grained helped account for the lack of an exact correspondence between grain size as described in drillers' lithologic logs and the relative size classes derived from SP-log analysis. For use in statistical and geostatistical analysis, the percentage of coarse-grained sediment was calculated for the entire thickness of each geologic unit for 218 wells (table 3). The percentage of coarse-grained sediment was calculated as the total thickness of coarse-grained intervals divided by the total thickness of the geologic unit. The global mean percentage of coarse-grained texture was 34 percent, with young alluvium being significantly more coarse than older alluvium or the Morales Formation (table 3).

Because the hydrologic-flow model was subdivided on the bassis of three geologic units, sediment texture was estimated at the nodes of a 2-D grid for each unit. The textural parameter represents an average value that applies to the entire thickness of the geologic unit. This grid node-based averaging provides a measure of spatial variability for the unit in the x,y dimensions, but eliminates any portrayal of textural variability in the z direction within the unit. The density of wells in the center of the groundwater basin is sufficient to model the texture of each geologic unit on a 250-m horizontal grid. Data density throughout the study region varied on the basis of the availability of data. This variable sample density did not appear to bias the statistics used to describe the x,y,z values. The data were not declustered prior to the geostatistical modeling. The grid was oriented with the long axis roughly parallel to Cuyama Valley axis and has a uniform cell spacing of 250 m in the x and y directions consisting of 300 cells in the x-direction and 135 in the y-direction. The textural data at wells represented x,y point values for each geologic unit.

Coarse-grained texture was extrapolated away from the well data for each geologic unit by using the geostatistical

Table 3. Summary of logs used for textural analysis by geologic unit.

[Qya, Younger alluvium; Qoa, Older alluvium; QTm, Morales formation]

Geologic unit (abbreviation)	Number of records[1]	Maximum thickness (feet)	Average thickness (feet)	Percentage coarse
Younger alluvium (Qya)	119	193	92	59
Older alluvium (Qoa)	154	354	171	36
Morales Formation (QTm)	120	1,384	754	31
All	235	1,637	868	34

[1]Records for each unit do not sum to the total shown in "All" because wells can penetrate more than one unit down hole.

method of ordinary kriging in a similar fashion to methods used by Burow and others (2004) and Faunt and others (2010). An advantage of using geostatistics instead of simple spatial interpolation methods, such as inverse-distance weighted interpolation, is that the geostatistical model is fitted to the observed spatial correlation structure, whereas simple interpolation methods are based on an assumed spatial correlation structure. Kriging is based on the assumption that the parameter being interpolated varies in a continuous manner from one location to the next, such that points that are near each other have a certain degree of spatial correlation, but points that are widely separated are not spatially correlated (Journel and Huijbregts, 1978; Isaaks and Srivastava, 1989). Anisotropy, or the directional component of the spatial dependence, in the spatial correlation structure can be obtained by combining several different models aligned along its principal axis to form a nested set of models.

2-D semivariograms that displayed differences in the percentage of coarse-grained sediment between pairs of points at different distances were developed in order to investigate the spatial correlation of the textural data (table 4). The semivariograms reflected the geometry and depositional environment of Cuyama Valley in that they typically have a horizontal range in kilometers along the axis of the valley and half that perpendicular to the valley axis (table 4). Typically, the semivariograms displayed a nugget, or variance at very close sample spacing, indicating textural variability at scales smaller than the distance between neighboring well data. Semivariograms were calculated by using a moving window with at least two nearest neighbors and an optimum of five nearest neighbors. The semivariograms were fitted with curves or variogram models that best fit the data. Each model included a nugget and used an exponential variogram model; in some cases the data were best fit using multiple, or nested, variagram models. Anisotropy that was observed in the semivariograms was best fit by setting the major anisotropic axis close to the trend of the valley axis, parallel to the main river channel, and the minor anisotropic axis perpendicular to this axis, close to the trend of the tributaries and fans (table 4).

2-D kriging was used to extrapolate coarse-grained texture to each x,y grid node for the entire thickness of the geologic unit. To augment the textural parameter for alluvial units Qya and Qoa, the digital elevation model was introduced as a second data set, and texture was computed by using co-kriging. Textural data for Qya and Qoa exhibited some correlation with elevation where these deposits were in channels or on alluvial fans. Co-kriging tended to improve the textural interpolation, especially in drainages with few or no well data, such that the primary texture variable was considerably undersampled.

The spatial dimensions of the search neighborhood were not constrained; therefore, for locations of the estimation grid having densely-spaced wells, the effective search neighborhood was relatively small. For locations of the estimation grid that contained widely-spaced wells, the effective search neighborhood expanded laterally until at least two texture values were reached. Although the estimation neighborhood used at least two values for each kriged estimate, most estimates in the corners and along the boundaries of the grid were extrapolated rather than interpolated values.

As is indicated by the nugget and range of the variograms, the assumption that texture at any point in heterogeneous alluvial sediments is related to texture at surrounding points several kilometers away might not always be valid. Therefore, in areas of sparse data, the texture maps are to be regarded as only showing general trends and averages. Conversely, in areas where nearby data are variable and there is a significant relative nugget in the variogram model, the 3-D kriging can produce smoothed estimates. This results because the kriging algorithm aims to find a least-squares estimate of the expected value; therefore, the more data that are included in the estimate, the smoother the estimate will be.

The spatial patterns of the percentage of coarse-grained texture are shown in texture maps of the three basin-fill units (figs. 22–24). The 2-D kriged estimates of percentage of coarse-grained texture showed significant heterogeneity in the texture of the sediments that reflects the depositional environment and the geomorphic evolution of the region since the Pliocene. The spatial structure of the kriged textural model for the young alluvium can be attributed to the alignment of the active drainages, whereas the textural models of the older units were less correlated to modern topography.

Table 4. Kriging parameters used for textural analysis.

[—, second dataset not used; DEM, digital elevation model; m, meters]

Geologic unit (abbreviation)	Method	Second dataset	Major[1] (meters)	Minor[2] (meters)	Direction[3] (degrees)	Sill, (percent)	Lag	Nugget, (percent)
Younger alluvium (Qya)	Co-kriging	DEM	19,200	11,500	105	10	12 lags of 1,600 m	6
Older alluvium (Qoa)	Co-kriging	DEM	14,400	8,900	107	3.5	12 lags of 1,200 m	9
Morales Formation (QTm)	Kriging	—	8,000	2,715	80	4.2	8 lags of 1,000 m	7

[1] Distance to the sill or correlation length along the major anisotropic axis.

[2] Distance to the sill or correlation length along the minor anisotropic axis.

[3] Direction reported in degrees measured clockwise from north.

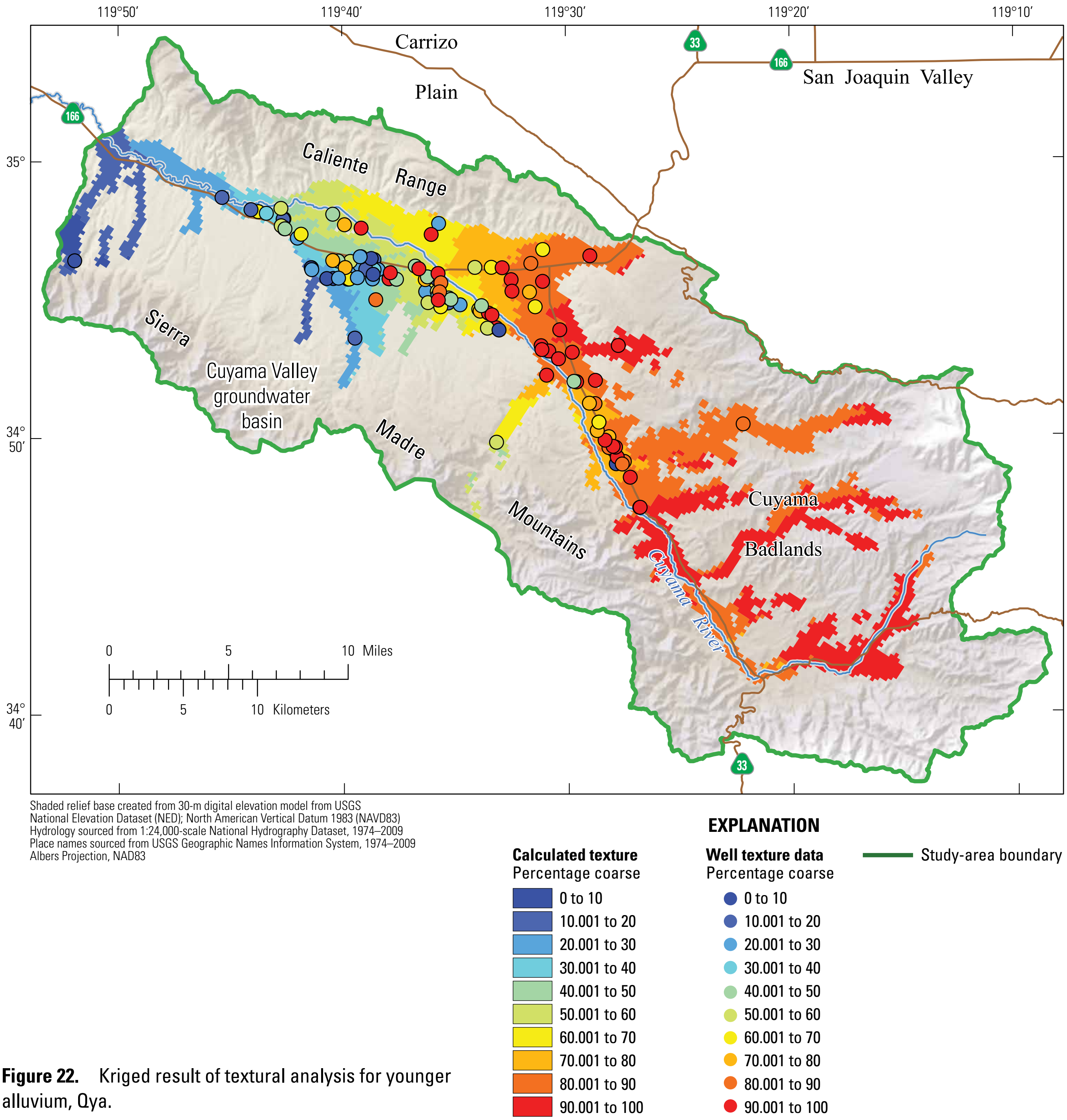

Figure 22. Kriged result of textural analysis for younger alluvium, Qya.

The texture model of Qya had the highest percentage of coarse deposits of the three units (fig. 22). The coarse-grained nature of the Qya reflects a number of factors, including the short distances between the sediment sources in the surrounding uplands and the sites of sediment deposition as well as the high-energy nature of Cuyama River and tributary creeks that transport sediments during winter storms and summer monsoonal rains. Because the basin is relatively small, the Cuyama River is able to carry a large bed load long distances through a large percentage of the valley. Coarse-grained sediment input also comes from several tributary drainages in the southeastern part of the study area that have relatively large catchment areas (fig. 22).

The texture model for Qoa differs in spatial structure from Qya in being overall much finer-grained and generally unrelated to the modern active drainages (fig. 23). Much of Qoa

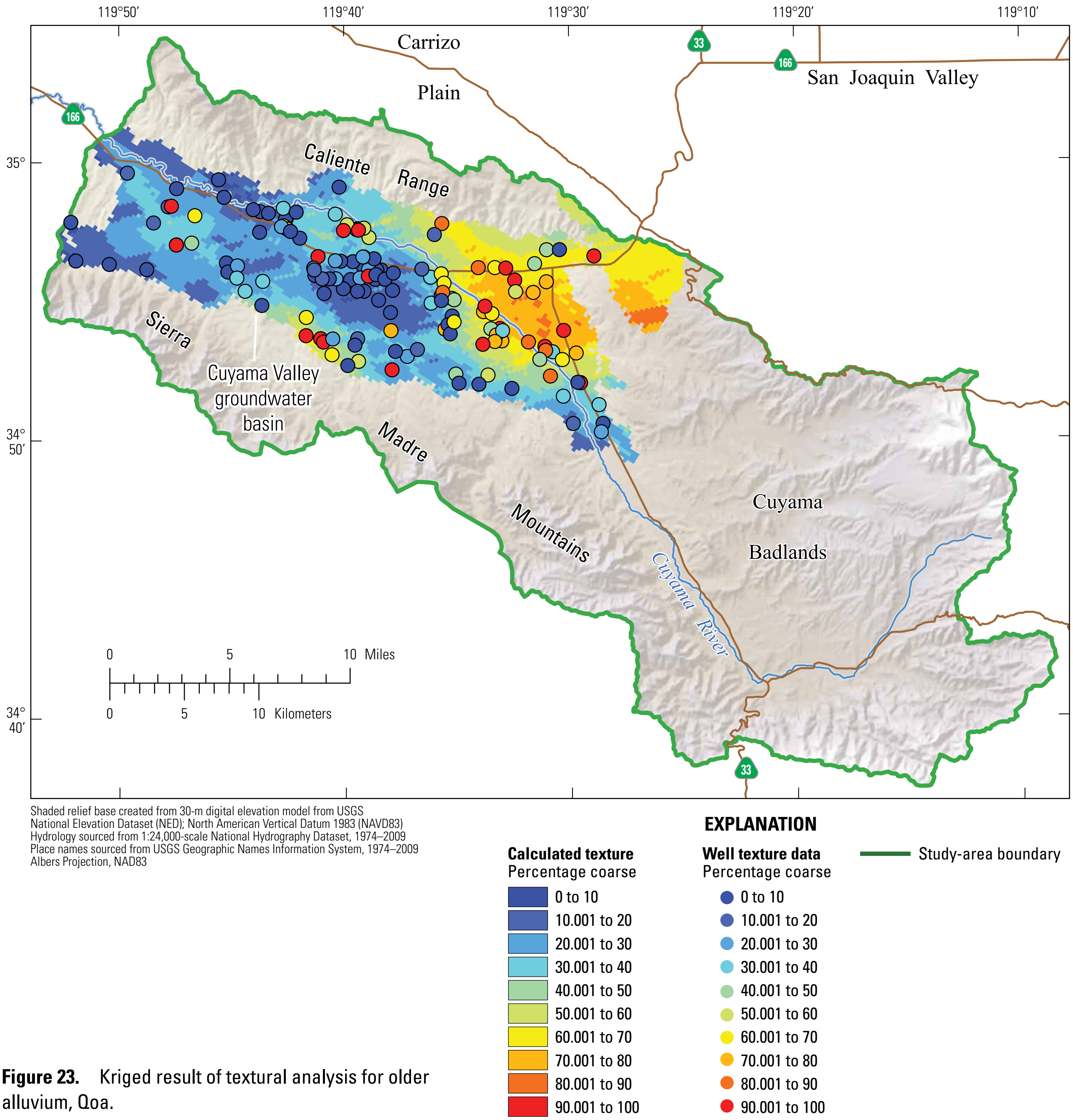

Figure 23. Kriged result of textural analysis for older alluvium, Qoa.

is derived from erosional reworking of uplifted parts of the Morales Formation. This reworking of previously-deposited sediment could account for the generally fine-grained nature of Qoa in the western half of the study area (fig. 23). Many of the wells throughout the valley are variable in their percentage of coarse-grained deposits in the Qoa, which could reflect the presence of local coarse-grained channels that affects the percentage of coarse-grained material when averaged over the entire thickness of the unit. A region of consistently coarse-grained material exists in the eastern part of the study area and could reflect an older stream channel alignment or the depositional site of sediments shed to the northwest off the uplifting Cuyama Badlands (fig. 23).

The QTm is much finer-grained than the overlying units (fig. 24). The QTm is particularly fine grained in the western half of Cuyama Valley, where surface geologic mapping identifies a lacustrine facies in this unit (Upson and Worts, 1951; Dibblee and Minch, 2005d; DeLong and others, 2008). This region of fine-grained material, and distinct fine-grained intervals within the Morales Formation, could reflect a

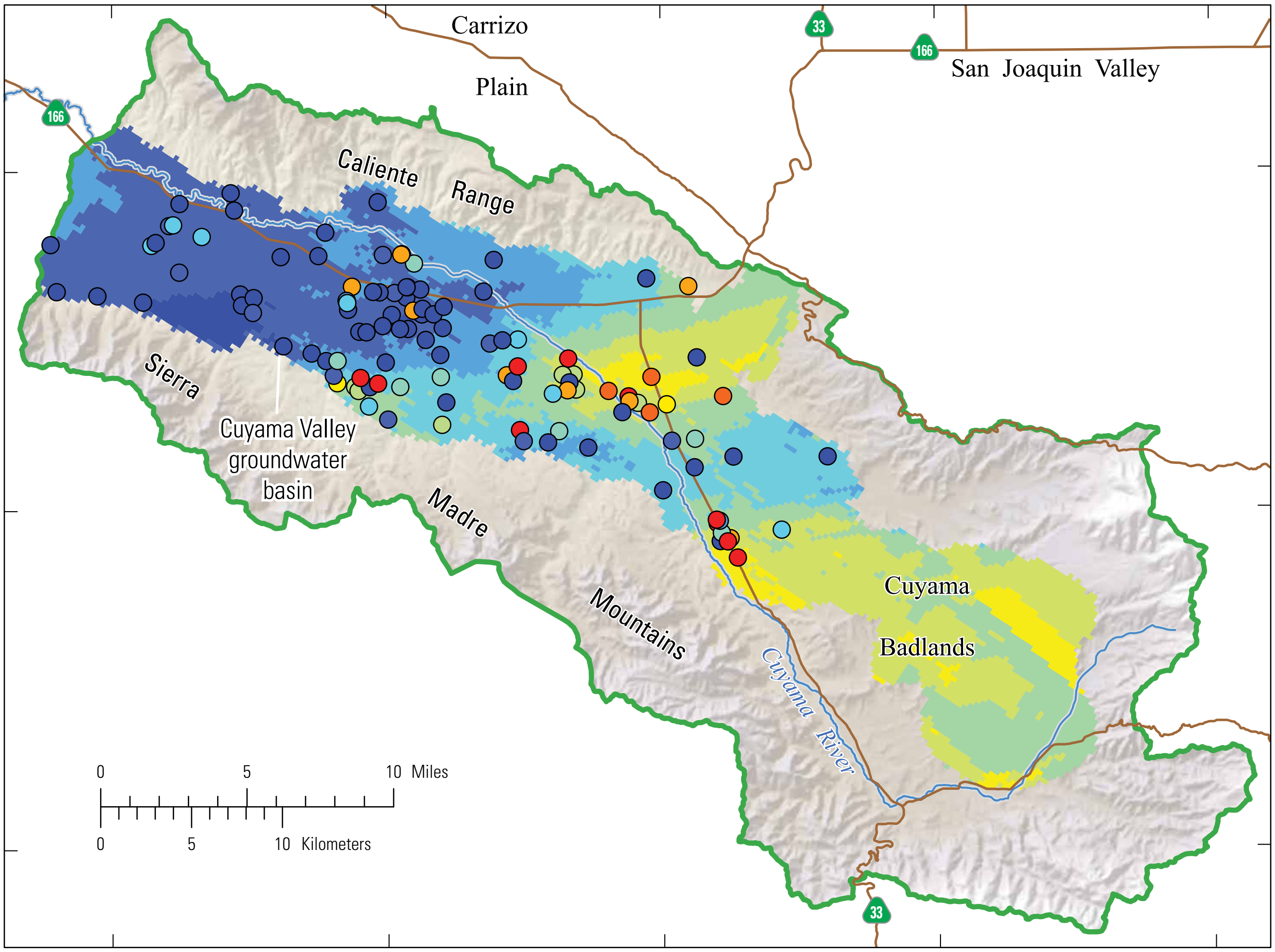

Figure 24. Kriged result of textural analysis for the Morales Formation, QTm.

relatively distant sediment supply and temporary disruption of sediment transport in the Cuyama River drainage as a result of episodic uplift of the Sierra Madre Mountains at the west end of the valley (Dibblee, 1976). There are broad regions of relatively coarse material in the vicinity of the Cuyama Badlands (fig. 24). These areas are generally unrelated to the modern active drainages and represent deposition of alluvial materials prior to the development of modern topography.

The modeled percentage of coarse-grained sediment for each of the three basin-filling units is shown in perspective view in figure 25 along the two lines of section from Singer and Swarzenski (1970; fig. 17). The percentage of coarse-grained sediment was calculated for the entire thickness of each basin-filling unit for 250-m grid cells throughout the Cuyama Valley study area. The modeled result is portrayed in figure 25 for only those grid nodes that fall along the two lines of section. In this view, the kriged textural results are portrayed in grid cells that have fixed x,y dimensions, but variable height that is governed by the modeled elevation of the top and base of each unit within the geologic framework model

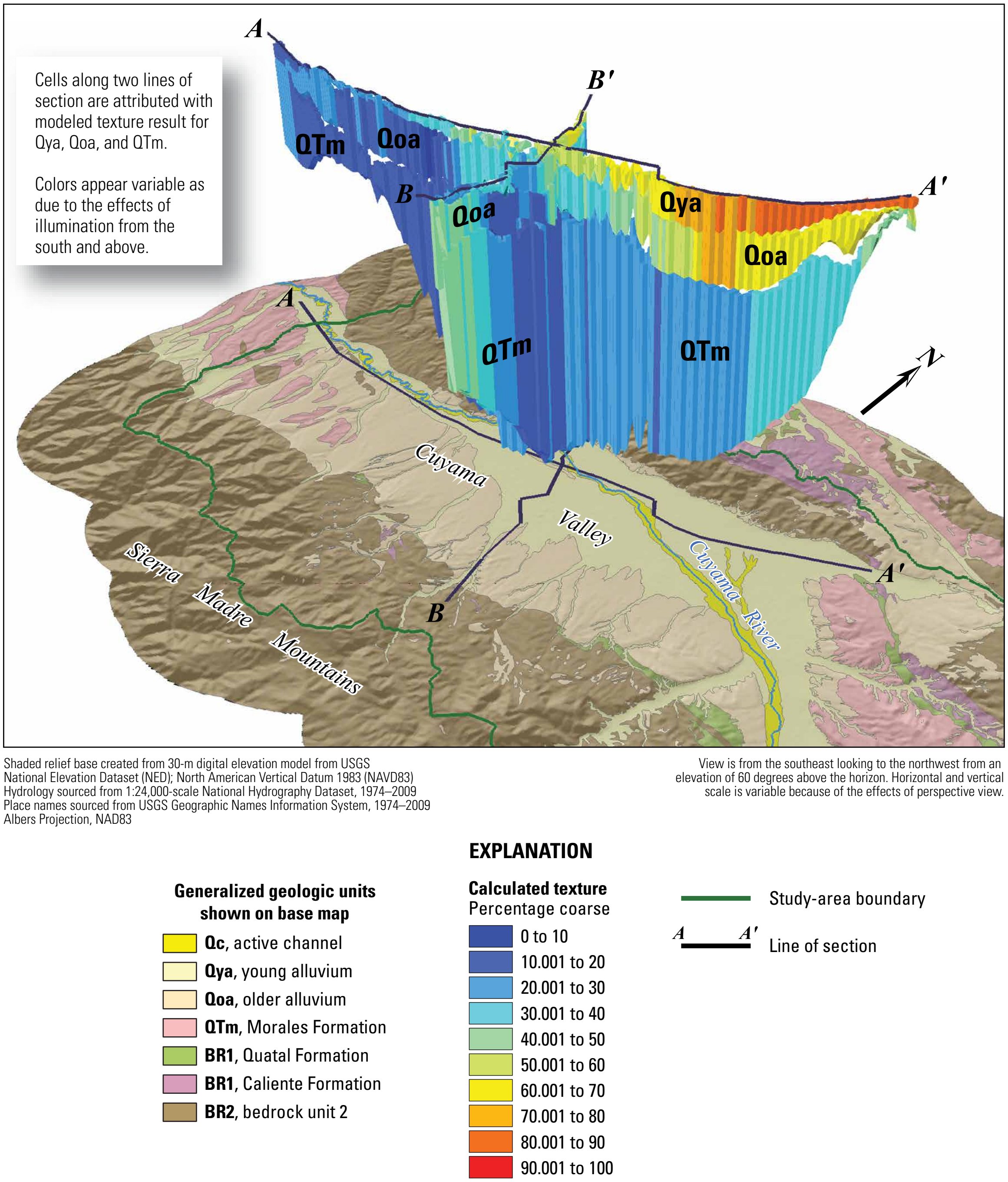

Figure 25. Perspective view showing result of kriged textural models for the younger alluvium, older alluvium, and Morales Formation units (Qya, Qoa, and QTm) along two vertical sections.

(fig. 25). Numerical effects resulting from the sampling of the stratigraphic unit tops and the textural models along the lines of section cause minor local gaps between grid cells between units. The geologic map and the map trace of the section are shown at an arbitrary depth below the modeled texture result for locational purposes (fig. 25).

Qya has the coarsest modeled grain size of the three basin-filling units; it is the coarsest in the vicinity of the active Cuyama River channel. Kriged textural results from Qoa are moderately coarse-grained in the eastern half of Cuyama Valley, but transition to fine-grained at the western end of the valley. Modeled texture results for the QTm portray it as being generally fine-grained, particularly at the west end of the valley (fig. 25). The south end of section *B-B'* shows a slight relative increase in the modeled percentage of coarse-grained sediment, which could reflect proximity to sediment sources along the uplifted southern edge of the basin.

Summary

Water-resource management concerns have prompted an evaluation of the hydrogeology and water availability of the Cuyama Valley groundwater basin by the U.S. Geological Survey (USGS), in cooperation with the Water Agency Division of the Santa Barbara County Department of Public Works. The eventual construction and use of a numerical hydrologic-flow model of the basin drives the need for (a) a conceptual understanding of the geologic setting of the Cuyama Valley groundwater basin; (b) the construction of three-dimensional digital models of the geologic framework of the basin; and (c) an analysis of the spatial variability of lithology and grain size to form the geologic basis for estimating the aquifer hydraulic properties. Previous work has outlined the overall shape of the basin, located many of the faults, and delineated and characterized aquifers in the saturated parts of the younger and older alluvium—units that historically have yielded most of the water pumped in the study area. This report builds on that work by creating three-dimensional digital datasets suitable for incorporation within a numerical hydrologic-flow model and includes greater detail for the deeper stratigraphic units of the groundwater basin, which were not previously investigated in detail.

A several hundred meter-thick section of Pliocene continental deposits and Pleistocene alluvial sediments constitutes the principal groundwater aquifer of the Cuyama Valley groundwater basin. This section can be subdivided into three principal stratigraphic units: Qya, younger alluvium; Qoa, older alluvium; and QTm, the Morales Formation. The two alluvial units are distinguished on the basis of degree of cementation and the amount of dissection and deformation. The QTm is an alluvial and fluvial deposit characterized by relatively fine-grain size, general lack of coarse channel deposits, and greater amounts of clay compared to the overlying section. Consolidated rocks that lie beneath the Morales Formation are generally non-water bearing.

A geologic framework model was constructed to represent the subsurface geometry of the stratigraphic units, Qya, Qoa, QTm, and a composite pre-QTm bedrock unit, by extracting and combining information from a variety of datasets, including existing lithologic and electrical geophysical logs from oil and gas wells and water wells, cross sections, and geologic maps. The framework model was constructed by creating gridded surfaces that represented the altitude of the top of each stratigraphic unit from the input data and then combining these surfaces within a three-dimensional geologic modeling software package. Data from electrical geophysical logs throughout the basin were combined with recent geologic mapping of the Cuyama area to consistently identify the Morales Formation and place the top of the unit within the geologic framework model some 400 to 600 feet deeper than previously published interpretations. The older alluvial unit, Qoa, was not subdivided from younger alluvium on previously published sections. Within the geologic framework model, Qoa is a locally thick unit that includes the lower parts of the previously defined undivided Qya and Qoa and the upper part of the previously defined Morales Formation.

Sediment grain-size data were analyzed in both two and three dimensions to help define textural variations in the Cuyama Valley groundwater basin and to identify areas with similar geologic materials that potentially have fairly uniform hydraulic properties. Sediment grain size was used to construct three-dimensional textural models that employed simple interpolation between drill holes and to construct two-dimensional textural models for each stratigraphic unit that incorporated spatial structure of the textural data. The percentage of coarse-grained sediment was calculated from well data for the entire thickness of the Qya, Qoa, and QTm units. These data were extrapolated away from the well data across the study area at 250-meter spacing by using geostatistical methods. The resultant textural models portrayed a coarse-grained younger alluvial unit localized along the Cuyama River and several tributary drainages and a finer-grained older alluvial unit whose textural variations were less tied to the location of the modern drainages. The underlying Morales Formation displayed a broad west-to-east transition from coarse to fine-grained deposits. The spatial distribution and modeled textural characteristics of the three basin-filling units are related to the Pliocene and Pleistocene tectonic evolution and uplift of the basin, the progressive narrowing of the valley, and the gradually increasing channelization of the Cuyama River drainage.

References Cited

Anderman, E.R., and Hill, M.C., 2000, MODFLOW-2000, The U.S. Geological Survey modular ground-water flow model—Documentation of the hydrogeologic-unit flow (HUF) package: U.S. Geological Survey Open-File Report 2000–342, 89 p.

Anderman, E.R., and Hill, M.C., 2003, MODFLOW-2000, The U.S. Geological Survey modular ground-water flow model—Three additions to the hydrogeologic-unit flow (HUF) package—Alternative storage for the uppermost active cells (STYP parameter type), flows in hydrogeologic units, and the hydraulic conductivity depth-dependence (KDEP) capability: U.S. Geological Survey Open-File Report 2003–347, 36 p. Accessed March 13, 2013, at *http://water.usgs.gov/nrp/gwsoftware/modflow2000/modflow2000.html.*

Argus, D.F., and Gordon, R.G., 2001, Present tectonic motion across the Coast Ranges and San Andreas fault system in central California: Geological Society of America Bulletin, v. 113, p. 1,580–1,592.

Barger, R.M., and Zulberti, J.L., 1952, Russell Ranch oil field: California Division of Oil and Gas, California Oil Fields Summary of Operations, v. 38, p. 5–10.

Bartow, J.A., 1990, Coarse-grained deltaic sedimentation in the Miocene Cuyama strike-slip basin, California Coast Ranges: Sedimentary Geology, v. 68, p. 17–38.

Bazeley, W.J.M., ed., 1988, Tertiary tectonics and sedimentation in the Cuyama basin, San Luis Obispo, Santa Barbara, and Ventura Counties, California: Society of Economic Paleontologists and Mineralogists, Pacific Section, Book 59, p. 87–98.

Belitz Kenneth, Phillips S.P., and Gronberg, J.M., 1993, Numerical simulation of ground-water flow in the central part of the Western San Joaquin Valley, California: U.S. Geological Survey Water-Supply Paper 2396, 69 p.

Bryant, W.A. (compiler), 2005, Digital Database of Quaternary and Younger Faults from the Fault Activity Map of California, version 2.0: accessed September, 2011 at *http://www.consrv.ca.gov/CGS/information/publications/QuaternaryFaults_ver2.htm*.

Burow, K.R., Shelton, J.L., Hevesi, J.A., and Weissmann, G.S., 2004, Hydrogeologic characterization of the Modesto area, San Joaquin Valley, California: U.S. Geological Survey Scientific Investigations Report 2004–5232, 54 p.

Calhoun, J.A., 1986, Structural geology of the Morales Canyon and Taylor Canyon region of the Cuyama basin, southern Coast Ranges, California: Corvallis, Oregon State University, M.S. thesis, 86 p., 18 pls., 9 figs.

California Department of Conservation, 2009, 2008 Annual Report of the State Oil and Gas Supervisor: Division of Oil, Gas and Geothermal Resources Publication PR06, 272 p., accessed February, 2010 at *ftp://ftp.consrv.ca.gov/pub/oil/annual_reports/2008/PR06_Annual_2008.pdf*.

California Department of Water Resources, 2003, California's Groundwater—Update 2003: California Department of Water Resources Bulletin 118, Cuyama Valley basin description, accessed May 09, 2012, at *http://www.water.ca.gov/pubs/groundwater/bulletin_118/basindescriptions/3-13.pdf*

Davis, T.L., Lagoe, M.B., Bazeley, W.J.M., Gordon, Stuart, McIntosh, Kirk, and Namson, J.S., 1988, Structure of the Cuyama Valley, Caliente Range, and Carrizo Plain and its significance to the structural style of the southern Coast Ranges and western Transverse Ranges, *in* Bazeley, W.J.M., ed., Tertiary tectonics and sedimentation in the Cuyama Basin, San Luis Obispo, Santa Barbara, and Ventura Counties, California: SEPM (Society for Sedimentary Geology), Pacific Section, v. 59, p. 159–161.

DeLong, S.B., Pelletier, J.D., and Arnold, L.J., 2008, Climate change triggered sedimentation and progressive tectonic uplift in a coupled piedmont-axial system—Cuyama Valley, California, USA: Earth Surface Processes and Landforms, v. 33, p. 1,033–1,046.

DeLong, S.B., Pelletier, J.D., and Arnold, L.J., 2011, Late Holocene alluvial history of the Cuyama River, California, USA: Geological Society of America Bulletin, v. 123, p. 2,160–2,176.

Dibblee, T.W., 1973, Regional geologic map of San Andreas and related faults in Carrizo Plain, Temblor, Caliente, and La Panza Ranges and vicinity, California: U.S. Geological Survey Miscellaneous Investigations Map I–757, scale 1:125,000.

Dibblee, T.W. Jr., 1976, The Rinconada and related faults in the southern Coast Ranges, California, and their tectonic significance: U.S. Geological Survey Professional Paper 981, 55 p.

Dibblee, T.W. Jr., 1982, Geology of the Alamo Mountain, Frazier Mountain, Lockwood Valley, Mount Pinos, and Cuyama Badlands areas, Southern California, *in* Fife, D.L. and Minch, J.A., eds., Geology and mineral wealth of the California Transverse Ranges; Mason Hill volume: South Coast Geological Society, p. 57–77.

Dibblee, T.W., Jr., 1995, Tectonic and depositional environment of middle and upper Cenozoic sequences of coastal southern California region, *in* Fritsche, A.E., ed., Cenozoic paleogeography of the western United States – II: SEPM (Society for Sedimentary Geology), Pacific Section, v. 75, p. 213–245.

Dibblee, T.W., and Minch, J.A., ed., 2005a, Geologic map of the Ballinger Canyon quadrangle, San Luis Obispo, Santa Barbara, Ventura, and Kern Counties, California: Dibblee Geological Foundation Map DF–170, scale 1:24,000.

Dibblee, T.W., and Minch, J.A., ed., 2005b, Geologic map of the Cuyama quadrangle, San Luis Obispo and Santa Barbara Counties, California: Dibblee Geological Foundation Map DF–176, scale 1:24,000.

Dibblee, T.W., and Minch, J.A., ed., 2005c, Geologic map of the New Cuyama quadrangle, San Luis Obispo and Santa Barbara Counties, California: Dibblee Geological Foundation Map DF–179, scale 1:24,000.

Dibblee, T.W., and Minch, J.A., ed., 2005d, Geologic map of the Peak Mountain quadrangle, San Luis Obispo and Santa Barbara Counties, California: Dibblee Geological Foundation Map DF–181, scale 1:24,000.

Dibblee, T.W., and Minch, J.A., ed., 2006, Geologic map of the Cuyama Peak quadrangle, Santa Barbara and Ventura Counties, California: Dibblee Geological Foundation Map DF–202, scale 1:24,000.

Dibblee, T.W., and Minch, J.A., ed., 2007, Geologic map of the Fox Mountain quadrangle, Santa Barbara County, California: Dibblee Geological Foundation Map DF–260, scale 1:24,000.

Ellis, B.J., 1994, Changing tectonic regimes in the southern Salinian block: extension, strike-slip faulting, compression and rotation in the Cuyama Valley, California: Corvallis, Oregon State University, Ph.D. dissertation, 141 p., 31 figs.

Ellis, B.J., and Spitz, H.M., 1987, Subsurface cross-section of the southeastern Cuyama basin, southern California, *in* Davis, T.L., and Namson, J.S., eds., Structural Evolution of the Western Transverse Ranges: SEPM (Society for Sedimentary Geology), Pacific Section, v. 48A, p. 77–84.

Ellis, B.J., Levi, Shaul, and Yeats, R.S., 1993, Magnetic stratigraphy of the Morales Formation: late Neogene clockwise rotation and compression in the Cuyama Basin, California Coast Ranges: Tectonics, v. 12, p.1170–1179.

Everett, R.R., Gibbs, D.R., Hanson, R.T., Sweetkind, D.S., Brandt, J.T., Falk, S.E. and Harich, C.R., 2013, Geology, water-quality, hydrology, and geomechanics of the Cuyama Valley groundwater basin, California, 2008–12: U.S. Geological Survey Scientific Investigations Report 2013–5108, 62 p.

Faunt, C.C., ed., 2009, Groundwater Availability of the Central Valley Aquifer, California: U.S. Geological Survey Professional Paper 1766, 225 p.

Faunt, C.C., Belitz, Kenneth, and Hanson, R.H., 2010, Development of a three-dimensional model of sedimentary texture in valley-fill deposits of Central Valley, California, USA: Hydrogeology, v. 18, p. 625–649

Faunt, C.C., Blainey, J.B., Hill, M.C., D'Agnese, F.A., and O'Brien, G.M., 2010, Chapter F. Transient flow model, *in* Belcher, W.R., and Sweetkind, D.S., eds., 2010., Death Valley regional groundwater flow system, Nevada and California—Hydrogeologic framework and transient: U.S. Geological Survey Professional Paper 1711, p. 251–344.

Fritsche, A.E., 1988, Origin and paleogeographic development of the Tertiary Cuyama depositional basin, southern California, *in* Bazeley, W.J.M., ed., Tertiary tectonics and sedimentation in the Cuyama basin, San Luis Obispo, Santa Barbara, and Ventura Counties, California: Pacific Section, Society of Economic Paleontologists and Mineralogists (SEPM), Cuyama symposium and field trip, Guidebook, April 16–18, 1988, v. 59, p. 159–162.

Graham, S.E., Mahony, T.M., Blissenbach, J.L., Mariant, J.J., and Wentworth, C.M., 1999, Regional geologic map of San Andreas and related faults in Carrizo Plain, Temblor, Caliente and La Panza Ranges and vicinity, California: A digital database: USGS Open-File Report 99–14, scale 1:125,000.

Hanson, R.T., Martin, Peter, Koczot, K M., 2003, Simulation of ground-water/surface-water flow in the Santa Clara-Calleguas basin, California: U.S. Geological Survey Water-Resources Investigation Report 02–4136, 214 p

Hanson, R.T., Li, Zhen, and Faunt C.C., 2004, Documentation of the Santa Clara Valley regional ground-water/surface-water flow model, Santa Clara County, California: U.S. Geological Survey Scientific Investigations Report 2004–5231, 75 p.

Hardebeck, J.L., and Michael, A.J., 2004, Stress orientations at intermediate angles to the San Andreas Fault, California: Journal of Geophysical Research, v. 109, B11303, doi:10.1029/2004JB003239.

Hill, M. L., Carlson, S.A., and Dibblee, T.W., Jr., 1958, Stratigraphy of Cuyama Valley-Caliente Range Area, California: American Association of Petroleum Geologists Bulletin, v. 42, p. 2,973–3,000.

Hudnut, K.W., Bock, Y., Galetzka, J.E., Webb, F.H., and Young, W.H., 2002, The Southern California Integrated GPS Network (SCIGN), *in* Fujinawa, Y., and Yoshida, A., eds., Seismotectonics in Convergent Plate Boundary: Terra Scientific Publishing Company, Toyko, p 167–189.

Isaaks, E.H., and Srivastava, R.M., 1989, An Introduction to Applied Geostatistics: Oxford University Press, New York, 561 p.

Johnson, D.E., and Pile, K.E., 2002, Well logging in non-technical language (2nd ed.): Tulsa, Penn Well Publishing Company, 289 p.

Journel, A.G., and Huijbregts, C.J., 1978, Mining Geostatistics: Academic Press, New York, 600 p.

Kellogg, K.S., Minor, S.A., and Cossette, P.M., 2008, Geologic map of the eastern three-quarters of the Cuyama 30′ x 60′ quadrangle, California: U.S. Geological Survey Scientific Investigations Map 3002, scale 1:100,000, 2 plates, 1 pamphlet, 23 p.

Keys, Scott, and MacCary, L.M., 1971, Application of borehole geophysics to water-resources investigations: U.S. Geological Survey Techniques of Water-Resources Investigations, Chapter E1, Book 2, 126 p.

Lagoe, M.B., 1984, Paleogeography of Monterey Formation, Cuyama Basin, California: American Association of Petroleum Geologists Bulletin, v. 68, p. 610–627.

Lagoe, M.B., 1987, Middle Cenozoic basin development, Cuyama Basin, California, *in* Ingersoll, R.V. and Ernst, W.G., eds., Cenozoic basin development of coastal California, Rubey Volume VI : Prentice-Hall, Englewood Cliffs, New Jersey, p. 172–206.

Laudon, Julie, and Belitz, Kenneth, 1991, Texture and depositional history of Late Pleistocene-Holocene alluvium in the central part of the western San Joaquin Valley, California: Bulletin of the Association of Engineering Geologists, v. 28, p. 73–88.

Meade, B.J., and Hager, B.H., 2005, Block models of crustal motion in southern California constrained by GPS measurements: Journal of Geophysical Research, v, 110, B03403, doi:10.1029/2004JB003209.

Nevins, B.B., 1982, Structural evolution of the Russell Ranch oil field and vicinity, southern Coast Ranges, California: Corvallis, Oregon State University, M.S. thesis, 76 p., 17 pls., 12 figs.

Page, R.W., 1986, Geology of the fresh ground-water basin of the Central Valley, California, with texture maps and sections: U.S. Geological Survey Professional Paper 1401-C, 54 p.

Phillips, S.P., and Belitz, Kenneth, 1991, Calibration of a textured-based model of a ground-water flow system, western San Joaquin Valley, California: Ground Water, v. 29, p. 702–715.

Pierotti, Bob, and Lewy, Richard, 1998, Evaluation of groundwater overdraft in the southern central coast region: California Department of Water Resources, Southern District, Technical Information Record SD–91–1, 13 p.

Schwing, H.F., 1982, Interaction between the Transverse Ranges and Salinian Block in the South Cuyama oil field, Cuyama Valley, California, *in* Fife, D.L., and Minch, J.A. eds., Geology and mineral wealth of the California Transverse Ranges; Mason Hill volume: South Coast Geological Society, p. 395–402.

Schwing, H.F., 1984, Subsurface Geology of the South Cuyama Oil Field and Adjacent Areas, Southern Coast Ranges, California: Corvallis, Oregon State University, M.S. thesis, 81 p., 19 pls., 10 figs.

Singer, J.A., and Swarzenski, W.V., 1970, Pumpage and ground-water storage depletion in Cuyama Valley California, 1947–66: U.S. Geological Survey Open-File Report 70–304, 24 p.

Spitz, H.M., 1986, Subsurface Geology of the Southeastern Cuyama Valley, Southern Coast Ranges, California: Corvallis, Oregon State University, M.S. thesis, 88 p., 20 pls., 12 figs.

Stanley, R.G., 1995, Central Coastal Province (011) with a section on Cuyama Basin, by M.E. Tennyson, *in* Gautier, D. L., Dolton, G.L., Takahashi, K.I., and Varnes, K.L., eds., 1995 National assessment of United States oil and gas resources—Results, methodology, and supporting data: U.S. Geological Survey Digital Data Series DDS–30, Release 2, one CD-ROM, accessed May 7, 2012 at *http://certmapper.cr.usgs.gov/data/noga95/prov11/text/prov11.pdf*

Sweetkind, D.S., Bova, S.C., Langenheim, V.E., Shumaker, L.E., and Scheirer, D.S., 2013, Digital Tabulation of Stratigraphic Data from Oil And Gas Wells in Cuyama Valley and surrounding areas, Central California: U.S. Geological Survey Open-File Report 2013–1084, 44 p.

Upson, J.E., and Worts, G.F., 1951, Ground water in the Cuyama Valley, California: U.S. Geological Survey Water Supply Paper 1110–B, 81 p.

Vedder, J.G., 1968, Geologic map of the Fox Mountain quadrangle, Santa Barbara County, California: U.S. Geological Survey Miscellaneous Investigations Map I–547, scale 1:24,000.

Vedder, J.G., and Repenning, C.A., 1975, Geologic map of Cuyama and New Cuyama Quadrangles, San Luis Obispo and Santa Barbara Counties, California, U.S. Geological Survey Miscellaneous Geologic Investigations Map I–876, scale 1:24,000, 2 plates.

Wyllie, M.R.J., 1957, The Fundamentals of Electric Log Interpetation (2d ed.): New York, New York, Academic Press Inc., 176 p.

Yeats, R.S., Calhoun, J.A., Nevins, B.B., Schwing, H.F., and H.M. Spitz, 1989, Russell Fault: Early strike-slip fault of California Coast Ranges: American Association of Petroleum Geologists Bulletin v. 73, p. 1,089–1,102.

Zulberti, J.L., 1954, South Cuyama oil field: California Division of Oil and Gas, California Oil Fields Summary of Operations, v. 40, p. 41–45.

Appendix

Appendix 1.

Interpreted depth to top of geologic units in oil and gas wells, Cuyama Valley

Data compiled within appendix 1 include well location information and subsurface geologic information, such as depths to the geologic unit tops, from oil and gas wells in the Cuyama Valley and surrounding areas. Well names and location data were obtained in a digital well-location database from the California Department of Conservation, Division of Oil, Gas and Geothermal Resources (CA DOGGR) (*ftp://ftp.consrv.ca.gov/pub/oil/GIS/* accessed February 2010). Oil and gas exploration holes in the database, and in this report, are referenced by American Petroleum Institute (API) well number, a unique, permanent, numeric identifier assigned to each well drilled for oil and gas in the United States. The numbers reported here are abbreviated versions of the full API well-number and consist of a three-digit county code followed in sequence by a five-digit unique well identification number within the county. County codes are as follows: 079, San Luis Obispo County; 083, Santa Barbara County; 111, Ventura County. Two wells do not have API numbers. The information contained in the CA DOGGR database includes API well number; operator; lease name and well number; section, township, and range; and latitude and longitude. Wells in appendix 1 are identified by API number and a well identifier, which was created by merging the lease name and well number.

Well locations, in meters, are reported in Albers projected coordinate system, North American Datum of 1983 (NAD 83), GRS 80 spheroid. Elevation at the well location, in feet, is reported relative to mean sea level. Values are reported in feet to maintain consistency with source geologic and geophysical data for which depths are reported in feet.

All geologic unit tops are reported in appendix 1 as measured depth—the depth as measured along the length of the borehole. Geologic unit tops with a depth of zero are exposed at land surface and indicate that the well spudded in the listed formation. Subsurface geologic units are listed in stratigraphic order, with stratigraphically highest units on the left and successively lower units to the right. Data columns for some formation tops are preceded by a “less than” symbol in a separate column (LT) that is used to denote cases where the top of the formation is above the start of the electric log, such that the top of the log only provides a maximum value for the drilled depth to the top of the stratigraphic unit. The symbol is listed in a separate column to avoid the appearance of non-numeric characters within the formation tops data column, facilitating use of these data within a geographic information system.

Data compiled within appendix 1 are presented as an EXCEL file that has the following information:

- API number.
- Well identifier.
- Easting, referenced to North American Datum of 1983 (NAD83).
- Northing, referenced to NAD83.
- Elevation of land surface at the well location, referenced to National Geodedic Vertical Datum of 1988 (NGVD88).
- Total depth of the well.
- Drilled depth to older alluvium, Qoa.
- Drilled depth to the Morales Formation, QTm.
- Drilled depth to the Quatal Formation, Tq.
- Drilled depth to bedrock units 1 or 2, BR1 or BR2.

Appendix 2.

Interpreted depth to top of geologic units in water wells, Cuyama Valley

Data compiled within appendix 2 include well location information and depths to geologic unit tops for older alluvium, Qoa, and the Morales Formation, QTm from water wells in the Cuyama Valley and surrounding areas. Well location data were obtained in a digital form from the US Geological Survey (USGS) National Water Information System web page (NWIS Web, *http://waterdata.usgs.gov/nwis/* accessed July 2012). Wells in appendix 2 are identified by a well identifier that take one of the following forms: (1) a well name, such as 10/25-19P1, from Upson and Worts (1951); (2) a well name, such as PT-18 or CUY-40, from Everett and others (2013); or (3) a well name, such as CUY-G-05, that is unique to this report. Some wells appear in both Upson and Worts (1951) and Everett and others and are given identifiers from both reports.

Well locations, in meters, are reported in Albers projected coordinate system, North American Datum of 1983 (NAD 83), GRS 80 spheroid. Elevation at the well location, in feet, is reported relative to mean sea level. Values are reported in feet to maintain consistency with source geologic and geophysical data for which depths are reported in feet.

All geologic unit tops are reported in appendix 2 as measured depth, the depth as measured along the length of the borehole. Geologic unit tops with a depth of zero are exposed at land surface and indicate that the well spudded in the listed formation. Some wells are interpreted to have bottomed within younger alluvium (Qya), such that the total depth of the log provides a minimum value for the drilled depth to the top of the underlying unit, Qoa. For these wells, interpreted depth to the top of Qoa is preceded by a "greater than" symbol in a separate column (GT) that is used to denote cases where the top of the formation is interpreted to lie below the bottom of the well. The symbol is listed in a separate column to avoid the appearance of non-numeric characters within the formation tops data column, facilitating use of these data within a geographic information system.

Data compiled within appendix 2 are presented as an EXCEL file that has the following information:

- Well identifier.
- Easting, referenced to North American Datum of 1983 (NAD83).
- Northing, referenced to NAD83.
- Elevation of land surface at the well location, referenced to National Geodedic Vertical Datum of 1988 (NGVD88).
- Total depth of the well.
- Drilled depth to older alluvium, Qoa.
- Drilled depth to the Morales Formation, QTm.
- Source of lithologic data.

References Cited

Everett, R.R., Gibbs, D.R., Hanson, R.T., Sweetkind, D.S., Brandt, J.T., Falk, S.E. and Harich, C.R., 2013, Geology, water-quality, hydrology, and geomechanics of the Cuyama Valley groundwater basin, California, 2008–12: U.S. Geological Survey Scientific Investigations Report 2013–5108, 62 p.

Appendix 3.

Sediment textural characteristics interpreted from electric logs from oil and gas wells, Cuyama Valley

Data compiled within appendix 3 include well location information and sediment textural characteristics as interpreted from electric logs from oil and gas wells in Cuyama Valley and surrounding areas. Well names and location data were obtained in a digital well location database from California Department of Conservation, Division of Oil, Gas and Geothermal Resources as described in appendix 1.

Interpreted sediment texture for down-hole intervals is reported along with a corresponding grain-size class. The geologic unit predicted to be present at each depth was determined by vertically intersecting the geologic framework model at the location of each well.

The EXCEL file that contains the sediment textural characteristics from oil and gas wells in Cuyama Valley has two worksheets. The first worksheet is labeled “Table A3_1 Well location” and contains the following information:

- American Petroleum Institute (API) well number.
- Well identifier, created by merging the lease name and well number.
- Easting, referenced to North American Datum of 1983 (NAD83).
- Northing, referenced to NAD83.
- Elevation of land surface at the well location, referenced to National Geodedic Vertical Datum of 1988 (NGVD88).
- Total depth of the well.

The second worksheet is labeled “Table A3_2 Texture” and contains the following information:

- API number.
- Interpreted lithology.
- Grain-size class.
- Top of interval.
- Base of interval.
- Interval thickness.
- Geologic unit from Framework.

Appendix 4.

Sediment textural characteristics interpreted from drillers’ lithologic logs from water wells, Cuyama Valley

Data compiled within appendix 4 include well location information and sediment textural characteristics as interpreted from drillers’ lithologic logs from water wells in Cuyama Valley and surrounding areas. Well names and location data were assigned in the fashion described in appendix 2.

The drillers’ lithologic description for down-hole intervals is reported along with a corresponding grain-size class and sorting parameter. Records for water wells obtained from the California Department of Water Resources are confidential. For these wells, the drillers’ lithologic descriptions were not tabulated; only the grain-size class and sorting parameter interpreted from the descriptions were tabulated. The stratigraphic unit predicted to be present at each depth was determined by vertically intersecting the geologic framework model at the location of each well.

The EXCEL file that contains the sediment textural characteristics from oil and gas wells in Cuyama Valley has two worksheets. The first worksheet is labeled “Table A4_1 Well location” and contains the following information:

- Well identifier.
- Easting, referenced to North American Datum of 1983 (NAD83).
- Northing, referenced to NAD83.
- Elevation of land surface at the well location, referenced to National Geodedic Vertical Datum of 1988 (NGVD88).
- Total depth of the well.
- Source of lithologic data.

The second worksheet is labeled “Table A4_2 Texture” and contains the following information:

- Well identifier.
- Top of interval.
- Base of interval.
- Interval thickness.
- Lithologic description.
- Grain-size class.
- Sorting.
- Geologic unit from Framework.

Prepared by the Sacramento Publishing Service Center.

For more information concerning this report, contact:

Director
U.S. Geological Survey
California Water Science Center
6000 J Street, Placer Hall
Sacramento, CA 95819
dc_ca@usgs.gov

or visit our Web site at:
http://ca.water.usgs.gov

Sweetkind and others—**Construction of 3-D Geologic Framework and Textural Models for Cuyama Valley Groundwater Basin, California**—SIR 2013-5127

science for a changing world

Prepared in cooperation with the County of Santa Barbara

Geology, Water-Quality, Hydrology, and Geomechanics of the Cuyama Valley Groundwater Basin, California, 2008–12

Scientific Investigations Report 2013–5108

U.S. Department of the Interior
U.S. Geological Survey

Cover. View of the Caliente Range, Cuyama Valley area, Santa Barbara and San Luis Obispo Counties, California. (Photography by Joseph Nawikas, U.S. Geological Survey.)

Geology, Water-Quality, Hydrology, and Geomechanics of the Cuyama Valley Groundwater Basin, California, 2008–12

By Rhett R. Everett, Dennis R. Gibbs, Randall T. Hanson, Donald S. Sweetkind, Justin T. Brandt, Sarah E. Falk, and Christopher R. Harich

Prepared in Cooperation with the County of Santa Barbara

Scientific Investigations Report 2013–5108

U.S. Department of the Interior
U.S. Geological Survey

U.S. Department of the Interior
SALLY JEWELL, Secretary

U.S. Geological Survey
Suzette M. Kimball, Acting Director

U.S. Geological Survey, Reston, Virginia: 2013

For more information on the USGS—the Federal source for science about the Earth, its natural and living resources, natural hazards, and the environment, visit *http://www.usgs.gov* or call 1–888–ASK–USGS.

For an overview of USGS information products, including maps, imagery, and publications, visit *http://www.usgs.gov/pubprod*.

To order this and other USGS information products, visit *http://store.usgs.gov*.

Suggested citation:
Everett, R.R., Gibbs, D.R., Hanson, R.T., Sweetkind, D.S., Brandt, J.T., Falk, S.E. and Harich, C.R., 2013, Geology, water-quality, hydrology, and geomechanics of the Cuyama Valley groundwater basin, California, 2008–12: U.S. Geological Survey Scientific Investigations Report 2013–5108, 62 p.

Contents

Figures

Tables

Conversion Factors, Datums, and Abbreviated Water-Quality Units

Inch/Pound to SI

Multiply	By	To obtain
	Length	
inch (in)	2.54	centimeter (cm)
foot (ft)	0.3048	meter (m)
mile (mi)	1.609	kilometer (km)
yard (yd)	0.9144	meter (m)
	Area	
acre	4,047	square meter (m^2)
square foot (ft^2)	0.09290	square meter (m^2)
square mile (mi^2)	2.590	square kilometer (km^2)
	Volume	
ounce, fluid (fl. oz)	0.02957	liter (L)
gallon (gal)	3.785	liter (L)
cubic inch (in^3)	16.39	cubic centimeter (cm^3)
cubic foot (ft^3)	0.02832	cubic meter (m^3)
acre-foot (acre-ft)	1,233	cubic meter (m^3)
	Flow rate	
acre-foot per day (acre-ft/d)	0.01427	cubic meter per second (m^3/s)
acre-foot per year (acre-ft/yr)	1,233	cubic meter per year (m^3/yr)
foot per second (ft/s)	0.3048	meter per second (m/s)
foot per minute (ft/min)	0.3048	meter per minute (m/min)
cubic foot per second (ft^3/s)	0.02832	cubic meter per second (m^3/s)
gallon per minute (gal/min)	0.06309	liter per second (L/s)
	Radioactivity	
picocurie per liter (pCi/L)	0.037	becquerel per liter (Bq/L)
	Specific capacity	
gallon per minute per foot [(gal/min)/ft)]	0.2070	liter per second per meter [(L/s)/m]
	Hydraulic conductivity	
foot per day (ft/d)	0.3048	meter per day (m/d)
	Hydraulic gradient	
foot per mile (ft/mi)	0.1894	meter per kilometer (m/km)
	Transmissivity*	
foot squared per day (ft^2/d)	0.09290	meter squared per day (m^2/d)

Temperature in degrees Celsius (°C) may be converted to degrees Fahrenheit (°F) as follows:

°F=(1.8×°C)+32

Temperature in degrees Fahrenheit (°F) may be converted to degrees Celsius (°C) as follows:

°C=(°F-32)/1.8

Vertical coordinate information is referenced to the North American Vertical Datum of 1988 (NAVD 88).

Horizontal coordinate information is referenced to the North American Datum of 1983 (NAD 83).

Altitude, as used in this report, refers to distance above the vertical datum.

Water-level measurements in this report are given in feet with reference to land-surface datum (lsd). Land-surface datum is a datum plane that is approximately at land surface at each well.

*Transmissivity: The standard unit for transmissivity is cubic foot per day per square foot times foot of aquifer thickness [(ft^3/d)/ft^2]ft. In this report, the mathematically reduced form, foot squared per day (ft^2/d), is used for convenience.

Specific conductance is given in microsiemens per centimeter at 25 degrees Celsius (µS/cm at 25 °C).

Concentrations of chemical constituents in water are given either in milligrams per liter (mg/L) or micrograms per liter (µg/L) which are equivalent to parts per million (ppm) or parts per billion (ppb), respectively.

Activities of radiochemical constituents in water are given in picocuries per liter (pCi/L).

Results for stable isotopes in water are reported in delta notation , *iE*, where the ratio of the rarer isotope of an element (*iE*) is expressed relative to the more common lighter isotope of that element, relative to a standard reference material, and expressed in *per mil*.

Abbreviations and Acronyms

bls	below land surface
CSU	combined standard uncertainty
CUY	Cuyama Valley study well
CVBR	Cuyama Valley Bell Road
CVFR	Cuyama Valley Foothill Road
CVKR	Cuyama Valley Kirschenmann Road
GPS	Global Positioning System
MCL	maximum contaminant level
MCL-US	maximum contaminant level (USEPA)
LSD	land surface datum
NWIS	National Water Information System (USGS)
OEHHA-PHG	Office of Environmental Health Hazard Assessment public health goal
SMCL	secondary maximum contaminant level
SMCL-CA	California Department of Public Health secondary maximum contaminant level
SMCL-US	secondary maximum contaminant level (USEPA)
U.S.	United States
USEPA	United States Environmental Protection Agency
USGS	United States Geological Survey

Acknowledgements

This study could not have been accomplished without the assistance of personnel from the Santa Barbara County Water Agency. In addition, we acknowledge the valuable participation of the residents and well owners of the Cuyama Valley who assisted in the study.

Finally, we acknowledge the valuable guidance of U.S. Geological Survey geologists and geophysicists of the Earth Surface Processes Group, Earthquake Hazards Group, Coastal Marine Geology Group, and Urban Hazards Group and thank them for their efforts supporting the selection of sites, collection of data, and subsequent analysis.

x

Geology, Water-Quality, Hydrology, and Geomechanics of the Cuyama Valley Groundwater Basin, California, 2008–12

By Rhett R. Everett, Dennis R. Gibbs, Randall T. Hanson, Donald S. Sweetkind, Justin T. Brandt, Sarah E. Falk, and Christopher R. Harich

Abstract

To assess the water resources of the Cuyama Valley groundwater basin in Santa Barbara County, California, a series of cooperative studies were undertaken by the U.S. Geological Survey and the Santa Barbara County Water Agency. Between 2008 and 2012, geologic, water-quality, hydrologic and geomechanical data were collected from selected sites throughout the Cuyama Valley groundwater basin.

Geologic data were collected from three multiple-well groundwater monitoring sites and included lithologic descriptions of the drill cuttings, borehole geophysical logs, temperature logs, as well as bulk density and sonic velocity measurements of whole-core samples.

Generalized lithologic characterization from the monitoring sites indicated the water-bearing units in the subsurface consist of unconsolidated to partly consolidated sand, gravel, silt, clay, and occasional cobbles within alluvial fan and stream deposits. Analysis of geophysical logs indicated alternating layers of finer- and coarser-grained material that range from less than 1 foot to more than 20 feet thick. On the basis of the geologic data collected, the principal water-bearing units beneath the monitoring-well sites were found to be composed of younger alluvium of Holocene age, older alluvium of Pleistocene age, and the Tertiary-Quaternary Morales Formation. At all three sites, the contact between the recent fill and younger alluvium is approximately 20 feet below land surface.

Water-quality samples were collected from 12 monitoring wells, 27 domestic and supply wells, 2 springs, and 4 surface-water sites and were analyzed for a variety of constituents that differed by site, but, in general, included trace elements; nutrients; dissolved organic carbon; major and minor ions; silica; total dissolved solids; alkalinity; total arsenic and iron; arsenic, chromium, and iron species; and isotopic tracers, including the stable isotopes of hydrogen and oxygen, activities of tritium, and carbon-14 abundance.

Of the 39 wells sampled, concentrations of total dissolved solids and sulfate from 38 and 37 well samples, respectively, were greater than the U.S. Environmental Protection Agency's secondary maximum contaminant levels. Concentrations greater than the maximum contaminant levels for nitrate were observed in five wells and were observed for arsenic in four wells.

Differences in the stable-isotopic values of hydrogen and oxygen among groundwater samples indicated that water does not move freely between different formations or between different zones within the Cuyama Valley. Variations in isotopic composition indicated that recharge is derived from several different sources. The age of the groundwater, expressed as time since recharge, was between 600 and 38,000 years before present. Detectable concentrations of tritium indicated that younger water, recharged since the early 1950s, is present in parts of the groundwater basin.

Hydrologic data were collected from 12 monitoring wells, 56 domestic and supply wells, 3 surface-water sites, and 4 rainfall-gaging stations. Rainfall in the valley averaged about 8 inches annually, whereas the mountains to the south received between 12 and 19 inches. Stream discharge records showed seasonal variability in surface-water flows ranging from no-flow to over 1,500 cubic feet per second. During periods when inflow to the valley exceeds outflow, there is potential recharge from stream losses to the groundwater system.

Water-level records included manual quarterly depth-to-water measurements collected from 68 wells, time-series data collected from 20 of those wells, and historic water levels from 16 wells. Hydrographs of the manual measurements showed declining water levels in 16 wells, mostly in the South-Main zone, and rising water levels in 14 wells, mostly in the Southern Ventucopa Uplands. Time-series hydrographs showed daily, seasonal, and longer-term effects associated with local pumping. Water-level data from the multiple-well monitoring sites indicated seasonal fluctuations as great as 80 feet and water-level differences between aquifers as great as 40 feet during peak pumping season. Hydrographs from the multiple-well groundwater monitoring sites showed vertical hydraulic gradients were upward during the winter months and downward during the irrigation season. Historic hydrographs showed water-level declines in the Southern-Main, Western Basin, Caliente Northern-Main, and Southern Sierra Madre zone ranging from 1 to 7 feet per year. Hydrographs of wells in the Southern Ventucopa Uplands zone showed several years with marked increases in water levels that corresponded to increased precipitation in the Cuyama Valley.

Investigation of hydraulic properties included hydraulic conductivity and transmissivity estimated from aquifer tests performed on 63 wells. Estimates of horizontal hydraulic

conductivity ranged from about 1.5 to 28 feet per day and decreased with depth. The median estimated hydraulic conductivity for the older alluvium was about five times that estimated for the Morales Formation. Estimates of transmissivity ranged from 560 to 163,400 gallons per day per foot and decreased with depth. The median estimated transmissivity for the younger alluvium was about three times that estimated for the older alluvium.

Geomechanical analysis included land-surface elevation changes at five continuously operating global positioning systems (GPS) and land-subsidence detection at five interferometric synthetic aperture radar (InSAR) reference points. Analysis of data collected from continuously operating GPS stations showed the mountains to the south and west moved upward about 1 millimeter (mm) annually, whereas the station in the center of the Southern-Main zone moved downward more than 7 mm annually, indicating subsidence. It is likely that this subsidence is inelastic (permanent) deformation and indicates reduced storage capacity in the aquifer sediments. Analysis of InSAR data showed local and regional changes that appeared to be dependent, in part, on the time span of the interferogram, seasonal variations in pumping, and tectonic uplift. Long-term InSAR time series showed a total maximum detected subsidence rate of approximately 12 mm per year at one location and approximately 8 mm per year at a second location, while short-term InSAR time series showed maximum subsidence of about 15 mm at one location and localized maximum uplift of about 10 mm at another location.

Introduction

Currently, groundwater is the sole source of water supply in the Cuyama Valley (fig. 1). Groundwater withdrawals, mainly for the irrigation of agricultural crops, have resulted in water-level declines of as much as 300 ft in some areas since the 1940s (California Department of Water Resources, 1998). The Cuyama Valley groundwater basin was identified in 1980 by the California Department of Water Resources (CA DWR) to be in the “critical condition of overdraft,” which indicates that a “continuation of present water management practices would probably result in significant adverse overdraft-related environmental, social or economic impact” (California Department of Water Resources, 2003). To provide for sustained beneficial use, it is necessary to define groundwater availability with respect to quantity and quality and to establish tools to allow water users and managers to efficiently utilize the available groundwater resources. The U.S. Geological Survey (USGS), in cooperation with the Santa Barbara County Water Agency, began a study in 2008 to assess the water resources of the Cuyama Valley groundwater basin. The study included a monitoring component (described in this report), a modeling component and a geologic framework component (presented in Sweetkind and others, 2013). As part of this study, the existing monitoring and modeling tools are being updated to provide water managers with the data and resources necessary to address the water-management issues.

Purpose and Scope

The primary purpose of this report is to present selected data that describe current groundwater conditions of the major aquifers in the Cuyama Valley groundwater basin. This report presents a summary of lithologic, geologic, geophysical, water-quality, hydrologic, and land-deformation data collected at three new multiple-well monitoring sites, selected domestic and supply wells (irrigation-supply and municipal-supply), springs, streams and various other sites in the Cuyama Valley during 2008–12. In addition to a summary of data collection, this report includes initial interpretations from these data. Geologic interpretation includes the depths of formation contacts based on lithologic and geophysical data collected at the multi-well monitoring sites. Water-quality interpretations include age dating and isotopic analysis. Hydrologic interpretations include definition of the depths of increased groundwater flow, determination of sources of recharge, and estimation of hydraulic properties. Interpretations of land deformation data include estimating the rate and cause of changes in land-surface elevation.

Description of Study Area

The Cuyama Valley groundwater basin is approximately 40 miles (mi) west of Bakersfield, California, in the southern Coast Ranges physiographic province (fig. 1). The 230 square mile (mi^2) basin lies near the intersection of San Luis Obispo, Santa Barbara, Ventura, and Kern counties. The Coast Ranges province lies west of the Great Valley and north of the west-trending Transverse Ranges. Although within the Coast Ranges, the Cuyama Valley has many of the climatic features of a desert basin, because it is surrounded by relatively high mountains. The Cuyama Valley basin is characterized by hot, dry summers and cold winters. Rainfall averages from 7 to 15 inches per year (in/yr) on the valley floor (California Department of Water Resources, 2003) to about 24 to 30 in/yr in the mountain headwaters of the Cuyama River and along the crest of the Sierra Madre Mountains.

Geologic Units

The Cuyama Valley groundwater basin is underlain by a sequence of unconsolidated to partly consolidated non-marine deposits including the Pliocene to Pleistocene Morales Formation and Pleistocene to recent alluvial and fluvial deposits (Hill and others, 1958; DeLong and others, 2008). These deposits unconformably overlie a late Cretaceous to middle Cenozoic succession of consolidated marine and non-marine sedimentary rocks, which in turn overlie crystalline granitic and gneissic rocks at depth (Hill and others, 1958; Lagoe, 1987). In terms of water-bearing properties, the

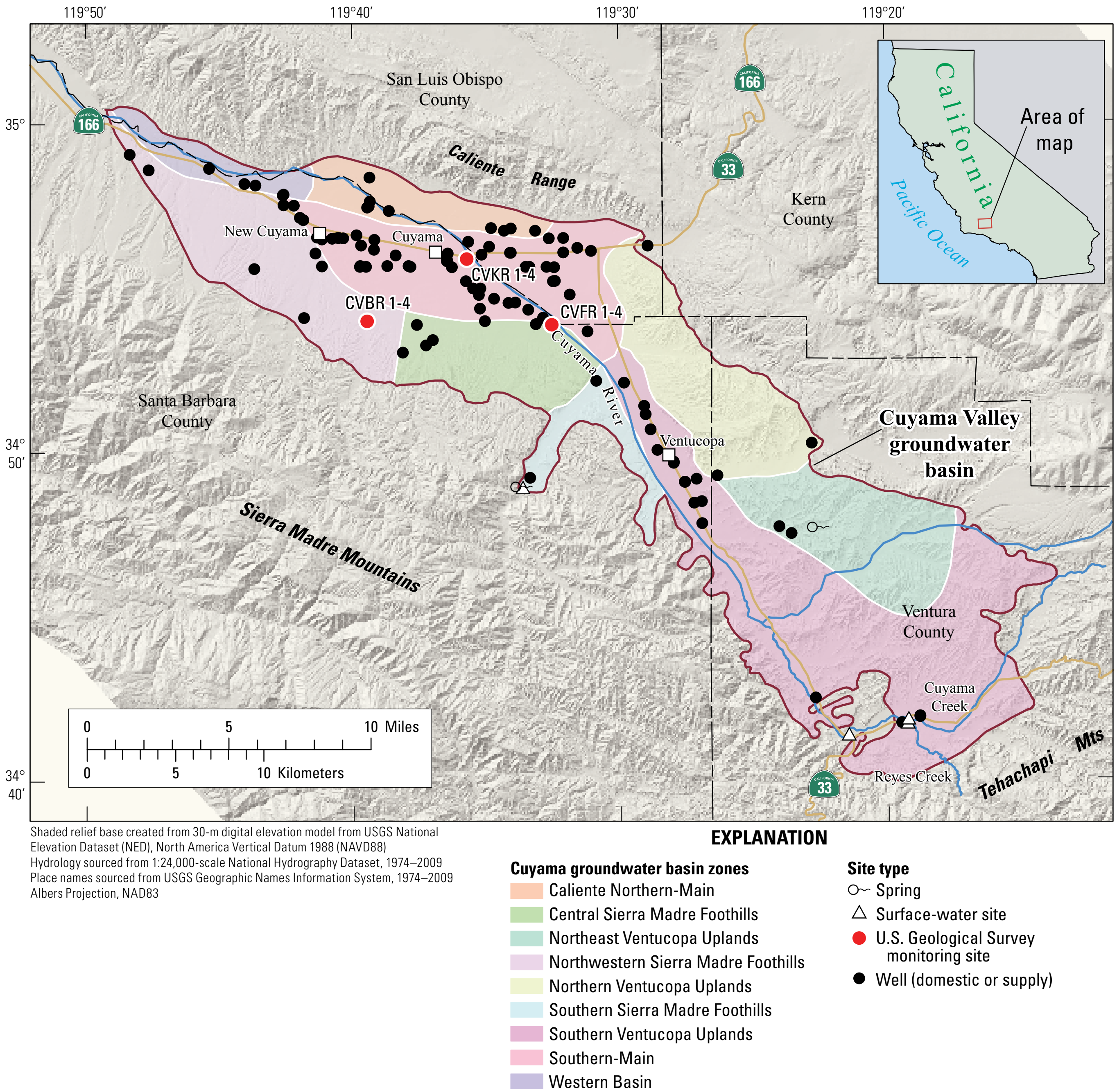

Figure 1. The location of Cuyama Valley, including multiple-well monitoring sites, selected domestic and supply wells, and hydrologic units, Cuyama Valley, Santa Barbara County, California.

geology of the Cuyama Valley can be generalized into four main units: (1) non-water-bearing rocks—the crystalline granitic rocks and all consolidated sedimentary rocks older than the Morales Formation, (2) the Morales Formation, (3) older alluvium of Pleistocene age, and (4) younger alluvium of Holocene age (Upson and Worts, 1951; Singer and Swarzenski, 1970). The aquifer system that is made up of the water-bearing portions of units 2–4 is described in more detail in the "Aquifer System" section.

The Morales Formation (QTm, fig. 2) is a Pliocene-Pleistocene fluvial deposit that is up to 5,000 feet thick and consists of massive- to thick-bedded, partly consolidated deposits of clay, silt, sand, and gravel (Hill and others, 1958; Ellis and others, 1993). The Morales Formation is widely exposed as badland topography to the east of the Cuyama River in the Ventucopa area (Dibblee, 1982; Dibblee and Minch, 2006; Kellogg and others, 2008). The geologic mapping of Dibblee (Dibblee, 1973; Dibblee and Minch, 2005 and 2006) included all young, deformed, non-marine

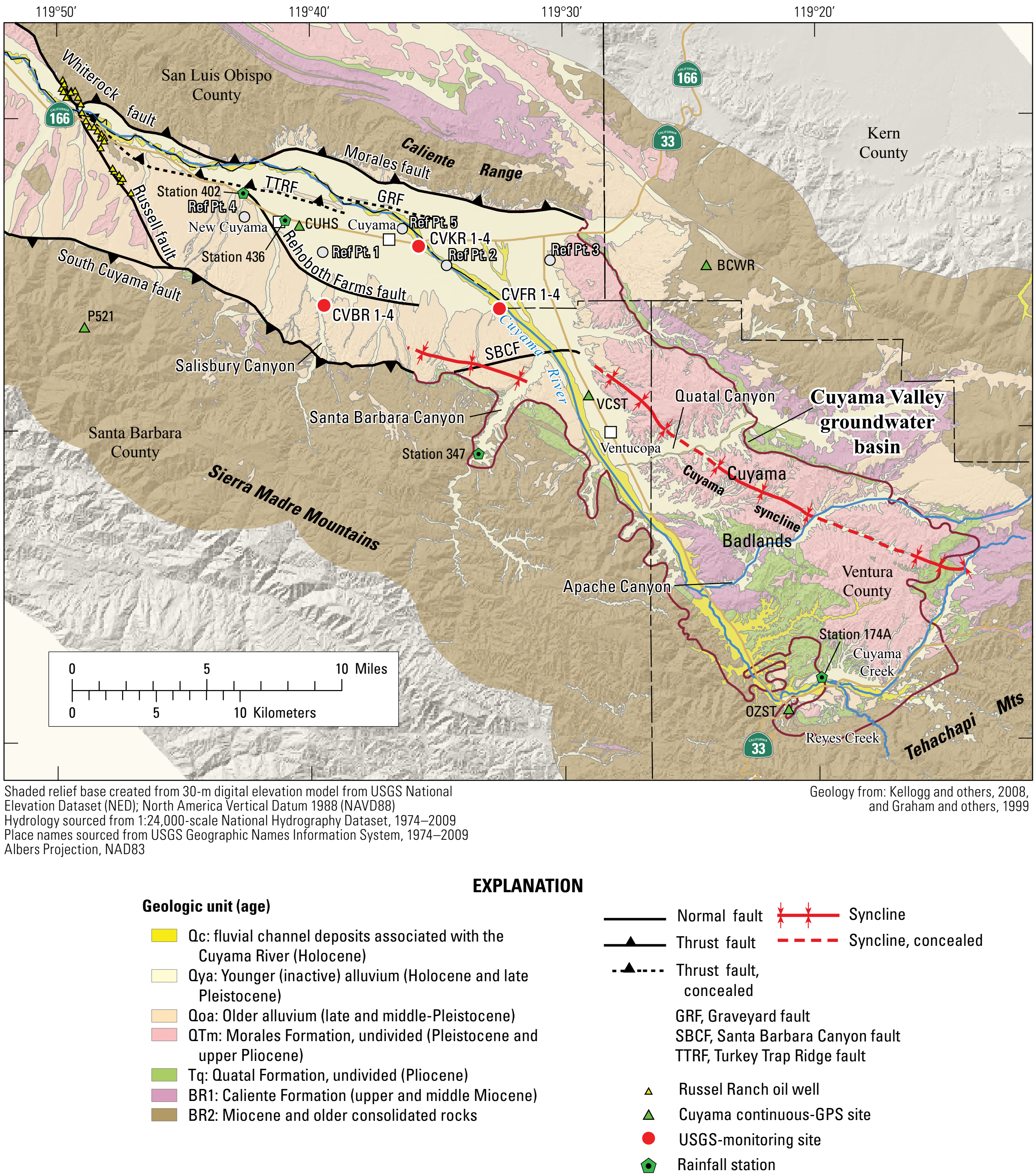

Figure 2. Geologic formation outcrops, faults, folds, InSAR reference points, continuously operating GPS stations, oil wells, and rainfall stations, Cuyama Valley, Santa Barbara County, California.

sediments of the Cuyama area in the Morales Formation; these maps portray the piedmont upland area along the south edge of the Cuyama Valley as being composed of exposed outcrops of Morales Formation. Subsequent workers (Vedder, 1968; Vedder and Repenning, 1975; Schwing, 1984; Spitz, 1986) classified the upper part of Dibblee's Morales Formation as "deformed older Quaternary alluvium." Using this classification, the Morales Formation is hundreds to greater than 1,000 ft below the surface on the south side of Cuyama Valley, rather than exposed at the surface.

Older alluvium (Qoa, fig. 2) consists of unconsolidated to partly consolidated sand, gravel, and boulders, with some clay (Vedder and Repenning, 1975; DeLong and others, 2008). The percentage of clay increases in the western part of the valley (Singer and Swarzenski, 1970; DeLong and others, 2008). Interpretation of geophysical logs from oil exploration wells indicated that this unit is typically 400 to 600 feet thick, but is as thick as 1,000 feet near the axis of Cuyama Valley (Schwing, 1984; Spitz, 1986). In the study area, older alluvium includes dissected alluvial fans, colluvial deposits, and sediments on multiple terraces and alluvial surfaces (Hill and others, 1958; DeLong and others, 2008). Older alluvial deposits are slightly deformed and are probably of late Pleistocene age, although in some places they could be Holocene (Vedder, 1968; DeLong and others, 2008). Older alluvium is exposed on the piedmont uplands along the south side of Cuyama Valley and locally at two fault-bounded ridges in the center of the valley (Vedder and Repenning, 1975; DeLong and others, 2008).

Younger alluvium (Qya, fig. 2) consists of unconsolidated sand, gravel, and boulders, with some clay deposited as alluvium in stream channels, floodplains, alluvial fans, and stream terraces. The unit is mainly Holocene in age, but locally can be late Pleistocene in part. Active stream deposits consist of river-bed gravels of the Cuyama River and other active channels (Vedder and Repenning, 1975; DeLong and others, 2008).

Geologic Structure

During Miocene and older time, the Cuyama Valley groundwater basin was the site of extensional and strike-slip deformation; older, inactive faults were buried by the Morales Formation and younger units (Yeats and others, 1989; fig. 2). During the Pliocene-Pleistocene, structural deformation of the Cuyama Valley changed to a predominantly compressional mode, resulting in the formation of folds and folding and thrust faults (Davis and others, 1988).

As a result of compression, the Cuyama Valley is currently a downfolded basin bounded to the north and south by faults. Miocene rocks of the Caliente Range to the north of Cuyama Valley are being thrust southward over older and younger alluvium on the Morales and Whiterock thrusts; similar-aged rocks in the Sierra Madre to the south of Cuyama Valley are being thrust northward over older alluvium on the South Cuyama fault (Vedder and Repenning, 1975; Davis and others, 1988; fig. 2).

The Morales Formation and older alluvium are deformed into tight synclines along the north and south margins of the basin near the bounding thrust faults (Spitz, 1986; Kellogg and others, 2008). The eastern part of the basin is underlain by the Cuyama syncline; its strike is parallel to the valley axis and the fold plunges toward the northwest (Ellis, 1994; Dibblee and Minch, 2006; Kellogg and others, 2008). The fold is exposed in outcrops in the Ventucopa area and the Cuyama Badlands to the east; beneath the central part of the valley, it is buried but known to be present from subsurface data from oil exploration wells (Spitz, 1986; Ellis, 1994).

Several ridges of older alluvium are mapped in the center of the Cuyama Valley, north of Highway 166 (Vedder and Repenning, 1975), on the north side on the Turkey Trap Ridge and Graveyard faults (fig. 2). These ridges trend slightly north-northwest and are oriented in a right-stepping, en echelon pattern. Upson and Worts (1951) suggested that these ridges were fault-related on the basis of their orientation and the presence of springs along the ridges. Vedder and Repenning (1975) mapped inferred reverse faults associated with these ridges; the faults cut alluvium and bring older alluvium to the surface. Seismic profiles collected across these ridges indicate that these faults cut the Morales Formation (Ellis, 1994), although their ultimate downdip projection is unknown.

Other faults, not obviously related to the overall compressional tectonics that affect the basin, have been inferred in the subsurface, primarily, on the basis of marked differences in water levels over short distances. One such fault (SBCF on fig. 2) is inferred to trend northeast-southwest near the mouth of the Santa Barbara Canyon (Singer and Swarzenski, 1970); similarly aligned structures are mapped in the piedmont upland to the west of Santa Barbara Canyon (Dibblee and Minch, 2007). Another fault (Rehoboth Farms fault on fig. 2) inferred to exist on the basis of water-level changes is in the west-central part of the valley; the inferred fault trends northwest-southeast near the town of New Cuyama and projects southeastward beneath the Salisbury Canyon drainage (Lane-Western Company, written commun., 1982).

Aquifer System

The main water-bearing deposits in the study area are the saturated portions of the younger and older alluvium and the Morales Formation (fig. 2). All rocks that are older than the Morales Formation were considered by previous investigators to be non-water-bearing (Upson and Worts, 1951; Singer and Swarzenski, 1970). The regional flow pattern of groundwater under natural conditions is northwestward, parallel to the central axis of the basin, similar to the orientation of the overlying Cuyama River, with a substantial component of flow northward from the Sierra Madre Mountains (Singer and Swarzenski, 1970). Historically, most of the water pumped from the study area was from the younger and older alluvium. Inspection of available geologic and geophysical logs indicated that the hydraulic conductivity, in general, decreases with depth.

Large-capacity wells perforated in the alluvium yield 1,000–3,000 gallons per minute (gpm) and have specific capacities of that range from 100 to 200 gpm per foot (Singer and Swarzenski, 1970). Yield and specific capacities generally tend to decrease with depth. Wells perforated in the younger alluvium have a median yield of 1,800 gpm and median specific capacity of 60 gpm per foot. Wells perforated in both the younger and older alluvium have a median yield of 1,200 gpm and median specific capacity of 40 gpm per foot. Wells perforated in the older alluvium have a median yield of 620 gpm and median specific capacity of 20 gpm per foot. Yield and specific capacities are less on the western half of the valley compared to the eastern half, indicating a spatial trend; however, a greater percentage of wells in the western part are perforated in the older alluvium.

The water-bearing properties of the Morales Formation are not well defined, but available data indicate that the hydraulic conductivity of the formation varies greatly both areally and with depth.

Wells perforated in the Morales Formation in the western part of the valley have specific capacities of 5–25 gpm per foot, whereas those in the north-central part of the valley have specific capacities of 25–50 gpm per foot (Singer and Swarzenski, 1970). Inspection of available geologic and geophysical logs indicated that the hydraulic conductivity of the Morales Formation decreases with depth.

Several faults that offset the basin-fill deposits, associated with measured water-level offsets, are inferred to impede groundwater movement (Upson and Worts, 1951; Singer and Swarzenski, 1970; fig. 2). Because the faults do not intersect land surface and are not readily apparent in the unconsolidated surface sediments, their locations have been inferred from well data and topographic features. The Graveyard and Turkey Trap Ridges faults on the northern side of the Cuyama Valley (fig. 2) are postulated from groundwater data by Upson and Worts (1951) and shown on the geologic map of Vedder and Repenning (1975). A fault on the south side of the basin, here called the Santa Barbara Canyon fault (fig. 2), was suggested by Singer and Swarzenski (1970) to be the cause of a steep hydraulic gradient in this part of Cuyama Valley, where water levels in the vicinity of Ventucopa were observed to be 100 feet higher than water levels 2 miles to the north. The fault is mapped in the uplifted piedmont older alluvium to the west of Santa Barbara Canyon (Dibblee and Minch, 2007) and is visible in outcrops to the west of the Cuyama River, but is not readily projected to the eastern side of the Cuyama River on the basis of geologic data. Water-level offsets along the valley were used to infer the location of the fault in the sediment (Sweetkind, 2013).

Historically, flowing springs were found along the trace of faults that parallel Graveyard and Turkey Trap Ridges (Santa Barbara County Planning and Development Department, 1994), and other springs have been reported along the South Cuyama and Santa Barbara fault. While many of the springs and seeps that flowed in 1946 have since dried up (Singer and Swarzenski, 1970), several springs still have seasonal flow. Two springs, one in the Southern Sierra Madre Foothills zone and another in the Northern Ventucopa Uplands zone (fig. 1), were sampled during the study.

This study required a better delineation of the groundwater basin than previously available. The basin was divided into nine groundwater subregional hydrologic zones (fig. 1). These zones separate the aquifers into regions that are fault bounded and where the response to the use, movement, and consumption of water is similar in specific parts of the aquifers, but differs from the other zones. In this context, Cuyama Valley can be considered a collection of zones that are partially connected, but have different geologic boundaries, hydrologic features and hydraulic properties, water quality and age of groundwater, and dominant aquifers that respond to natural and anthropogenic stresses differently.

Accessing Data

Users of the data presented in this report are encouraged to access information through the USGS National Water Information System (NWIS) web page (NWIS Web) at *http://waterdata.usgs.gov/nwis/*. NWIS Web serves as an interface to a database of site information and groundwater, surface-water, and water-quality data collected throughout the 50 states and elsewhere. NWIS Web is updated from the database on a regularly scheduled basis. Data can be retrieved by category and geographic area, and the retrieval can be selectively refined by a specific location or parameter field. NWIS Web can output water-level and water-quality graphs, site maps, and data tables (in HTML and ASCII format) and can be used to develop site-selection lists. Updates to data presented in this report after publication will be made to the NWIS. Additional data could be available on the project web site at *http://ca.water.usgs.gov/projects/cuyama/*. Formal requests for specific data may be directed to the U.S. Geological Survey California Water Science Center, Public Information Officer in Sacramento, California.

Description of the Monitoring Network

Most information presented in this report focuses on three multiple-well monitoring sites installed between December 2008 and October 2009 within the study area (fig. 1). Data collected from the monitoring sites provided information on vertical differences in hydraulic properties, water levels, and water chemistry at the same location; these data can be used to characterize the three-dimensional groundwater system. Existing wells (domestic and supply) were incorporated into the monitoring network to help meet additional needs (fig. 1). Table 1 lists all wells referenced in this report, including information on the well location by zone, and data collected from each well site. Well-identification and well-construction information for groundwater wells in the monitoring network are presented in table 2. Supporting data were collected from four surface-water sites and two springs; related site-identification information and available data for these sites are presented in table 3.

Table 1. Selected characteristics and data availability for wells in the Cuyama Valley groundwater basin, Santa Barbara County, California.

[See figures 1, 8, 15, and 25 for well locations. **Abbreviations**: CVKR, Cuyama Valley Kirschenmann Road; CVBR, Cuyama Valley Bell Road, CVFR, Cuyama Valley Foothill Road; CUY, Cuyama Valley study well; PT, Pump test well; x, data are available; —, data not available]

Common well name	Site identification number	Cuyama groundwater-basin zones	Water-quality data	Discrete (manual) water-level measurements	Time-series (automated) water-level measurements	Aquifer-test data
CVKR-1	345552119354201	Southern-Main	x	x	x	x
CVKR-2	345552119354202	Southern-Main	x	x	x	x
CVKR-3	345552119354203	Southern-Main	x	x	x	x
CVKR-4	345552119354204	Southern-Main	x	x	x	x
CVBR-1	345359119392701	Northwestern Sierra Madre Foothills	x	x	x	x
CVBR-2	345359119392702	Northwestern Sierra Madre Foothills	x	x	x	x
CVBR-3	345359119392703	Northwestern Sierra Madre Foothills	x	x	x	x
CVBR-4	345359119392704	Northwestern Sierra Madre Foothills	x	x	x	x
CVFR-1	345351119323101	Central Sierra Madre Foothills	x	x	x	x
CVFR-2	345351119323102	Central Sierra Madre Foothills	x	x	x	x
CVFR-3	345351119323103	Central Sierra Madre Foothills	x	x	x	x
CVFR-4	345351119323104	Central Sierra Madre Foothills	x	x	x	x
CUY-01	345838119452001	Western Basin	x	x	—	—
CUY-02	345603119411901	Northwestern Sierra Madre Foothills	x	x	x	—
CUY-03	345100119290001	Southern Ventucopa Uplands	x	x	—	—
CUY-04	345602119362401	Southern-Main	x	x	x	—
CUY-05	345600119400001	Southern-Main	x	x	x	—
CUY-06	345300119310001	Southern-Main	x	x	—	—
CUY-07	345538119332201	Southern-Main	x	x	x	—
CUY-08	345405119325101	Southern-Main	x	x	—	—
CUY-11	344143119193001	Southern Ventucopa Uplands	x	x	—	—
CUY-12	345100119290002	Southern Ventucopa Uplands	x	x	x	—
CUY-13	344910119270501	Southern Ventucopa Uplands	x	x	—	—
CUY-14	345338119324801	Central Sierra Madre Foothills	x	—	—	—
CUY-16	345540119410901	Northwestern Sierra Madre Foothills	x	x	—	—
CUY-17	344729119233501	Northeast Ventucopa Uplands	x	x	—	—
CUY-18	344859119280801	Southern Ventucopa Uplands	x	x	—	—
CUY-19	345003119283501	Southern Ventucopa Uplands	x	x	—	—
CUY-20	345615119285501	Outside basin boundary	x	x	—	—
CUY-21	345359119350201	Central Sierra Madre Foothills	x	x	—	—
CUY-22	345552119362901	Southern-Main	x	x	—	—
CUY-23	345539119393901	Southern-Main	x	x	—	—
CUY-24	345325119365603	Central Sierra Madre Foothills	x	x	—	—
CUY-25	345302119380701	Central Sierra Madre Foothills	x	x	—	—
CUY-26	345753119421701	Western Basin	x	x	—	—
CUY-27	345539119394001	Southern-Main	—	x	—	—
CUY-28	344900119332201	Southern Sierra Madre Foothills	x	—	—	—
CUY-30	344156119184801	Southern Ventucopa Uplands	—	x	—	—
CUY-31	344154119184801	Southern Ventucopa Uplands	—	x	—	—
CUY-32	344231119224101	Southern Ventucopa Uplands	—	x	—	—
CUY-33	344828119265301	Southern Ventucopa Uplands	—	x	—	—
CUY-34	344843119272401	Southern Ventucopa Uplands	—	x	—	—
CUY-35	344825119271001	Southern Ventucopa Uplands	—	x	x	—

Table 1. Selected characteristics and data availability for wells in the Cuyama Valley groundwater basin, Santa Barbara County, California.—Continued

[See figures 1, 8, 15, and 25 for well locations. **Abbreviations**: CVKR, Cuyama Valley Kirschenmann Road; CVBR, Cuyama Valley Bell Road, CVFR, Cuyama Valley Foothill Road; CUY, Cuyama Valley study well; PT, Pump test well; x, data are available; —, data not available]

Common well name	Site identification number	Cuyama groundwater-basin zones	Water-quality data	Discrete (manual) water-level measurements	Time-series (automated) water-level measurements	Aquifer-test data
CUY-36	344742119240201	Northeast Ventucopa Uplands	—	x	—	—
CUY-38	345040119285101	Southern Ventucopa Uplands	—	x	—	—
CUY-39	344944119275701	Southern Ventucopa Uplands	—	x	—	—
CUY-40	344939119275901	Southern Ventucopa Uplands	—	x	—	—
CUY-42	344904119273101	Southern Ventucopa Uplands	—	x	—	—
CUY-43	344904119273401	Southern Ventucopa Uplands	—	x	—	—
CUY-44	344915119262001	Northern Ventucopa Uplands	—	x	—	—
CUY-45	345209119304901	Southern Sierra Madre Foothills	—	x	—	—
CUY-46	345206119294701	Southern Ventucopa Uplands	—	x	—	—
CUY-47	344940119330501	Southern Sierra Madre Foothills	—	x	—	—
CUY-48	345315119371501	Central Sierra Madre Foothills	—	x	—	—
CUY-49	345353119373601	Central Sierra Madre Foothills	—	x	—	—
CUY-50	345600119351001	Southern-Main	—	x	—	—
CUY-51	345606119310301	Southern-Main	—	x	—	—
CUY-52	345511119322801	Southern-Main	—	x	—	—
CUY-53	345447119315101	Southern-Main	—	x	—	—
CUY-54	345512119354101	Southern-Main	—	x	—	—
CUY-55	345631119402901	Southern-Main	—	x	x	—
CUY-56	345709119415501	Southern-Main	—	x	—	—
CUY-57	345618119393701	Southern-Main	—	x	—	—
CUY-58	345540119394301	Southern-Main	—	x	—	—
CUY-59	345538119374601	Southern-Main	—	x	—	—
CUY-60	345808119433501	Western Basin	—	x	x	—
CUY-61	345604119340201	Southern-Main	x	—	—	—
CUY-62	345822119391801	Caliente Northern-Main	—	x	—	—
CUY-63	345721119383401	Caliente Northern-Main	x	—	—	—
CUY-64	345540119384201	Southern-Main	x	—	—	—
CUY-73	345014119224901	Northern Ventucopa Uplands	—	x	—	—
CUY-74	344749119265301	Southern Ventucopa Uplands	—	x	—	—
CUY-75	345637119394701	Southern-Main	—	x	—	—
PT-01	—	Southern-Main	—	—	—	x
PT-02	—	Southern-Main	—	—	—	x
PT-03	—	Caliente Northern-Main	—	—	—	x
PT-04	—	Caliente Northern-Main	—	—	—	x
PT-05	—	Caliente Northern-Main	—	—	—	x
PT-07	—	Southern-Main	—	—	—	x
PT-08	—	Southern-Main	—	—	—	x
PT-09	—	Southern-Main	—	—	—	x
PT-10	—	Southern-Main	—	—	—	x
PT-11	—	Southern-Main	—	—	—	x
PT-12	—	Southern-Main	—	—	—	x
PT-13	—	Southern-Main	—	—	—	x
PT-14	—	Southern-Main	—	—	—	x
PT-15	—	Southern-Main	—	—	—	x

Table 1. Selected characteristics and data availability for wells in the Cuyama Valley groundwater basin, Santa Barbara County, California.—Continued

[See figures 1, 8, 15, and 25 for well locations. **Abbreviations**: CVKR, Cuyama Valley Kirschenmann Road; CVBR, Cuyama Valley Bell Road, CVFR, Cuyama Valley Foothill Road; CUY, Cuyama Valley study well; PT, Pump test well; x, data are available; —, data not available]

Common well name	Site identification number	Cuyama groundwater-basin zones	Water-quality data	Discrete (manual) water-level measurements	Time-series (automated) water-level measurements	Aquifer-test data
PT-16	—	Southern-Main	—	—	—	x
PT-17	—	Southern-Main	—	—	—	x
PT-18	—	Southern-Main	—	—	—	x
PT-19	—	Southern-Main	—	—	—	x
PT-20	—	Southern-Main	—	—	—	x
PT-21	—	Southern-Main	—	—	—	x
PT-22	—	Southern-Main	—	—	—	x
PT-23	—	Southern-Main	—	—	—	x
PT-24	—	Southern-Main	—	—	—	x
PT-25	—	Central Sierra Madre Foothills	—	—	—	x
PT-26	—	Southern-Main	—	—	—	x
PT-27	—	Caliente Northern-Main	—	—	—	x
PT-28	—	Caliente Northern-Main	—	—	—	x
PT-30	—	Southern-Main	—	—	—	x
PT-31	—	Southern-Main	—	—	—	x
PT-32	—	Southern-Main	—	—	—	x
PT-34	—	Southern-Main	—	—	—	x
PT-35	—	Southern-Main	—	—	—	x
PT-36	—	Southern-Main	—	—	—	x
PT-37	—	Southern-Main	—	—	—	x
PT-38	—	Southern-Main	—	—	—	x
PT-39	—	Southern-Main	—	—	—	x
PT-40	—	Southern-Main	—	—	—	x
PT-41	—	Southern-Main	—	—	—	x
PT-42	—	Southern-Main	—	—	—	x
PT-43	—	Southern-Main	—	—	—	x
PT-44	—	Southern-Main	—	—	—	x
PT-45	—	Southern-Main	—	—	—	x
PT-46	—	Northwestern Sierra Madre Foothills	—	—	—	x
PT-47	—	Northwestern Sierra Madre Foothills	—	—	—	x
PT-48	—	Northwestern Sierra Madre Foothills	—	—	—	x
PT-49	—	Western Basin	—	—	—	x
PT-50	—	Western Basin	—	—	—	x
PT-51	—	Western Basin	—	—	—	x
PT-52	—	Western Basin	—	—	—	x
PT-53	—	Northwestern Sierra Madre Foothills	—	—	—	x
PT-54	—	Northwestern Sierra Madre Foothills	—	—	—	x

Each of the multiple-well monitoring sites consists of four 2-inch diameter wells installed at different depths in the same borehole. Individual wells are screened over a specific 20-foot interval and isolated from other wells by a low-permeability bentonite grout. The construction of these wells enables the collection of depth-specific water-quality, water-level, and aquifer hydraulic-property data. Well-construction information for the three multiple-well monitoring sites is summarized in table 2.

Boreholes at each site were drilled by the USGS Western Region Research Drilling Unit using the mud-rotary method. Borehole diameter decreased with depth, ranging in diameter from 14-3/4 to 4-1/2 inches. After total hole depth was attained, geophysical log surveys were completed, and the

Table 2. Summary of well completion for selected wells, Cuyama Valley, Santa Barbara County, California.

[See figures 1, 8, 15, and 25 for well locations. **Abbreviations**: CVKR, Cuyama Valley Kirschenmann Road; CVBR, Cuyama Valley Bell Road, CVFR, Cuyama Valley Foothill Road; CUY, Cuyama Valley study well; ft bls, feet below land surface; —, data not available; * denotes data that were reported to the U.S. Geological Survey from various sources and are not stored in the National Water Information System database. Qya, Younger alluvium; Qoa, Older alluvium; QTm, Morales]

Common well name	Site identification number	Depth to bottom of well (ft bls)	Depth to top of perforations (ft bls)	Depth to bottom of perforations (ft bls)	Depth to top of sand pack (ft bls)	Depth to bottom of sand pack (ft bls)	Formation at top of screen	Formation at bottom of screen
CVKR-1	345552119354201	980	960	980	944	1,000	Qoa	Qoa
CVKR-2	345552119354202	780	760	780	728	800	Qoa	Qoa
CVKR-3	345552119354203	620	600	620	575	627	Qoa	Qoa
CVKR-4	345552119354204	460	440	460	417	471	Qoa	Qoa
CVBR-1	345359119392701	850	830	850	807	858	QTm	QTm
CVBR-2	345359119392702	750	730	750	702	767	QTm	QTm
CVBR-3	345359119392703	560	540	560	518	581	Qoa	Qoa
CVBR-4	345359119392704	380	360	380	303	403	Qoa	Qoa
CVFR-1	345351119323101	980	960	980	935	1,000	QTm	QTm
CVFR-2	345351119323102	830	810	830	787	839	QTm	QTm
CVFR-3	345351119323103	700	680	700	660	720	QTm	QTm
CVFR-4	345351119323104	610	590	610	568	625	QTm	QTm
CUY-01	345838119452001	188	45	125	—	—	Qoa	Qoa
CUY-02	345603119411901	790	340	790	—	—	Qoa	QTm
CUY-03	345100119290001	—	75*	200*	—	—	Qya	Qya
CUY-04	345602119362401	720	420	720	—	—	Qya	Qoa
CUY-05	345600119400001	—	100*	300*	—	—	Qya	Qya
CUY-06	345300119310001	800	640	800	—	—	QTm	QTm
CUY-07	345538119332201	750	250	750	—	—	Qya	Qoa
CUY-08	345405119325101	550	100*	400*	—	—	Qya	Qoa
CUY-11	344143119193001	357	100*	357*	—	—	Below QTm	Below QTm
CUY-12	345100119290002	93	50*	150*	—	—	Qya	Qya
CUY-13	344910119270501	233	100*	233*	—	—	Qya	QTm
CUY-14	345338119324801	1,100	580	1,100	—	—	Qya	Qoa
CUY-16	345540119410901	880	380	880	—	—	Qoa	QTm
CUY-17	344729119233501	400	300	400	—	—	Below QTm	Below QTm
CUY-18	344859119280801	—	100*	212*	—	—	Undetermined	Undetermined
CUY-19	345003119283501	198	87*	198*	—	—	Qya	Qya
CUY-20	345615119285501	155	100*	155*	—	—	Undetermined	Undetermined
CUY-21	345359119350201	805	620	800	—	—	QTm	QTm
CUY-22	345552119362901	1,000	401	1,000	—	—	Qya	Qoa
CUY-23	345539119393901	2,120	400	2,120	—	—	Qya	Qoa
CUY-24	345325119365603	500	300	500	—	—	Qoa	Qoa
CUY-25	345302119380701	750	325*	400*	—	—	Qoa	Qoa
CUY-26	345753119421701	—	100*	215*	—	—	Qya	Qoa
CUY-27	345539119394001	993	144	993	—	—	Qya	QTm
CUY-28	344900119332201	—	—	—	—	—	Undetermined	Undetermined
CUY-30	344156119184801	73	100*	500*	—	—	Undetermined	Undetermined
CUY-31	344154119184801	140	40	140	—	—	Undetermined	Undetermined
CUY-32	344231119224101	125	65	125*	—	—	Undetermined	Undetermined
CUY-33	344828119265301	360	50*	372*	—	—	Qya	QTm
CUY-34	344843119272401	284	120	302	—	—	Qya	QTm

Table 2. Summary of well completion for selected wells, Cuyama Valley, Santa Barbara County, California.—Continued

[See figures 1, 8, 15, and 25 for well locations. **Abbreviations**: CVKR, Cuyama Valley Kirschenmann Road; CVBR, Cuyama Valley Bell Road, CVFR, Cuyama Valley Foothill Road; CUY, Cuyama Valley study well; ft bls, feet below land surface; —, data not available; * denotes data that were reported to the U.S. Geological Survey from various sources and are not stored in the National Water Information System database. Qya, Younger alluvium; Qoa, Older alluvium; QTm, Morales]

Common well name	Site identification number	Depth to bottom of well (ft bls)	Depth to top of perforations (ft bls)	Depth to bottom of perforations (ft bls)	Depth to top of sand pack (ft bls)	Depth to bottom of sand pack (ft bls)	Formation at top of screen	Formation at bottom of screen
CUY-35	344825119271001	220	100*	175*	—	—	Qya	Qya
CUY-36	344742119240201	435	255	435	—	—	Undetermined	Undetermined
CUY-38	345040119285101	200	120	200	—	—	Qya	Qya
CUY-39	344944119275701	212	100*	212*	—	—	Qya	Qya
CUY-40	344939119275901	200	50*	200*	—	—	Qya	Qya
CUY-42	344904119273101	160.7	100*	174*	—	—	Qya	Qoa
CUY-43	344904119273401	225	125	225	—	—	Qya	Qoa
CUY-44	344915119262001	230	100*	235*	—	—	QTm	QTm
CUY-45	345209119304901	230	100*	300*	—	—	Qya	Qoa
CUY-46	345206119294701	175	120*	175*	—	—	Qya	Qya
CUY-47	344940119330501	151	31	151	—	—	Undetermined	Undetermined
CUY-48	345315119371501	—	425*	500*	—	—	Qoa	Qoa
CUY-49	345353119373601	750	425*	500*	—	—	Qoa	Qoa
CUY-50	345600119351001	—	50*	300*	—	—	Qya	Qya
CUY-51	345606119310301	800	50*	800*	—	—	Qya	QTm
CUY-52	345511119322801	1,008	484	1,008	—	—	Qoa	QTm
CUY-53	345447119315101	—	50*	500*	—	—	Qya	Qoa
CUY-54	345512119354101	239	124*	370*	—	—	Qya	Qoa
CUY-55	345631119402901	425	100*	441*	—	—	Qya	Qoa
CUY-56	345709119415501	240	58*	237*	—	—	Qya	Qoa
CUY-57	345618119393701	1,004	160	1,004	—	—	Qya	QTm
CUY-58	345540119394301	—	150*	500*	—	—	Qya	Qoa
CUY-59	345538119374601	—	306	620	—	—	Qya	Qoa
CUY-60	345808119433501	215	100*	215*	—	—	Qya	Qoa
CUY-61	345604119340201	—	50*	745*	—	—	Qya	Qoa
CUY-62	345822119391801	238	108	232	—	—	Qya	Qoa
CUY-63	345721119383401	634	200	628	—	—	Qya	Qoa
CUY-64	345540119384201	—	150*	425*	—	—	Qya	Qoa
CUY-73	345014119224901	232	100*	232*	—	—	Qoa	Qoa
CUY-74	344749119265301	—	100*	290*	—	—	Qya	QTm
CUY-75	345637119394701	646	166	640	—	—	Qya	Qoa
PT-01	—	392	50*	392*	—	—	Qya	Qoa
PT-02	—	194	97*	319*	—	—	Qya	Qya
PT-03	—	346	50*	346*	—	—	Qya	Qya
PT-04	—	288	50*	288*	—	—	Qya	Qya
PT-05	—	203.5	50*	304*	—	—	Qya	Qya
PT-07	—	316	112*	310*	—	—	Qya	Qya
PT-08	—	—	110*	371*	—	—	Qya	Qya
PT-09	—	656	108*	656*	—	—	Qya	Qoa
PT-10	—	298.5	50*	337*	—	—	Qya	Qya
PT-11	—	623	94*	623*	—	—	Qya	Qoa
PT-12	—	—	50*	600*	—	—	Qya	Qoa
PT-13	—	660	108	660*	—	—	Qya	Qoa

Table 2. Summary of well completion for selected wells, Cuyama Valley, Santa Barbara County, California.—Continued

[See figures 1, 8, 15, and 25 for well locations. **Abbreviations**: CVKR, Cuyama Valley Kirschenmann Road; CVBR, Cuyama Valley Bell Road, CVFR, Cuyama Valley Foothill Road; CUY, Cuyama Valley study well; ft bls, feet below land surface; —, data not available; * denotes data that were reported to the U.S. Geological Survey from various sources and are not stored in the National Water Information System database. Qya, Younger alluvium; Qoa, Older alluvium; QTm, Morales]

Common well name	Site identification number	Depth to bottom of well (ft bls)	Depth to top of perforations (ft bls)	Depth to bottom of perforations (ft bls)	Depth to top of sand pack (ft bls)	Depth to bottom of sand pack (ft bls)	Formation at top of screen	Formation at bottom of screen
PT-14	—	810	175	810	—	—	Qya	Qoa
PT-15	—	666	119*	665*	—	—	Qya	Qoa
PT-16	—	239	124*	370*	—	—	Qya	Qoa
PT-17	—	186	120*	369*	—	—	Qya	Qya
PT-18	—	417	50*	417*	—	—	Qya	Qya
PT-19	—	—	50*	400*	—	—	Qya	Qya
PT-20	—	—	100*	359*	—	—	Qoa	Qoa
PT-21	—	370	100*	370*	—	—	Qya	Qoa
PT-22	—	400	100*	400*	—	—	Qya	Qya
PT-23	—	—	156*	351*	—	—	Qya	Qya
PT-24	—	333	100*	204*	—	—	Qya	Qya
PT-25	—	390	190*	390*	—	—	Qoa	Qoa
PT-26	—	204	100*	204*	—	—	Qya	Qoa
PT-27	—	222	42*	218*	—	—	Qoa	Qoa
PT-28	—	380	33*	212*	—	—	Qoa	Qoa
PT-30	—	508	226	—	—	—	Qya	Qoa
PT-31	—	409	108*	308*	—	—	Qya	Qya
PT-32	—	240	58*	237*	—	—	Qya	Qoa
PT-34	—	465	173	465*	—	—	Qya	Qoa
PT-35	—	350	128	350*	—	—	Qya	Qoa
PT-36	—	441	100*	441*	—	—	Qya	Qoa
PT-37	—	407	133*	407*	—	—	Qya	Qya
PT-38	—	514	133*	514*	—	—	Qya	Qoa
PT-39	—	—	166*	454*	—	—	Qya	Qoa
PT-40	—	371	50*	190*	—	—	Qya	Qya
PT-41	—	—	150*	310*	—	—	Qya	Qya
PT-42	—	—	130*	322*	—	—	Qya	Qya
PT-43	—	278	130*	278*	—	—	Qya	Qya
PT-44	—	720	420	720	—	—	Qya	Qoa
PT-45	—	298	53*	275*	—	—	Qya	Qya
PT-46	—	1,006	196	1003*	—	—	Qoa	QTm
PT-47	—	603	224*	560*	—	—	Qoa	Qoa
PT-48	—	404	100	404*	—	—	Qoa	QTm
PT-49	—	215	100*	215*	—	—	Qya	Qoa
PT-50	—	378	36*	117*	—	—	Qya	Qya
PT-51	—	138	40*	138*	—	—	Qya	Qya
PT-52	—	294	40*	294*	—	—	Qya	Qoa
PT-53	—	110	57*	128*	—	—	Qoa	Qoa
PT-54	—	700	125	625*	—	—	Qoa	Qoa

Table 3. Site identification and data availability for selected springs and surface-water sites in the Cuyama Valley groundwater basin, Santa Barbara County, California

[See figure 8 for locations. An "x" denotes data are available. **Abbreviations**: mm/dd/yyyy, month, day, year; SP, spring site; SW, surface water site; —, data not available]

Common site name	Site type	Site identification number	Sub-region	Site description	Water-chemistry data	Discharge data	Discharge data start (mm/dd/yyyy)
SP-01	Spring	344740119224801	Northeast Ventucopa Uplands	Quail Creek Spring	x	—	—
SP-02	Spring	344857119334701	Southern Sierra Madre Foothills	Reyes Creek Spring	x	—	—
SW-01	Surface water	344143119191701	Southern Ventucopa Uplands	Reyes Creek at Lockwood Valley Road near Ventucopa	x	—	—
SW-02	Surface water	344147119191601	Southern Ventucopa Uplands	Cuyama River at Lockwood Valley Road near Ventucopa	x	—	—
SW-03	Surface water	11136600	Southern Sierra Madre Foothills	Santa Barbara Canyon Creek near Ventucopa	x	x	9/30/2009
SW-04	Surface water	11136500	Outside basin boundary	Cuyama River near Ventucopa	x	x	5/15/2009
SW-05	Surface water	11136800	Outside basin boundary	Cuyama River below Buckhorn Canyon near Santa Maria	—	x	2/10/1962

monitoring wells were installed. The monitoring wells were constructed by using flush-threaded, 2-inch-diameter, schedule 80 polyvinyl chloride (PVC) casing. The screened interval for each monitoring well typically consisted of a 20-foot section of slotted PVC (slot size is 0.020 inch) at the bottom. Once the well was lowered to the desired depth, a filter pack was tremied around the screened interval using No. 3 Monterey sand. A low-permeability bentonite grout was then tremied in place to seal the borehole and effectively isolate the screened interval of the monitoring well. The process was repeated for each successive well. Well-construction diagrams for each multiple-well monitoring site are presented in figures 3–5.

After completion, drilling fluid was evacuated from each monitoring well by using compressed air. Extensive airlifting and a surging technique with compressed air were employed to further develop the filter pack surrounding the well. Specific conductance, pH, temperature, apparent color, and turbidity, along with the discharge rate and total volume, were recorded during this process. Development was continuous until no discernible drilling mud was present and field measurements had stabilized.

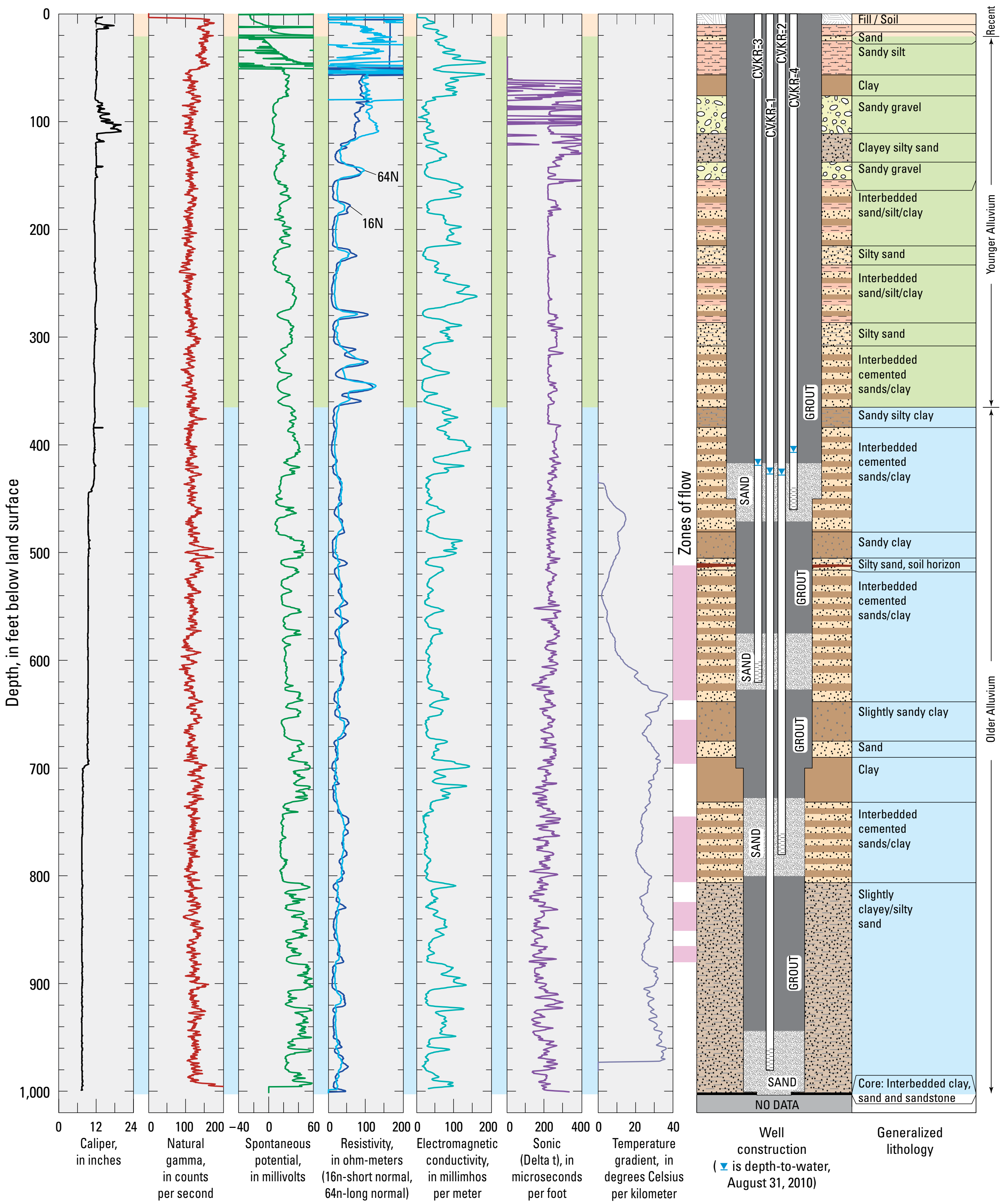

Figure 3. Geophysical logs, well-construction diagram, and generalized lithologic description for multiple-well monitoring site Cuyama Valley Kirschenmann Road (CVKR), Cuyama Valley, Santa Barbara County, California.

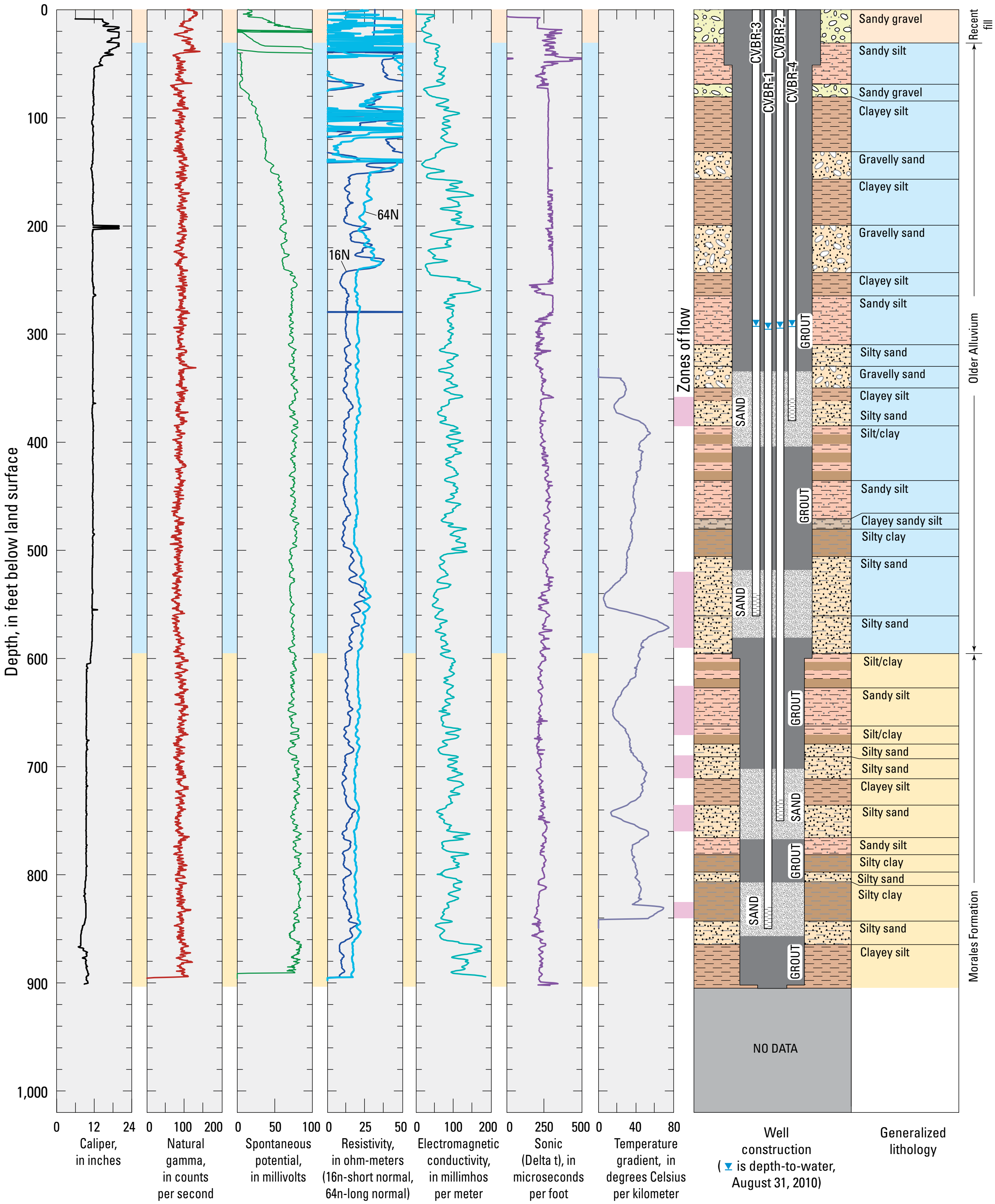

Figure 4. Geophysical logs, well-construction diagram, and generalized lithologic description for multiple-well monitoring site Cuyama Valley Bell Road (CVBR), Cuyama Valley, Santa Barbara County, California.

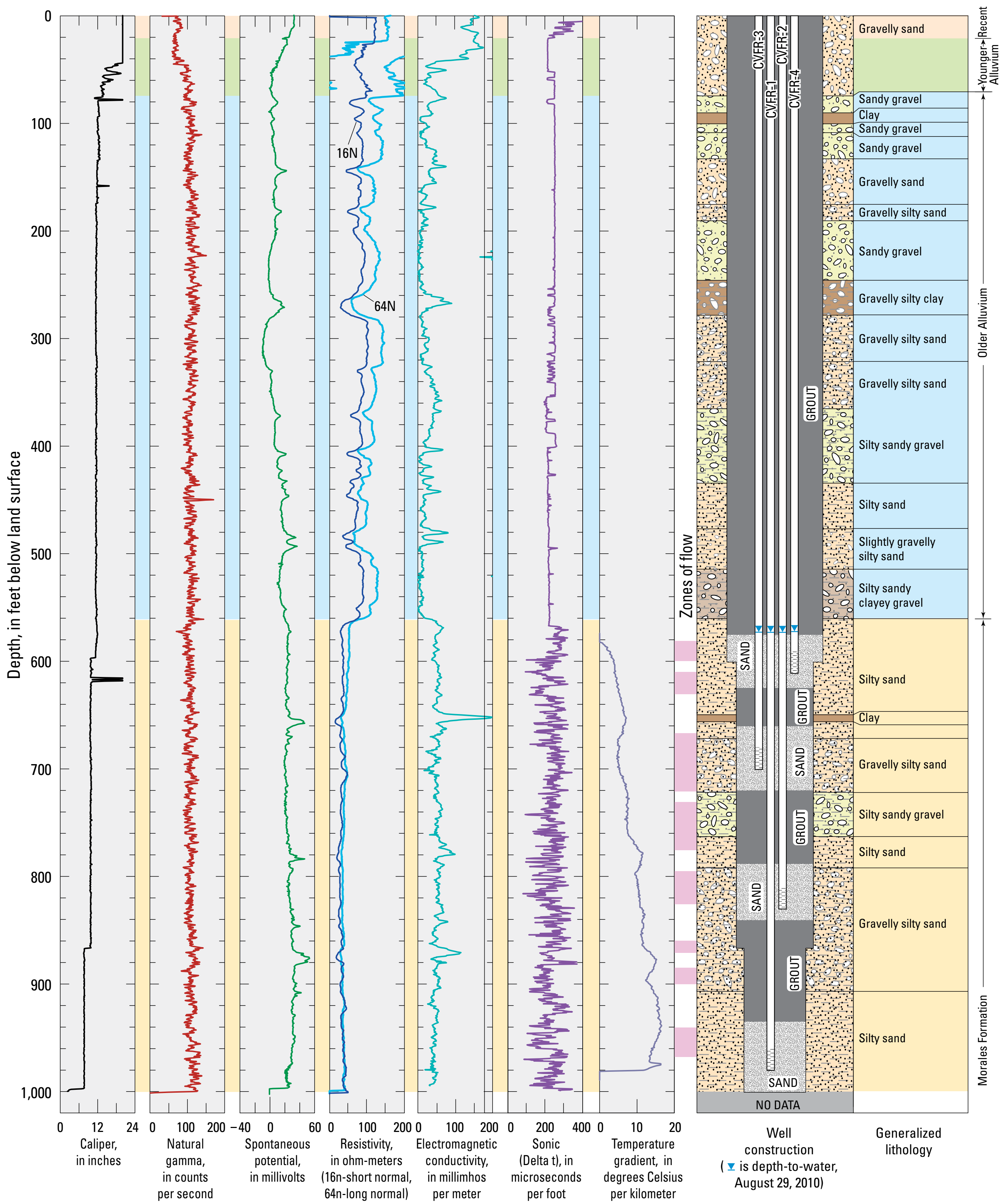

Figure 5. Geophysical logs, well-construction diagram, and generalized lithologic description for multiple-well monitoring site Cuyama Valley Foothill Road (CVFR), Cuyama Valley, Santa Barbara County, California.

Geology

Geologic information was collected to characterize and correlate stratigraphic units and boundaries associated with the aquifer system. Geologic information for each multiple-well monitoring site included lithologic cutting descriptions and a suite of geophysical logs. At two locations, CVKR and CVBR, whole core samples were collected.

Lithologic Descriptions

Detailed lithologic logs were compiled from descriptions of drill cuttings or whole core samples collected at each borehole site and from observations recorded during drilling. Cuttings samples (tables 4–6), termed “sieved drill cuttings,” were composited from 20-foot depth intervals and sieved at the borehole surface by using a No. 120 sieve (0.125-mm screen opening). Additional cutting samples, termed “shaker cuttings,” were collected at 10-ft depth intervals from a No. 60 screen (0.250-mm screen opening) mounted on the drill rig’s shaker tank.

Sieve and shaker cuttings were first described in the field. Subsequently, samples were examined in greater detail in the office by using a microscope and characterized by grain size, texture, sorting, rounding, color, and other features.

Texture descriptions followed the National Research Council (National Research Council, 1947) grain-size classification shown in figure 6. This classification allows for correlation of grain-size terms (such as “sand”) to size limits in millimeters or inches. For samples containing gravel, the terms “silt” and “clay” are used in lieu of “mud.” Color, determined on moist samples, followed the numerical color designations in Munsell Soil Color Charts (Munsell Color, 1994). Lithologic logs from the sieved drill cuttings are presented in tables 4–6.

The generalized lithology next to each monitoring site diagram (figs. 3–5) was compiled by grouping similar lithologic units, as determined from the detailed lithologic logs from the sieved and shaker samples. The lithologic units were categorized into textural groups, such as gravels or sands (fig. 6), on the basis of estimated percentages of gravel and sand and the ratios of sand, silt, and clay present following the nomenclature of Folk (1954). Information collected from borehole geophysical logs also was used to help identify contact depths between major lithologic units.

Geophysical Logs

Borehole geophysical surveys provided information about the nature of the lithologic units and the water chemistry and flow patterns of groundwater. Geophysical log surveys were done shortly after attaining total hole depth in the uncased, fluid-filled borehole. These surveys included caliper, bulk-natural gamma, spontaneous potential, 16- and 64-inch normal resistivity, electromagnetic induction, and acoustic logs. High-resolution temperature logs were performed in the deepest completed well at each site at a later date. Geophysical logs for each multiple-well monitoring site are presented in figures 3–5.

Calipers were used to measure the diameter of the borehole. The caliper log can be used to identify the depth intervals of consolidated layers, washed-out sand, or the presence of swelling clay. Caliper logs also are useful in the construction of multiple-well sites by providing accurate borehole-volume calculations for placement of sand filter packs and environmental sealing materials.

Bulk natural-gamma logs measure the intensity of gamma-rays emitted from the natural decay of potassium-40 and of the daughter products of uranium and thorium (Schlumberger, 1972). Gamma logs are used primarily to define lithology indicators and for correlation of geologic units among boreholes within the same region. Typically, increases in gamma-ray emissions are observed in clay, feldspar-rich sand and gravel, and granite.

The spontaneous potential (SP) log measures the difference in electrical potentials, as a voltage, that develops at the contacts between different formations, such as shale or clay beds and a sand aquifer. Spontaneous potential is a function of the chemical activities of fluids in the borehole and adjacent rocks, the temperature, and the type and quantity of clay present; therefore, SP logs are directly influenced by the drilling fluid in undeveloped water wells. If the drilling fluid in the borehole is fresher than the native interstitial water, there is a negative spontaneous potential opposite sand beds—this is the so-called standard response. If the salinities are reversed, the spontaneous-potential response is reversed also (Keys and MacCary, 1983). SP logs are not directly related to porosity or permeability.

Resistivity tools measure the apparent resistivity of a volume of material surrounding the borehole under the direct application of an electric current (Keys and MacCary, 1983). These logs are used to determine formation and fluid resistivity and to estimate formation porosity. In general, low resistivity indicates water with higher concentrations of dissolved solids or fine-grained deposits such as silt, clay, and shale; high resistivity indicates water with lower concentrations of dissolved solids or coarser material, such as sand or gravel.

The 16-in. normal resistivity probe measures the apparent resistivity of material surrounding the borehole that was most likely invaded with drilling fluid. The 64-in. normal resistivity probe measures the apparent resistivity at a greater radius, which is considered to be representative of material that is saturated with formation water beyond the invaded zone. Comparison of the two logs is a useful indicator of aquifer zones with relatively high total dissolved solids.

Electromagnetic (EM) induction logs yield detailed information about the vertical electrical conductivity of the formation and pore water (McNeill, 1986). Electrical conductivity is affected by the porosity, permeability, clay and silt content of the sand-and-gravel aquifers, and the dissolved-solids concentration of the groundwater in the aquifer. EM induction logs can help identify water-bearing units to

Table 4. Lithologic log from sieved drill cuttings (0.125-millimeter screen opening) from multiple-well monitoring site Cuyama Valley Kirschenmann Road (CVKR).

Depth (ft)		Description
From	To	
0	20	Sand (S); fine to coarse sand; well sorted; angular to subangular; very pale brown (10YR 7/4)
20	40	Sand (S); fine to medium sand; well sorted; angular to subangular; yellowish brown (10YR 5/4)
40	60	Clayey sand (cS); fine to coarse sand with clay; well sorted; subangular; yellowish brown (10YR 5/4)
60	80	Slightly gravelly sand ((g)S); medium sand with granules to small pebbles; well sorted; subangular; yellowish brown (10YR 5/4)
80	100	Gravelly sand (gS); fine to coarse sand with granules to medium pebbles; poorly sorted; subrounded to subangular; yellowish brown (10YR 5/4)
100	120	Gravelly sand (gS); very fine to coarse sand with granules to small pebbles; poorly sorted; subrounded to subangular; yellowish brown (10YR 5/4)
120	140	Gravelly sand (gS); fine to coarse sand with granules to medium pebbles; poorly sorted; subrounded to subangular; yellowish brown (10YR 5/4)
140	160	Slightly gravelly sand ((g)S); very fine to very coarse sand with minor small pebbles; poorly sorted; subrounded to subangular; yellowish brown (10YR 5/4)
160	180	Slightly gravelly sand ((g)S); fine to coarse sand with minor granules; poorly sorted; subrounded to subangular; yellowish brown (10YR 5/4)
180	200	Sand (S); medium to very coarse sand; moderately sorted; subrounded to subangular; yellowish brown (10YR 5/4)
200	220	Slightly gravelly sand ((g)S); fine to very coarse sand with granules to small pebbles; poorly sorted; subrounded to subangular; yellowish brown (10YR 5/4)
220	240	Gravelly sand (gS); fine to coarse sand with granules; poorly sorted; subrounded to subangular; yellowish brown (10YR 5/4)
240	260	Slightly gravelly clayey sand ((g)mS); medium to coarse sand with clay and small pebbles; poorly sorted; subrounded to subangular; yellowish brown (10YR 5/4)
260	280	Clayey sand (cS); medium sand with clay; very well sorted; rounded to subrounded; yellowish brown (10YR 5/4)
280	300	Clayey sand (cS); medium sand with clay; very well sorted; rounded to subrounded; yellowish brown (10YR 5/4)
300	320	Sand (S); fine to medium sand; well sorted; subrounded to subangular; yellowish brown (10YR 5/4)
320	340	Sand (S); fine to medium sand; well sorted; subrounded to subangular; yellowish brown (10YR 5/4)
340	360	Sand (S); fine to medium sand; well sorted; subrounded to subangular; yellowish brown (10YR 5/4)
360	380	Slightly gravelly sand ((g)S); medium to coarse sand with minor granules; well sorted; subrounded to subangular; yellowish brown (10YR 5/4)
380	400	Sand (S); medium to coarse sand; well sorted; subrounded to subangular; yellowish brown (10YR 5/4)
400	420	Sand (S); medium to coarse sand; well sorted; subrounded to subangular; yellowish brown (10YR 5/4)
420	440	Sand (S); medium to coarse sand; well sorted; subrounded to subangular; yellowish brown (10YR 5/4)
440	460	Sand (S); medium to very coarse sand; well sorted; rounded to subrounded; yellowish brown (10YR 5/4)
460	480	Sand (S); medium to very coarse sand; well sorted; rounded to subrounded; yellowish brown (10YR 5/4)
480	500	Sand (S); fine to medium sand; well sorted; rounded to subrounded; yellowish brown (10YR 5/4)
500	520	Sand (S); very fine to medium sand; moderately sorted; subrounded to subangular; yellowish brown (10YR 5/4)
520	540	Sand (S); very fine to medium sand; moderately sorted; subrounded to subangular; yellowish brown (10YR 5/4)
540	560	Sand (S); very fine to medium sand; moderately sorted; subrounded to subangular; yellowish brown (10YR 5/4)
560	580	Sand (S); very fine to medium sand; moderately sorted; subrounded to subangular; yellowish brown (10YR 5/4)
580	600	Sand (S); very fine to medium sand; moderately sorted; subrounded to subangular; yellowish brown (10YR 5/4)
600	620	Sand (S); fine to medium sand; well sorted; subangular; yellowish brown (10YR 5/4)
620	640	Sand (S); fine to coarse sand; well sorted; subangular; yellowish brown (10YR 5/4)
640	660	Sand (S); fine to coarse sand; well sorted; subangular; yellowish brown (10YR 5/4)
660	680	Sand (S); fine to coarse sand; moderately sorted; subangular; yellowish brown (10YR 5/4)
680	700	Sand (S); fine to coarse sand; moderately sorted; subangular; yellowish brown (10YR 5/4)
700	720	Sand (S); fine to coarse sand; moderately sorted; subangular; yellowish brown (10YR 5/4)
720	740	Sand (S); fine to coarse sand; moderately sorted; subangular; yellowish brown (10YR 5/4)
740	760	Sand (S); fine to coarse sand; moderately sorted; subangular; yellowish brown (10YR 5/4)
760	780	Sand (S); fine to coarse sand; moderately sorted; subangular; yellowish brown (10YR 5/4)
780	800	Sand (S); fine to coarse sand; moderately sorted; subangular; yellowish brown (10YR 5/4)
800	820	Sand (S); fine to coarse sand; moderately sorted; subrounded to subangular; yellowish brown (10YR 5/4)
820	840	Sand (S); fine to coarse sand; moderately sorted; subrounded to subangular; yellowish brown (10YR 5/4)
840	860	Sand (S); fine to medium sand; well sorted; subangular; yellowish brown (10YR 5/4)
860	880	Sand (S); fine to coarse sand; moderately sorted; angular to subangular; yellowish brown (10YR 5/4)
880	900	Sand (S); fine to coarse sand; moderately sorted; angular to subangular; yellowish brown (10YR 5/4)
900	920	Sand (S); fine to coarse sand; moderately sorted; angular to subangular; yellowish brown (10YR 5/4)
920	940	Sand (S); fine to coarse sand; moderately sorted; subangular; yellowish brown (10YR 5/4)
940	960	Sand (S); fine to coarse sand; moderately sorted; subangular; yellowish brown (10YR 5/4)
960	980	Sand (S); fine to coarse sand; well to moderately sorted; subangular; yellowish brown (10YR 5/4)
980	1,000	Sand (S); fine to coarse sand; well to moderately sorted; subangular; yellowish brown (10YR 5/4)
980	1,000	Sand (S); medium to coarse sand with trace granules; well sorted; angular to subangular; yellowish brown (10YR 5/4)

Table 5. Lithologic log from sieved drill cuttings (0.125-millimeter screen opening) from multiple-well monitoring site Cuyama Valley Bell Road (CVBR).

Depth (ft)		Description
From	To	
0	19	Slightly gravelly sand ((g)S); medium to coarse sand with minor small pebbles; well to moderately sorted; subrounded to subangular; light yellowish brown (2.5Y 6/4)
19	39	Gravelly sand (gS); medium to very coarse sand with granules to medium pebbles; moderately sorted; subrounded to subangular; light yellowish brown (2.5Y 6/4)
39	60	Sand (S); fine to medium sand; well sorted; subrounded to subangular; light yellowish brown (2.5Y 6/4)
60	80	Sand (S); fine to coarse sand; moderately sorted; subrounded to subangular; light yellowish brown (2.5Y 6/4)
80	100	Sand (S); fine to coarse sand; moderately sorted; subrounded to subangular; light yellowish brown (2.5Y 6/4)
100	120	Sand (S); fine to coarse sand; moderately sorted; subrounded to subangular; light yellowish brown (2.5Y 6/4)
120	140	Sand (S); fine to coarse sand; moderately to poorly sorted; subrounded to subangular; light yellowish brown (2.5Y 6/4)
140	160	Sand (S); fine to very coarse sand with minor clay; poorly sorted; subrounded to subangular; light yellowish brown (2.5Y 6/4)
160	180	Sandy clay (sC); clay with very fine to medium sand; moderately sorted; light yellowish brown (2.5Y 6/4)
180	200	Sandy clay (sC); clay with fine to medium sand and trace coarse sand; moderately sorted; light yellowish brown (2.5Y 6/4)
200	220	Sand (S); fine to coarse sand; moderately to poorly sorted; subrounded to subangular; light yellowish brown (2.5Y 6/4)
220	240	Sand (S); fine to very coarse sand; poorly sorted; subrounded to subangular; light yellowish brown (2.5Y 6/4)
240	260	Silty sand (zS); medium to coarse sand with silt; moderately sorted; subrounded to subangular; light yellowish brown (2.5Y 6/4)
260	280	Slightly gravelly sand ((g)S); fine to very coarse sand with small amounts of medium pebbles; poorly sorted; subrounded to subangular; light yellowish brown (2.5Y 6/4)
280	300	Sand (S); fine to coarse sand; moderately to poorly sorted; subrounded to subangular; light yellowish brown (2.5Y 6/4)
300	320	Sand (S); fine to coarse sand; moderately sorted; rounded to subrounded; light yellowish brown (2.5Y 6/4)
320	340	Silty sand (zS); fine to coarse sand with silt; moderately to poorly sorted; rounded to subrounded; light yellowish brown (2.5Y 6/4)
340	360	Slightly gravelly silty sand ((g)mS); fine to coarse sand with silt and small pebbles; poorly to very poorly sorted; subrounded to subangular; light yellowish brown (2.5Y 6/4)
360	380	Sand (S); very fine to coarse sand; moderately to poorly sorted; subrounded to subangular; light yellowish brown (2.5Y 6/4)
380	400	Silty sand (zS); very fine to coarse sand with silt; moderately to poorly sorted; subrounded to subangular; light yellowish brown (2.5Y 6/4)
400	420	Silty sand (zS); very fine to coarse sand with silt; moderately to poorly sorted; subrounded to subangular; light yellowish brown (2.5Y 6/4)
420	440	Silty sand (zS); very fine to coarse sand with silt; moderately to poorly sorted; subrounded to subangular; light yellowish brown (2.5Y 6/4)
440	460	Silty sand (zS); very fine to coarse sand with silt; moderately to poorly sorted; subrounded to subangular; light yellowish brown (2.5Y 6/4)
460	480	Sand (S); fine to coarse sand; moderately sorted; rounded to subrounded; light yellowish brown (2.5Y 6/4)
480	500	Sand (S); fine to medium sand; well sorted; rounded to subrounded; light yellowish brown (2.5Y 6/4)
500	520	Sand (S); fine to coarse sand; well sorted; rounded to subrounded; light yellowish brown (2.5Y 6/4)
520	540	Sand (S); fine to coarse sand; well sorted; rounded to subrounded; light yellowish brown (2.5Y 6/4)
540	560	Sand (S); fine to coarse sand; moderately sorted; subrounded to subangular; light yellowish brown (2.5Y 6/4)
560	580	Sand (S); fine to coarse sand; moderately sorted; subrounded to subangular; light yellowish brown (2.5Y 6/4)
580	600	Sand (S); fine to very coarse sand; moderately to poorly sorted; subrounded to subangular; light yellowish brown (2.5Y 6/4)
600	620	Sand (S); very fine to medium sand; well to moderately sorted; subrounded to subangular; light yellowish brown (2.5Y 6/4)
620	640	Sand (S); very fine to medium sand; well to moderately sorted; subrounded to subangular; light yellowish brown (2.5Y 6/4)
640	660	Sand (S); very fine to medium sand; well to moderately sorted; subrounded to subangular; light yellowish brown (2.5Y 6/4)
660	680	Sand (S); fine to coarse sand; moderately sorted; subrounded to subangular; light yellowish brown (2.5Y 6/4)
680	700	Sand (S); fine to coarse sand; moderately sorted; subrounded to subangular; light yellowish brown (2.5Y 6/4)
700	720	Sand (S); fine to coarse sand; moderately sorted; subrounded to subangular; light yellowish brown (2.5Y 6/4)
720	740	Sand (S); fine to coarse sand; moderately sorted; subrounded to subangular; light yellowish brown (2.5Y 6/4)
740	760	Sand (S); medium to coarse sand; well sorted; subrounded to subangular; light yellowish brown (2.5Y 6/4)
760	780	Sand (S); fine to coarse sand; moderately sorted; subrounded to subangular; light yellowish brown (2.5Y 6/4)
780	800	Sand (S); fine to coarse sand; moderately sorted; subrounded to subangular; light yellowish brown (2.5Y 6/4)
800	820	Sand (S); fine to coarse sand; moderately sorted; subrounded to subangular; light yellowish brown (2.5Y 6/4)
820	840	Sand (S); fine to medium sand; well sorted; subrounded to subangular; light yellowish brown (2.5Y 6/4)
840	860	Sand (S); fine to coarse sand; moderately sorted; subrounded to subangular; light yellowish brown (2.5Y 6/4)
860	880	Sand (S); fine to coarse sand; moderately sorted; subrounded to subangular; light yellowish brown (2.5Y 6/4)

Table 6. Lithologic log from sieved drill cuttings (0.125-millimeter screen opening) from multiple-well monitoring site Cuyama Valley Foothill Road (CVFR).

Depth (ft)		Description
From	To	
0	20	Sand (S); medium to coarse sand; well sorted; angular to subangular; light yellowish brown (2.5Y 6/3)
20	40	Slightly gravelly sand ((g)S); fine to coarse sand with minor amounts of medium pebbles; moderately sorted; angular to subangular; light olive brown (2.5Y 5/4)
40	60	Slightly gravelly sand ((g)S); fine to very coarse sand with minor amounts of granules; poorly sorted; subangular; light olive brown (2.5Y 5/3)
60	80	Sandy gravel (sG); small to medium pebbles with medium to very coarse sand; poorly sorted; subrounded to subangular; light olive brown (2.5Y 5/4)
80	100	Gravelly sand (gS); fine to coarse sand with granules to medium pebbles; poorly sorted; angular to subangular; light olive brown (2.5Y 5/4)
100	120	Sandy gravel (sG); small to medium pebbles with very fine to coarse sand; very poorly sorted; angular to subangular; light olive brown (2.5Y 5/4)
120	140	Gravelly sand (gS); very fine to coarse sand with granules to medium pebbles; very poorly sorted; angular to subangular; light olive brown (2.5Y 5/4)
140	160	Sandy gravel (sG); small to large pebbles with very fine to coarse sand; very poorly sorted; subrounded to subangular; yellowish brown (10YR 5/4)
160	180	Gravelly sand (gS); very fine to coarse sand with small to medium pebbles; poorly sorted; angular to subangular; yellowish brown (10YR 5/4)
180	200	Sandy gravel (sG); granules to very large pebbles with very fine to coarse sand; very poorly sorted; angular; yellowish brown (10YR 5/4)
200	220	Sandy gravel (sG); granules to medium pebbles with very fine to medium sand; poorly sorted; angular to very angular; yellowish brown (10YR 5/4)
220	240	Gravelly silty sand (gmS); fine to coarse sand with silt and small to medium pebbles; poorly sorted; subrounded to subangular; yellowish brown (10YR 5/4)
240	260	Gravelly silty sand (gmS); fine to coarse sand with silt and small pebbles; poorly sorted; subrounded to subangular; yellowish brown (10YR 5/4)
260	280	Gravelly sand (gS); medium to coarse sand with small pebbles; moderately sorted; subrounded to subangular; yellowish brown (10YR 5/4)
280	300	Sand (S); fine to medium sand; well sorted; subangular to subrounded; yellowish brown (10YR 5/4)
300	320	Sand (S); very fine to coarse sand; moderately sorted; rounded to subrounded; yellowish brown (10YR 5/4)
320	340	Sand (S); very fine to coarse sand; moderately sorted; angular to subangular; yellowish brown (10YR 5/4)
340	360	Slightly gravelly sand ((g)S); very fine to coarse sand with minor granules to small pebbles; poorly sorted; subrounded to subangular; yellowish brown (10YR 5/4)
360	380	Slightly gravelly sand ((g)S); very fine to very coarse sand with minor granules and clay; poorly sorted; angular to subangular; yellowish brown (10YR 5/4)
380	400	Sand (S); very fine to coarse sand; moderately to poorly sorted; subangular to subrounded; yellowish brown (10YR 5/4)
400	420	Gravelly sand (gS); very fine to coarse sand with granules; moderately sorted; angular to subangular; yellowish brown (10YR 5/4)
420	440	Gravelly sand (gS); very fine to coarse sand with granules; moderately sorted; angular to subangular; yellowish brown (10YR 5/4)
440	460	Sand (S); fine to coarse sand; moderately sorted; angular to subangular; yellowish brown (10YR 5/4)
460	480	Slightly gravelly sand ((g)S); fine to coarse sand with small amounts of granules; moderately sorted; angular to subangular; yellowish brown (10YR 5/4)
480	500	Sand (S); fine to coarse sand; moderately sorted; angular to subangular; yellowish brown (10YR 5/4)
500	520	Sand (S); fine to coarse sand; moderately sorted; angular to subangular; yellowish brown (10YR 5/4)
520	540	Sand (S); fine to coarse sand; moderately sorted; angular to subangular; yellowish brown (10YR 5/4)
540	560	Sand (S); fine to coarse sand; moderately sorted; angular to subangular; yellowish brown (10YR 5/4)
560	580	Sand (S); fine to coarse sand; moderately sorted; angular to subangular; yellowish brown (10YR 5/4)
580	600	Sand (S); fine to coarse sand; moderately sorted; angular to subangular; yellowish brown (10YR 5/4)
600	620	Sand (S); fine to coarse sand; moderately sorted; subrounded to subangular; yellowish brown (10YR 5/4)
620	640	Sand (S); fine to very coarse sand; moderately to poorly sorted; angular; yellowish brown (10YR 5/4)
640	660	Gravelly sand (gS); fine to very coarse sand with granules; poorly sorted; angular; yellowish brown (10YR 5/4)
660	680	Sand (S); fine to very coarse sand; poorly sorted; angular; yellowish brown (10YR 5/4)
680	700	Gravelly sand (gS); medium to very coarse sand with granules; moderately sorted; angular to subangular; yellowish brown (10YR 5/4)
700	720	Gravelly sand (gS); medium to very coarse sand with granules; moderately sorted; angular to subangular; yellowish brown (10YR 5/4)
720	740	Gravelly sand (gS); fine to very coarse sand with granules; poorly sorted; angular to subangular; yellowish brown (10YR 5/4)
740	760	Gravelly sand (gS); fine to very coarse sand with granules; poorly sorted; angular to subangular; yellowish brown (10YR 5/4)
760	780	Gravelly sand (gS); medium to very coarse sand with granules; moderately sorted; angular to subangular; yellowish brown (10YR 5/4)
780	800	Sand (S); fine to very coarse sand; moderately sorted; subrounded to subangular; yellowish brown (10YR 5/4)
800	820	Sand (S); fine to coarse sand; moderately sorted; subrounded to subangular; yellowish brown (10YR 5/4)
820	840	Gravelly sand (gS); fine to very coarse sand with granules to small pebbles; poorly sorted; subrounded to subangular; yellowish brown (10YR 5/4)

Table 6. Lithologic log from sieved drill cuttings (0.125-millimeter screen opening) from multiple-well monitoring site Cuyama Valley Foothill Road (CVFR).—Continued

Depth (ft) From	Depth (ft) To	Description
840	860	Gravelly sand (gS); fine to coarse sand with granules; moderately to poorly sorted; subrounded to subangular; yellowish brown (10YR 5/4)
860	879	Sand (S); fine to very coarse sand; moderately to poorly sorted; subrounded to subangular; yellowish brown (10YR 5/4)
879	899	Slightly gravelly sand ((g)S); fine to medium sand with minor small pebbles; moderately sorted; subrounded to subangular; yellowish brown (10YR 5/4)
899	919	Sand (S); very fine to very coarse sand; poorly sorted; subrounded to subangular; yellowish brown (10YR 5/4)
919	939	Sand (S); very fine to medium sand; well to moderately sorted; subrounded to subangular; yellowish brown (10YR 5/4)
939	959	Sand (S); very fine to medium sand; well to moderately sorted; subrounded to subangular; yellowish brown (10YR 5/4)
959	979	Sand (S); fine to coarse sand; well to moderately sorted; subrounded to subangular; yellowish brown (10YR 5/4)
979	1,000	Sand (S); medium sand; very well sorted; subrounded to subangular; yellowish brown (10YR 5/4)

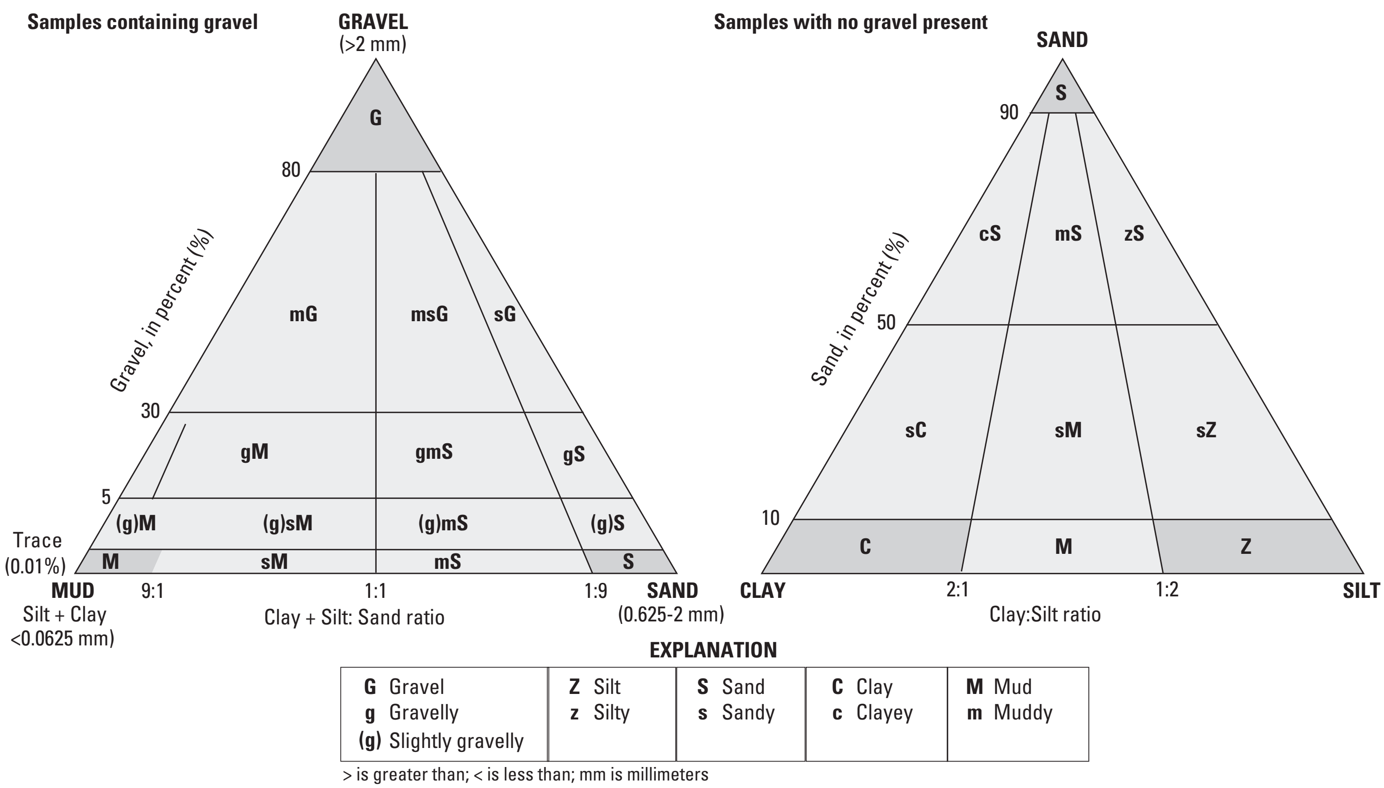

Figure 6. Rock-type nomenclature used for lithologic-log descriptions.

determine optimum depths for the placement of monitoring well screens and can help identify temporal changes in water quality through sequential logging (Williams and others, 1993).

An acoustic (sonic) log measures the time it takes for a pulsed compressional sound wave to travel from a downhole source to downhole receivers. The sonic tool used has two receivers, near and far, that recorded the arrival time of the compressional sound wave. The difference in arrival times between the receivers, or delta t, can be related to the physical properties of the adjacent material. In unconsolidated material, sonic logs principally are used to identify contacts between lithologic units that were penetrated by the borehole.

Temperature Logs

High-resolution borehole temperature logs were collected in the deepest well at each multiple-well monitoring site on June 24, 2010. To ensure that the water temperature was characteristic of ambient groundwater conditions, logging was performed several months after the site had been constructed, developed, and sampled for water-quality to allow sufficient time for the water column in the well to equilibrate with the surrounding material. Generally, groundwater temperature increases with depth, and the global average is about 25 degrees Celsius (°C) per kilometer. The geothermal gradient in sedimentary basins generally exceeds this average because of the relatively low thermal conductivity of sedimentary materials (Ingebritsen and Sanford, 1998). Perturbations in the geothermal gradient in temperature logs can provide information about geologic formations as well as horizontal and vertical groundwater-flow patterns. Groundwater temperature is related to factors such as lithology (which affects thermal conductance), depth, recharge source, and residence time within the aquifer. Measured temperature logs, when expressed as a measured vertical temperature gradient and compared with the geothermal gradient, can be used to identify potential zones of groundwater flow. Depth intervals where the temperature gradient is concave upward, or increases more quickly than the geothermal gradient, are consistent with the cooling influence of groundwater flow through relatively permeable units. Depth intervals exhibiting greater temperature perturbation (relatively large increases in temperature gradient with depth) can be interpreted as zones of greater flow.

Changes in the temperature gradients were used, in conjunction with other logs, to identify discrete flow zones at each monitoring site (see figs. 3, 4 and 5). At the CVKR site (fig. 3), five flow zones were identified: (1) 513–637 ft, (2) 655–695 ft, (3) 745–804 ft, (4) 823–850 ft, and (5) 865–880 ft below land surface. A comparison of the magnitude of the vertical change in temperature gradient with depth among flow zones indicated a general decrease in flow with increasing depth and that the majority of flow at the CVKR site is in the shallowest zone. This zone not only is the thickest, but also showed the greatest temperature perturbation. At the CVBR site (fig. 4), six flow zones were identified: (1) 357–385 ft, (2) 520–590 ft, (3) 625–670 ft, (4) 690–710 ft, (5) 735–760 ft, and (6) 825–840 ft below land surface. A comparison of the flow zones indicated a general decrease in flow with increasing depth and that a majority of the flow is in zone 2. Similar in nature to the zone of greatest flow at CVKR site, zone 2 is the thickest at CVBR and also showed the greatest temperature perturbation. At the CVFR site (fig. 5), eight flow zones were identified: (1) 580–600 ft, (2) 610–630 ft, (3) 667–720 ft, (4) 730–775 ft, (5) 795–825 ft, (6) 860–870 ft, (7) 885–900 ft, and (8) 940–967 ft below land surface. Overall, differences in flow among zones at CVFR were less apparent than at the other sites, as was indicated by a relatively small perturbation in the gradient. The majority of flow at CVFR could be in the deepest zones (7 and 8), unlike the CVKR and CVBR sites. Although the deeper zones at CVFR are not as thick as some of the shallower zones, they exhibited greater fluctuations in the temperature gradient.

Core Measurements

Core samples were collected from the bottom of the borehole at the CVKR and CVBR sites. The cores were collected in 3-inch-diameter thin-walled metal tubes. Each coring “push” retrieved a cylinder of sediment as long as 3 feet. The locations, depths, and the total recovery of these core samples are given in table 7. The CVKR core was analyzed for bulk density and sonic velocity (fig. 7) by using a multi-sensor core log scanner (Kayen and others, 1999). The CVKR core varied in density from approximately 1.5–2.7 grams per cubic centimeter. Density changes indicated seven distinct layers within the 2.8 feet of recovered sediment. On the basis of a visual inspection of the top and bottom of the core, and the density measurements, the core was characterized as interbedded clay, sand, and sandstone. The CVBR core was not analyzed with a multi-sensor core log scanner. The top of the core contained clay and minor fine sands, and the bottom of the core contained a silty very fine to medium sand. For any future use, the cores were sealed and are stored under refrigerated conditions at the USGS core storage facility in Menlo Park, California.

Geology at the Monitoring Well Sites

Geologic maps of the Cuyama Valley (Vedder and Repenning, 1975; Kellogg and others, 2008) show two units of Holocene and Pleistocene-aged alluvial deposits, termed younger and older alluvium, underlying the three monitoring-well sites. Interpretive geologic cross sections, which were based in part on deep oil and gas exploration wells, showed that these alluvial deposits extend to a depth of approximately 1,000 ft bls beneath the monitoring-well sites (Vedder and Repenning, 1975). These alluvial deposits are underlain by the weakly to moderately indurated arkosic Morales Formation of Pleistocene to upper Pliocene age. The three multiple-well monitoring sites test different sections of the basin-fill alluvial stratigraphy relative to their locations within the basin (fig. 1). The CVKR site is in the main axis of Cuyama Valley in younger alluvium, west of the active alluvial channel of the Cuyama River. The CVFR site, 3.8 miles to the southeast of CVKR at the northern edge of the Central Sierra Madre Foothills zone, is also west of the active alluvial channel of the Cuyama River, but is close to the mapped contact between

Table 7. Summary of cores collected from multiple-well monitoring sites, Cuyama Valley groundwater basin, Santa Barbara County, California.

[See table 1 for definitions of common well names. **Abbreviations**: —, data not available; ft bls, feet below land surface; %, percent; F, fine; VF, very fine; M, medium; C, coarse]

Common well name	Core ID (site-core#-section)	Top of core interval (ft bls)	Bottom of core interval (ft bls)	Total core-interval length (ft)	Total recovery (%)	Description
CVKR	CVKR-1C-1	1,000.5	1,003.5	3	93	Interbedded clay, sand, and sandstone throughout
CVBR	CVBR-1C-1	903	906	3	88	Top: clay with minor sand (F); Bottom: Silty sand (VF-M with trace C)
CVFR	—	—	—	—	—	No core collected

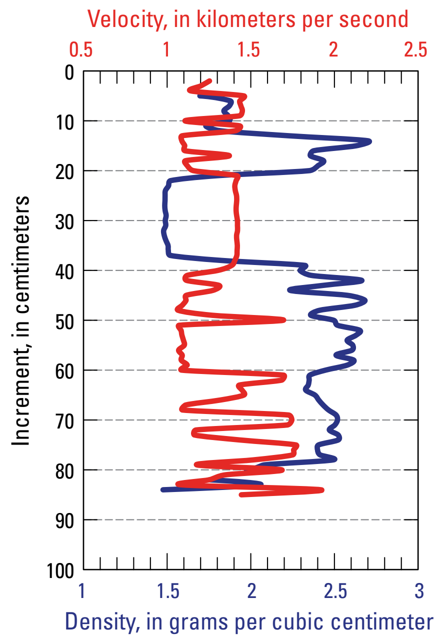

Figure 7. Sonic velocity and bulk density of core CVKR-1C-1 collected from the bottom of the Cuyama Valley Kirschenmann Road (CVKR) borehole, Cuyama Valley, Santa Barbara County, California.

younger and older alluvium. The CVBR site is in the alluvial uplands that lie to the north of the Sierra Madre Mountains and south of Cuyama Valley, next to the Salisbury Canyon drainage. The well site is in older alluvium; the site is above and to the west of the young alluvial fill in the main part of the valley.

Lithologic and borehole geophysical logs aided distinguishing among the younger and older alluvium and the underlying Morales Formation. Younger alluvium in Cuyama Valley tends to be the coarsest-grained deposit, typically consisting of unconsolidated sand, gravel, and boulders, with some clay. These coarse-grained deposits tended to yield the greatest response on borehole resistivity logs and, where thin clays were present, indicated large SP-log deflections as well. By contrast, the relatively fine-grained, massively bedded Morales Formation typically yielded a subdued response on SP and resistivity logs. The older alluvium produced an intermediate response on borehole geophysical logs. Similar to the younger alluvium, the older alluvium contains unconsolidated to partly consolidated sand, gravel, and boulders, but the older alluvium also contains a significant amount of fine-grained arkosic sands and clays that are derived from erosional reworking of the underlying Morales Formation.

The CVKR borehole penetrated terrestrial siliciclastic sediments that are alluvial fan and stream deposits. The geophysical logs indicated a distinct drop-off in resistivity at about 365 ft bls, which was interpreted as the contact of younger alluvium overlying more consolidated older alluvium. Sediments encountered in the CVKR borehole at depths of 365–620 ft bls, correlating to the top of the Older Alluvium, were much more consolidated than expected from the descriptions of these units published on the geologic maps. A paleosol (buried soil horizon) was encountered at the CVKR site at approximately 505 ft bls, further subdividing the sequence of consolidated older alluvium (fig. 3). The highest level of natural gamma radioactivity was observed within, and just above, this paleosol. This paleosol was not encountered at the other drill sites.

On the basis of an absence of distinctive changes in either the geophysical logs or mineralogy of the sediments, the CVKR wellbore did not reach the Morales Formation. The core collected from the bottom of the borehole contained interbedded clay, sand, and sandstone. Two oil and gas exploration holes drilled 1,500 ft and 4,300 ft to the northwest of the CVKR borehole have geophysical logs that begin about 1,400 ft bls (California Division of Oil, Gas and Geothermal Resources, accessed in July 2009, at *http://owr.conservation.ca.gov/WellSearch/WellSearch.aspx*). Geophysical logs from these wells showed they were both in Morales Formation at this depth. If similar conditions exist beneath the CVKR site, this places a lower bound on the thickness of older alluvium at the CVKR site.

The CVBR borehole penetrated terrestrial siliciclastic sediments that are alluvial fan and stream deposits (fig. 4). The well penetrated an upper 30-ft thick section of sandy gravel with high and variable resistivity on borehole geophysical logs that can be interpreted as recent deposits (fig. 4). This thin layer of younger alluvium, consistent with the position of this well, is in the uplands on the southern edge of the valley, which are mapped as underlain by older alluvial deposits. The geophysical logs had an interval of moderate resistivity response between 30 ft bls and 240 ft bls that we interpreted as more consolidated older alluvium (fig. 4). The interval between 260 ft bls and 595 ft bls is characterized by silty sands, with some intervals of gravelly sands, and generally low-resistivity values on borehole geophysical logs. This interval was interpreted to be part of the older alluvium; it could correlate to the older, deformed alluvium of Vedder and Repenning (1975). This interval appeared to be lithologically similar to the underlying Morales Formation and could be composed, in large part, from sediments derived from erosion of the Morales Formation.

The contact between the older alluvium and the Morales Formation at CVBR was interpreted to be at about 595 ft bls and was below the deepest elevated resistivity values (fig. 4). Below this point, resistivity values were generally low, and the lithology is uniformly silty clay. No distinctive changes in the mineralogy of the sediments were observed at this site. The core collected from the bottom of the borehole contained a clay with minor fine sand and a silty very fine to medium sand. An oil and gas exploration well 2,900 ft to the northwest of CVBR was reported to have an electric-log response interpreted as Morales Formation at 840 ft bls, where the geophysical logging of this hole began (California Division of Oil, Gas and Geothermal Resources, accessed on July, 2009, at *http://owr.conservation.ca.gov/WellSearch/WellSearch.aspx*). The top of the Morales Formation in this oil and gas exploration well is shallower than 840 ft bls, which is generally consistent with the interpreted top of the Morales in CVBR.

The CVFR borehole penetrated terrestrial siliciclastic sediments that are alluvial fan and stream deposits (fig. 5). The upper 75 ft of the hole are characterized by sandy gravel, granules to medium pebbles, and medium to very coarse sand with relatively high values of resistivity; this interval can be interpreted as recent deposits and younger alluvium. Deposits below 75 ft bls are also coarse-grained, but contain minor amounts of silt and clay and had less resistivity on geophysical logs; these deposits were interpreted as older, more consolidated alluvium. The relatively thin interval of younger alluvium is consistent with the location of this well near the mapped surface expression of the contact between younger and older alluvium.

The contact between the older alluvium and the underlying Morales Formation at CVFR was interpreted to be at 560 ft bls on the basis of the lack of pebbles and gravel and overall drop in resistivity values to consistently low values below this depth (fig. 5). No distinctive changes in the mineralogy of the sediments were observed at this site.

Geophysical logs from well CUY-06, on the east side of the Cuyama River 1.25 mi east-southeast of the CVFR site, showed a similar drop in resistivity at about 600 ft bls, which was interpreted as the depth of the contact between the older alluvium and the Morales Formation. Geophysical logs from an oil and gas exploration hole drilled 1-mi east-southeast of the CVFR borehole (California Division of Oil, Gas and Geothermal Resources, accessed on July, 2009, at *http://owr.conservation.ca.gov/WellSearch/WellSearch.aspx*) showed high resistivity values typical of younger alluvium to a depth of 1,100 ft bls, below which an abrupt drop in resistivity values to low values typical of the Morales Formation was observed. This well, very close to the active channel of the Cuyama River, could record the local presence of a channel scoured through the older alluvium, placing young alluvial channel fill directly on the Morales Formation.

Water-Quality

Groundwater samples were collected from the 12 monitoring wells (4 wells at each of the 3 multiple-well monitoring sites), 27 selected domestic and supply wells, and 2 springs (fig. 8). In addition, four surface-water samples were collected (fig. 8). Samples were analyzed for as many as 53 constituents, including field parameters (water temperature, specific conductance, pH, dissolved oxygen, and alkalinity); major and minor ions; nitrate; trace elements; stable isotopes of hydrogen and oxygen; tritium and carbon-14 activities; and species of arsenic, iron, and chromium. Selected water-quality constituents results are presented. Water-quality results not presented in this report are available through the USGS NWIS web site.

Field and Laboratory Methods

Sampling was done by USGS personnel, and all samples were collected, handled, and preserved following written USGS field procedures (U.S. Geological Survey, variously dated). Prior to sampling, water-level measurements were made, and at least three well-casing volumes were purged from the well. For monitoring wells, a portable submersible pump was used for purging and sampling the well; for domestic and supply wells, samples were collected from the discharge of the installed pump before it entered a storage tank or any treatment. Specific conductance, pH, and temperature were monitored during the purging process. Samples were collected only after these parameters had stabilized. Stability was attained when three successive measurements taken at intervals of 5 minutes or more differed by less than 5 percent for specific conductance, 0.1 units for pH, and 0.2°C for temperature. Purge logs, field measurements, and other information related to sample collection are on file at the USGS office in San Diego, California.

During sample collection, water from the pump was diverted into a special sample-collection chamber designed to minimize contamination. Most water samples intended for routine analyses (major and minor ions, nutrients, and trace elements) were pressure-filtered in the field through a polyethersulfone (PES) membrane capsule filter having a pore size of 0.45 µm. Laboratory samples intended for the analysis of pH, specific conductance, and acid-neutralizing capacity were not filtered. Polyethylene bottles were used to contain most samples and were rinsed three times with filtered native water prior to filling. Samples for nutrient determinations were collected in dark, opaque polyethylene bottles and preserved on ice to inhibit bacterial growth. Samples for cations and selected trace element determinations were collected in acid-rinsed polyethylene bottles and preserved by acidifying the sample to a pH less than 2 with a small volume of concentrated nitric acid. Samples for anion determination were collected in a natural polyethylene bottle and did not require preservation. Samples were shipped to the USGS National Water Quality Laboratory (NWQL) in Lakewood, Colorado, for analysis following standard methods outlined by Fishman and Friedman (1989), Fishman (1993), Struzeski and others (1996), Garbarino (1999), and Garbarino and others (2006).

Water samples for analysis of stable isotopes of hydrogen and oxygen (δ^2H and $\delta^{18}O$) were collected in 60-mL glass bottles. These samples were not filtered. The bottles were not rinsed, but were sealed with a special polyseal (conical) cap to minimize exchange with the atmosphere. These samples were shipped to the USGS Stable Isotope Laboratory in Reston, Virginia, for analysis according to methods outlined by Coplen

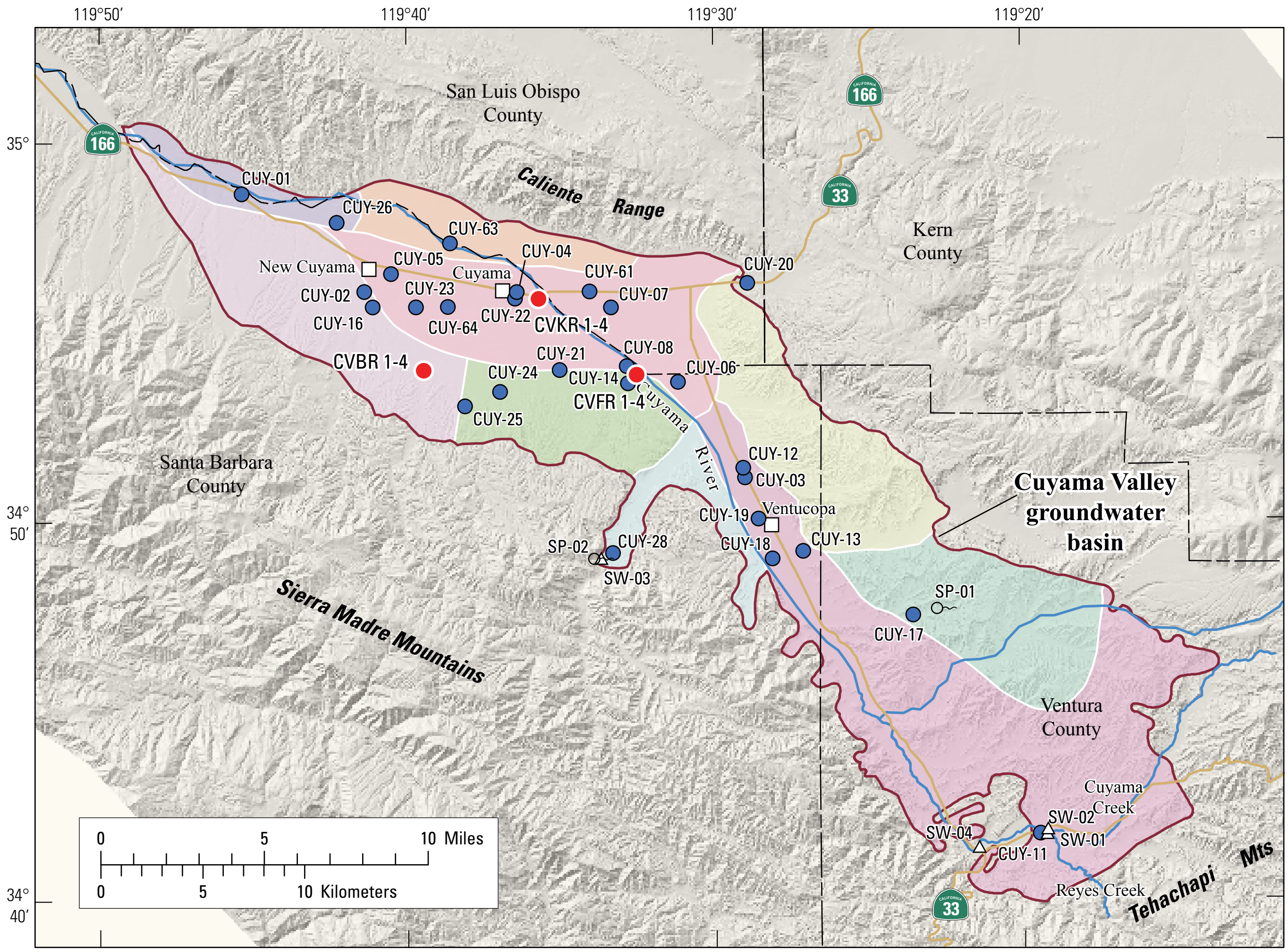

Shaded relief base created from 30-m digital elevation model from USGS National Elevation Dataset (NED), North America Vertical Datum 1988 (NAVD88)
Hydrology sourced from 1:24,000-scale National Hydrography Dataset, 1974–2009
Place names sourced from USGS Geographic Names Information System, 1974–2009
Albers Projection, NAD83

EXPLANATION

Cuyama groundwater basin zones
- Caliente Northern-Main
- Central Sierra Madre Foothills
- Northeast Ventucopa Uplands
- Northwestern Sierra Madre Foothills
- Northern Ventucopa Uplands
- Southern Sierra Madre Foothills
- Southern Ventucopa Uplands
- Southern-Main
- Western Basin

Site type
- Spring
- Surface-water site
- U.S. Geological Survey monitoring site
- Water-quality site

Figure 8. The location of multiple-well monitoring sites, domestic and supply wells, springs, and surface water sites with available water-quality data, Cuyama Valley, Santa Barbara County, California.

and others (1991). The results of these determinations are expressed in terms of per mil relative to Vienna Standard Mean Ocean Water (Gonfiantini, 1984). The estimates of precision (two-sigma) for δ^2H and δ^{18}O are 2 are 0.2 per mil, respectively.

Water samples intended for the analysis of tritium were collected in one-L polyethylene bottles. The samples were not filtered. Bottles were not rinsed and care was taken not to aerate the sample during collection. Samples were sealed with a polyseal (conical) cap to minimize exchange with the atmosphere. These samples were analyzed at the USGS Isotope Tracers Laboratory in Menlo Park, California, or at the University of Miami (through arrangements with the NWQL), by gas counting (or liquid scintillation) after electrolytic enrichment as described by Ostlund and Dorsey (1977) and Ostlund and others (1987). The activity of tritium is reported in terms of picocuries per liter (pCi/L) plus or minus the 1 sigma combined standard uncertainty (CSU). Tritium values less than the sample-specific critical level (ssLC) are reported as non-detections.

Water samples for analysis of δ^{13}C and carbon-14 isotopes were collected in either a 500-milliliter (mL) or one-liter (L) plastic coated glass bottle fitted with a polyseal cone cap. Samples were filtered in the field through PES membrane capsule filter having a pore size of 0.45 micrometer (µm). The bottle was bottom-filled and allowed to overflow to several times the bottle volume, then sealed with a special Teflon-septa cap and held on ice. $\delta^{13}C$ and carbon-14 of the dissolved inorganic carbon were analyzed by the National Ocean Sciences Accelerator Mass Spectrometry Facility (NOSAMS) in Woods Hole, Mass., by accelerator mass spectrometry (through arrangements with the NWQL). Results of the $\delta^{13}C$ determination are reported in per mil relative to the Vienna PeeDee belemnite standard (Coplen, 1994). The activity of carbon-14 expressed as percent modern carbon (pmc) is reported with a 1-sigma estimate of precision relative to the 1950 National Bureau of Standards (NBS) oxalic acid standard (Stuiver and Polach, 1977; Wigley and Muller, 1981).

Water samples intended for analysis of chromium species were collected by using a 10-mL syringe with an attached 0.45-µm disk filter. After the syringe was thoroughly rinsed and filled with native water, 4 mL were forced through the disk filter; the next 2 mL of native water was slowly filtered into a small centrifuge vial and analyzed for total chromium. Hexavalent chromium, Cr (VI), was then collected by attaching a small cation-exchange column to the syringe filter, and after conditioning the column with 2 mL of sample water, two mL were collected in a second centrifuge vial. Vials for both constituents were preserved with 7.5 Normal (N) nitric acid (Ball and McCleskey, 2003a and 2003b). Water samples intended for analysis of arsenic and iron species were filtered into 250-mL polyethylene bottles that were covered with tape to prevent light exposure and preserved with 6 N hydrochloric acid. Total chromium, total arsenic, total iron, and the dissolved concentration of either the reduced or the oxidized species of the element were analyzed at the USGS National Research Program (NRP) Trace Metal Laboratory (TML) in Boulder, Colorado, by using various techniques of ultraviolet visible (UV-VIS) spectrophotometer and atomic absorbance spectroscopy (Stookey, 1970; Ball and McCleskey, 2003a and 2003b; McCleskey and others, 2003).

Comparison Benchmarks

Concentrations of constituents detected in groundwater samples were compared with U.S Environmental Protection Agency (USEPA) and California Department of Public Health (CDPH) regulatory and non-regulatory drinking-water health-based benchmarks and benchmarks established for aesthetic purposes (California Department of Public Health, 2012a and 2012b; U.S. Environmental Protection Agency, 2012a and 2012b). The chemical data presented in this report are meant to characterize the quality of the untreated groundwater within the primary aquifer system of the Cuyama Valley groundwater basin and are not intended to represent the treated drinking water delivered to consumers by water purveyors. The chemical composition of treated drinking water can differ from untreated groundwater because treated drinking water can be subjected to disinfection, filtration, mixing with other waters or exposure to the atmosphere prior to its delivery to consumers. Comparisons of untreated groundwater to benchmarks are for illustrative purposes only and are not indicative of compliance or non-compliance with drinking-water regulations. Three benchmarks—maximum contaminant level, secondary maximum contaminant level, and public health goal—are used for comparisons. The maximum contaminant level (MCL) is a legally enforceable standard that applies to public-water systems and is designed to protect public health by limiting the levels of contaminants in drinking water. MCLs established by the USEPA are the minimum standards with which states are required to comply, and individual states may choose to set more stringent standards. The CDPH has established MCLs for additional constituents not regulated by the USEPA, as well as lowered the benchmark concentrations for a number of constituents with MCLs established by the USEPA. In this report, a benchmark set by the USEPA is labeled “MCL-US,” and one set by the CDPH that is more stringent than the MCL-US is labeled “MCL-CA.” The secondary maximum contaminant level (SMCL) is a non-enforceable standard applied to constituents that affect the aesthetic qualities of drinking water, such as taste, odor, and color, or the technical qualities of drinking water, such as scaling and staining. Both the USEPA and the CDPH define SMCLs, but unlike MCLs, SMCLs established by the CDPH are not required to be at least as stringent as those established by USEPA. In this report, the USEPA SMCLs (SMCL-US) are used unless the SMCLs established by the CDPH (SMCL-CA) have a lower value. The public health goal (PHG) is a non-enforceable standard set by the California Office of Environmental Health Hazard Assessment (OEHHA). In this report, the public health goal (OEHHA-PHG) is listed for hexavalent chromium (Cr-VI), which does not have a MCL or SMCL; for constituents that have a MCL, the OEHHA-PHG is typically orders of magnitude lower than the MCL. The benchmark type and benchmark level are included in all tables with water-quality data.

Selected Chemical Attributes

Water-quality data indicated that the groundwater in the alluvial aquifer system generally has high concentrations of total dissolved solids and sulfate. Concentrations greater than the SMCL-US for total dissolved solids (greater than 500 mg/L) were observed in samples collected from 38 of 39 wells (97 percent); concentrations greater than the SMCL-US for sulfate (greater than 250 mg/L) were observed in samples collected from 37 of 39 wells (95 percent; table 8).

Table 8. Results for analyses of major and minor ions, silica, and total dissolved solids in samples collected from selected sites, Cuyama Valley groundwater basin, Santa Barbara County, California.

Table available separately as Microsoft Excel® at http://pubs.usgs.gov/sir/2013/5108.

Concentrations greater than the MCL-US for nitrate were observed in 5 of the 39 wells (13 percent; table 9). Concentrations greater than the MCL-US for arsenic were observed in 4 of 33 wells (12 percent; table 10). Concentrations of fluoride greater than the MCL-CA of 2 mg/L were observed in one well (CUY-20; table 8).

Table 9. Results for analyses of stable isotopes, tritium and carbon-14, estimated age since recharge, and nitrate in samples collected from selected sites, Cuyama Valley groundwater basin, Santa Barbara County, California.

Table available separately as Microsoft Excel® at http://pubs.usgs.gov/sir/2013/5108.

Table 10. Results for analyses of arsenic, iron, and chromium speciation and dissolved oxygen in samples collected from selected well sites, Cuyama Valley, Santa Barbara County, California.

Table available separately as Microsoft Excel® at http://pubs.usgs.gov/sir/2013/5108.

Five wells (CVKR-2, CVBR-1, CVBR-2, CVBR-3, CUY21) had concentrations of manganese greater than the SMCL-US of 50 µg/L; one of these wells (CUY-21) also had concentrations of iron greater than the SMCL-US of 300 µg/L (table 10). One well (CUY-20) had concentrations of chloride greater than the SMCL-US of 250 mg/L (table 8), and one well (CVKR-4) had concentrations of aluminum greater than the SMCL-US of 50 mg/L (table 10).

Major Ions

Piper diagrams show the relative abundance of major cations and anions (on a charge equivalent basis) as a percentage of the total ion content of the water (Piper, 1944). Piper diagrams often are used to define groundwater type (Hem, 1992). In this report, the dominant cation and anion species are used to describe the water type of a water sample when a single cation or anion composes more than 60 percent of the total cations or anions, respectively. Where no one cation or anion exceeds 60 percent, the first and second most abundant cations or anions are given for description purposes.

The samples from CVKR were characterized as calcium-magnesium sulfate waters (fig. 9*A*) and had total dissolved-solids concentrations ranging from 1,480 to 1,930 mg/L (table 8). The samples from CVBR were calcium-magnesium sulfate waters and had total dissolved-solids concentrations ranging from 772 to 1,560 mg/L. The samples from CVFR also were calcium-magnesium sulfate waters and had total dissolved-solids concentrations ranging from 1,140 to 1,480 mg/L. At the CVFR site, total dissolved-solids increased with depth, but the highest concentrations were observed in samples collected from the shallowest wells at the CVKR and CVBR sites. The majority of the other groundwater samples also were calcium-magnesium sulfate waters (fig. 9*B*). A few samples had a lesser abundance of calcium and magnesium and a greater abundance of sodium (fig.9*B*), which is consistent with loss of calcium and magnesium from solution by means of ion exchange with sodium attached to clays; this process is commonly observed in groundwater with longer residence times and abundant clays in the subsurface.

Nitrate

Samples from all 12 monitoring wells, 27 additional wells, 2 springs, and 2 surface-water sites were analyzed for nitrate. Nitrate concentrations reported as nitrogen (NO_3-N) ranged from less than 0.02 to 45.3 mg/L (table 9). Five of the samples (CVKR-4, CUY-04, -07, -20, and -61) had concentrations greater than the MCL-US of 10 mg/L.

At the CVKR site, nitrate concentrations ranged from 0.45 to 15.2 mg/L and decreased with depth. At the CVBR site, nitrate concentrations were 1.01 mg/L in the shallowest well and were below the detection limit of 0.04 in the three deeper wells. At the CVFR site, nitrate concentrations ranged from estimated values of 0.53 to 1.37 mg/L and, generally, increased with depth.

Irrigation return flows are a possible source of the high nitrate concentrations detected in the Cuyama Valley groundwater basin. A majority of the agricultural activity within the Cuyama Groundwater basin lies within the Caliente Northern-Main and Southern-Main zones and within the northern half of the Southern Ventucopa Uplands. Four of the wells (CVKR-4, CUY-4, -07, -61) where the nitrate levels were greater than the MCL were in the Southern-Main zone (fig. 8) in the center of the agricultural land-use area. A decrease in concentrations with depth at the CVKR site, in the center of the Southern-Main zone, indicated the source of higher nitrate concentrations is likely to be near the surface. Four wells (CUY-2, -16, -21, -28), where the observed nitrate levels were the lowest, below 0.15 mg/L, were south of the Southern-Main zone, outside of the agricultural-use area. Low concentrations of nitrate, less than 0.02 mg/L, in the surface-water samples indicated that surface-water recharge was not a source of high nitrate.

Isotope Analyses

Oxygen-18 (^{18}O) and deuterium (^{2}H) are naturally occurring stable isotopes of oxygen and hydrogen. The isotopic ratios are expressed in delta notation (δ) as per mil (parts per thousand) differences relative to the standard known as Vienna Standard Mean Ocean Water (VSMOW) (Gonfiantini, 1978). The δ^2H and $\delta^{18}O$ composition of precipitation throughout the world is linearly correlated because most of the world's precipitation is derived from the evaporation of seawater. This linear relationship is known as the global meteoric water line (Craig, 1961). The stable isotope ratios of oxygen and hydrogen in groundwater reflect the altitude, latitude, and temperature of recharge and the extent of evaporation before the water entered the groundwater system. Isotope ratios were analyzed from water samples collected from all of the monitoring sites, 21 selected wells, 4 surface-water collection sites, and 2 springs.

The isotope samples from the three deeper CVKR wells became progressively lighter (more negative), indicating that groundwater does not move freely between the different flow paths of the older alluvium and that the units within the

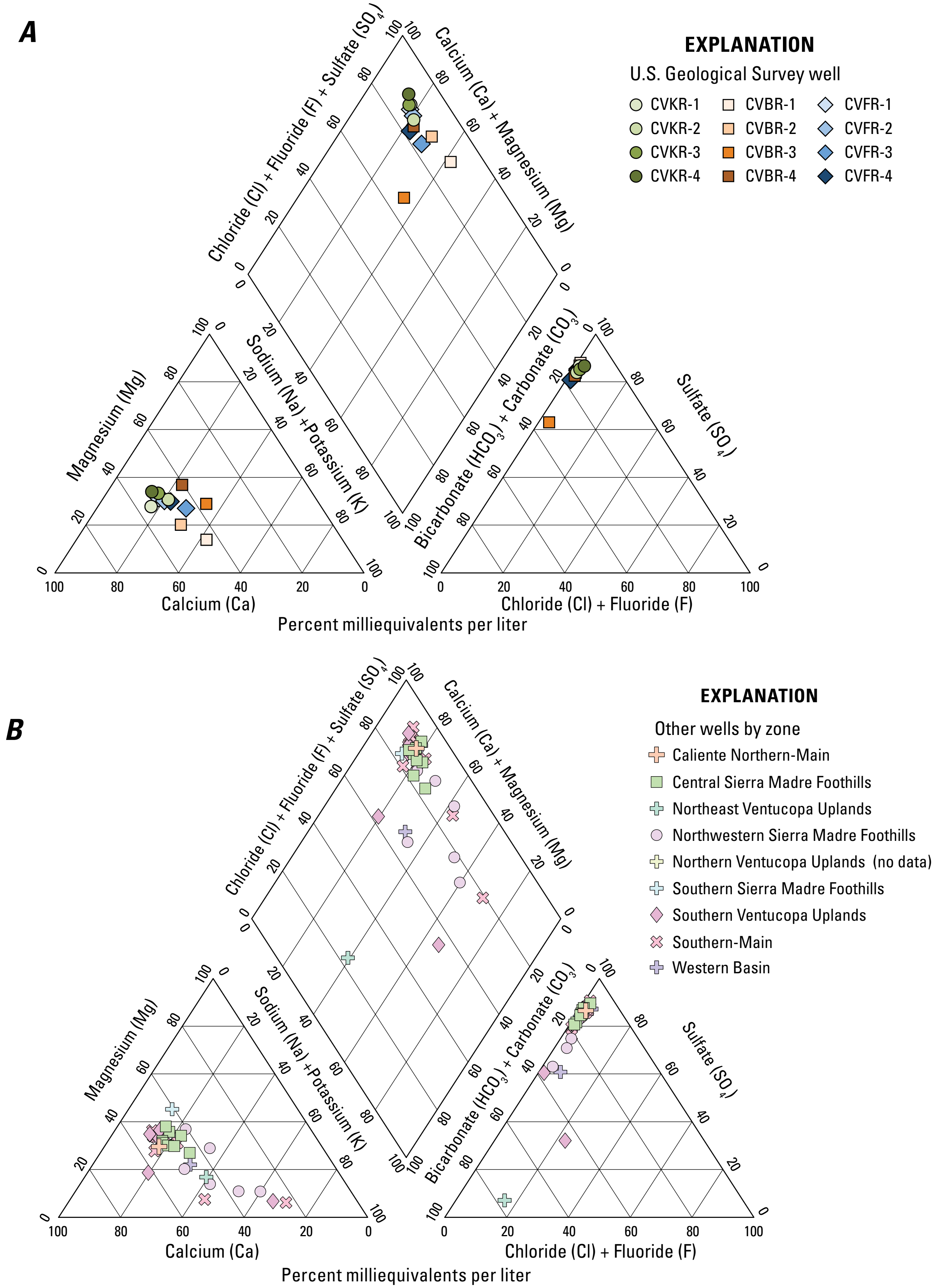

Figure 9. Piper diagrams depicting major-ion composition for groundwater samples, Cuyama Valley, California, collected from *A*, the selected multiple-well monitoring sites; and *B*, multiple-well monitoring sites, domestic and supply wells grouped by zone.

formations could have different sources of recharge (fig. 10*A*). The isotopic composition of the sample from the shallow well (CVKR-4) was similar to the composition of a surface-water sample collected from the nearby Cuyama River (SW-02), indicating a larger contribution from surface-water sources to this shallower depth interval than to the deeper wells at this site.

The isotope samples from the four CVBR wells were, in general, lighter in deuterium than the CVKR wells (fig. 10*A*). The range in values among the four wells also indicated that groundwater does not move freely between the older alluvium and the Morales Formation and that the units could have different sources of recharge.

The isotope samples from the four CVFR wells were the heaviest (least negative) from the three multiple-well monitoring sites (fig. 10*A*). The slightly different isotopic composition of the sample from the deep well (CVFR-1) indicated that groundwater might not move freely between units within the Morales Formation. The isotopic compositions of the four samples were between the compositions of the two surface-water samples collected from the nearby Cuyama River (SW-02 and SW-04), indicating the source of recharge could be the Cuyama River. The substantial difference in isotopic values between the SW-02 and SW-04 sites, which were relatively near each other on the Cuyama River, could reflect that SW-04 was sampled in late August, when evaporative effects on surface water would be expected to be greatest; in contrast, SW-02 was sampled in early April. Evaporation causes isotopic values to move to the right of the meteoric water line, and the isotopic composition of SW-04 is consistent with evaporative modification (fig. 10*A*). Because streamflow is higher in the spring, when evaporative effects are less, it is logical that recharge from Cuyama River water would have an isotopic composition closer to SW-02, a spring value, than SW-04, a summer value.

Restricted movement of water between units was also supported by the wide variability among the isotope samples from the other supply wells in the basin (fig. 10*B*). Samples from the Central Sierra Madre Foothills tended to be heavier (less negative) than most of the other samples. Samples from the Southern Ventucopa Uplands were similar to each other, indicating the same source of recharge. Samples from the Southern-Main and Northwestern Sierra Madre zone were typically lighter than samples from the Southern Ventucopa Uplands zone and trended along or below the meteoric water line, with the latter zone being lighter in deuterium. Isotope ratios for most samples from the Southern-Main zone were between the lightest samples from the Central Sierra Madre Foothills and most of the samples from the Southern Ventucopa Uplands, indicating that water in most of the Southern-Main zone could include a mixture of sources of recharge from the other two zones. Samples from the Southern-Main zone showed greater variation in isotope values than the other zones (fig. 10*B*), which is consistent with groundwater in this zone being derived from a variety of upgradient recharge sources.

Age Dating

Water samples from all of the wells at the CVKR, CVBR, and CVFR sites were analyzed for tritium and carbon-14. Ten other wells (CUY-01 through -08,-11, and -12) were analyzed for tritium, and twenty wells (CUY-01 through -08,-11, -12, and -17 through 26) and one spring (SP-01) were analyzed for carbon-14 (table 9). Tritium and carbon-14 activities provide information about the age (time since recharge) of groundwater. Tritium is a short-lived radioactive isotope of hydrogen; therefore, tritium concentrations above the detection level (0.3 picocuries per liter) indicate the presence of water recharged since the early 1950s, or recent recharge (Plummer and others, 1993; Clark and Fritz, 1997).

Samples from CVKR-3, CVKR-4, and CVBR-3 contained tritium concentrations near the detection level of 0.3 pCi/L, indicating recent recharge. Samples from CVKR-1, CVKR-2, CVBR-1, CVBR-2 and CVBR-4 contained concentrations less than 0.3 pCi/L, indicating that the water from these wells was recharged prior to the early 1950s. Post-1950s recharge in CVKR-3 and CVKR-4 was supported by relatively high NO_3-N concentrations in samples from these wells (table 9). Samples from all four wells at the CVFR site contained relatively high concentrations of tritium, indicating that the water from these wells contains water recharged since the 1950s. Tritium concentrations at the CVFR site increased with depth. The presence of modern water throughout the depth profile is most likely caused by local pumping. Pumping at depth can alter the natural flow paths and draw younger water from the edges of the basin under the shallower, non-pumped units or can draw younger water down to the pumped depths from above. Greater groundwater flows in the deeper depth intervals are consistent with the measured temperature gradients at CVKR and CVBR; however, fluctuations in temperature gradients at CVFR were greatly subdued relative to these sites, indicating lateral groundwater fluxes at CVFR are relatively modest. However, the isotopic data from CVFR were consistent with recharge derived from Cuyama River water at all depths. Because the CVFR site has an unsaturated zone that is nearly 570 ft thick with some clay layers (fig. 5), it is most likely that recharge from the Cuyama River followed horizontal and vertical flow paths through the saturated aquifer between the river and CVFR to reach these monitoring wells.

Tritium was detected in 14 of the 20 water samples collected from other wells (table 9). Tritium concentrations in these samples ranged from 0.43 to 9.0 pCi/L. The presence of tritium in most of the wells indicated that recent recharge contributes to the water resources in all zones in the Cuyama Valley groundwater basin.

Carbon-14 is a radioactive isotope of carbon with a half-life of about 5,700 years (Godwin, 1962). Carbon-14 activities are used to determine the age (time since recharge) of groundwater on time scales ranging from recent to more than 20,000 years before present (Izbicki and Michel, 2003). Carbon-14 ages presented in this report do not account for changes in carbon-14 activities resulting from chemical

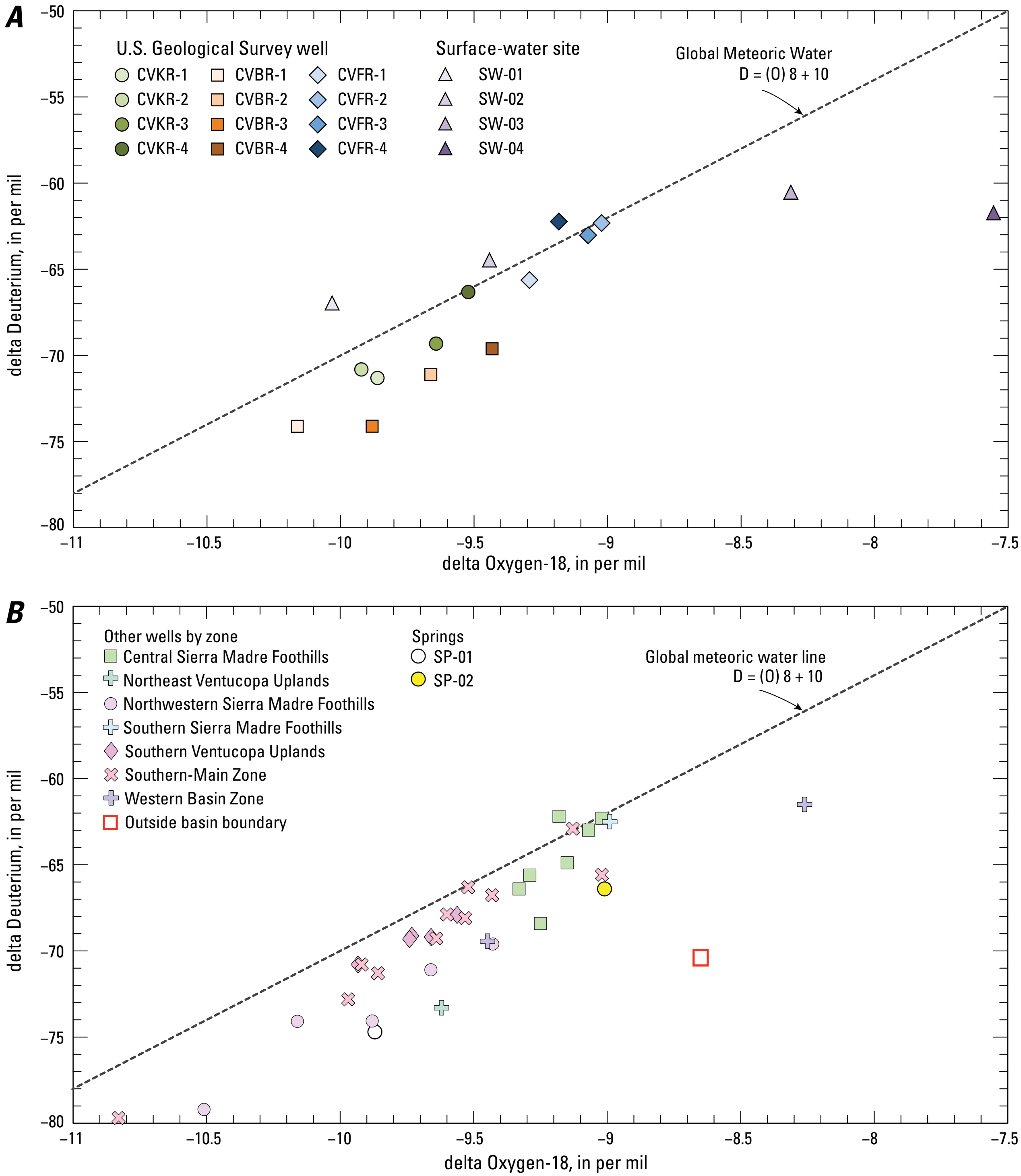

Figure 10. Isotopic composition of water samples, Cuyama Valley, California, collected from *A*, selected multiple-well monitoring sites and surface-water sites, and *B*, multiple-well monitoring sites, domestic and supply wells, grouped by zone and springs.

reactions or mixing and, therefore, are considered uncorrected ages. In general, uncorrected carbon-14 ages are older than the actual ages of the water after correction. Uncorrected ages (in years before present) were calculated by multiplying 8,033 by the natural log (ln) of the percent modern carbon expressed as a decimal as shown in the following equation (Stuiver and Polach, 1977):

Estimated age = 8,033 * ln (percent modern carbon/100 percent)

Uncertainties in the initial value of carbon-14 in recharge waters add uncertainties to the groundwater-age estimations using carbon-14; without more comprehensive geochemical modeling, the carbon-14 ages are to be treated as relative estimates of age rather than accurate, absolute estimates of age. Water from the CVKR and CVFR monitoring wells (near the Cuyama River) was found to be younger than the water from the CVBR monitoring wells (4 miles away from the Cuyama River). Estimated carbon-14 ages for the CVKR, CVBR, and CVFR sites ranged from 3,600 to 6,400, 20,900 to 31,200, and 2,700 to 3,100 years before present, respectively. Estimated ages increased with depth at the CVKR and CVBR sites. The samples from CVKR-3 and -4, CVBR-3, and CVFR-1, -2, -3, and -4 contained water with detectable tritium (recent recharge) and an uncorrected carbon-14 age of more than 2,700 years before present, indicating that these wells receive groundwater of different ages that are mixed in the sampled groundwater. In these mixed samples, tritium activities were less than 0.55 pCi/L in CVKR-3, and -4, and CVBR-3; these samples could contain relatively small amounts of modern water. The carbon-14 value in CVBR-3 was an order of magnitude less than in CVKR-3, -4; this comparison indicated that the water at CVBR-3 is primarily very old with a small fraction of modern water and that CVKR-3 and -4 could contain mixtures of water that do not span as wide a range of ages. The samples from CVFR had tritium activities that were an order of magnitude higher than CVKR-3, and -4, and CVBR-3; consequently, fractions of modern water in CVFR wells are likely to be much larger than in CVKR-3, and -4, and CVBR-3.

Estimated carbon-14 ages for the other 20 sites ranged from 600 (CUY-03) to 38,300 (CUY-23) years before present (table 9). In general, the youngest water was found in wells in the Southern Ventucopa Uplands; this zone is a source of recharge for the Cuyama Valley and the presence of younger water is expected. The oldest water was found in wells in the Southern-Main, Northwestern Sierra Madre Foothills, and Central Sierra Madre Foothills zones. This is in contrast to the observation of Singer and Swarzenski (1970) that a substantial component of regional flow was northward from the Sierra Madre Mountains. If a significant portion of the flow is from the Sierra Madres, water in this flow path would be expected to be younger than what was observed, unless formations deeper than the Morales Formation, previously thought to be non-water-bearing, are contributing to groundwater discharge from the Sierra Madres toward the Southern-Main zone.

Arsenic, Iron, and Chromium Species

Arsenic, chromium, and iron can be different species depending on the oxidation-reduction state of the groundwater. The oxidized and reduced species have different solubilities in groundwater and can have different effects on human health. The relative proportions of the oxidized and reduced species of each element can be used to aid in interpretation of the oxidation–reduction conditions of the aquifer, which affect the mobility of many constituents. Concentrations of dissolved arsenic, chromium, and iron, and the dissolved concentration of either the reduced or the oxidized species of the element are reported in table 10. The concentration of the other species can be calculated by difference. The concentrations measured by the NWQL are considered to be more accurate determinations of dissolved arsenic, iron, and chromium. For some samples, the concentrations of total arsenic, total iron, and total chromium were measured by the TML and the NWQL using different sample collection and analytical methods; therefore, the total concentrations reported from the TML in table 10 could be different than those reported by the NWQL. The data from TML were primarily used to identify the predominant oxidation-reduction species present in the samples, which is useful for understanding the geochemical environment and processes affecting trace-element concentrations in the system.

Concentrations of total arsenic [As(T)] were greater than the MCL-US of 10 micrograms per liter (µg/L) in well samples analyzed at the NWQL from 4 of 33 wells. The highest concentration of arsenic, 67.1 µg/L, was in well CUY-23, which is in the Southern-Main zone and screened in both the younger and older alluvium; this sample had the oldest groundwater age in the study area, with no detected tritium, and an uncorrected carbon-14 age of 38,300 years before present (table 9), as well as the deepest bottom of perforations at 2,120 ft bls (table 2). Concentrations of arsenic in the CVBR-2 and CVBR-1 samples were 58.1 and 37.7 µg/L, respectively. The CVBR multiple-well monitoring site is in the Northwestern Sierra Madre Foothills zone, and both wells are screened in the Morales Formation and have uncorrected carbon-14 ages older than 25,000 years before present. An arsenic concentration of 44.0 µg/L was observed in well CUY-02, which is in the Northwestern Sierra Madre Foothills, is screened in both the older alluvium and Morales Formation, and contained water that had an uncorrected carbon-14 age of 33,400 years before present. The next highest concentrations of arsenic in groundwater—8.6 and 5.6 µg/L—were measured for CVBR-3, which is in the Northwestern Sierra Madre Foothills and screened in the older alluvium, followed by CUY-21, with a total arsenic concentration of 3.5 ug/L, which is in the Central Sierra Madre Foothills and screened in the Morales. The surface-water sample collected from the Cuyama River at site SW-04 in the southern end of the Southern Ventucopa Uplands contained a total concentration of 0.51 µg/L, indicating that surface-water recharge potentially is not a source of the arsenic. The four highest concentrations of arsenic were found in water that is older than 25,000 years, indicating that arsenic concentrations are higher in groundwater that has had more time to mobilize the arsenic.

Concentrations of total chromium [Cr(T)] ranged from no detections to 2.2 µg/L, less than the MCL-CA threshold 50 µg/L. The highest concentration of Cr(T), 2.2 µg/L, was observed in well CUY-20, which is outside of the basin boundary (fig. 8). All of the wells inside the basin had concentrations of Cr(T) less than or equal to 1.3 µg/L. Concentrations of hexavalent chromium [Cr(VI)], however, were greater than the OEHHA-PHG of 0.02 µg/L in 20 of the samples. Concentrations of Cr(VI) ranged from 0.1 to 1.7 µg/L. Concentrations of Cr(VI) were greater than the concentrations of Cr(T) in five of the samples. The difference in values can be attributed to the different methods of analysis used and the level of error (0.1 µg/L for each method) in the laboratory analysis. In these five samples, all concentrations of Cr(VI) and Cr(T)) were very near the detection limit (0.1 µg/L), and the laboratory measurement error can account for the differences. The three remaining samples had detections of Cr(VI) below the reporting limit of 0.1 µg/L.

Hydrology

Hydrologic data analyzed as part of this study included rainfall records, stream-discharge records, water-level records, and estimates of hydraulic properties. Rainfall records include monthly and annual rainfall totals and provide information on seasonal and annual variability in precipitation. Stream-discharge records include daily mean discharge measurements from three stream gaging stations and provide information on seasonal variability in surface-water flows and the potential stream losses (recharge) to the groundwater system. Water-level records include quarterly manual depth-to-water measurements collected from the 12 monitoring wells and 55 domestic and supply wells and time-series data collected from the monitoring wells and 8 domestic and supply wells. Water-level measurements, manual and time-series, provide information on the seasonal responses of the aquifer system to pumping. Estimates of hydraulic properties include hydraulic conductivity and transmissivity estimated from aquifer tests performed on the 12 monitoring wells and 51 domestic and supply wells. Estimates of hydraulic properties of the Cuyama Valley aquifer provide insight into the rates of groundwater movement.

Rainfall Gaging Stations

The annual rainfall data in this report are presented by “water year.” A water year is defined as the 12-month period from October 1 of any given year through September 30 of the following year. The water year is designated by the calendar year in which it ends. Thus, the year ending September 30, 1999, is called the “water year 1999.” Historical yearly and monthly rainfall totals from three rainfall gages operating in Santa Barbara County and one rainfall gage operating in Ventura County are shown in figures 11 and 12, respectively. The Caltrans, New Cuyama gage (Station 402), and the Cuyama Fire Station gage (Station 436) are near the city of New Cuyama; the Santa Barbara Canyon gage (Station 347) is in Santa Barbara County; and the Ozena Guard Station (NWS) gage (Station 174A) is near the Cuyama River in the southern half of the Southern Ventucopa Uplands (fig. 2). Rainfall records for Stations 402 and 436 are available from water-year 1955 to the present. Records for Station 347 are available from water-year 1905 through water-year 1980, and from water-year 1997 to the present. Rainfall records for Station 174A are available from water-year 1980 through July 2008. The official monthly and yearly rainfall records for the Santa Barbara County stations are published by the Santa Barbara County Flood Control District. The data are available for public access at *http://www.countyofsb.org/pwd/*. The monthly and yearly rainfall records for the Ventura County stations are published by the Ventura County Watershed Protection District and are available for public access at *http://www.vcwatershed.net/hydrodata*.

Analysis of the annual rainfall showed that Stations 402 and 436, in the valley, received less rainfall than Stations 347 and 174A in the uplands to the south (fig. 11). Stations 402 and 436 received approximately the same amount of rainfall. Annual totals for the two sites averaged 8 inches and range from less than 2 inches (Station 436) to over 20 inches (Station 402) per year. Station 174A typically received the most rainfall. Annual rainfall totals at Stations 174A averaged almost 19 inches and ranged from about 5 to over 44 inches per year. Annual rainfall totals at Stations 347 averaged over 12 inches and ranged from about 4 to over 32 inches per year.

Averaging the total annual rainfall from all stations since records began at multiple sites in 1954 indicated that the highest annual rainfall in the Cuyama Valley was during water-years 1958, 1969, 1978, 1983, 1995, and 1998 (fig. 11). Records from the only station to exist prior to 1954 (Station 347) showed an annual rainfall of over 32 inches during water year 1941, the highest observed at that station.

Streamflow Gaging Stations

Daily discharge data from three streamflow gaging stations in the Cuyama Valley drainage are available (figs. 13–14). Two gaging stations are on the Cuyama River: one is south of Ventucopa and measures surface-water flow into the valley from the Cuyama River, and the second site is near Buckhorn Canyon, west of the valley, and measures all surface flow out of the valley. The third gaging station is in Santa Barbara Canyon. The station on the Cuyama River near Ventucopa (SW-04) has historic data from October 1945 through September 1958. The site was reestablished on August 24, 2009. The station near Buckhorn Canyon (SW-05) was established on October 1, 1959. The station in Santa Barbara Canyon (SW-03) was established on October 1, 2009.

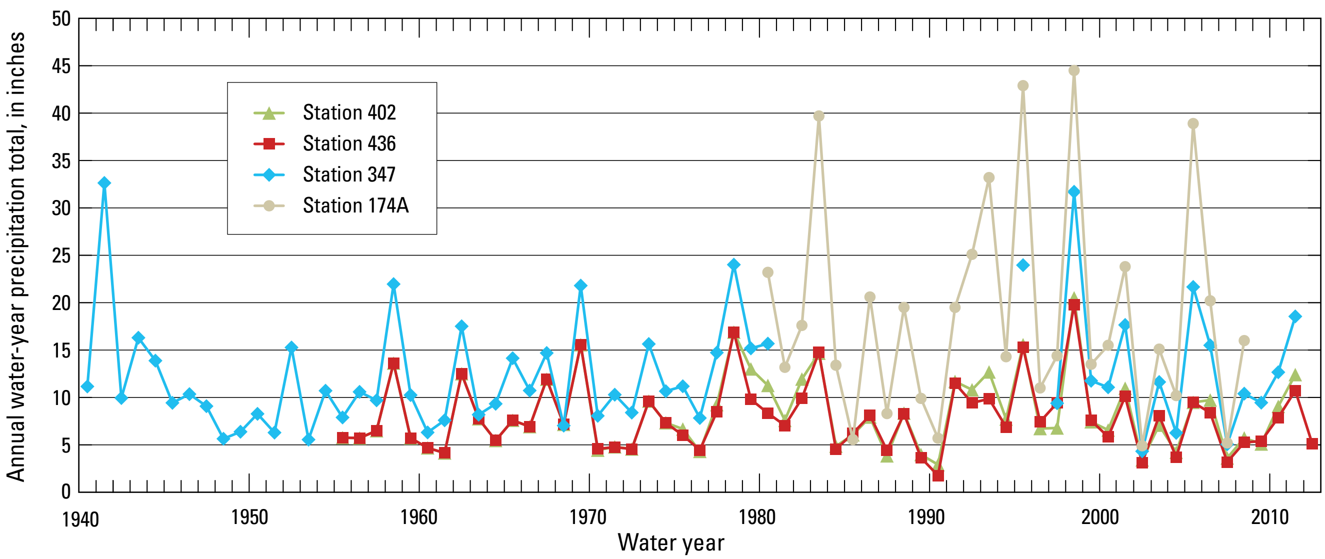

Figure 11. Historic annual rainfall graphs from four rainfall stations in the study area, Cuyama Valley, Santa Barbara County, California.

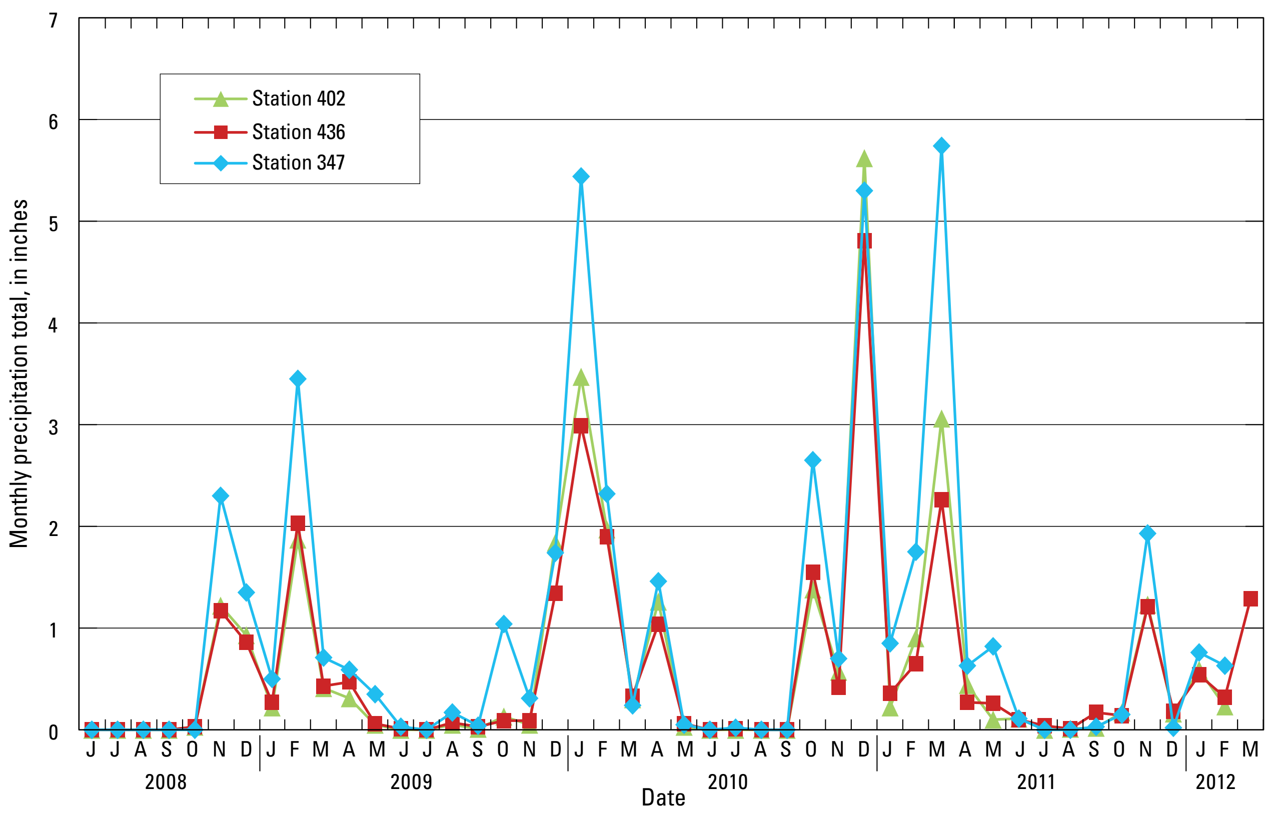

Figure 12. Monthly rainfall graphs for three rainfall stations in the study area from June 2008 to March 2012, Cuyama Valley, Santa Barbara County, California.

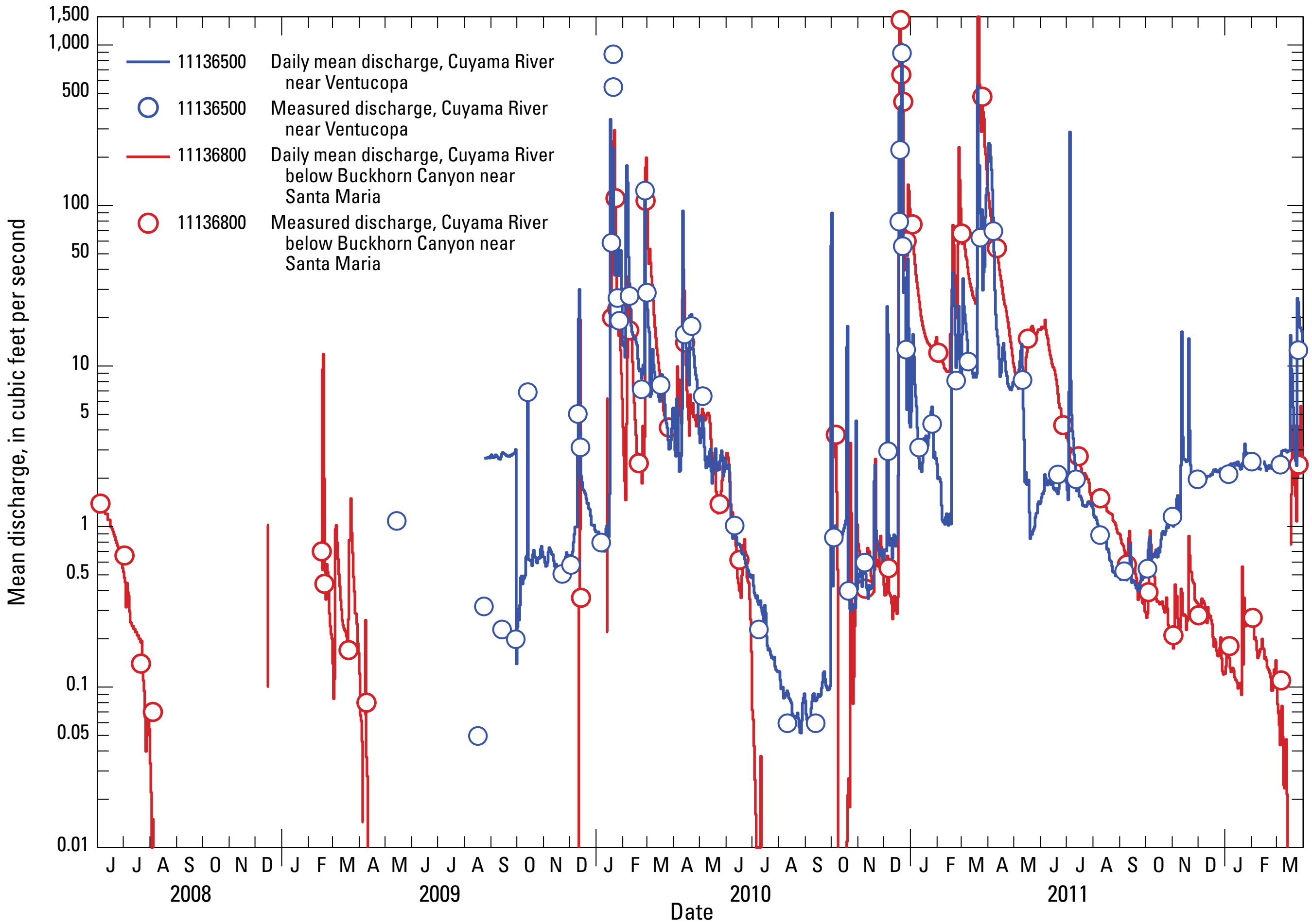

Figure 13. Daily discharge graphs for two streamflow gaging stations (11136500 and 11136800) on the Cuyama River, Cuyama Valley, Santa Barbara County, California.

Locations of these gaging stations, with the exception of SW-05, are shown in figure 1. Data collected from these sites are available online at *http://waterdata.usgs.gov/ca/nwis*.

Cuyama River

Records from the Ventucopa station (fig. 13) showed the streamflow is perennial, but varies seasonally. Higher flow, averaging between 2 and 200 cubic feet per second (cfs), generally is observed during the wet season, or December through May; lower flow, averaging below 2 cfs, is observed during the dry season, or the remainder of the year. Flow observed during the dry season of 2011 was greater than that of 2010. Three flow events exceeding 100 cfs were observed between September 2009 and March 2012. High flows of 875 and 1,020 cfs were observed in January and December of 2010, respectively. A sustained increase in flow was observed between March 20 and April 9, 2011. While four distinct peaks were observed, flows exceeded 30 cfs during the entire period and averaged 136 cfs for the 21-day period.

Records from the Buckhorn Canyon station showed the streamflow is not continuous and varies seasonally. Higher flow, averaging between 2 and 200 cfs is observed through most of the wet season, while flow during the dry season averaged less than 2 cfs, and it is typically dry late in the season. Flows exceeding 1500 cfs were observed during the wet season of 2011, but high flows were typically below 200 cfs.

Periods when the inflow from the Cuyama River (SW-04) was equal to or greater than the Cuyama River outflow (SW-05) indicated that the surface water was recharging the groundwater system. Simplistically, it can be assumed that if the inflow and outflow along the Cuyama River are equal, then the total of all other inflow to the Cuyama Valley, such as from Apache, Quanta, Santa Barbara, and Salisbury Canyon, represents the total amount of potential recharge. In general, surface water flowing into the Cuyama Valley from the Cuyama River is about equal to the amount of water flowing out, indicating that some degree of recharge from streams is typical. There are periods when outflow exceeds inflow, which indicate some combination of significant input

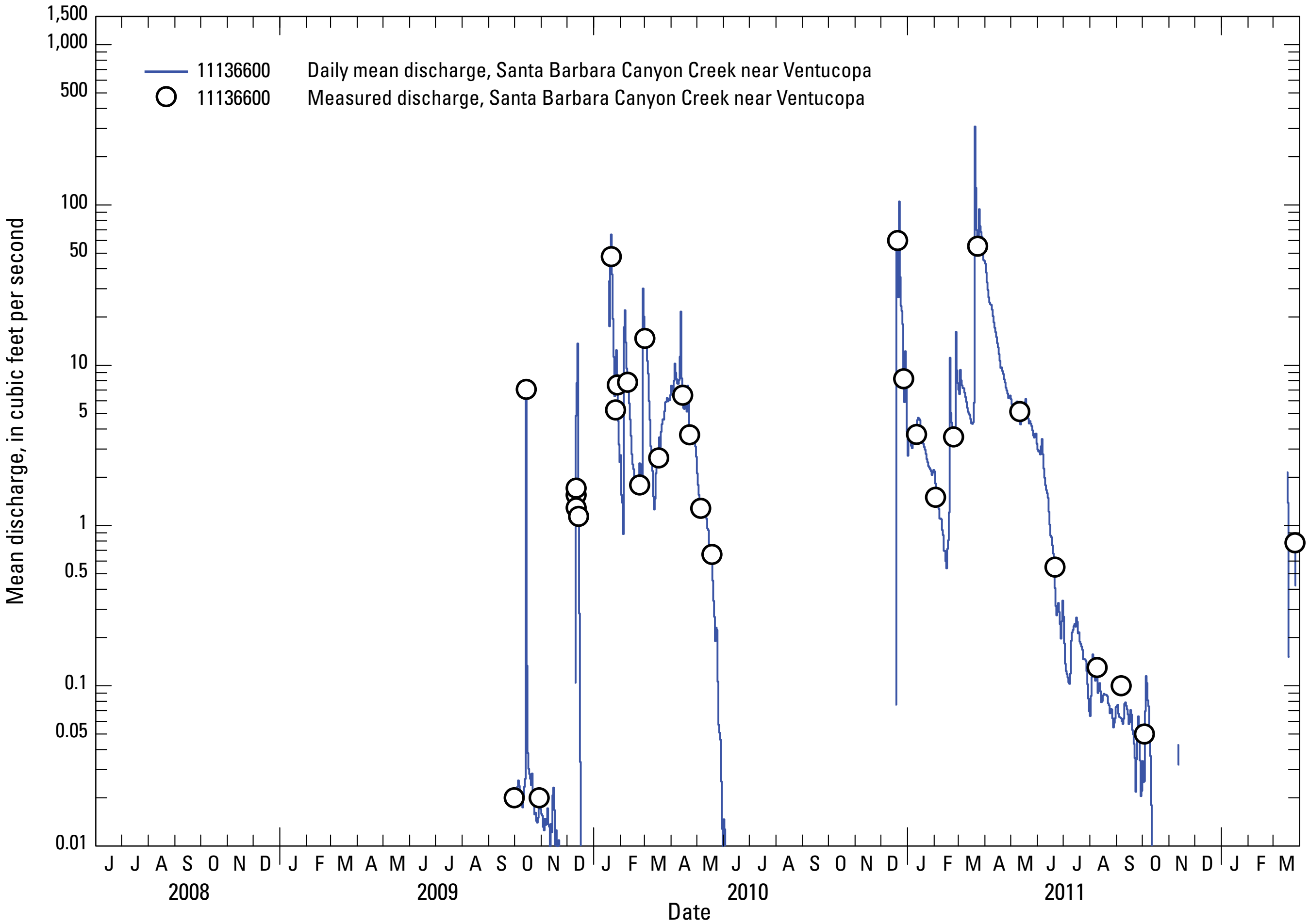

Figure 14. Daily discharge graphs for streamflow gaging stations (11136600) in Santa Barbara Canyon, Cuyama Valley, Santa Barbara County, California.

from tributaries, baseflow, and return flow from bank storage. Periods when inflow exceeds outflow indicate significant recharge from streams; the longest such period was from October 2011 to March 2012 (fig. 13).

Santa Barbara Canyon

Santa Barbara Canyon drains the southwest flanks of the Sierra Madre Mountains and represents the largest of the surrounding watersheds that flow into Cuyama Valley as a tributary to the Cuyama River (fig. 14). Streamflow records showed seasonality, with continuous flow generally ranging between 1 and 20 cfs through most of the wet season and no flow during the dry season. Flow was observed during the dry season of 2011, but was less than 0.5 cfs. The highest flow on record at this site, about 300 cfs, was measured in late March of 2011.

Groundwater Levels

Water levels, measured as depth to water below land surface, were routinely measured in all 12 monitoring wells and in an additional 56 selected wells in the Cuyama Valley (table 1). Thirty-three of the additional wells had water-level records prior to January 1, 2008; some records date as far back as August 1941 (table 11). Twenty of the wells were equipped with instrumentation to automatically measure and record the depth to water at regular time intervals (time-series; table 1). The water-level measurements in this report are given in feet with reference to land-surface datum (LSD). LSD is a datum plane that is approximately at land surface at each well. The elevation of the land-surface datum is given in table 11. Users of the data are encouraged to access site information through the USGS NWIS Web at *http://waterdata.usgs.gov/nwis/*.

Table 11. Summary of sites with manual water-level measurements including period of record, number of observation, and minimum and maximum observed water levels for selected wells, Cuyama Valley, Santa Barbara County, California.

Table available separately as Microsoft Excel® at http://pubs.usgs.gov/sir/2013/5108.

Manual Measurements

Manual water-level measurements were typically taken once every 3 months in all wells shown in figure 15. Water levels were measured and recorded to within 0.01 foot by using a calibrated electric or steel tape. A summary of the available water-level data is presented in table 11, including land-surface elevation, period of record, number of measurements, and the minimum and maximum observed water levels.

Hydrographs for most wells showed seasonal fluctuations in water levels. Water levels generally declined during the summer months, coinciding with the peak of the agricultural season, and recovered during the winter months, when agricultural pumping is at a minimum. Several wells on the outer edges of the basin and in the Southern Ventucopa Uplands showed delayed responses, with the highest levels in the summer and lowest in the winter.

A comparison of the highest annual measured water levels since January 2008 in the 56 domestic and supply wells showed that 16 wells had a declining trend, 7 wells had an upward trend, 8 wells had a reversal from downward to upward trends, 1 well had a reversal from upward to downward trend, and 9 wells showed no trend. Records from the remaining 15 wells were insufficient to determine a trend. Water-level declines in the 16 wells with downward trends ranged from about 6 feet in several wells to over 30 feet (CUY-07). Downward water-level trends were observed in five zones; 7 of the 16 wells were in the Southern-Main zone (CUY-04, -06, -07, -50, -51, -56, and -59), 4 were in the Central Sierra Madre Foothills (CUY-21, -24, -25, and -48), and 3 were in the Southern Ventucopa Uplands (CUY-03, -12, and -46). Water-level increases in the seven wells with upward trends ranged from less than 1 foot in several wells to about 8 feet (CUY-47). Two of the seven wells showing upward trends were in the Southern Ventucopa Uplands (CUY-31, and -35), two were in the Northeast Ventucopa Uplands (CUY-17, and -36), two were in the Southern-Main zone (CUY-08, and -27), and one was in the Southern Sierra Madre Foothills (CUY-47). The eight wells showing a reversal from declining to rising water levels were all in the Southern Ventucopa Uplands (CUY-13, -19, -30, -38, -39, -40, -42, and -43). Water levels declined from 2008 through the summer of 2010, began to rise early in 2012, and continued to rise throughout the summer of 2012. The observed rise in these wells ranged from 5 to 15 feet. The rise in water level indicated that the aquifers receive recharge under certain conditions; this rise only in the Southern Ventucopa Uplands indicates that the water table in this zone could be relatively well-connected with recharge sources.

Time-Series Water Levels

All 12 monitoring wells and 8 additional wells were equipped with instrumentation to automatically measure and record the depth to water at regular time intervals, typically every hour or 15 minutes (fig. 15). The computed unit values, and daily maximum, minimum, and median values for all time-series water-level data for these sites are available through the USGS NWIS Web. Periodic manual measurements of water levels were made to verify the time-series data. Seventeen wells with time-series water-level data are presented as time-series plots. Three wells (CUY-04,-55, and -60) with time-series records shorter than 6 months are not presented in this report.

Time-series data presented in this report are the computed hourly unit values, as opposed to daily statistical values. Including the computed hourly values, even those water levels affected by pumping can cause the hydrograph to appear cluttered or "fuzzy," especially when the x-axis is compressed. The hourly data display the entire range of water levels observed in the well under static and pumping conditions, and indicate when pumping and recovery are occurring. Most data gaps, denoted in grey on the hydrographs, were caused by the water level in the well dropping below the level of the sensor; consequently, the water level during these gaps is known to be deeper than the last measurement before the data gap.

The pumping of nearby irrigation wells directly influenced water levels in all of the CVKR (fig. 16) and CVBR (fig. 17) wells. During the period of record (2009–12), data showed a seasonal pattern, with water levels declining between March and August, coinciding with the peak of the agricultural season, and rising between September and February, when nearby irrigation and related pumping were at a minimum.

At the CVKR site, water levels in the three deeper wells (CVKR-1, -2, and -3) varied as much as 60 feet between March and August, while water levels in the shallowest well (CVKR-4) varied by about 25 ft over the same period (fig. 16). Water levels showed a decline in the seasonally high levels over the period of record. Manual measurements made in late February 2012 showed a decline of over 30 feet compared to those made in early March 2009. Vertical hydraulic gradients were upward during the winter months and reversed to downward gradients during the irrigation season.

Seasonal patterns at the CVBR site were similar to those at the CVKR site. Water levels in the three deeper wells (CVBR-1, -2, and -3) varied by as much as 90 feet between March and August, while water levels in the shallowest well (CVBR-4) varied by about 40 ft over the same period (fig. 17). Water levels showed a decline in the seasonally high levels over the period of record. Manual measurements made in late February of 2011 showed a decline of about 5 feet compared to those made in early March of 2010. Vertical hydraulic gradients were upward during the winter months and reversed to downward gradients during the irrigation season. Short-term fluctuations in water levels were larger at CVBR than CVKR, which is consistent with CVBR being more strongly affected by pumping in close proximity to the monitoring wells than CVKR.

Observations at the CVFR site indicated that water levels did not show short-term (daily) variability from nearby pumping as seen at the other sites, but did show similar

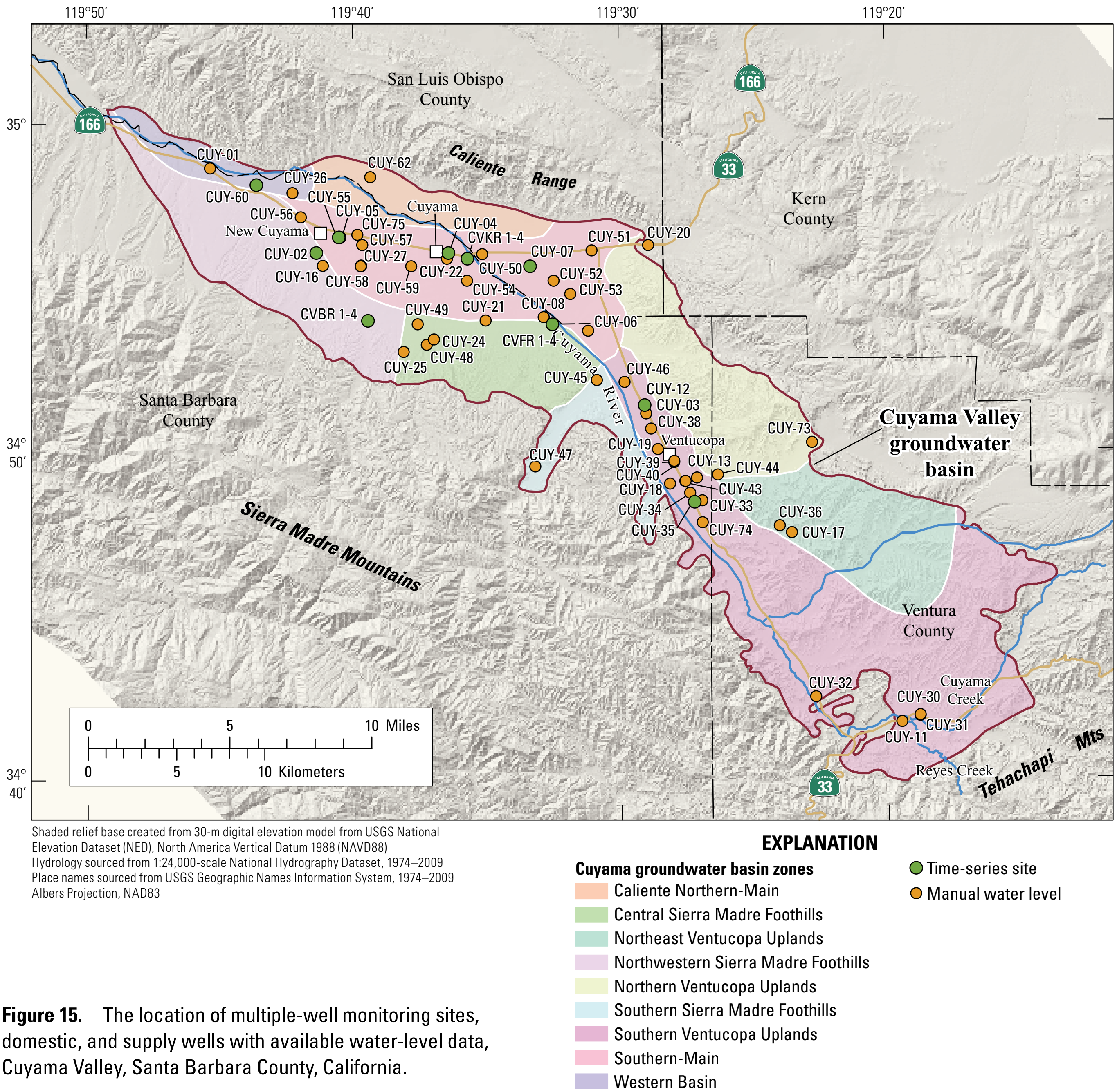

Figure 15. The location of multiple-well monitoring sites, domestic, and supply wells with available water-level data, Cuyama Valley, Santa Barbara County, California.

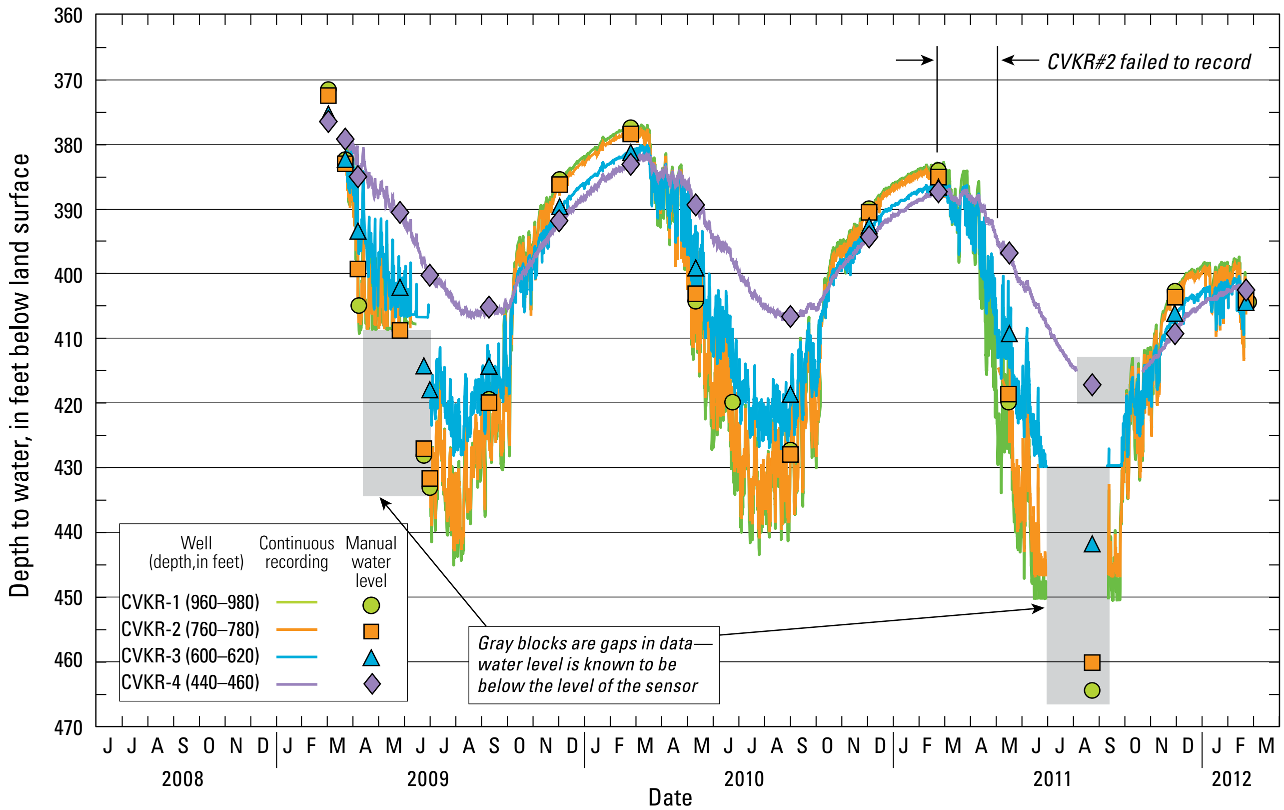

Figure 16. Water-level hydrograph from multiple-well monitoring site Cuyama Valley Kirschenmann Road (CVKR) from April 8, 2009, to February 20, 2012, Cuyama Valley, California.

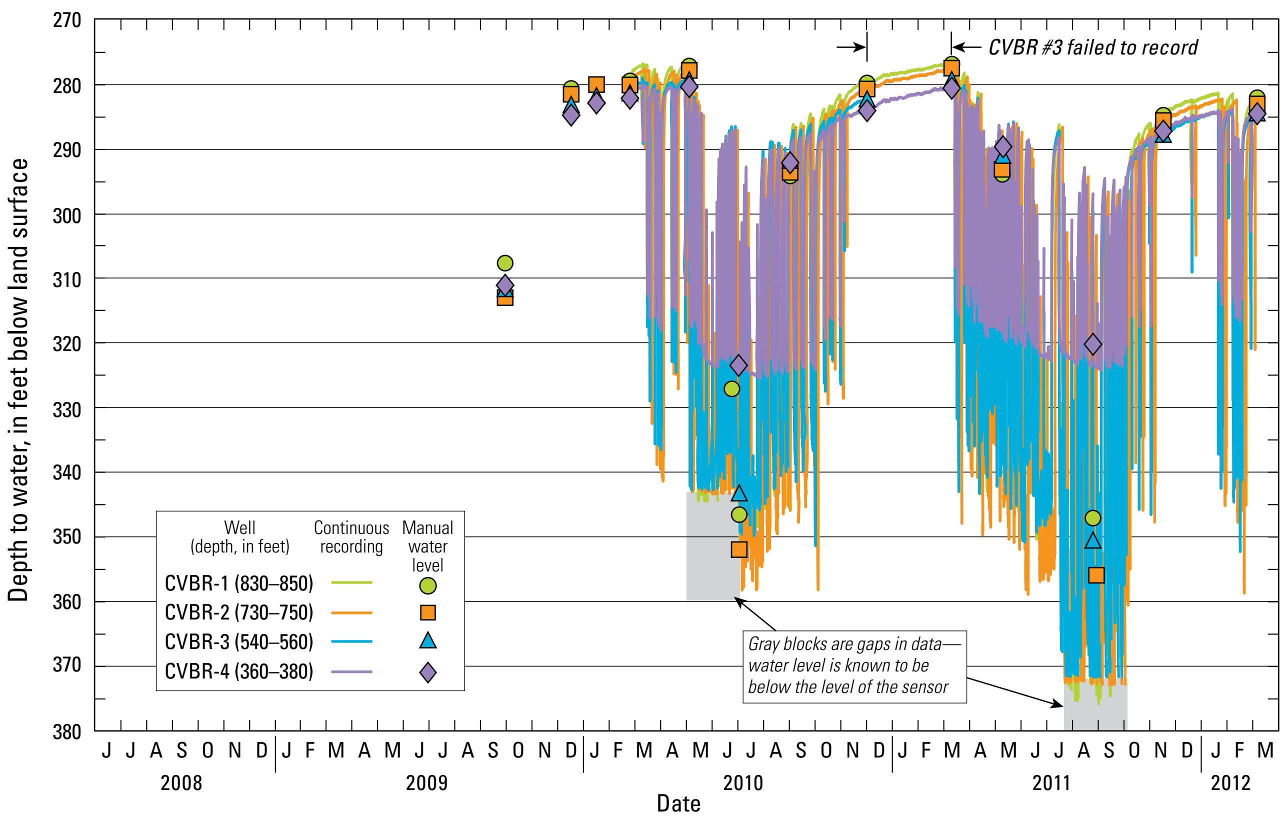

Figure 17. Water-level hydrograph from multiple-well monitoring site Cuyama Valley Bell Road (CVBR) from September 29, 2009, to March 5, 2012, Cuyama Valley, California.

seasonal and longer-term changes. Similar to CVKR and CVBR, the vertical hydraulic gradients were upward during the winter months and reversed to downward gradients during the irrigation season; however, the gradients at the CVFR site were notably smaller. The gradient reversal at this location indicated that water levels at this site were influenced by local pumping but were not as strongly affected as CVKR and CVBR. Seasonal water levels in the wells varied about 15 feet between March and September (fig. 18). Water levels showed a decline in the seasonally high levels over the period of record by about 10 feet per year.

Time-series data from well CUY-02 (fig. 19) in the Northwestern Sierra Madre Foothills zone showed no discernible trend over the period of record. Seasonally high water levels rose slightly between 2009 and 2010, were similar between 2010 and 2011, then declined by almost 25 ft between 2011 and 2012; this pattern correlates to the relative duration of seasonal pumping of the well, which was apparent on the hydrograph (fig. 19). In 2009, daily pumping in this well started in late June and continued for about 5 months. Because of the data gap between early August 2009 and April 2010, caused by a probe failure, the entire pumping season did not show, but manual water-level measurements indicated pumping stopped sometime before mid-November. This pumping cycle correlated with the observed rise. In 2010, daily pumping in this well covered the same period: pumping started in early June and continued until early November. Comparison of the daily records, however, indicated the pump was operated more frequently during the first 30 days of operation in 2010 than in 2009. This pumping cycle correlated with the observed static water levels. In 2011, daily pumping in this well covered a longer time span: pumping started a month earlier, in mid-May, and continued through November. A comparison of the daily records indicated the pump was operated more during 2011 than 2010. This pumping cycle correlated with the observed decrease in water levels. The increased irrigational pumping

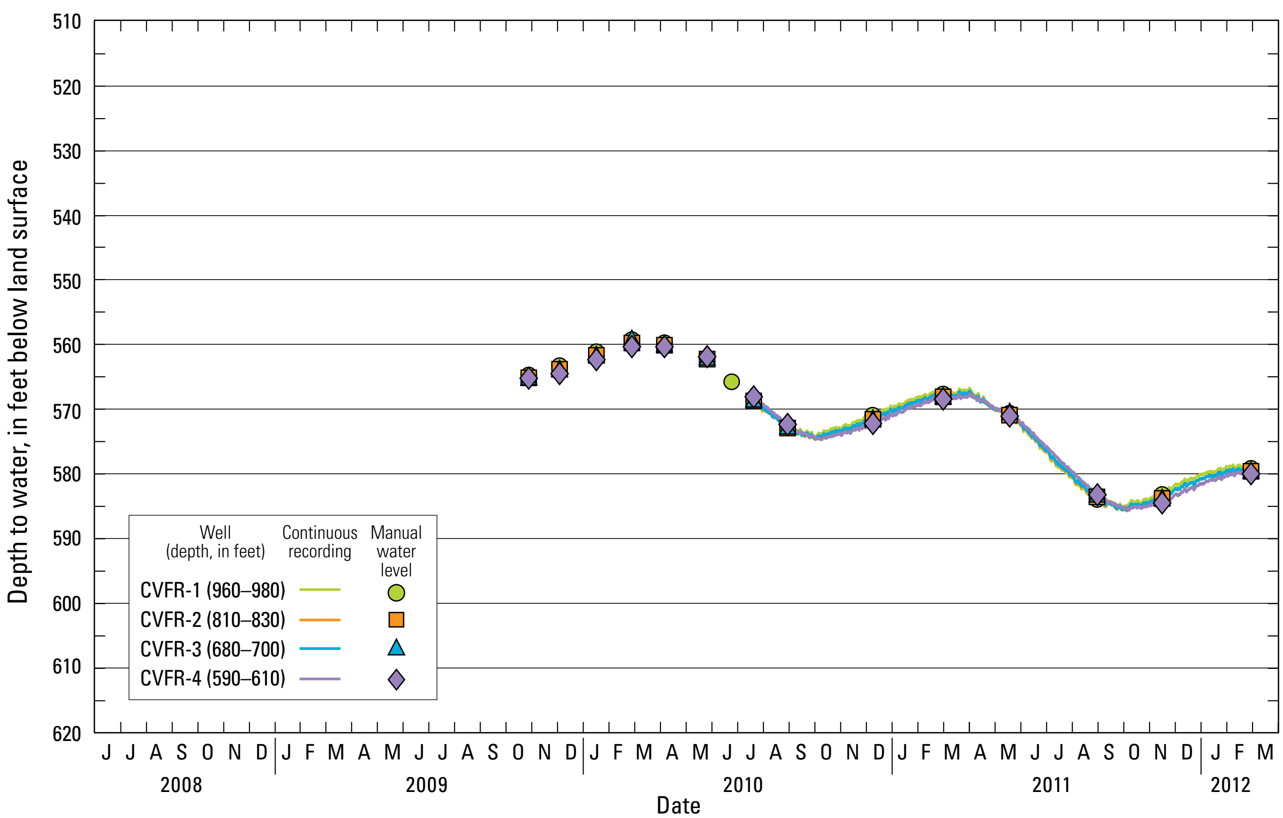

Figure 18. Water-level hydrograph from multiple-well monitoring site Cuyama Valley Foothill Road (CVFR) from October 27, 2009, to February 28, 2012, Cuyama Valley, California.

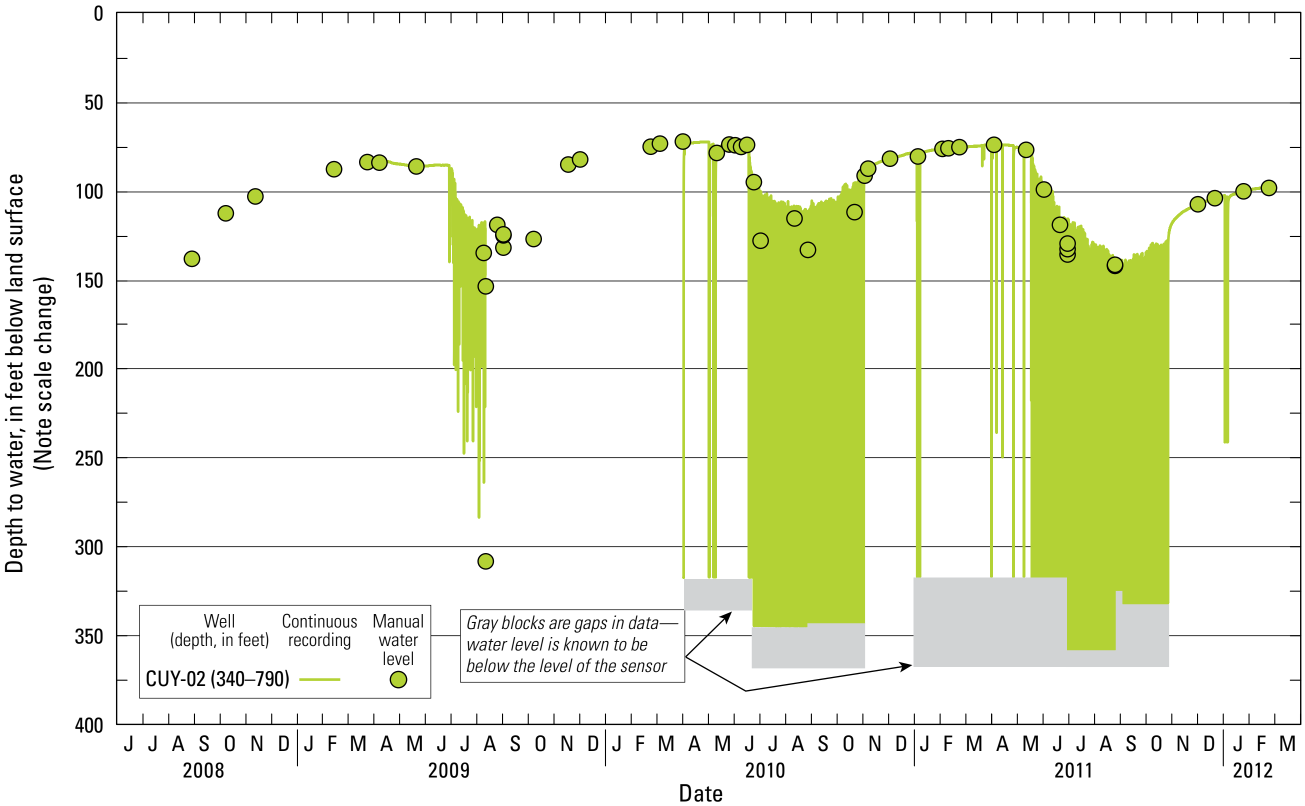

Figure 19. Water-level hydrograph from CUY-02, from January 1, 2008, to March 23, 2012, Cuyama Valley, California.

of other wells in the Northwestern Sierra Madre Foothills zone, reported during the summer of 2011 by several residents, also could have contributed to the observed decline in water levels. Irrespective of cause, the change in the pumping, and possibly recharge, conditions between 2010 and 2011 in the Northwestern Sierra Madre Foothills zone resulted in changes from static and overdraft conditions; these patterns were evident in both CVBR and CUY-02.

Time-series data from wells CUY-05 (fig. 20) and CUY-07 (fig. 21) in the Southern Main zone showed a more detailed record of the steady decline in water level than was observed in the manual measurements. These hydrographs showed the seasonal highs and lows that are expected, and the year-to-year seasonal highs showed a steady decline in water levels. A decline of approximately 2.5 feet per year was observed at CUY-05 (fig. 20) between 2010 and 2012, and a decline of about 7 feet per year was observed at CUY-07 (fig. 21) between 2010 and 2012. Water levels in well CUY-05 showed high daily variability associated with the active pumping during the period of record, while water levels in the non-pumped well CUY-07 showed low daily variability. The lower variability in CUY-07 likely reflected the effects of regional pumping rather than local pumping effects near CUY-07.

Time-series water-level data from two wells, CUY-12 and CUY-35 in the Southern Ventucopa Uplands zone, showed a rise in water levels during the spring of 2012 compared to earlier spring high water levels. At CUY-12 (fig. 22), the 3 to 4 foot per year of decline in water levels observed over the previous 2 years did not continue into 2012. Generally, increasing water levels at CUY-35 (fig. 23) corresponded with the high-flow events observed at the stream gage station on the Cuyama River near Ventucopa (11136500) between December 2009 and February 2012 (fig. 13). At CUY-35 (fig. 23), an increase of approximately 27 feet corresponded with a high-flow event in late March and early April 2011. A water-level increase of over 5 feet was observed at CUY-35 shortly after a December 2010 flow event. The correspondence of rising groundwater and river levels indicates that the Southern Ventucopa Uplands zone is strongly hydraulically connected to the Cuyama River.

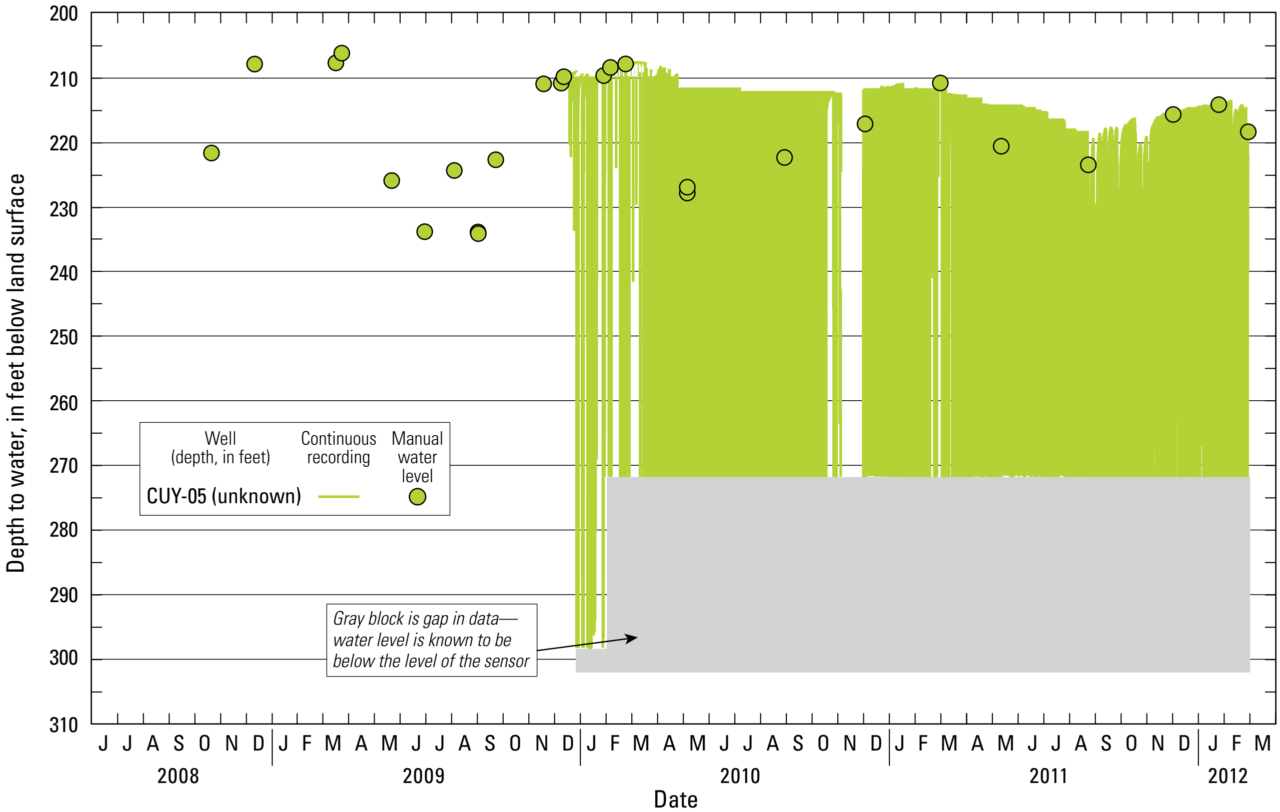

Figure 20. Water-level hydrograph from CUY-05, from January 1, 2008, to February 28, 2012, Cuyama Valley, California.

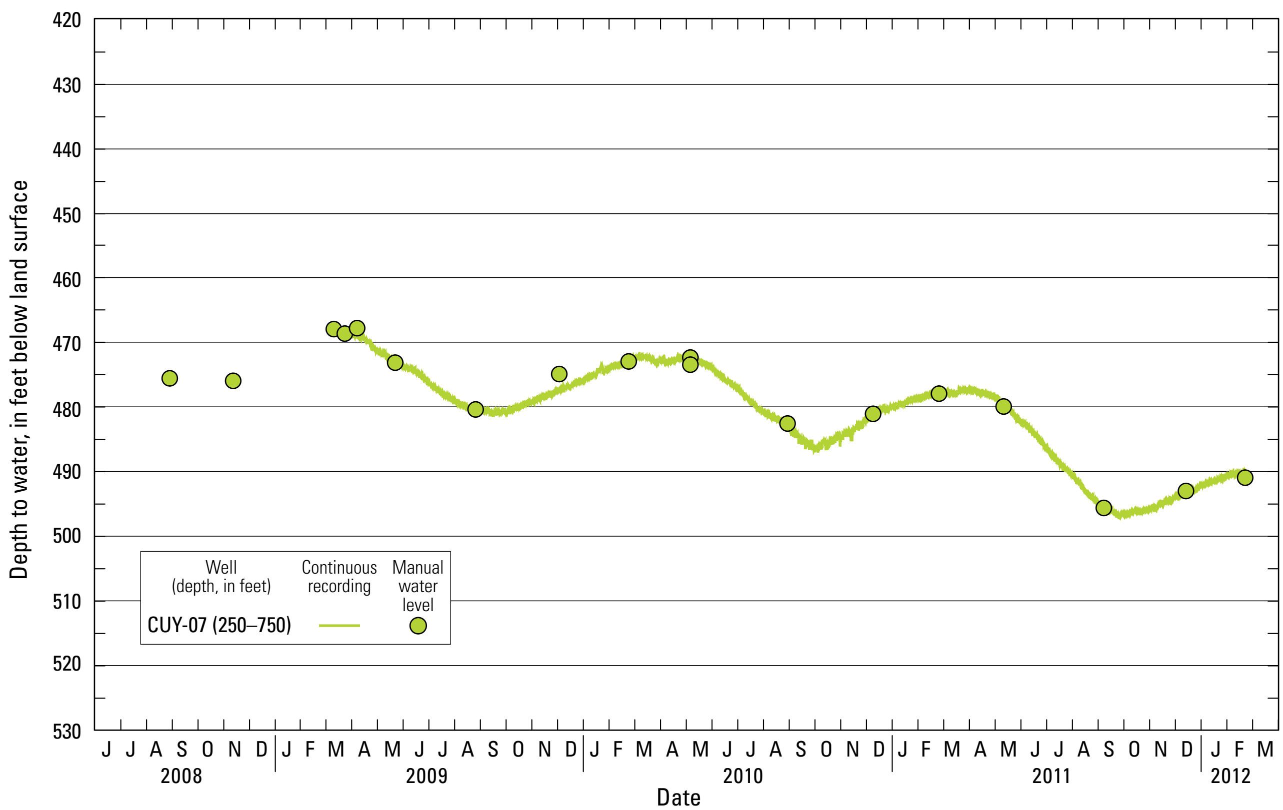

Figure 21. Water-level hydrograph from CUY-07, from January 1, 2008, to February 21, 2012, Cuyama Valley, California.

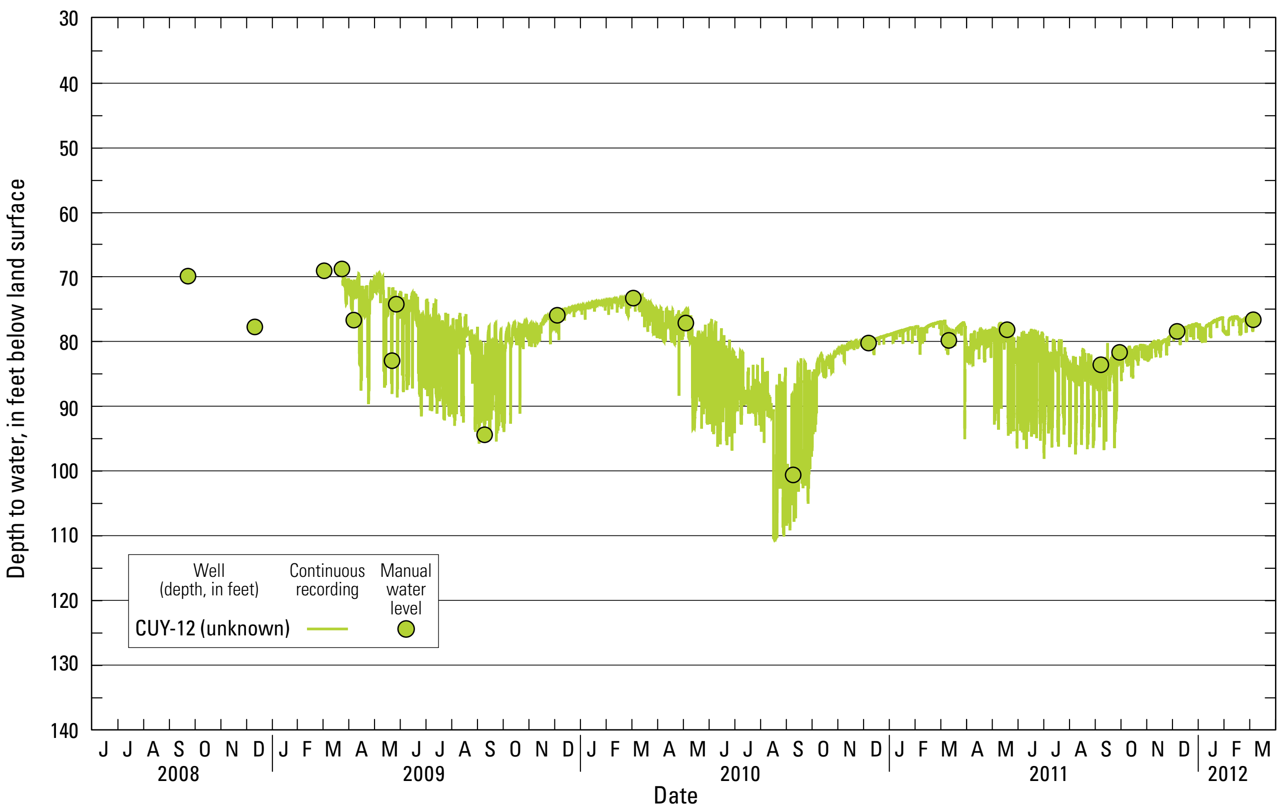

Figure 22. Water-level hydrograph from CUY-12, from January 1, 2008, to March 5, 2012, Cuyama Valley, California.

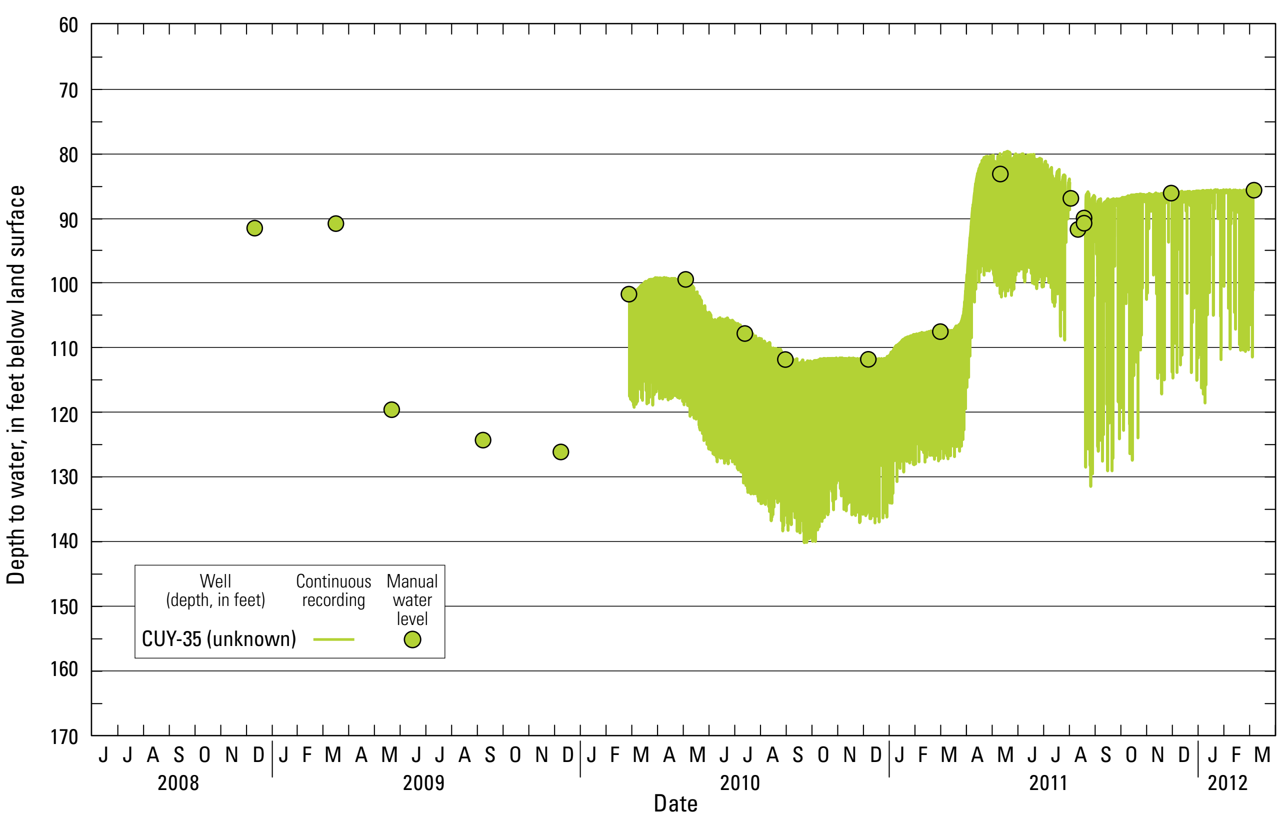

Figure 23. Water-level hydrograph from CUY-35, from January 1, 2008, to March 6, 2012, Valley, California.

Historic Water Levels

Historic water-level data, some dating back to the early 1940s, were compiled for 16 sites in the Cuyama Valley. Analysis of the long-term trends indicated that 10 wells showed a declining trend, 3 wells showed no trend, and 3 wells showed a rising trend (fig. 24).

All six wells in the South-Main zone showed declines over the period of record. Well CUY-04 showed the largest decline—over 300 feet between 1960 and 2001, for an average decline of over 7 ft per year. Well CUY-75 declined nearly 200 ft from 1954 to 2007, for an average decline of almost 4 ft per year. Wells CUY-27, -54, and -56 declined about 100 feet over the period of record, for an average decline of between 1 and 2 ft per year. Large water-level declines were not limited to the South-Main zone. Well CUY-62, in the Caliente Northern-Main zone, declined over 100 feet between 1947 and 2007, for an average decline of almost 2 ft per year. Well CUY-60, in the Western Basin zone, declined over 80 ft between 1945 and 2012, an average decline of over 1 ft per year. Well CUY-24, in the Central Sierra Madre foothills zone, declined approximately 30 feet between 1983 and 2012, for an average decline of about 1 ft per year.

Two of the wells that showed an increase in water levels, CUY-13 and -74, are in the Southern Ventucopa Uplands zone, which further indicated that this zone can respond quickly to periods of increased recharge. The third well that had an increase in water levels, well CUY-36, is in the Northeast Ventucopa Uplands zone. The record for well CUY-36 was limited, and it cannot be determined if the fluctuations in water levels that were observed in the Southern Ventucopa Uplands also occurred in this well.

Wells CUY-13, -30, -39, -46, and -74, in the Southern Ventucopa Uplands, showed cyclical fluctuations in water levels. Declines in water levels over a 5 to 12 year period were followed by a marked rise. Well CUY-74 showed an increase in water level of over 116 feet between December 1977 and May 1978. Other rapid increases in water levels over a short time included 58 feet over 3 months in 1958, 74 ft over 2 months in 1969, and 68 feet over 4 months in 1983. Well CUY-32, also in the Southern Ventucopa Uplands, did not show cyclical fluctuations in water levels.

Increases in water levels observed in the Southern Ventucopa Uplands corresponded to increased annual precipitation. The marked water-level rises in well CUY-74 observed in 1958, 1969, 1978, and 1983 correlated with above average rain-fall totals during the respective years. Although increases in water levels were associated with increased precipitation (fig. 11), all of the marked increases were associated with annual rainfall totals exceeding 20 in/yr at either Station 347 or 174A. The 25-ft rise in water level at CUY-35 (fig. 23) in late March 2011 correlated with an above average monthly rainfall of over 5 inches at Station 34 (fig. 12). A similar monthly rainfall in December 2010 also correlated to an increase in water level of 5 ft at CUY-35. This indicated that recharge to the aquifer system in the Southern Ventucopa Uplands is highly dependent on periods of increased annual rainfall and stream levels.

Aquifer Tests

Aquifer tests were performed on the monitoring wells and selected domestic and supply wells in the Cuyama Valley groundwater basin (fig. 25). Slug tests on the monitoring wells were done by using physical displacement. Historic pump test data for 51 wells were collected and analyzed to estimate the aquifer transmissivity.

Slug Tests

Hydraulic conductivity estimates for the aquifer materials proximate to the screened intervals of the three multiple-well monitoring sites (CVKR, CVBR, and CVFR) were obtained by using physical displacement “slug” tests. These tests are useful for determining aquifer properties around small-diameter wells that have short screened intervals. Unlike longer-term tests, the results are based on small changes in water level measured over short periods and, therefore, represent the hydraulic response from only a small volume of aquifer material next to the well screen.

The slug used for the displacement of volume was a 1.05-inch outer diameter PVC pipe 63 inches long. The pipe was filled with sand for weight and sealed at both ends with pointed capes. The slug displacement was 0.0327 cubic feet (ft^3), which resulted in an equivalent head displacement of approximately 1.50 ft in a 2-inch well. The initial head displacement observed for some tests differed from the calculated equivalent head displacement. The cause of the difference is uncertain. The observed initial head displacement was used for processing the results.

Computations were performed by using existing spreadsheet-based tools (Halford and Kuniansky, 2002). The selection of the most appropriate method to analyze the data was based on a preliminary analysis of the slug test data and comparison with predicted responses from different methods. Wells CVKR-1, -2, and -3 were analyzed by using methods developed by James Butler of the Kansas Geological Survey (Butler and others, 2003) for formations of high hydraulic conductivity. All other wells were analyzed by using methods developed by Green and Shapiro (1998), with the exception of CVFR-4 . The water level in CVFR-4 was below the top of the sand pack at the time of testing; therefore, it was considered unconfined and was analyzed by using methods developed by Bouwer and Rice (1976) for unconfined wells.

The following assumptions were made for the interpretation of slug test data: the volume of water is displaced instantaneously at $t = 0$, and the well is of finite diameter and

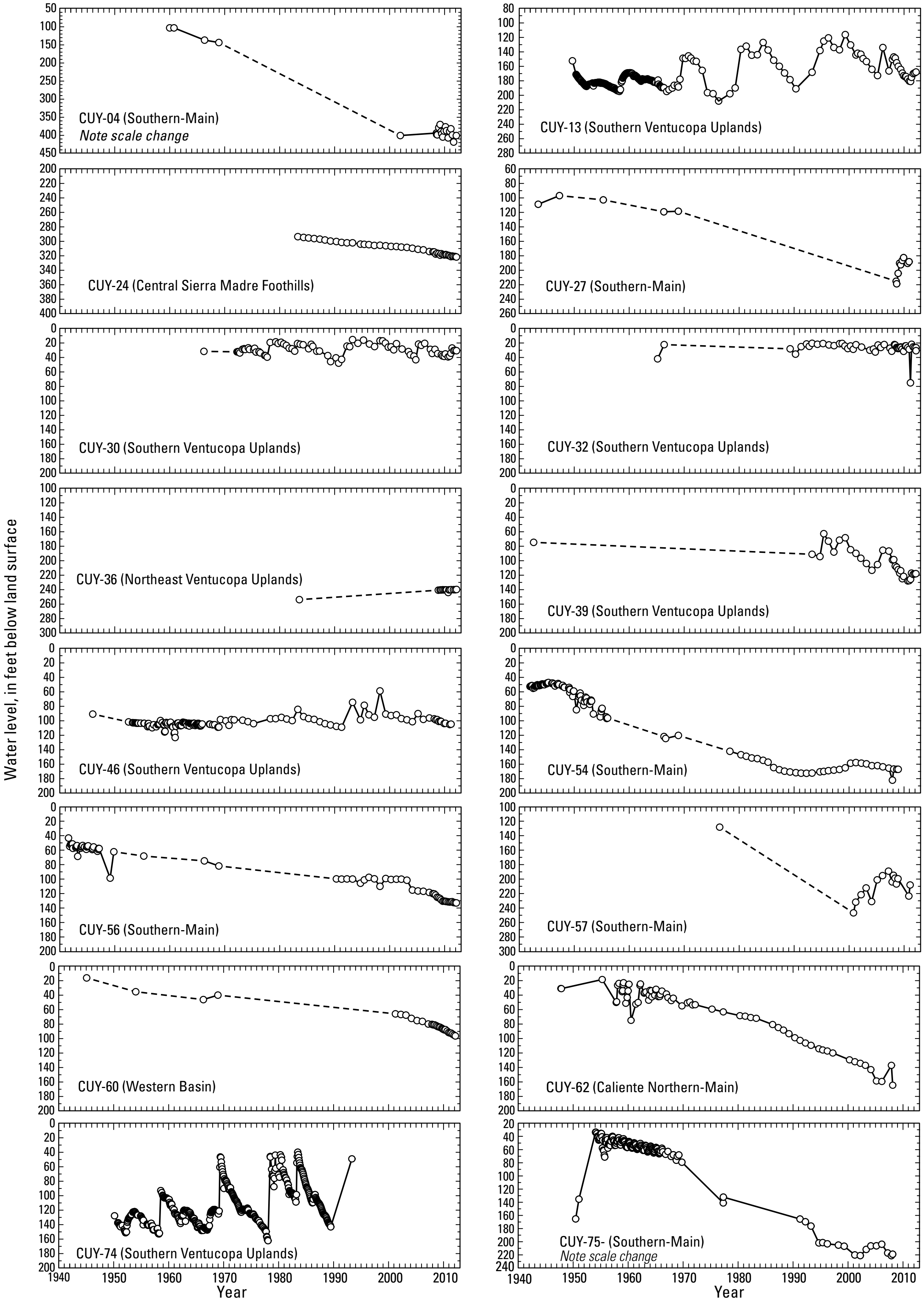

Figure 24. Historic water-level hydrographs from 16 selected domestic and supply wells, Cuyama Valley, Santa Barbara County, California.

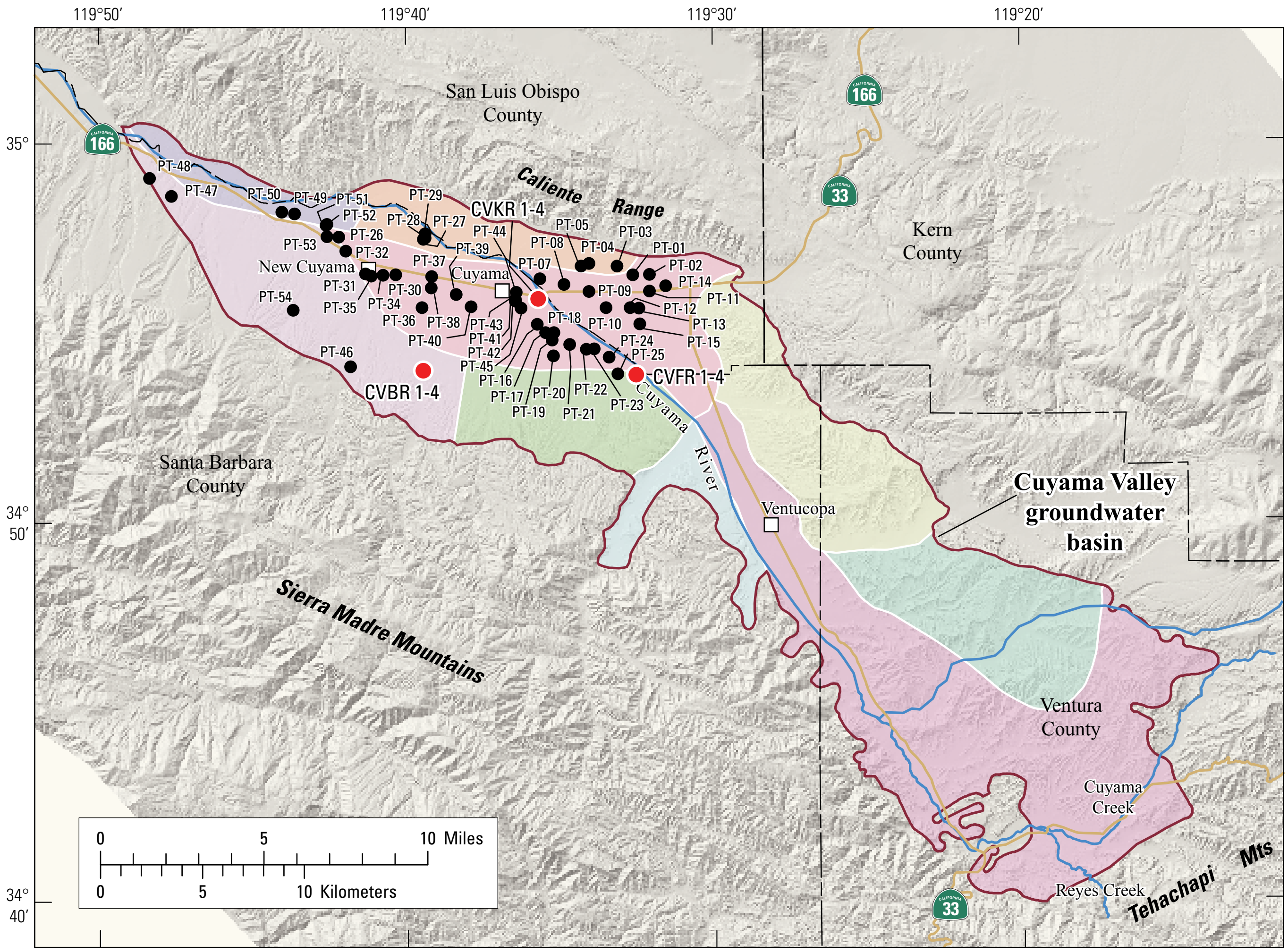

Shaded relief base created from 30-m digital elevation model from USGS National Elevation Dataset (NED), North America Vertical Datum 1988 (NAVD88)
Hydrology sourced from 1:24,000-scale National Hydrography Dataset, 1974–2009
Place names sourced from USGS Geographic Names Information System, 1974–2009
Albers Projection, NAD83

EXPLANATION

Cuyama groundwater basin zones

- Caliente Northern-Main
- Central Sierra Madre Foothills
- Northeast Ventucopa Uplands
- Northwestern Sierra Madre Foothills
- Northern Ventucopa Uplands
- Southern Sierra Madre Foothills
- Southern Ventucopa Uplands
- Southern-Main
- Western Basin

Site type

- U.S. Geological Survey monitoring site
- Pump-test site

Figure 25. The location of multiple-well monitoring sites, domestic and supply wells with aquifer test data, Cuyama Valley, Santa Barbara County, California.

fully penetrates the aquifer. It is also assumed that the aquifer is confined, homogeneous, isotropic, and of uniform thickness; the flow within each aquifer is horizontal and radially symmetric; and that the response is influenced over the entire screened interval. Thus, for these calculations, the aquifer thickness is assumed to equal the length of the screened interval of the monitoring well.

For wells analyzed after Butler and others (2003), the type curve can be automatically or manually fit to match the observed response by using the spreadsheet tool to adjust the dimensionless dampening coefficient and the hydraulic conductivity. The accuracy of the fit between the match curve and the measured response curve is characterized best by the residual standard error. For wells analyzed after Green and Shapiro (1998), the type curve can be automatically or manually fit to match the observed response by adjusting the storage coefficient and the hydraulic conductivity. For wells analyzed after Bouwer and Rice (1976), the type curve can be automatically or manually fit to match the observed response by adjusting the hydraulic conductivity (K).

Slug tests from each well were analyzed and grouped on the basis of the shape of each type curve. Similarly shaped type curves were grouped together. For each approach, the individual tests were manually examined; tests that contained errors were removed from the batch. For each well, the results from all valid tests were averaged to estimate K for the given well. Common errors included measured displacements varying greatly from the calculated equivalent head displacement, irregular recoveries, and tests containing anomalous readings.

Slug test results from the monitoring wells indicated that horizontal hydraulic conductivities ranged from about 1.5 feet per day (ft/d) for the CVBR-4 well to 28 ft/d for the CVKR-3 well (table 12). The median hydraulic conductivity of 15 ft/d observed for the wells in the older alluvium was almost five times greater than the median hydraulic conductivity observed in the Morales Formation (3.1 ft/d). The relatively low hydraulic conductivity values estimated in the Morales Formation probably reflect the greater degree of cementation and induration. None of the wells tested was screened in the younger alluvium.

Pump Tests

To better understand hydraulic properties of the local aquifer system, transmissivity (T) of the aquifer was estimated at 51 wells screened in the water-bearing units of the Cuyama Valley groundwater basin (table 13). The data used for the analysis were from historical pump efficiency tests performed on irrigation wells between 1941 and 1966. Data from these tests were analyzed by using the Jacob's equations to estimate T of the aquifer material around the well (Jacob, 1946). Most of the tests were done by Pacific Gas and Electric (PG&E) as a service to the customers for the purpose of maximizing the well efficiency and aiding in the protection of the electrical grid. Water pumping accounts for approximately 80 percent of the energy consumed by PG&E's agricultural customers and is a significant load to the electrical system (Pacific Gas and Electric, 2006). PG&E has performed free well-efficiency tests of water-pumping systems for their customers since 1911. The data—date and time, static and pumping water levels, total lift, discharge, specific capacity, kilowatt input, kilowatt-hour per acre-foot (ac-ft), and plant efficiency—were provided to the USGS for analysis. The overall condition of the well was not noted; it was assumed that wells were fully developed and in good working condition.

A common approach for analyzing short-term single-well pumping test data is the use of the Jacob's Method (Jacob, 1946) to estimate the transmissivity of the aquifer. Although this method makes various assumptions (including the aquifer is infinitely large, homogeneous, isotropic, confined, and unconsolidated), it still provides a reasonable first-order approximation of the transmissivity of the aquifer near the well. Because drawdown data seldom fall in a straight line when plotted on a linear time scale (Bear, 1979), the method assumes that steady-state conditions are eventually reached, and the time since pumping began is plotted on a log cycle. It is assumed from the PG&E data that the reported water level was measured after a static condition had been reached, and the pump was allowed to run for at least one log-time cycle (for example, 1, 10, 100; or 30, 300 min, and so on). This technique allows for an estimation of transmissivity from specific capacity by taking the flow rate and drawdown of a well, at one log cycle apart, and applying Jacob's Equation for straight-line drawdown, as shown (Roscoe Moss Company, 1990).

Table 13. Summary of pump-test estimates of hydraulic properties for selected well sites, Cuyama Valley, Santa Barbara County, California.

Table available separately as Microsoft Excel® at http://pubs.usgs.gov/sir/2013/5108.

Table 12. Summary of slug-test estimates of hydraulic properties for selected multiple-well monitoring sites, Cuyama Valley, Santa Barbara County, California.

[Depth in feet below land surface, see table 1 for definitions of common well names. **Abbreviations**: Qoa, Older alluvium; QTm, Morales Formation; ft/day, feet per day; USGS, U.S. Geological Survey]

Common well name	Tested by	Number of tests	Date of test (mm/dd/yyyy)	Top of screen	Bottom of screen	Formation at top of screen	Formation at bottom of screen	Method of analysis	Hydraulic conductivity (ft/d)
CVKR-1	USGS	17	3/22/2009	960	980	Qoa	Qoa	Butler, Garnett and Healey, 2003	18
CVKR-2	USGS	17	3/23/2009	760	780	Qoa	Qoa	Butler, Garnett and Healey, 2003	22
CVKR-3	USGS	14	3/23/2009	600	620	Qoa	Qoa	Butler, Garnett and Healey, 2003	28
CVKR-4	USGS	15	3/23/2009	440	460	Qoa	Qoa	Greene and Shapiro, 1998	9.3
CVBR-1	USGS	20	11/4/2009	830	850	QTm	QTm	Greene and Shapiro, 1998	3.3
CVBR-2	USGS	19	11/5/2009	730	750	QTm	QTm	Greene and Shapiro, 1998	2.6
CVBR-3	USGS	17	11/5/2009	540	560	Qoa	Qoa	Greene and Shapiro, 1998	12
CVBR-4	USGS	18	11/4/2009	360	380	Qoa	Qoa	Greene and Shapiro, 1998	1.5
CVFR-1	USGS	20	11/4/2009	960	980	QTm	QTm	Greene and Shapiro, 1998	9.9
CVFR-2	USGS	20	11/5/2009	810	830	QTm	QTm	Greene and Shapiro, 1998	3.0
CVFR-3	USGS	20	11/5/2009	680	700	QTm	QTm	Greene and Shapiro, 1998	6.8
CVFR-4	USGS	20	11/5/2009	590	610	QTm	QTm	Bouwer and Rice, 1976	1.6

$$T = \frac{2.303}{4\pi} x \frac{Q}{\Delta s}$$

where

T is transmissivity (gallons per day per foot or square meters per day),

Δs is drawdown (feet or meters),

Q is well discharge (gallons per minute or liters per second).

Adding the conversion from gallons per minute (gpm) to gallons per day (gpd) allows for the flow (Q) to be entered in the standard unit of gpm while transmissivity (T) is calculated in the conventional units of gallons per day per foot (gpd/ft). Simplifying the resulting equation yields the following:

$$T = \frac{264Q}{\Delta s}$$

The median transmissivity estimates from pump-test analyses of the supply wells ranged from 560 to 163,400 gallons per day per foot (gal/d/ft). The median transmissivity of 15,700 gal/d/ft for wells in the younger alluvium was three times that of the older alluvium (5,000 gal/d/ft). Wells screened in both the younger and older alluvium had a median transmissivity of 11,300 gal/d/ft. Data from wells screened solely in the Morales Formation were not available to be analyzed; however, transmissivity estimates from two wells screened in both the older alluvium and Morales Formation averaged 4,900 gal/d/ft.

Pump tests were repeated for some wells over a span of several years. Analysis of the results indicated that transmissivity typically decreased over time, with a few exceptions. These temporal changes in transmissivity are likely due to physical deterioration of the well, but could also be influenced by declines in water levels over time, the loss of storage due to land subsidence, or both.

Geomechanical Activity

Geomechanical data collected from the study area included continuously operating global positioning system (GPS) and interferometric synthetic aperture radar (InSAR) data. The geomechanical data were used to estimate the rate of vertical land movement in the Cuyama Valley groundwater basin to determine if it is subsiding. Data from 5 GPS stations and 133 unique interferograms were analyzed. Estimates of land subsidence for the Cuyama Valley provided insight into the response of the aquifer system to groundwater withdrawal.

GPS Data

The horizontal and vertical motion of the Earth's tectonic activity in California is monitored by a continuously operating network of GPS stations that are operated by various groups, including government agencies and education consortiums. Stations within the Cuyama study area were installed as part of Southern California Integrated GPS Network (SCIGN), which was designed to monitor plate boundary deformation and seismic hazards throughout Southern California (Hudnut and others, 2002). The GPS stations generally were constructed by using a stable monument embedded in the ground to a depth of approximately 10 meters to minimize signal noise and employ a standard choke ring antenna for the GPS receiver (Hudnut and others, 2002). The receiver detects signals transmitted by GPS satellites in orbit around the earth and determines the distance between the satellites to the receiver based on the travel time of the signal (U.S. Geological Survey Earthquakes Hazards Program, 2012). The station position (latitude, longitude, and elevation) is determined by triangulation of the distances to at least four GPS satellites (U.S. Geological Survey Earthquakes Hazards Program, 2012).

Variations in the position of a GPS station can result from tectonic motion and from deformation associated with fluid pumping from anthropogenic activities—in this case, groundwater withdrawal. A study of continuous GPS data from sites in southern California determined that measured seasonal horizontal and vertical motion across a basin were consistent with simple elastic movement of the basin material responding to aquifer pumping and recharge (Bawden and others, 2001). “GPS sites on the margin… undergo seasonal horizontal motion toward and away from the basin, while sites within the basin undergo seasonal uplift and subsidence.” (Bawden and others, 2001, pg. 814). Seasonal motion showing fluctuating compression and expansion of the aquifer sediment is a result of elastic, or reversible, deformation and is the result of fluctuations in the pore-fluid pressure in the aquifer sediments that are less any previous maximum fluctuations (Galloway and others, 1999). Generally, elastic deformation is correlated with water-level changes and associated pumping. Inelastic, or irreversible, deformation occurs when the pore-fluid pressure is reduced to a value lower than the previous minimum pressure; in response, the aquifer sediments are permanently rearranged and the pore volume is reduced (Galloway and others, 1999). Generally, inelastic deformation is indicated by a multi-year trend of decline in the elevation of the land surface and does not correlate with water level recovery.

The GPS stations used for the study, shown in figure 2, were Cuyama Valley High School (CUHS), Ventucopa Station (VCST), McPherson_CS2008 (P521), Bitter Creek Wildlife Refuge (BCWR), and OZST_SCGN_CS2000 (OZST). GPS stations within the Cuyama Valley study area are maintained by the USGS, and the data are available online at *http://earthquake.usgs.gov/monitoring/gps/* (accessed July 12, 2012). Post-processing of data collected from the GPS network stations can include cleaning, filtering, and de-trending for each position component (north, east, and up for a local Cartesian coordinate system). The data were cleaned to remove outliers that deviate significantly relative to an average position measurement, filtered to remove systemic errors that increase the signal noise, and de-trended to remove the regional tectonic signal (N. King, oral commun., 2012). Regionally, filtered data were the most appropriate for comparison with estimates of subsidence from InSAR (see next section, “InSAR Data”).

Comparison of the annual velocity in the north and east directions for all GPS stations in the Cuyama study area indicated the land surface is moving northwest at an average rate of almost 36 millimeters per year (mm/yr; table 14). The stations in the valley (CUHS, VCST, and OZST) are moving northwest at nearly the same velocity (about 25 mm/yr). P521, in the mountains to the west of the basin, is moving at a slightly faster velocity (about 29 mm/yr) toward the northwest direction; BWCR, in the hills to the east of the basin, is moving at a slightly slower velocity (about 22 mm/yr) toward the northwest. This indicates that there is movement consistent with the San Andreas fault system, with regional compression still occurring around this “pull-apart” basin.

The annual velocity in the up direction for all GPS monitoring stations was positive, with the exception of CUHS, indicating a general net upward motion for the land surface in the region. The annual velocity at VCST, OZST, and BCWR was 0.7 mm/yr (table 14), indicating the valley is moving upward at the same rate as the area to the east and slightly slower than the mountains to the west (annual velocity at P521 was 1.3 mm/yr). The annual velocity at CUHS is −7.5 mm/yr, indicating significant downward motion at this location relative to the region. The daily land surface position in the up coordinate for CUHS (raw data from the USGS Earthquakes Hazard Program) showed a downward trend over the period of record and cyclic variability over shorter periods (fig. 26). The measured displacement at CUHS between December 5, 2002, and May 22, 2008, was −40 mm. It is likely that this downward trend, or subsidence, represents inelastic deformation and indicates compaction and reduced storage capacity of the aquifer sediments; a significant component of the seasonal fluctuations represented elastic deformation, as evidenced by various periods of partial recovery.

The cyclic variability in the daily land surface position in the north, east, and up directions for CUHS also indicated the aquifer sediments in the area had experienced elastic deformation. The variability in the north and east directions of the de-trended data correlated with the variability in the up direction (fig. 27). As noted by Bawden and others (2001), elastic deformation in a basin will result in horizontal motion near the edge of the basin as the surface is pulled inward toward the center of subsidence and pushed outward during expansion. Cyclic deformation at CUHS in the north and east direction indicated elastic deformation of the aquifer sediments. The cyclic variation in the position of the land surface at CUHS also correlated with water-level measurements in nearby wells, which supports the conclusion that elastic deformation was caused by groundwater withdrawals. Water levels at well CUY-57 from 2000 to 2008 followed the de-trended up data; higher water levels occurred close in time to surface expansion, and lower water levels occurred close in time to surface compression (fig. 27). In 2011, motion in all directions increased substantially and corresponded to compression of the aquifer sediments (fig. 27). Likewise, in 2011, water levels from CUY-05 and CUY-58 sharply declined, and the surface compressed at the highest rate during the period of record (fig. 27).

InSAR Data

Interferometric synthetic aperture radar (InSAR) is a satellite-based remote sensing technique that can detect centimeter-level land-surface deformation over hundreds of square kilometers at a spatial resolution (pixel size) of 90 meters or better and a height resolution of 5–10 mm (Bawden and others, 2003). Synthetic aperture radar (SAR) imagery is produced by reflecting radar signals off a target area and measuring the two-way travel time to the satellite. SAR imagery has two components: amplitude and phase. The amplitude is the measure of the RADAR signal intensity returned to the satellite and shows roads, mountains, and other features because of their varying reflective properties. The phase component is the percentage of the sine wavelength that intersects the land-surface and is proportional to the line-of-site distance from the land surface to the satellite (range).

There are two forms of interferometric processing: conventional and persistent scatterer (PS InSAR). The conventional InSAR technique uses two SAR scenes of the same area taken at different times and differences the

Table 14. Annual velocities and associated uncertainties for selected GPS monitoring stations in the Cuyama study area, reported from the regionally filtered data from the U.S. Geological Survey Earthquakes Hazard Program for the period of record, Cuyama Valley, Santa Barbara County, California.

[mm/yy; millimeters per year]

GPS monitoring station	P521 (McPherson_CS2008)		CUHS (Cuyama Valley High School)		VCST (Ventucopa Station)		OZST (OZST_SCGN_CS2000)		BCWR (Bitter Creek Wildlife Refuge)	
	Velocity (mm/yr)	Uncertainty (mm/yr)	Velocity (mm/yr)	Uncertainty (mm/yr)	Velocity (mm/yr)	Uncertainty (mm/yr)	Velocity (mm/yr)	Uncertainty (mm/yr)	Velocity (mm/yr)	Uncertainty (mm/yr)
North	29.10	0.50	24.70	0.30	24.50	0.30	24.60	0.30	21.50	0.30
East	–27.40	0.50	–28.00	0.30	–25.10	0.30	–26.80	0.30	–22.00	0.30
Up	1.30	0.50	–7.50	0.30	0.70	0.30	0.70	0.30	0.70	0.30

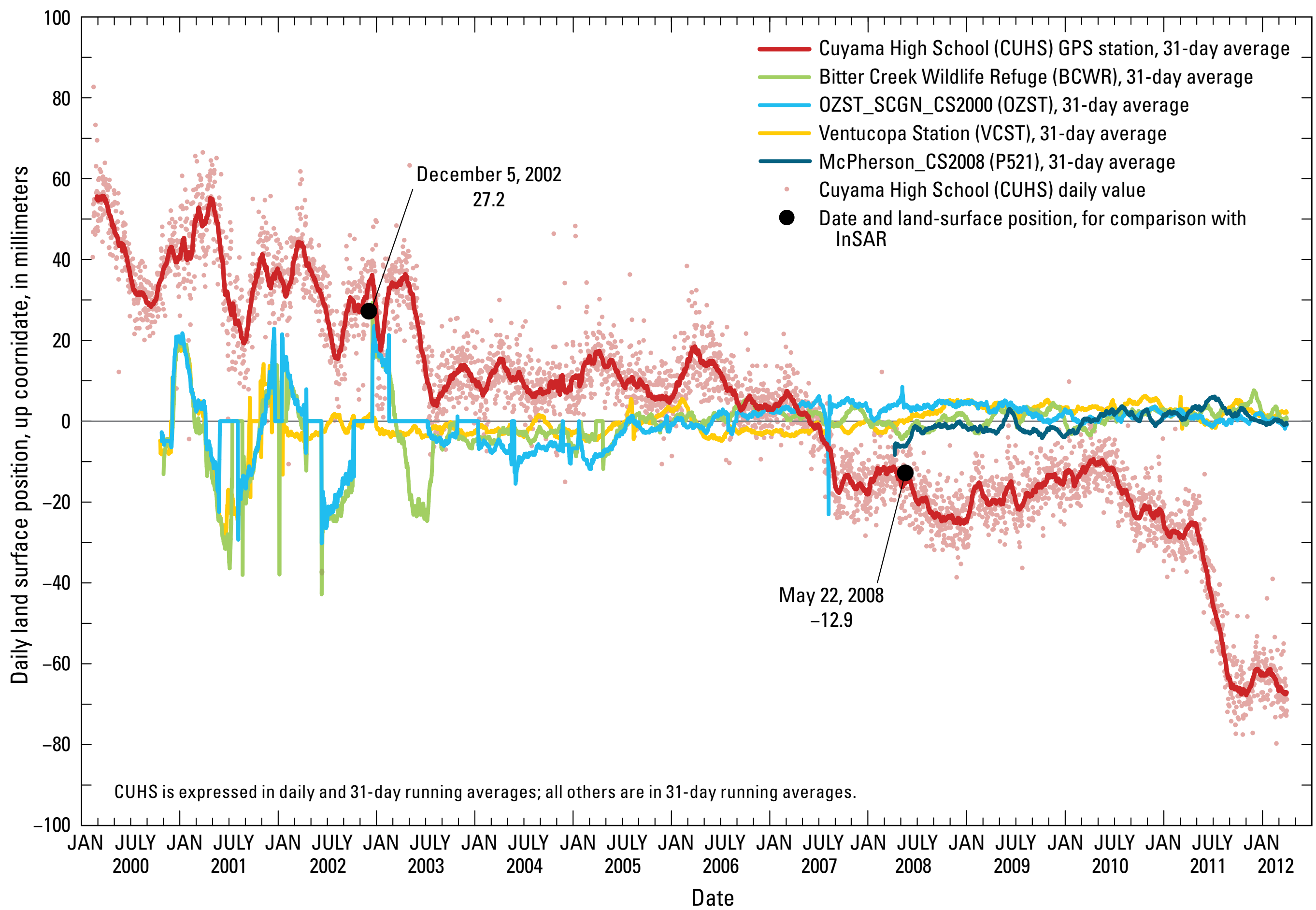

Figure 26. Land-surface position, up coordinate, in millimeters, for the GPS stations Cuyama High School (CUHS), Ventucopa Station (VCST), McPherson_CS2008 (P521), Bitter Creek Wildlife Refuge (BCWR), and OZST_SCGN_CS2000 (OZST), Cuyama Valley, Santa Barbara County, California.

phase portion of the SAR signal, resulting in maps called interferograms that show relative land-surface elevation change (range change) between the two SAR acquisition dates (Sneed and Brandt, 2007). If the land surface has moved away from the satellite (subsidence), a slightly longer portion of the wavelength is reflected back to the satellite. Conversely, if the land surface has moved closer to the satellite (uplift), a slightly shorter portion of the wavelength is reflected back to the satellite. The PS InSAR technique requires many more SAR —usually 20 or more—that are processed together to determine, in part, the amplitude variance across the entire data stack (all of the SAR images) for each pixel. Pixels with relatively high amplitude variance (in time) are filtered from the data set, resulting in a list of relatively “stable” points, or persistent scatterers (PS). The differential phase is then calculated in a manner identical to that of conventional InSAR, except that the differential phase is only calculated for each “stable” point, rather than across the entire image.

InSAR signal quality is dependent on topography, ground cover, land-use practices, atmospheric artifacts, time span of the interferogram, and orbit geometry, among other factors. Areas with high topographic relief can result in blocked radar signal in the line-of-sight (shadows). Densely forested areas are prone to poor signal quality because RADAR cannot effectively penetrate thick vegetation, and it either gets absorbed or reflects back to the satellite from random depths within the canopy, which leads to spatially incoherent signals. Certain land-use practices, such as farming, also cause spatially incoherent signal. The tilling, plowing, or flooding of farm fields causes large and non-uniform land-surface change that affect the amount of RADAR signal reflected back to the satellite and cannot be resolved with InSAR. Urban centers, however, generally have high signal quality because roads and buildings have high reflectivity (amplitude) and remain relatively uniform throughout the InSAR timescale. Non-uniform atmospheric water-vapor, such as clouds or fog, slows the radar signal, causing a phase shift that can lead to inappropriate deformation interpretations. Atmospheric artifacts can be identified by using multiple independent interferogram pairs, or by stacking interferograms.

Stacking interferograms involves adding together several back-to-back shorter term images into a longer term time series for either select points or for the entire image. Long time span interferograms (generally 2 years or more) usually

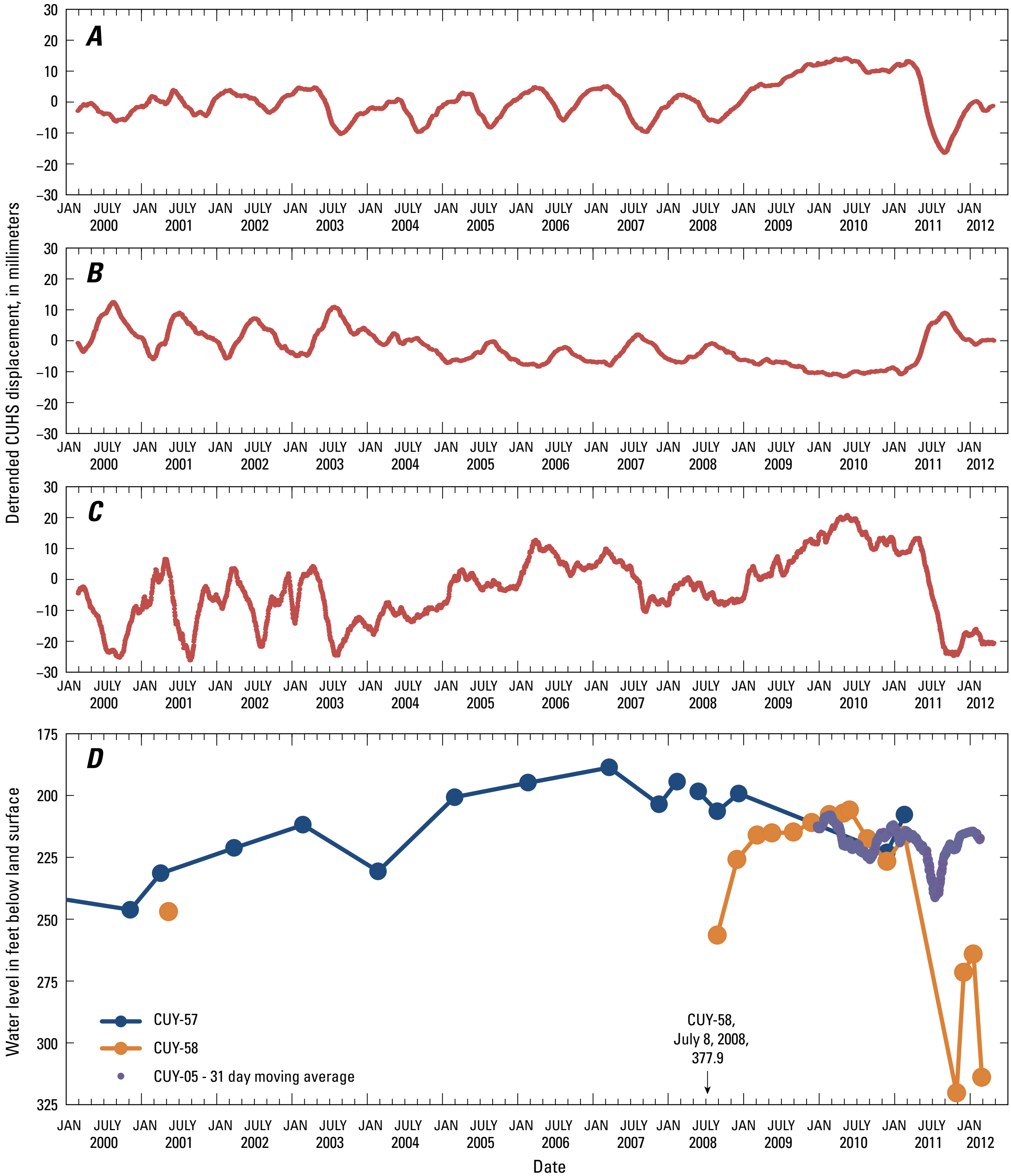

Figure 27. Daily detrended land-surface position, in millimeters, for the GPS station Cuyama High School (CUHS) for the *A*, north; *B*, east; and *C*, up direction; and *D*, water levels in selected wells near CUHS, in feet below land surface, Cuyama Valley, Santa Barbara County, California.

have poor signal quality because more non-uniform change is likely to have occurred in both urban and non-urban areas and are, therefore, generally not used (Sneed and Brandt, 2007). Stacking is very beneficial in reducing these time-dependent errors. The agricultural fields in the study area produce significant random noise across the imagery, which obscures good-quality points. The PS InSAR technique has the inherent ability to account for many of the anthropogenic effects because pixels with relatively high amplitude variance are removed early in the processing. The use of multiple, independent interferograms and stacking were used in the interpretation of both the conventional and PS InSAR imagery to account for atmospheric and time-dependent errors.

Strict orbital control is required to precisely control the look angle and position of the satellite. Successful application of the InSAR technique is contingent on looking at the same point on the land-surface from the same position in space, such that the horizontal distance between each satellite pass, or perpendicular baseline, is minimized. Perpendicular baselines generally greater than about 200 meters (m) usually produce excessive topographic effects (Sneed and Brandt, 2007). The relatively flat topography of the study area, however, allowed some images with perpendicular baselines of up to about 500 m to be successfully interpreted.

Understanding an interferogram image is not intuitive. An interferogram is a map that represents the change in the line-of-site distance between the land-surface and the satellite. This change is manifested as a set of repeating color fringes that indicate the magnitude and direction of deformation. In the case of ENVISAT (C-band), each complete color fringe (for example, purple, blue, cyan, green, yellow, red) represents 28.3 millimeters (mm) of deformation. The progression of colors indicates whether the change is uplift or subsidence. For example, a change resulting in a mound-shaped increase of 85 mm in height would appear as concentric rings alternating in color. Starting from outside the “bulls-eye” and working inward, there would be three complete color fringes; the colors would progress from red to yellow through purple, then the sequence would repeat twice more, indicating about 85 mm of uplift (three fringes times 28.3 mm is equal to 84.9 mm). If the shape were a depression, the color sequence would be reversed. One might think of the different colors as lines of topography, but instead of elevation, the changing colors represent the magnitude and direction of deformation. The more deformation there is, the larger number of color fringes are drawn.

For this study, data from the European Space Agency’s (ESA) ENVISAT satellite were acquired through the InSAR and GeoEarthScope data archives. These archives are operated through UNAVCO, a consortium of educational, public, and non-profit institutions whose goal is to use various precision land- and space-based technologies to identify and understand land deformation across the United States. For the period of this study, the side-looking 5.6 centimeter (cm) wavelength satellite orbited the earth at an altitude of approximately 800 kilometer (km) and had a 35-day repeat cycle. Tight orbital control is required in order to precisely control the look angle and position of the satellite, which consumes relatively large quantities of fuel. In October 2010, however, ESA made adjustments to ENVISAT’s orbit parameters in an attempt to extend its lifespan by 3 years, primarily by reducing fuel consumption. As a consequence, the satellite look angle is no longer controlled. Although the orbital changes did not affect the functionality of the SAR instruments, the lack of tight orbital control makes interferogram generation using post October 2010 data unlikely.

For this study, 30 SAR images were used to produce a total of 152 interferograms (77 conventional, and 75 PS InSAR), 42 of which (20 conventional, and 22 PS InSAR) were of sufficient quality for interpretation. Both the conventional and PS InSAR techniques were used to produce 19 interferogram pairs; in all, 133 unique interferograms were generated. The 133 interferograms spanned from December 5, 2002, to May 22, 2008, and each represented differences in time ranging from 35 to 665 days. No compatible SAR data were available from June 2008 to September 2010.

Data from the continuous GPS site CUHS (fig. 2) were used to calibrate InSAR interpretations. However, day-to-day GPS height solutions varied by as much as about plus or minus 13 mm likely because of variable atmospheric conditions, random walk noise, and other effects not directly related to land-surface-elevation change (Zerbini and others, 2001; Williams and others, 2004; Langbein, 2008). To minimize this high-frequency variability to allow better correlation of GPS heights to InSAR measurements, a correction was used: the height values for the 15 days prior to and following the observed date were combined into a 31-day running average. The relatively large day-to-day variations in GPS heights were thus minimized, while maintaining a height resolution similar to that of InSAR (within about 5 mm) and the long-term deformation magnitudes evident in the GPS data.

The construction of the InSAR time series involved selecting interferograms on the basis of image quality and the minimization of time gaps and overlaps and combining them to form longer-term time series. Various combinations of 28 of the previously mentioned 42 interferograms were combined into 8 different time series. Each time series contained between 8 and 11 interferograms. Gaps or overlaps were never more than 70 days and were accounted for by using simple linear interpolation (for example, if the subsidence rate before a 35-day gap was 50 mm/yr, and it was 30 mm/yr after the gap, a rate of 40 mm/yr (or approximately 4 mm) was added to the time series for that period). The resultant time series (fig. 28) was the average of these eight individually constructed time series.

Five points were selected from the Cuyama Valley on the basis of geographic distribution and proximity to wells. The resultant InSAR time series (fig. 28*B*) for these five points (fig. 29) showed a total maximum detected subsidence of about 65 mm between December 5, 2002, and May 22, 2008, at point five (which, if constant, would extrapolate to a rate about 12 mm/yr) compared to about 40 mm (about 8 mm/yr) at CUHS

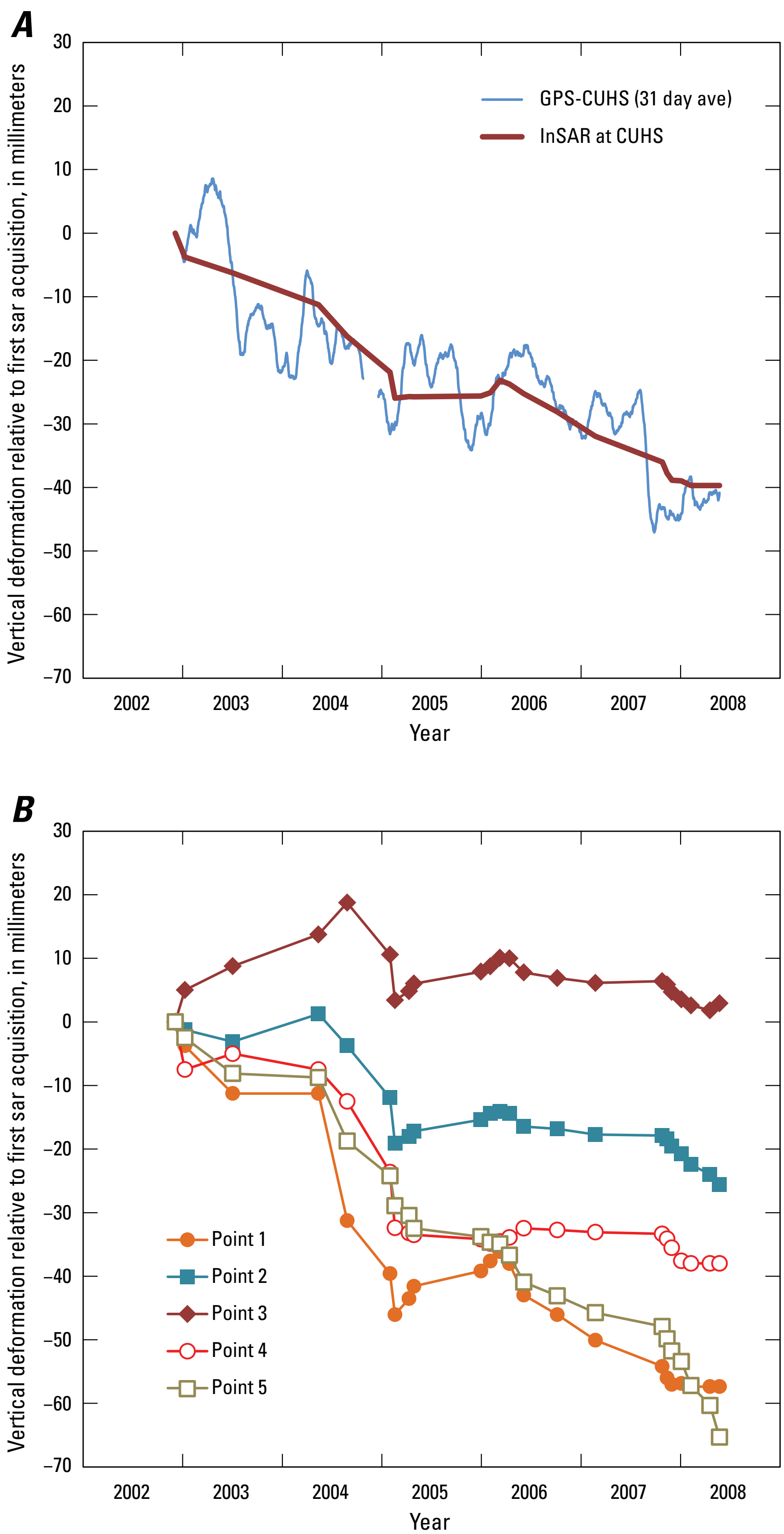

Figure 28. Vertical deformation in Cuyama Valley, Santa Barbara County, California, relative to *A*, first SAR acquisition for the Cuyama High School (CUHS) continuous GPS station; and *B*, selected reference points.

(fig. 28*A*), which is approximately 7 km to the east of point five. An interferogram spanning December 5, 2002–January 9, 2003, that was used in the construction of the averaged time series indicated a local short-term maximum subsidence magnitude of approximately 15 mm near point four. Two interferograms not used in the construction of the long-term time series spanning December 9, 2004–January 13, 2005, and December 29, 2005–February 2, 2006, (fig. 28*B*) indicated a local maximum uplift of approximately 10 mm (about 100 mm/yr) at points one and three, respectively. Interferograms between December 5, 2002, and May 22, 2008, showed the area of primary deformation approximately 3 kilometers to the southeast of the GPS site CUHS. The size and location of this feature appeared to be dependent, in part, on the timespan of the interferogram, which could reflect seasonal variations in pumping (figs. 29 and 30). Interferograms beginning in summer and ending in winter generally showed uplift (fig. 30*B*). Interferograms beginning in winter or spring and ending in summer or fall generally showed subsidence (figs. 29*A*–*B*, 30*A*, 31).

A qualitative analysis of the InSAR imagery, with respect to nearby faulting and oil-field production, was also completed (fig. 31). The primary faults in question were the Morales fault on the northern boundary of Cuyama Valley, the Russell fault to the west, the Rehoboth fault in the central portion of the basin, and the South Cuyama fault on the southern boundary of Cuyama Valley (fig. 31). In a few interferograms, there was an apparent deformation to the north of the range-front Morales fault, but this is more likely attributed to the parallax effect from relatively large perpendicular baselines than true land-surface elevation change because the signal mirrors that of the topography and is not consistent throughout the InSAR time span. The South Cuyama fault on the southern boundary of the basin showed no tendency to create sharp phase-change ramps (lineaments) in interferograms parallel to the fault itself. Both the Morales and South Cuyama faults are thrust faults, with older alluvium and the Morales Formation extending beneath exposed consolidated rocks in the range blocks. It is likely that these faults showed no INSAR response because the basin-fill units were not truncated below the map-view trace of the fault. The Santa Barbara Canyon fault is too far to the south and east of the primary deforming areas to show a fault-related

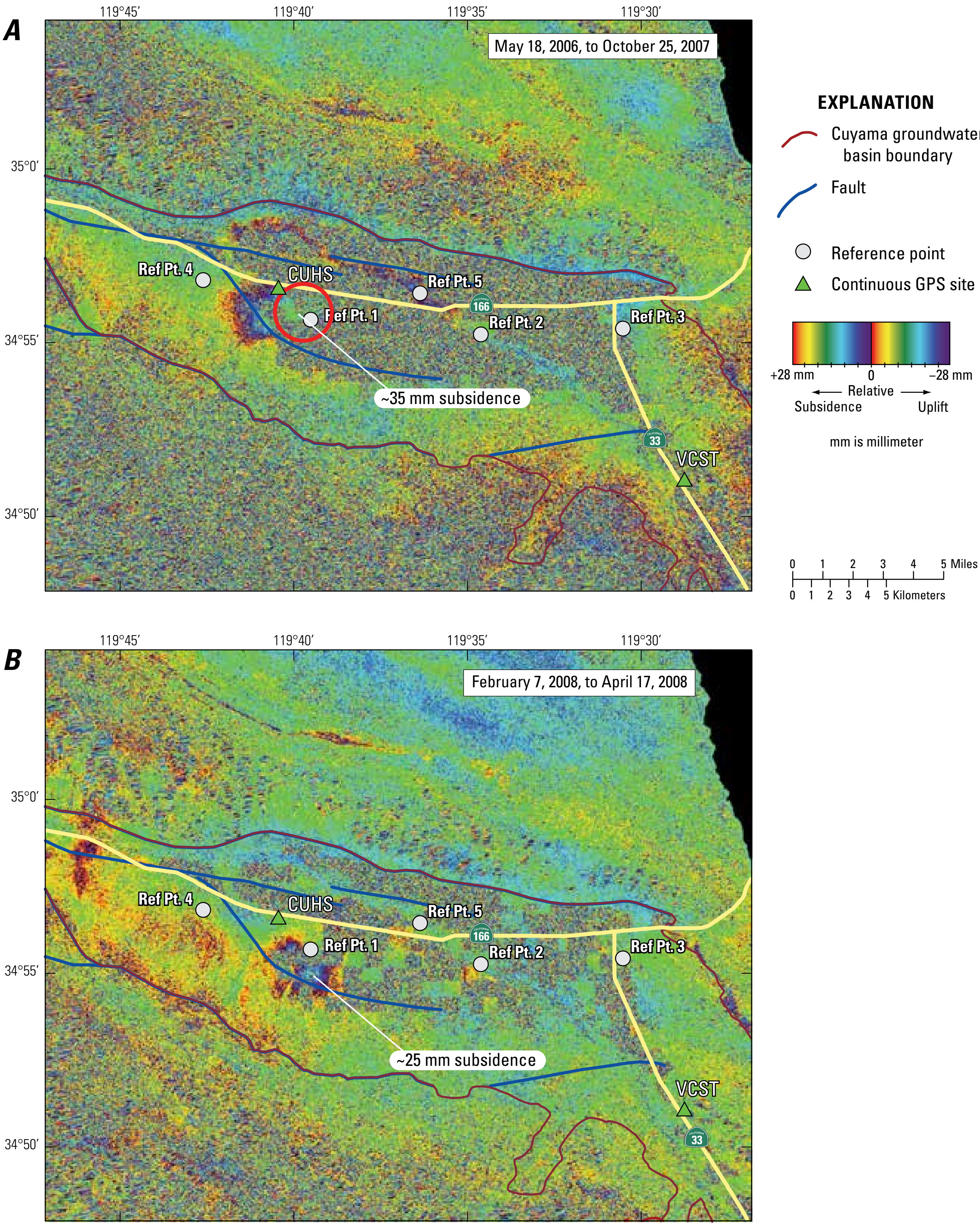

Figure 29. Conventional InSAR interferogram images for Cuyama Valley, Santa Barbara County, California, from *A*, May 18, 2006, to October 25, 2007; and *B*, February 7, 2008, to April 17, 2008.

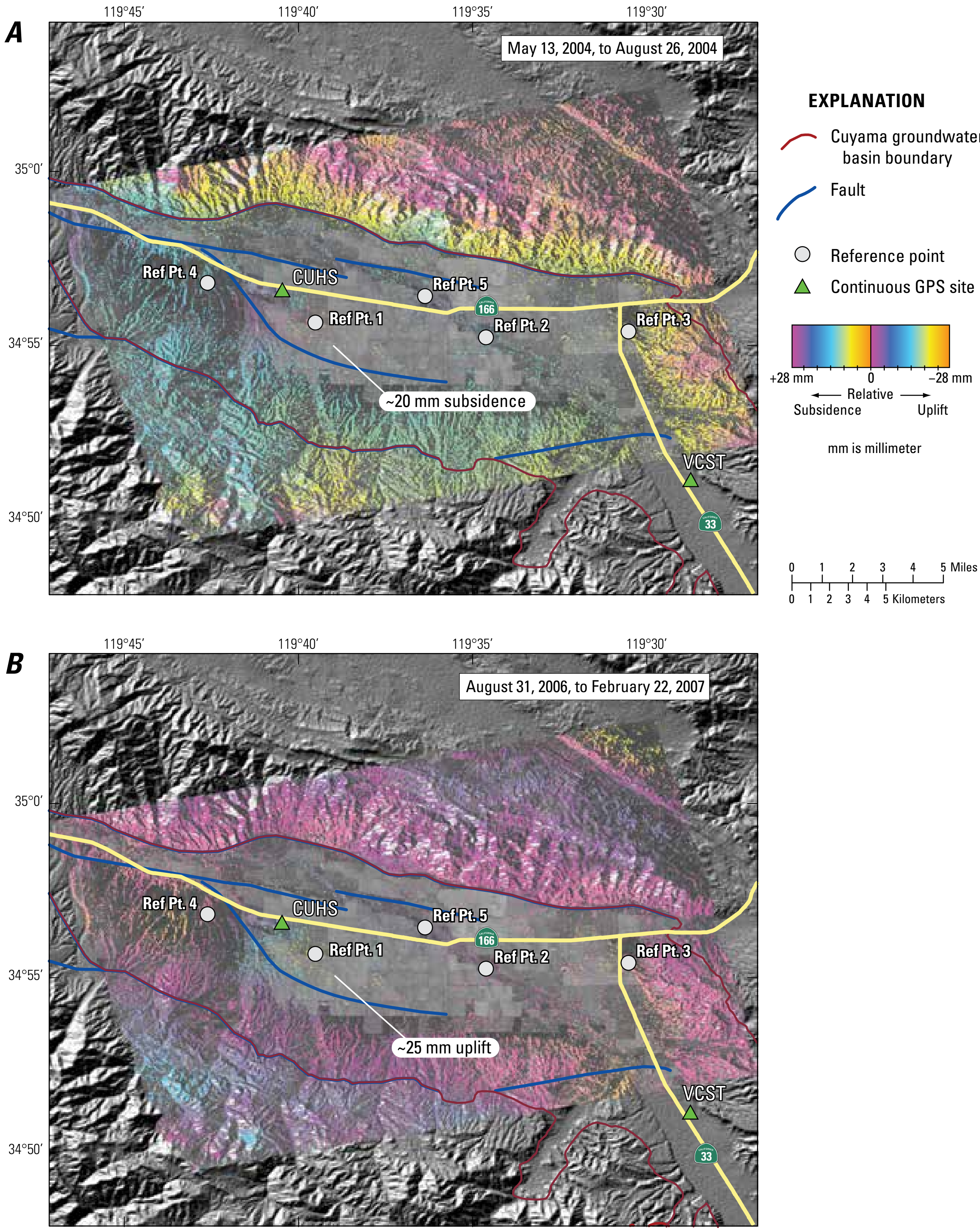

Figure 30. Persistent scatterer InSAR interferogram images for Cuyama Valley, Santa Barbara County, California, from *A*, May 13, 2004, to August 26, 2004; and *B*, August 31, 2006, to February 22, 2007.

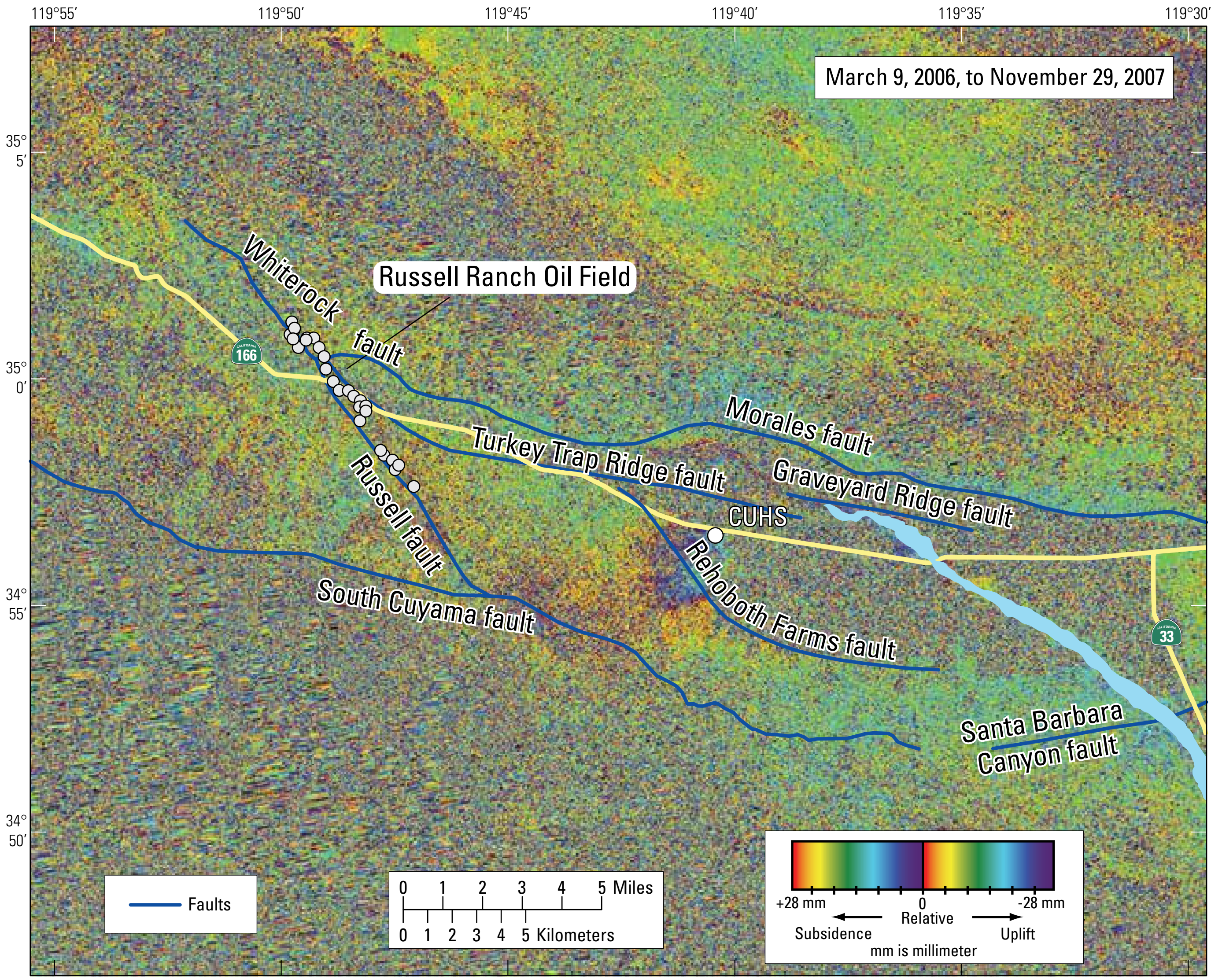

Figure 31. Persistent scatterer InSAR interferogram images for Cuyama Valley, Santa Barbara County, California, from March 9, 2006, to November 29, 2007.

response. The Rehoboth Farms fault trends northwest/southeast and approximately bisects Cuyama Valley. It is apparent from InSAR that this fault is not a significant barrier to groundwater flow because the majority of interferograms showed symmetrical subsidence or uplift on both sides of this fault. The last fault that is of concern in the study area is the Russell fault, which runs roughly parallel to the Russell Ranch oil field. Similar to the other faults, the Russell fault did not appear to be acting as a barrier to groundwater flow. As with the South Cuyama fault, the primary areas of deformation did not typically extend far enough to the west to be truncated by the Russell fault, if it were to act as a groundwater-flow barrier. Subsidence detected by InSAR did not appear to be caused by hydrocarbon extraction from the Russell Ranch oil field because the primary subsidence feature lies 10 kilometers or more to the east of the 8-km long by 1-km wide oil field. Subsidence caused by oil and gas extraction is largely restricted to the area of the oil field itself, as compared to the regional-scale subsidence that is typical of regional groundwater-extraction effects (Coplin and others, 1999).

Summary and Conclusions

To better assess the water resources of the Cuyama Valley groundwater basin, Santa Barbara County, California, geologic, lithologic, geophysical, water-quality, and hydraulic data were collected from three groundwater multiple-well monitoring sites constructed in Cuyama Valley. Additional water-quality and hydraulic data were collected and compiled from 2008 to 2012 from selected domestic and supply wells, springs, and surface-water sites. Geomechanical processes in the Cuyama Valley were also analyzed.

Three multiple-well monitoring sites, CVKR, CVBR, and CVFR, were installed in the study area to test specific conditions related to the geologic and hydrologic system. Data collected from multiple-well monitoring sites wells provided information on vertical differences in geology, water-quality, water levels, and hydraulic properties at the same location; these vertical profiles at multiple locations helped characterize the three-dimensional groundwater system.

Analysis of the generalized lithologic characterization and geophysical logs collected from the monitoring sites indicated the water-bearing units are composed of alternating layers of alluvial fan and stream deposits consisting of unconsolidated to partly consolidated sand, gravel, silt, clay, and occasional cobbles that range from less than 1 foot to more than 20 feet thick. At the CVKR site, the contact of younger and older alluvium is 365 ft bls; the contact of the older alluvium and the Morales Formation is deeper than 1,003 ft bls. At the CVBR site, the contact of recent and older alluvium is 30 ft bls; the contact of the older alluvium and the Morales Formation is 595 ft bls. At the CVFR site, the contact of younger and older alluvium is 75 ft bls; the contact of the older alluvium and the Morales Formation is 560 ft bls. Thus, structure, deposition, and erosion have resulted in considerable variation in the depth and thickness of these units in the valley.

Deviations in temperature-gradient logs indicated that the local geothermal gradient is influenced by the movement of groundwater. Changes in the temperature gradients were used to identify several flow zones at each site. At the CVKR and CVBR sites, flow generally decreased with depth, whereas at the CVFR site, a majority of the flow is in the deeper zones.

Water-quality samples indicated poor water quality, with respect to total dissolved solids and sulfate, throughout the Cuyama Valley, whereas poor water quality with respect to other constituents was less prevalent. Concentrations greater than the USEPA secondary drinking-water standard (SMCL) were observed for total dissolved solids in 97 percent of the samples and for sulfate in 95 percent of the samples. Concentrations greater than the USEPA primary drinking standard (MCL) were observed for nitrate in 13 percent the samples and for arsenic in 12 percent of the samples. Concentrations of total chromium [Cr(T)] were not greater than the MCL-CA of 50 µg/L in any of the samples; however, concentrations of hexavalent chromium [Cr(VI)] greater than the PHG were observed in 95 percent of the samples (the PHG is a non-regulatory threshold, and PHGs are typically orders of magnitude lower than MCLs). Nitrate concentrations decreased with depth at the CVKR site, indicating the source was near surface. Four of the five wells where nitrate levels were greater than the MCL were in the Southern-Main zone in center of the agricultural land-use area. Wells with the lowest nitrate levels were on the edges of the agricultural land-use areas, indicating the source of nitrate was likely from irrigation return flows. Low concentrations of nitrate (NO_3-N), less than 0.02 mg/L, in the surface-water samples indicated that natural surface-water recharge was not a source of high nitrate concentrations.

The isotope data indicated that groundwater does not move freely among the different flow-paths within the older alluvium or the Morales Formations, and that these units could have different sources of recharge. The range in isotope values observed at the different depths at the CVKR, CVBR, and CVBR indicated the water does not readily flow vertically between the water-bearing units. The relation between isotope values and depths also indicated that these units could have different sources of recharge. Variations in isotope values among the three monitoring sites indicated movement of water between different zones also could be restricted. The isotope samples from the four CVBR wells were, in general, lighter in deuterium than the CVKR wells, whereas isotope samples from the four CVFR wells were the heaviest collected in the basin. Comparison of values from other supply wells in the basin also supported restricted lateral flow between zones that could be controlled by the structural compartments of the basin.

Tritium concentrations and carbon activities showed a wide range in groundwater age for the basin. Concentrations of tritium in the samples ranged from 0.9 to 9.0 pCi/L, while time since recharge ranged between 600 and 38,000 years before present. The youngest water was collected in the Southern Ventucopa Uplands, and the oldest water was collected in the Northwestern Sierra Madre Foothills. Tritium concentrations in samples indicated the presence of some recent recharge in the CVKR-3, CVKR-4, and CVBR-3 wells and the absence of modern water in the CVKR-1, CVKR-2, and CVBR-3 wells. Tritium concentrations in samples from all four CVFR indicated a higher percentage of recent recharge. Tritium levels at the CVFR site increased with depth, indicating that the percentage of younger water at depth was most likely caused by local pumping. Estimated carbon-14 ages for the CVKR, CVBR, and CVFR sites ranged from 2,700 to 31,200 years before present. Samples from CVKR-3 and 4, CVBR-3, and CVFR-1, -2, -3, and -4 were all older than 2,700 years before present but also contained detectable levels of tritium, indicating that water from these wells is a mix of differently aged groundwater from different sources.

Arsenic concentrations ranged from less than 0.2 to 71.4 µg/l. The highest concentration sample was collected from a well in the Southern-Main zone that was screened in both the younger and older alluvium. A surface-water sample collected from the Cuyama River contained arsenic concentrations of 0.51 µg/l. Variation in the concentration of arsenic across zones and formations was observed. Elevated arsenic concentrations were observed in water recharged more than 22,000 years before present, indicating that arsenic concentrations are higher in groundwater that has had more time to mobilize the arsenic.

Water-level data indicated water levels fluctuated seasonally by as much as 80 feet, and water-level differences between aquifers were as great as 40 feet during the peak of the pumping season. Hydrographs showed downward vertical hydraulic gradients during the peak of the pumping season. The water-level hydrographs indicated different water-level changes and relations between aquifers in different parts of the basin. A comparison of the highest level observed each year since January 2008 showed a variation in water-level trends, with some levels declining, some rising, and some reversing. Declines from 6 to over 30 feet were observed in the Southern-Main zone and Central Sierra Madre Foothills. Rises in water levels from less than 1 to about 8 feet were observed the Southern Ventucopa Uplands and Northeast Ventucopa Uplands. Reversal from declining to rising water levels was only observed in the Southern Ventucopa Uplands and indicated that this zone could have the only viable source of recharge (from the Cuyama River) for the Cuyama Valley under the current conditions.

Time-series water-level data showed a seasonal pattern of declining levels coinciding with the peak of the agricultural season and rising water levels when nearby irrigation and related pumping were at a minimum. The pumping of nearby irrigation wells directly influenced water levels in all of the CVKR and CVBR wells. Water-level data from all of the monitoring sites showed a decline in the seasonally high levels over the period of record and showed a vertical hydraulic gradient reversal from upward during the winter months to downward during the irrigation season. Observations at the CVKR site showed water levels in the three deeper wells varied by as much as 60 ft seasonally, while water levels in the shallowest well varied by about 25 ft. Water levels in all wells showed a decline of over 20 ft between 2009 and 2012. Observations at the CVBR site showed water levels in the three deeper wells varied by as much as 90 ft seasonally, while water levels in the shallowest well varied by about 40 ft. Water levels in all wells showed a decline of over 5 ft between 2010 and 2012. Observations at the CVFR site showed water levels in all wells varied by as much as 15 ft seasonally. Water levels in all wells showed a decline of over 20 ft between 2010 and 2012.

Water-level rises and declines observed in the Sierra Madre Foothills zone correlated to the duration of seasonal pumping of the wells. Increased pumping in 2011 resulted in a water-level decline of over 25 ft in 1 year. Changes in the pumping, and possible the recharge, conditions between 2010 and 2011 in Northwestern Sierra Madre Foothills zone can be the difference between static and overdraft conditions. Time-series data from two wells in the Southern Main Zone showed a detailed record of the steady decline in water level. The hydrographs showed the seasonal highs and lows that were expected; however, the year-to-year seasonal high showed a steady decline in water levels of approximately 2.5 and 7 ft per year. Time-series data from two wells showed a rise in water levels in the Southern Ventucopa Uplands zone during the spring of 2012. Observations showed the rise began in late March 2012 and rose over the 25 ft in one well in about 1 month. This marked rise in water level over a short period indicated that this zone responds quickly to periods of increased recharge, possibly from the Cuyama River.

Historic water level data, dating back to the early 1940s, showed long-term trends. Data indicated that nine wells had declining water levels, four wells had relatively static levels, and three wells had rising water levels. All of the wells in the wells in the South-Main zone had declines in water levels over the period of record. The largest decline of 300 ft, averaging 7.25 ft per year, was observed between 1960 and 2001. However, large declines in water levels were not limited to the Southern Main zone. In the Caliente Northern-Main zone, a decline of over 130 feet, for an average decline of 1.7 ft per year, was observed. In the Western Basin zone, a decline of over 80 ft, for an average decline of 1.2 ft per year, was observed. In the Southern Sierra Madre zone, a decline of over 30 ft, for an average decline of 0.9 ft per year, was observed. Declines were not observed in all zones of the basin. Two of the wells in the Southern Ventucopa Uplands zone showed an increase in water levels, while five others showed slow declines followed by a marked rise in water levels—over 100 ft in one case—indicating that this zone responds quickly to periods of increased recharge.

Slug-test data from the monitoring wells indicated that horizontal hydraulic conductivities range from 1.5 to 28 ft/day. The median hydraulic conductivity of 15 ft/day observed for the wells in the older alluvium was almost five times higher than the median hydraulic conductivity of 3.1 ft/day in the Morales formation. Pump-test data from supply wells indicated that transmissivities range from 560 to 163,400 gal/d/ft. The median transmissivity of 15,700 gal/d/ft for the wells in the younger alluvium was three times higher than the median transmissivity of 5,000 gal/d/ft in the older alluvium. Tests were repeated on some wells over a span of several years. Analysis of the results indicated that hydraulic conductivity typically decreased over time. These temporal changes in hydraulic conductivity are likely due to well performance, but also could be influenced by the declines in water levels over time.

Daily discharge data from stream-flow gaging stations in the Cuyama Valley drainage showed the stream flows vary seasonally. Records from the Cuyama River, where it enters and exits the basin, showed a higher flow, averaging between 2 and 200 cubic feet per second (cfs), through most of the winter months, while there was lower flow, below 2 cfs, during the summer months. Summer flow rates in 2011 were greater than in 2010. High flows of almost 900 cfs were observed in January and December of 2010. Changes in water levels in well CUY-35, in the Southern Ventucopa Uplands, correlated with high-flow events, while the extended-flow event corresponded with the 25-foot increase in water level at this well. In general, surface water flowing into the valley from the Cuyama River was equal to the amount of water flowing out of the valley, indicating that all other sources of inflow to the Cuyama Valley would be sources of recharge. Starting in October 2011, there was a net increase of inflow into the valley along the Cuyama River compared to the outflow, indicating that surface water was recharging the groundwater system.

Data collected from continuously operating GPS stations indicated that the Cuyama study area is slowly moving northwest. Stations in the mountains to the west of the valley, in the hills to the east of the valley, and in the Southern Ventucopa uplands showed a net upward motion for the land surface in the region. The CUHS, in the Southern-Main zone showed an annual velocity of −7.5 mm/yr (downward), indicating significant downward motion at this location relative to the region. The cyclic variability in the daily land-surface position in the lateral and vertical directions for CUHS indicated the aquifer sediments in the area had experienced elastic deformation. However, a longer-term downward trend likely represents inelastic deformation and indicates reduced storage capacity in the aquifer sediments. In 2011, motion in all the directions increased substantially and corresponded to compression of the aquifer sediments. The cyclic variation in the position of the land surface at CUHS also correlated with water-level measurements in nearby wells, which supports the conclusion that elastic deformation was caused by groundwater withdrawals.

InSAR data showed local and regional changes that appeared to be dependent, in part, on both the time span of the interferogram, seasonal variations in pumping, and geological uplift. Long-term InSAR time series showed a total detected subsidence rate of approximately 12 mm per year at one location, while short InSAR time series showed uplift of approximately 10 mm per year at several locations. The resultant InSAR time series for five selected points showed a total maximum detected subsidence of about 40 mm (about 8 mm/yr) at CUHS. Interferograms showed that a local maximum deformation bowl typically forms approximately 3 kilometers to the southeast of the CUHS GPS site. The size and location of this feature appear to be dependent, in part, on both the timespan of the interferogram and seasonal variations in pumping. A qualitative analysis of the InSAR imagery with respect to nearby faulting production showed the Rehoboth Farms fault trend is not a significant barrier to groundwater flow because the majority of interferograms showed symmetrical subsidence or uplift on both sides of this fault. A qualitative analysis with respect to the local Russell Ranch oil field, which runs roughly parallel to the Russell fault, indicated that subsidence did not appear to be caused by hydrocarbon extraction and that the fault did not appear to be a contributing barrier to groundwater flow.

References Cited

Ball, J.W., and McCleskey, R.B., 2003a, A new cation-exchange method for accurate field speciation of hexavalent chromium: U.S. Geological Survey Water-Resources Investigations Report 03–4018, 17 p.

Ball, J.W., and McCleskey, R.B., 2003b, A new cation-exchange method for accurate field speciation of hexavalent chromium: Talanta, v. 61, p. 305–313.

Bawden, G.W., Sneed M., Stork S.V., and Galloway D.L., 2003, Measuring Human Induced Land Subsidence from Space: U.S. Geological Survey Fact Sheet 069–03, 4 p.

Bawden, G.W., Thatcher, W., Stein, R.S., Hudnut, K.W., and Peltzer, G., 2001, Tectonic contraction across Los Angeles after removal of groundwater pumping effects: Nature, v. 412, p. 812–815.

Bear, Jacob, 1979, Hydraulics of Groundwater: New York, McGraw-Hill, 569 p.

Bouwer, Herman and Rice, R.C., 1976, A slug test for determining hydraulic conductivity of unconfined aquifers with completely or partially penetrating wells: Water Resources Research v. 12 no. 3, p.423–428.

Butler, J.J., Jr., Garnett, E.J., and Healey,J.M., 2003, Analysis of slug tests in formations of high hydraulic conductivity: Ground Water, v. 41, no. 5, p. 620–630.

California Department of Public Health, 2012a, California drinking water-related laws—Drinking water-related regulations, Title 22: California Department of Public Health, accessed February 28, 2013, at *http://www.CDPH.ca.gov/certlic/drinkingwater/Pages/Lawbook.aspx*.

California Department of Public Health, 2012b, Drinking water notification levels—Notification levels: California Department of Public Health, accessed February 28, 2013, at *http://www.CDPH.ca.gov/certlic/drinkingwater/Pages/NotificationLevels.aspx*.

California Department of Water Resources—Southern District, 1998, Evaluation of Groundwater Overdraft in the Southern Central Coast Region, Technical Information Record SD-98-1.

California Department of Water Resources, 2003, California's Groundwater: Bulletin 118 Update 2003. Chapter 6: Basic Groundwater Concepts. Retrieved May 1, 2012, from *http://www.water.ca.gov/pubs/groundwater/bulletin_118/california%27s_groundwater__bulletin_118_-_update_2003_/bulletin118-chapter6.pdf*.

Clark, I.D., and Fritz, P., 1997, Environmental isotopes in hydrogeology: Boca Raton, Fla., CRC Press LLC, 328 p.

Coplen, T.B., 1994, Reporting of stable hydrogen, carbon, and oxygen isotopic abundances: Pure and Applied Chemistry, v. 66, p. 273–276.

Coplen, T.B., Wildman, J.D., and Chen, J., 1991, Improvements in the gaseous hydrogen-water equilibration technique for hydrogen isotope ratio analysis: Analytical Chemistry, v. 63, p. 910–912.

Coplin, L.S., and Galloway, D.L., 1999, Houston-Galveston, Texas—Managing coastal subsidence, in Land subsidence in the United States: U.S. Geological Survey Circular 1182, p. 35–48.

Craig, H., 1961, Isotopic variations in meteoric waters: Science, v. 133, p. 1702–1703.

Davis, T.L., Lagoe, M.B., Bazeley, W.J.M., Gordon, Stuart, Mcintosh, Kirk, and Namson, J.S., 1988, Structure of the Cuyama Valley, Caliente Range, and Carrizo Plain and its significance to the structural style of the southern Coast Ranges and western Transverse Ranges, in Bazeley, W.J.M., ed., Tertiary Tectonics and Sedimentation in the Cuyama Basin, San Louis Obispo, Santa Barbara, and Ventura Counties, California: Society of Economic Paleontologists and Mineralogists, Pacific Section, v. 59, p. 159–161.

DeLong, S.B., Pelletier, J.D., and Arnold, L.J., 2008, Climate change triggered sedimentation and progressive tectonic uplift in a coupled piedmont-axial system: Cuyama Valley, California, USA: Earth Surface Processes and Landforms, v. 33, no. 7, p. 1033–1046.

Dibblee, T.W., Jr., 1973, Regional geologic map of San Andreas and related faults in Carrizo Plain, Temblor, Caliente, and La Panza Ranges and vicinity, California: U.S. Geological Survey Miscellaneous Investigations Series Map I-757, scale 1:125,000.

Dibblee, T.W., Jr., 1982, Geology of the Alamo Mountain, Frazier Mountain, Lockwood Valley, Mount Pinos, and Cuyama badlands areas, southern California, in Fife, D.L., and Minch, J.A., eds., Geology and mineral wealth of the California Transverse Ranges (Mason Hill volume): Santa Ana, California, South Coast Geological Society, p. 57–77.

Dibblee, T.W., Jr., and Minch, J.A., ed., 2005, Geologic map of the New Cuyama quadrangle, San Luis Obispo and Santa Barbara Counties, California: Thomas W. Dibblee, Jr. Geological Foundation Map DF–179, scale 1:24,000.

Dibblee, T.W., Jr., and Minch, J.A., ed., 2006, Geologic map of the Cuyama Peak quadrangle, Santa Barbara and Ventura Counties, California: Thomas W. Dibblee, Jr. Geological Foundation Map DF–202, scale 1:24,000.

Dibblee, T.W., Jr., and Minch, J.A., ed., 2007, Geologic map of the Fox Mountain quadrangle, Santa Barbara County, California: Thomas W. Dibblee, Jr. Geological Foundation Map DF–260 , scale 1:24,000.

Ellis, B.J., 1994, Changing Tectonic Regimes in the Southern Salinian Block: Extension, Strike-Slip Faulting, Compression and Rotation in the Cuyama Valley, California: Corvallis, Oregon State University, Ph.D. dissertation, 141 p., 31 figs.

Ellis, B.J., Levi, Shaul, and Yeats, R.S., 1993, Magnetic stratigraphy of the Morales formation: Late Neogene clockwise rotation and compression in the Cuyama Basin, California Coast Ranges: Tectonics, v. 12, p. 1170–1179.

Fishman, M.J., 1993, Methods of analysis by the U.S. Geological Survey National Water Quality Laboratory—Determination of inorganic and organic constituents in water and fluvial sediments: U.S. Geological Survey Open-File Report 93–125, 217 p.

Fishman, M.J., and Friedman, L.C., 1989, Methods for determination of inorganic substances in water and fluvial sediments: U.S. Geological Survey Techniques of Water-Resources Investigations, book 5, chap. A1, 545 p.

Folk, R.L., 1954, The distinction between grain size and mineral composition in sedimentary-rocks: Journal of Geology, v. 62, no. 4, p. 344–359.

Galloway, D.L., Jones, D.R., and Ingebritsen, S.E., 1999, Land subsidence in the United States: U.S. Geological Survey Circular 1182, 175 p. *http://pubs.usgs.gov/circ/circ1182/*, accessed March 22, 2012

Garbarino, J.R., 1999, Methods of analysis by the U.S. Geological Survey National Water Quality Laboratory—Determination of dissolved arsenic, boron, lithium, selenium, strontium, thallium, and vanadium using inductively coupled plasma-mass spectrometry: U.S. Geological Survey Open-File Report 99–093, 31 p.

Garbarino, J.R., Kanagy, L.K., and Cree, M.E., 2006, Determination of elements in natural-water, biota, sediment and soil samples using collision/reaction cell inductively coupled plasma-mass spectrometry: U.S. Geological Survey Techniques and Methods, book 5, sec. B, chap.1, 88

Godwin, H, 1962, Half-life of radiocarbon: Nature ,v.195, p. 984.

Gonfiantini, R., 1978, Standards for stable isotope measurements in natural compounds: Nature, v. 271, p. 534–536.

Gonfiantini, R., 1984, Advisory group meeting on stable isotope reference samples for geochemical and hydrological investigations, Vienna, September 19–21, 1983: International Atomic Energy Agency, Vienna, 77 p.

Graham, S.E., Mahony, T.M., Blissenbach, J.L., Mariant, J.J., and Wentworth, C.M., 1999, Regional geologic map of San Andreas and related faults in Carrizo Plain, Temblor, Caliente and La Panza Ranges and vicinity, California—A digital database: U.S. Geological Survey Open-File Report 99–14, scale 1:125,000.

Greene, E.A. and Shapiro, A.M., 1998, AIRSLUG: A FORTRAN program for the computation of type curves to estimate transmissivity and storativity of prematurely terminated air-pressurized slug tests: Ground Water, v. 36, no.2, p. 373–376.

Halford, K. J., and Kuniansky, Eve L., 2002, Documentation of Spreadsheets for the Analysis of Aquifer-Test and Slug-Test Data: U.S. Geological Survey Open-File Report 02–197, 54 p.

Hem, J.D., 1992, Study and interpretation of the chemical characteristics of natural water, third edition: U.S. Geological Survey Water Supply Paper 2254, 264 p.

Hill, M.L., Carlson, S.A., and Dibblee, T.W., Jr., 1958, Stratigraphy of Cuyama Valley–Caliente Range area, California: American Association of Petroleum Geologists Bulletin, v. 42, no. 12, p. 2,973–3,000.

Hudnut, K. W., Bock, Y., Galetzka, J.E., Webb, F.H., and Young, W.H., 2002, The Southern California Integrated GPS Network (SCIGN), in Seismotectonics in Convergent Plate Boundary, edited by Y. Fujinawa and A. Yoshida: Toyko, Terra Scientific Publishing Company, p. 167–189.
Ingebritsen, S.E., and Sanford, W.E., 1998, Groundwater in geologic processes: New York, New York, Cambridge University Press, 341 p.

Izbicki, J. A. and Michel, R. L., 2003, Movement and Age of Ground Water in the Western Part of the Mojave Desert, Southern California, USA: U.S. Geological Survey Water-Resources Investigations Report 03–4314, 35 p.

Jacob, C. E., 1946, Drawdown test to determine effective radius of artesian well: American Society of Civil Engineers Proceedings, v. 72, May.

Kayen, R.E., Edwards, B.D., and Lee, H.J., 1999, Nondestructive laboratory measurement of geotechnical and geoacoustic properties through intact core-liner, in Nondestructive and Automated Testing for Soil and Rock Properties, 1999: West Conshohocken, Pa., American Society for Testing and Materials, STP 1350, p. 83–94.

Kellogg, K.S., Minor, S.A., and Cossette, P.M., 2008, Geologic Map of the Eastern Three-Quarters of the Cuyama 30' x 60' Quadrangle, California: U.S. Geological Survey Scientific Investigations Map 3002, scale 1:100,000, 2 plates, 1 pamphlet, 23 p.

Keys, W.S., and MacCary, L.M., 1983, Application of bore-hole geophysics to water-resources investigations: U.S. Geological SurveyTechniques of Water-Resources Investigations, book 2, chap. E1, 126 p.

Lagoe, M.B., 1987, Middle Cenozoic basin development, Cuyama Basin, California, in Ingersoll, R.V. and Ernst, W.G., eds., Cenozoic basin development of coastal California, Rubey Volume VI : Englewood Cliffs, New Jersey, Prentice-Hall, p. 172–206.

Langbein, John, 2008, Noise in GPS displacement measurements from Southern California and Southern Nevada: Journal of Geophysical Research, v. 113, B05405, 12 p.

McCleskey, R.B., Nordstrom, D.K., and Ball, J.W., 2003, Metal interferences and their removal prior to the determination of As(T) and As(III) in acid mine waters by hydride generation atomic absorption spectrometry: U.S. Geological Survey Water-Resources Investigations Report 03–4117, 14 p. Available at *http://pubs.usgs.gov/wri/wri03-4117/WRI034117.pdf*

McNeill, J.D., 1986, Geonics EM39 borehole conductivity meter-theory of operation: Mississauga, Ontario, Geonics Ltd., Technical Note 20, 11 p.

Munsell Color, 1994, Munsell soil color charts: Baltimore, Md., Munsell Color, Inc.

National Research Council, 1947, Report of the Subcommittee on Sediment Terminology: American Geophysical Union Transactions, v. 28, no. 6, p. 936–938.

Ostlund, H.G., Craig, H., Broecker, W.S., and Spencer, D., 1987, Geosecs Atlantic, Pacific, and Indian Ocean Expeditions, Shorebased Data and Graphics, v. 7, p. 7–19.

Ostlund, H.G. and Dorsey, H.G., 1977, Rapid electrolytic enrichment and hydrogen gas proportional counting of tritium, in Low-Radioactivity Measurements and Applications: Proceedings of the International Conference on Low-Radioactivity Measurements and Application, October 6–10, 1975, The High Tatras, Czechoslovakia, p. 55–60.

Pacific Gas and Electric Company, 2006, PG&E's Energy Management Solutions for Pumps & Pumping Systems: C-0492 ver. September 2006, 2p.

Piper, A.M., 1944, A graphic procedure in the geochemical interpretation of water analyses: American Geophysical Union Transactions, v. 25, p. 914–923.

Plummer, L.N., Michel, R.L., Thurman, E.M., and Glynn, P.D., 1993, Environmental tracers for age dating young ground water, in Alley, W.M., ed., Regional ground-water quality: New York, Van Nostrand Reinhold, p. 255–294.

Roscoe Moss Company, 1990, Handbook of Groundwater Development, Wiley-Interscience, p. 493.

Santa Barbara County Planning and Development Department, 1994, Santa Barbara County Comprehensive Plan, 77 p.

Schlumberger, 1972, Log interpretation, volume I—principles: New York, Schlumberger Limited, 113 p.

Schwing, H.F., 1984, Subsurface geology of the South Cuyama oil field and adjacent areas, southern Coast Ranges, California: Corvallis, Oregon State University, M.S. thesis, 81 p., 19 pls., 10 figs.

Singer, J.A., and Swarzenski, W.V., 1970, Pumpage and ground-water storage depletion in Cuyama Valley California, 1947–66: U.S. Geological Survey Open-Rile Report 70–304, 24 p.

Spitz, H.M., 1986, Subsurface Geology of the southeastern Cuyama Valley, southern Coast Ranges, California: Corvallis, Oregon State University, M.S. thesis, 88 p., 20 pls., 12 figs.

Sneed, Michelle., Brandt, J.T., 2007, Detection and measurement of land subsidence using global positioning system surveying and interferometric synthetic aperture radar, Coachella Valley, California, 1996–2005: U.S. Geological Survey Scientific Investigations Report 2007–5251, 31 p.

Stookey, L.L., 1970, FerroZine—A new spectrophotometric reagent for iron: Analytical Chemistry, v. 42, p. 779–781.

Stuiver, M., and Polach, H.A., 1977, Reporting of 14C data: Radiocarbon, v. 19, p. 355–363.

Struzeski, T.M., DeGiacomo, W.J., and Zayhowski, E.J., 1996, Methods of analysis by the U.S. Geological Survey National Water Quality Laboratory— Determination of dissolved aluminum and boron in water by inductively coupled plasma-atomic emission spectrometry: U.S. Geological Survey Open-File Report 96–149, 17 p.

Sweetkind, D.S., Faunt, C.C., and Hanson, R.T., 2013, Construction of 3-D geologic framework and textural models for Cuyama Valley groundwater basin, California: U.S. Geological Survey Scientific Investigations Series Report 2013-5127, 46 p.

Upson, J.E. and Worts, G.F., Jr, 1951, Groundwater in the Cuyama Valley California: US Geological Survey Water-Supply Paper 1110-B, 81 p., 1 plate.

U.S. Environmental Protection Agency, 2012a, National Primary Drinking Water Regulations, accessed April 1, 2012, at *http://water.epa.gov/drink/contaminants/index.cfm*

U.S. Environmental Protection Agency, 2012b, Drinking water contaminants, accessed April 1, 2012, at *http://www.epa.gov/safewater/contaminants/index.html*

U.S. Geological Survey Earthquakes Hazards Program, 2012, About GPS: accessed May 2012 at *http://earthquake.usgs.gov/monitoring/gps/about.php*

U.S. Geological Survey, variously dated, National field manual for the collection of water-quality data: U.S. Geological Survey Techniques of Water-Resources Investigations, book 9, chap. A1–A9, accessed January 17, 2013, at *http://water.usgs.gov/owq/FieldManual/*

Vedder, J.G., 1968, Geologic map of the Fox Mountain quadrangle, Santa Barbara County, California: U.S. Geological Survey Miscellaneous Investigations Map I-547, scale 1:24,000.

Vedder, J.G., and Repenning, C.A., 1975, Geologic map of the Cuyama and New Cuyama quadrangles, San Luis Obispo and Santa Barbara Counties, California: U.S. Geological Survey Miscellaneous Investigations Map I–876, scale 1:24,000.

Wigley, T.M.L., and Muller, A.B., 1981, Fractionation corrections in radiocarbon dating: Radiocarbon, v. 23, p. 173–190.

Williams, J.H., Lapham, W.W., and Barringer, T.H., 1993, Application of electromagnetic logging to contamination investigations in glacial sand-and-gravel aquifers: Groundwater Monitoring Review, v. 13, no. 3, p. 129–138.

Williams, S.D.P., Bock, Yehuda, Fang, Peng, Jamason, Paul, Nikolaidis, R.M., Prawirodirdjo, Linette, Miller, Meghan, and Johnson, D.J., 2004, Error analysis of continuous GPS position time series: Journal of Geophysical Research, v. 109, B03412, 19 p.

Yeats, R.S., Calhoun, J.A., Nevins, B.B., Schwing, H.F., and Spitz, H. M., 1989, Russell Fault; early strike-slip fault of California Coast Ranges: American Association of Petroleum Geologists Bulletin, v. 73, p. 1089–1102.

Zerbini, Susanna, Richter, Bernd, Negusisi, Monia, Romagnoli, Claudia, Simon, Dietrich, Domenichini, Francesco, and Schwahn, Wolfgang, 2001, Height and gravity variations by continuous GPS, gravity and environmental parameter observations in the southern Po Plain, near Bologna, Italy: Earth and Planetary Science Letters, v. 192, no. 3, p. 267–279.

Prepared by the Sacramento Publishing Service Center.

For more information concerning this report, contact:

Director
U.S. Geological Survey
California Water Science Center
6000 J Street, Placer Hall
Sacramento, CA 95819
dc_ca@usgs.gov

or visit our Web site at:
http://ca.water.usgs.gov

Everett and others—**Geology, Water-Quality, Hydrology, and Geomechanics of the Cuyama Valley Groundwater Basin, California, 2008–12**—SIR 2013-5108

Prepared in cooperation with the Water Agency Division of the Santa Barbara County Department of Public Works

Kirschenmann Road Multi-Well Monitoring Site, Cuyama Valley, Santa Barbara County, California

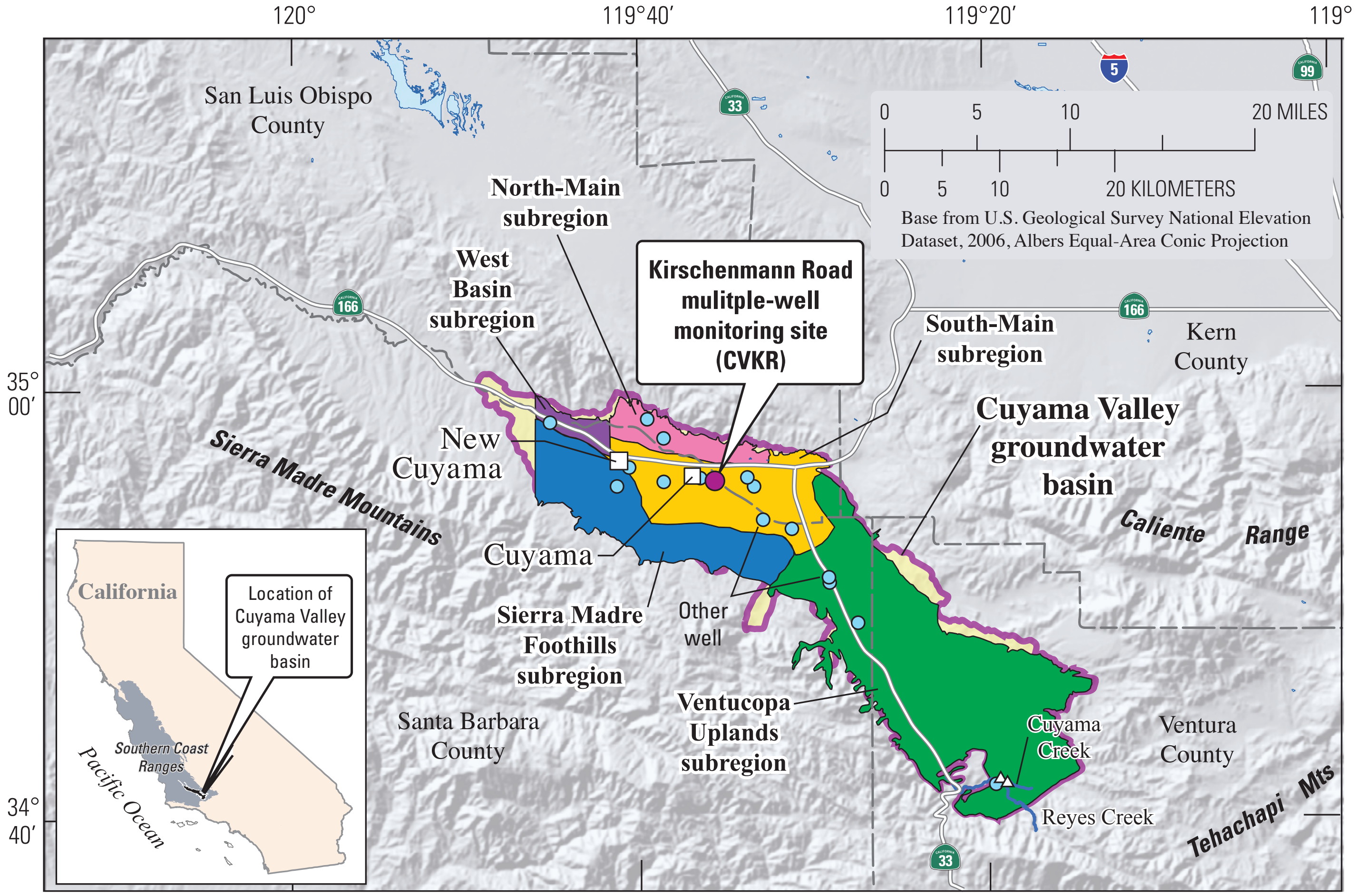

Figure 1. Location of multiple-aquifer monitoring-well site (CVKR), selected supply and irrigation wells, and surface-water water-quality collection sites Cuyama Creek and Reyes Creek, Cuyama Valley, California.

Introduction

The U.S. Geological Survey (USGS), in cooperation with the Water Agency Division of the Santa Barbara County Department of Public Works, is evaluating the geohydrology and water availability of the Cuyama Valley, California (fig. 1). As part of this evaluation, the USGS installed the Cuyama Valley Kirschenmann Road multiple-well monitoring site (CVKR) in the South-Main subregion of the Cuyama Valley (fig. 1). The CVKR well site is designed to allow for the collection of depth-specific water-level and water-quality data. Data collected at this site provides information about the geology, hydrology, geophysics, and geochemistry of the local aquifer system, thus, enhancing the understanding of the geohydrologic framework of the Cuyama Valley. This report presents the construction information and initial geohydrologic data collected from the CVKR monitoring site, along with a brief comparison to selected supply and irrigation wells from the major subregions of the Cuyama Valley (fig. 1).

Well Completion

The CVKR borehole was drilled to a depth of 1,003.5 feet below land surface (ft bls) using direct mud-rotary drilling techniques. Drill cuttings were collected throughout the drilling process and a core sample was collected from the bottom of the borehole to determine the lithology (fig. 2). To assist in the identification of lithologic and stratigraphic units, geophysical logs were collected from the borehole prior to well construction in accordance with the protocols established by the USGS National Field Manual (U.S. Geological Survey, variously dated, book 2). Four 2-inch-diameter wells, were installed with screened intervals from 960 to 980 (CVKR-1), 760 to 780 (CVKR-2), 600 to 620 (CVKR-3), and 440 to 460 (CVKR-4) ft bls (fig. 2). A filter pack of #3 sand was installed around each screen and a low-permeability bentonite grout was placed between the filter packs to vertically isolate each of the wells. Installation of multiple wells within a single borehole allows for analysis of the hydrologic properties of discrete vertical zones within the multiple-aquifer system as well as the collection of depth-specific water-quality samples.

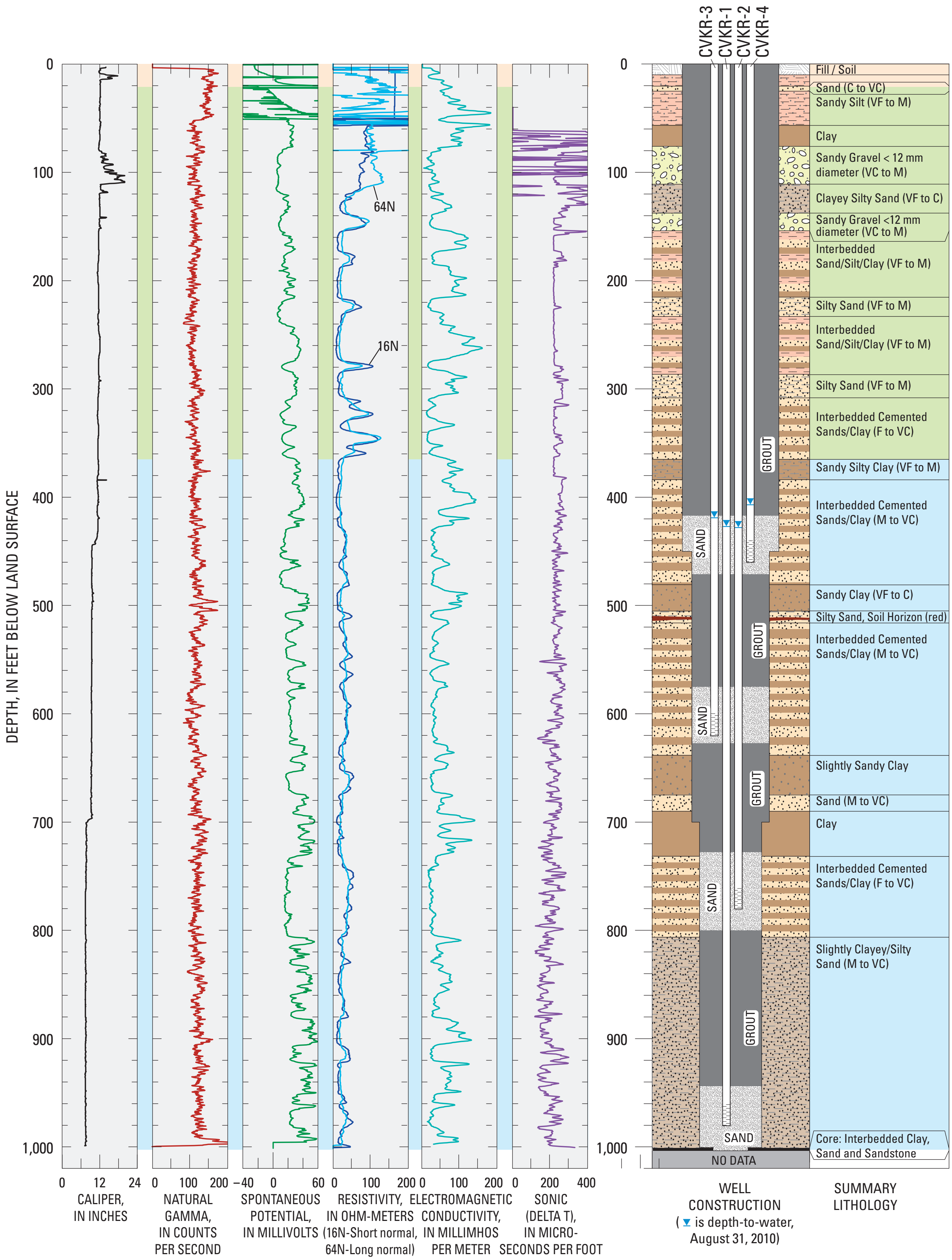

Figure 2. Well construction, summary lithology, and geophysical-log data from multiple-well monitoring site CVKR, Cuyama Valley, California. Abbreviations: VF, very fine; F, fine; M, medium; C, coarse; VC, very coarse.

Geology

Singer and Swarzenski (1970) generalized the geology of the Cuyama Valley into four main units: (1) non-water-bearing rocks—the basement complex and all sedimentary rocks older than the Morales

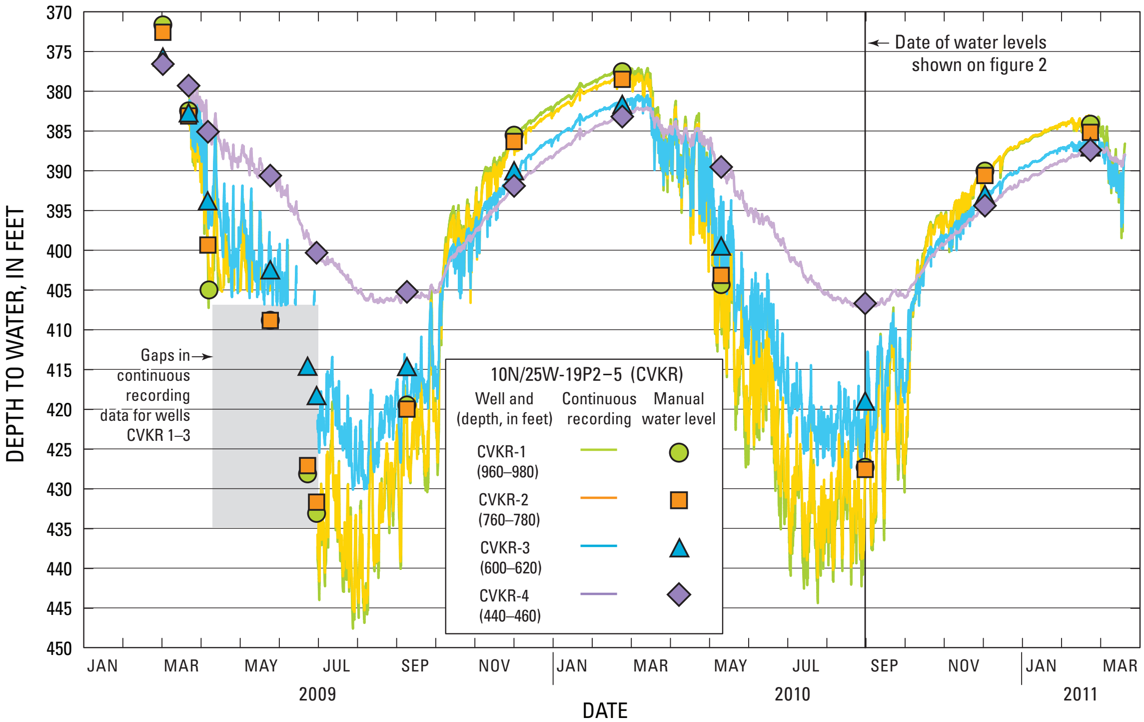

Figure 3. Water-level hydrograph from multiple-well monitoring site CVKR from March 1, 2009 to March 20, 2011, Cuyama Valley, California.

Formation, (2) the Morales Formation of Pleistocene to Pliocene age, (3) older alluvium of Pleistocene age, and (4) younger alluvium of Holocene age. Cross sections accompanying the geologic maps of Vedder and Repenning (1975), which were based, in part, on deep oil and gas exploration wells, show that older and younger alluvial deposits are generally about 1,000 feet thick in the vicinity of CVKR borehole. As evidenced by the drill cuttings and geophysical logs, the CVKR borehole penetrated terrestrial siliciclastic sediments that are alluvial fan and stream deposits (fig. 2). The borehole encountered younger alluvium from land surface to about 360 ft bls and older alluvium from about 360 ft bls to the bottom the hole. The Morales Formation was not encountered in this borehole. Sediments encountered in the CVKR borehole at intermediate depths of 360 to 620 ft bls were much more consolidated than expected from the descriptions of these older alluvium units published on the geologic maps. Drill cuttings collected at about 505 ft bls were reddish in color, suggesting the presence of a paleosol (buried soil horizon), which represents a period of non-deposition (fig. 2). The highest levels of natural gamma occur within, and just above, this paleosol. Below 720 feet there is a general decrease in sonic Delta T, indicating an increase in cementation and induration. The three feet of core collected from the bottom of the borehole contained interbedded clay, sand, and sandstone.

Hydrology

Each of the four wells at the CVKR site was equipped with instrumentation to automatically measure and record the depth to water at regular time intervals (fig. 3). Periodic manual measurements of water levels were made to verify the continuously-monitored data (fig. 3). The pumping of nearby irrigation wells influenced water levels in all of the CVKR wells. Over the period of record (2009-2011), data showed a seasonal pattern, with water levels declining between March and August, coinciding with the peak of the agricultural season, and rising between September and February, when nearby irrigation and related pumping was at a minimum. Seasonal water levels in the three deeper wells (CVKR-1, 2 and 3) varied as much as 60 feet between March and August, while water levels in the shallowest well (CVKR-4) varied by about 25 ft over the same period. Water levels showed a decline in the seasonally high levels over the period of record. Manual measurements made in late February of 2011 showed a decline of over 10 feet compared to those made in early March of 2009. Vertical water-level gradients were upward during the winter months and reversed to downward gradients during the irrigation season.

Slug tests were performed on each of the wells, in accordance with the protocols established by the USGS National Field Manual (U.S. Geological Survey, variously dated, book 3), to estimate the hydraulic conductivity of the aquifer material next to the screened interval. The shallowest well (CVKR-4) had the lowest estimated hydraulic conductivity value of 9.3 feet per day (ft/day), well CVKR-3 had the highest estimated hydraulic conductivity value of 28 ft/day, and wells CVKR-2 and CVKR-1 had slightly lower values of 22 and 18.1 ft/day, respectively.

Geochemistry

Water samples were collected in accordance with the protocols established by the USGS National Field Manual (U.S. Geological Survey, variously dated, book 9) and were analyzed for major-ion chemistry, stable isotopes of hydrogen (deuterium) and oxygen (oxygen-18), tritium, and carbon-14 to delineate the type, source, and age of the groundwater. Analyses were performed by the USGS National Water Quality Laboratory (NWQL) in Lakewood, Colorado; the USGS Stable Isotope Laboratory in Reston, Virginia; and the National Ocean Sciences AMS Facility in Woods Hole, Massachusetts, following standard methods outlined by Fishman (1993), Copland and others (1991), Ostlund and Dorsey (1977), and Coplen (1994).

The samples from the CVKR wells were found to be calcium-magnesium-sulfate waters (fig. 4). Water-quality characteristics of all four samples were similar to each other and to samples from other wells in the South-Main subregion (fig. 1).

Nitrate concentrations, reported as nitrogen (NO_3-N), in the shallow well (CVKR-4) were 15 milligrams per liter (mg/L); CVKR-3 had a NO_3-N concentration of 7 mg/L (table 1). Irrigation return flows are a possible source of the high NO_3-N concentrations in the shallower wells.

The stable isotopes oxygen-18 and deuterium in groundwater reflect the altitude, latitude, and temperature of recharge and the extent of evaporation before water entered the groundwater system. The isotope samples from the three deeper wells are progressively lighter (more negative), indicating that groundwater does not move freely between the different layers. Restricted movement of water between the layers also is supported by wide variation in isotope values in water from the other water-supply and irrigation wells in South-Main subregion. The three deeper CVKR wells are most similar to samples from the Sierra Madre and Ventucopa subregions (fig. 1), indicating that these subregions could be the main source of recharge for the South-Main subregion. The isotopic composition of the sample from the

Table 1. Selected water-chemistry constituents for the CVKR monitoring site, Cuyama Valley, California. Abbreviations: ND denotes no detection.

State and local well number	Screened interval (feet below land surface)	Total dissolved solids (milligrams per liter)	Nitrate plus nitrite, as nitrogen (milligrams per liter)	Delta deuterium (δD per mil)	Delta oxygen-18 ($\delta^{18}O$ per mil)	Tritium (picocuries per liter	Uncorrected carbon-14 age (years before present)
10N/25W-19P2 (CVKR-1)	960 - 980	1,580	ND	−71.3	−9.86	ND	6,300
10N/25W-19P3 (CVKR-2)	760 - 780	1,500	0.54	−70.8	−9.92	ND	4,600
10N/25W-19P4 (CVKR-3)	600 - 620	1,560	7.0	−69.3	−9.64	0.3	3,700
10N/25W-19P5 (CVKR-4)	440 - 460	1,820	15.2	−66.3	−9.52	0.5	3,600

shallow well (CVKR-4) is similar to the composition of a surface-water sample collected from Cuyama Creek, indicating the creek could be the source of recharge for this subregion.

Tritium and carbon-14 are radioactive isotopes that provide information about the age (time since recharge) of groundwater. Water from the four CVKR wells contained low levels of tritium, ranging from 0 (non-detection) to 0.5 picocuries per liter. Samples from CVKR-3 and CVKR-4 had low tritium concentrations, indicating the presence of at least some recent recharge; however, the samples from CVKR-1 and CVKR-2 contained no detectable tritium, indicating that the water from these wells was recharged prior to the early 1950s. The uncorrected carbon-14 ages of the water collected from the wells increased with depth and ranged from 3,600 to 6,300 years before present (table 1). Water samples collected from other wells in the Cuyama Basin contained levels of carbon-14 representative of water recharged between 600 (Ventucopa Uplands) to 33,400 (Sierra Madre Foothills) years before present.

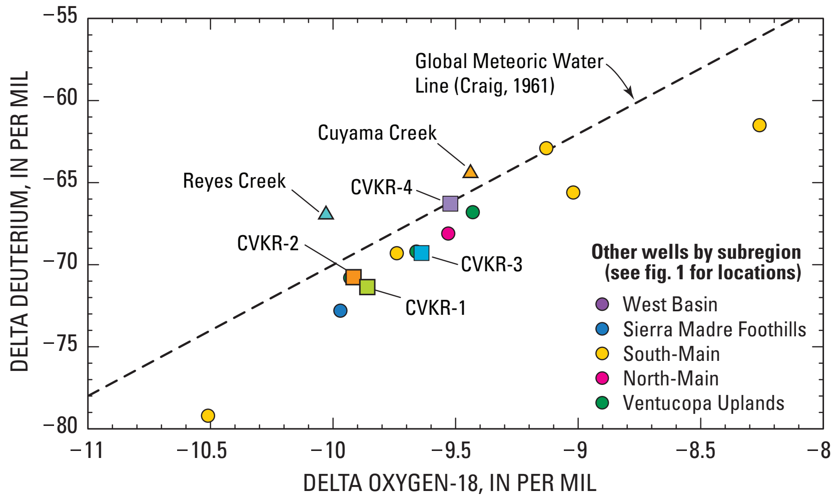

Figure 5. Isotopic composition of groundwater collected from multiple-well monitoring site CVKR, and selected water-supply and irrigation wells and surface water collected from Cuyama and Reyes Creeks, Cuyama Valley, California.

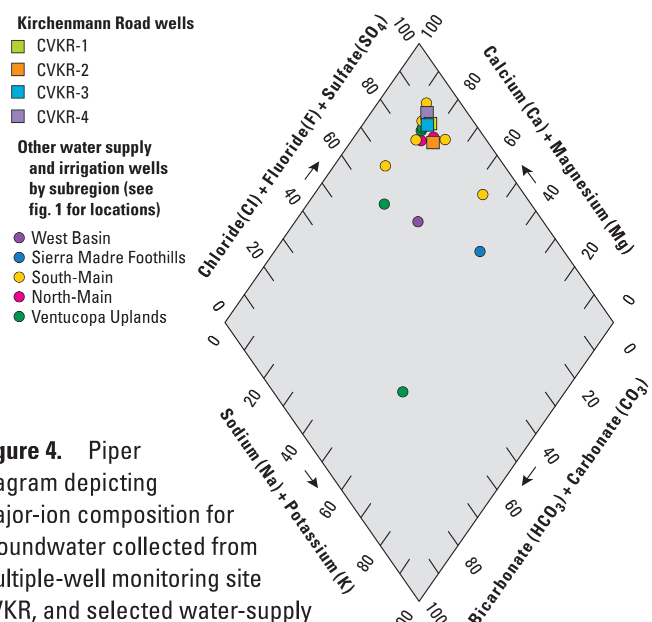

Figure 4. Piper diagram depicting major-ion composition for groundwater collected from multiple-well monitoring site CVKR, and selected water-supply and irrigation wells, Cuyama Valley, California.

References

Coplen, T.B., 1994, Reporting of stable hydrogen, carbon, and oxygen isotopic abundances: Pure & Applied Chemistry, v. 66, p. 273–276.

Coplen, T.B., Wildman, J.D., and Chen, J., 1991, Improvements in the gaseous hydrogen-water equilibration technique for hydrogen isotope ratio analysis: Analytical Chemistry, v. 63, p. 910–912.

Craig, H., (1961). "Isotopic variations in meteoric waters". Science, 133, 1702-1703.

Fishman, M.J., ed., 1993, Methods of analysis by the U.S. Geological Survey National Water Quality Laboratory--Determination of inorganic and organic constituents in water and fluvial sediments: U.S. Geological Survey Open-File Report 93-125, 217 p.

Ostlund, H.G. and Dorsey, H.G., 1977, Rapid electrolytic enrichment and hydrogen gas proportional counting of tritium, in Low-Radioactivity Measurements and Applications: Proceedings of the International Conference on Low-Radioactivity Measurements and Application, October 6–10, 1975, The High Tatras, Czechoslovakia, p. 55–60.

Singer, J.A., and Swarzenski, W.V., 1970, Pumpage and ground-water storage depletion in Cuyama Valley California, 1947-66: U.S. Geological Survey Open-File Report 70-304, 24 p.

U.S. Geological Survey, variously dated, National field manual for the collection of water-quality data: U.S. Geological Survey Techniques of Water-Resources Investigations, books 2,3, and 9, available online at http://pubs.water.usgs.gov/twri/.

Vedder, J.G., and Repenning, C.A., 1975, Geologic map of the Cuyama and New Cuyama quadrangles, San Luis Obispo and Santa Barbara Counties, California: U.S. Geological Survey Miscellaneous Investigations Map I-876, scale 1:24,000.

By R.R. Everett, R.T. Hanson, and D.S. Sweetkind

Technical Contacts:

Rhett R. Everett
Randall T. Hanson

U.S. Geological Survey
4165 Spruance Road, Suite 200
San Diego, CA 92101

Don Sweetkind

U.S Geological Survey,
Denver Federal Center, MS 973
Lakewood, CO 80225-0046

Table A1_1. Interpreted depth to top of geologic units in oil and gas wells, Cuyama Valley.

[API Number, American Petroleum Institute well number. Northing and easting are in Albers projected coordinates, referenced to North American Datum of 1983 (NAD83). Elevations are referenced to North American Vertical Datum of 1988 (NAVD 88). LT, less than, shown in the table with the symbol <, indicating that the top of the formation is interpreted to be shallower than the listed depth; ---, no data were interpreted for that unit. Qoa, older alluvium, QTm, Morales Formation, Tq, Quatal Formation, BR1 or BR2, bedrock units 1 or 2.]

API Number	Well indentifier	Easting (meters)	Northing (meters)	Elevation (feet)	Total depth (feet)	Drilled depth togeologic unit top (feet)						
						LT	Qoa	LT	QTm	LT	Tq	BR1 or BR2
07900119	Mettler A-1-13	44522	1320757	2,496	3,602	---	---	---	1,100	---	---	---
07900123	Russell C-1	30304	1324811	2,126	2,748	---	---	---	850	---	---	---
07900124	Russell C-2	31490	1323273	2,114	12,981	---	---	<	600	---	---	---
07900125	Russell C 3	32957	1323838	2,156	11,292	---	---	---	1,294	---	---	---
07900149	Brownson, Cuyama 1	13251	1330829	1,722	2,124	---	---	---	120	---	---	---
07900152	I Lee Burch 1	30667	1323815	2,105	1,438	---	---	---	700	---	---	---
07900183	Mettler 64-16	41012	1321528	2,393	3,602	---	---	---	2,900	---	---	---
07900184	Russell 12-18	36139	1321769	2,237	5,706	---	---	---	910	---	3,750	---
07900345	Ballinger Canyon Unit 1	47298	1316414	3,254	11,981	---	---	---	0	---	2,920	---
07900888	Chorum 67-10	13586	1332582	2,315	2,175	---	---	---	1,450	---	---	---
07900889	Whitney 47-10	13182	1332582	2,319	2,217	---	---	---	1,000	---	---	---
07900950	F.R.Anderson 28-24	15352	1328514	1,772	3,559	---	---	---	700	---	---	---
07900958	Indian 3	14698	1328605	1,761	4,774	---	---	---	100	---	---	---
07900971	Sloan C 71-26	15300	1328927	1,813	3,453	---	---	---	1,450	---	---	---
07900974	Sloan C 83-26	15482	1328440	1,790	3,430	---	---	---	1,500	---	---	---
07900983	Kosanke 86-23	14933	1329046	1,796	4,783	---	---	---	100	---	---	---
07900986	Chas Holmes 1	14662	1328716	1,767	946	---	---	---	450	---	---	---
07900990	Kosanke 9	14960	1328600	1,767	4,306	---	---	---	100	---	---	---
07901002	Wood-Callahan 13B-25	15764	1328530	2,298	2,682	---	---	---	2,450	---	---	---
07901018	F.R.Anderson 65-25A	16130	1327640	1,876	3,720	---	---	---	1,350	---	---	---
07901035	Indian 4	14322	1329794	1,767	3,434	---	---	---	90	---	---	---
07901038	Roussey Seismic 1	43647	1318607	2,422	708	---	---	---	800	---	---	---
07920769	Federal 1-7	37748	1322903	2,662	12,304	---	---	---	3,820	---	---	---
08300076	S.C.U. 83-6	27745	1314993	2,464	4,727	---	---	---	660	---	---	---
08300112	S.C.U. 58-31	27158	1315606	2,461	4,545	---	---	---	160	---	---	---
08300322	S.C.U. 14-31	26339	1316420	2,559	4,655	---	---	---	100	---	---	---
08300425	S.C.U. 73-6	27547	1314993	2,419	4,600	<	400	<	400	---	2,255	2,370

08300655	S.C.U. 61-6	27354	1315402	2,447	4,730	<	400	<	400	---	2,280	2,330
08300686	A.H. Heller 63-6	27350	1314988	2,431	4,510	---	---	---	480	---	---	---
08300738	S.C.U. 13-31	26342	1316621	2,565	3,579	---	---	---	150	---	---	---
08300741	Homan A 84-35	24541	1316417	2,881	4,875	---	---	---	550	---	---	2,470
08300788	S.C.U. 83-36	26142	1316622	2,640	4,780	---	---	---	710	---	2,395	2,440
08301027	S.C.U. 57-25	25555	1317434	2,606	4,620	---	---	---	1,200	---	---	---
08301030	S.C.U. 36-25	25149	1317635	2,602	4,705	---	---	---	1,310	---	---	---
08303031	R. R. U. 13-5	18308	1324672	2,044	3,325	---	---	---	100	---	---	---
08303037	Russell 18-5	18318	1323655	2,129	3,440	---	---	---	820	---	1,490	1,580
08303044	Russell 28-5	18518	1323669	2,097	4,218	---	---	---	820	---	---	1,480
08303047	R. R. U. 33-31	17107	1326290	1,885	3,170	---	---	---	1,200	---	---	---
08303048	Russell 38-5	18710	1323658	2,115	3,391	---	---	---	890	---	---	---
08303052	Russell A 43-8	18930	1323088	2,179	4,847	---	---	---	950	---	---	---
08303076	R. R. U. 73-6	17911	1324670	2,049	3,340	---	---	---	100	---	---	---
08303090	R. R. U. 123-31	17027	1326330	1,877	3,100	---	---	---	1,100	---	---	---
08303099	R. R. U. 48-5	18883	1323645	2,093	3,375	---	---	---	980	---	---	---
08303107	R. R. U. 83-6	18109	1324671	2,060	3,345	---	---	---	100	---	---	---
08303109	F.R.Anderson 73-36	16337	1326320	1,916	5,636	---	---	---	100	---	---	---
08303120	Russell A 23-9	20092	1323028	2,113	5,085	---	---	---	1,300	---	---	1,770
08303123	Russell A 34-6	17107	1324447	2,140	3,451	---	---	---	670	---	---	---
08303124	Russell A 42-5	18871	1324844	1,930	3,921	---	---	---	1,360	---	---	1,570
08303128	Russell A 53-6	17493	1324635	2,105	1,200	---	---	---	100	---	---	---
08303129	Russell A 53-8	19094	1323078	2,148	3,470	---	---	---	970	---	---	---
08303132	Russell A 83-8	19670	1322986	2,161	3,711	---	---	---	1,220	---	---	---
08303136	Russell A 138-5	18725	1323613	2,113	1,470	---	---	---	900	---	---	---
08303144	R. R. U. 23-31	16912	1326311	1,898	3,564	---	---	---	570	---	---	---
08303147	Indian 2	13782	1328678	1,757	4,143	---	---	---	90	---	---	---
08303150	Kirschenmann 87-22	32542	1319091	2,256	8,754	<	600	---	750	---	4,350	4,470
08303151	Seaboard-Richfield-Kirschenman 78-22	32372	1318838	2,265	10,097	<	550	---	1,100	---	4,900	5,000
08303164	F.K. Perkins 218-31	26331	1315592	2,631	2,800	---	---	---	900	---	---	---
08303165	Buzzard 1 1-25	25585	1318066	2,445	5,847	---	---	---	1,400	---	---	2,850
08303168	Baker No 1	28753	1317817	2,318	7,610	---	0	<	800	---	3,460	3,560
08303169	Cox 13-5	27938	1314991	2,535	5,706	---	0	<	300	---	2,400	2,460

08303170	Cox 35-5	28330	1314571	2,721	5,988	---	0	---	570	---	2,940	3,100
08303171	Cox 44-5	28520	1314786	2,659	6,015	---	---	---	760	---	2,900	2,990
08303172	Cox 55-5	28708	1314562	2,703	6,451	---	0	---	550	---	1,850	1,980
08303173	Cox 84-5	29331	1314772	2,684	8,208	---	0	<	500	---	3,090	3,140
08303174	Fisher 1	23525	1315162	2,889	9,505	---	---	---	2,990	---	---	---
08303177	J. G. Herren A 37-35	23532	1315730	2,706	4,598	---	---	---	1,760	---	---	---
08303185	S.C.U. 72-1	25925	1315201	2,602	4,175	---	---	---	980	---	---	---
08303186	Hibberd 81-1	26126	1315405	2,647	4,197	---	---	---	900	---	---	---
08303189	S.C.U. 10-36	24751	1317230	2,697	4,865	---	---	---	1,150	---	---	---
08303197	S.C.U. 13-36	24746	1316623	2,860	4,715	---	---	---	920	---	---	---
08303207	Perkins 18-31	26328	1315607	2,621	4,484	---	---	---	880	---	---	---
08303213	S.C.U. 22-36	24949	1316828	2,891	4,900	---	---	---	1,120	---	---	---
08303214	S.C.U. 23-6	26531	1314998	2,538	4,120	---	---	---	960	---	---	---
08303218	S.C.U. 25-31	26546	1316215	2,528	4,629	---	---	---	100	---	---	---
08303222	S.C.U. 27-25	24953	1317429	2,623	4,788	---	---	---	1,310	---	---	---
08303229	S.C.U. 31-36	25149	1317028	2,743	4,875	---	---	---	1,160	---	---	---
08303234	S.C.U. 33-6	26741	1314998	2,501	4,246	---	---	---	780	---	---	---
08303246	Heath 38-25	25151	1317232	2,690	4,264	---	---	---	1,150	---	2,480	2,520
08303257	S.C.U. 43-1	25324	1315000	2,665	4,430	---	---	---	1,500	---	---	---
08303258	Johnston 43-6	26951	1314998	2,479	4,400	---	---	---	670	---	---	---
08303267	Perkins 45-31	26935	1316216	2,478	4,605	---	0	<	400	---	2,370	2,420
08303274	S.C.U. 47-31	26961	1315810	2,496	4,579	---	---	---	140	---	---	---
08303275	S.C.U. 48-25	25351	1317231	2,665	4,850	---	---	---	1,130	---	---	---
08303281	S.C.U. 53-1	25523	1315000	2,637	4,301	---	---	---	1,400	---	---	---
08303282	A.H. Heller 53-6	27198	1314991	2,468	4,516	---	---	---	500	---	---	---
08303287	S.C.U. 54-31	27168	1316418	2,445	4,574	---	0	<	300	---	2,450	2,500
08303288	S.C.U. 54-35	23944	1316422	2,552	4,360	---	---	---	820	---	---	---
08303302	S.C.U. 63-1	25723	1315000	2,611	4,565	---	---	---	1,350	---	---	---
08303311	S.C.U. 66-35	24138	1316014	2,609	4,590	---	---	---	900	---	---	---
08303320	S.C.U. 72-6	27551	1315198	2,412	4,450	---	---	---	140	---	---	---
08303321	S.C.U. (Homan A) 72-35	24351	1316827	2,704	4,480	---	---	---	730	---	---	---
08303323	S.C.U. 73-1	25923	1314999	2,597	4,193	---	---	---	1,400	---	---	---
08303329	S.C.U. 75-35	24342	1316218	2,716	4,430	---	---	---	890	---	---	---
08303340	Homan A 81-35	24551	1317030	2,660	4,675	---	---	---	900	---	2,220	2,290

08303358	Cox 46-5	28514	1314375	2,734	6,483	---	0	---	540	---	2,920	3,000
08303359	H.U. 13-6	26322	1314997	2,558	4,267	---	---	---	1,000	---	---	---
08303362	S.C.U. 83-1	26122	1314999	2,573	4,228	---	---	---	1,120	---	---	---
08303372	S.C.U. 75-31	27562	1316213	2,390	4,425	<	400	<	400	---	2,440	2,510
08304102	Conklin 1	14894	1322043	2,458	1,570	---	---	<	200	---	1,150	---
08304104	Russell A 55-7	17466	1322691	2,275	3,292	---	---	<	200	---	1,100	---
08304105	Russell A 77-7	17879	1322220	2,335	3,646	---	---	<	400	---	1,220	---
08304106	Victoria Wood 1	11694	1322579	2,486	3,942	---	---	<	250	---	1,930	---
08304107	Wood 1	11698	1322606	2,489	3,020	---	---	---	---	---	---	2,300
08304110	Gerard-Callaway 46-16	10925	1320889	2,866	5,545	---	---	---	---	---	---	4,227
08304116	Norris Richardson 1	14353	1319764	2,843	4,849	---	---	---	---	---	---	2,080
08304117	Hinsdale 34-18	17023	1321143	2,491	3,355	---	---	<	200	---	1,634	---
08304118	Plaugher 1	16793	1320321	2,633	2,690	---	---	<	550	---	2,020	---
08304123	Russell (Shell) 1	10286	1325819	2,056	2,539	---	---	<	300	---	900	---
08304136	Wilrich Richardson 1	16005	1321209	2,455	1,393	---	---	<	200	---	1,260	1,300
08304137	Richardson 2	15745	1320843	2,532	1,663	---	---	<	200	---	1,440	1,480
08304142	Russell A 25-10 (Nevins: 21-5)	21655	1322622	2,142	5,340	---	---	---	200	---	---	1,735
08304143	Russell 45-24	25389	1319257	2,272	7,264	---	---	---	1,200	---	3,400	3,480
08304144	Russell A 52-22	22200	1319867	2,432	6,259	---	---	---	600	---	2,140	2,300
08304145	Russell A 55-22	22302	1319259	2,528	6,097	---	---	---	1,150	---	2,950	3,030
08304148	Elliott 88 84-34	22931	1315535	2,820	6,030	---	---	---	3,150	---	---	---
08304149	Schaeffer 1	28436	1320298	2,164	8,680	<	500	---	590	---	3,740	3,800
08304152	James Wilson No 1	19856	1321724	2,221	5,518	---	---	---	1,150	---	---	---
08304155	Smith Ranch 2	18764	1321062	2,428	4,465	---	---	<	200	---	1,350	---
08304156	Kirschenmann No 1	25139	1322915	1,999	7,096	---	---	---	1,270	---	4,600	---
08304157	Patterson 41-5	9124	1325217	2,191	4,291	---	---	<	300	---	2,600	---
08304158	Kirschenmann No 1?	25523	1323332	1,998	5,127	---	470	---	1,400	---	5,000	---
08304160	Sesnon-Richfield-Russell A 44-23	23767	1319453	2,347	6,437	---	---	---	1,080	---	2,850	---
08304161	Russell A 83-22	22940	1319668	2,450	5,600	---	---	---	1,200	---	2,860	2,910
08304162	Smith Ranch 1	19638	1321729	2,215	3,990	---	---	---	1,120	---	---	---
08304163	Steele No 1	21577	1323076	2,099	5,173	---	0	<	1,000	---	2,750	2,800
08304164	Kirschenmann 1	26413	1321978	2,056	7,788	---	---	---	650	---	4,850	4,902

08304170	Dixon A-1	45338	1308674	3,103	3,382	---	0	---	---	<	400	---
08304171	James No 1	30343	1312989	2,815	11,336	---	0	---	600	---	2,890	2,950
08304172	Lundstrom-Becker No 1	33305	1312702	2,802	10,434	---	0	<	400	---	2,680	2,900
08304173	Wegis Reyes A-1	39740	1312358	2,855	6,049	---	0	---	770	---	3,415	3,485
08304174	Wegis Reyes B-1	37792	1311809	2,789	7,500	---	0	<	400	---	3,160	3,270
08304175	Hickey 1	47693	1309067	2,840	6,817	---	---	<	300	---	1,480	---
08304180	USL-CDFPT 86X	35647	1311035	3,068	5,636	---	---	---	---	---	---	0
08304181	Cuyama 85-16	30908	1311291	3,028	6,956	---	---	---	2,380	---	---	3,480
08304184	Dougherty No 55	35161	1311388	3,121	6,502	---	---	---	---	---	---	0
08304189	Bandini 51-17	28790	1312099	3,053	7,020	---	---	---	3,000	---	---	---
08304192	Pickrell 21-16	29776	1312125	3,028	9,315	---	---	---	1,700	---	3,800	3,980
08304195	Dougherty No 1	35750	1311463	3,020	6,515	---	---	---	530	---	---	---
08304196	Norris No 1	43214	1313400	2,677	11,508	---	---	---	530	---	2,240	---
08304201	Wilshire No 1	29287	1313711	2,817	9,569	---	0	<	500	---	2,700	2,770
08304208	Sterling USL 83X-17	39131	1311737	2,882	6,039	---	0	<	300	---	2,900	2,960
08304264	Cuyama Oil Company 1	10109	1326748	1,939	1,612	---	---	<	200	---	1,300	---
08304265	Homan C-1	19139	1317531	3,197	7,697	---	---	---	3,170	---	---	---
08304266	Kirschenmann 37-22	31716	1318978	2,269	9,159	<	600	---	900	---	4,410	4,470
08304267	F. K. Perkins 1-27	32407	1317371	2,354	11,883	---	190	---	700	---	3,590	3,750
08304268	F. K. Perkins 24-27	31429	1317975	2,327	10,306	<	500	---	600	---	3,800	3,850
08304269	Perkins 33-26	33338	1318025	2,309	12,090	<	500	---	1,000	---	4,600	---
08304270	Perkins 33-35	33207	1316541	2,410	13,106	<	500	---	800	---	3,730	4,000
08304271	F. K. Perkins 66-28	30043	1318135	2,311	9,295	<	500	---	900	---	3,820	3,890
08304272	F. K. Perkins 84-28	30995	1317967	2,331	10,267	<	500	---	600	---	3,730	3,760
08304273	Russell C-5	30046	1322045	2,139	9,808	---	---	---	---	---	---	6,230
08304277	Russell A 78-11	24341	1321917	2,089	6,506	---	---	---	1,200	---	3,570	3,610
08304278	Russell A 87-22	22908	1318853	2,480	5,026	---	---	---	1,170	---	2,800	2,850
08304318	Landry 1	14681	1321207	2,600	3,108	---	---	<	200	---	1,550	---
08304354	Christian 1	10384	1326530	2,041	1,604	---	---	<	200	---	1,300	---
08304365	Russell 33-7	26878	1323270	2,019	8,124	---	---	---	650	---	---	5,980
08304506	Kirschenmann 67-22	32229	1319082	2,261	9,631	---	400	---	1,100	---	4,590	4,660
08304518	Clayton 14-4	49714	1315156	3,187	7,259	---	---	---	0	---	910	1,260
08304519	Humble-Lundstrom 48-2	33535	1313936	2,675	11,175	---	0	<	500	---	3,030	3,300
08304523	George Noonan 1	37206	1315113	2,495	4,045	---	---	---	540	---	3,150	---

08304552	Goehring 1	32831	1318776	2,270	7,601	<	450	---	800	---	---	4,840
08320191	Russell 41-15	22132	1321678	2,215	4,761	---	---	---	1,200	---	2,500	---
08320687	U.S. Miller 1	29785	1314969	2,653	8,400	---	0	<	850	---	3,320	3,380
08320908	Perkins 255-33	30206	1316127	2,458	8,345	<	850	<	850	---	3,720	3,770
08321118	Federal 1-15	41337	1311457	3,145	6,008	---	0	---	1,220	---	3,630	3,780
08321299	Reserve-Wright 1	42910	1315219	2,521	14,175	---	---	<	1,500	---	---	---
08321334	Chevron-Sulpetro Wylie U.S.L. 1	37629	1314141	2,601	11,408	---	0	---	580	---	2,720	2,770
08321607	Chambers Federal 1-2	42890	1314847	2,525	15,283	<	600	---	1,050	---	3,700	3,830
08321608	Perkins Ranch 1	29147	1317784	2,327	7,500	---	0	<	1,300	---	3,740	3,850
08321657	USA 1-5	28822	1315278	2,569	4,972	---	0	<	600	---	2,470	2,540
08321997	Russell 81X-24	35577	1320030	2,244	12,764	---	---	<	1,400	---	4,550	---
08322092	Koch-Russell 24X-19	36245	1319531	2,265	12,970	---	---	<	1,400	---	4,370	---
08322097	Mccray 1	27712	1318895	2,226	9,099	---	0	<	1,000	---	---	3,200
08322161	Mitchell 1	12705	1322735	2,363	3,002	---	---	<	400	---	1,340	1,470
08322170	Los Amigos 1A	6918	1323799	2,560	5,743	---	---	<	700	---	3,620	3,980
08322237	Federal 1-20	49321	1310960	3,279	9,900	---	---	---	0	---	3,050	---
08322267	Los Padres 76X-32	49460	1306651	3,019	3,480	---	---	---	100	---	265	---
11106128	Tarver-Volk 1	83828	1287065	4,766	3,012	---	---	---	---	---	---	0
11106130	Hattie Russell 1	64530	1284965	5,981	9,748	---	---	---	---	---	---	0
11106131	Cuyama-Piru 1	80866	1290494	5,343	4,740	---	---	---	---	---	---	0
11106132	Cuyama-Piru 1	81455	1290389	5,367	5,220	---	---	---	---	---	---	0
11106133	Jamieson 11-7	67504	1295994	4,232	2,852	---	---	---	---	---	---	25
11106134	Jamieson 54-7	68087	1295500	4,307	3,214	---	---	---	---	---	---	25
11106135	M-T 1	57632	1291402	3,964	653	---	---	---	---	---	---	0
11106138	Wright 54-18	58306	1293835	3,856	4,537	---	0	---	---	---	50	---
11106139	Smith 1	60198	1292008	3,629	5,286	---	---	---	---	---	---	25
11106140	D&B 1	57915	1291425	3,910	1,501	---	---	---	---	---	---	0
11106144	R-S 1	57491	1291266	3,942	954	---	---	---	---	---	---	0
11106145	Reyes 64-12	57040	1295519	3,536	4,045	---	---	---	---	---	50	---
11106151	Round Springs Unit 1	59741	1298777	4,004	4,010	---	---	---	---	---	0	---
11106152	Apache Unit 2	58865	1299184	4,058	3,404	---	---	---	---	---	0	---
11106153	Adams US 1	53049	1299647	3,249	5,938	---	---	---	---	---	---	25
11106154	Apache Unit 1	53913	1301030	4,082	10,563	---	---	---	---	---	---	0

11106155	Dixon B-1	57435	1300260	3,937	3,150	---	---	---	---	---	---	0
11106156	Explorer 1	50571	1305783	3,095	1,220	---	---	---	54	---	765	---
11106157	Brubaker 1	51926	1299445	3,311	3,290	---	---	---	---	---	---	25
11106158	Thompson 1	51154	1304568	3,152	810	---	---	---	90	---	780	---
11106161	Curyea 32	64422	1309204	4,304	584	---	---	---	---	---	---	100
11106162	Curyea 54	61603	1308815	4,061	974	---	---	---	---	---	---	100
11106163	Well No. 1, Stone	56604	1308687	3,567	257	---	---	---	---	---	50	---
11106164	Adams Drilling & Oil Company 1	53725	1314911	3,931	2,207	---	---	---	---	---	---	0
11106165	Adams Drilling & Oil Company 2	53583	1314604	3,936	785	---	---	---	---	---	---	0
11106166	Gillbergh A 2	54493	1310976	4,385	3,335	---	---	---	0	---	1,040	---
11106167	Quatal Unit 1	51971	1306942	3,206	4,010	---	---	---	100	---	1,740	1,960
11106168	Blue Diamond 1	52500	1313229	3,557	5,875	---	---	---	---	---	---	0
noAPI1	Cox 82-6	28008	1315099	2,515	4,550	---	---	---	30	---	---	---
noAPI2	South Cuyama unit 13-5	27949	1314997	2,544	5,232	---	---	---	690	---	---	---

Table A2_1. Interpreted depth to top of geologic units in water wells, Cuyama Valley.

[Northing and easting are in Albers projected coordinates, referenced to North American Datum of 1983 (NAD83). Elevations are referenced to North American Vertical Datum of 1988 (NAVD 88). GT, greater than, shown in the table with the symbol >, indicating that the top of the formation is interpreted to be deeper than the listed depth; ---, no data were interpreted for that unit. Qoa, older alluvium, QTm, Morales Formation.]

Well Identifier	Easting (meters)	Northing (meters)	Elevation (feet)	Total depth (feet)	Drilled depth to geologic unit top (feet)			Source of lithologic data[1]
					GT	Qoa	QTm	
CUY-G-01	43982	1313919	2,585	800	---	290	450	CA-DWR
CUY-G-02	43528	1314011	2,567	810	---	390	610	CA-DWR
CUY-G-03	45653	1312157	2,690	700	---	360	---	CA-DWR
CUY-G-04	31061	1313270	2,661	500	---	120	---	CA-DWR
CUY-G-06	35888	1318912	2,292	980	---	610	---	CA-DWR
CUY-02	28012	1319500	2,172	820	---	266	---	CA-DWR
CUY-G-08	48121	1307406	2,917	130	>	130	---	CA-DWR
CUY-G-09	27372	1321782	2,082	300	>	300	---	CA-DWR
CUY-G-11	31055	1322063	2,135	913	---	315	---	CA-DWR
CUY-G-13	45453	1309109	2,974	600	---	0	---	CA-DWR
CUY-G-14	47446	1309119	2,823	280	---	250	---	CA-DWR
CUY-G-15	47399	1308372	2,851	312	---	202	---	CA-DWR
CUY-G-16	48749	1314287	2,994	560	---	108	---	CA-DWR
CUY-G-17	50227	1303379	3,084	252	---	230	---	CA-DWR
CUY-G-18	48935	1306302	2,992	245	>	245	---	CA-DWR
CUY-G-19	33387	1319187	2,262	1,068	---	545	---	CA-DWR
CUY-G-21	43525	1314632	2,549	803	---	430	---	CA-DWR
CUY-G-22	30613	1319953	2,225	1,300	---	460	995	CA-DWR
CUY-G-23	29833	1319950	2,219	1,004	---	355	450	CA-DWR
CUY-G-24	29418	1320009	2,206	1,004	---	480	680	CA-DWR
PT-19	36953	1317520	2,331	970	---	434	---	CA-DWR
CUY-G-27	44216	1312272	2,627	798	---	---	---	CA-DWR
CUY-64	32077	1318778	2,269	1,015	---	415	---	CA-DWR
CUY-12	46647	1310857	2,740	200	---	175	---	CA-DWR
CUY-G-29	48456	1306362	2,962	385	---	218	---	CA-DWR
CUY-G-30	49791	1306587	3,052	255	---	250	---	CA-DWR
CUY-G-31	26243	1322158	2,051	403	---	235	---	CA-DWR

CUY-G-32	48444	1307300	2,930	243	>	243	---	CA-DWR
CUY-G-33	31164	1318856	2,284	703	---	360	---	CA-DWR
CUY-G-34	26035	1322353	2,041	340	---	155	---	CA-DWR
CUY-G-35	47208	1311938	2,882	343	---	120	---	CA-DWR
CUY-G-37	19673	1322878	2,176	540	---	0	---	CA-DWR
CUY-35	49475	1305373	2,997	302	---	275	---	CA-DWR
CUY-G-39	50198	1303375	3,082	248	---	241	---	CA-DWR
CUY-G-40	46183	1311818	2,748	270	>	270	---	CA-DWR
CUY-G-41	37786	1317089	2,362	1,125	---	493	---	CA-DWR
CUY-G-42	36656	1319199	2,284	1,165	---	545	---	CA-DWR
CUY-G-43	48468	1307214	2,934	220	---	210	---	CA-DWR
PT-18	37368	1317524	2,338	1,205	---	652	---	CA-DWR
CUY-G-46	36790	1318510	2,296	1,138	---	262	---	CA-DWR
CUY-G-47	45523	1315322	2,659	1,220	---	454	---	CA-DWR
CUY-40	48311	1307628	2,915	275	---	255	---	CA-DWR
CUY-G-48	31407	1320265	2,220	1,220	---	590	---	CA-DWR
CUY-G-49	48121	1308135	2,890	204	>	204	---	CA-DWR
CUY-G-50	29503	1323134	2,085	840	---	420	---	CA-DWR
CUY-G-52	30292	1322423	2,120	970	---	440	---	CA-DWR
CUY-G-54	48566	1307433	2,933	270	---	240	---	CA-DWR
CUY-G-55	48402	1307490	2,926	267	>	275	---	CA-DWR
CUY-G-56	25895	1322300	2,046	420	---	219	---	CA-DWR
CUY-G-57	32099	1320146	2,216	1,210	---	560	---	CA-DWR
CUY-G-59	45781	1311847	2,704	300	>	300	---	CA-DWR
CUY-G-61	47862	1307906	2,882	160	>	160	---	CA-DWR
CUY-G-62	57553	1308870	3,648	400	---	175	---	CA-DWR
CUY-G-63	26013	1323525	1,991	560	---	320	---	CA-DWR
CUY-06	43429	1315076	2,534	800	---	500	---	CA-DWR
10/24-19F1	46831	1320334	2,682	811	---	225	---	Upson and Worts (1951)
10/25-14Q1	43670	1320755	2,429	506	---	145	---	Upson and Worts (1951)
10/25-20H1 (PT-09)	39095	1319552	2,333	656	---	648	---	Upson and Worts (1951)
10/25-22E1	40933	1319529	2,364	659	---	514	---	Upson and Worts (1951)

10/25-23E1 (PT-14)	42869	1319818	2,378	810	---	380	---	Upson and Worts (1951)
10/25-26E1	42778	1317891	2,432	845	---	409	---	Upson and Worts (1951)
10/25-27G1 (PT-15)	41594	1317948	2,415	666	---	446	---	Upson and Worts (1951)
10/25-30F1 (CUY-54)	36561	1317925	2,319	376	---	408	---	Upson and Worts (1951)
10/26-18F1 (CUY-56)	27135	1321527	2,095	240	---	158	---	Upson and Worts (1951)
10/26-21Q1	30532	1318753	2,296	993	---	183	---	Upson and Worts (1951)
10/26-22E1 (PT-38)	31344	1319707	2,239	514	---	358	---	Upson and Worts (1951)
10/26-22J2	32301	1319400	2,245	575	---	420	---	Upson and Worts (1951)
10/26-22K1	31747	1319429	2,254	507	---	410	---	Upson and Worts (1951)
10/26-9R1 (PT-27)	31033	1322161	2,133	222	---	212	---	Upson and Worts (1951)
10/26-9R2 (PT-28)	30957	1322099	2,133	380	---	176	---	Upson and Worts (1951)
10/27-11A2	24480	1323309	1,972	533	---	175	---	Upson and Worts (1951)
10/27-11C1 (PT-50)	24010	1323444	1,966	378	---	221	---	Upson and Worts (1951)
10/27-12E1	25042	1323198	1,996	248	---	127	---	Upson and Worts (1951)
9/24-19F1 (CUY-03)	46745	1310392	2,757	113	>	113	---	Upson and Worts (1951)
9/24-30B2	47458	1309122	2,824	190	>	190	---	Upson and Worts (1951)
9/25-111	43914	1312272	2,635	368	---	328	---	Upson and Worts (1951)
9/26-4J1	30822	1314358	2,587	327	---	38	---	Upson and Worts (1951)
CUY-G-65	40192	1316417	2,421	1,098	---	733	---	CA-DWR
CUY-G-66	36620	1317348	2,340	1,020	---	422	---	CA-DWR
CUY-G-67	35309	1319458	2,281	1,020	---	694	---	CA-DWR

[1]CA-DWR, California Department of Water Resources; Upson and Worts (1951), Upson, J.E., and Worts, G.F., 1951, Ground water in the Cuyama Valley, California: U.S. Geological Survey Water Supply Paper 1110–B, 81 p.

Table A3_2. Textural characteristics for down-hole intervals, oil and gas wells, Cuyama Valley.

[API Number, American Petroleum Institute well number. Qya, younger alluvium; Qoa, older alluvium, QTm, Morales Formation.]

API Number	Interpreted texture	Grain-size class	Top of interval (feet)	Base of interval (feet)	Interval thickness (feet)	Geologic Unit from framework
7900119	fine massive	fine	530	906	376	Qoa
7900119	fine massive	fine	906	1,102	196	QTm
7900119	very fine massive	fine	1,102	1,438	336	QTm
7900119	fine interbedded	fine	1,438	1,475	37	QTm
7900119	very fine interbedded	fine	1,475	1,505	30	QTm
7900119	fine massive	fine	1,505	1,555	50	QTm
7900119	very fine massive	fine	1,555	1,716	161	QTm
7900184	medium massive	coarse	220	318	98	Qya
7900184	coarse massive	coarse	318	340	22	Qya
7900184	medium massive	coarse	340	348	8	Qya
7900184	medium massive	coarse	348	446	98	Qoa
7900184	fine massive	fine	446	825	379	Qoa
7900184	very fine massive	fine	825	910	85	Qoa
7900184	very fine interbedded	fine	910	938	28	Qoa
7900184	very fine interbedded	fine	938	1,717	779	QTm
7900184	very fine massive	fine	1,717	1,999	282	QTm
7900184	very fine interbedded	fine	1,999	2,273	274	QTm
7900184	very fine massive	fine	2,273	2,495	222	QTm
7900184	fine interbedded	fine	2,495	2,690	195	QTm
7900184	very fine interbedded	fine	2,690	2,775	85	QTm
7900184	fine interbedded	fine	2,775	3,075	300	QTm
7900184	fine massive	fine	3,075	3,090	15	QTm
7900184	very fine massive	fine	3,090	3,130	40	QTm
7900185	very fine interbedded	fine	300	570	270	Qoa
7900185	fine massive	fine	570	596	26	Qoa
7900185	very fine interbedded	fine	596	620	24	Qoa
7900185	fine massive	fine	620	641	21	Qoa
7900185	very fine interbedded	fine	641	773	132	Qoa

7900185	fine massive	fine	773	800	27	Qoa
7900185	very fine massive	fine	800	830	30	QTm
7900185	fine interbedded	fine	830	867	37	QTm
7900185	very fine interbedded	fine	867	1,290	423	QTm
7900185	very fine massive	fine	1,290	1,518	228	QTm
7900185	fine massive	fine	1,518	1,562	44	QTm
7900185	very fine massive	fine	1,562	1,595	33	QTm
7900185	fine massive	fine	1,595	1,750	155	QTm
7900185	very fine massive	fine	1,750	1,785	35	QTm
7900189	fine massive	fine	242	634	392	Qoa
7900189	fine interbedded	fine	634	712	78	QTm
7900189	very fine interbedded	fine	712	838	126	QTm
7900189	very fine massive	fine	838	908	70	QTm
7900189	very fine interbedded	fine	908	964	56	QTm
7900189	very fine massive	fine	964	1,037	74	QTm
7900189	very fine interbedded	fine	1,037	1,094	57	QTm
7900189	very fine massive	fine	1,094	1,149	56	QTm
7900189	very fine interbedded	fine	1,149	1,220	71	QTm
7900189	very fine massive	fine	1,220	1,330	110	QTm
7900189	very fine interbedded	fine	1,330	1,385	55	QTm
7900189	fine interbedded	fine	1,385	1,495	110	QTm
7900189	fine massive	fine	1,495	1,502	7	QTm
7900189	very fine massive	fine	1,502	1,515	13	QTm
7900189	medium massive	coarse	1,515	1,540	25	QTm
7900345	fine interbedded	fine	626	775	149	QTm
7900345	very fine interbedded	fine	775	1,220	445	QTm
7900345	very fine massive	fine	1,220	1,240	20	QTm
7900345	very fine interbedded	fine	1,240	1,339	99	QTm
7900345	very fine massive	fine	1,339	1,371	32	QTm
7900345	very fine interbedded	fine	1,371	1,541	170	QTm
7900345	very fine massive	fine	1,541	1,578	37	QTm
7900345	very fine interbedded	fine	1,578	1,648	70	QTm
7900345	fine interbedded	fine	1,648	2,060	412	QTm
7900345	very fine interbedded	fine	2,060	2,273	213	QTm

7900345	very fine massive	fine	2,273	2,347	74	QTm
7900345	very fine interbedded	fine	2,347	2,453	106	QTm
7900345	very fine massive	fine	2,453	2,572	119	QTm
7901038	coarse interbedded	coarse	30	74	44	Qya
7901038	medium interbedded	coarse	74	226	152	Qya
7901038	fine interbedded	fine	519	562	43	Qoa
7901038	medium interbedded	coarse	562	615	53	Qoa
7901038	coarse interbedded	coarse	615	690	75	Qoa
7901038	medium interbedded	coarse	690	720	30	Qoa
7901039	medium interbedded	coarse	226	519	293	Qoa
8300425	coarse interbedded	coarse	372	479	107	Qoa
8300425	coarse massive	coarse	571	600	29	QTm
8300425	medium interbedded	coarse	600	617	17	QTm
8300425	fine interbedded	fine	617	649	32	QTm
8300425	medium massive	coarse	649	662	13	QTm
8300425	fine interbedded	fine	662	712	50	QTm
8300425	medium interbedded	coarse	712	750	38	QTm
8300425	fine interbedded	fine	750	800	50	QTm
8300425	medium interbedded	coarse	800	910	110	QTm
8300425	medium massive	coarse	910	929	19	QTm
8300425	medium interbedded	coarse	929	1,005	76	QTm
8300425	medium massive	coarse	1,005	1,033	28	QTm
8300425	coarse massive	coarse	1,033	1,063	30	QTm
8300425	coarse interbedded	coarse	1,063	1,154	91	QTm
8300425	medium interbedded	coarse	1,154	1,184	30	QTm
8300425	medium massive	coarse	1,184	1,214	30	QTm
8300425	medium interbedded	coarse	1,214	1,325	111	QTm
8300425	coarse interbedded	coarse	1,325	1,380	55	QTm
8300425	medium interbedded	coarse	1,380	1,692	312	QTm
8300425	fine interbedded	fine	1,692	1,926	234	QTm
8300425	medium interbedded	coarse	1,926	1,952	26	QTm
8300425	fine interbedded	fine	1,952	1,991	39	QTm
8300425	medium massive	coarse	1,991	2,032	41	QTm
8300425	medium interbedded	coarse	2,032	2,086	54	QTm

8300425	medium massive	coarse	2,086	2,112	26	QTm
8300425	medium interbedded	coarse	2,112	2,195	83	QTm
8300425	medium massive	coarse	2,195	2,215	20	QTm
8300425	fine interbedded	fine	2,215	2,235	20	QTm
8300425	medium massive	coarse	2,235	2,255	20	QTm
8300426	coarse interbedded	coarse	479	571	92	QTm
8300655	fine interbedded	fine	350	390	40	QTm
8300655	medium interbedded	coarse	390	431	41	QTm
8300655	fine interbedded	fine	431	467	36	QTm
8300655	medium interbedded	coarse	467	500	33	QTm
8300655	fine interbedded	fine	500	588	88	QTm
8300655	fine massive	fine	588	614	26	QTm
8300655	fine interbedded	fine	614	715	101	QTm
8300655	medium interbedded	coarse	715	780	65	QTm
8300655	fine interbedded	fine	780	850	70	QTm
8300655	medium massive	coarse	850	883	33	QTm
8300655	fine interbedded	fine	883	1,072	189	QTm
8300655	fine massive	fine	1,072	1,090	18	QTm
8300655	medium massive	coarse	1,090	1,119	29	QTm
8300655	fine massive	fine	1,119	1,158	39	QTm
8300655	fine interbedded	fine	1,158	1,265	107	QTm
8300655	very fine interbedded	fine	1,265	1,318	53	QTm
8300655	fine interbedded	fine	1,318	1,378	60	QTm
8300655	fine massive	fine	1,378	1,434	56	QTm
8300655	fine interbedded	fine	1,434	1,728	294	QTm
8300655	very fine massive	fine	1,728	1,740	12	QTm
8300655	fine interbedded	fine	1,740	1,793	53	QTm
8300655	very fine interbedded	fine	1,793	1,815	22	QTm
8300655	very fine massive	fine	1,815	1,932	117	QTm
8300655	very fine interbedded	fine	1,932	1,972	40	QTm
8300655	fine interbedded	fine	1,972	2,020	48	QTm
8300655	fine massive	fine	2,020	2,072	52	QTm
8300655	fine interbedded	fine	2,072	2,206	134	QTm
8300655	fine massive	fine	2,206	2,228	22	QTm

8300655	fine interbedded	fine	2,228	2,278	50	QTm
8300788	very fine interbedded	fine	825	998	173	QTm
8300788	fine interbedded	fine	998	1,623	625	QTm
8300788	fine massive	fine	1,623	1,660	37	QTm
8300788	fine interbedded	fine	1,660	2,223	563	QTm
8300788	fine massive	fine	2,223	2,265	42	QTm
8300788	fine interbedded	fine	2,265	2,313	48	QTm
8300788	fine massive	fine	2,313	2,360	47	QTm
8300788	fine interbedded	fine	2,360	2,585	225	QTm
8303037	fine interbedded	fine	200	270	70	Qoa
8303037	medium massive	coarse	270	375	105	Qoa
8303037	fine massive	fine	375	764	389	Qoa
8303037	fine massive	fine	764	815	51	QTm
8303037	fine interbedded	fine	815	1,190	375	QTm
8303037	medium interbedded	coarse	1,190	1,330	140	QTm
8303037	very fine interbedded	fine	1,330	1,420	90	QTm
8303037	very fine massive	fine	1,420	1,580	160	QTm
8303044	medium massive	coarse	250	784	534	Qoa
8303044	medium massive	coarse	784	800	16	QTm
8303044	fine interbedded	fine	800	845	45	QTm
8303044	medium interbedded	coarse	845	910	65	QTm
8303044	fine interbedded	fine	910	1,040	130	QTm
8303044	medium interbedded	coarse	1,040	1,085	45	QTm
8303044	fine interbedded	fine	1,085	1,210	125	QTm
8303044	medium interbedded	coarse	1,210	1,300	90	QTm
8303044	very fine massive	fine	1,300	1,490	190	QTm
8303108	fine massive	fine	78	97	20	Qoa
8303108	very fine interbedded	fine	97	120	23	Qoa
8303108	fine interbedded	fine	120	174	54	Qoa
8303108	very fine massive	fine	174	181	7	Qoa
8303108	fine interbedded	fine	181	191	10	Qoa
8303108	medium interbedded	coarse	191	220	29	Qoa
8303108	fine massive	fine	220	237	17	Qoa
8303108	medium massive	coarse	237	245	8	Qoa

8303108	fine interbedded	fine	245	272	27	Qoa
8303108	medium massive	coarse	272	282	10	Qoa
8303108	fine massive	fine	282	300	18	Qoa
8303108	medium interbedded	coarse	300	338	38	Qoa
8303108	medium massive	coarse	338	349	12	Qoa
8303108	fine interbedded	fine	349	395	46	Qoa
8303108	very fine interbedded	fine	395	470	75	Qoa
8303108	fine massive	fine	470	504	34	Qoa
8303108	very fine interbedded	fine	504	522	18	Qoa
8303108	very fine massive	fine	522	541	19	Qoa
8303108	very fine interbedded	fine	541	582	41	Qoa
8303108	very fine massive	fine	582	600	18	Qoa
8303108	very fine interbedded	fine	600	664	64	Qoa
8303108	fine massive	fine	664	680	16	Qoa
8303108	very fine massive	fine	680	690	10	Qoa
8303108	fine interbedded	fine	690	756	66	Qoa
8303108	fine massive	fine	756	790	34	Qoa
8303108	very fine massive	fine	790	800	10	Qoa
8303108	fine massive	fine	800	810	10	Qoa
8303108	very fine massive	fine	810	820	10	Qoa
8303108	fine massive	fine	820	841	21	Qoa
8303108	very fine massive	fine	841	929	89	Qoa
8303108	fine massive	fine	929	989	60	Qoa
8303120	medium massive	coarse	280	780	500	Qoa
8303120	fine massive	fine	780	840	60	Qoa
8303120	medium massive	coarse	840	875	35	Qoa
8303120	fine massive	fine	875	890	15	Qoa
8303120	medium massive	coarse	890	950	60	Qoa
8303120	fine massive	fine	950	1,161	211	Qoa
8303120	fine massive	fine	1,161	1,250	89	QTm
8303120	medium interbedded	coarse	1,250	1,360	110	QTm
8303120	fine interbedded	fine	1,360	1,440	80	QTm
8303120	coarse massive	coarse	1,440	1,455	15	QTm
8303120	medium interbedded	coarse	1,455	1,505	50	QTm

8303120	fine interbedded	fine	1,505	1,645	140	QTm
8303120	medium interbedded	coarse	1,645	1,662	17	QTm
8303120	fine interbedded	fine	1,662	1,695	33	QTm
8303120	very fine interbedded	fine	1,695	1,770	75	QTm
8303124	fine interbedded	fine	190	298	108	Qoa
8303124	very fine massive	fine	298	640	342	Qoa
8303124	fine massive	fine	640	790	150	Qoa
8303124	very fine interbedded	fine	790	880	90	Qoa
8303124	fine interbedded	fine	880	942	62	Qoa
8303124	fine interbedded	fine	942	1,030	88	QTm
8303124	fine massive	fine	1,030	1,350	320	QTm
8303124	fine interbedded	fine	1,350	1,428	78	QTm
8303124	very fine interbedded	fine	1,428	1,495	67	QTm
8303168	fine interbedded	fine	770	797	27	Qoa
8303168	fine interbedded	fine	797	1,570	773	QTm
8303168	fine massive	fine	1,570	1,675	105	QTm
8303168	very fine massive	fine	1,675	1,695	20	QTm
8303168	fine massive	fine	1,695	1,708	13	QTm
8303168	very fine massive	fine	1,708	1,740	32	QTm
8303168	fine interbedded	fine	1,740	1,765	25	QTm
8303168	fine massive	fine	1,765	1,810	45	QTm
8303168	very fine interbedded	fine	1,810	1,920	110	QTm
8303168	fine massive	fine	1,920	2,020	100	QTm
8303168	very fine massive	fine	2,020	2,035	15	QTm
8303168	fine interbedded	fine	2,035	2,098	63	QTm
8303168	very fine massive	fine	2,098	2,119	21	QTm
8303168	fine massive	fine	2,119	2,170	51	QTm
8303168	fine interbedded	fine	2,170	2,482	312	QTm
8303168	fine massive	fine	2,482	2,519	37	QTm
8303168	fine interbedded	fine	2,519	2,740	221	QTm
8303168	fine massive	fine	2,740	2,792	52	QTm
8303168	fine interbedded	fine	2,792	3,335	543	QTm
8303168	fine massive	fine	3,335	3,460	125	QTm
8303168	fine interbedded	fine	3,460	3,550	90	QTm

8303171	medium interbedded	coarse	365	420	55	Qoa
8303171	coarse interbedded	coarse	420	550	130	Qoa
8303171	medium interbedded	coarse	550	653	103	Qoa
8303171	medium interbedded	coarse	653	845	192	QTm
8303171	fine interbedded	fine	845	1,051	206	QTm
8303171	medium massive	coarse	1,051	1,105	54	QTm
8303171	medium interbedded	coarse	1,105	1,132	27	QTm
8303171	coarse massive	coarse	1,132	1,186	54	QTm
8303171	medium interbedded	coarse	1,186	1,260	74	QTm
8303171	medium massive	coarse	1,260	1,280	20	QTm
8303171	medium interbedded	coarse	1,280	1,328	48	QTm
8303171	coarse massive	coarse	1,328	1,362	34	QTm
8303171	medium interbedded	coarse	1,362	1,420	58	QTm
8303171	coarse massive	coarse	1,420	1,435	15	QTm
8303171	medium interbedded	coarse	1,435	1,453	18	QTm
8303171	coarse massive	coarse	1,453	1,495	42	QTm
8303171	fine interbedded	fine	1,495	1,580	85	QTm
8303171	fine massive	fine	1,580	1,610	30	QTm
8303171	coarse massive	coarse	1,610	1,645	35	QTm
8303171	medium massive	coarse	1,645	1,760	115	QTm
8303171	medium interbedded	coarse	1,760	1,842	82	QTm
8303171	fine interbedded	fine	1,842	1,960	118	QTm
8303171	fine massive	fine	1,960	1,995	35	QTm
8303171	medium massive	coarse	1,995	2,035	40	QTm
8303171	medium interbedded	coarse	2,035	2,121	86	QTm
8303171	fine interbedded	fine	2,121	2,185	64	QTm
8303171	medium interbedded	coarse	2,185	2,270	85	QTm
8303171	fine interbedded	fine	2,270	2,333	63	QTm
8303171	fine massive	fine	2,333	2,475	142	QTm
8303171	very fine massive	fine	2,475	2,570	95	QTm
8303171	fine interbedded	fine	2,570	2,610	40	QTm
8303171	fine massive	fine	2,610	2,670	60	QTm
8303171	very fine massive	fine	2,670	2,690	20	QTm
8303172	medium interbedded	coarse	385	460	75	Qoa

8303172	coarse interbedded	coarse	460	528	68	Qoa
8303172	medium interbedded	coarse	528	623	95	Qoa
8303172	medium interbedded	coarse	623	687	64	QTm
8303172	fine massive	fine	687	767	80	QTm
8303172	medium massive	coarse	767	808	41	QTm
8303172	fine interbedded	fine	808	948	140	QTm
8303172	medium interbedded	coarse	948	1,053	105	QTm
8303172	fine massive	fine	1,053	1,099	46	QTm
8303172	medium interbedded	coarse	1,099	1,265	166	QTm
8303172	fine interbedded	fine	1,265	1,380	115	QTm
8303172	medium interbedded	coarse	1,380	1,550	170	QTm
8303172	fine interbedded	fine	1,550	1,610	60	QTm
8303172	medium interbedded	coarse	1,610	1,750	140	QTm
8303172	fine massive	fine	1,750	1,800	50	QTm
8303172	fine interbedded	fine	1,800	1,850	50	QTm
8303172	fine massive	fine	1,850	1,980	130	QTm
8303172	medium interbedded	coarse	1,980	2,100	120	QTm
8303172	fine interbedded	fine	2,100	2,320	220	QTm
8303172	medium interbedded	coarse	2,320	2,575	255	QTm
8303173	fine interbedded	fine	530	587	57	Qoa
8303173	medium interbedded	coarse	587	621	34	Qoa
8303173	fine interbedded	fine	621	666	45	Qoa
8303173	fine interbedded	fine	666	820	154	QTm
8303173	very fine interbedded	fine	820	1,109	289	QTm
8303173	fine interbedded	fine	1,109	1,275	166	QTm
8303173	very fine interbedded	fine	1,275	1,303	28	QTm
8303173	fine interbedded	fine	1,303	1,493	190	QTm
8303173	fine massive	fine	1,493	1,518	25	QTm
8303173	fine interbedded	fine	1,518	1,649	131	QTm
8303173	fine massive	fine	1,649	1,675	26	QTm
8303173	very fine interbedded	fine	1,675	1,700	25	QTm
8303173	fine interbedded	fine	1,700	1,910	210	QTm
8303173	medium massive	coarse	1,910	2,040	130	QTm
8303173	fine interbedded	fine	2,040	2,130	90	QTm

8303173	very fine massive	fine	2,130	2,225	95	QTm
8303173	fine massive	fine	2,225	2,340	115	QTm
8303173	very fine massive	fine	2,340	2,385	45	QTm
8303267	very fine interbedded	fine	355	882	527	QTm
8303267	very fine massive	fine	882	1,002	120	QTm
8303267	very fine interbedded	fine	1,002	1,085	83	QTm
8303267	fine massive	fine	1,085	1,115	30	QTm
8303267	fine interbedded	fine	1,115	1,139	24	QTm
8303267	fine massive	fine	1,139	1,180	41	QTm
8303267	very fine massive	fine	1,180	1,218	38	QTm
8303267	fine interbedded	fine	1,218	1,329	111	QTm
8303267	very fine interbedded	fine	1,329	1,455	126	QTm
8303267	fine massive	fine	1,455	1,490	35	QTm
8303267	very fine interbedded	fine	1,490	1,607	117	QTm
8303267	fine massive	fine	1,607	1,642	35	QTm
8303267	fine interbedded	fine	1,642	1,660	18	QTm
8303267	fine massive	fine	1,660	1,700	40	QTm
8303267	fine interbedded	fine	1,700	1,956	256	QTm
8303267	very fine massive	fine	1,956	2,259	303	QTm
8303267	fine interbedded	fine	2,259	2,301	42	QTm
8303267	fine massive	fine	2,301	2,367	66	QTm
8303267	very fine massive	fine	2,367	2,420	53	QTm
8303340	very fine interbedded	fine	505	535	30	Qoa
8303340	fine interbedded	fine	535	642	107	Qoa
8303340	fine massive	fine	642	740	98	Qoa
8303340	fine interbedded	fine	740	902	162	Qoa
8303340	very fine interbedded	fine	902	1,075	173	QTm
8303340	fine interbedded	fine	1,075	1,235	160	QTm
8303340	very fine interbedded	fine	1,235	1,285	50	QTm
8303340	fine massive	fine	1,285	1,355	70	QTm
8303340	very fine interbedded	fine	1,355	1,400	45	QTm
8303340	fine interbedded	fine	1,400	1,450	50	QTm
8303340	fine massive	fine	1,450	1,600	150	QTm
8303340	very fine interbedded	fine	1,600	1,860	260	QTm

8303340	fine interbedded	fine	1,860	1,945	85	QTm
8303340	fine massive	fine	1,945	2,220	275	QTm
8303340	very fine massive	fine	2,220	2,280	60	QTm
8303372	fine interbedded	fine	265	281	16	Qoa
8303372	medium interbedded	coarse	281	313	32	Qoa
8303372	fine massive	fine	313	340	27	Qoa
8303372	medium interbedded	coarse	340	384	44	Qoa
8303372	medium interbedded	coarse	384	426	42	QTm
8303372	fine massive	fine	426	448	22	QTm
8303372	medium massive	coarse	448	460	12	QTm
8303372	medium interbedded	coarse	460	580	120	QTm
8303372	fine massive	fine	580	598	18	QTm
8303372	medium interbedded	coarse	598	612	14	QTm
8303372	fine massive	fine	612	661	49	QTm
8303372	medium interbedded	coarse	661	758	97	QTm
8303372	fine interbedded	fine	758	795	37	QTm
8303372	medium interbedded	coarse	795	936	141	QTm
8303372	fine interbedded	fine	936	1,000	64	QTm
8303372	medium interbedded	coarse	1,000	1,031	31	QTm
8303372	fine interbedded	fine	1,031	1,108	77	QTm
8303372	medium interbedded	coarse	1,108	1,214	106	QTm
8303372	fine interbedded	fine	1,214	1,235	21	QTm
8303372	medium massive	coarse	1,235	1,250	15	QTm
8303372	fine interbedded	fine	1,250	1,310	60	QTm
8303372	medium interbedded	coarse	1,310	1,390	80	QTm
8303372	fine interbedded	fine	1,390	1,490	100	QTm
8303372	very fine interbedded	fine	1,490	1,520	30	QTm
8303372	medium interbedded	coarse	1,520	1,559	39	QTm
8303372	fine interbedded	fine	1,559	1,590	31	QTm
8303372	very fine interbedded	fine	1,590	1,676	86	QTm
8303372	medium interbedded	coarse	1,676	1,736	60	QTm
8303372	medium massive	coarse	1,736	1,770	34	QTm
8303372	fine interbedded	fine	1,770	2,000	230	QTm
8303372	fine massive	fine	2,000	2,292	292	QTm

8303372	very fine interbedded	fine	2,292	2,325	33	QTm
8303372	fine interbedded	fine	2,325	2,399	74	QTm
8303372	medium interbedded	coarse	2,399	2,440	41	QTm
8304104	fine massive	fine	240	450	210	QTm
8304104	very fine massive	fine	450	470	20	QTm
8304104	fine interbedded	fine	470	592	122	QTm
8304104	very fine interbedded	fine	592	670	78	QTm
8304104	fine massive	fine	670	689	19	QTm
8304104	very fine massive	fine	689	708	19	QTm
8304104	fine interbedded	fine	708	753	45	QTm
8304104	very fine massive	fine	753	771	18	QTm
8304104	very fine interbedded	fine	771	790	19	QTm
8304104	fine massive	fine	790	809	19	QTm
8304104	very fine interbedded	fine	809	918	109	QTm
8304104	fine massive	fine	918	938	20	QTm
8304104	very fine massive	fine	938	979	41	QTm
8304104	fine interbedded	fine	979	1,088	109	QTm
8304104	very fine massive	fine	1,088	1,120	33	QTm
8304106	fine massive	fine	210	263	53	Qoa
8304106	fine interbedded	fine	263	410	147	Qoa
8304106	fine massive	fine	410	427	17	Qoa
8304106	fine massive	fine	427	452	25	QTm
8304106	very fine massive	fine	452	473	21	QTm
8304106	fine interbedded	fine	473	525	52	QTm
8304106	very fine interbedded	fine	525	566	41	QTm
8304106	very fine massive	fine	566	583	17	QTm
8304106	fine interbedded	fine	583	650	67	QTm
8304106	very fine interbedded	fine	650	989	339	QTm
8304106	very fine massive	fine	989	1,017	28	QTm
8304106	very fine interbedded	fine	1,017	1,276	259	QTm
8304108	fine interbedded	fine	210	335	125	Qoa
8304108	fine interbedded	fine	335	560	225	QTm
8304108	very fine massive	fine	560	590	30	QTm
8304108	fine interbedded	fine	590	620	30	QTm

8304108	very fine massive	fine	620	634	14	QTm
8304108	fine massive	fine	634	712	78	QTm
8304108	very fine massive	fine	712	835	123	QTm
8304108	fine massive	fine	835	870	35	QTm
8304108	very fine massive	fine	870	970	100	QTm
8304108	fine massive	fine	970	1,145	175	QTm
8304108	very fine massive	fine	1,145	1,198	53	QTm
8304108	fine massive	fine	1,198	1,225	27	QTm
8304108	very fine massive	fine	1,225	1,295	70	QTm
8304108	fine massive	fine	1,295	1,325	30	QTm
8304108	very fine massive	fine	1,325	1,395	70	QTm
8304108	fine massive	fine	1,395	1,470	75	QTm
8304108	very fine massive	fine	1,470	1,619	149	QTm
8304108	fine massive	fine	1,619	1,648	29	QTm
8304108	very fine massive	fine	1,648	1,915	267	QTm
8304116	very fine massive	fine	215	354	139	Qoa
8304116	very fine massive	fine	354	1,841	1,486	QTm
8304144	fine massive	fine	395	598	203	Qoa
8304144	very fine massive	fine	598	768	170	Qoa
8304144	very fine massive	fine	768	790	22	QTm
8304144	fine interbedded	fine	790	840	50	QTm
8304144	very fine interbedded	fine	840	969	129	QTm
8304144	very fine massive	fine	969	1,270	301	QTm
8304144	fine massive	fine	1,270	1,325	55	QTm
8304144	very fine interbedded	fine	1,325	1,480	155	QTm
8304144	fine massive	fine	1,480	1,510	30	QTm
8304144	very fine massive	fine	1,510	1,555	45	QTm
8304144	fine interbedded	fine	1,555	1,702	147	QTm
8304144	very fine massive	fine	1,702	1,720	18	QTm
8304144	fine massive	fine	1,720	1,770	50	QTm
8304144	very fine massive	fine	1,770	1,790	20	QTm
8304144	very fine interbedded	fine	1,790	1,855	65	QTm
8304144	fine interbedded	fine	1,855	1,995	140	QTm
8304144	very fine massive	fine	1,995	2,015	20	QTm

8304144	fine massive	fine	2,015	2,025	10	QTm
8304144	very fine massive	fine	2,025	2,045	20	QTm
8304144	fine massive	fine	2,045	2,062	17	QTm
8304144	very fine massive	fine	2,062	2,092	30	QTm
8304144	fine interbedded	fine	2,092	2,138	46	QTm
8304144	very fine massive	fine	2,138	2,309	171	QTm
8304144	fine massive	fine	2,309	2,340	31	QTm
8304144	fine interbedded	fine	2,340	2,390	50	QTm
8304144	very fine massive	fine	2,390	2,450	60	QTm
8304144	fine massive	fine	2,450	2,530	80	QTm
8304144	very fine massive	fine	2,530	2,539	9	QTm
8304144	fine massive	fine	2,539	2,570	31	QTm
8304144	very fine massive	fine	2,570	2,589	19	QTm
8304144	fine massive	fine	2,589	2,663	74	QTm
8304144	fine interbedded	fine	2,663	2,758	95	QTm
8304144	medium interbedded	coarse	2,758	2,828	70	QTm
8304144	fine massive	fine	2,828	2,880	52	QTm
8304145	very fine interbedded	fine	50	130	80	Qoa
8304145	fine interbedded	fine	130	230	100	Qoa
8304145	medium massive	coarse	230	252	22	Qoa
8304145	fine interbedded	fine	252	365	113	Qoa
8304145	very fine massive	fine	365	430	65	Qoa
8304145	fine massive	fine	430	718	288	Qoa
8304145	very fine interbedded	fine	718	845	127	Qoa
8304145	fine massive	fine	845	870	25	Qoa
8304145	very fine massive	fine	870	1,109	239	Qoa
8304145	very fine massive	fine	1,109	1,130	21	QTm
8304145	very fine interbedded	fine	1,130	1,198	68	QTm
8304145	fine massive	fine	1,198	1,225	27	QTm
8304145	very fine massive	fine	1,225	1,250	25	QTm
8304145	fine massive	fine	1,250	1,275	25	QTm
8304145	very fine massive	fine	1,275	1,318	43	QTm
8304145	fine interbedded	fine	1,318	1,508	190	QTm
8304145	very fine interbedded	fine	1,508	2,025	517	QTm

8304145	fine massive	fine	2,025	2,070	45	QTm
8304145	fine interbedded	fine	2,070	2,240	170	QTm
8304145	very fine massive	fine	2,240	2,260	20	QTm
8304145	fine interbedded	fine	2,260	2,352	92	QTm
8304145	medium massive	coarse	2,352	2,440	88	QTm
8304149	medium interbedded	coarse	505	630	125	Qoa
8304149	medium interbedded	coarse	630	1,730	1,100	QTm
8304149	medium massive	coarse	1,730	1,754	24	QTm
8304149	medium interbedded	coarse	1,754	1,881	127	QTm
8304149	medium massive	coarse	1,881	1,902	21	QTm
8304149	medium interbedded	coarse	1,902	2,028	126	QTm
8304149	coarse massive	coarse	2,028	2,046	18	QTm
8304149	coarse interbedded	coarse	2,046	2,070	24	QTm
8304149	coarse massive	coarse	2,070	2,095	25	QTm
8304149	coarse interbedded	coarse	2,095	2,110	15	QTm
8304149	medium interbedded	coarse	2,110	2,957	847	QTm
8304149	coarse interbedded	coarse	2,957	3,002	45	QTm
8304149	medium interbedded	coarse	3,002	3,080	78	QTm
8304149	coarse interbedded	coarse	3,080	3,104	24	QTm
8304149	fine interbedded	fine	3,104	3,133	29	QTm
8304149	medium interbedded	coarse	3,133	3,164	31	QTm
8304149	fine massive	fine	3,164	3,197	33	QTm
8304149	medium interbedded	coarse	3,197	3,248	51	QTm
8304149	coarse interbedded	coarse	3,248	3,275	27	QTm
8304149	fine interbedded	fine	3,275	3,289	14	QTm
8304149	coarse massive	coarse	3,289	3,320	31	QTm
8304149	medium interbedded	coarse	3,320	3,382	62	QTm
8304149	fine interbedded	fine	3,382	3,399	17	QTm
8304149	coarse interbedded	coarse	3,399	3,438	39	QTm
8304149	fine interbedded	fine	3,438	3,633	195	QTm
8304149	medium interbedded	coarse	3,633	3,663	30	QTm
8304149	fine interbedded	fine	3,663	3,693	30	QTm
8304149	coarse interbedded	coarse	3,693	3,732	39	QTm
8304149	fine interbedded	fine	3,732	3,803	71	QTm

8304149	coarse interbedded	coarse	3,803	3,889	86	QTm
8304149	coarse massive	coarse	3,889	3,911	22	QTm
8304149	fine interbedded	fine	3,911	3,945	34	QTm
8304149	coarse interbedded	coarse	3,945	3,990	45	QTm
8304149	fine interbedded	fine	3,990	4,004	14	QTm
8304149	coarse interbedded	coarse	4,004	4,033	29	QTm
8304149	coarse massive	coarse	4,033	4,059	26	QTm
8304149	medium interbedded	coarse	4,059	4,083	24	QTm
8304149	coarse interbedded	coarse	4,083	4,103	20	QTm
8304149	fine interbedded	fine	4,103	4,130	27	QTm
8304149	fine massive	fine	4,130	4,150	20	QTm
8304149	fine interbedded	fine	4,150	4,201	51	QTm
8304149	fine massive	fine	4,201	4,240	39	QTm
8304149	fine interbedded	fine	4,240	4,265	25	QTm
8304149	medium massive	coarse	4,265	4,283	18	QTm
8304149	fine interbedded	fine	4,283	4,327	44	QTm
8304149	medium interbedded	coarse	4,327	4,346	19	QTm
8304149	fine interbedded	fine	4,346	4,380	34	QTm
8304149	medium interbedded	coarse	4,380	4,437	57	QTm
8304149	fine interbedded	fine	4,437	4,480	43	QTm
8304149	medium interbedded	coarse	4,480	4,509	29	QTm
8304149	fine interbedded	fine	4,509	4,544	35	QTm
8304149	medium interbedded	coarse	4,544	4,575	31	QTm
8304149	fine interbedded	fine	4,575	4,600	25	QTm
8304149	medium interbedded	coarse	4,600	4,627	27	QTm
8304149	coarse interbedded	coarse	4,627	4,670	43	QTm
8304155	medium interbedded	coarse	210	468	258	Qoa
8304155	fine massive	fine	468	490	22	Qoa
8304155	medium interbedded	coarse	490	777	287	Qoa
8304155	fine massive	fine	777	800	23	Qoa
8304155	medium interbedded	coarse	800	868	68	Qoa
8304155	fine interbedded	fine	868	888	20	Qoa
8304155	fine massive	fine	888	907	19	QTm
8304155	very fine massive	fine	907	937	30	QTm

8304155	fine interbedded	fine	937	1,020	83	QTm
8304155	very fine interbedded	fine	1,020	1,045	25	QTm
8304155	fine interbedded	fine	1,045	1,179	134	QTm
8304155	very fine massive	fine	1,179	1,203	24	QTm
8304155	fine interbedded	fine	1,203	1,220	17	QTm
8304155	medium interbedded	coarse	1,220	1,249	29	QTm
8304155	very fine massive	fine	1,249	1,259	10	QTm
8304155	medium interbedded	coarse	1,259	1,290	31	QTm
8304155	fine interbedded	fine	1,290	1,309	19	QTm
8304155	very fine massive	fine	1,309	1,320	11	QTm
8304155	fine interbedded	fine	1,320	1,350	30	QTm
8304155	very fine massive	fine	1,350	1,408	58	QTm
8304161	fine interbedded	fine	240	820	580	Qoa
8304161	medium massive	coarse	820	1,005	185	Qoa
8304161	fine interbedded	fine	1,005	1,145	140	Qoa
8304161	fine interbedded	fine	1,145	1,255	110	QTm
8304161	fine massive	fine	1,255	1,490	235	QTm
8304161	fine interbedded	fine	1,490	1,782	292	QTm
8304161	medium massive	coarse	1,782	1,820	38	QTm
8304161	very fine massive	fine	1,820	1,843	23	QTm
8304161	fine interbedded	fine	1,843	2,006	163	QTm
8304161	fine massive	fine	2,006	2,068	62	QTm
8304161	fine interbedded	fine	2,068	2,280	212	QTm
8304161	very fine interbedded	fine	2,280	2,400	120	QTm
8304161	fine interbedded	fine	2,400	2,510	110	QTm
8304161	very fine massive	fine	2,510	2,587	77	QTm
8304161	fine interbedded	fine	2,587	2,615	28	QTm
8304161	fine massive	fine	2,615	2,655	40	QTm
8304161	fine interbedded	fine	2,655	2,802	147	QTm
8304161	medium massive	coarse	2,802	2,859	57	QTm
8304161	very fine massive	fine	2,859	2,910	51	QTm
8304164	fine interbedded	fine	530	535	5	Qoa
8304164	fine massive	fine	535	540	5	Qoa
8304164	fine interbedded	fine	540	595	55	Qoa

8304164	fine massive	fine	595	605	10	Qoa
8304164	fine interbedded	fine	605	620	15	Qoa
8304164	fine massive	fine	620	630	10	Qoa
8304164	fine interbedded	fine	630	748	118	Qoa
8304164	fine interbedded	fine	748	800	52	QTm
8304164	fine massive	fine	800	905	105	QTm
8304164	fine interbedded	fine	905	980	75	QTm
8304164	fine massive	fine	980	1,000	20	QTm
8304164	very fine massive	fine	1,000	1,005	5	QTm
8304164	fine massive	fine	1,005	1,020	15	QTm
8304164	very fine massive	fine	1,020	1,027	7	QTm
8304164	fine massive	fine	1,027	1,035	8	QTm
8304164	very fine massive	fine	1,035	1,045	10	QTm
8304164	fine massive	fine	1,045	1,057	12	QTm
8304164	fine interbedded	fine	1,057	1,205	148	QTm
8304164	fine massive	fine	1,205	1,240	35	QTm
8304164	fine interbedded	fine	1,240	1,285	45	QTm
8304164	fine massive	fine	1,285	1,330	45	QTm
8304164	fine interbedded	fine	1,330	1,390	60	QTm
8304164	fine massive	fine	1,390	1,420	30	QTm
8304164	fine interbedded	fine	1,420	1,480	60	QTm
8304164	fine massive	fine	1,480	1,510	30	QTm
8304164	fine interbedded	fine	1,510	1,550	40	QTm
8304164	very fine massive	fine	1,550	1,575	25	QTm
8304164	fine massive	fine	1,575	1,585	10	QTm
8304164	very fine massive	fine	1,585	1,600	15	QTm
8304164	fine massive	fine	1,600	1,620	20	QTm
8304164	very fine massive	fine	1,620	1,630	10	QTm
8304164	fine interbedded	fine	1,630	1,680	50	QTm
8304164	fine massive	fine	1,680	1,690	10	QTm
8304164	very fine interbedded	fine	1,690	1,720	30	QTm
8304164	fine massive	fine	1,720	1,735	15	QTm
8304164	very fine massive	fine	1,735	1,765	30	QTm
8304164	very fine interbedded	fine	1,765	1,890	125	QTm

8304164	very fine massive	fine	1,890	1,905	15	QTm
8304164	very fine interbedded	fine	1,905	2,235	330	QTm
8304164	fine massive	fine	2,235	2,245	10	QTm
8304164	very fine massive	fine	2,245	2,270	25	QTm
8304164	very fine interbedded	fine	2,270	2,455	185	QTm
8304164	very fine massive	fine	2,455	2,495	40	QTm
8304164	fine massive	fine	2,495	2,505	10	QTm
8304164	very fine massive	fine	2,505	2,510	5	QTm
8304164	fine massive	fine	2,510	2,525	15	QTm
8304164	very fine massive	fine	2,525	2,530	5	QTm
8304164	very fine interbedded	fine	2,530	2,745	215	QTm
8304164	fine massive	fine	2,745	2,755	10	QTm
8304164	very fine massive	fine	2,755	2,820	65	QTm
8304164	fine massive	fine	2,820	2,825	5	QTm
8304164	very fine massive	fine	2,825	2,830	5	QTm
8304164	fine massive	fine	2,830	2,850	20	QTm
8304164	very fine interbedded	fine	2,850	3,150	300	QTm
8304164	very fine massive	fine	3,150	3,260	110	QTm
8304164	very fine interbedded	fine	3,260	3,360	100	QTm
8304164	very fine massive	fine	3,360	3,410	50	QTm
8304164	very fine interbedded	fine	3,410	3,530	120	QTm
8304164	very fine massive	fine	3,530	3,605	75	QTm
8304164	very fine interbedded	fine	3,605	3,630	25	QTm
8304164	very fine massive	fine	3,630	3,685	55	QTm
8304171	very fine interbedded	fine	500	529	29	Qoa
8304171	fine interbedded	fine	529	682	153	Qoa
8304171	fine interbedded	fine	682	780	98	QTm
8304171	fine massive	fine	780	873	93	QTm
8304171	fine interbedded	fine	873	1,033	160	QTm
8304171	medium massive	coarse	1,033	1,102	69	QTm
8304171	fine interbedded	fine	1,102	1,275	173	QTm
8304171	medium massive	coarse	1,275	1,304	29	QTm
8304171	fine interbedded	fine	1,304	1,459	155	QTm
8304171	medium massive	coarse	1,459	1,485	26	QTm

8304171	fine interbedded	fine	1,485	1,635	150	QTm
8304171	very fine interbedded	fine	1,635	1,673	38	QTm
8304171	medium massive	coarse	1,673	1,703	30	QTm
8304171	fine interbedded	fine	1,703	1,735	32	QTm
8304171	medium massive	coarse	1,735	1,755	20	QTm
8304171	fine interbedded	fine	1,755	1,788	33	QTm
8304171	very fine massive	fine	1,788	1,810	22	QTm
8304171	very fine interbedded	fine	1,810	1,850	40	QTm
8304171	fine interbedded	fine	1,850	2,033	183	QTm
8304171	medium massive	coarse	2,033	2,060	27	QTm
8304171	fine interbedded	fine	2,060	2,105	45	QTm
8304171	medium interbedded	coarse	2,105	2,155	50	QTm
8304171	fine interbedded	fine	2,155	2,211	56	QTm
8304171	very fine interbedded	fine	2,211	2,297	86	QTm
8304171	fine interbedded	fine	2,297	2,332	35	QTm
8304171	medium massive	coarse	2,332	2,390	58	QTm
8304171	fine massive	fine	2,390	2,450	60	QTm
8304171	fine interbedded	fine	2,450	2,510	60	QTm
8304171	very fine massive	fine	2,510	2,542	32	QTm
8304171	fine massive	fine	2,542	2,570	28	QTm
8304171	very fine massive	fine	2,570	2,605	35	QTm
8304171	fine massive	fine	2,605	2,620	15	QTm
8304171	very fine massive	fine	2,620	2,738	118	QTm
8304171	medium interbedded	coarse	2,738	2,778	40	QTm
8304171	fine interbedded	fine	2,778	2,900	122	QTm
8304172	medium interbedded	coarse	350	370	20	Qoa
8304172	coarse massive	coarse	370	400	30	Qoa
8304172	medium interbedded	coarse	400	775	375	Qoa
8304172	fine interbedded	fine	775	814	39	Qoa
8304172	fine interbedded	fine	814	964	150	QTm
8304172	medium interbedded	coarse	964	1,035	71	QTm
8304172	fine massive	fine	1,035	1,095	60	QTm
8304172	medium massive	coarse	1,095	1,132	37	QTm
8304172	fine massive	fine	1,132	1,203	71	QTm

8304172	medium interbedded	coarse	1,203	1,258	55	QTm
8304172	fine interbedded	fine	1,258	1,330	72	QTm
8304172	medium massive	coarse	1,330	1,375	45	QTm
8304172	fine interbedded	fine	1,375	1,445	70	QTm
8304172	medium interbedded	coarse	1,445	1,487	42	QTm
8304172	fine massive	fine	1,487	1,520	33	QTm
8304172	medium massive	coarse	1,520	1,548	28	QTm
8304172	fine interbedded	fine	1,548	1,610	62	QTm
8304172	medium interbedded	coarse	1,610	2,081	471	QTm
8304172	fine massive	fine	2,081	2,093	12	QTm
8304172	medium interbedded	coarse	2,093	2,118	25	QTm
8304172	fine massive	fine	2,118	2,133	15	QTm
8304172	medium interbedded	coarse	2,133	2,370	237	QTm
8304172	fine interbedded	fine	2,370	2,440	70	QTm
8304172	medium interbedded	coarse	2,440	2,500	60	QTm
8304172	fine interbedded	fine	2,500	2,709	209	QTm
8304172	medium interbedded	coarse	2,709	2,845	136	QTm
8304173	medium interbedded	coarse	218	254	36	Qoa
8304173	coarse interbedded	coarse	254	290	36	Qoa
8304173	medium interbedded	coarse	290	361	71	Qoa
8304173	coarse interbedded	coarse	361	394	33	Qoa
8304173	medium interbedded	coarse	394	478	84	Qoa
8304173	fine interbedded	fine	478	593	115	Qoa
8304173	medium interbedded	coarse	593	620	27	Qoa
8304173	fine interbedded	fine	620	705	85	QTm
8304173	fine interbedded	fine	705	768	63	QTm
8304173	very fine massive	fine	768	784	16	QTm
8304173	fine interbedded	fine	784	848	64	QTm
8304173	very fine massive	fine	848	863	15	QTm
8304173	medium interbedded	coarse	863	882	19	QTm
8304173	fine interbedded	fine	882	938	56	QTm
8304173	fine massive	fine	938	978	40	QTm
8304173	fine interbedded	fine	978	1,106	128	QTm
8304173	medium interbedded	coarse	1,106	1,142	36	QTm

8304173	fine interbedded	fine	1,142	1,205	63	QTm
8304173	medium interbedded	coarse	1,205	1,550	345	QTm
8304173	fine interbedded	fine	1,309	1,550	241	QTm
8304173	medium interbedded	coarse	1,309	1,372	63	QTm
8304173	medium massive	coarse	1,372	1,387	15	QTm
8304173	fine interbedded	fine	1,387	1,432	45	QTm
8304173	medium massive	coarse	1,432	1,468	36	QTm
8304173	fine interbedded	fine	1,468	1,512	44	QTm
8304173	medium interbedded	coarse	1,512	1,540	28	QTm
8304173	very fine massive	fine	1,540	1,555	15	QTm
8304173	medium massive	coarse	1,555	1,575	20	QTm
8304173	medium interbedded	coarse	1,575	1,614	39	QTm
8304173	fine interbedded	fine	1,614	1,702	88	QTm
8304173	medium massive	coarse	1,702	1,730	28	QTm
8304173	fine interbedded	fine	1,730	1,762	32	QTm
8304173	medium interbedded	coarse	1,762	1,881	119	QTm
8304173	fine interbedded	fine	1,881	2,016	135	QTm
8304173	medium interbedded	coarse	2,016	2,062	46	QTm
8304174	fine interbedded	fine	370	390	20	Qoa
8304174	fine interbedded	fine	390	438	48	Qoa
8304174	medium interbedded	coarse	438	575	137	QTm
8304174	fine interbedded	fine	575	719	144	QTm
8304174	very fine interbedded	fine	719	891	172	QTm
8304174	very fine massive	fine	891	1,222	331	QTm
8304174	fine massive	fine	1,222	1,238	16	QTm
8304174	very fine massive	fine	1,238	1,259	21	QTm
8304174	fine massive	fine	1,259	1,279	20	QTm
8304174	very fine massive	fine	1,279	1,463	184	QTm
8304174	fine massive	fine	1,463	1,545	82	QTm
8304194	very fine massive	fine	20	38	18	Qya
8304194	fine massive	fine	38	58	20	Qya
8304194	medium massive	coarse	58	130	72	Qya
8304196	coarse massive	coarse	90	240	150	Qoa
8304196	medium massive	coarse	240	300	60	Qoa

8304196	fine massive	fine	300	423	123	Qoa
8304196	very fine massive	fine	423	480	57	Qoa
8304196	fine massive	fine	480	530	50	Qoa
8304196	very fine massive	fine	530	548	18	Qoa
8304196	fine interbedded	fine	548	577	29	Qoa
8304196	fine interbedded	fine	577	748	171	QTm
8304196	fine massive	fine	748	805	57	QTm
8304196	very fine interbedded	fine	805	2,293	1,488	QTm
8304201	very fine massive	fine	483	505	22	QTm
8304201	fine massive	fine	505	533	28	QTm
8304201	medium massive	coarse	533	752	219	QTm
8304201	fine interbedded	fine	752	845	93	QTm
8304201	medium massive	coarse	845	935	90	QTm
8304201	fine interbedded	fine	935	1,048	113	QTm
8304201	fine massive	fine	1,048	1,082	34	QTm
8304201	fine interbedded	fine	1,082	1,248	166	QTm
8304201	medium massive	coarse	1,248	1,445	197	QTm
8304201	fine interbedded	fine	1,445	1,482	37	QTm
8304201	medium massive	coarse	1,482	1,505	23	QTm
8304201	very fine interbedded	fine	1,505	1,540	35	QTm
8304201	fine massive	fine	1,540	1,567	27	QTm
8304201	very fine interbedded	fine	1,567	1,600	33	QTm
8304201	fine massive	fine	1,600	1,678	78	QTm
8304201	medium interbedded	coarse	1,678	1,810	132	QTm
8304201	fine interbedded	fine	1,810	1,983	173	QTm
8304201	medium interbedded	coarse	1,983	2,045	62	QTm
8304201	fine massive	fine	2,045	2,183	138	QTm
8304201	fine interbedded	fine	2,183	2,260	77	QTm
8304201	fine massive	fine	2,260	2,326	66	QTm
8304201	fine interbedded	fine	2,326	2,389	63	QTm
8304201	fine massive	fine	2,389	2,410	21	QTm
8304201	fine interbedded	fine	2,410	2,450	40	QTm
8304201	medium interbedded	coarse	2,450	2,490	40	QTm
8304201	medium massive	coarse	2,490	2,520	30	QTm

8304201	medium interbedded	coarse	2,520	2,580	60	QTm
8304201	medium massive	coarse	2,580	2,680	100	QTm
8304201	fine massive	fine	2,680	2,760	80	QTm
8304201	fine interbedded	fine	2,760	2,815	55	QTm
8304208	fine interbedded	fine	340	358	18	Qoa
8304208	fine interbedded	fine	358	950	592	QTm
8304208	very fine massive	fine	950	1,022	72	QTm
8304208	fine interbedded	fine	1,022	1,195	173	QTm
8304208	very fine massive	fine	1,195	1,220	25	QTm
8304208	fine interbedded	fine	1,220	1,595	375	QTm
8304266	medium interbedded	coarse	500	830	330	Qoa
8304266	medium interbedded	coarse	830	904	74	QTm
8304266	fine interbedded	fine	904	1,140	236	QTm
8304266	medium interbedded	coarse	1,140	2,020	880	QTm
8304266	medium massive	coarse	2,020	2,038	18	QTm
8304266	medium interbedded	coarse	2,038	2,375	337	QTm
8304266	fine interbedded	fine	2,375	2,407	32	QTm
8304266	medium interbedded	coarse	2,407	2,430	23	QTm
8304266	medium massive	coarse	2,430	2,463	33	QTm
8304266	fine massive	fine	2,463	2,490	27	QTm
8304266	medium interbedded	coarse	2,490	2,518	28	QTm
8304266	fine massive	fine	2,518	2,540	22	QTm
8304266	medium interbedded	coarse	2,540	2,565	25	QTm
8304266	fine massive	fine	2,565	2,613	48	QTm
8304266	medium massive	coarse	2,613	2,740	127	QTm
8304266	fine massive	fine	2,740	2,760	20	QTm
8304266	medium interbedded	coarse	2,760	3,064	304	QTm
8304266	medium massive	coarse	3,064	3,093	29	QTm
8304266	fine interbedded	fine	3,093	3,140	47	QTm
8304266	medium interbedded	coarse	3,140	3,638	498	QTm
8304266	fine interbedded	fine	3,638	3,752	114	QTm
8304266	medium interbedded	coarse	3,752	3,831	79	QTm
8304266	medium massive	coarse	3,831	3,989	158	QTm
8304266	medium interbedded	coarse	3,989	4,051	62	QTm

8304266	medium massive	coarse	4,051	4,269	218	QTm
8304266	medium interbedded	coarse	4,269	4,280	11	QTm
8304266	coarse interbedded	coarse	4,280	4,412	132	QTm
8304267	very fine interbedded	fine	25	55	30	Qya
8304267	medium interbedded	coarse	55	190	135	Qya
8304267	fine interbedded	fine	190	727	537	Qoa
8304267	very fine interbedded	fine	727	778	51	Qoa
8304267	very fine interbedded	fine	778	1,880	1,102	QTm
8304267	fine interbedded	fine	1,880	2,738	858	QTm
8304267	fine massive	fine	2,738	2,792	54	QTm
8304267	very fine massive	fine	2,792	2,835	43	QTm
8304267	fine interbedded	fine	2,835	3,091	256	QTm
8304267	very fine interbedded	fine	3,091	3,150	59	QTm
8304267	fine interbedded	fine	3,150	3,345	195	QTm
8304267	very fine massive	fine	3,345	3,400	55	QTm
8304267	fine interbedded	fine	3,400	3,715	315	QTm
8304267	very fine massive	fine	3,715	3,745	30	QTm
8304268	very fine interbedded	fine	500	580	80	Qoa
8304268	fine interbedded	fine	580	702	122	Qoa
8304268	fine interbedded	fine	702	1,162	460	QTm
8304268	very fine interbedded	fine	1,162	1,262	100	QTm
8304268	fine interbedded	fine	1,262	1,311	49	QTm
8304268	very fine interbedded	fine	1,311	1,428	117	QTm
8304268	fine interbedded	fine	1,428	1,818	390	QTm
8304268	very fine massive	fine	1,818	1,840	22	QTm
8304268	fine interbedded	fine	1,840	2,145	305	QTm
8304268	very fine massive	fine	2,145	2,177	32	QTm
8304268	fine interbedded	fine	2,177	2,290	113	QTm
8304268	fine massive	fine	2,290	2,338	48	QTm
8304268	fine interbedded	fine	2,338	2,452	114	QTm
8304268	very fine massive	fine	2,452	5,475	3,023	QTm
8304268	fine massive	fine	2,608	5,475	2,867	QTm
8304268	very fine massive	fine	2,608	2,670	62	QTm
8304268	fine massive	fine	2,670	3,330	660	QTm

8304268	fine interbedded	fine	3,330	3,545	215	QTm
8304268	fine massive	fine	3,545	3,577	32	QTm
8304268	fine interbedded	fine	3,577	3,643	66	QTm
8304268	fine massive	fine	3,643	3,675	32	QTm
8304268	fine interbedded	fine	3,675	3,855	180	QTm
8304269	fine interbedded	fine	495	892	397	Qoa
8304269	fine interbedded	fine	892	983	91	QTm
8304269	very fine interbedded	fine	983	2,078	1,095	QTm
8304269	fine interbedded	fine	2,078	2,144	66	QTm
8304269	very fine interbedded	fine	2,144	2,247	103	QTm
8304269	fine interbedded	fine	2,247	2,354	107	QTm
8304269	very fine massive	fine	2,354	2,400	46	QTm
8304269	fine interbedded	fine	2,400	2,640	240	QTm
8304269	very fine interbedded	fine	2,640	3,310	670	QTm
8304269	very fine massive	fine	3,310	3,385	75	QTm
8304269	fine interbedded	fine	3,385	3,745	360	QTm
8304269	very fine interbedded	fine	3,745	3,836	91	QTm
8304269	fine interbedded	fine	3,836	4,288	452	QTm
8304270	fine interbedded	fine	530	827	297	Qoa
8304270	fine interbedded	fine	827	2,715	1,888	QTm
8304270	medium interbedded	coarse	2,715	2,767	52	QTm
8304270	fine interbedded	fine	2,767	2,850	83	QTm
8304270	fine massive	fine	2,850	2,900	50	QTm
8304270	very fine massive	fine	2,900	2,940	40	QTm
8304270	fine interbedded	fine	2,940	3,070	130	QTm
8304270	fine massive	fine	3,070	3,195	125	QTm
8304270	very fine massive	fine	3,195	3,213	18	QTm
8304270	fine massive	fine	3,213	3,335	122	QTm
8304270	very fine massive	fine	3,335	3,350	15	QTm
8304270	fine massive	fine	3,350	3,410	60	QTm
8304270	fine interbedded	fine	3,410	3,450	40	QTm
8304270	fine massive	fine	3,450	3,565	115	QTm
8304270	fine interbedded	fine	3,565	3,663	98	QTm
8304270	medium massive	coarse	3,663	3,715	52	QTm

8304270	fine interbedded	fine	3,715	3,740	25	QTm
8304270	medium interbedded	coarse	3,740	3,772	32	QTm
8304271	very fine interbedded	fine	500	545	45	Qoa
8304271	fine interbedded	fine	545	843	298	Qoa
8304271	fine interbedded	fine	843	1,109	266	QTm
8304271	very fine interbedded	fine	1,109	1,202	93	QTm
8304271	fine interbedded	fine	1,202	1,638	436	QTm
8304271	medium interbedded	coarse	1,638	1,719	81	QTm
8304271	fine interbedded	fine	1,719	1,762	43	QTm
8304271	medium interbedded	coarse	1,762	1,825	63	QTm
8304271	fine interbedded	fine	1,825	2,350	525	QTm
8304271	fine massive	fine	2,350	2,410	60	QTm
8304271	very fine massive	fine	2,410	2,430	20	QTm
8304271	fine massive	fine	2,430	2,493	63	QTm
8304271	fine interbedded	fine	2,493	2,540	47	QTm
8304271	very fine interbedded	fine	2,540	2,590	50	QTm
8304271	fine massive	fine	2,590	2,695	105	QTm
8304271	fine interbedded	fine	2,695	2,730	35	QTm
8304271	fine massive	fine	2,730	2,748	18	QTm
8304271	very fine massive	fine	2,748	2,768	20	QTm
8304271	fine massive	fine	2,768	2,950	182	QTm
8304271	fine interbedded	fine	2,950	3,329	379	QTm
8304271	fine massive	fine	3,329	3,375	46	QTm
8304271	fine interbedded	fine	3,375	3,561	186	QTm
8304271	medium interbedded	coarse	3,561	3,598	37	QTm
8304271	fine interbedded	fine	3,598	3,670	72	QTm
8304271	medium interbedded	coarse	3,670	3,703	33	QTm
8304271	fine interbedded	fine	3,703	3,737	34	QTm
8304271	medium massive	coarse	3,737	3,760	23	QTm
8304271	very fine massive	fine	3,760	3,771	11	QTm
8304271	medium massive	coarse	3,771	3,823	52	QTm
8304272	fine interbedded	fine	527	658	131	Qoa
8304272	very fine massive	fine	658	685	27	Qoa
8304272	fine interbedded	fine	685	719	34	Qoa

8304272	fine interbedded	fine	719	1,267	549	QTm
8304272	very fine interbedded	fine	1,267	1,302	35	QTm
8304272	fine interbedded	fine	1,302	1,889	587	QTm
8304272	medium interbedded	coarse	1,889	1,935	46	QTm
8304272	fine interbedded	fine	1,935	2,513	578	QTm
8304272	fine massive	fine	2,513	2,550	37	QTm
8304272	fine interbedded	fine	2,550	2,573	23	QTm
8304272	very fine massive	fine	2,573	2,605	32	QTm
8304272	fine massive	fine	2,605	2,632	27	QTm
8304272	fine interbedded	fine	2,632	2,676	44	QTm
8304272	fine massive	fine	2,676	2,705	29	QTm
8304272	very fine massive	fine	2,705	2,716	11	QTm
8304272	fine massive	fine	2,716	2,730	14	QTm
8304272	fine interbedded	fine	2,730	2,769	39	QTm
8304272	fine massive	fine	2,769	2,904	135	QTm
8304272	fine interbedded	fine	2,904	2,930	26	QTm
8304272	fine massive	fine	2,930	3,114	184	QTm
8304272	fine interbedded	fine	3,114	3,165	51	QTm
8304272	fine massive	fine	3,165	3,204	39	QTm
8304272	fine interbedded	fine	3,204	3,328	124	QTm
8304272	fine massive	fine	3,328	3,348	20	QTm
8304272	fine interbedded	fine	3,348	3,382	34	QTm
8304272	fine massive	fine	3,382	3,411	29	QTm
8304272	fine interbedded	fine	3,411	3,440	29	QTm
8304272	fine massive	fine	3,440	3,470	30	QTm
8304272	fine interbedded	fine	3,470	3,503	33	QTm
8304272	medium massive	coarse	3,503	3,525	22	QTm
8304272	fine interbedded	fine	3,525	3,542	17	QTm
8304272	medium massive	coarse	3,542	3,556	14	QTm
8304272	fine interbedded	fine	3,556	3,602	46	QTm
8304272	medium interbedded	coarse	3,602	3,639	37	QTm
8304272	fine interbedded	fine	3,639	3,819	180	QTm
8304273	medium massive	coarse	530	635	105	Qoa
8304273	fine massive	fine	635	646	11	Qoa

8304273	fine massive	fine	646	815	169	QTm
8304273	medium massive	coarse	815	928	113	QTm
8304273	fine massive	fine	928	990	62	QTm
8304273	medium massive	coarse	990	1,068	78	QTm
8304273	fine massive	fine	1,068	1,108	40	QTm
8304273	medium massive	coarse	1,108	1,242	134	QTm
8304273	fine massive	fine	1,242	1,315	73	QTm
8304273	medium massive	coarse	1,315	1,432	117	QTm
8304273	fine massive	fine	1,432	1,476	44	QTm
8304273	fine interbedded	fine	1,476	1,620	144	QTm
8304273	fine massive	fine	1,620	1,862	242	QTm
8304273	fine interbedded	fine	1,862	1,939	77	QTm
8304273	fine massive	fine	1,939	2,117	178	QTm
8304273	very fine massive	fine	2,117	2,188	71	QTm
8304273	very fine interbedded	fine	2,188	2,610	422	QTm
8304273	fine massive	fine	2,610	2,688	78	QTm
8304273	fine interbedded	fine	2,688	3,225	537	QTm
8304273	very fine interbedded	fine	3,225	3,482	257	QTm
8304273	fine interbedded	fine	3,482	3,925	443	QTm
8304273	medium interbedded	coarse	3,925	4,073	148	QTm
8304273	fine interbedded	fine	4,073	4,417	344	QTm
8304273	medium interbedded	coarse	4,417	4,545	128	QTm
8304273	fine interbedded	fine	4,545	4,687	142	QTm
8304273	medium interbedded	coarse	4,687	4,785	98	QTm
8304273	fine interbedded	fine	4,785	4,856	71	QTm
8304277	fine interbedded	fine	352	400	48	Qoa
8304277	very fine interbedded	fine	400	481	81	Qoa
8304277	very fine massive	fine	481	540	59	Qoa
8304277	fine massive	fine	540	551	11	Qoa
8304277	very fine interbedded	fine	551	589	38	Qoa
8304277	very fine massive	fine	589	609	20	Qoa
8304277	very fine interbedded	fine	609	721	112	Qoa
8304277	very fine massive	fine	721	749	29	Qoa
8304277	very fine interbedded	fine	749	818	69	Qoa

8304277	very fine massive	fine	818	829	11	Qoa
8304277	very fine interbedded	fine	829	915	86	Qoa
8304277	very fine interbedded	fine	915	957	42	QTm
8304277	very fine massive	fine	957	974	17	QTm
8304277	very fine interbedded	fine	974	1,012	38	QTm
8304277	fine interbedded	fine	1,012	1,030	18	QTm
8304277	very fine massive	fine	1,030	1,063	33	QTm
8304277	fine interbedded	fine	1,063	1,071	8	QTm
8304277	very fine interbedded	fine	1,071	1,083	12	QTm
8304277	very fine massive	fine	1,083	1,110	27	QTm
8304277	very fine interbedded	fine	1,110	1,148	38	QTm
8304277	very fine massive	fine	1,148	1,183	35	QTm
8304277	fine interbedded	fine	1,183	1,243	60	QTm
8304277	very fine massive	fine	1,243	1,293	51	QTm
8304277	very fine interbedded	fine	1,293	1,329	36	QTm
8304277	very fine massive	fine	1,329	1,348	19	QTm
8304277	very fine interbedded	fine	1,348	1,365	17	QTm
8304277	very fine massive	fine	1,365	1,393	28	QTm
8304277	very fine interbedded	fine	1,393	1,480	87	QTm
8304277	fine interbedded	fine	1,480	1,595	115	QTm
8304277	very fine interbedded	fine	1,595	1,638	43	QTm
8304277	fine interbedded	fine	1,638	1,768	130	QTm
8304277	fine massive	fine	1,768	1,840	72	QTm
8304277	very fine massive	fine	1,840	1,859	19	QTm
8304277	very fine interbedded	fine	1,859	1,918	59	QTm
8304277	fine massive	fine	1,918	1,930	12	QTm
8304277	very fine interbedded	fine	1,930	1,952	22	QTm
8304277	very fine massive	fine	1,952	1,966	14	QTm
8304277	fine massive	fine	1,966	2,004	38	QTm
8304277	very fine massive	fine	2,004	2,017	13	QTm
8304277	very fine interbedded	fine	2,017	2,078	61	QTm
8304277	fine massive	fine	2,078	2,106	28	QTm
8304277	very fine massive	fine	2,106	2,210	104	QTm
8304277	very fine interbedded	fine	2,210	2,228	18	QTm

8304277	fine massive	fine	2,228	2,250	22	QTm
8304277	very fine massive	fine	2,250	2,288	38	QTm
8304277	very fine interbedded	fine	2,288	2,300	12	QTm
8304277	very fine massive	fine	2,300	2,360	60	QTm
8304277	very fine interbedded	fine	2,360	2,367	7	QTm
8304277	very fine massive	fine	2,367	2,410	43	QTm
8304277	very fine interbedded	fine	2,410	2,475	65	QTm
8304277	very fine massive	fine	2,475	2,507	32	QTm
8304277	medium massive	coarse	2,507	2,536	29	QTm
8304277	very fine massive	fine	2,536	2,555	20	QTm
8304277	fine interbedded	fine	2,555	2,569	14	QTm
8304277	very fine massive	fine	2,569	2,590	21	QTm
8304277	medium massive	coarse	2,590	2,613	23	QTm
8304277	very fine massive	fine	2,613	2,620	7	QTm
8304278	medium massive	coarse	400	665	265	Qoa
8304278	fine massive	fine	665	960	295	Qoa
8304278	fine interbedded	fine	960	1,129	169	Qoa
8304278	fine interbedded	fine	1,129	1,930	801	QTm
8304278	medium interbedded	coarse	1,930	2,085	155	QTm
8304278	fine interbedded	fine	2,085	2,170	85	QTm
8304278	fine massive	fine	2,170	2,225	55	QTm
8304278	medium massive	coarse	2,225	2,260	35	QTm
8304280	fine interbedded	fine	570	708	138	QTm
8304280	fine massive	fine	708	791	83	QTm
8304280	fine interbedded	fine	791	866	75	QTm
8304280	medium massive	coarse	866	888	22	QTm
8304280	fine massive	fine	888	921	33	QTm
8304280	medium massive	coarse	921	944	23	QTm
8304280	fine massive	fine	944	960	16	QTm
8304280	medium massive	coarse	960	987	27	QTm
8304280	fine interbedded	fine	987	1,213	226	QTm
8304280	very fine massive	fine	1,213	1,242	29	QTm
8304280	fine interbedded	fine	1,242	1,372	130	QTm
8304280	very fine massive	fine	1,372	1,392	20	QTm

8304280	fine interbedded	fine	1,392	1,493	101	QTm
8304280	very fine massive	fine	1,493	1,513	20	QTm
8304280	fine massive	fine	1,513	1,533	20	QTm
8304280	very fine massive	fine	1,533	1,553	21	QTm
8304280	fine interbedded	fine	1,553	1,590	37	QTm
8304354	fine massive	fine	198	660	462	QTm
8304365	very fine massive	fine	315	370	55	Qoa
8304365	fine massive	fine	370	745	375	Qoa
8304365	fine massive	fine	745	1,753	1,008	QTm
8304365	fine interbedded	fine	1,753	1,791	38	QTm
8304365	fine massive	fine	1,791	2,950	1,159	QTm
8304365	very fine massive	fine	2,950	4,444	1,494	QTm
8304365	very fine interbedded	fine	4,444	4,734	290	QTm
8304506	fine interbedded	fine	334	407	73	Qya
8304506	fine interbedded	fine	407	787	381	Qoa
8304506	fine interbedded	fine	787	1,840	1,053	QTm
8304506	medium interbedded	coarse	1,840	1,868	28	QTm
8304506	fine massive	fine	1,868	1,888	20	QTm
8304506	fine interbedded	fine	1,888	1,959	71	QTm
8304506	medium interbedded	coarse	1,959	1,986	27	QTm
8304506	fine interbedded	fine	1,986	2,065	79	QTm
8304506	fine massive	fine	2,065	2,114	49	QTm
8304506	fine interbedded	fine	2,114	2,238	124	QTm
8304506	medium massive	coarse	2,238	2,253	15	QTm
8304506	fine interbedded	fine	2,253	2,327	74	QTm
8304506	fine massive	fine	2,327	2,346	19	QTm
8304506	medium massive	coarse	2,346	2,359	13	QTm
8304506	fine interbedded	fine	2,359	2,370	11	QTm
8304506	medium massive	coarse	2,370	2,387	17	QTm
8304506	fine interbedded	fine	2,387	2,407	20	QTm
8304506	fine massive	fine	2,407	2,420	13	QTm
8304506	medium interbedded	coarse	2,420	2,436	16	QTm
8304506	fine interbedded	fine	2,436	2,532	96	QTm
8304506	fine massive	fine	2,532	2,553	21	QTm

8304506	fine interbedded	fine	2,553	2,643	90	QTm
8304506	fine massive	fine	2,643	2,662	19	QTm
8304506	fine interbedded	fine	2,662	2,681	19	QTm
8304506	fine massive	fine	2,681	2,708	27	QTm
8304506	fine interbedded	fine	2,708	2,738	30	QTm
8304506	fine massive	fine	2,738	2,761	23	QTm
8304506	fine interbedded	fine	2,761	2,790	29	QTm
8304506	fine massive	fine	2,790	2,830	40	QTm
8304506	fine interbedded	fine	2,830	3,305	475	QTm
8304506	fine massive	fine	3,305	3,339	34	QTm
8304506	fine interbedded	fine	3,339	3,390	51	QTm
8304506	fine massive	fine	3,390	3,405	15	QTm
8304506	fine interbedded	fine	3,405	3,441	36	QTm
8304506	fine massive	fine	3,441	3,458	17	QTm
8304506	fine interbedded	fine	3,458	3,481	23	QTm
8304506	fine massive	fine	3,481	3,513	32	QTm
8304506	fine interbedded	fine	3,513	3,532	19	QTm
8304506	fine massive	fine	3,532	3,605	73	QTm
8304506	fine interbedded	fine	3,605	3,851	246	QTm
8304506	fine massive	fine	3,851	3,876	25	QTm
8304506	fine interbedded	fine	3,876	4,168	292	QTm
8304506	fine massive	fine	4,168	4,234	66	QTm
8304506	medium interbedded	coarse	4,234	4,271	37	QTm
8304506	fine interbedded	fine	4,271	4,350	79	QTm
8304506	medium interbedded	coarse	4,350	4,383	33	QTm
8304506	medium massive	coarse	4,383	4,410	27	QTm
8304506	medium interbedded	coarse	4,410	4,468	58	QTm
8304506	fine interbedded	fine	4,468	4,485	17	QTm
8304506	medium interbedded	coarse	4,485	4,518	33	QTm
8304519	fine interbedded	fine	440	719	279	Qoa
8304519	fine interbedded	fine	719	801	83	QTm
8304519	very fine interbedded	fine	801	817	16	QTm
8304519	fine interbedded	fine	817	960	143	QTm
8304519	fine massive	fine	960	978	18	QTm

8304519	very fine interbedded	fine	978	1,298	320	QTm
8304519	fine interbedded	fine	1,298	1,488	190	QTm
8304519	very fine interbedded	fine	1,488	1,675	187	QTm
8304519	fine interbedded	fine	1,675	1,980	305	QTm
8304519	very fine interbedded	fine	1,980	2,028	48	QTm
8304519	fine interbedded	fine	2,028	2,170	142	QTm
8304519	very fine interbedded	fine	2,170	2,396	226	QTm
8304519	fine interbedded	fine	2,396	2,506	110	QTm
8304519	fine massive	fine	2,506	2,530	24	QTm
8304519	fine interbedded	fine	2,530	2,592	62	QTm
8304519	fine massive	fine	2,592	2,648	56	QTm
8304519	very fine massive	fine	2,648	2,662	14	QTm
8304519	fine massive	fine	2,662	2,720	58	QTm
8304519	fine interbedded	fine	2,720	3,030	310	QTm
8304519	very fine massive	fine	3,030	3,060	30	QTm
8304523	very fine interbedded	fine	335	574	239	Qoa
8304523	very fine interbedded	fine	574	2,450	1,876	QTm
8304523	fine interbedded	fine	2,450	2,705	255	QTm
8304523	very fine interbedded	fine	2,705	2,897	192	QTm
8304552	very fine interbedded	fine	535	804	269	Qoa
8304552	very fine interbedded	fine	804	2,580	1,776	QTm
8304552	fine interbedded	fine	2,580	2,595	15	QTm
8304552	very fine interbedded	fine	2,595	2,660	65	QTm
8304552	fine interbedded	fine	2,660	2,698	38	QTm
8304552	very fine interbedded	fine	2,698	2,830	132	QTm
8304552	very fine massive	fine	2,830	2,864	34	QTm
8304552	very fine interbedded	fine	2,864	3,027	163	QTm
8304552	very fine massive	fine	3,027	3,098	71	QTm
8304552	very fine interbedded	fine	3,098	3,415	317	QTm
8304552	very fine massive	fine	3,415	3,509	94	QTm
8304552	very fine interbedded	fine	3,509	4,255	746	QTm
8304552	very fine massive	fine	4,255	4,355	100	QTm
8304552	very fine interbedded	fine	4,355	4,433	77	QTm
8320687	medium interbedded	coarse	830	898	68	QTm

8320687	coarse interbedded	coarse	898	931	33	QTm
8320687	medium interbedded	coarse	931	1,145	214	QTm
8320687	medium massive	coarse	1,145	1,189	44	QTm
8320687	medium interbedded	coarse	1,189	1,212	23	QTm
8320687	medium massive	coarse	1,212	1,230	18	QTm
8320687	medium interbedded	coarse	1,230	2,036	806	QTm
8320687	medium massive	coarse	2,036	2,055	19	QTm
8320687	medium interbedded	coarse	2,055	2,108	53	QTm
8320687	medium massive	coarse	2,108	2,132	24	QTm
8320687	medium interbedded	coarse	2,132	2,208	76	QTm
8320687	medium massive	coarse	2,208	2,318	110	QTm
8320687	medium interbedded	coarse	2,318	2,550	232	QTm
8320687	coarse interbedded	coarse	2,550	2,595	45	QTm
8320687	medium interbedded	coarse	2,595	2,743	148	QTm
8320687	medium massive	coarse	2,743	2,790	47	QTm
8320687	medium interbedded	coarse	2,790	2,840	50	QTm
8320687	medium massive	coarse	2,840	2,978	138	QTm
8320687	medium interbedded	coarse	2,978	3,141	163	QTm
8320687	medium massive	coarse	3,141	3,199	58	QTm
8320908	very fine interbedded	fine	835	1,061	226	QTm
8320908	fine interbedded	fine	1,061	2,162	1,101	QTm
8320908	fine massive	fine	2,162	2,211	49	QTm
8320908	very fine interbedded	fine	2,211	2,222	11	QTm
8320908	fine interbedded	fine	2,222	2,314	92	QTm
8320908	fine massive	fine	2,314	2,360	46	QTm
8320908	fine interbedded	fine	2,360	2,905	545	QTm
8320908	very fine massive	fine	2,905	2,920	15	QTm
8320908	fine interbedded	fine	2,920	2,973	53	QTm
8320908	fine massive	fine	2,973	3,025	52	QTm
8320908	fine interbedded	fine	3,025	3,118	93	QTm
8320908	very fine interbedded	fine	3,118	3,134	16	QTm
8320908	fine massive	fine	3,134	3,156	22	QTm
8320908	fine interbedded	fine	3,148	3,208	60	QTm
8320908	very fine massive	fine	3,148	3,156	8	QTm

8320908	fine massive	fine	3,208	3,260	52	QTm
8320908	fine interbedded	fine	3,260	3,404	144	QTm
8320908	fine massive	fine	3,404	3,434	30	QTm
8320908	fine interbedded	fine	3,434	3,540	106	QTm
8321118	very fine interbedded	fine	620	710	90	Qoa
8321118	fine interbedded	fine	710	930	220	Qoa
8321118	very fine interbedded	fine	930	978	48	Qoa
8321118	fine interbedded	fine	978	1,065	87	Qoa
8321118	very fine interbedded	fine	1,065	1,120	55	QTm
8321118	fine interbedded	fine	1,120	1,358	238	QTm
8321118	very fine massive	fine	1,358	1,445	87	QTm
8321118	fine massive	fine	1,445	1,470	25	QTm
8321118	very fine massive	fine	1,470	1,528	58	QTm
8321118	fine interbedded	fine	1,528	1,600	72	QTm
8321118	very fine massive	fine	1,600	1,710	110	QTm
8321118	fine massive	fine	1,710	1,730	20	QTm
8321118	very fine massive	fine	1,730	1,755	25	QTm
8321118	fine massive	fine	1,755	1,785	30	QTm
8321118	very fine massive	fine	1,785	1,810	25	QTm
8321118	fine massive	fine	1,810	1,865	55	QTm
8321118	very fine massive	fine	1,865	1,900	35	QTm
8321118	fine interbedded	fine	1,900	2,035	135	QTm
8321118	fine massive	fine	2,035	2,095	60	QTm
8321118	very fine massive	fine	2,095	2,129	34	QTm
8321608	very fine interbedded	fine	834	1,066	232	QTm
8321608	fine interbedded	fine	1,066	2,830	1,764	QTm
8321608	very fine interbedded	fine	2,830	2,876	46	QTm
8321608	fine interbedded	fine	2,876	2,903	27	QTm
8321608	very fine massive	fine	2,903	2,920	17	QTm
8321608	fine interbedded	fine	2,920	2,935	15	QTm
8321608	very fine massive	fine	2,935	2,946	11	QTm
8321608	fine interbedded	fine	2,946	2,975	29	QTm
8321608	fine massive	fine	2,975	3,025	50	QTm
8321608	fine interbedded	fine	3,025	3,118	93	QTm

8321608	very fine interbedded	fine	3,118	3,135	17	QTm
8321608	fine massive	fine	3,135	3,157	22	QTm
8321608	very fine massive	fine	3,157	3,183	26	QTm
8321608	fine interbedded	fine	3,183	3,208	25	QTm
8321608	fine massive	fine	3,208	3,260	52	QTm
8321608	fine interbedded	fine	3,260	3,405	145	QTm
8321608	fine massive	fine	3,405	3,435	30	QTm
8321608	fine interbedded	fine	3,435	3,535	100	QTm
8321608	fine massive	fine	3,535	3,603	67	QTm
8321657	medium interbedded	coarse	645	1,368	723	QTm
8321657	medium massive	coarse	1,368	1,470	102	QTm
8321657	medium interbedded	coarse	1,470	1,985	515	QTm
8321657	medium massive	coarse	1,985	2,150	165	QTm
8321657	medium interbedded	coarse	2,150	2,430	280	QTm
8321657	medium massive	coarse	2,430	2,472	42	QTm
8321997	very fine massive	fine	1,335	2,100	765	QTm
8321997	very fine interbedded	fine	2,100	2,262	162	QTm
8321997	fine massive	fine	2,262	2,278	16	QTm
8321997	very fine interbedded	fine	2,278	2,448	170	QTm
8321997	very fine massive	fine	2,448	3,030	582	QTm
8321997	fine massive	fine	3,030	3,145	115	QTm
8321997	very fine massive	fine	3,145	4,460	1,315	QTm
8321997	fine massive	fine	4,460	4,564	104	QTm
8322237	medium interbedded	coarse	1,500	1,525	25	QTm
8322237	fine interbedded	fine	1,525	2,555	1,030	QTm
8322237	very fine interbedded	fine	2,555	2,608	53	QTm
8322237	fine interbedded	fine	2,608	2,858	250	QTm
11106166	fine interbedded	fine	257	738	481	QTm
11106166	very fine interbedded	fine	738	823	85	QTm
11106167	fine interbedded	fine	309	332	23	QTm
11106167	medium interbedded	coarse	332	517	185	QTm
11106167	fine interbedded	fine	517	700	183	QTm
11106167	medium interbedded	coarse	700	845	145	QTm
11106167	fine interbedded	fine	845	1,515	670	QTm

11106167	medium interbedded	coarse	1,515	1,545	30	QTm
11106167	medium massive	coarse	1,545	1,570	25	QTm
11106167	medium interbedded	coarse	1,570	1,637	67	QTm

Table A4_2. Textural characteristics for down-hole intervals, water wells, Cuyama Valley.

[---, confidential record, driller's lithologic description not shown. Qya, younger alluvium; Qoa, older alluvium; QTm, Morales Formation; nd, formation not determined.]

Well Identifier	Top of interval (feet)	Base of interval (feet)	Interval thickness (feet)	Lithologic description	Grain-size class	Sorting	Geologic Unit from framework
CUY-G-01	0	20	20	---	coarse	unsorted	Qya
CUY-G-01	20	40	20	---	coarse	unsorted	Qya
CUY-G-01	40	70	30	---	coarse	unsorted	Qya
CUY-G-01	70	100	30	---	coarse	sorted	Qya
CUY-G-01	100	130	30	---	coarse	sorted	Qya
CUY-G-01	130	150	20	---	coarse	sorted	Qya
CUY-G-01	150	180	30	---	coarse	sorted	Qya
CUY-G-01	180	211	31	---	coarse	unsorted	Qya
CUY-G-01	211	241	30	---	coarse	unsorted	Qya
CUY-G-01	241	270	29	---	coarse	unsorted	Qya
CUY-G-01	270	290	20	---	coarse	sorted	Qya
CUY-G-01	290	364	74	---	coarse	unsorted	Qoa
CUY-G-01	364	450	86	---	coarse	unsorted	Qoa
CUY-G-01	450	581	131	---	fine	unsorted	QTm
CUY-G-01	581	629	48	---	fine	unsorted	QTm
CUY-G-01	629	635	6	---	fine	unsorted	QTm
CUY-G-01	635	670	35	---	fine	unsorted	QTm
CUY-G-01	670	690	20	---	fine	unsorted	QTm
CUY-G-01	690	800	110	---	coarse	unsorted	QTm
CUY-G-02	0	30	30	---	fine	sorted	Qya
CUY-G-02	30	60	30	---	coarse	sorted	Qya
CUY-G-02	60	120	60	---	coarse	unsorted	Qya
CUY-G-02	120	150	30	---	coarse	unsorted	Qya
CUY-G-02	150	210	60	---	coarse	unsorted	Qya
CUY-G-02	210	270	60	---	coarse	unsorted	Qya
CUY-G-02	270	330	60	---	coarse	sorted	Qya
CUY-G-02	330	371	41	---	coarse	unsorted	Qoa

CUY-G-02	371	390	19	---	coarse	unsorted	Qoa
CUY-G-02	390	420	30	---	fine	unsorted	Qoa
CUY-G-02	420	568	148	---	coarse	unsorted	QTm
CUY-G-02	568	610	42	---	coarse	unsorted	QTm
CUY-G-02	610	635	25	---	fine	unsorted	QTm
CUY-G-02	635	720	85	---	coarse	sorted	QTm
CUY-G-02	720	810	90	---	coarse	unsorted	QTm
CUY-G-03	0	180	180	---	coarse	unsorted	Qya
CUY-G-03	180	269	89	---	coarse	unsorted	Qya
CUY-G-03	269	302	33	---	coarse	unsorted	Qoa
CUY-G-03	302	360	58	---	coarse	unsorted	QTm
CUY-G-03	360	430	70	---	fine	unsorted	QTm
CUY-G-03	430	460	30	---	fine	unsorted	QTm
CUY-G-03	460	650	190	---	fine	unsorted	QTm
CUY-G-03	650	700	50	---	fine	unsorted	QTm
CUY-G-04	0	3	3	---	coarse	sorted	Qoa
CUY-G-04	3	8	5	---	coarse	sorted	Qoa
CUY-G-04	8	30	22	---	coarse	sorted	Qoa
CUY-G-04	30	38	8	---	coarse	sorted	Qoa
CUY-G-04	38	40	2	---	coarse	sorted	Qoa
CUY-G-04	40	90	50	---	coarse	sorted	Qoa
CUY-G-04	90	100	10	---	coarse	sorted	Qoa
CUY-G-04	100	120	20	---	coarse	unsorted	Qoa
CUY-G-04	120	145	25	---	fine	unsorted	Qoa
CUY-G-04	145	200	55	---	coarse	sorted	Qoa
CUY-G-04	200	205	5	---	fine	unsorted	Qoa
CUY-G-04	205	320	115	---	coarse	sorted	Qoa
CUY-G-04	320	334	14	---	fine	sorted	Qoa
CUY-G-04	334	500	166	---	fine	unsorted	Qoa
CUY-G-05	0	3	3	---	coarse	sorted	Qya
CUY-G-05	3	5	2	---	fine	sorted	Qya
CUY-G-05	5	40	35	---	coarse	unsorted	Qya
CUY-G-05	40	70	30	---	fine	unsorted	Qya
CUY-G-05	70	80	10	---	coarse	unsorted	Qya

CUY-G-05	80	85	5	---	fine	unsorted	Qya
CUY-G-05	85	87	2	---	coarse	sorted	Qya
CUY-G-05	87	95	8	---	fine	sorted	Qya
CUY-G-05	95	110	15	---	coarse	sorted	Qya
CUY-G-05	110	135	25	---	coarse	unsorted	Qya
CUY-G-05	135	160	25	---	fine	unsorted	Qya
CUY-G-05	160	180	20	---	coarse	unsorted	Qya
CUY-G-05	180	195	15	---	fine	unsorted	Qya
CUY-G-05	195	300	105	---	coarse	unsorted	Qya
CUY-G-06	0	50	50	---	fine	unsorted	Qya
CUY-G-06	50	60	10	---	coarse	sorted	Qya
CUY-G-06	60	70	10	---	fine	unsorted	Qya
CUY-G-06	70	100	30	---	coarse	unsorted	Qya
CUY-G-06	100	130	30	---	coarse	unsorted	Qya
CUY-G-06	130	160	30	---	fine	sorted	Qya
CUY-G-06	160	180	20	---	coarse	unsorted	Qya
CUY-G-06	180	200	20	---	fine	sorted	Qya
CUY-G-06	200	220	20	---	coarse	unsorted	Qya
CUY-G-06	220	280	60	---	fine	sorted	Qya
CUY-G-06	280	300	20	---	fine	unsorted	Qya
CUY-G-06	300	310	10	---	fine	sorted	Qya
CUY-G-06	310	330	20	---	fine	unsorted	Qya
CUY-G-06	330	340	10	---	coarse	unsorted	Qya
CUY-G-06	340	350	10	---	fine	unsorted	Qya
CUY-G-06	350	360	10	---	coarse	unsorted	Qya
CUY-G-06	360	380	20	---	coarse	unsorted	Qya
CUY-G-06	380	390	10	---	fine	sorted	Qya
CUY-G-06	390	410	20	---	fine	unsorted	Qya
CUY-G-06	410	420	10	---	coarse	unsorted	Qya
CUY-G-06	420	430	10	---	fine	sorted	Qya
CUY-G-06	430	450	20	---	coarse	unsorted	Qya
CUY-G-06	450	460	10	---	coarse	unsorted	Qya
CUY-G-06	460	490	30	---	coarse	unsorted	Qya
CUY-G-06	490	510	20	---	coarse	unsorted	Qya

CUY-G-06	510	520	10	---	coarse	sorted	Qya
CUY-G-06	520	530	10	---	coarse	unsorted	Qya
CUY-G-06	530	540	10	---	coarse	unsorted	Qya
CUY-G-06	540	570	30	---	fine	sorted	Qya
CUY-G-06	570	610	40	---	coarse	unsorted	Qoa
CUY-G-06	610	640	30	---	fine	sorted	Qoa
CUY-G-06	640	700	60	---	fine	unsorted	Qoa
CUY-G-06	700	750	50	---	fine	sorted	Qoa
CUY-G-06	750	760	10	---	fine	sorted	Qoa
CUY-G-06	760	770	10	---	fine	sorted	Qoa
CUY-G-06	770	800	30	---	fine	unsorted	Qoa
CUY-G-06	800	810	10	---	fine	sorted	Qoa
CUY-G-06	810	855	45	---	fine	unsorted	Qoa
CUY-G-06	855	875	20	---	fine	unsorted	Qoa
CUY-G-06	875	955	80	---	coarse	unsorted	Qoa
CUY-G-06	955	965	10	---	fine	sorted	Qoa
CUY-G-06	965	970	5	---	coarse	unsorted	Qoa
CUY-G-06	970	980	10	---	fine	sorted	Qoa
CUY-02	0	50	50	---	nd	nd	Qya
CUY-02	50	177	127	---	fine	unsorted	Qya
CUY-02	177	253	76	---	fine	unsorted	Qoa
CUY-02	253	266	13	---	coarse	unsorted	Qoa
CUY-02	266	334	68	---	fine	sorted	Qoa
CUY-02	334	360	26	---	coarse	unsorted	Qoa
CUY-02	360	380	20	---	fine	unsorted	Qoa
CUY-02	380	410	30	---	fine	sorted	Qoa
CUY-02	410	490	80	---	coarse	unsorted	Qoa
CUY-02	490	563	73	---	fine	sorted	Qoa
CUY-02	563	633	70	---	coarse	unsorted	Qoa
CUY-02	633	669	36	---	fine	sorted	Qoa
CUY-02	669	702	33	---	fine	unsorted	QTm
CUY-02	702	723	21	---	coarse	unsorted	QTm
CUY-02	723	747	24	---	fine	sorted	QTm
CUY-02	747	765	18	---	coarse	unsorted	QTm

CUY-02	765	820	55	---	fine	unsorted	QTm
CUY-01	0	6	6	---	fine	unsorted	Qya
CUY-01	6	33	27	---	fine	sorted	Qya
CUY-01	33	37	4	---	coarse	sorted	Qya
CUY-01	37	47	10	---	fine	sorted	Qya
CUY-01	47	53	6	---	coarse	unsorted	Qya
CUY-01	53	65	12	---	coarse	unsorted	Qya
CUY-01	65	87	22	---	fine	sorted	Qya
CUY-01	87	88	1	---	coarse	sorted	Qya
CUY-01	88	121	33	---	fine	sorted	Qya
CUY-01	121	122	1	---	coarse	sorted	Qya
CUY-01	122	131	9	---	fine	sorted	Qya
CUY-01	131	164	33	---	fine	sorted	Qoa
CUY-01	164	179	15	---	fine	sorted	Qoa
CUY-01	179	188	9	---	fine	sorted	Qoa
CUY-G-07	0	42	42	---	fine	sorted	Qya
CUY-G-07	42	80	38	---	coarse	unsorted	Qya
CUY-G-07	80	85	5	---	fine	sorted	Qya
CUY-G-07	85	95	10	---	fine	sorted	Qya
CUY-G-07	95	103	8	---	coarse	unsorted	Qya
CUY-G-07	103	112	9	---	fine	sorted	Qya
CUY-G-07	112	118	6	---	coarse	unsorted	Qya
CUY-G-07	118	128	10	---	fine	sorted	Qya
CUY-G-07	128	135	7	---	fine	sorted	Qoa
CUY-G-07	135	155	20	---	coarse	unsorted	Qoa
CUY-G-08	0	11	11	---	fine	sorted	Qya
CUY-G-08	11	73	62	---	coarse	sorted	Qya
CUY-G-08	73	79	6	---	coarse	sorted	Qya
CUY-G-08	79	83	4	---	coarse	sorted	Qya
CUY-G-08	83	96	13	---	coarse	sorted	Qya
CUY-G-08	96	101	5	---	coarse	sorted	Qya
CUY-G-08	101	109	8	---	coarse	sorted	Qya
CUY-G-08	109	111	2	---	coarse	sorted	Qya
CUY-G-08	111	122	11	---	coarse	sorted	Qya

CUY-G-08	122	130	8	---	fine	sorted	Qya
CUY-G-09	0	37	37	---	fine	unsorted	Qya
CUY-G-09	37	44	7	---	fine	unsorted	Qya
CUY-G-09	44	51	7	---	fine	sorted	Qya
CUY-G-09	51	140	89	---	coarse	unsorted	Qya
CUY-G-09	140	160	20	---	fine	unsorted	Qya
CUY-G-09	160	168	8	---	coarse	unsorted	Qya
CUY-G-09	168	173	5	---	coarse	unsorted	Qya
CUY-G-09	173	196	23	---	coarse	unsorted	Qya
CUY-G-09	196	209	13	---	coarse	unsorted	Qya
CUY-G-09	209	221	12	---	coarse	unsorted	Qya
CUY-G-09	221	238	17	---	coarse	unsorted	Qya
CUY-G-09	238	249	11	---	coarse	unsorted	Qya
CUY-G-09	249	263	14	---	coarse	unsorted	Qya
CUY-G-09	263	278	15	---	fine	unsorted	Qya
CUY-G-09	278	288	10	---	coarse	unsorted	Qya
CUY-G-09	288	300	12	---	fine	sorted	Qya
CUY-G-10	0	4	4	---	fine	sorted	Qya
CUY-G-10	4	20	16	---	fine	sorted	Qya
CUY-G-10	20	50	30	---	fine	sorted	Qya
CUY-G-10	50	58	8	---	fine	sorted	Qya
CUY-G-10	58	88	30	---	fine	sorted	Qya
CUY-G-10	88	115	27	---	coarse	sorted	Qya
CUY-G-10	115	120	5	---	fine	sorted	Qya
CUY-G-10	120	140	20	---	fine	sorted	Qya
CUY-G-10	140	144	4	---	coarse	sorted	Qya
CUY-G-10	144	164	20	---	fine	sorted	Qya
CUY-G-10	164	168	4	---	coarse	sorted	Qya
CUY-G-10	168	180	12	---	fine	unsorted	Qya
CUY-G-10	180	204	24	---	coarse	sorted	Qya
CUY-G-10	204	222	18	---	fine	sorted	Qya
CUY-G-10	222	226	4	---	fine	sorted	Qya
CUY-G-10	226	234	8	---	fine	sorted	Qya
CUY-G-10	234	240	6	---	fine	sorted	Qoa

CUY-G-10	240	266	26	---	coarse	unsorted	Qoa
CUY-G-10	266	274	8	---	fine	unsorted	Qoa
CUY-G-10	274	348	74	---	coarse	sorted	Qoa
CUY-16	0	50	50	---	fine	unsorted	Qoa
CUY-16	50	82	32	---	fine	sorted	Qoa
CUY-16	82	91	9	---	coarse	unsorted	Qoa
CUY-16	91	105	14	---	coarse	unsorted	Qoa
CUY-16	105	116	11	---	fine	unsorted	Qoa
CUY-16	116	118	2	---	coarse	unsorted	Qoa
CUY-16	118	124	6	---	fine	unsorted	Qoa
CUY-16	124	137	13	---	fine	unsorted	Qoa
CUY-16	137	139	2	---	coarse	unsorted	Qoa
CUY-16	139	147	8	---	fine	unsorted	Qoa
CUY-16	147	153	6	---	fine	unsorted	Qoa
CUY-16	153	162	9	---	coarse	unsorted	Qoa
CUY-16	162	176	14	---	fine	unsorted	Qoa
CUY-16	176	181	5	---	fine	unsorted	Qoa
CUY-16	181	195	14	---	fine	sorted	Qoa
CUY-16	195	211	16	---	fine	unsorted	Qoa
CUY-16	211	223	12	---	fine	sorted	Qoa
CUY-16	223	229	6	---	fine	sorted	Qoa
CUY-16	229	235	6	---	coarse	unsorted	Qoa
CUY-16	235	256	21	---	fine	sorted	Qoa
CUY-16	256	273	17	---	fine	sorted	Qoa
CUY-16	273	281	8	---	fine	unsorted	Qoa
CUY-16	281	302	21	---	fine	unsorted	Qoa
CUY-16	302	356	54	---	fine	sorted	Qoa
CUY-16	356	402	46	---	fine	sorted	Qoa
CUY-16	402	406	4	---	coarse	unsorted	Qoa
CUY-16	406	525	119	---	fine	sorted	Qoa
CUY-16	525	532	7	---	fine	unsorted	Qoa
CUY-16	532	563	31	---	fine	sorted	Qoa
CUY-16	563	572	9	---	fine	unsorted	Qoa
CUY-16	572	665	93	---	fine	sorted	Qoa

CUY-16	665	700	35	---	fine	sorted	Qoa
CUY-16	700	761	61	---	fine	sorted	QTm
CUY-16	761	764	3	---	fine	sorted	QTm
CUY-16	764	776	12	---	fine	sorted	QTm
CUY-16	776	824	48	---	fine	unsorted	QTm
CUY-16	824	935	111	---	fine	sorted	QTm
CUY-16	935	941	6	---	fine	sorted	QTm
CUY-16	941	1,021	80	---	fine	sorted	QTm
CUY-G-11	0	125	125	---	coarse	unsorted	Qoa
CUY-G-11	125	170	45	---	coarse	unsorted	Qoa
CUY-G-11	170	200	30	---	fine	unsorted	Qoa
CUY-G-11	200	226	26	---	coarse	sorted	Qoa
CUY-G-11	226	260	34	---	coarse	unsorted	Qoa
CUY-G-11	260	315	55	---	coarse	sorted	Qoa
CUY-G-11	315	460	145	---	coarse	sorted	Qoa
CUY-G-11	460	480	20	---	coarse	unsorted	Qoa
CUY-G-11	480	510	30	---	coarse	sorted	Qoa
CUY-G-11	510	570	60	---	coarse	unsorted	Qoa
CUY-G-11	570	630	60	---	coarse	sorted	Qoa
CUY-G-11	630	656	26	---	coarse	sorted	Qoa
CUY-G-11	656	775	119	---	coarse	sorted	QTm
CUY-G-11	775	810	35	---	fine	sorted	QTm
CUY-G-11	810	890	80	---	coarse	unsorted	QTm
CUY-G-11	890	913	23	---	coarse	unsorted	QTm
CUY-G-68	0	10	10	---	coarse	unsorted	Qoa
CUY-G-68	10	30	20	---	coarse	unsorted	Qoa
CUY-G-68	30	110	80	---	fine	unsorted	Qoa
CUY-G-68	110	160	50	---	fine	unsorted	Qoa
CUY-G-68	160	220	60	---	fine	unsorted	Qoa
CUY-G-68	220	250	30	---	coarse	unsorted	Qoa
CUY-G-68	250	270	20	---	coarse	unsorted	Qoa
CUY-G-68	270	360	90	---	fine	unsorted	Qoa
CUY-G-68	360	380	20	---	fine	sorted	Qoa
CUY-G-68	380	420	40	---	fine	unsorted	Qoa

CUY-G-68	420	440	20	---	fine	unsorted	QTm
CUY-G-68	440	480	40	---	coarse	unsorted	QTm
CUY-G-68	480	535	55	---	fine	unsorted	QTm
CUY-G-68	535	560	25	---	fine	sorted	QTm
CUY-G-68	560	620	60	---	coarse	sorted	QTm
CUY-G-68	620	700	80	---	fine	unsorted	QTm
CUY-G-12	0	2	2	---	fine	unsorted	Qya
CUY-G-12	2	20	18	---	fine	unsorted	Qya
CUY-G-12	20	30	10	---	coarse	unsorted	Qya
CUY-G-12	30	40	10	---	coarse	unsorted	Qya
CUY-G-12	40	55	15	---	fine	unsorted	Qya
CUY-G-12	55	80	25	---	coarse	unsorted	Qya
CUY-G-12	80	114	34	---	fine	unsorted	Qya
CUY-G-12	114	140	26	---	coarse	unsorted	Qya
CUY-G-12	140	180	40	---	fine	sorted	Qya
CUY-G-12	180	183	3	---	coarse	unsorted	Qya
CUY-G-12	183	275	92	---	fine	unsorted	Qya
CUY-G-12	275	280	5	---	coarse	unsorted	Qya
CUY-G-12	280	315	35	---	fine	unsorted	Qya
CUY-G-12	315	335	20	---	coarse	sorted	Qya
CUY-G-12	335	357	22	---	fine	unsorted	Qya
CUY-G-12	357	395	38	---	coarse	sorted	Qya
CUY-G-12	395	410	15	---	fine	unsorted	Qya
CUY-G-12	410	480	70	---	coarse	sorted	Qya
CUY-G-12	480	525	45	---	fine	unsorted	Qya
CUY-G-12	525	550	25	---	coarse	unsorted	Qya
CUY-G-12	550	603	53	---	coarse	sorted	Qya
CUY-G-13	0	1	1	---	fine	unsorted	Qoa
CUY-G-13	1	15	14	---	coarse	sorted	Qoa
CUY-G-13	15	35	20	---	coarse	sorted	Qoa
CUY-G-13	35	70	35	---	fine	sorted	Qoa
CUY-G-13	70	80	10	---	fine	sorted	Qoa
CUY-G-13	80	94	14	---	fine	sorted	Qoa
CUY-G-13	94	96	2	---	coarse	sorted	Qoa

CUY-G-13	96	135	39	---	fine	sorted	Qoa
CUY-G-13	135	197	62	---	fine	sorted	Qoa
CUY-G-13	197	206	9	---	coarse	sorted	Qoa
CUY-G-13	206	211	5	---	fine	sorted	Qoa
CUY-G-13	211	213	2	---	coarse	sorted	Qoa
CUY-G-13	213	219	6	---	fine	sorted	Qoa
CUY-G-13	219	225	6	---	coarse	sorted	Qoa
CUY-G-13	225	260	35	---	fine	sorted	Qoa
CUY-G-13	260	314	54	---	fine	unsorted	Qoa
CUY-G-13	314	320	6	---	coarse	sorted	Qoa
CUY-G-13	320	326	6	---	fine	sorted	Qoa
CUY-G-13	326	335	9	---	coarse	sorted	Qoa
CUY-G-13	335	360	25	---	fine	sorted	Qoa
CUY-G-13	360	372	12	---	fine	sorted	Qoa
CUY-G-13	372	389	17	---	fine	sorted	Qoa
CUY-G-13	389	400	11	---	fine	sorted	Qoa
CUY-G-13	400	420	20	---	fine	unsorted	QTm
CUY-G-13	420	451	31	---	fine	sorted	QTm
CUY-G-13	451	500	49	---	coarse	sorted	QTm
CUY-G-13	500	520	20	---	fine	sorted	QTm
CUY-G-13	520	580	60	---	coarse	unsorted	QTm
CUY-G-13	580	600	20	---	fine	sorted	QTm
CUY-G-69	0	2	2	---	fine	unsorted	Qoa
CUY-G-69	2	20	18	---	coarse	sorted	Qoa
CUY-G-69	20	60	40	---	coarse	sorted	Qoa
CUY-G-69	60	77	17	---	fine	unsorted	Qoa
CUY-G-69	77	85	8	---	coarse	sorted	Qoa
CUY-G-69	85	120	35	---	fine	unsorted	Qoa
CUY-G-69	120	160	40	---	fine	unsorted	Qoa
CUY-G-69	160	210	50	---	coarse	sorted	Qoa
CUY-G-69	210	215	5	---	fine	unsorted	Qoa
CUY-G-69	215	270	55	---	fine	unsorted	Qoa
CUY-G-69	270	305	35	---	coarse	sorted	Qoa
CUY-G-69	305	435	130	---	fine	unsorted	Qoa

CUY-G-69	435	440	5	---	fine	unsorted	Qoa
CUY-G-69	440	455	15	---	fine	sorted	Qoa
CUY-G-69	455	460	5	---	fine	unsorted	Qoa
CUY-G-69	460	472	12	---	fine	sorted	Qoa
CUY-G-69	472	480	8	---	fine	unsorted	Qoa
CUY-G-69	480	503	23	---	fine	sorted	Qoa
CUY-G-14	0	1	1	---	fine	unsorted	Qya
CUY-G-14	1	20	19	---	coarse	unsorted	Qya
CUY-G-14	20	70	50	---	coarse	unsorted	Qya
CUY-G-14	70	100	30	---	coarse	unsorted	Qya
CUY-G-14	100	120	20	---	fine	unsorted	Qya
CUY-G-14	120	160	40	---	coarse	unsorted	Qya
CUY-G-14	160	170	10	---	coarse	unsorted	Qya
CUY-G-14	170	190	20	---	fine	unsorted	Qya
CUY-G-14	190	200	10	---	fine	unsorted	Qya
CUY-G-14	200	213	13	---	fine	unsorted	Qya
CUY-G-14	213	260	47	---	fine	unsorted	Qoa
CUY-G-14	260	280	20	---	fine	unsorted	Qoa
CUY-G-15	0	27	27	---	coarse	sorted	Qya
CUY-G-15	27	81	54	---	coarse	unsorted	Qya
CUY-G-15	81	82	1	---	coarse	unsorted	Qya
CUY-G-15	82	95	13	---	coarse	unsorted	Qya
CUY-G-15	95	102	7	---	coarse	unsorted	Qya
CUY-G-15	102	105	3	---	coarse	sorted	Qya
CUY-G-15	105	122	17	---	coarse	unsorted	Qya
CUY-G-15	122	144	22	---	fine	unsorted	Qya
CUY-G-15	144	155	11	---	coarse	unsorted	Qya
CUY-G-15	155	157	2	---	coarse	unsorted	Qya
CUY-G-15	157	191	34	---	fine	unsorted	Qya
CUY-G-15	191	202	11	---	coarse	sorted	Qoa
CUY-G-15	202	220	18	---	fine	unsorted	Qoa
CUY-G-15	220	221	1	---	coarse	sorted	Qoa
CUY-G-15	221	231	10	---	fine	sorted	Qoa
CUY-G-15	231	234	3	---	coarse	sorted	Qoa

CUY-G-15	234	243	9	---	fine	unsorted	Qoa
CUY-G-15	243	245	2	---	coarse	unsorted	Qoa
CUY-G-15	245	293	48	---	fine	unsorted	Qoa
CUY-G-15	293	307	14	---	coarse	unsorted	Qoa
CUY-G-15	307	312	5	---	coarse	sorted	Qoa
CUY-G-16	0	2	2	---	fine	unsorted	Qya
CUY-G-16	2	4	2	---	coarse	unsorted	Qya
CUY-G-16	4	39	35	---	coarse	unsorted	Qya
CUY-G-16	39	68	29	---	coarse	unsorted	QTm
CUY-G-16	68	83	15	---	coarse	unsorted	QTm
CUY-G-16	83	108	25	---	coarse	unsorted	QTm
CUY-G-16	108	145	37	---	coarse	unsorted	QTm
CUY-G-16	145	178	33	---	fine	unsorted	QTm
CUY-G-16	178	210	32	---	coarse	unsorted	QTm
CUY-G-16	210	280	70	---	coarse	unsorted	QTm
CUY-G-16	280	385	105	---	coarse	unsorted	QTm
CUY-G-16	385	480	95	---	coarse	unsorted	QTm
CUY-G-16	480	560	80	---	coarse	unsorted	QTm
CUY-G-17	0	35	35	---	coarse	unsorted	Qya
CUY-G-17	35	95	60	---	coarse	sorted	Qya
CUY-G-17	95	230	135	---	coarse	unsorted	Qya
CUY-G-17	230	252	22	---	fine	unsorted	Qya
CUY-G-70	0	30	30	---	fine	unsorted	Qoa
CUY-G-70	30	33	3	---	fine	unsorted	Qoa
CUY-G-70	33	140	107	---	coarse	unsorted	Qoa
CUY-G-70	140	145	5	---	fine	sorted	Qoa
CUY-G-70	145	180	35	---	coarse	unsorted	Qoa
CUY-G-70	180	200	20	---	fine	sorted	Qoa
CUY-G-70	200	250	50	---	coarse	unsorted	Qoa
CUY-G-70	250	260	10	---	fine	sorted	Qoa
CUY-G-70	260	280	20	---	coarse	unsorted	Qoa
CUY-G-70	280	290	10	---	fine	unsorted	Qoa
CUY-G-70	290	300	10	---	coarse	sorted	Qoa
CUY-G-70	300	320	20	---	fine	unsorted	Qoa

CUY-G-70	320	370	50	---	coarse	unsorted	Qoa
CUY-G-70	370	390	20	---	coarse	sorted	Qoa
CUY-G-70	390	400	10	---	fine	unsorted	Qoa
CUY-G-70	400	410	10	---	coarse	sorted	Qoa
CUY-G-70	410	420	10	---	fine	sorted	Qoa
CUY-G-70	420	450	30	---	fine	unsorted	Qoa
CUY-G-70	450	515	65	---	coarse	unsorted	Qoa
CUY-G-70	515	540	25	---	coarse	unsorted	QTm
CUY-G-70	540	580	40	---	fine	sorted	QTm
CUY-G-70	580	590	10	---	coarse	unsorted	QTm
CUY-G-70	590	600	10	---	fine	sorted	QTm
CUY-G-70	600	690	90	---	coarse	unsorted	QTm
CUY-G-70	690	770	80	---	coarse	sorted	QTm
CUY-G-70	770	800	30	---	coarse	unsorted	QTm
CUY-G-18	0	2	2	---	fine	unsorted	Qya
CUY-G-18	2	26	24	---	coarse	sorted	Qya
CUY-G-18	26	42	16	---	fine	sorted	Qya
CUY-G-18	42	82	40	---	coarse	unsorted	Qya
CUY-G-18	82	101	19	---	fine	sorted	Qya
CUY-G-18	101	130	29	---	coarse	sorted	Qya
CUY-G-18	130	230	100	---	coarse	sorted	Qya
CUY-G-18	230	245	15	---	coarse	sorted	Qoa
CUY-G-19	0	135	135	---	coarse	sorted	Qoa
CUY-G-19	135	188	53	---	coarse	unsorted	Qya
CUY-G-19	188	196	8	---	coarse	unsorted	Qya
CUY-G-19	196	390	194	---	coarse	unsorted	Qya
CUY-G-19	390	395	5	---	coarse	unsorted	Qya
CUY-G-19	395	410	15	---	coarse	unsorted	Qya
CUY-G-19	410	415	5	---	coarse	unsorted	Qya
CUY-G-19	415	472	57	---	coarse	unsorted	Qya
CUY-G-19	472	502	30	---	fine	unsorted	Qya
CUY-G-19	502	525	23	---	fine	unsorted	Qoa
CUY-G-19	525	529	4	---	coarse	unsorted	Qoa
CUY-G-19	529	538	9	---	fine	unsorted	Qoa

CUY-G-19	538	542	4	---	coarse	unsorted	Qoa
CUY-G-19	542	545	3	---	coarse	unsorted	Qoa
CUY-G-19	545	576	31	---	fine	sorted	Qoa
CUY-G-19	576	620	44	---	fine	unsorted	Qoa
CUY-G-19	620	666	46	---	fine	sorted	Qoa
CUY-G-19	666	729	63	---	fine	unsorted	Qoa
CUY-G-19	729	745	16	---	fine	sorted	Qoa
CUY-G-19	745	774	29	---	fine	unsorted	Qoa
CUY-G-19	774	800	26	---	fine	sorted	Qoa
CUY-G-19	800	810	10	---	fine	unsorted	Qoa
CUY-G-19	810	830	20	---	fine	sorted	Qoa
CUY-G-19	830	833	3	---	coarse	unsorted	Qoa
CUY-G-19	833	887	54	---	fine	unsorted	Qoa
CUY-G-19	887	1,024	137	---	fine	unsorted	QTm
CUY-G-19	1,024	1,068	44	---	fine	unsorted	QTm
CUY-G-20	0	25	25	---	fine	sorted	Qya
CUY-G-20	25	50	25	---	fine	unsorted	Qya
CUY-G-20	50	53	3	---	coarse	unsorted	Qya
CUY-G-20	53	57	4	---	fine	unsorted	Qya
CUY-G-20	57	60	3	---	coarse	unsorted	Qya
CUY-G-20	60	70	10	---	fine	unsorted	Qya
CUY-G-20	70	90	20	---	coarse	unsorted	Qya
CUY-G-20	90	185	95	---	coarse	sorted	Qya
CUY-G-20	185	195	10	---	fine	unsorted	Qya
CUY-G-20	195	200	5	---	coarse	sorted	Qya
CUY-G-22	0	15	15	---	coarse	unsorted	Qya
CUY-G-22	15	62	47	---	coarse	unsorted	Qya
CUY-G-22	62	73	11	---	coarse	unsorted	Qya
CUY-G-22	73	209	136	---	coarse	unsorted	Qya
CUY-G-22	209	305	96	---	coarse	unsorted	Qya
CUY-G-22	305	315	10	---	coarse	unsorted	Qya
CUY-G-22	315	377	62	---	coarse	unsorted	Qya
CUY-G-22	377	430	53	---	coarse	unsorted	Qoa
CUY-G-22	430	450	20	---	fine	unsorted	Qoa

CUY-G-22	450	480	30	---	coarse	unsorted	Qoa
CUY-G-22	480	572	92	---	coarse	unsorted	Qoa
CUY-G-22	572	695	123	---	coarse	unsorted	QTm
CUY-G-22	695	710	15	---	coarse	unsorted	QTm
CUY-G-22	710	803	93	---	coarse	unsorted	QTm
CUY-G-71	0	14	14	---	fine	unsorted	Qya
CUY-G-71	14	25	11	---	coarse	sorted	Qya
CUY-G-71	25	32	7	---	fine	unsorted	Qya
CUY-G-71	32	60	28	---	coarse	unsorted	Qya
CUY-G-71	60	80	20	---	coarse	unsorted	Qya
CUY-G-71	80	103	23	---	fine	sorted	Qya
CUY-G-71	103	113	10	---	coarse	sorted	Qya
CUY-G-71	113	124	11	---	fine	unsorted	Qya
CUY-G-71	124	154	30	---	fine	unsorted	Qya
CUY-G-71	154	210	56	---	fine	unsorted	Qya
CUY-G-71	210	265	55	---	coarse	unsorted	Qya
CUY-G-71	265	285	20	---	fine	unsorted	Qya
CUY-G-71	285	306	21	---	coarse	unsorted	Qya
CUY-G-71	306	316	10	---	fine	sorted	Qya
CUY-G-71	316	387	71	---	coarse	unsorted	Qya
CUY-G-71	387	398	11	---	coarse	unsorted	Qoa
CUY-G-71	398	418	20	---	fine	sorted	Qoa
CUY-G-71	418	438	20	---	coarse	sorted	Qoa
CUY-G-71	438	488	50	---	fine	unsorted	Qoa
CUY-G-71	488	542	54	---	fine	sorted	Qoa
CUY-G-71	542	567	25	---	coarse	unsorted	Qoa
CUY-G-71	567	630	63	---	fine	sorted	Qoa
CUY-G-71	630	636	6	---	coarse	sorted	Qoa
CUY-G-71	636	774	138	---	fine	unsorted	Qoa
CUY-G-71	774	815	41	---	coarse	unsorted	Qoa
CUY-G-71	815	835	20	---	fine	unsorted	Qoa
CUY-G-71	835	846	11	---	coarse	sorted	Qoa
CUY-G-71	846	904	58	---	fine	sorted	Qoa
CUY-G-71	904	924	20	---	coarse	unsorted	Qoa

CUY-G-71	924	938	14	---	fine	unsorted	Qoa
CUY-G-71	938	993	55	---	coarse	unsorted	Qoa
CUY-G-71	993	1,025	32	---	fine	sorted	QTm
CUY-G-71	1,025	1,043	18	---	fine	sorted	QTm
CUY-G-21	0	15	15	---	fine	unsorted	Qya
CUY-G-21	15	32	17	---	coarse	sorted	Qya
CUY-G-21	32	35	3	---	fine	unsorted	Qya
CUY-G-21	35	57	22	---	coarse	unsorted	Qya
CUY-G-21	57	125	68	---	coarse	unsorted	Qya
CUY-G-21	125	180	55	---	fine	unsorted	Qya
CUY-G-21	180	205	25	---	coarse	unsorted	Qya
CUY-G-21	205	215	10	---	fine	sorted	Qya
CUY-G-21	215	335	120	---	coarse	unsorted	Qya
CUY-G-21	335	433	98	---	fine	unsorted	Qya
CUY-G-21	433	460	27	---	fine	unsorted	Qoa
CUY-G-21	460	473	13	---	fine	sorted	Qoa
CUY-G-21	473	530	57	---	fine	sorted	Qoa
CUY-G-21	530	608	78	---	fine	unsorted	Qoa
CUY-G-21	608	774	166	---	fine	sorted	Qoa
CUY-G-21	774	942	168	---	fine	sorted	QTm
CUY-G-21	942	995	53	---	coarse	unsorted	QTm
CUY-G-21	995	1,130	135	---	fine	sorted	QTm
CUY-G-21	1,130	1,145	15	---	fine	unsorted	QTm
CUY-G-21	1,145	1,300	155	---	fine	sorted	QTm
CUY-G-23	1	12	11	---	fine	unsorted	Qya
CUY-G-23	12	32	20	---	coarse	unsorted	Qya
CUY-G-23	32	175	143	---	fine	unsorted	Qya
CUY-G-23	175	215	40	---	coarse	unsorted	Qya
CUY-G-23	215	227	12	---	fine	sorted	Qya
CUY-G-23	227	260	33	---	coarse	unsorted	Qya
CUY-G-23	260	320	60	---	coarse	unsorted	Qya
CUY-G-23	320	342	22	---	coarse	unsorted	Qya
CUY-G-23	342	355	13	---	coarse	unsorted	Qya
CUY-G-23	355	390	35	---	fine	unsorted	Qya

CUY-G-23	390	420	30	---	fine	unsorted	Qoa
CUY-G-23	420	450	30	---	fine	unsorted	Qoa
CUY-G-23	450	722	272	---	fine	sorted	QTm
CUY-G-23	722	766	44	---	fine	sorted	QTm
CUY-G-23	766	865	99	---	fine	sorted	QTm
CUY-G-23	865	870	5	---	fine	unsorted	QTm
CUY-G-23	870	879	9	---	coarse	unsorted	QTm
CUY-G-23	879	885	6	---	fine	sorted	QTm
CUY-G-23	885	888	3	---	coarse	unsorted	QTm
CUY-G-23	888	1,004	116	---	fine	sorted	QTm
CUY-G-24	0	23	23	---	fine	unsorted	Qya
CUY-G-24	23	30	7	---	fine	unsorted	Qya
CUY-G-24	30	50	20	---	coarse	unsorted	Qya
CUY-G-24	50	93	43	---	coarse	unsorted	Qya
CUY-G-24	93	130	37	---	fine	unsorted	Qya
CUY-G-24	130	155	25	---	coarse	unsorted	Qya
CUY-G-24	155	235	80	---	coarse	unsorted	Qya
CUY-G-24	235	360	125	---	coarse	unsorted	Qya
CUY-G-24	360	395	35	---	fine	unsorted	Qya
CUY-G-24	395	480	85	---	coarse	unsorted	Qoa
CUY-G-24	480	680	200	---	fine	unsorted	Qoa
CUY-G-24	680	705	25	---	fine	unsorted	Qoa
CUY-G-24	705	750	45	---	fine	unsorted	QTm
CUY-G-24	750	817	67	---	fine	sorted	QTm
CUY-G-24	817	867	50	---	fine	sorted	QTm
CUY-G-24	867	887	20	---	coarse	unsorted	QTm
CUY-G-24	887	930	43	---	fine	sorted	QTm
CUY-G-24	930	936	6	---	fine	unsorted	QTm
CUY-G-24	936	1,004	68	---	fine	sorted	QTm
CUY-G-72	0	6	6	---	fine	unsorted	Qoa
CUY-G-72	6	12	6	---	coarse	sorted	Qoa
CUY-G-72	12	20	8	---	fine	unsorted	Qoa
CUY-G-72	20	30	10	---	fine	unsorted	Qoa
CUY-G-72	30	40	10	---	coarse	unsorted	Qoa

CUY-G-72	40	45	5	---	fine	sorted	Qoa
CUY-G-72	45	50	5	---	coarse	unsorted	Qoa
CUY-G-72	50	62	12	---	fine	unsorted	Qoa
CUY-G-72	62	82	20	---	coarse	unsorted	Qoa
CUY-G-72	82	89	7	---	coarse	unsorted	Qoa
CUY-G-72	89	99	10	---	fine	unsorted	Qoa
CUY-G-72	99	115	16	---	fine	unsorted	Qoa
CUY-G-72	115	123	8	---	fine	unsorted	Qoa
CUY-G-72	123	143	20	---	fine	unsorted	Qoa
CUY-G-72	143	160	17	---	coarse	unsorted	Qoa
CUY-G-72	160	168	8	---	fine	unsorted	Qoa
CUY-G-72	168	276	108	---	coarse	unsorted	Qoa
CUY-G-72	276	420	144	---	coarse	unsorted	Qoa
CUY-G-72	420	430	10	---	coarse	unsorted	Qoa
CUY-G-72	430	490	60	---	coarse	unsorted	Qoa
CUY-G-72	490	495	5	---	fine	sorted	Qoa
CUY-G-72	495	515	20	---	fine	sorted	QTm
CUY-G-72	515	635	120	---	coarse	unsorted	QTm
CUY-G-72	635	670	35	---	fine	unsorted	QTm
CUY-G-72	670	775	105	---	coarse	unsorted	QTm
CUY-G-72	775	800	25	---	fine	unsorted	QTm
CUY-G-72	800	875	75	---	fine	sorted	QTm
CUY-G-72	875	900	25	---	coarse	unsorted	QTm
CUY-G-72	900	910	10	---	fine	sorted	QTm
CUY-G-72	910	924	14	---	fine	unsorted	QTm
CUY-G-25	0	7	7	---	fine	unsorted	Qya
CUY-G-25	7	20	13	---	coarse	unsorted	Qya
CUY-G-25	20	45	25	---	coarse	sorted	Qya
CUY-G-25	45	150	105	---	coarse	unsorted	Qya
CUY-G-25	150	186	36	---	coarse	unsorted	Qya
CUY-G-25	186	261	75	---	fine	unsorted	Qya
CUY-G-25	261	280	19	---	coarse	unsorted	Qya
CUY-G-25	280	337	57	---	coarse	sorted	Qya
CUY-G-25	337	365	28	---	coarse	unsorted	Qya

CUY-G-25	365	419	54	---	coarse	sorted	Qya
CUY-G-25	419	469	50	---	fine	unsorted	Qya
CUY-G-25	469	490	21	---	fine	unsorted	Qoa
CUY-G-25	490	590	100	---	coarse	unsorted	Qoa
CUY-G-25	590	600	10	---	fine	sorted	Qoa
CUY-G-73	0	20	20	---	fine	unsorted	Qoa
CUY-G-73	20	100	80	---	coarse	sorted	Qoa
CUY-G-73	100	140	40	---	fine	sorted	Qoa
CUY-G-73	140	210	70	---	coarse	unsorted	Qoa
CUY-G-73	210	238	28	---	coarse	sorted	Qoa
CUY-G-73	238	260	22	---	coarse	unsorted	Qoa
CUY-G-73	260	286	26	---	coarse	sorted	Qoa
CUY-G-73	286	327	41	---	coarse	sorted	Qoa
CUY-G-73	327	376	49	---	coarse	unsorted	Qoa
CUY-G-73	376	455	79	---	coarse	sorted	Qoa
CUY-G-73	455	502	47	---	fine	unsorted	Qoa
CUY-G-73	502	580	78	---	coarse	sorted	Qoa
CUY-G-73	580	638	58	---	fine	unsorted	Qoa
CUY-G-73	638	700	62	---	coarse	unsorted	QTm
CUY-G-73	700	728	28	---	fine	sorted	QTm
CUY-G-73	728	750	22	---	coarse	sorted	QTm
CUY-G-73	750	820	70	---	coarse	unsorted	QTm
CUY-G-26	0	60	60	---	coarse	unsorted	Qya
CUY-G-26	60	83	23	---	coarse	sorted	Qya
CUY-G-26	83	130	47	---	coarse	unsorted	Qya
CUY-G-26	130	155	25	---	coarse	sorted	Qya
CUY-G-26	155	177	22	---	coarse	sorted	Qya
CUY-G-26	177	199	22	---	coarse	unsorted	Qya
CUY-G-26	199	233	34	---	coarse	sorted	Qya
CUY-G-26	233	265	32	---	coarse	unsorted	Qya
CUY-G-26	265	282	17	---	coarse	unsorted	Qya
CUY-G-26	282	310	28	---	coarse	unsorted	Qya
CUY-G-26	310	334	24	---	coarse	sorted	Qya
CUY-G-26	334	360	26	---	coarse	sorted	Qya

CUY-G-26	360	429	69	---	coarse	sorted	Qya
CUY-G-26	429	450	21	---	coarse	unsorted	Qya
CUY-G-26	450	475	25	---	coarse	sorted	Qya
CUY-G-26	475	505	30	---	coarse	sorted	Qya
CUY-G-26	505	520	15	---	fine	sorted	Qya
CUY-G-26	520	529	9	---	coarse	sorted	Qya
CUY-G-26	529	554	25	---	coarse	sorted	Qya
CUY-G-26	554	588	34	---	coarse	sorted	Qoa
CUY-G-26	588	610	22	---	fine	sorted	Qoa
PT-19	0	80	80	---	coarse	unsorted	Qya
PT-19	80	86	6	---	fine	unsorted	Qya
PT-19	86	101	15	---	fine	unsorted	Qya
PT-19	101	113	12	---	coarse	unsorted	Qya
PT-19	113	115	2	---	fine	sorted	Qya
PT-19	115	128	13	---	coarse	unsorted	Qya
PT-19	128	139	11	---	fine	unsorted	Qya
PT-19	139	141	2	---	coarse	unsorted	Qya
PT-19	141	150	9	---	fine	unsorted	Qya
PT-19	150	155	5	---	coarse	unsorted	Qya
PT-19	155	158	3	---	fine	sorted	Qya
PT-19	158	170	12	---	coarse	unsorted	Qya
PT-19	170	191	21	---	fine	unsorted	Qya
PT-19	191	205	14	---	fine	sorted	Qya
PT-19	205	215	10	---	coarse	sorted	Qya
PT-19	215	225	10	---	fine	sorted	Qya
PT-19	225	228	3	---	fine	sorted	Qya
PT-19	228	230	2	---	coarse	unsorted	Qya
PT-19	230	235	5	---	fine	sorted	Qya
PT-19	235	245	10	---	coarse	unsorted	Qya
PT-19	245	250	5	---	fine	sorted	Qya
PT-19	250	258	8	---	coarse	sorted	Qya
PT-19	258	260	2	---	fine	sorted	Qya
PT-19	260	262	2	---	coarse	unsorted	Qya
PT-19	262	276	14	---	fine	unsorted	Qya

PT-19	276	284	8	---	coarse	unsorted	Qya
PT-19	284	290	6	---	fine	unsorted	Qya
PT-19	290	300	10	---	fine	unsorted	Qya
PT-19	300	318	18	---	fine	unsorted	Qya
PT-19	318	320	2	---	fine	unsorted	Qya
PT-19	320	337	17	---	coarse	unsorted	Qya
PT-19	337	354	17	---	fine	sorted	Qya
PT-19	354	358	4	---	coarse	unsorted	Qya
PT-19	358	371	13	---	fine	sorted	Qya
PT-19	371	373	2	---	coarse	unsorted	Qya
PT-19	373	390	17	---	coarse	unsorted	Qya
PT-19	390	434	44	---	coarse	unsorted	Qya
PT-19	434	485	51	---	fine	sorted	Qya
PT-19	485	490	5	---	fine	unsorted	Qya
PT-19	490	515	25	---	fine	sorted	Qya
PT-19	515	518	3	---	coarse	unsorted	Qya
PT-19	518	520	2	---	fine	unsorted	Qya
PT-19	520	528	8	---	fine	sorted	Qya
PT-19	528	536	8	---	fine	sorted	Qoa
PT-19	536	545	9	---	coarse	unsorted	Qoa
PT-19	545	558	13	---	fine	sorted	Qoa
PT-19	558	628	70	---	coarse	unsorted	Qoa
PT-19	628	675	47	---	fine	sorted	Qoa
PT-19	675	737	62	---	coarse	unsorted	Qoa
PT-19	737	859	122	---	fine	unsorted	Qoa
PT-19	859	875	16	---	fine	unsorted	Qoa
PT-19	875	916	41	---	fine	unsorted	Qoa
PT-19	916	919	3	---	coarse	sorted	Qoa
PT-19	919	935	16	---	fine	sorted	Qoa
PT-19	935	945	10	---	fine	unsorted	Qoa
PT-19	945	947	2	---	fine	sorted	Qoa
PT-19	947	950	3	---	fine	sorted	Qoa
PT-19	950	970	20	---	fine	sorted	Qoa
CUY-G-27	0	4	4	---	fine	unsorted	Qya

CUY-G-27	4	189	193	---	coarse	unsorted	Qya
CUY-G-27	189	250	53	---	coarse	unsorted	Qoa
CUY-G-27	250	253	3	---	fine	sorted	Qoa
CUY-G-27	253	270	17	---	coarse	unsorted	Qoa
CUY-G-27	270	295	25	---	fine	unsorted	Qoa
CUY-G-27	295	331	36	---	coarse	unsorted	Qoa
CUY-G-27	331	400	69	---	coarse	unsorted	QTm
CUY-G-27	400	409	9	---	fine	unsorted	QTm
CUY-G-27	409	445	36	---	coarse	unsorted	QTm
CUY-G-27	445	458	13	---	fine	unsorted	QTm
CUY-G-27	458	510	52	---	coarse	sorted	QTm
CUY-G-27	510	518	8	---	coarse	unsorted	QTm
CUY-G-27	518	521	3	---	coarse	sorted	QTm
CUY-G-27	521	524	3	---	coarse	unsorted	QTm
CUY-G-27	524	528	4	---	fine	unsorted	QTm
CUY-G-27	528	534	6	---	coarse	unsorted	QTm
CUY-G-27	534	571	37	---	coarse	unsorted	QTm
CUY-G-27	571	582	11	---	fine	unsorted	QTm
CUY-G-27	582	586	4	---	coarse	unsorted	QTm
CUY-G-27	586	592	6	---	coarse	unsorted	QTm
CUY-G-27	592	620	28	---	coarse	unsorted	QTm
CUY-G-27	620	634	14	---	fine	unsorted	QTm
CUY-G-27	634	639	5	---	coarse	sorted	QTm
CUY-G-27	639	653	14	---	fine	unsorted	QTm
CUY-G-27	653	660	7	---	fine	sorted	QTm
CUY-G-27	660	690	30	---	fine	unsorted	QTm
CUY-G-27	690	710	20	---	coarse	unsorted	QTm
CUY-G-27	710	716	6	---	fine	unsorted	QTm
CUY-G-27	716	718	2	---	coarse	sorted	QTm
CUY-G-27	718	720	2	---	fine	unsorted	QTm
CUY-G-27	720	724	4	---	coarse	sorted	QTm
CUY-G-27	724	730	6	---	fine	sorted	QTm
CUY-G-27	730	790	60	---	coarse	unsorted	QTm
CUY-G-27	790	798	8	---	fine	sorted	QTm

CUY-64	0	2	2	---	fine	unsorted	Qya
CUY-64	2	18	16	---	fine	sorted	Qya
CUY-64	18	34	16	---	coarse	unsorted	Qya
CUY-64	34	48	14	---	fine	sorted	Qya
CUY-64	48	56	8	---	coarse	unsorted	Qya
CUY-64	56	115	59	---	fine	sorted	Qya
CUY-64	115	118	3	---	coarse	sorted	Qya
CUY-64	118	175	57	---	fine	sorted	Qya
CUY-64	175	183	8	---	coarse	unsorted	Qya
CUY-64	183	190	7	---	fine	sorted	Qya
CUY-64	190	193	3	---	coarse	sorted	Qya
CUY-64	193	310	117	---	fine	sorted	Qya
CUY-64	310	330	20	---	coarse	sorted	Qya
CUY-64	330	345	15	---	fine	sorted	Qya
CUY-64	345	354	9	---	coarse	sorted	Qya
CUY-64	354	356	2	---	fine	sorted	Qya
CUY-64	356	365	9	---	coarse	sorted	Qya
CUY-64	365	378	13	---	fine	sorted	Qya
CUY-64	378	383	5	---	coarse	unsorted	Qya
CUY-64	383	405	22	---	fine	sorted	Qya
CUY-64	405	415	10	---	coarse	unsorted	Qoa
CUY-64	415	425	10	---	fine	sorted	Qoa
CUY-64	425	440	15	---	fine	sorted	Qoa
CUY-64	440	445	5	---	fine	sorted	Qoa
CUY-64	445	520	75	---	fine	sorted	Qoa
CUY-64	520	525	5	---	fine	sorted	Qoa
CUY-64	525	560	35	---	fine	unsorted	Qoa
CUY-64	560	565	5	---	fine	unsorted	Qoa
CUY-64	565	618	53	---	fine	sorted	Qoa
CUY-64	618	627	9	---	fine	sorted	Qoa
CUY-64	627	643	16	---	fine	sorted	Qoa
CUY-64	643	648	5	---	fine	unsorted	Qoa
CUY-64	648	657	9	---	fine	sorted	Qoa
CUY-64	657	662	5	---	fine	unsorted	Qoa

CUY-64	662	667	5	---	fine	unsorted	Qoa
CUY-64	667	676	9	---	fine	sorted	Qoa
CUY-64	676	682	6	---	coarse	sorted	Qoa
CUY-64	682	700	18	---	fine	sorted	Qoa
CUY-64	700	703	3	---	coarse	unsorted	Qoa
CUY-64	703	720	17	---	fine	sorted	Qoa
CUY-64	720	765	45	---	fine	unsorted	Qoa
CUY-64	765	780	15	---	fine	sorted	Qoa
CUY-64	780	787	7	---	fine	unsorted	Qoa
CUY-64	787	800	13	---	fine	sorted	QTm
CUY-64	800	810	10	---	fine	unsorted	QTm
CUY-64	810	813	3	---	fine	sorted	QTm
CUY-64	813	860	47	---	fine	sorted	QTm
CUY-64	860	867	7	---	fine	unsorted	QTm
CUY-64	867	874	7	---	fine	sorted	QTm
CUY-64	874	875	1	---	coarse	sorted	QTm
CUY-64	875	878	3	---	fine	sorted	QTm
CUY-64	878	883	5	---	fine	unsorted	QTm
CUY-64	883	892	9	---	coarse	sorted	QTm
CUY-64	892	898	6	---	fine	unsorted	QTm
CUY-64	898	947	49	---	fine	sorted	QTm
CUY-64	947	950	3	---	fine	unsorted	QTm
CUY-64	950	953	3	---	fine	sorted	QTm
CUY-64	953	956	3	---	coarse	sorted	QTm
CUY-64	956	965	9	---	fine	sorted	QTm
CUY-64	965	973	8	---	fine	unsorted	QTm
CUY-64	973	982	9	---	fine	sorted	QTm
CUY-64	982	1,015	33	---	fine	unsorted	QTm
CUY-12	0	20	20	---	fine	unsorted	Qya
CUY-12	20	90	70	---	coarse	unsorted	Qya
CUY-12	90	148	58	---	coarse	unsorted	Qya
CUY-12	148	160	12	---	coarse	unsorted	Qoa
CUY-12	160	165	5	---	fine	sorted	Qoa
CUY-12	165	195	30	---	coarse	unsorted	Qoa

CUY-12	195	256	61	---	fine	sorted	Qoa
CUY-12	256	260	4	---	fine	sorted	QTm
CUY-G-28	0	1	1	---	fine	unsorted	Qya
CUY-G-28	1	45	44	---	fine	sorted	Qya
CUY-G-28	45	52	7	---	coarse	sorted	Qya
CUY-G-28	52	59	7	---	fine	sorted	Qya
CUY-G-28	59	65	6	---	fine	sorted	Qoa
CUY-G-28	65	70	5	---	coarse	unsorted	Qoa
CUY-G-28	70	73	3	---	fine	sorted	Qoa
CUY-G-28	73	77	4	---	coarse	sorted	Qoa
CUY-G-28	77	93	16	---	fine	sorted	Qoa
CUY-G-28	93	107	14	---	coarse	sorted	Qoa
CUY-G-28	107	112	5	---	fine	sorted	Qoa
CUY-G-28	112	160	48	---	fine	unsorted	Qoa
CUY-G-28	160	170	10	---	coarse	unsorted	Qoa
CUY-G-28	170	175	5	---	fine	sorted	Qoa
CUY-G-28	175	220	45	---	fine	unsorted	Qoa
CUY-G-28	220	260	40	---	fine	unsorted	Qoa
CUY-G-28	260	300	40	---	fine	unsorted	Qoa
CUY-G-28	300	495	195	---	nd	nd	Qoa
CUY-G-28	495	510	15	---	coarse	sorted	Qoa
CUY-G-28	510	540	30	---	fine	unsorted	Qoa
CUY-G-28	540	560	20	---	coarse	sorted	Qoa
CUY-G-28	560	571	11	---	fine	unsorted	Qoa
CUY-G-28	571	593	22	---	fine	unsorted	QTm
CUY-G-28	579	610	31	---	coarse	sorted	QTm
CUY-G-28	593	607	14	---	fine	unsorted	QTm
CUY-G-28	607	579	-28	---	coarse	sorted	QTm
CUY-G-28	610	624	14	---	coarse	sorted	QTm
CUY-G-28	624	637	13	---	fine	unsorted	QTm
CUY-G-28	637	641	4	---	coarse	sorted	QTm
CUY-G-28	641	650	9	---	fine	sorted	QTm
CUY-G-74	0	10	10	---	fine	sorted	Qoa
CUY-G-74	10	80	70	---	coarse	unsorted	Qoa

CUY-G-74	80	84	4	---	coarse	unsorted	Qoa
CUY-G-74	84	95	11	---	fine	sorted	Qoa
CUY-G-74	95	160	65	---	coarse	unsorted	Qoa
CUY-G-74	160	200	40	---	coarse	sorted	Qoa
CUY-G-74	200	210	10	---	coarse	sorted	Qoa
CUY-G-74	210	220	10	---	coarse	sorted	Qoa
CUY-G-74	220	226	6	---	coarse	sorted	Qoa
CUY-G-74	226	230	4	---	coarse	sorted	Qoa
CUY-G-74	230	237	7	---	coarse	unsorted	Qoa
CUY-G-74	237	240	3	---	fine	sorted	Qoa
CUY-G-74	240	290	50	---	coarse	sorted	Qoa
CUY-G-74	290	320	30	---	fine	unsorted	Qoa
CUY-G-74	320	345	25	---	coarse	sorted	Qoa
CUY-G-74	345	360	15	---	coarse	sorted	Qoa
CUY-G-74	360	380	20	---	fine	unsorted	Qoa
CUY-G-74	380	395	15	---	coarse	sorted	Qoa
CUY-G-74	395	435	40	---	coarse	sorted	Qoa
CUY-G-74	435	540	105	---	coarse	unsorted	Qoa
CUY-G-74	540	590	50	---	coarse	sorted	Qoa
CUY-G-74	590	600	10	---	fine	unsorted	QTm
CUY-G-74	600	680	80	---	coarse	sorted	QTm
CUY-G-74	680	705	25	---	coarse	sorted	QTm
CUY-G-74	705	720	15	---	coarse	sorted	QTm
CUY-G-74	720	740	20	---	coarse	sorted	QTm
CUY-G-74	740	755	15	---	coarse	sorted	QTm
CUY-G-74	755	785	30	---	coarse	sorted	QTm
CUY-G-29	0	3	3	---	fine	unsorted	Qya
CUY-G-29	3	8	5	---	fine	sorted	Qya
CUY-G-29	8	85	77	---	fine	sorted	Qya
CUY-G-29	85	105	20	---	fine	sorted	Qya
CUY-G-29	105	140	35	---	fine	sorted	Qya
CUY-G-29	140	210	70	---	fine	sorted	Qya
CUY-G-29	210	218	8	---	fine	sorted	Qya
CUY-G-29	218	227	9	---	fine	unsorted	Qya

CUY-G-29	227	245	18	---	fine	sorted	QTm
CUY-G-29	245	257	12	---	fine	unsorted	QTm
CUY-G-29	257	280	23	---	fine	sorted	QTm
CUY-G-29	280	301	21	---	fine	unsorted	QTm
CUY-G-29	301	323	22	---	fine	sorted	QTm
CUY-G-29	323	341	18	---	fine	unsorted	QTm
CUY-G-29	341	365	24	---	fine	sorted	QTm
CUY-G-29	365	375	10	---	fine	unsorted	QTm
CUY-G-29	375	385	10	---	fine	sorted	QTm
CUY-G-103	0	10	10	---	fine	sorted	Qoa
CUY-G-103	10	140	130	---	fine	unsorted	Qoa
CUY-G-103	140	210	70	---	coarse	unsorted	Qoa
CUY-G-103	210	235	25	---	coarse	unsorted	Qoa
CUY-G-30	0	80	80	---	coarse	unsorted	Qya
CUY-G-30	80	105	25	---	fine	unsorted	Qya
CUY-G-30	105	140	35	---	coarse	unsorted	Qya
CUY-G-30	140	150	10	---	fine	unsorted	Qya
CUY-G-30	150	157	7	---	coarse	unsorted	Qya
CUY-G-30	157	160	3	---	fine	sorted	Qya
CUY-G-30	160	200	40	---	coarse	unsorted	Qya
CUY-G-30	200	230	30	---	coarse	unsorted	Qya
CUY-G-30	230	250	20	---	coarse	unsorted	QTm
CUY-G-30	250	255	5	---	fine	sorted	QTm
CUY-G-31	0	35	35	---	fine	unsorted	Qya
CUY-G-31	35	128	93	---	coarse	sorted	Qya
CUY-G-31	128	140	12	---	coarse	sorted	Qoa
CUY-G-31	140	150	10	---	fine	sorted	Qoa
CUY-G-31	150	160	10	---	coarse	sorted	Qoa
CUY-G-31	160	165	5	---	fine	sorted	Qoa
CUY-G-31	165	235	70	---	coarse	unsorted	Qoa
CUY-G-31	235	403	168	---	fine	sorted	Qoa
CUY-G-32	0	1	1	---	coarse	sorted	Qya
CUY-G-32	1	180	179	---	coarse	unsorted	Qya
CUY-G-32	180	200	20	---	fine	unsorted	Qya

CUY-G-32	200	230	30	---	coarse	unsorted	Qya
CUY-G-32	230	243	13	---	coarse	unsorted	QTm
CUY-G-75	0	10	10	---	coarse	unsorted	Qya
CUY-G-75	10	85	75	---	fine	sorted	Qya
CUY-G-75	85	115	30	---	fine	unsorted	QTm
CUY-G-75	115	120	5	---	coarse	sorted	QTm
CUY-G-75	120	180	60	---	fine	unsorted	QTm
CUY-G-75	180	200	20	---	coarse	sorted	QTm
CUY-G-75	200	220	20	---	fine	sorted	QTm
CUY-G-75	220	260	40	---	coarse	unsorted	QTm
CUY-G-75	260	300	40	---	fine	sorted	QTm
CUY-G-75	300	360	60	---	coarse	unsorted	QTm
CUY-G-33	0	3	3	---	fine	unsorted	Qya
CUY-G-33	3	10	7	---	fine	sorted	Qya
CUY-G-33	10	35	25	---	coarse	sorted	Qya
CUY-G-33	35	65	30	---	fine	sorted	Qya
CUY-G-33	65	75	10	---	coarse	sorted	Qya
CUY-G-33	75	125	50	---	fine	unsorted	Qya
CUY-G-33	125	130	5	---	coarse	sorted	Qya
CUY-G-33	130	170	40	---	fine	sorted	Qya
CUY-G-33	170	215	45	---	coarse	sorted	Qya
CUY-G-33	215	295	80	---	fine	unsorted	Qya
CUY-G-33	295	341	46	---	fine	unsorted	Qya
CUY-G-33	341	358	17	---	fine	unsorted	Qoa
CUY-G-33	358	360	2	---	coarse	sorted	Qoa
CUY-G-33	360	370	10	---	fine	sorted	Qoa
CUY-G-33	370	380	10	---	fine	unsorted	Qoa
CUY-G-33	380	385	5	---	fine	sorted	Qoa
CUY-G-33	385	396	11	---	coarse	unsorted	Qoa
CUY-G-33	396	416	20	---	fine	sorted	Qoa
CUY-G-33	416	430	14	---	coarse	unsorted	Qoa
CUY-G-33	430	435	5	---	fine	sorted	Qoa
CUY-G-33	435	464	29	---	fine	unsorted	Qoa
CUY-G-33	464	469	5	---	coarse	sorted	Qoa

CUY-G-33	469	497	28	---	fine	sorted	Qoa
CUY-G-33	497	500	3	---	coarse	sorted	Qoa
CUY-G-33	500	510	10	---	fine	sorted	Qoa
CUY-G-33	510	515	5	---	coarse	sorted	Qoa
CUY-G-33	515	555	40	---	fine	unsorted	Qoa
CUY-G-33	555	560	5	---	coarse	sorted	Qoa
CUY-G-33	560	595	35	---	fine	sorted	Qoa
CUY-G-33	595	600	5	---	coarse	sorted	Qoa
CUY-G-33	600	611	11	---	fine	sorted	Qoa
CUY-G-33	611	622	11	---	coarse	sorted	Qoa
CUY-G-33	622	630	8	---	fine	sorted	Qoa
CUY-G-33	630	635	5	---	coarse	sorted	Qoa
CUY-G-33	635	644	9	---	fine	unsorted	Qoa
CUY-G-33	644	662	18	---	coarse	sorted	Qoa
CUY-G-33	662	703	41	---	fine	sorted	Qoa
CUY-G-76	0	3	3	---	fine	unsorted	Qoa
CUY-G-76	3	10	7	---	coarse	unsorted	Qoa
CUY-G-76	10	15	5	---	fine	sorted	Qoa
CUY-G-76	15	17	2	---	coarse	sorted	Qoa
CUY-G-76	17	70	53	---	fine	unsorted	Qoa
CUY-G-76	70	89	19	---	coarse	sorted	Qoa
CUY-G-76	89	91	2	---	fine	sorted	Qoa
CUY-G-76	91	103	12	---	coarse	sorted	Qoa
CUY-G-76	103	115	12	---	fine	sorted	Qoa
CUY-G-76	115	128	13	---	coarse	sorted	Qoa
CUY-G-76	128	140	12	---	coarse	unsorted	Qoa
CUY-G-76	140	150	10	---	fine	sorted	Qoa
CUY-G-76	150	160	10	---	fine	unsorted	Qoa
CUY-G-76	160	170	10	---	fine	sorted	Qoa
CUY-G-76	170	180	10	---	fine	unsorted	Qoa
CUY-G-76	180	190	10	---	fine	sorted	Qoa
CUY-G-76	190	195	5	---	coarse	sorted	Qoa
CUY-G-76	195	223	28	---	fine	sorted	Qoa
CUY-G-34	0	2	2	---	fine	unsorted	Qya

CUY-G-34	2	20	18	---	fine	sorted	Qya
CUY-G-34	20	30	10	---	coarse	sorted	Qya
CUY-G-34	30	38	8	---	coarse	sorted	Qya
CUY-G-34	38	45	7	---	fine	sorted	Qya
CUY-G-34	45	70	25	---	fine	unsorted	Qya
CUY-G-34	70	85	15	---	coarse	sorted	Qya
CUY-G-34	85	90	5	---	fine	unsorted	Qya
CUY-G-34	90	97	7	---	coarse	sorted	Qya
CUY-G-34	97	100	3	---	fine	unsorted	Qya
CUY-G-34	100	105	5	---	coarse	sorted	Qya
CUY-G-34	105	120	15	---	fine	unsorted	Qya
CUY-G-34	120	130	10	---	coarse	sorted	Qya
CUY-G-34	130	155	25	---	coarse	sorted	Qya
CUY-G-34	155	160	5	---	fine	sorted	Qoa
CUY-G-34	160	170	10	---	fine	sorted	Qoa
CUY-G-34	170	191	21	---	coarse	unsorted	Qoa
CUY-G-34	191	205	14	---	coarse	unsorted	Qoa
CUY-G-34	205	225	20	---	coarse	unsorted	Qoa
CUY-G-34	225	230	5	---	fine	unsorted	Qoa
CUY-G-34	230	290	60	---	coarse	unsorted	Qoa
CUY-G-34	290	340	50	---	fine	sorted	Qoa
CUY-G-35	0	3	3	---	coarse	sorted	Qya
CUY-G-35	3	120	117	---	coarse	unsorted	Qya
CUY-G-35	120	135	15	---	fine	sorted	QTm
CUY-G-35	135	140	5	---	fine	unsorted	QTm
CUY-G-35	140	150	10	---	fine	sorted	QTm
CUY-G-35	150	185	35	---	coarse	unsorted	QTm
CUY-G-35	185	190	5	---	coarse	sorted	QTm
CUY-G-35	190	194	4	---	fine	sorted	QTm
CUY-G-35	194	197	3	---	coarse	sorted	QTm
CUY-G-35	197	205	8	---	fine	sorted	QTm
CUY-G-35	205	207	2	---	coarse	sorted	QTm
CUY-G-35	207	225	18	---	fine	sorted	QTm
CUY-G-35	225	227	2	---	coarse	sorted	QTm

CUY-G-35	227	244	17	---	fine	unsorted	QTm
CUY-G-35	244	290	46	---	coarse	unsorted	QTm
CUY-G-35	290	343	53	---	fine	unsorted	QTm
CUY-G-36	0	3	3	---	coarse	sorted	Qya
CUY-G-36	3	30	27	---	coarse	sorted	Qya
CUY-G-36	30	40	10	---	fine	unsorted	Qya
CUY-G-36	40	45	5	---	coarse	sorted	Qya
CUY-G-36	45	60	15	---	fine	unsorted	Qya
CUY-G-36	60	75	15	---	coarse	sorted	Qya
CUY-G-36	75	90	15	---	fine	sorted	Qya
CUY-G-36	90	100	10	---	coarse	sorted	Qya
CUY-G-36	100	120	20	---	fine	unsorted	Qya
CUY-G-36	120	360	240	---	fine	unsorted	Qya
CUY-G-36	360	440	80	---	coarse	sorted	Qya
CUY-G-36	440	505	65	---	coarse	unsorted	Qoa
CUY-G-36	505	603	98	---	coarse	unsorted	Qoa
CUY-G-37	0	1	1	---	fine	unsorted	Qya
CUY-G-37	1	45	44	---	fine	unsorted	Qya
CUY-G-37	45	60	15	---	fine	unsorted	Qoa
CUY-G-37	60	80	20	---	fine	sorted	Qoa
CUY-G-37	80	120	40	---	fine	sorted	Qoa
CUY-G-37	120	180	60	---	fine	unsorted	QTm
CUY-G-37	180	200	20	---	fine	unsorted	QTm
CUY-G-37	200	220	20	---	fine	sorted	QTm
CUY-G-37	220	260	40	---	fine	unsorted	QTm
CUY-G-37	260	280	20	---	coarse	sorted	QTm
CUY-G-37	280	300	20	---	fine	unsorted	QTm
CUY-G-37	300	320	20	---	fine	sorted	QTm
CUY-G-37	320	340	20	---	fine	sorted	QTm
CUY-G-37	340	365	25	---	fine	sorted	QTm
CUY-G-37	365	380	15	---	fine	unsorted	QTm
CUY-G-37	380	540	160	---	fine	sorted	QTm
CUY-35	0	20	20	---	coarse	sorted	Qya
CUY-35	20	132	112	---	coarse	unsorted	Qya

CUY-35	132	165	33	---	coarse	sorted	Qya
CUY-35	165	197	32	---	coarse	unsorted	Qya
CUY-35	197	275	78	---	coarse	unsorted	Qoa
CUY-35	275	302	27	---	coarse	unsorted	Qoa
CUY-G-77	0	51	51	---	coarse	unsorted	Qoa
CUY-G-77	51	62	11	---	coarse	sorted	Qoa
CUY-G-77	62	76	14	---	fine	unsorted	Qoa
CUY-G-77	76	100	24	---	coarse	unsorted	Qoa
CUY-G-77	100	170	70	---	fine	unsorted	Qoa
CUY-G-77	170	295	125	---	fine	unsorted	Qoa
CUY-G-77	295	310	15	---	coarse	unsorted	Qoa
CUY-G-77	310	327	17	---	fine	unsorted	Qoa
CUY-G-77	327	374	47	---	coarse	unsorted	Qoa
CUY-G-77	374	408	34	---	fine	unsorted	Qoa
CUY-G-77	408	451	43	---	coarse	unsorted	Qoa
CUY-G-77	451	473	22	---	fine	unsorted	Qoa
CUY-G-77	473	508	35	---	coarse	unsorted	Qoa
CUY-G-77	508	568	60	---	fine	unsorted	Qoa
CUY-G-77	568	614	46	---	fine	sorted	Qoa
CUY-G-77	614	650	36	---	fine	unsorted	Qoa
CUY-G-77	650	677	27	---	fine	sorted	Qoa
CUY-G-77	677	745	68	---	coarse	unsorted	Qoa
CUY-G-78	0	124	124	---	coarse	unsorted	Qya
CUY-G-78	124	198	74	---	fine	unsorted	Qya
CUY-G-78	198	312	114	---	fine	unsorted	Qya
CUY-G-78	312	360	48	---	fine	unsorted	Qya
CUY-G-78	360	408	48	---	coarse	unsorted	Qya
CUY-G-78	408	440	32	---	fine	sorted	Qya
CUY-G-78	440	476	36	---	fine	sorted	Qoa
CUY-G-78	476	602	126	---	fine	unsorted	Qoa
CUY-G-78	602	654	52	---	fine	unsorted	Qoa
CUY-G-78	654	676	22	---	coarse	unsorted	Qoa
CUY-G-78	676	719	43	---	fine	sorted	Qoa
CUY-G-78	719	775	56	---	coarse	unsorted	Qoa

CUY-G-78	775	834	59	---	fine	sorted	Qoa
CUY-G-78	834	892	58	---	fine	unsorted	Qoa
CUY-G-78	892	973	81	---	fine	unsorted	Qoa
CUY-G-78	973	1,024	51	---	coarse	unsorted	Qoa
CUY-G-78	1,024	1,100	76	---	fine	unsorted	Qoa
CUY-G-39	0	35	35	---	coarse	unsorted	Qya
CUY-G-39	35	210	175	---	coarse	unsorted	Qya
CUY-G-39	210	214	4	---	fine	sorted	QTm
CUY-G-39	214	229	15	---	coarse	unsorted	QTm
CUY-G-39	229	236	7	---	fine	unsorted	QTm
CUY-G-39	236	241	5	---	coarse	unsorted	QTm
CUY-G-39	241	248	7	---	fine	unsorted	QTm
CUY-G-40	0	40	40	---	coarse	unsorted	Qya
CUY-G-40	40	90	50	---	coarse	unsorted	Qya
CUY-G-40	90	120	30	---	fine	unsorted	Qya
CUY-G-40	120	130	10	---	fine	sorted	Qya
CUY-G-40	130	140	10	---	fine	unsorted	Qya
CUY-G-40	140	170	30	---	coarse	unsorted	Qya
CUY-G-40	170	180	10	---	coarse	unsorted	Qya
CUY-G-40	180	230	50	---	fine	unsorted	Qya
CUY-G-40	230	240	10	---	fine	unsorted	Qya
CUY-G-40	240	270	30	---	fine	sorted	Qya
CUY-G-41	0	224	224	---	coarse	unsorted	Qya
CUY-G-41	224	256	32	---	coarse	unsorted	Qya
CUY-G-41	256	269	13	---	coarse	unsorted	Qoa
CUY-G-41	269	376	107	---	coarse	unsorted	Qoa
CUY-G-41	376	493	117	---	coarse	unsorted	Qoa
CUY-G-41	493	584	91	---	fine	unsorted	QTm
CUY-G-41	584	670	86	---	coarse	unsorted	QTm
CUY-G-41	670	737	67	---	fine	unsorted	QTm
CUY-G-41	737	811	74	---	coarse	unsorted	QTm
CUY-G-41	811	920	109	---	fine	unsorted	QTm
CUY-G-41	920	1,061	141	---	coarse	unsorted	QTm
CUY-G-41	1,061	1,125	64	---	coarse	unsorted	QTm

CUY-G-42	0	70	70	---	coarse	unsorted	QTm
CUY-G-42	70	131	61	---	coarse	unsorted	Qya
CUY-G-42	131	204	73	---	fine	unsorted	Qya
CUY-G-42	204	233	29	---	fine	unsorted	Qya
CUY-G-42	233	377	144	---	fine	unsorted	Qoa
CUY-G-42	377	482	105	---	coarse	unsorted	QTm
CUY-G-42	482	545	63	---	coarse	unsorted	QTm
CUY-G-42	545	580	35	---	fine	sorted	QTm
CUY-G-42	580	631	51	---	coarse	unsorted	QTm
CUY-G-42	631	774	143	---	fine	unsorted	QTm
CUY-G-42	774	800	26	---	coarse	unsorted	QTm
CUY-G-42	800	854	54	---	fine	unsorted	QTm
CUY-G-42	854	935	81	---	coarse	unsorted	QTm
CUY-G-42	935	953	18	---	fine	unsorted	QTm
CUY-G-42	953	1,019	66	---	coarse	unsorted	QTm
CUY-G-42	1,019	1,035	16	---	fine	unsorted	QTm
CUY-G-42	1,035	1,081	46	---	coarse	unsorted	QTm
CUY-G-42	1,081	1,125	44	---	fine	unsorted	QTm
CUY-G-42	1,125	1,165	40	---	coarse	unsorted	QTm
CUY-G-43	0	17	17	---	fine	unsorted	Qya
CUY-G-43	17	124	107	---	coarse	unsorted	Qya
CUY-G-43	124	165	41	---	fine	unsorted	Qya
CUY-G-43	165	210	45	---	coarse	unsorted	Qya
CUY-G-43	210	220	10	---	fine	unsorted	Qya
CUY-G-38	0	264	264	---	coarse	unsorted	Qoa
CUY-G-38	264	292	28	---	fine	sorted	Qoa
CUY-G-38	292	347	55	---	coarse	unsorted	Qoa
CUY-G-38	347	402	55	---	fine	sorted	Qoa
CUY-G-38	402	453	51	---	coarse	unsorted	Qoa
CUY-G-38	453	499	46	---	fine	unsorted	Qoa
CUY-G-38	499	790	291	---	fine	unsorted	QTm
CUY-G-38	790	844	54	---	coarse	unsorted	QTm
CUY-G-38	844	1,200	356	---	fine	unsorted	QTm
PT-18	0	86	86	---	fine	unsorted	Qya

PT-18	86	124	38	---	coarse	unsorted	Qya
PT-18	124	217	93	---	fine	unsorted	Qya
PT-18	217	269	52	---	coarse	unsorted	Qya
PT-18	269	295	26	---	fine	unsorted	Qya
PT-18	295	328	33	---	coarse	unsorted	Qya
PT-18	328	342	14	---	fine	unsorted	Qya
PT-18	342	370	28	---	coarse	unsorted	Qya
PT-18	370	398	28	---	fine	unsorted	Qya
PT-18	398	487	89	---	coarse	unsorted	Qya
PT-18	487	528	41	---	fine	unsorted	Qya
PT-18	528	551	23	---	fine	unsorted	Qoa
PT-18	551	598	47	---	coarse	unsorted	Qoa
PT-18	598	652	54	---	fine	unsorted	Qoa
PT-18	652	684	32	---	fine	unsorted	Qoa
PT-18	684	709	25	---	coarse	unsorted	Qoa
PT-18	709	748	39	---	fine	unsorted	Qoa
PT-18	748	803	55	---	coarse	unsorted	Qoa
PT-18	803	829	26	---	fine	unsorted	Qoa
PT-18	829	851	22	---	coarse	unsorted	Qoa
PT-18	851	900	49	---	fine	unsorted	Qoa
PT-18	900	921	21	---	coarse	unsorted	Qoa
PT-18	921	934	13	---	fine	unsorted	Qoa
PT-18	934	949	15	---	coarse	unsorted	Qoa
PT-18	949	990	41	---	fine	unsorted	Qoa
PT-18	990	1,002	12	---	coarse	unsorted	Qoa
PT-18	1,002	1,026	24	---	fine	unsorted	Qoa
PT-18	1,026	1,037	11	---	coarse	unsorted	Qoa
PT-18	1,037	1,062	25	---	coarse	unsorted	QTm
PT-18	1,062	1,093	31	---	fine	unsorted	QTm
PT-18	1,093	1,137	44	---	fine	unsorted	QTm
PT-18	1,137	1,178	41	---	coarse	unsorted	QTm
PT-18	1,178	1,205	27	---	fine	unsorted	QTm
CUY-G-44	0	157	157	---	coarse	unsorted	Qya
CUY-G-44	157	246	89	---	coarse	unsorted	Qya

CUY-G-44	246	357	111	---	coarse	unsorted	Qya
CUY-G-44	357	390	33	---	fine	unsorted	Qya
CUY-G-44	390	466	76	---	coarse	unsorted	Qya
CUY-G-44	466	546	80	---	coarse	unsorted	Qoa
CUY-G-44	546	585	39	---	fine	unsorted	Qoa
CUY-G-44	585	624	39	---	coarse	unsorted	Qoa
CUY-G-44	624	666	42	---	fine	unsorted	Qoa
CUY-G-44	666	753	87	---	coarse	unsorted	Qoa
CUY-G-44	753	780	27	---	fine	unsorted	Qoa
CUY-G-44	780	876	96	---	coarse	unsorted	Qoa
CUY-G-44	876	927	51	---	fine	unsorted	Qoa
CUY-G-44	927	949	22	---	coarse	unsorted	Qoa
CUY-G-44	949	958	9	---	fine	unsorted	Qoa
CUY-G-44	958	1,026	68	---	coarse	unsorted	Qoa
CUY-G-44	1,026	1,041	15	---	fine	unsorted	Qoa
CUY-G-44	1,041	1,088	47	---	coarse	unsorted	Qoa
CUY-G-44	1,088	1,127	39	---	fine	unsorted	Qoa
CUY-G-44	1,127	1,143	16	---	coarse	unsorted	Qoa
CUY-G-44	1,143	1,200	57	---	fine	unsorted	Qoa
CUY-G-79	0	8	8	---	coarse	unsorted	Qoa
CUY-G-79	8	19	11	---	fine	unsorted	Qoa
CUY-G-79	19	27	8	---	fine	unsorted	Qoa
CUY-G-79	27	31	4	---	fine	unsorted	Qoa
CUY-G-79	31	38	7	---	coarse	unsorted	Qoa
CUY-G-79	38	41	3	---	fine	unsorted	Qoa
CUY-G-79	41	46	5	---	fine	sorted	Qoa
CUY-G-79	46	60	14	---	fine	unsorted	Qoa
CUY-G-79	60	62	2	---	coarse	unsorted	Qoa
CUY-G-79	62	86	24	---	fine	sorted	Qoa
CUY-G-79	86	100	14	---	fine	unsorted	Qoa
CUY-G-79	100	104	4	---	coarse	unsorted	Qoa
CUY-G-79	104	121	17	---	fine	unsorted	Qoa
CUY-G-79	121	137	16	---	coarse	unsorted	Qoa
CUY-G-79	137	143	6	---	fine	sorted	Qoa

CUY-G-79	143	152	9	---	coarse	unsorted	Qoa
CUY-G-79	152	158	6	---	fine	unsorted	Qoa
CUY-G-79	158	166	8	---	fine	unsorted	Qoa
CUY-G-79	166	177	11	---	fine	sorted	Qoa
CUY-G-79	177	180	3	---	coarse	unsorted	Qoa
CUY-G-79	180	192	12	---	fine	unsorted	Qoa
CUY-G-79	192	208	16	---	coarse	unsorted	Qoa
CUY-G-79	208	214	6	---	fine	sorted	Qoa
CUY-G-79	214	218	4	---	fine	unsorted	Qoa
CUY-G-79	218	229	11	---	coarse	unsorted	Qoa
CUY-G-79	229	241	12	---	fine	unsorted	Qoa
CUY-G-79	241	246	5	---	coarse	sorted	Qoa
CUY-G-79	246	260	14	---	fine	unsorted	Qoa
CUY-G-79	260	263	3	---	coarse	sorted	Qoa
CUY-G-79	263	277	14	---	fine	unsorted	Qoa
CUY-G-79	277	282	5	---	fine	sorted	Qoa
CUY-G-79	282	288	6	---	coarse	sorted	Qoa
CUY-G-79	288	293	5	---	fine	unsorted	Qoa
CUY-G-79	293	336	43	---	fine	unsorted	Qoa
CUY-G-79	336	344	8	---	fine	sorted	Qoa
CUY-G-80	0	15	15	---	fine	sorted	QTm
CUY-G-80	15	260	245	---	fine	unsorted	QTm
CUY-G-80	260	265	5	---	coarse	sorted	QTm
CUY-G-80	265	520	255	---	fine	unsorted	QTm
CUY-G-45	0	20	20	---	coarse	unsorted	QTm
CUY-G-45	20	60	40	---	fine	unsorted	QTm
CUY-G-45	60	85	25	---	fine	unsorted	QTm
CUY-G-45	85	95	10	---	coarse	unsorted	QTm
CUY-G-45	95	120	25	---	fine	unsorted	QTm
CUY-G-45	120	180	60	---	fine	unsorted	QTm
CUY-G-45	180	300	120	---	fine	unsorted	QTm
CUY-G-45	300	360	60	---	fine	unsorted	QTm
CUY-G-45	360	430	70	---	coarse	unsorted	QTm
CUY-G-45	430	500	70	---	fine	unsorted	QTm

CUY-G-45	500	535	35	---	coarse	unsorted	QTm
CUY-G-45	535	660	125	---	fine	unsorted	QTm
CUY-G-45	660	720	60	---	coarse	unsorted	QTm
CUY-G-45	720	800	80	---	fine	sorted	QTm
CUY-G-46	0	20	20	---	coarse	unsorted	Qya
CUY-G-46	20	79	59	---	coarse	unsorted	Qya
CUY-G-46	79	107	28	---	coarse	unsorted	Qya
CUY-G-46	107	236	129	---	coarse	unsorted	Qya
CUY-G-46	236	262	26	---	coarse	unsorted	Qya
CUY-G-46	262	298	36	---	fine	unsorted	Qya
CUY-G-46	298	334	36	---	coarse	unsorted	Qya
CUY-G-46	334	356	22	---	fine	unsorted	Qya
CUY-G-46	356	449	93	---	coarse	unsorted	Qya
CUY-G-46	449	507	58	---	coarse	unsorted	Qoa
CUY-G-46	507	600	93	---	fine	unsorted	Qoa
CUY-G-46	600	619	19	---	coarse	unsorted	Qoa
CUY-G-46	619	643	24	---	fine	unsorted	Qoa
CUY-G-46	643	666	23	---	coarse	unsorted	Qoa
CUY-G-46	666	695	29	---	fine	unsorted	Qoa
CUY-G-46	695	736	41	---	coarse	unsorted	Qoa
CUY-G-46	736	763	27	---	fine	unsorted	Qoa
CUY-G-46	763	786	23	---	coarse	unsorted	Qoa
CUY-G-46	786	799	13	---	fine	unsorted	Qoa
CUY-G-46	799	838	39	---	coarse	unsorted	Qoa
CUY-G-46	838	847	9	---	fine	unsorted	Qoa
CUY-G-46	847	862	15	---	coarse	unsorted	Qoa
CUY-G-46	862	876	14	---	fine	unsorted	Qoa
CUY-G-46	876	912	36	---	coarse	unsorted	Qoa
CUY-G-46	912	920	8	---	fine	unsorted	Qoa
CUY-G-46	920	941	21	---	coarse	unsorted	Qoa
CUY-G-46	941	950	9	---	fine	unsorted	Qoa
CUY-G-46	950	1,076	126	---	coarse	unsorted	Qoa
CUY-G-46	1,076	1,101	25	---	fine	unsorted	Qoa
CUY-G-46	1,101	1,138	37	---	coarse	unsorted	Qoa

CUY-G-47	0	75	75	---	coarse	unsorted	Qya
CUY-G-47	75	139	64	---	coarse	unsorted	Qya
CUY-G-47	139	180	41	---	coarse	unsorted	Qya
CUY-G-47	180	200	20	---	coarse	unsorted	Qya
CUY-G-47	200	261	61	---	coarse	unsorted	Qya
CUY-G-47	261	290	29	---	coarse	unsorted	Qya
CUY-G-47	290	317	27	---	coarse	unsorted	Qya
CUY-G-47	317	348	31	---	coarse	unsorted	Qya
CUY-G-47	348	396	48	---	coarse	unsorted	Qya
CUY-G-47	396	404	8	---	coarse	unsorted	Qya
CUY-G-47	404	454	50	---	coarse	unsorted	Qoa
CUY-G-47	454	488	34	---	coarse	unsorted	Qoa
CUY-G-47	488	495	7	---	coarse	unsorted	Qoa
CUY-G-47	495	510	15	---	coarse	unsorted	QTm
CUY-G-47	510	600	90	---	coarse	unsorted	QTm
CUY-G-47	600	607	7	---	coarse	unsorted	QTm
CUY-G-47	607	643	36	---	coarse	unsorted	QTm
CUY-G-47	643	683	40	---	coarse	unsorted	QTm
CUY-G-47	683	709	26	---	coarse	unsorted	QTm
CUY-G-47	709	792	83	---	coarse	unsorted	QTm
CUY-G-47	792	797	5	---	coarse	unsorted	QTm
CUY-G-47	797	878	81	---	coarse	unsorted	QTm
CUY-G-47	878	891	13	---	coarse	unsorted	QTm
CUY-G-47	891	1,064	173	---	coarse	unsorted	QTm
CUY-G-47	1,064	1,075	11	---	coarse	unsorted	QTm
CUY-G-47	1,075	1,125	50	---	coarse	unsorted	QTm
CUY-G-47	1,125	1,186	61	---	fine	unsorted	QTm
CUY-G-47	1,186	1,220	34	---	coarse	unsorted	QTm
CUY-40	0	10	10	---	fine	unsorted	Qya
CUY-40	10	50	40	---	coarse	unsorted	Qya
CUY-40	50	100	50	---	coarse	unsorted	Qya
CUY-40	100	160	60	---	coarse	sorted	Qya
CUY-40	160	200	40	---	coarse	unsorted	Qya
CUY-40	200	240	40	---	coarse	unsorted	Qya

CUY-40	240	255	15	---	coarse	unsorted	QTm
CUY-40	255	275	20	---	fine	sorted	QTm
CUY-G-48	0	40	40	---	fine	sorted	Qya
CUY-G-48	40	90	50	---	coarse	unsorted	Qya
CUY-G-48	90	110	20	---	coarse	unsorted	Qya
CUY-G-48	110	190	80	---	fine	sorted	Qya
CUY-G-48	190	210	20	---	fine	sorted	Qya
CUY-G-48	210	230	20	---	coarse	unsorted	Qya
CUY-G-48	230	310	80	---	fine	sorted	Qya
CUY-G-48	310	330	20	---	coarse	unsorted	Qya
CUY-G-48	330	400	70	---	fine	sorted	Qya
CUY-G-48	400	466	66	---	coarse	unsorted	Qya
CUY-G-48	466	520	54	---	coarse	unsorted	Qoa
CUY-G-48	520	530	10	---	fine	sorted	Qoa
CUY-G-48	530	540	10	---	coarse	unsorted	Qoa
CUY-G-48	540	590	50	---	fine	sorted	Qoa
CUY-G-48	590	902	312	---	fine	unsorted	Qoa
CUY-G-48	902	1,220	318	---	fine	unsorted	QTm
CUY-G-49	0	70	70	---	coarse	unsorted	Qya
CUY-G-49	70	85	15	---	fine	sorted	Qya
CUY-G-49	85	175	90	---	coarse	unsorted	Qya
CUY-G-49	175	204	29	---	fine	unsorted	Qya
CUY-G-81	0	3	3	---	fine	unsorted	Qoa
CUY-G-81	3	10	7	---	coarse	unsorted	Qoa
CUY-G-81	10	15	5	---	coarse	sorted	Qoa
CUY-G-81	15	20	5	---	coarse	unsorted	Qoa
CUY-G-81	20	25	5	---	coarse	sorted	Qoa
CUY-G-81	25	45	20	---	coarse	unsorted	Qoa
CUY-G-81	45	50	5	---	coarse	sorted	Qoa
CUY-G-81	50	60	10	---	fine	sorted	Qoa
CUY-G-81	60	65	5	---	coarse	sorted	Qoa
CUY-G-81	65	130	65	---	fine	sorted	Qoa
CUY-G-81	130	170	40	---	coarse	sorted	Qoa
CUY-G-81	170	195	25	---	coarse	sorted	Qoa

CUY-G-81	195	210	15	---	fine	sorted	Qoa
CUY-G-81	210	225	15	---	coarse	sorted	Qoa
CUY-G-81	225	310	85	---	coarse	sorted	Qoa
CUY-G-81	310	330	20	---	coarse	sorted	Qoa
CUY-G-81	330	340	10	---	coarse	sorted	Qoa
CUY-G-81	340	380	40	---	coarse	sorted	Qoa
CUY-G-81	380	440	60	---	coarse	sorted	Qoa
CUY-G-81	440	500	60	---	coarse	sorted	Qoa
CUY-G-81	500	520	20	---	coarse	sorted	Qoa
CUY-G-81	520	580	60	---	fine	sorted	Qoa
CUY-G-81	580	600	20	---	coarse	sorted	Qoa
CUY-G-81	600	610	10	---	fine	sorted	Qoa
CUY-G-81	610	620	10	---	fine	sorted	QTm
CUY-G-81	620	640	20	---	coarse	sorted	QTm
CUY-G-81	640	645	5	---	fine	sorted	QTm
CUY-G-81	645	650	5	---	coarse	sorted	QTm
CUY-G-81	650	660	10	---	fine	sorted	QTm
CUY-G-50	0	30	30	---	fine	unsorted	Qya
CUY-G-50	30	40	10	---	coarse	sorted	Qya
CUY-G-50	40	50	10	---	coarse	sorted	Qya
CUY-G-50	50	60	10	---	coarse	unsorted	Qya
CUY-G-50	60	80	20	---	fine	sorted	Qya
CUY-G-50	80	90	10	---	coarse	unsorted	Qya
CUY-G-50	90	140	50	---	fine	sorted	Qya
CUY-G-50	140	150	10	---	fine	unsorted	Qya
CUY-G-50	150	160	10	---	coarse	unsorted	Qya
CUY-G-50	160	170	10	---	coarse	unsorted	Qya
CUY-G-50	170	180	10	---	coarse	unsorted	Qya
CUY-G-50	180	190	10	---	coarse	sorted	Qya
CUY-G-50	190	200	10	---	fine	sorted	Qya
CUY-G-50	200	210	10	---	fine	unsorted	Qya
CUY-G-50	210	220	10	---	coarse	sorted	Qya
CUY-G-50	220	230	10	---	fine	sorted	Qya
CUY-G-50	230	246	16	---	coarse	sorted	Qya

CUY-G-50	246	260	14	---	coarse	sorted	Qoa
CUY-G-50	260	270	10	---	fine	unsorted	Qoa
CUY-G-50	270	280	10	---	fine	sorted	Qoa
CUY-G-50	280	300	20	---	fine	unsorted	Qoa
CUY-G-50	300	310	10	---	coarse	sorted	Qoa
CUY-G-50	310	320	10	---	fine	sorted	Qoa
CUY-G-50	320	330	10	---	fine	sorted	Qoa
CUY-G-50	330	340	10	---	fine	unsorted	Qoa
CUY-G-50	340	350	10	---	coarse	sorted	Qoa
CUY-G-50	350	360	10	---	fine	sorted	Qoa
CUY-G-50	360	370	10	---	fine	unsorted	Qoa
CUY-G-50	370	390	20	---	coarse	sorted	Qoa
CUY-G-50	390	420	30	---	fine	unsorted	Qoa
CUY-G-50	420	430	10	---	fine	sorted	Qoa
CUY-G-50	430	440	10	---	fine	unsorted	Qoa
CUY-G-50	440	450	10	---	fine	unsorted	Qoa
CUY-G-50	450	460	10	---	fine	unsorted	Qoa
CUY-G-50	460	470	10	---	coarse	unsorted	Qoa
CUY-G-50	470	480	10	---	coarse	sorted	Qoa
CUY-G-50	480	499	19	---	coarse	sorted	Qoa
CUY-G-50	499	510	11	---	fine	sorted	Qoa
CUY-G-50	510	520	10	---	fine	unsorted	Qoa
CUY-G-50	520	540	20	---	coarse	sorted	Qoa
CUY-G-50	540	560	20	---	fine	sorted	Qoa
CUY-G-50	560	570	10	---	fine	unsorted	Qoa
CUY-G-50	570	590	20	---	coarse	sorted	Qoa
CUY-G-50	590	640	50	---	fine	unsorted	Qoa
CUY-G-50	640	650	10	---	coarse	unsorted	Qoa
CUY-G-50	650	660	10	---	coarse	unsorted	Qoa
CUY-G-50	660	670	10	---	fine	unsorted	Qoa
CUY-G-50	670	690	20	---	coarse	sorted	Qoa
CUY-G-50	690	700	10	---	fine	sorted	Qoa
CUY-G-50	700	710	10	---	coarse	sorted	Qoa
CUY-G-50	710	720	10	---	fine	sorted	Qoa

CUY-G-50	720	730	10	---	fine	sorted	Qoa
CUY-G-50	730	740	10	---	coarse	sorted	Qoa
CUY-G-50	740	750	10	---	fine	sorted	Qoa
CUY-G-50	750	760	10	---	fine	unsorted	Qoa
CUY-G-50	760	770	10	---	fine	sorted	Qoa
CUY-G-50	770	840	70	---	fine	sorted	Qoa
CUY-G-82	0	30	30	---	fine	sorted	Qoa
CUY-G-82	30	60	30	---	fine	unsorted	Qoa
CUY-G-82	60	110	50	---	coarse	unsorted	Qoa
CUY-G-82	110	130	20	---	coarse	unsorted	Qoa
CUY-G-82	130	140	10	---	fine	unsorted	Qoa
CUY-G-82	140	150	10	---	fine	sorted	Qoa
CUY-G-82	150	180	30	---	fine	unsorted	Qoa
CUY-G-82	180	210	30	---	fine	sorted	Qoa
CUY-G-82	210	230	20	---	coarse	unsorted	Qoa
CUY-G-82	230	250	20	---	fine	unsorted	Qoa
CUY-G-82	250	280	30	---	fine	unsorted	Qoa
CUY-G-82	280	300	20	---	fine	unsorted	Qoa
CUY-G-82	300	370	70	---	coarse	unsorted	Qoa
CUY-G-82	370	410	40	---	fine	sorted	Qoa
CUY-G-82	410	430	20	---	coarse	unsorted	Qoa
CUY-G-82	430	460	30	---	fine	unsorted	Qoa
CUY-G-82	460	510	50	---	coarse	unsorted	Qoa
CUY-G-82	510	520	10	---	fine	sorted	Qoa
CUY-G-82	520	630	110	---	coarse	unsorted	Qoa
CUY-G-82	630	640	10	---	fine	unsorted	Qoa
CUY-G-82	640	699	59	---	coarse	unsorted	Qoa
CUY-G-82	699	830	131	---	coarse	unsorted	QTm
CUY-G-82	830	890	60	---	fine	unsorted	QTm
CUY-G-82	890	970	80	---	fine	unsorted	QTm
CUY-G-82	970	980	10	---	fine	sorted	QTm
CUY-G-82	980	988	8	---	coarse	sorted	QTm
CUY-G-52	0	20	20	---	coarse	unsorted	Qya
CUY-G-52	20	60	40	---	coarse	unsorted	Qya

CUY-G-52	60	70	10	---	fine	sorted	Qya
CUY-G-52	70	90	20	---	fine	sorted	Qya
CUY-G-52	90	120	30	---	coarse	unsorted	Qoa
CUY-G-52	120	130	10	---	fine	sorted	Qoa
CUY-G-52	130	140	10	---	coarse	sorted	Qoa
CUY-G-52	140	150	10	---	fine	sorted	Qoa
CUY-G-52	150	200	50	---	coarse	unsorted	Qoa
CUY-G-52	200	210	10	---	fine	sorted	Qoa
CUY-G-52	210	220	10	---	coarse	unsorted	Qoa
CUY-G-52	220	240	20	---	coarse	sorted	Qoa
CUY-G-52	240	260	20	---	coarse	unsorted	Qoa
CUY-G-52	260	270	10	---	fine	unsorted	Qoa
CUY-G-52	270	300	30	---	coarse	unsorted	Qoa
CUY-G-52	300	310	10	---	fine	sorted	Qoa
CUY-G-52	310	340	30	---	coarse	sorted	Qoa
CUY-G-52	340	370	30	---	fine	unsorted	Qoa
CUY-G-52	370	400	30	---	coarse	unsorted	Qoa
CUY-G-52	400	440	40	---	coarse	unsorted	Qoa
CUY-G-52	440	460	20	---	fine	sorted	Qoa
CUY-G-52	460	480	20	---	fine	unsorted	Qoa
CUY-G-52	480	500	20	---	fine	sorted	Qoa
CUY-G-52	500	530	30	---	coarse	unsorted	Qoa
CUY-G-52	530	540	10	---	fine	sorted	Qoa
CUY-G-52	540	550	10	---	fine	unsorted	Qoa
CUY-G-52	550	560	10	---	fine	sorted	Qoa
CUY-G-52	560	580	20	---	coarse	unsorted	Qoa
CUY-G-52	580	590	10	---	fine	sorted	Qoa
CUY-G-52	590	620	30	---	coarse	unsorted	Qoa
CUY-G-52	620	630	10	---	fine	unsorted	Qoa
CUY-G-52	630	650	20	---	coarse	unsorted	Qoa
CUY-G-52	650	710	60	---	coarse	unsorted	Qoa
CUY-G-52	710	740	30	---	fine	sorted	Qoa
CUY-G-52	740	760	20	---	coarse	unsorted	Qoa
CUY-G-52	760	770	10	---	fine	unsorted	Qoa

CUY-G-52	770	780	10	---	fine	unsorted	Qoa
CUY-G-52	780	820	40	---	fine	sorted	Qoa
CUY-G-52	820	850	30	---	fine	unsorted	Qoa
CUY-G-52	850	890	40	---	fine	unsorted	Qoa
CUY-G-52	890	910	20	---	fine	sorted	Qoa
CUY-G-52	910	940	30	---	coarse	unsorted	Qoa
CUY-G-52	940	970	30	---	fine	sorted	Qoa
CUY-G-53	0	40	40	---	fine	unsorted	Qya
CUY-G-53	40	140	100	---	coarse	sorted	Qya
CUY-G-53	140	150	10	---	fine	sorted	Qya
CUY-G-53	150	195	45	---	coarse	sorted	Qya
CUY-G-53	195	200	5	---	fine	sorted	Qya
CUY-G-53	200	295	95	---	coarse	sorted	Qya
CUY-G-53	295	305	10	---	fine	sorted	Qya
CUY-G-53	305	345	40	---	coarse	sorted	Qya
CUY-G-53	345	350	5	---	fine	sorted	Qya
CUY-G-53	350	443	93	---	coarse	sorted	Qya
CUY-G-53	443	530	87	---	coarse	sorted	Qoa
CUY-G-53	530	555	25	---	fine	sorted	Qoa
CUY-G-53	555	630	75	---	coarse	sorted	Qoa
CUY-G-53	630	640	10	---	fine	sorted	Qoa
CUY-G-53	640	715	75	---	coarse	sorted	Qoa
CUY-G-53	715	740	25	---	fine	sorted	Qoa
CUY-G-53	740	760	20	---	coarse	sorted	Qoa
CUY-G-53	760	770	10	---	fine	sorted	Qoa
CUY-G-53	770	890	120	---	coarse	sorted	Qoa
CUY-G-53	890	895	5	---	fine	sorted	Qoa
CUY-G-53	895	920	25	---	coarse	sorted	Qoa
CUY-G-53	920	930	10	---	fine	sorted	Qoa
CUY-G-53	930	1,000	70	---	coarse	sorted	Qoa
CUY-G-53	1,000	1,020	20	---	fine	unsorted	Qoa
CUY-G-54	0	8	8	---	fine	unsorted	Qya
CUY-G-54	8	240	232	---	coarse	unsorted	Qya
CUY-G-54	240	270	30	---	fine	unsorted	QTm

CUY-G-55	0	20	20	---	fine	unsorted	Qya
CUY-G-55	20	245	225	---	coarse	unsorted	Qya
CUY-G-55	245	275	30	---	coarse	unsorted	QTm
CUY-G-83	0	15	15	---	fine	unsorted	QTm
CUY-G-83	15	25	10	---	fine	sorted	QTm
CUY-G-83	25	30	5	---	coarse	sorted	QTm
CUY-G-83	30	45	15	---	coarse	sorted	QTm
CUY-G-83	45	60	15	---	coarse	unsorted	QTm
CUY-G-83	60	75	15	---	coarse	unsorted	QTm
CUY-G-83	75	90	15	---	fine	sorted	QTm
CUY-G-83	90	115	25	---	coarse	sorted	QTm
CUY-G-83	115	120	5	---	fine	sorted	QTm
CUY-G-83	120	135	15	---	coarse	sorted	QTm
CUY-G-83	135	140	5	---	fine	sorted	QTm
CUY-G-83	140	155	15	---	coarse	unsorted	QTm
CUY-G-83	155	160	5	---	fine	sorted	QTm
CUY-G-83	160	165	5	---	coarse	sorted	QTm
CUY-G-83	165	175	10	---	fine	sorted	QTm
CUY-G-83	175	185	10	---	coarse	sorted	QTm
CUY-G-83	185	190	5	---	fine	sorted	QTm
CUY-G-83	190	210	20	---	fine	unsorted	QTm
CUY-G-56	0	20	20	---	coarse	unsorted	Qoa
CUY-G-56	20	25	5	---	fine	unsorted	Qoa
CUY-G-56	25	42	17	---	fine	unsorted	Qoa
CUY-G-56	42	110	68	---	coarse	unsorted	Qoa
CUY-G-56	110	122	12	---	fine	unsorted	Qoa
CUY-G-56	122	127	5	---	fine	unsorted	Qoa
CUY-G-56	127	161	34	---	fine	unsorted	Qoa
CUY-G-56	161	178	17	---	fine	unsorted	Qoa
CUY-G-56	178	203	25	---	fine	unsorted	Qoa
CUY-G-56	203	219	16	---	fine	unsorted	Qoa
CUY-G-56	219	420	201	---	fine	sorted	Qoa
CUY-G-57	0	50	50	---	nd	nd	Qya
CUY-G-57	50	70	20	---	fine	sorted	Qya

CUY-G-57	70	80	10	---	fine	unsorted	Qya
CUY-G-57	80	90	10	---	fine	sorted	Qya
CUY-G-57	90	110	20	---	fine	sorted	Qya
CUY-G-57	110	140	30	---	fine	unsorted	Qya
CUY-G-57	140	150	10	---	fine	sorted	Qya
CUY-G-57	150	180	30	---	fine	sorted	Qya
CUY-G-57	180	210	30	---	fine	sorted	Qya
CUY-G-57	210	220	10	---	fine	sorted	Qya
CUY-G-57	220	240	20	---	fine	unsorted	Qya
CUY-G-57	240	260	20	---	fine	sorted	Qya
CUY-G-57	260	270	10	---	coarse	unsorted	Qya
CUY-G-57	270	340	70	---	fine	sorted	Qya
CUY-G-57	340	350	10	---	fine	unsorted	Qya
CUY-G-57	350	360	10	---	fine	unsorted	Qya
CUY-G-57	360	370	10	---	fine	sorted	Qya
CUY-G-57	370	380	10	---	fine	unsorted	Qya
CUY-G-57	380	390	10	---	fine	sorted	Qya
CUY-G-57	390	410	20	---	fine	unsorted	Qya
CUY-G-57	410	420	10	---	fine	sorted	Qya
CUY-G-57	420	430	10	---	fine	sorted	Qya
CUY-G-57	430	480	50	---	fine	sorted	Qya
CUY-G-57	480	500	20	---	fine	unsorted	Qya
CUY-G-57	500	510	10	---	fine	unsorted	Qoa
CUY-G-57	510	530	20	---	fine	sorted	Qoa
CUY-G-57	530	540	10	---	coarse	unsorted	Qoa
CUY-G-57	540	560	20	---	fine	unsorted	Qoa
CUY-G-57	560	580	20	---	fine	sorted	Qoa
CUY-G-57	580	620	40	---	fine	unsorted	Qoa
CUY-G-57	620	630	10	---	fine	unsorted	Qoa
CUY-G-57	630	640	10	---	fine	unsorted	Qoa
CUY-G-57	640	660	20	---	fine	unsorted	Qoa
CUY-G-57	660	680	20	---	fine	sorted	Qoa
CUY-G-57	680	730	50	---	fine	sorted	Qoa
CUY-G-57	730	1,030	300	---	fine	sorted	Qoa

CUY-G-57	1,030	1,210	180	---	fine	sorted	QTm
CUY-G-58	0	60	60	---	coarse	unsorted	Qya
CUY-G-58	60	80	20	---	coarse	unsorted	Qya
CUY-G-58	80	90	10	---	coarse	unsorted	Qya
CUY-G-58	90	100	10	---	coarse	unsorted	Qya
CUY-G-58	100	110	10	---	coarse	unsorted	Qya
CUY-G-58	110	120	10	---	coarse	unsorted	Qya
CUY-G-58	120	140	20	---	coarse	unsorted	Qya
CUY-G-58	140	160	20	---	coarse	unsorted	Qya
CUY-G-58	160	170	10	---	coarse	unsorted	Qya
CUY-G-58	170	180	10	---	coarse	unsorted	Qya
CUY-G-58	180	190	10	---	coarse	unsorted	Qya
CUY-G-58	190	200	10	---	coarse	unsorted	Qya
CUY-G-58	200	220	20	---	coarse	sorted	Qya
CUY-G-58	220	240	20	---	coarse	unsorted	Qya
CUY-G-58	240	250	10	---	coarse	unsorted	Qya
CUY-G-58	250	260	10	---	coarse	unsorted	Qya
CUY-G-58	260	270	10	---	coarse	sorted	Qya
CUY-G-58	270	280	10	---	coarse	unsorted	Qya
CUY-G-58	280	289	9	---	coarse	sorted	Qya
CUY-G-58	289	310	21	---	coarse	sorted	Qoa
CUY-G-58	310	320	10	---	coarse	unsorted	Qoa
CUY-G-58	320	330	10	---	coarse	unsorted	Qoa
CUY-G-58	330	340	10	---	coarse	unsorted	Qoa
CUY-G-58	340	360	20	---	fine	unsorted	Qoa
CUY-G-58	360	370	10	---	fine	unsorted	Qoa
CUY-G-58	370	380	10	---	fine	unsorted	Qoa
CUY-G-58	380	400	20	---	fine	unsorted	Qoa
CUY-G-58	400	410	10	---	coarse	unsorted	Qoa
CUY-G-58	410	460	50	---	coarse	unsorted	Qoa
CUY-G-58	460	470	10	---	coarse	unsorted	Qoa
CUY-G-58	470	480	10	---	fine	unsorted	Qoa
CUY-G-58	480	500	20	---	fine	unsorted	Qoa
CUY-G-58	500	510	10	---	fine	unsorted	Qoa

CUY-G-58	510	520	10	---	fine	unsorted	Qoa
CUY-G-58	520	530	10	---	coarse	unsorted	Qoa
CUY-G-58	530	540	10	---	coarse	unsorted	Qoa
CUY-G-58	540	570	30	---	coarse	unsorted	Qoa
CUY-G-58	570	580	10	---	coarse	unsorted	Qoa
CUY-G-58	580	600	20	---	coarse	unsorted	Qoa
CUY-G-58	600	620	20	---	coarse	unsorted	Qoa
CUY-G-58	620	630	10	---	fine	unsorted	Qoa
CUY-G-58	630	650	20	---	fine	unsorted	Qoa
CUY-G-58	650	660	10	---	fine	unsorted	Qoa
CUY-G-58	660	680	20	---	fine	unsorted	Qoa
CUY-G-58	680	690	10	---	coarse	unsorted	Qoa
CUY-G-58	690	700	10	---	coarse	unsorted	Qoa
CUY-G-58	700	710	10	---	coarse	unsorted	Qoa
CUY-G-58	710	730	20	---	coarse	unsorted	Qoa
CUY-G-58	730	740	10	---	coarse	unsorted	Qoa
CUY-G-58	740	750	10	---	coarse	unsorted	Qoa
CUY-G-58	750	760	10	---	coarse	unsorted	Qoa
CUY-G-58	760	780	20	---	coarse	unsorted	Qoa
CUY-G-58	780	790	10	---	coarse	unsorted	Qoa
CUY-G-58	790	800	10	---	coarse	unsorted	Qoa
CUY-G-58	800	810	10	---	fine	unsorted	Qoa
CUY-G-58	810	820	10	---	fine	unsorted	Qoa
CUY-G-58	820	830	10	---	coarse	unsorted	Qoa
CUY-G-58	830	840	10	---	coarse	unsorted	Qoa
CUY-G-58	840	850	10	---	fine	unsorted	Qoa
CUY-G-58	850	860	10	---	fine	unsorted	Qoa
CUY-G-58	860	870	10	---	fine	unsorted	Qoa
CUY-G-58	870	880	10	---	coarse	unsorted	Qoa
CUY-G-58	880	890	10	---	coarse	unsorted	Qoa
CUY-G-58	890	910	20	---	fine	unsorted	Qoa
CUY-G-58	910	920	10	---	fine	unsorted	Qoa
CUY-G-58	920	930	10	---	fine	unsorted	Qoa
CUY-G-58	930	940	10	---	fine	unsorted	Qoa

CUY-G-58	940	950	10	---	coarse	unsorted	Qoa
CUY-G-58	950	960	10	---	fine	unsorted	Qoa
CUY-G-58	960	970	10	---	fine	unsorted	Qoa
CUY-G-58	970	980	10	---	fine	sorted	Qoa
CUY-G-59	0	110	110	---	coarse	unsorted	Qya
CUY-G-59	110	115	5	---	fine	sorted	Qya
CUY-G-59	115	135	20	---	coarse	sorted	Qya
CUY-G-59	135	137	2	---	fine	sorted	Qya
CUY-G-59	137	145	8	---	fine	sorted	Qya
CUY-G-59	145	248	103	---	fine	sorted	Qya
CUY-G-59	248	262	14	---	fine	sorted	Qya
CUY-G-59	262	300	38	---	fine	sorted	Qoa
CUY-G-60	0	6	6	---	fine	sorted	Qya
CUY-G-60	6	48	42	---	coarse	unsorted	Qya
CUY-G-60	48	55	7	---	fine	sorted	Qya
CUY-G-60	55	168	113	---	coarse	unsorted	Qya
CUY-G-60	168	173	5	---	fine	sorted	Qya
CUY-G-60	173	255	82	---	coarse	unsorted	Qya
CUY-G-60	255	260	5	---	fine	sorted	Qya
CUY-G-60	260	302	42	---	coarse	unsorted	Qya
CUY-G-60	302	365	63	---	coarse	unsorted	Qoa
CUY-G-60	365	440	75	---	fine	sorted	Qoa
CUY-G-60	440	503	63	---	coarse	unsorted	Qoa
CUY-G-60	503	515	12	---	fine	sorted	Qoa
CUY-G-60	515	561	46	---	coarse	unsorted	Qoa
CUY-G-60	561	587	26	---	coarse	unsorted	QTm
CUY-G-60	587	594	7	---	fine	sorted	QTm
CUY-G-60	594	676	82	---	coarse	unsorted	QTm
CUY-G-60	676	681	5	---	fine	sorted	QTm
CUY-G-60	681	760	79	---	coarse	unsorted	QTm
CUY-G-84	0	9	9	---	fine	sorted	QTm
CUY-G-84	9	20	11	---	fine	unsorted	QTm
CUY-G-84	20	32	12	---	coarse	unsorted	QTm
CUY-G-84	32	40	8	---	fine	unsorted	QTm

CUY-G-84	40	45	5	---	coarse	sorted	QTm
CUY-G-84	45	102	57	---	coarse	unsorted	QTm
CUY-G-84	102	120	18	---	coarse	unsorted	QTm
CUY-G-84	120	255	135	---	coarse	unsorted	QTm
CUY-G-84	255	265	10	---	coarse	unsorted	QTm
CUY-G-84	265	332	67	---	fine	unsorted	QTm
CUY-G-84	332	346	14	---	coarse	unsorted	QTm
CUY-G-84	346	420	74	---	fine	unsorted	QTm
CUY-G-84	420	436	16	---	coarse	unsorted	QTm
CUY-G-84	436	464	28	---	fine	unsorted	QTm
CUY-G-84	464	472	8	---	coarse	unsorted	QTm
CUY-G-84	472	475	3	---	fine	unsorted	QTm
CUY-G-84	475	478	3	---	coarse	unsorted	QTm
CUY-G-84	478	480	2	---	fine	unsorted	QTm
CUY-G-84	480	485	5	---	coarse	unsorted	QTm
CUY-G-84	485	490	5	---	fine	unsorted	QTm
CUY-G-84	490	496	6	---	coarse	unsorted	QTm
CUY-G-84	496	520	24	---	fine	unsorted	QTm
CUY-G-61	0	10	10	---	fine	unsorted	Qya
CUY-G-61	10	120	110	---	coarse	unsorted	Qya
CUY-G-61	120	160	40	---	coarse	sorted	Qya
CUY-G-85	0	3	3	---	fine	unsorted	Qoa
CUY-G-85	3	10	7	---	coarse	unsorted	Qoa
CUY-G-85	10	22	12	---	coarse	unsorted	Qoa
CUY-G-85	22	27	5	---	coarse	sorted	Qoa
CUY-G-85	27	95	68	---	fine	sorted	Qoa
CUY-G-85	95	105	10	---	coarse	sorted	Qoa
CUY-G-85	105	135	30	---	fine	sorted	Qoa
CUY-G-85	135	145	10	---	coarse	sorted	Qoa
CUY-G-85	145	160	15	---	fine	unsorted	Qoa
CUY-G-85	160	185	25	---	coarse	unsorted	Qoa
CUY-G-85	185	260	75	---	fine	unsorted	Qoa
CUY-G-85	260	295	35	---	coarse	sorted	Qoa
CUY-G-85	295	305	10	---	coarse	unsorted	Qoa

CUY-G-85	305	315	10	---	fine	unsorted	Qoa
CUY-G-85	315	325	10	---	coarse	unsorted	Qoa
CUY-G-85	325	335	10	---	fine	unsorted	Qoa
CUY-G-85	335	365	30	---	coarse	unsorted	Qoa
CUY-G-85	365	405	40	---	fine	unsorted	Qoa
CUY-G-85	405	443	38	---	coarse	sorted	QTm
CUY-G-85	443	500	57	---	coarse	sorted	QTm
CUY-G-86	0	4	4	---	coarse	sorted	Qoa
CUY-G-86	4	40	36	---	coarse	unsorted	Qoa
CUY-G-86	40	55	15	---	fine	sorted	Qoa
CUY-G-86	55	61	6	---	coarse	unsorted	Qoa
CUY-G-86	61	67	6	---	fine	sorted	Qoa
CUY-G-86	67	75	8	---	coarse	unsorted	Qoa
CUY-G-86	75	87	12	---	coarse	sorted	Qoa
CUY-G-86	87	97	10	---	fine	sorted	Qoa
CUY-G-86	97	118	21	---	coarse	sorted	Qoa
CUY-G-86	118	135	17	---	fine	sorted	Qoa
CUY-G-86	135	155	20	---	coarse	sorted	Qoa
CUY-G-86	155	173	18	---	fine	sorted	Qoa
CUY-G-86	173	187	14	---	coarse	sorted	Qoa
CUY-G-86	187	198	11	---	fine	sorted	Qoa
CUY-G-86	198	510	312	---	fine	unsorted	Qoa
CUY-G-87	0	4	4	---	coarse	sorted	Qoa
CUY-G-87	4	87	83	---	coarse	unsorted	Qoa
CUY-G-87	87	360	273	---	fine	sorted	Qoa
CUY-G-87	360	369	9	---	coarse	unsorted	Qoa
CUY-G-87	369	575	206	---	fine	sorted	Qoa
CUY-G-87	575	585	10	---	coarse	unsorted	Qoa
CUY-G-87	585	608	23	---	fine	sorted	Qoa
CUY-G-62	0	50	50	---	coarse	sorted	Qoa
CUY-G-62	50	100	50	---	coarse	unsorted	Qya
CUY-G-62	100	125	25	---	coarse	unsorted	Qya
CUY-G-62	125	155	30	---	fine	unsorted	Qya
CUY-G-62	155	175	20	---	coarse	sorted	Qya

CUY-G-62	175	235	60	---	coarse	unsorted	QTm
CUY-G-62	235	305	70	---	fine	unsorted	QTm
CUY-G-62	305	335	30	---	coarse	unsorted	QTm
CUY-G-62	335	380	45	---	fine	unsorted	QTm
CUY-G-62	380	400	20	---	fine	sorted	QTm
CUY-G-63	0	100	100	---	fine	sorted	Qya
CUY-G-63	100	220	120	---	coarse	sorted	Qya
CUY-G-63	220	230	10	---	coarse	unsorted	Qya
CUY-G-63	230	240	10	---	fine	sorted	Qya
CUY-G-63	240	245	5	---	coarse	unsorted	Qya
CUY-G-63	245	260	15	---	coarse	unsorted	Qoa
CUY-G-63	260	280	20	---	coarse	unsorted	Qoa
CUY-G-63	280	300	20	---	coarse	unsorted	Qoa
CUY-G-63	300	320	20	---	coarse	unsorted	Qoa
CUY-G-63	320	410	90	---	fine	unsorted	Qoa
CUY-G-63	410	420	10	---	coarse	sorted	Qoa
CUY-G-63	420	440	20	---	fine	sorted	Qoa
CUY-G-63	440	480	40	---	fine	sorted	Qoa
CUY-G-63	480	520	40	---	fine	unsorted	Qoa
CUY-G-63	520	560	40	---	coarse	unsorted	Qoa
10/24-19F1	0	15	15	surface sand and gravel	fine	unsorted	Qya
10/24-19F1	15	137	152	sand and gravel	coarse	unsorted	Qya
10/24-19F1	137	177	40	sand and gravel	coarse	unsorted	Qoa
10/24-19F1	177	225	48	sand and gravel	coarse	unsorted	QTm
10/24-19F1	225	240	15	clay, sandy	fine	sorted	QTm
10/24-19F1	240	410	170	sand, gravel, and boulders	coarse	unsorted	QTm
10/24-19F1	410	485	75	gravel and boulders	coarse	unsorted	QTm
10/24-19F1	485	675	190	clay, gravel and boulders	fine	unsorted	QTm
10/24-19F1	675	811	136	gravel and boulders	coarse	unsorted	QTm
10/25-14Q1	0	42	42	surface sand	fine	sorted	Qya
10/25-14Q1	42	145	103	sand, gravel, and boulders	coarse	unsorted	Qya
10/25-14Q1	145	355	210	sandy clay, and streaks of gravel	fine	unsorted	Qoa
10/25-14Q1	355	506	151	sand, gravel and boulders	coarse	unsorted	Qoa

10/25-19P1	0	14	14	soil	fine	unsorted	Qya
10/25-19P1	14	17	3	sand	coarse	sorted	Qya
10/25-19P1	17	42	25	clay, sandy, hard	fine	sorted	Qya
10/25-19P1	42	60	18	clay, brown	fine	sorted	Qya
10/25-19P1	60	64	4	clay, sandy, and gravel, “free”	fine	unsorted	Qya
10/25-19P1	64	73	9	clay, sandy	fine	sorted	Qya
10/25-19P1	73	77	4	gravel	coarse	sorted	Qya
10/25-19P1	77	87	10	clay, sandy, and gravel	fine	unsorted	Qya
10/25-19P1	87	94	7	clay and small boulders	fine	unsorted	Qya
10/25-19P1	94	98	4	sand, gravel, and boulders	coarse	unsorted	Qya
10/25-19P1	98	101	3	boulders	coarse	sorted	Qya
10/25-19P1	101	115	14	sand and boulders	coarse	unsorted	Qya
10/25-19P1	115	120	5	sand	coarse	sorted	Qya
10/25-19P1	120	133	13	sand, gravel, and boulders	coarse	unsorted	Qya
10/25-19P1	133	144	11	clay, sandy, gravel, and boulders	fine	unsorted	Qya
10/25-19P1	144	201	57	clay, sandy, and gravel	fine	unsorted	Qya
10/25-19P1	201	207	6	sand and gravel	coarse	unsorted	Qya
10/25-19P1	207	230	23	clay, sandy, and gravel, “free streaks”	fine	unsorted	Qya
10/25-19P1	230	240	10	clay, sandy	fine	sorted	Qya
10/25-19P1	240	246	6	sand and gravel	coarse	unsorted	Qya
10/25-19P1	246	284	38	clay, sandy, gravel and boulders	fine	unsorted	Qya
10/25-19P1	284	289	5	clay, sticky	fine	sorted	Qya
10/25-19P1	289	320	31	clay, sandy, and gravel, “free streaks”	fine	unsorted	Qya
10/25-19P1	320	355	35	clay, sandy, gravel, and boulders	fine	unsorted	Qya
10/25-19P1	355	384	29	clay, sandy	fine	sorted	Qya
10/25-19P1	384	392	8	clay, sandy, and gravel, “free streaks”	fine	unsorted	Qya
10/25-19P1	392	411	19	clay, sandy, gravel, and boulders	fine	unsorted	Qya
10/25-19P1	411	418	7	clay, sandy	fine	sorted	Qya

10/25-20H1 (PT-09)	0	187	187	sand and coarse gravel	coarse	unsorted	Qya
10/25-20H1 (PT-09)	187	435	248	clay and coarse gravel	fine	unsorted	Qya
10/25-20H1 (PT-09)	435	585	150	gravel, coarse	coarse	sorted	Qya
10/25-20H1 (PT-09)	585	626	41	gravel, coarse with some clay	coarse	unsorted	Qoa
10/25-20H1 (PT-09)	626	648	22	gravel, coarse	coarse	sorted	Qoa
10/25-20H1 (PT-09)	648	656	8	clay and coarse gravel	fine	unsorted	Qoa
10/25-21G1	0	234	234	sand and coarse gravel	coarse	unsorted	Qya
10/25-21G1	234	314	80	clay and coarse gravel with streaks of sand	fine	unsorted	Qya
10/25-21G1	314	381	67	clay and coarse gravel	fine	unsorted	Qya
10/25-21G1	381	466	85	gravel, coarse	coarse	sorted	Qya
10/25-21G1	466	492	26	gravel, coarse	coarse	sorted	Qoa
10/25-21G1	492	567	75	clay and coarse gravel	fine	unsorted	Qoa
10/25-21G1	567	618	51	sand and coarse gravel	coarse	unsorted	Qoa
10/25-21G1	618	657	39	gravel, coarse	coarse	sorted	Qoa
10/25-22E1	0	19	19	sand and coarse gravel	coarse	unsorted	Qya
10/25-22E1	19	36	17	sand and boulders	coarse	unsorted	Qya
10/25-22E1	36	43	7	sand and coarse gravel	coarse	unsorted	Qya
10/25-22E1	43	100	57	sand and boulders	coarse	unsorted	Qya
10/25-22E1	100	159	59	sand and course gravel	coarse	unsorted	Qya
10/25-22E1	159	226	67	sand and boulders	coarse	unsorted	Qya
10/25-22E1	226	329	103	sand and coarse gravel	coarse	unsorted	Qya
10/25-22E1	329	380	51	sand and boulders	coarse	unsorted	Qya
10/25-22E1	380	410	30	sand and coarse gravel	coarse	unsorted	Qya
10/25-22E1	410	450	40	sand and boulders	coarse	unsorted	Qya
10/25-22E1	450	475	25	sand and coarse gravel	coarse	unsorted	Qya
10/25-22E1	475	514	39	sand and boulders	coarse	unsorted	Qya
10/25-22E1	514	605	91	sand and boulders with streaks of clay	coarse	unsorted	Qoa

10/25-22E1	605	659	54	sand and coarse gravel	coarse	unsorted	Qoa
10/25-22P1 (PT-13)	0	50	50	sand and coarse gravel	coarse	unsorted	Qya
10/25-22P1 (PT-13)	50	157	107	gravel, coarse	coarse	sorted	Qya
10/25-22P1 (PT-13)	157	455	298	gravel, coarse with streaks of clay	coarse	unsorted	Qya
10/25-22P1 (PT-13)	455	602	147	gravel, coarse	coarse	sorted	Qoa
10/25-22P1 (PT-13)	602	660	58	gravel, coarse, with streaks of clay	coarse	unsorted	Qoa
10/25-23E1 (PT-14)	0	52	52	surface soil	fine	unsorted	Qya
10/25-23E1 (PT-14)	52	202	150	sand, gravel and boulders	coarse	unsorted	Qya
10/25-23E1 (PT-14)	202	330	128	sand, gravel, and boulders with streaks of clay	coarse	unsorted	Qya
10/25-23E1 (PT-14)	330	380	50	sand and gravel, hard	coarse	unsorted	Qoa
10/25-23E1 (PT-14)	380	435	55	clay, sand, and gravel	fine	unsorted	Qoa
10/25-23E1 (PT-14)	435	486	51	clay, sand, gravel, and boulders	fine	unsorted	Qoa
10/25-23E1 (PT-14)	486	558	72	sand, hard, with streaks of clay	coarse	unsorted	Qoa
10/25-23E1 (PT-14)	558	600	42	clay, sandy, with streaks of gravel	fine	unsorted	Qoa
10/25-23E1 (PT-14)	600	640	40	sand, gravel and boulders	coarse	unsorted	Qoa
10/25-23E1 (PT-14)	640	747	107	clay, sand, and gravel	fine	unsorted	Qoa
10/25-23E1 (PT-14)	747	810	63	sand, gravel, and boulders	coarse	unsorted	Qoa
10/25-26E1	0	40	40	soil	fine	unsorted	Qya

10/25-26E1	40	131	91	gravel and boulders	coarse	unsorted	Qya
10/25-26E1	131	160	29	sand, sticky	coarse	unsorted	Qya
10/25-26E1	160	196	36	gravel, water-bearing	coarse	sorted	Qya
10/25-26E1	196	236	40	clay	fine	sorted	Qya
10/25-26E1	236	291	55	gravel, water-bearing	coarse	sorted	Qya
10/25-26E1	291	318	27	clay and boulders, hard	fine	unsorted	Qya
10/25-26E1	318	323	5	gravel, water-bearing	coarse	sorted	Qya
10/25-26E1	323	330	7	boulders	coarse	sorted	Qya
10/25-26E1	330	372	42	gravel, water-bearing	coarse	sorted	Qya
10/25-26E1	372	379	7	clay	fine	sorted	Qya
10/25-26E1	379	409	30	gravel, water-bearing	coarse	sorted	Qoa
10/25-26E1	409	424	15	sandstone	coarse	sorted	Qoa
10/25-26E1	424	467	43	gravel, water-bearing	coarse	sorted	Qoa
10/25-26E1	467	476	9	clay	fine	sorted	Qoa
10/25-26E1	476	492	16	gravel	coarse	sorted	Qoa
10/25-26E1	492	501	9	clay	fine	sorted	Qoa
10/25-26E1	501	563	62	clay, sandy	fine	sorted	Qoa
10/25-26E1	563	578	15	sand, “poor”, not water-bearing	coarse	unsorted	Qoa
10/25-26E1	578	612	34	clay and “poor” sand	fine	unsorted	Qoa
10/25-26E1	612	845	233	sand, water-bearing	coarse	sorted	Qoa
10/25-27G1 (PT-15)	0	121	121	sand with some gravel	coarse	unsorted	Qya
10/25-27G1 (PT-15)	121	413	292	gravel with streaks of clay	coarse	unsorted	Qya
10/25-27G1 (PT-15)	413	446	33	gravel	coarse	sorted	Qya
10/25-27G1 (PT-15)	446	549	103	clay and gravel	fine	unsorted	Qoa
10/25-27G1 (PT-15)	549	666	117	sand and gravel	coarse	unsorted	Qoa
10/25-30E1	0	52	52	soil	fine	unsorted	Qya
10/25-30E1	52	68	16	sand and boulders as much as 8 inches in diameter	coarse	unsorted	Qya
10/25-30E1	68	76	8	clay, sandy, soft, red	fine	sorted	Qya

10/25-30E1	76	78	2	sand and cobbles as much as 2 inches in diameter	coarse	unsorted	Qya
10/25-30E1	78	105	27	clay, sandy, red,	fine	sorted	Qya
10/25-30E1	105	108	3	sand and gravel as much as 1 inch in diameter	coarse	unsorted	Qya
10/25-30E1	108	149	41	clay, sandy, red	fine	sorted	Qya
10/25-30E1	149	161	12	sand, “muddy,” and cobbles as much as 6 inches in diameter	fine	unsorted	Qya
10/25-30E1	161	167	6	clay, sandy, red	fine	sorted	Qya
10/25-30E1	167	175	8	sand “muddy” and gravel	fine	unsorted	Qya
10/25-30E1	175	178	3	clay, sandy, red	fine	sorted	Qya
10/25-30E1	178	182	4	sand, “muddy,” and cobbles as much as 3 inches in diameter	fine	unsorted	Qya
10/25-30E1	182	193	11	clay, sandy, tough, brown	fine	sorted	Qya
10/25-30E1	193	217	24	clay, sandy, hard	fine	sorted	Qya
10/25-30E1	217	218	1	sand and cobbles as much as 3 inches in diameter	coarse	unsorted	Qya
10/25-30E1	218	219	1	sand, packed	coarse	sorted	Qya
10/25-30E1	219	223	4	sand and cobbles as much as 4 inches in diameter.	coarse	unsorted	Qya
10/25-30E1	223	251	28	clay, sandy, brown	fine	sorted	Qya
10/25-30E1	251	256	5	clay, tough, gray	fine	sorted	Qya
10/25-30E1	256	263	7	clay, red with gray streaks	fine	sorted	Qya
10/25-30E1	263	266	3	sand and gravel	coarse	unsorted	Qya
10/25-30E1	266	303	37	clay, tough, brown	fine	sorted	Qya
10/25-30E1	303	308	5	sand and cobbles as much as 3 inches in diameter	coarse	unsorted	Qya
10/25-30E1	308	328	20	clay, sandy, with gravel	fine	unsorted	Qya
10/25-30E1	328	333	5	clay, tough, red	fine	sorted	Qya
10/25-30E1	333	335	2	sand, coarse	coarse	sorted	Qya
10/25-30E1	335	358	23	clay, sandy, red	fine	sorted	Qya
10/25-30E1	358	360	2	sand, coarse	coarse	sorted	Qya
10/25-30E1	360	405	45	sand, packed	coarse	sorted	Qya
10/25-30E1	405	410	5	clay	fine	sorted	Qya
10/25-30E1	410	417	7	clay, tough, red	fine	sorted	Qya

10/25-30E1	417	424	7	sand, packed	coarse	sorted	Qya
10/25-30F1 (CUY-54)	0	15	15	soil	fine	unsorted	Qya
10/25-30F1 (CUY-54)	15	32	17	sand, packed, non water-bearing	coarse	sorted	Qya
10/25-30F1 (CUY-54)	32	35	3	sand, “free”	coarse	sorted	Qya
10/25-30F1 (CUY-54)	35	97	62	sand, packed, non water-bearing	coarse	sorted	Qya
10/25-30F1 (CUY-54)	97	161	64	sand and boulders	coarse	unsorted	Qya
10/25-30F1 (CUY-54)	161	170	9	clay, sandy	fine	sorted	Qya
10/25-30F1 (CUY-54)	170	180	10	sand and boulders	coarse	unsorted	Qya
10/25-30F1 (CUY-54)	180	210	30	clay with streaks of sand	fine	unsorted	Qya
10/25-30F1 (CUY-54)	210	227	17	sand, not water-bearing	coarse	sorted	Qya
10/25-30F1 (CUY-54)	227	243	16	clay	fine	sorted	Qya
10/25-30F1 (CUY-54)	243	248	5	sand and gravel	coarse	unsorted	Qya
10/25-30F1 (CUY-54)	248	260	12	clay with streaks of sand	fine	unsorted	Qya
10/25-30F1 (CUY-54)	260	274	14	clay	fine	sorted	Qya
10/25-30F1 (CUY-54)	274	282	8	sand and boulders	coarse	unsorted	Qya
10/25-30F1 (CUY-54)	282	296	14	clay with streaks of sand	fine	unsorted	Qya
10/25-30F1 (CUY-54)	296	335	39	clay with streaks of shale	fine	unsorted	Qya

10/25-30F1 (CUY-54)	335	341	6	boulders	coarse	sorted	Qya
10/25-30F1 (CUY-54)	341	356	15	shale with streaks of sand	fine	unsorted	Qya
10/25-30F1 (CUY-54)	356	362	6	sand and boulders	coarse	unsorted	Qya
10/25-30F1 (CUY-54)	362	376	14	gravel, cemented	coarse	sorted	Qya
10/25-30R1	0	30	30	soil	fine	unsorted	Qya
10/25-30R1	30	35	5	sand and boulders	coarse	unsorted	Qya
10/25-30R1	35	63	28	silt, packed	fine	sorted	Qya
10/25-30R1	63	74	11	sand, gravel and boulders	coarse	unsorted	Qya
10/25-30R1	74	99	25	clay, silty, soft	fine	sorted	Qya
10/25-30R1	99	138	39	sand, gravel, and boulders	coarse	unsorted	Qya
10/25-30R1	138	270	132	clay, yellow	fine	sorted	Qya
10/25-30R1	270	273	3	clay, sandy, soft	fine	sorted	Qya
10/25-30R1	273	277	4	clay, tough, yellow	fine	sorted	Qya
10/25-30R1	277	278	1	clay, sandy, soft	fine	sorted	Qya
10/25-30R1	278	282	4	clay, tough	fine	sorted	Qya
10/25-30R1	282	283	1	clay, sandy, soft	fine	sorted	Qya
10/25-30R1	283	287	4	clay, tough, yellow	fine	sorted	Qya
10/25-30R1	287	288	1	clay, sandy, soft	fine	sorted	Qya
10/25-30R1	288	292	4	clay, tough, yellow	fine	sorted	Qya
10/25-30R1	292	293	1	clay, sandy, soft	fine	sorted	Qya
10/25-30R1	293	297	4	clay, tough	fine	sorted	Qya
10/25-30R1	297	298	1	clay, sandy, soft	fine	sorted	Qya
10/25-30R1	298	301	3	clay, tough, yellow	fine	sorted	Qya
10/25-30R1	301	304	3	gravel and boulders	coarse	unsorted	Qya
10/25-30R1	304	305	1	sandstone	coarse	sorted	Qya
10/25-30R1	305	318	13	clay, sandy	fine	sorted	Qya
10/25-30R1	318	342	24	clay, gray	fine	sorted	Qya
10/25-30R1	342	354	12	clay, tough, yellow	fine	sorted	Qya
10/25-30R1	354	360	6	sand, gravel and boulders	coarse	unsorted	Qya
10/25-30R1	360	372	12	clay, tough, yellow	fine	sorted	Qya

10/25-31B1	0	15	15	soil	fine	unsorted	Qya
10/25-31B1	15	136	121	sand, not water-bearing	coarse	sorted	Qya
10/25-31B1	136	146	10	sand, free	coarse	sorted	Qya
10/25-31B1	146	170	24	clay, sandy	fine	sorted	Qya
10/25-31B1	170	180	10	sand, free	coarse	sorted	Qya
10/25-31B1	180	187	7	clay, sandy	fine	sorted	Qya
10/25-31B1	187	194	7	sand and boulders	coarse	unsorted	Qya
10/25-31B1	194	205	11	clay and sand, not water-bearing	fine	unsorted	Qya
10/25-31B1	205	208	3	cap rock	nd	nd	Qya
10/25-31B1	208	214	6	clay and boulders	fine	unsorted	Qya
10/25-31B1	214	220	6	sand, not water-bearing	coarse	sorted	Qya
10/25-31B1	220	224	4	clay	fine	sorted	Qya
10/25-31B1	224	236	12	clay and sand	fine	unsorted	Qya
10/25-31B1	236	266	30	sand, not water-bearing	coarse	sorted	Qya
10/25-31B1	266	270	4	clay	fine	sorted	Qya
10/25-31B1	270	276	6	sand and boulders	coarse	unsorted	Qya
10/25-31B1	276	282	6	sand, not water-bearing	coarse	sorted	Qya
10/25-31B1	282	297	15	clay and boulders	fine	unsorted	Qya
10/25-31B1	297	304	7	sandstone	coarse	sorted	Qya
10/25-31B1	304	310	6	gravel, cemented	coarse	sorted	Qya
10/25-31B1	310	320	10	sand and boulder	coarse	unsorted	Qya
10/25-31B1	320	340	20	clay, sand, and boulders	fine	unsorted	Qya
10/25-31B1	340	350	10	sand, fine	coarse	sorted	Qya
10/25-31B1	350	359	9	sand, not water-bearing	coarse	sorted	Qya
10/25-31H2 (CUY-G	0	150	150	silt	fine	sorted	Qoa
10/25-31H2 (CUY-G	150	157	7	clay, tough	fine	sorted	Qoa
10/25-31H2 (CUY-G	157	159	2	sand	coarse	sorted	Qoa
10/25-31H2 (CUY-G	159	297	138	clay	fine	sorted	Qoa
10/25-31H2 (CUY-G	297	299	2	gravel and boulders	coarse	unsorted	Qoa
10/25-31H2 (CUY-G	299	305	6	sandstone,	coarse	sorted	Qoa
10/25-31H2 (CUY-G	305	380	75	clay	fine	sorted	Qoa
10/25-31H2 (CUY-G	380	387	7	clay, soft	fine	sorted	Qoa
10/25-31H2 (CUY-G	387	404	17	clay	fine	sorted	Qoa

10/25-32C1	0	75	75	sandy loam	fine	unsorted	Qya
10/25-32C1	75	85	10	sand and gravel, water-bearing	coarse	unsorted	Qya
10/25-32C1	85	105	20	gravel, good	coarse	sorted	Qya
10/25-32C1	105	140	35	clay and sand	fine	unsorted	Qya
10/25-32C1	140	142	2	gravel	coarse	sorted	Qya
10/25-32C1	142	147	5	gravel, fine	coarse	sorted	Qya
10/25-32C1	147	194	47	clay and muck	fine	unsorted	Qya
10/25-32C1	194	200	6	sand and “good” gravel	coarse	unsorted	Qya
10/25-33D1 (PT-23)	0	60	60	soil	fine	unsorted	Qya
10/25-33D1 (PT-23)	60	142	82	sand and boulders as much as 6 inches in diameter	coarse	unsorted	Qya
10/25-33D1 (PT-23)	142	153	11	clay, sandy, soft	fine	sorted	Qya
10/25-33D1 (PT-23)	153	157	4	gravel and cobbles as much as 4 inches in diameter	coarse	unsorted	Qya
10/25-33D1 (PT-23)	157	171	14	clay, tough, red	fine	sorted	Qya
10/25-33D1 (PT-23)	171	175	4	gravel and cobbles as much as 2 inches in diameter	coarse	unsorted	Qya
10/25-33D1 (PT-23)	175	177	2	clay, red	fine	sorted	Qya
10/25-33D1 (PT-23)	177	183	6	gravel and boulders as much as 6 inches in diameter	coarse	unsorted	Qya
10/25-33D1 (PT-23)	183	195	12	clay, sandy, red	fine	sorted	Qya
10/25-33D1 (PT-23)	195	223	28	gravel and boulders as much as 6 inches in diameter	coarse	unsorted	Qya
10/25-33D1 (PT-23)	223	226	3	clay, sandy, red	fine	sorted	Qya
10/25-33D1 (PT-23)	226	241	15	gravel and boulders as much as 6 inches in diameter	coarse	unsorted	Qya

10/25-33D1 (PT-23)	241	244	3	clay, red	fine	sorted	Qya
10/25-33D1 (PT-23)	244	285	41	gravel and cobbles as much as 3 inches	coarse	unsorted	Qya
10/25-33D1 (PT-23)	285	297	12	clay, red	fine	sorted	Qya
10/25-33D1 (PT-23)	297	313	16	gravel and boulders as much as 6 inches in diameter	coarse	unsorted	Qya
10/25-33D1 (PT-23)	313	317	4	clay, red	fine	sorted	Qya
10/25-33D1 (PT-23)	317	324	7	gravel and cobbles as much as 3 inches in diameter	coarse	unsorted	Qya
10/25-33D1 (PT-23)	324	330	6	clay, tough, blue	fine	sorted	Qya
10/25-33D1 (PT-23)	330	354	24	gravel and boulders as much as 8 inches in diameter	coarse	unsorted	Qya
10/25-35C1	0	1	1	soil	fine	unsorted	Qya
10/25-35C1	1	2	1	boulders	coarse	sorted	Qya
10/25-35C1	2	9	7	clay, sandy	fine	sorted	Qya
10/25-35C1	9	10	1	boulders	coarse	sorted	Qya
10/25-35C1	10	52	42	clay, sandy	fine	sorted	Qya
10/25-35C1	52	69	17	sand and gravel	coarse	unsorted	Qya
10/25-35C1	69	79	10	boulders	coarse	sorted	Qya
10/25-35C1	79	91	12	gravel	coarse	sorted	Qya
10/25-35C1	91	94	3	clay, yellow	fine	sorted	Qya
10/25-35C1	94	99	5	gravel	coarse	sorted	Qya
10/25-35C1	99	136	37	gravel and boulders	coarse	unsorted	Qya
10/25-35C1	136	156	20	gravel with streaks of clay	coarse	unsorted	Qya
10/25-35C1	156	172	16	clay, yellow	fine	sorted	Qya
10/25-35C1	172	184	12	gravel	coarse	sorted	Qya
10/25-35C1	184	196	12	clay, yellow	fine	sorted	Qya
10/25-35C1	196	236	40	gravel	coarse	sorted	Qya
10/26-18F1 (CUY-56)	0	14	14	soil	fine	unsorted	Qya

10/26-18F1 (CUY-56)	14	22	8	boulders, as much as 8 inches in diameter not water-bearing	coarse	sorted	Qya
10/26-18F1 (CUY-56)	22	58	36	clay, sand and gravel streaks	fine	unsorted	Qya
10/26-18F1 (CUY-56)	58	60	2	gravel and boulders as much as 6 inches in diameter, water-bearing	coarse	unsorted	Qya
10/26-18F1 (CUY-56)	60	75	15	clay, sandy, yellow	fine	sorted	Qya
10/26-18F1 (CUY-56)	75	85	10	boulders, loose, an much as 10 inches in diameter	coarse	sorted	Qya
10/26-18F1 (CUY-56)	85	99	14	clay, yellow	fine	sorted	Qya
10/26-18F1 (CUY-56)	99	100	1	gravel and boulders an much as 6 inches in diameter	coarse	unsorted	Qya
10/26-18F1 (CUY-56)	100	112	12	clay, yellow	fine	sorted	Qya
10/26-18F1 (CUY-56)	112	114	2	gravel, coarse, as much as 0.5 inches in diameter	coarse	unsorted	Qya
10/26-18F1 (CUY-56)	114	133	19	clay, yellow	fine	sorted	Qya
10/26-18F1 (CUY-56)	133	135	2	sandstone	coarse	sorted	Qya
10/26-18F1 (CUY-56)	135	142	7	clay and boulders, brown	fine	unsorted	Qya
10/26-18F1 (CUY-56)	142	145	3	gravel as much as 1 inch in diameter	coarse	unsorted	Qya
10/26-18F1 (CUY-56)	145	150	5	sand and gravel, cemented	coarse	unsorted	Qya
10/26-18F1 (CUY-56)	150	151	1	cobbles as much as 4 inches in diameter	coarse	sorted	Qya
10/26-18F1 (CUY-56)	151	156	5	clay, brown	fine	sorted	Qya

10/26-18F1 (CUY-56)	156	158	2	gravel and cobbles as much as 3 inches in diameter	coarse	unsorted	Qya
10/26-18F1 (CUY-56)	158	180	22	clay, hard, brown with cobbles	fine	unsorted	Qoa
10/26-18F1 (CUY-56)	180	205	25	clay, blue	fine	sorted	Qoa
10/26-18F1 (CUY-56)	205	210	5	clay, yellow	fine	sorted	Qoa
10/26-18F1 (CUY-56)	210	217	7	clay, blue	fine	sorted	Qoa
10/26-18F1 (CUY-56)	217	228	11	clay, yellow	fine	sorted	Qoa
10/26-18F1 (CUY-56)	228	240	12	clay, tough, blue	fine	sorted	Qoa
10/26-21Q1	0	10	10	soil	fine	unsorted	Qya
10/26-21Q1	10	64	54	clay, sandy and boulders	fine	unsorted	Qya
10/26-21Q1	64	117	53	clay, sandy, yellow	fine	sorted	Qya
10/26-21Q1	117	126	9	clay, sandy and gravel; yellow	fine	unsorted	Qya
10/26-21Q1	126	150	24	clay, sandy, yellow	fine	sorted	Qya
10/26-21Q1	150	172	22	clay and boulders, yellow	fine	unsorted	Qya
10/26-21Q1	172	183	11	sand and gravel; not water-bearing,	coarse	unsorted	Qya
10/26-21Q1	183	236	53	clay, yellow	fine	sorted	Qya
10/26-21Q1	236	341	105	clay, yellow	fine	sorted	Qoa
10/26-21Q1	341	392	51	clay, yellow, with streaks of sand	fine	unsorted	Qoa
10/26-21Q1	392	520	128	clay and sand in streaks, yellow-gray	fine	unsorted	Qoa
10/26-21Q1	520	692	172	clay, sandy, gray-blue	fine	sorted	Qoa
10/26-21Q1	692	762	70	clay and sand in streaks, blue-gray	fine	unsorted	Qoa
10/26-21Q1	762	804	42	clay, gray, with streaks of sand	fine	unsorted	Qoa
10/26-21Q1	804	810	6	sand, white	coarse	sorted	Qoa
10/26-21Q1	810	860	50	clay, blue	fine	sorted	QTm

10/26-21Q1	860	865	5	sand	coarse	sorted	QTm
10/26-21Q1	865	963	98	clay, sandy, blue	fine	sorted	QTm
10/26-21Q1	963	970	7	sand, blue-white	coarse	sorted	QTm
10/26-21Q1	970	993	23	clay, blue	fine	sorted	QTm
10/26-22A1	0	5	5	soil	fine	unsorted	Qya
10/26-22A1	5	32	27	clay, sandy	fine	sorted	Qya
10/26-22A1	32	35	3	sand	coarse	sorted	Qya
10/26-22A1	35	69	34	clay, sandy	fine	sorted	Qya
10/26-22A1	69	79	10	clay, sandy, blue	fine	sorted	Qya
10/26-22A1	79	93	14	sand	coarse	sorted	Qya
10/26-22A1	93	181	88	clay, sandy, with streaks of sand	fine	unsorted	Qya
10/26-22A1	181	189	8	sand	coarse	sorted	Qya
10/26-22A1	189	210	21	“shale”	fine	sorted	Qya
10/26-22A1	210	216	6	sand	coarse	sorted	Qya
10/26-22A1	216	235	19	clay	fine	sorted	Qya
10/26-22A1	235	240	5	sand	coarse	sorted	Qya
10/26-22A1	240	251	11	clay	fine	sorted	Qya
10/26-22A1	251	257	6	sand	coarse	sorted	Qya
10/26-22A1	257	260	3	clay	fine	sorted	Qya
10/26-22A1	260	266	6	sand	coarse	sorted	Qya
10/26-22A1	266	281	15	clay and “shale”	fine	unsorted	Qya
10/26-22A1	281	288	7	sand	coarse	sorted	Qya
10/26-22A1	288	293	5	“shale”	fine	sorted	Qya
10/26-22A1	293	305	12	sand	coarse	sorted	Qya
10/26-22A1	305	328	23	clay	fine	sorted	Qya
10/26-22A1	328	333	5	sand	coarse	sorted	Qya
10/26-22A1	333	350	17	clay	fine	sorted	Qya
10/26-22A1	350	381	31	clay with streaks of sand	fine	unsorted	Qya
10/26-22A1	381	396	15	“shale”	fine	sorted	Qya
10/26-22A1	396	402	6	sand	coarse	sorted	Qya
10/26-22A1	402	422	20	clay with streaks of sand	fine	unsorted	Qya
10/26-22A1	422	423	1	“shale”	fine	sorted	Qya
10/26-22D1	0	15	15	soil	fine	unsorted	Qya

10/26-22D1	15	28	13	sand, not water-bearing	coarse	sorted	Qya
10/26-22D1	28	40	12	sand and gravel	coarse	unsorted	Qya
10/26-22D1	40	60	20	clay	fine	sorted	Qya
10/26-22D1	60	65	5	sand and gravel	coarse	unsorted	Qya
10/26-22D1	65	112	47	clay	fine	sorted	Qya
10/26-22D1	112	116	4	gravel, cemented	coarse	sorted	Qya
10/26-22D1	116	124	8	clay	fine	sorted	Qya
10/26-22D1	124	126	2	gravel, cemented	coarse	sorted	Qya
10/26-22D1	126	132	6	sand and gravel	coarse	unsorted	Qya
10/26-22D1	132	152	20	clay and boulders	fine	unsorted	Qya
10/26-22D1	152	160	8	clay	fine	sorted	Qya
10/26-22D1	160	170	10	clay and boulders	fine	unsorted	Qya
10/26-22D1	170	187	17	shale	fine	sorted	Qya
10/26-22D1	187	196	9	sand and gravel, “free”	coarse	unsorted	Qya
10/26-22D1	196	218	22	shale with streaks of sand	fine	unsorted	Qya
10/26-22D1	218	230	12	clay	fine	sorted	Qya
10/26-22D1	230	235	5	sand	coarse	sorted	Qya
10/26-22D1	235	322	87	clay with streaks of sand	fine	unsorted	Qya
10/26-22D1	322	326	4	gravel, cemented	coarse	sorted	Qya
10/26-22D1	326	334	8	clay, dry	fine	sorted	Qya
10/26-22D1	334	349	15	gravel, cemented	coarse	sorted	Qya
10/26-22D1	349	358	9	clay with streaks of sand	fine	unsorted	Qya
10/26-22D1	358	362	4	gravel, cemented	coarse	sorted	Qya
10/26-22D1	362	385	23	clay with streaks of sand	fine	unsorted	Qya
10/26-22D1	385	387	2	gravel, cemented	coarse	sorted	Qya
10/26-22D1	387	390	3	sand	coarse	sorted	Qya
10/26-22D1	390	404	14	clay and shale	fine	unsorted	Qya
10/26-22D1	404	407	3	gravel, cemented	coarse	sorted	Qya
10/26-22E1 (PT-38)	0	6	6	soil	fine	unsorted	Qya
10/26-22E1 (PT-38)	6	28	22	sand, dry	coarse	sorted	Qya
10/26-22E1 (PT-38)	28	30	2	clay	fine	sorted	Qya

10/26-22E1 (PT-38)	30	53	23	clay with streaks of sand	fine	unsorted	Qya
10/26-22E1 (PT-38)	53	56	3	gravel, cemented	coarse	sorted	Qya
10/26-22E1 (PT-38)	56	75	19	clay and sand	fine	unsorted	Qya
10/26-22E1 (PT-38)	75	78	3	shale and clay	fine	sorted	Qya
10/26-22E1 (PT-38)	78	85	7	clay with streaks of sand	fine	unsorted	Qya
10/26-22E1 (PT-38)	85	91	6	clay and sand, dry	fine	unsorted	Qya
10/26-22E1 (PT-38)	91	93	2	sand, packed	coarse	sorted	Qya
10/26-22E1 (PT-38)	93	95	2	sand	coarse	sorted	Qya
10/26-22E1 (PT-38)	95	104	9	shale	fine	sorted	Qya
10/26-22E1 (PT-38)	104	126	22	sand, dry	coarse	sorted	Qya
10/26-22E1 (PT-38)	126	138	12	clay and gravel	fine	unsorted	Qya
10/26-22E1 (PT-38)	138	140	2	shale, brown	fine	sorted	Qya
10/26-22E1 (PT-38)	140	150	10	shale and clay	fine	sorted	Qya
10/26-22E1 (PT-38)	150	162	12	shale, brown	fine	sorted	Qya
10/26-22E1 (PT-38)	162	165	3	sand, “free”	coarse	sorted	Qya
10/26-22E1 (PT-38)	165	182	17	clay and sand	fine	unsorted	Qya
10/26-22E1 (PT-38)	182	185	3	shale	fine	sorted	Qya

10/26-22E1 (PT-38)	185	195	10	sand “free”	coarse	sorted	Qya
10/26-22E1 (PT-38)	195	198	3	shale, brown	fine	sorted	Qya
10/26-22E1 (PT-38)	198	210	12	clay and sand	fine	unsorted	Qya
10/26-22E1 (PT-38)	210	214	4	shale, brown	fine	sorted	Qya
10/26-22E1 (PT-38)	214	220	6	sand, fine	coarse	sorted	Qya
10/26-22E1 (PT-38)	220	232	12	clay and sand	fine	unsorted	Qya
10/26-22E1 (PT-38)	232	245	13	sand, “free”	coarse	sorted	Qya
10/26-22E1 (PT-38)	245	250	5	clay and sand	fine	unsorted	Qya
10/26-22E1 (PT-38)	250	260	10	sand, dry	coarse	sorted	Qya
10/26-22E1 (PT-38)	260	282	22	shale and sand	fine	unsorted	Qya
10/26-22E1 (PT-38)	282	290	8	shale	fine	sorted	Qya
10/26-22E1 (PT-38)	290	295	5	shale and sand	fine	unsorted	Qya
10/26-22E1 (PT-38)	295	300	5	shale	fine	sorted	Qya
10/26-22E1 (PT-38)	300	316	16	shale and sand	fine	unsorted	Qya
10/26-22E1 (PT-38)	316	321	5	shale	fine	sorted	Qya
10/26-22E1 (PT-38)	321	330	9	shale and sand	fine	unsorted	Qya
10/26-22E1 (PT-38)	330	332	2	shale	fine	sorted	Qya

10/26-22E1 (PT-38)	332	340	8	shale and sand	fine	unsorted	Qya
10/26-22E1 (PT-38)	340	354	14	shale	fine	sorted	Qya
10/26-22E1 (PT-38)	354	358	4	clay and sand	fine	unsorted	Qya
10/26-22E1 (PT-38)	358	366	8	clay	fine	sorted	Qya
10/26-22E1 (PT-38)	366	394	28	clay and sand	fine	unsorted	Qya
10/26-22E1 (PT-38)	394	877	483	clay and sand	fine	unsorted	Qoa
10/26-22E1 (PT-38)	382	405	23	clay and sand	fine	unsorted	Qoa
10/26-22E1 (PT-38)	405	415	10	clay	fine	sorted	Qoa
10/26-22E1 (PT-38)	415	420	5	clay and sand	fine	unsorted	Qoa
10/26-22E1 (PT-38)	420	428	8	shale	fine	sorted	Qoa
10/26-22E1 (PT-38)	428	430	2	sand	coarse	sorted	Qoa
10/26-22E1 (PT-38)	430	437	7	shale	fine	sorted	Qoa
10/26-22E1 (PT-38)	437	450	13	clay and sand	fine	unsorted	Qoa
10/26-22E1 (PT-38)	450	455	5	clay	fine	sorted	Qoa
10/26-22E1 (PT-38)	455	460	5	shale	fine	sorted	Qoa
10/26-22E1 (PT-38)	460	470	10	clay and sand	fine	unsorted	Qoa
10/26-22E1 (PT-38)	470	492	22	sand, dry	coarse	sorted	Qoa

10/26-22E1 (PT-38)	492	498	6	clay and sand	fine	unsorted	Qoa
10/26-22E1 (PT-38)	498	500	2	sand	coarse	sorted	Qoa
10/26-22E1 (PT-38)	500	510	10	clay and shale	fine	unsorted	Qoa
10/26-22E1 (PT-38)	510	514	4	shale	fine	sorted	Qoa
10/26-22J1 (PT-39)	0	4	4	soil	fine	unsorted	Qya
10/26-22J1 (PT-39)	4	17	13	clay, sandy	fine	sorted	Qya
10/26-22J1 (PT-39)	17	23	6	sand	coarse	sorted	Qya
10/26-22J1 (PT-39)	23	48	25	clay, sandy	fine	sorted	Qya
10/26-22J1 (PT-39)	48	56	8	shale with streaks of sand	fine	unsorted	Qya
10/26-22J1 (PT-39)	56	68	12	clay	fine	sorted	Qya
10/26-22J1 (PT-39)	68	95	27	shale with streaks of sand	fine	unsorted	Qya
10/26-22J1 (PT-39)	95	107	12	clay sandy	fine	unsorted	Qya
10/26-22J1 (PT-39)	107	120	13	shale	fine	sorted	Qya
10/26-22J1 (PT-39)	120	135	15	sand and gravel	coarse	unsorted	Qya
10/26-22J1 (PT-39)	135	154	19	clay	fine	sorted	Qya
10/26-22J1 (PT-39)	154	198	44	shale with streaks of sand	fine	unsorted	Qya
10/26-22J1 (PT-39)	198	215	17	sand, dry	coarse	sorted	Qya

10/26-22J1 (PT-39)	215	224	9	sand with streaks of clay	coarse	unsorted	Qya
10/26-22J1 (PT-39)	224	251	27	sand and gravel with streaks of shale	coarse	unsorted	Qya
10/26-22J1 (PT-39)	251	264	13	shale	fine	sorted	Qya
10/26-22J1 (PT-39)	264	270	6	clay, sandy	fine	sorted	Qya
10/26-22J1 (PT-39)	270	276	6	sand and gravel	coarse	unsorted	Qya
10/26-22J1 (PT-39)	276	281	5	clay, sandy	fine	sorted	Qya
10/26-22J1 (PT-39)	281	293	12	clay and sand in streaks	fine	unsorted	Qya
10/26-22J1 (PT-39)	293	315	22	shale	fine	sorted	Qya
10/26-22J1 (PT-39)	315	322	7	clay, sandy, dry	fine	sorted	Qya
10/26-22J1 (PT-39)	322	332	10	clay and sand, gray	fine	unsorted	Qya
10/26-22J1 (PT-39)	332	346	14	sand “free”	coarse	sorted	Qya
10/26-22J1 (PT-39)	346	359	13	clay with streaks of sand	fine	unsorted	Qya
10/26-22J1 (PT-39)	359	369	10	clay, sand and gravel	fine	unsorted	Qya
10/26-22J1 (PT-39)	369	376	7	sand, coarse	coarse	sorted	Qya
10/26-22J1 (PT-39)	376	392	16	clay with streaks of sand	fine	unsorted	Qya
10/26-22J1 (PT-39)	392	398	6	sand	coarse	sorted	Qya
10/26-22J1 (PT-39)	398	410	12	clay	fine	sorted	Qya

10/26-22J1 (PT-39)	410	423	13	shale with streaks of sand	fine	unsorted	Qya
10/26-22J1 (PT-39)	423	465	42	shale with streaks of sand	fine	unsorted	Qoa
10/26-22J2	0	15	15	soil	fine	unsorted	Qya
10/26-22J2	15	35	20	sand, fine, packed	coarse	sorted	Qya
10/26-22J2	35	48	13	sand, coarse	coarse	sorted	Qya
10/26-22J2	48	57	9	shale, sandy	fine	unsorted	Qya
10/26-22J2	57	79	22	shale with streaks of clay	fine	sorted	Qya
10/26-22J2	79	88	9	clay and gravel	fine	unsorted	Qya
10/26-22J2	88	115	27	shale, sandy	fine	unsorted	Qya
10/26-22J2	115	145	30	shale with streaks of clay	fine	sorted	Qya
10/26-22J2	145	168	23	clay, sand, and boulders	fine	unsorted	Qya
10/26-22J2	168	195	27	sand with streaks of clay	coarse	unsorted	Qya
10/26-22J2	195	236	41	sand, coarse, and gravel	coarse	unsorted	Qya
10/26-22J2	236	246	10	clay and gravel	fine	unsorted	Qya
10/26-22J2	246	313	67	clay	fine	sorted	Qya
10/26-22J2	313	345	32	sand and gravel with streaks of clay	coarse	unsorted	Qya
10/26-22J2	345	380	35	clay	fine	sorted	Qya
10/26-22J2	380	420	40	clay with some gravel	fine	unsorted	Qya
10/26-22J2	420	430	10	shale	fine	sorted	Qoa
10/26-22J2	430	451	21	clay	fine	sorted	Qoa
10/26-22J2	451	475	24	shale with streaks of clay	fine	sorted	Qoa
10/26-22J2	475	482	7	shale, hard	fine	sorted	Qoa
10/26-22J2	482	506	24	clay with streaks of shale	fine	unsorted	Qoa
10/26-22J2	506	525	19	shale	fine	sorted	Qoa
10/26-22J2	525	575	50	clay, blue	fine	sorted	Qoa
10/26-22K1	0	50	50	soil	fine	unsorted	Qya
10/26-22K1	50	55	5	gravel, dry	coarse	sorted	Qya
10/26-22K1	55	88	33	clay, sandy	fine	sorted	Qya
10/26-22K1	88	100	12	clay with streaks of mud	fine	unsorted	Qya
10/26-22K1	100	105	5	sand and gravel	coarse	unsorted	Qya
10/26-22K1	105	112	7	clay and gravel	fine	unsorted	Qya

10/26-22K1	112	161	49	clay, sandy	fine	sorted	Qya
10/26-22K1	161	170	9	shale	fine	sorted	Qya
10/26-22K1	170	175	5	clay, sandy	fine	sorted	Qya
10/26-22K1	175	190	15	clay, sandy	fine	sorted	Qya
10/26-22K1	190	194	4	shale	fine	sorted	Qya
10/26-22K1	194	199	5	sand with streaks of clay	coarse	unsorted	Qya
10/26-22K1	199	219	20	gravel, cemented	coarse	sorted	Qya
10/26-22K1	219	248	29	clay	fine	sorted	Qya
10/26-22K1	248	268	20	clay with streaks of sand	fine	unsorted	Qya
10/26-22K1	268	274	6	shale and gravel	fine	unsorted	Qya
10/26-22K1	274	285	11	clay with streaks of sand	fine	unsorted	Qya
10/26-22K1	285	291	6	gravel, cemented	coarse	sorted	Qya
10/26-22K1	291	330	39	clay with streaks of sand	fine	unsorted	Qya
10/26-22K1	330	337	7	clay	fine	sorted	Qya
10/26-22K1	337	350	13	gravel	coarse	sorted	Qya
10/26-22K1	350	410	60	clay with streaks of sand	fine	unsorted	Qya
10/26-22K1	410	418	8	gravel, cemented	coarse	sorted	Qoa
10/26-22K1	418	423	5	clay	fine	sorted	Qoa
10/26-22K1	423	427	4	gravel, tight	coarse	sorted	Qoa
10/26-22K1	427	438	11	clay	fine	sorted	Qoa
10/26-22K1	438	445	7	gravel, tight	coarse	sorted	Qoa
10/26-22K1	445	449	4	clay	fine	sorted	Qoa
10/26-22K1	449	452	3	sand and gravel	coarse	unsorted	Qoa
10/26-22K1	452	458	6	shale and gravel	fine	unsorted	Qoa
10/26-22K1	458	470	12	clay with streaks of sand	fine	unsorted	Qoa
10/26-22K1	470	491	21	shale	fine	sorted	Qoa
10/26-22K1	491	496	5	clay	fine	sorted	Qoa
10/26-22K1	496	498	2	gravel, cemented	coarse	sorted	Qoa
10/26-22K1	498	505	7	clay with streaks of sand	fine	unsorted	Qoa
10/26-22K1	505	507	2	gravel, cemented	coarse	sorted	Qoa
10/26-23P1 (PT-40)	0	8	8	soil	fine	unsorted	Qya
10/26-23P1 (PT-40)	8	50	42	sand, dry	coarse	sorted	Qya

10/26-23P1 (PT-40)	50	55	5	sand, coarse	coarse	sorted	Qya
10/26-23P1 (PT-40)	55	65	10	sand, dry	coarse	sorted	Qya
10/26-23P1 (PT-40)	65	69	4	sand, coarse	coarse	sorted	Qya
10/26-23P1 (PT-40)	69	96	27	clay and sand	fine	unsorted	Qya
10/26-23P1 (PT-40)	96	100	4	sand, coarse	coarse	sorted	Qya
10/26-23P1 (PT-40)	100	152	52	sand, dry	coarse	sorted	Qya
10/26-23P1 (PT-40)	152	166	14	sand, “free”	coarse	sorted	Qya
10/26-23P1 (PT-40)	166	200	34	sand, dry	coarse	sorted	Qya
10/26-23P1 (PT-40)	200	222	22	sand, “free”	coarse	sorted	Qya
10/26-23P1 (PT-40)	222	226	4	gravel, cemented	coarse	sorted	Qya
10/26-23P1 (PT-40)	226	231	5	sand, dry	coarse	sorted	Qya
10/26-23P1 (PT-40)	231	250	19	sand, “free”	coarse	sorted	Qya
10/26-23P1 (PT-40)	250	264	14	sand, coarse	coarse	sorted	Qya
10/26-23P1 (PT-40)	264	271	7	sand, dry	coarse	sorted	Qya
10/26-23P1 (PT-40)	271	285	14	sand, coarse	coarse	sorted	Qya
10/26-23P1 (PT-40)	285	304	19	sand, dry	coarse	sorted	Qya
10/26-23P1 (PT-40)	304	314	10	sand, “free”	coarse	sorted	Qya

10/26-23P1 (PT-40)	314	326	12	sand, dry	coarse	sorted	Qya
10/26-23P1 (PT-40)	326	332	6	sand, “free”	coarse	sorted	Qya
10/26-23P1 (PT-40)	332	356	24	sand, dry	coarse	sorted	Qya
10/26-23P1 (PT-40)	356	360	4	sand, “free”	coarse	sorted	Qya
10/26-23P1 (PT-40)	360	371	11	sand, dry	coarse	sorted	Qya
10/26-23R1	0	20	20	soil	fine	unsorted	Qya
10/26-23R1	20	67	47	sand, hard, with streaks of clay	coarse	unsorted	Qya
10/26-23R1	67	76	9	clay, sandy, and gravel; “free” streaks	fine	unsorted	Qya
10/26-23R1	76	95	19	clay, sandy, with small gravel	fine	unsorted	Qya
10/26-23R1	95	98	3	sand, “free”	coarse	sorted	Qya
10/26-23R1	98	120	22	clay, sandy; gravel, and small boulders, “free” streaks	fine	unsorted	Qya
10/26-23R1	120	125	5	clay, sandy, hard; and small gravel	fine	unsorted	Qya
10/26-23R1	125	133	8	sand, gravel, and boulders, cemented	coarse	unsorted	Qya
10/26-23R1	133	145	12	clay sandy, and small boulders, “free” streaks	fine	unsorted	Qya
10/26-23R1	145	154	9	sand and small gravel	coarse	unsorted	Qya
10/26-23R1	154	178	24	clay, sandy, and small gravel, “free” streaks,	fine	unsorted	Qya
10/26-23R1	178	184	6	sand	coarse	sorted	Qya
10/26-23R1	184	228	44	sand and gravel	coarse	unsorted	Qya
10/26-23R1	228	232	4	sand and gravel, cemented	coarse	unsorted	Qya
10/26-23R1	232	238	6	sand	coarse	sorted	Qya
10/26-23R1	238	245	7	clay, sandy, “free” streaks	fine	sorted	Qya
10/26-23R1	245	252	7	sand	coarse	sorted	Qya
10/26-23R1	252	272	20	sand, hard, with little clay	coarse	unsorted	Qya
10/26-23R1	272	280	8	sand	coarse	sorted	Qya

10/26-23R1	280	284	4	sand, cemented	coarse	sorted	Qya
10/26-23R1	284	304	20	clay, sandy, and gravel, “free” streaks”	fine	unsorted	Qya
10/26-23R1	304	330	26	clay, sandy, and gravel, hard	fine	unsorted	Qya
10/26-23R1	330	350	20	clay, sandy and gravel, hard, “free” streaks	fine	unsorted	Qya
10/26-23R1	350	355	5	sand	coarse	sorted	Qya
10/26-23R1	355	368	13	clay, sandy, hard	fine	sorted	Qya
10/26-23R1	368	390	22	clay, sandy, hard streaks	fine	unsorted	Qya
10/26-23R1	390	395	5	clay, sandy, “free”	fine	sorted	Qya
10/26-23R1	395	414	19	sand, cemented	coarse	sorted	Qya
10/26-23R1	414	433	19	clay, sandy and small gravel, cemented	fine	unsorted	Qya
10/26-24R1 (PT-41)	0	20	20	soil	fine	unsorted	Qya
10/26-24R1 (PT-41)	20	45	25	sand, fine	coarse	sorted	Qya
10/26-24R1 (PT-41)	45	67	22	sand, coarse	coarse	sorted	Qya
10/26-24R1 (PT-41)	67	123	56	sand, coarse and small gravel	coarse	unsorted	Qya
10/26-24R1 (PT-41)	123	126	3	shale, hard	fine	sorted	Qya
10/26-24R1 (PT-41)	126	135	9	sand, fine, hard-packed	coarse	sorted	Qya
10/26-24R1 (PT-41)	135	141	6	sand, cemented	coarse	sorted	Qya
10/26-24R1 (PT-41)	141	154	13	boulders, hard	coarse	sorted	Qya
10/26-24R1 (PT-41)	154	198	44	sand, coarse, with streaks of shale	coarse	unsorted	Qya
10/26-24R1 (PT-41)	198	233	35	sand, coarse, with streaks of clay	coarse	unsorted	Qya
10/26-24R1 (PT-41)	233	275	42	clay and sand	fine	unsorted	Qya

10/26-24R1 (PT-41)	275	278	3	boulders, hard	coarse	sorted	Qya
10/26-24R1 (PT-41)	278	298	20	clay, yellow	fine	sorted	Qya
10/26-9R1 (PT-27)	0	24	24	soil	fine	unsorted	Qoa
10/26-9R1 (PT-27)	24	28	4	clay	fine	sorted	Qoa
10/26-9R1 (PT-27)	28	40	12	sand and boulders	coarse	unsorted	Qoa
10/26-9R1 (PT-27)	40	48	8	gravel, cemented	coarse	sorted	Qoa
10/26-9R1 (PT-27)	48	60	12	sand and boulders	coarse	unsorted	Qoa
10/26-9R1 (PT-27)	60	68	8	gravel, cemented	coarse	sorted	Qoa
10/26-9R1 (PT-27)	68	82	14	sand and gravel	coarse	unsorted	Qoa
10/26-9R1 (PT-27)	82	92	10	clay	fine	sorted	Qoa
10/26-9R1 (PT-27)	92	101	9	clay, sandy	fine	sorted	Qoa
10/26-9R1 (PT-27)	101	114	13	sand, fine	coarse	sorted	Qoa
10/26-9R1 (PT-27)	114	118	4	clay and boulders	fine	unsorted	Qoa
10/26-9R1 (PT-27)	118	126	8	sand and gravel	coarse	unsorted	Qoa
10/26-9R1 (PT-27)	126	133	7	clay	fine	sorted	Qoa
10/26-9R1 (PT-27)	133	136	3	sand and gravel	coarse	unsorted	Qoa
10/26-9R1 (PT-27)	136	145	9	clay and boulders	fine	unsorted	Qoa

10/26-9R1 (PT-27)	145	154	9	sand and gravel	coarse	unsorted	Qoa
10/26-9R1 (PT-27)	154	159	5	clay	fine	sorted	Qoa
10/26-9R1 (PT-27)	159	161	2	sand and gravel	coarse	unsorted	Qoa
10/26-9R1 (PT-27)	161	180	19	clay, blue	fine	sorted	Qoa
10/26-9R1 (PT-27)	180	188	8	sand, gravel, and boulders	coarse	unsorted	Qoa
10/26-9R1 (PT-27)	188	204	16	clay, blue	fine	sorted	Qoa
10/26-9R1 (PT-27)	204	208	4	gravel and boulders	coarse	unsorted	Qoa
10/26-9R1 (PT-27)	208	212	4	clay and boulders	fine	unsorted	Qoa
10/26-9R1 (PT-27)	212	219	7	gravel, cemented	coarse	sorted	Qoa
10/26-9R1 (PT-27)	219	222	3	clay and boulders, not water-bearing	fine	unsorted	Qoa
10/26-9R2 (PT-28)	0	33	33	clay	fine	sorted	Qoa
10/26-9R2 (PT-28)	33	48	15	gravel, “free”	coarse	sorted	Qoa
10/26-9R2 (PT-28)	48	54	6	gravel, “tight”	coarse	sorted	Qoa
10/26-9R2 (PT-28)	54	99	45	clay, blue and brown	fine	sorted	Qoa
10/26-9R2 (PT-28)	99	109	10	gravel, “free”	coarse	sorted	Qoa
10/26-9R2 (PT-28)	109	120	11	clay	fine	sorted	Qoa
10/26-9R2 (PT-28)	120	129	9	gravel, “free”	coarse	sorted	Qoa

10/26-9R2 (PT-28)	129	157	28	clay	fine	sorted	Qoa
10/26-9R2 (PT-28)	157	166	9	gravel	coarse	sorted	Qoa
10/26-9R2 (PT-28)	166	176	10	clay	fine	sorted	Qoa
10/26-9R2 (PT-28)	176	202	26	older continental deposits gravel, “tight”	coarse	unsorted	Qoa
10/26-9R2 (PT-28)	202	230	28	clay	fine	sorted	Qoa
10/26-9R2 (PT-28)	230	240	10	clay with some gravel	fine	unsorted	Qoa
10/26-9R2 (PT-28)	240	250	10	clay, blue	fine	sorted	Qoa
10/26-9R2 (PT-28)	250	275	25	clay, brown	fine	sorted	Qoa
10/26-9R2 (PT-28)	275	289	14	gravel, tight	coarse	sorted	Qoa
10/26-9R2 (PT-28)	289	320	31	sand and boulders, hard	coarse	unsorted	Qoa
10/26-9R2 (PT-28)	320	335	15	clay, brown	fine	sorted	Qoa
10/26-9R2 (PT-28)	335	355	20	clay, sandy, red	fine	sorted	Qoa
10/26-9R2 (PT-28)	355	360	5	clay, sticky, brown,	fine	sorted	Qoa
10/26-9R2 (PT-28)	360	370	10	clay, blue	fine	sorted	Qoa
10/26-9R2 (PT-28)	370	380	10	clay, sticky, brown	fine	sorted	Qoa
10/27-11A2	0	20	20	soil	fine	unsorted	Qya
10/27-11A2	20	55	35	clay with sand and gravel	fine	unsorted	Qya
10/27-11A2	55	115	60	sand and gravel	coarse	unsorted	Qya

10/27-11A2	115	175	60	sand and gravel with streaks of clay	coarse	unsorted	Qya
10/27-11A2	175	226	51	clay	fine	sorted	Qoa
10/27-11A2	226	265	39	clay and gravel	fine	unsorted	Qoa
10/27-11A2	265	280	15	clay, sand, and gravel	fine	unsorted	Qoa
10/27-11A2	280	490	210	clay, sticky, yellow,	fine	sorted	Qoa
10/27-11A2	490	533	43	clay, sandy, yellow	fine	sorted	Qoa
10/27-11C1 (PT-50)	0	26	26	soil	fine	unsorted	Qya
10/27-11C1 (PT-50)	26	28	2	clay, blue	fine	sorted	Qya
10/27-11C1 (PT-50)	28	46	18	clay, gray, with soft streaks	fine	unsorted	Qya
10/27-11C1 (PT-50)	46	47	1	clay, blue	fine	sorted	Qya
10/27-11C1 (PT-50)	47	57	10	clay, black	fine	sorted	Qya
10/27-11C1 (PT-50)	57	62	5	sand and gravel	coarse	unsorted	Qya
10/27-11C1 (PT-50)	62	83	21	clay, black, and boulders	fine	unsorted	Qya
10/27-11C1 (PT-50)	83	90	7	sand and cobbles up to 2 inches in diameter	coarse	unsorted	Qya
10/27-11C1 (PT-50)	90	97	7	clay, black, and boulders	fine	unsorted	Qya
10/27-11C1 (PT-50)	97	100	3	sand with cobbles up to 3 inches in diameter	coarse	unsorted	Qya
10/27-11C1 (PT-50)	100	131	31	clay, yellow-brown, and cobbles	fine	unsorted	Qya
10/27-11C1 (PT-50)	131	221	90	clay, yellow-brown, and cobbles	fine	unsorted	Qoa
10/27-11C1 (PT-50)	221	378	157	clay, blue	fine	sorted	Qoa
10/27-12E1	0	33	33	clay	fine	sorted	Qya

10/27-12E1	33	37	4	sand	coarse	sorted	Qya
10/27-12E1	37	64	27	clay	fine	sorted	Qya
10/27-12E1	64	70	6	sand and gravel	coarse	unsorted	Qya
10/27-12E1	70	84	14	clay, blue	fine	sorted	Qya
10/27-12E1	84	127	43	gravel	coarse	sorted	Qya
10/27-12E1	127	177	50	shale, hard,	fine	sorted	Qya
10/27-12E1	177	187	10	sand and boulders, hard	coarse	unsorted	Qya
10/27-12E1	187	217	30	clay, brown	fine	sorted	Qoa
10/27-12E1	217	219	2	clay, blue	fine	sorted	Qoa
10/27-12E1	219	228	9	clay, yellow, and coarse sand	fine	unsorted	Qoa
10/27-12E1	228	248	20	clay, blue	fine	sorted	Qoa
10/27-12J1 (PT-51)	0	36	36	clay	fine	sorted	Qya
10/27-12J1 (PT-51)	36	40	4	gravel	coarse	sorted	Qya
10/27-12J1 (PT-51)	40	42	2	clay	fine	sorted	Qya
10/27-12J1 (PT-51)	42	47	5	gravel	coarse	sorted	Qya
10/27-12J1 (PT-51)	47	53	6	clay	fine	sorted	Qya
10/27-12J1 (PT-51)	53	68	15	gravel	coarse	sorted	Qya
10/27-12J1 (PT-51)	68	70	2	clay	fine	sorted	Qya
10/27-12J1 (PT-51)	70	97	27	gravel	coarse	sorted	Qya
10/27-12J1 (PT-51)	97	106	9	clay	fine	sorted	Qoa
10/27-12J1 (PT-51)	106	134	28	gravel	coarse	sorted	Qoa
10/27-12J1 (PT-51)	134	138	4	clay	fine	sorted	Qoa

10/27-12J2 PT-52)	0	71	71	no record	nd	nd	Qya
10/27-12J2 PT-52)	71	85	14	sand	coarse	sorted	Qya
10/27-12J2 PT-52)	85	131	46	no record	nd	nd	Qoa
10/27-12J2 PT-52)	131	132	1	sand	coarse	sorted	Qoa
10/27-12J2 PT-52)	132	182	50	no record	nd	nd	Qoa
10/27-12J2 PT-52)	182	184	2	sand	coarse	sorted	Qoa
10/27-12J2 PT-52)	184	188	4	no record	nd	nd	Qoa
10/27-12J2 PT-52)	188	191	3	sand	coarse	sorted	Qoa
10/27-12J2 PT-52)	191	253	62	no record	nd	nd	Qoa
10/27-12J2 PT-52)	253	258	5	sand	coarse	sorted	Qoa
10/27-12J2 PT-52)	258	290	32	no record	nd	nd	Qoa
10/27-12J2 PT-52)	290	294	4	sand	coarse	sorted	Qoa
10/27-12R1 (PT-53)	0	36	36	soil	fine	unsorted	Qya
10/27-12R1 (PT-53)	36	42	6	sand, water-bearing	coarse	sorted	Qya
10/27-12R1 (PT-53)	42	67	25	gravel and boulders as much as 6 inches in diameter	coarse	unsorted	Qya
10/27-12R1 (PT-53)	67	72	5	clay, brown	fine	sorted	Qya
10/27-12R1 (PT-53)	72	76	4	sand and boulders as much as 6 inches in diameter	coarse	unsorted	Qya

10/27-12R1 (PT-53)	76	108	32	clay, yellow	fine	sorted	Qya
10/27-12R1 (PT-53)	108	110	2	sand and boulders as much as 6 inches in diameter	coarse	unsorted	Qya
10/27-12R1 (PT-53)	110	131	21	clay, brown	fine	sorted	Qya
CUY-G-89	0	5	5	clay and gravel	fine	unsorted	nd
CUY-G-89	5	41	36	decomposed granite	coarse	sorted	nd
CUY-G-89	41	43	2	clay	fine	sorted	nd
CUY-G-89	43	78	35	decomposed granite and loose rock	coarse	unsorted	nd
CUY-G-89	78	116	38	clay, gravel and boulders	fine	unsorted	nd
CUY-G-89	116	124	8	sandstone	coarse	sorted	nd
CUY-G-89	124	145	21	hard, sandy shale	fine	sorted	nd
CUY-G-89	145	171	26	clay, gravel and boulders	fine	unsorted	nd
CUY-G-89	171	215	44	shale streaks sandstone	fine	unsorted	nd
CUY-G-90	0	3	3	soil and gravel	fine	unsorted	nd
CUY-G-90	3	91	88	decomposed granite	coarse	sorted	nd
CUY-G-90	91	102	11	clay and gravel	fine	unsorted	nd
CUY-G-90	102	160	58	decomposed granite	coarse	sorted	nd
CUY-G-91	0	60	60	silty sand (sp), moist, brown to red, medium dense, poorly graded, no waste or odor	fine	unsorted	nd
CUY-G-92	0	50	50	silty sand (sp), yellow brown, medium dense, poorly graded, no waste or gas odor	fine	unsorted	nd
CUY-G-92	50	60	10	scattered sandstone fragments	coarse	unsorted	nd
9/24-19F1 (CUY-03)	0	27	27	soil, brown	fine	unsorted	Qya
9/24-19F1 (CUY-03)	27	64	37	gravel, fine, dry	coarse	sorted	Qya
9/24-19F1 (CUY-03)	64	67	3	gravel, fine, “small water seepage”	coarse	sorted	Qya
9/24-19F1 (CUY-03)	67	74	7	gravel, fine, dry	coarse	sorted	Qya

9/24-19F1 (CUY-03)	74	77	3	gravel, coarse, water-bearing	coarse	sorted	Qya
9/24-19F1 (CUY-03)	77	85	8	sand, coarse, water-bearing	coarse	sorted	Qya
9/24-19F1 (CUY-03)	85	91	6	gravel, fine, water-bearing,	coarse	sorted	Qya
9/24-19F1 (CUY-03)	91	97	6	clay and gravel, dry	fine	unsorted	Qya
9/24-19F1 (CUY-03)	97	113	16	gravel, fine, water-bearing	coarse	sorted	Qya
9/24-30B2	0	50	50	silt and sand	fine	unsorted	Qya
9/24-30B2	50	169	119	sand and gravel, “good”	coarse	unsorted	Qya
9/24-30B2	169	180	11	clay, sandy	fine	sorted	Qya
9/24-30B2	180	190	10	quicksand	coarse	sorted	Qya
9/25-111	0	262	262	sand, gravel and boulders; occasional layers of clay	coarse	unsorted	Qya
9/25-111	262	328	66	sand, gravel and boulders; occasional layers of clay	coarse	unsorted	Qoa
9/25-111	328	330	2	clay, sticky, dark	fine	sorted	Qoa
9/25-111	330	332	2	gravel	coarse	sorted	Qoa
9/25-111	332	334	2	sand, hard	coarse	sorted	Qoa
9/25-111	334	347	13	sand, gravel, and boulders; water-bearing	coarse	unsorted	Qoa
9/25-111	347	349	2	clay, yellow	fine	sorted	Qoa
9/25-111	349	358	9	“shale”, muddy	fine	sorted	Qoa
9/25-111	358	366	8	sand and gravel	coarse	unsorted	Qoa
9/25-111	366	368	2	clay, sandy, light-colored	fine	sorted	Qoa
9/25-3D1	0	82	82	No record, (bases of alluvium and terrace deposits probably within this unit)	nd	nd	Qya
9/25-3D1	82	190	108	No record, (bases of alluvium and terrace deposits probably within this unit)	nd	nd	Qoa
9/25-3D1	190	197	7	gravel, coarse, dry	coarse	sorted	Qoa
9/25-3D1	197	211	14	gravel, coarse, water-bearing	coarse	sorted	Qoa
9/25-3D1	211	250	39	gravel, coarse, and boulders	coarse	unsorted	Qoa

9/26-4J1	0	3	3	soil	fine	unsorted	Qoa
9/26-4J1	3	10	7	sand and gravel, brown	coarse	unsorted	Qoa
9/26-4J1	10	20	10	clay, yellow	fine	sorted	Qoa
9/26-4J1	20	38	18	clay, yellow, and boulders	fine	unsorted	Qoa
9/26-4J1	38	65	27	clay, hard, yellow, and fine sand	fine	unsorted	Qoa
9/26-4J1	65	85	20	clay, yellow	fine	sorted	Qoa
9/26-4J1	85	197	112	clay, yellow, and streaks of sand	fine	unsorted	Qoa
9/26-4J1	197	200	3	sand, hard	coarse	sorted	Qoa
9/26-4J1	200	260	60	clay and sand	fine	unsorted	Qoa
9/26-4J1	260	283	23	clay, hard, yellow	fine	sorted	Qoa
9/26-4J1	283	295	12	sand, water-bearing	coarse	sorted	Qoa
9/26-4J1	295	297	2	clay, yellow	fine	sorted	Qoa
9/26-4J1	297	302	5	sand, water-bearing, “about 3 gpm”	coarse	sorted	Qoa
9/26-4J1	302	304	2	clay, yellow	fine	sorted	Qoa
9/26-4J1	304	309	5	sand, water-bearing,	coarse	sorted	Qoa
9/26-4J1	309	327	18	clay	fine	sorted	Qoa
CUY-G-64	0	10	10	---	fine	unsorted	Qya
CUY-G-64	10	40	30	---	coarse	unsorted	Qya
CUY-G-64	40	60	20	---	fine	sorted	Qya
CUY-G-64	60	70	10	---	coarse	unsorted	Qya
CUY-G-64	70	135	65	---	fine	sorted	Qya
CUY-G-64	135	165	30	---	fine	unsorted	Qya
CUY-G-64	165	180	15	---	coarse	unsorted	Qya
CUY-G-64	180	188	8	---	fine	sorted	Qya
CUY-G-64	188	200	12	---	coarse	unsorted	Qya
CUY-G-64	200	220	20	---	fine	unsorted	Qya
CUY-G-64	220	255	35	---	coarse	unsorted	Qya
CUY-G-64	255	346	91	---	fine	sorted	Qya
CUY-G-64	346	357	11	---	coarse	unsorted	Qya
CUY-G-64	357	368	11	---	fine	sorted	Qya
CUY-G-64	368	380	12	---	coarse	unsorted	Qya
CUY-G-64	380	466	86	---	fine	unsorted	Qya

CUY-G-64	466	505	39	---	fine	unsorted	Qoa
CUY-G-64	505	685	180	---	fine	unsorted	Qoa
CUY-G-64	685	690	5	---	coarse	unsorted	Qoa
CUY-G-64	690	720	30	---	fine	sorted	Qoa
CUY-G-64	720	770	50	---	fine	unsorted	Qoa
CUY-G-64	770	880	110	---	coarse	unsorted	Qoa
CUY-G-64	880	902	22	---	fine	sorted	Qoa
CUY-G-64	902	960	58	---	fine	sorted	QTm
CUY-G-64	960	1,066	106	---	fine	sorted	QTm
CUY-G-65	0	10	10	---	fine	sorted	Qya
CUY-G-65	10	70	60	---	coarse	unsorted	Qya
CUY-G-65	70	284	214	---	coarse	unsorted	Qya
CUY-G-65	284	377	93	---	coarse	sorted	Qya
CUY-G-65	377	544	167	---	coarse	unsorted	Qya
CUY-G-65	544	600	56	---	coarse	unsorted	Qya
CUY-G-65	600	733	133	---	coarse	unsorted	QTm
CUY-G-65	733	842	109	---	coarse	sorted	QTm
CUY-G-65	842	1,097	255	---	coarse	unsorted	QTm
CUY-G-66	0	302	302	---	coarse	sorted	Qya
CUY-G-66	302	422	120	---	coarse	unsorted	Qya
CUY-G-66	422	433	11	---	fine	unsorted	Qya
CUY-G-66	433	563	130	---	fine	unsorted	Qoa
CUY-G-66	563	623	60	---	fine	sorted	Qoa
CUY-G-66	623	683	60	---	fine	unsorted	Qoa
CUY-G-66	683	780	97	---	fine	sorted	Qoa
CUY-G-66	780	1,020	240	---	fine	unsorted	Qoa
CUY-G-67	0	8	8	---	fine	sorted	Qya
CUY-G-67	8	80	72	---	coarse	sorted	Qya
CUY-G-67	80	90	10	---	coarse	sorted	Qya
CUY-G-67	90	162	72	---	coarse	sorted	Qya
CUY-G-67	162	224	62	---	coarse	unsorted	Qya
CUY-G-67	224	185	409	---	coarse	unsorted	Qya
CUY-G-67	185	694	61	---	coarse	unsorted	Qoa
CUY-G-67	694	744	50	---	fine	unsorted	Qoa

CUY-G-67	744	1,020	276	---	fine	unsorted	Qoa
CUY-G-93	0	2	2	---	fine	unsorted	Qoa
CUY-G-93	2	35	33	---	coarse	unsorted	Qoa
CUY-G-93	35	45	10	---	fine	sorted	Qoa
CUY-G-93	45	100	55	---	coarse	unsorted	Qoa
CUY-G-93	100	115	15	---	fine	sorted	Qoa
CUY-G-93	115	130	15	---	coarse	unsorted	Qoa
CUY-G-93	130	170	40	---	fine	unsorted	Qoa
CUY-G-93	170	185	15	---	coarse	unsorted	Qoa
CUY-G-93	185	205	20	---	fine	sorted	Qoa
CUY-G-93	205	240	35	---	coarse	unsorted	Qoa
CUY-G-93	240	250	10	---	fine	sorted	Qoa
CUY-G-93	250	265	15	---	coarse	unsorted	Qoa
CUY-G-93	265	335	70	---	fine	unsorted	Qoa
CUY-G-93	335	375	40	---	coarse	sorted	Qoa
CUY-G-93	375	380	5	---	coarse	unsorted	Qoa
CUY-G-93	380	455	75	---	fine	unsorted	Qoa
CUY-G-93	455	580	125	---	coarse	sorted	Qoa
CUY-G-93	580	620	40	---	coarse	sorted	Qoa
CUY-G-93	620	725	105	---	coarse	sorted	Qoa
CUY-G-93	725	730	5	---	fine	sorted	Qoa
CUY-G-93	730	750	20	---	coarse	unsorted	Qoa
CUY-G-93	750	760	10	---	coarse	unsorted	QTm
CUY-G-94	0	42	42	---	coarse	sorted	Qoa
CUY-G-94	42	52	10	---	coarse	unsorted	Qoa
CUY-G-94	52	62	10	---	coarse	unsorted	Qoa
CUY-G-94	62	92	30	---	coarse	unsorted	Qoa
CUY-G-94	92	123	31	---	coarse	unsorted	Qoa
CUY-G-94	123	133	10	---	coarse	unsorted	Qoa
CUY-G-94	133	155	22	---	coarse	unsorted	Qoa
CUY-G-94	155	165	10	---	coarse	unsorted	Qoa
CUY-G-94	165	175	10	---	coarse	unsorted	Qoa
CUY-G-94	175	216	41	---	coarse	unsorted	Qoa
CUY-G-94	216	226	10	---	fine	unsorted	Qoa

CUY-G-94	226	310	84	---	coarse	unsorted	Qoa
CUY-G-94	310	340	30	---	coarse	unsorted	Qoa
CUY-G-94	340	373	33	---	coarse	unsorted	Qoa
CUY-G-94	373	468	95	---	coarse	unsorted	Qoa
CUY-G-94	468	500	32	---	fine	sorted	QTm
CUY-G-94	500	522	22	---	coarse	unsorted	QTm
CUY-G-94	522	553	31	---	coarse	unsorted	QTm
CUY-G-94	553	563	10	---	coarse	sorted	QTm
CUY-G-94	563	573	10	---	coarse	unsorted	QTm
CUY-G-94	573	583	10	---	coarse	unsorted	QTm
CUY-G-94	583	657	74	---	fine	unsorted	QTm
CUY-G-94	657	688	31	---	coarse	unsorted	QTm
CUY-G-94	688	700	12	---	fine	unsorted	QTm
CUY-G-94	700	732	32	---	coarse	unsorted	QTm
CUY-G-94	732	752	20	---	coarse	unsorted	QTm
CUY-G-94	752	863	111	---	fine	unsorted	QTm
CUY-G-94	863	935	72	---	fine	unsorted	QTm
CUY-G-94	935	996	61	---	fine	unsorted	QTm
CUY-G-94	996	1,010	14	---	fine	unsorted	QTm
CUY-G-95	0	3	3	Top soil	fine	unsorted	Qya
CUY-G-95	3	6	3	Brown silt	fine	sorted	Qya
CUY-G-95	6	9	3	Large rock with silt	coarse	unsorted	Qya
CUY-G-95	9	12	3	Coarse gravel and rock with silt	coarse	unsorted	Qya
CUY-G-95	12	16	4	Fine to coarse sand and gravel with silt	coarse	unsorted	Qya
CUY-G-95	16	93	77	Brown silt with very sandy silt	fine	unsorted	Qya
CUY-G-95	93	210	117	Brown silty clay with some very sandy clay streaks	fine	unsorted	Qya
CUY-G-95	210	246	36	Brown and gray clay with some very sandy clay streaks	fine	unsorted	Qya

CUY-G-95	246	271	25	Brown and gray clay with some very sandy clay streaks	fine	unsorted	Qoa
CUY-G-95	271	283	12	Medium to coarse sand to medium to coarse gravel - tight	coarse	unsorted	Qoa
CUY-G-95	283	301	18	Gray clay	fine	sorted	Qoa
CUY-G-95	301	305	4	Medium to coarse sand to medium to coarse gravel - slight tight	coarse	unsorted	Qoa
CUY-G-95	305	316	11	Gray clay with sandy clay stringers	fine	unsorted	Qoa
CUY-G-95	316	320	4	Medium to coarse sand to medium gravel	coarse	unsorted	Qoa
CUY-G-96	0	2	2	Top soil	fine	unsorted	Qya
CUY-G-96	2	12	10	Rock and boulder mixed with silt	coarse	unsorted	Qya
CUY-G-96	12	22	10	Brown silt with some rock	fine	unsorted	Qya
CUY-G-96	22	218	196	Brown and gray clay with sand stringers; water changed to yellow color	fine	unsorted	Qya
CUY-G-96	218	225	7	fine to coarse sand to medium fine gravel	coarse	unsorted	Qya
CUY-G-96	225	246	21	very sandy clay with sand lenses	fine	unsorted	Qya
CUY-G-96	246	322	76	very sandy clay with sand lenses	fine	unsorted	Qoa
CUY-G-96	322	328	6	Medium to coarse sand to medium coarse gravel - blue	coarse	unsorted	Qoa
CUY-G-96	328	344	16	clayey medium to coarse sand to medium coarse gravel	fine	unsorted	Qoa

CUY-G-96	344	348	4	Medium to coarse sand to medium coarse gravel - blue	coarse	unsorted	Qoa
CUY-G-96	348	370	22	Blue gray clay with sand stringers	fine	unsorted	Qoa
CUY-G-97	0	2	2	Sandy top soil	fine	unsorted	Qoa
CUY-G-97	2	6	4	Brown silt with large rock	fine	unsorted	Qoa
CUY-G-97	6	136	130	Brown silty clay	fine	sorted	Qoa
CUY-G-97	136	283	147	Sandy clay with clay lenses	fine	unsorted	Qoa
CUY-G-97	283	300	17	Very sandy tan clay	fine	unsorted	Qoa
CUY-G-97	300	311	11	Fine to coarse sand to medium coarse gravel - tan	coarse	unsorted	Qoa
CUY-G-97	311	353	42	Gray and tan clay with sandy clay lenses	fine	unsorted	Qoa
CUY-G-97	353	376	23	Fine to coarse sand to medium coarse gravel - blue, tight	coarse	unsorted	Qoa
CUY-G-97	376	394	18	Blue gray clay with sand base; soft	fine	unsorted	Qoa
CUY-G-97	394	398	4	Medium to coarse sand to medium fine gravel - blue	coarse	unsorted	Qoa
CUY-G-97	398	412	14	Blue gray clay soft	fine	sorted	Qoa
CUY-G-97	412	420	8	Medium to coarse sand to medium gravel - blue	coarse	unsorted	Qoa
CUY-G-98	0	2	2	Sandy top soil	fine	unsorted	Qya
CUY-G-98	2	17	15	Brown sandy silt with rocks and boulders	fine	unsorted	Qya
CUY-G-98	17	18	1	Cemented clay and sand	fine	unsorted	Qya
CUY-G-98	18	21	3	silt with rocks and boulders	fine	unsorted	Qya
CUY-G-98	21	177	156	Tan clay with sand lenses	fine	unsorted	Qya
CUY-G-98	177	253	76	Tan clay with sand lenses	fine	unsorted	Qoa
CUY-G-98	253	266	13	Fine to coarse sand to medium gravel - tan	coarse	unsorted	Qoa
CUY-G-98	266	334	68	tan to gray clay	fine	unsorted	Qoa

CUY-G-98	334	360	26	Medium Fine to coarse sand to medium gravel - gray	coarse	unsorted	Qoa
CUY-G-98	360	380	20	Gray clay with sand stringers	fine	unsorted	Qoa
CUY-G-98	380	410	30	Gray clay	fine	sorted	Qoa
CUY-G-98	410	490	80	Fine to coarse sand mixed with clay	fine	unsorted	Qoa
CUY-G-98	490	563	73	Gray clay	fine	sorted	Qoa
CUY-G-98	563	633	70	Medium to coarse sand to medium coarse gravel with some clay lenses - slightly loose - took lots of water	coarse	unsorted	Qoa
CUY-G-98	633	669	36	Gray clay	fine	sorted	Qoa
CUY-G-98	669	702	33	Gray clay with sand stringers - dirty	fine	unsorted	QTm
CUY-G-98	702	723	21	very fine to medium coarse sand	coarse	unsorted	QTm
CUY-G-98	723	747	24	Gray clay -- slightly tight	fine	sorted	QTm
CUY-G-98	747	765	18	very fine to medium coarse sand - gray	coarse	unsorted	QTm
CUY-G-98	765	820	55	gray clay and tight	fine	sorted	QTm
CUY-G-101	0	3	3	very sandy top soil	fine	unsorted	Qya
CUY-G-101	3	18	15	silt and gravel with rocks	coarse	unsorted	Qya
CUY-G-101	18	19	1	Cemented clay	fine	sorted	Qya
CUY-G-101	19	35	16	sand, gravel, rocks with silt	coarse	unsorted	Qya
CUY-G-101	35	40	5	tan clay	fine	sorted	Qya
CUY-G-101	40	70	30	tan clay	fine	sorted	Qya
CUY-G-101	70	142	72	tan clay with sand base	fine	unsorted	Qya
CUY-G-101	142	145	3	very cemented sand and gravel	coarse	unsorted	Qya
CUY-G-101	145	175	30	tan clay	fine	sorted	Qya
CUY-G-101	175	196	21	Fine to coarse sand to medium gravel - tight	coarse	unsorted	Qoa

CUY-G-101	196	229	33	tan and gray clay	fine	sorted	Qoa
CUY-G-101	229	298	69	Fine to coarse sand to fine gravel with clay	fine	unsorted	Qoa
CUY-G-101	298	418	120	tan and gray clay with sand lenses	fine	unsorted	Qoa
CUY-G-101	418	429	11	Medium to coarse sand to fine gravel -tight	coarse	unsorted	Qoa
CUY-G-101	429	490	61	Gray clay	fine	sorted	Qoa
CUY-G-101	490	500	10	Medium to coarse sand to fine gravel -tight	coarse	unsorted	Qoa
CUY-G-101	500	590	90	gray clay with sand	fine	unsorted	Qoa
CUY-G-101	590	605	15	Medium to coarse sand to fine gravel -tight	coarse	unsorted	Qoa
CUY-G-101	605	627	22	Gray clay with sand stringers	fine	unsorted	Qoa
CUY-G-101	627	652	25	Medium fine to coarse sand to medium gravel -tight	coarse	unsorted	Qoa
CUY-G-101	652	710	58	Gray clay	fine	sorted	Qoa
CUY-G-101	710	734	24	Fine to coarse sand to fine gravel - tight	coarse	unsorted	QTm
CUY-G-101	734	747	13	Gray clay	fine	sorted	QTm
CUY-G-101	747	763	16	very fine to coarse sand - tight	coarse	unsorted	QTm
CUY-G-101	763	800	37	Gray clay	fine	sorted	QTm
CUY-G-101	800	811	11	very fine to coarse sand - tight	coarse	unsorted	QTm
CUY-G-101	811	820	9	Gray clay - tight	fine	unsorted	Qya
CUY-G-102	0	2	2	Top soil	fine	unsorted	Qya
CUY-G-102	2	6	4	Brown sandy silt	fine	unsorted	Qya
CUY-G-102	6	43	37	Brown silt with rocks and boulder with sand lenses	fine	unsorted	Qya
CUY-G-102	43	54	11	brown clay	fine	sorted	Qya
CUY-G-102	54	63	9	hard cemented sand and rock	coarse	unsorted	Qya

CUY-G-102	63	110	47	brown and tan clay with sand base	fine	unsorted	Qya
CUY-G-102	110	117	7	fine to coarse sand	coarse	unsorted	Qya
CUY-G-102	117	127	10	tan clay	fine	sorted	Qya
CUY-G-102	127	132	5	very hard rock	coarse	unsorted	Qya
CUY-G-102	132	169	37	brown clay	fine	sorted	Qya
CUY-G-102	169	189	20	very hard rock and sandstone	coarse	unsorted	Qya
CUY-G-102	189	199	10	brown clay	fine	sorted	Qya
CUY-G-102	199	210	11	fine to coarse sand with some medium coarse gravel	coarse	unsorted	Qya
CUY-G-102	210	230	20	tan clay	fine	sorted	Qya
CUY-G-102	230	244	14	fine to coarse sand with some medium coarse gravel	coarse	unsorted	Qya